Distortional Mechanics of Thin-Walled Structural Elements

Andreassen, Michael Joachim; Nielsen, Leif Otto; Jönsson, Jeppe

Publication date:
2012

Document Version
Publisher's PDF, also known as Version of record

Distortional Mechanics of Thin-Walled Structural Elements

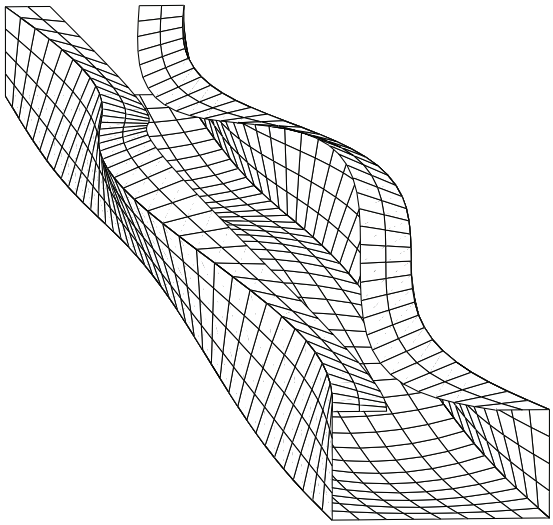

Michael Joachim Andreassen

PhD Thesis

Department of Civil Engineering

2012

DTU Civil Engineering Report R-273 (UK)
September 2012

DTU Civil Engineering
Department of Civil Engineering

Distortional Mechanics of Thin-Walled Structural Elements

Distortional Mechanics of Thin-Walled Structural Elements

PhD dissertation

DTU Byg, Department of Civil Engineering
Section of Structural Engineering
Technical University of Denmark
Brovej – Building 118
2800 Kgs. Lyngby

Byg report R–273
ISBN: 9788778773555

Typeset in LaTeX

To Nikoline, Pauline & Filippa

Preface

This thesis is a partial fulfilment of the requirements for the Ph.D. degree. The work is performed at DTU Byg, Department of Civil Engineering, Section of Structural Engineering at the Technical University of Denmark. The main supervisor was Professor Jeppe Jönsson together with supervisor Associate Professor Leif Otto Nielsen both affiliated with DTU Byg. Additionally, there was a good collaboration with Professor Nuno Silvestre and Professor Dinar Camotim both affiliated with Instituto Superior Técnico, Department of Civil Engineering and Architecture at the Technical University of Lisbon.

The thesis was submitted the 22th of June 2012 and defended at a public defence at DTU the 27th of September 2012. Official opponents were Professor Henrik Stang, Technical University of Denmark, Professor Nuno Silvestre, Technical University of Lisbon, and Professor Jens Schneider, Technical University of Darmstadt. Subsequently the Ph.D. degree was awarded from the Technical University of Denmark.

Compared to the original submitted version of the thesis, several minor editorial corrections are implemented as well as several minor comments from the opponents during the defence. A single paper on which the thesis is based is changed from submitted to published.

Kgs. Lyngby, November 2012

Michael Joachim Andreassen

Acknowledgements

A gratitude is directed to several people who have been an invaluable help and assisted me throughout the project.

A very special gratitude goes to professor Jeppe Jönsson, my teacher and mentor, who is due to much of what I am today as researcher. The extensive scientific knowledge, patience, the spirit to meet the rigorous analysis and synthesis and pursuit of perfection are aspects of his personality that I have learned from. I want to thank you for your presence in many joyful moments and for your cooperation and guidance. Moral values, unconditional and invaluable support at work as well as private are some aspects that I appreciate very much.

Also a thanks goes to associate professor Leif Otto Nielsen for his extensive scientific knowledge, kindness and guidance throughout the project.

I would also like to thank Otto Mønsteds Fond, Larsen og Nielsen Fonden, Berg Nielsens legat, Rudolph Als Fondet, Erik Hegenhofts Legat, Fabrikant Vilhelm Pedersen og hustrus Legat, Ingeniør Alexandre Haynman and hustru Nina Haynmans Fond and Lemvigh-Müller Fonden for the funding of a six month research stay at the Technical University of Lisbon in 2010.

Further I wish to express my gratitude to professor Nuno Silvestre and professor Dinar Camotim for making my external research stay possible. Professor Nuno Silvestre is greatly acknowledged for his hospitality during my stay in Portugal and I really enjoyed the delightful acquaintance and the valuable discussions I have had with you and the IST research group especially Dinar Camotim, Cilmar Basaglia, Nuno Silva, Pedro Natário and Rui Bebiano.

I am also grateful to the anonymous reviewers from Thin-Walled Structures for giving challenging comments and suggestions.

An extensive gratitude goes to my wife, assistant professor, PhD, Katrine Alling Andreassen for her great patience and support as well as the maintenance of calm and stability for our family.

Last, but not least, I am very grateful for the always unconditional loving support and encouragement from my dear three daughters Nikoline, Pauline and Filippa.

Abstract

In several industries such as civil, mechanical, and aerospace, thin-walled structures are often used due to the high strength and effective use of the materials. Because of the increased consumption there has been increasing focus on optimizing and more detailed calculations. However, finely detailed calculations will be very time consuming, if not impossible, due to the large amount of degrees of freedom needed. The present thesis deals with a novel mode-based approach concerning more detailed calculation in the context of distortion of the cross section which model distortion by a limited number of degrees of freedom. This means that the classical Vlasov thin-walled beam theory for open and closed cross sections is generalized as part of a semi-discretization process by including distortional displacement fields. A novel finite-element-based displacement approach is used in combination with a weak formulation of the shear constraints and constrained wall widths. The weak formulation of the shear constraints enables analysis of both open and closed cell cross-sections by allowing constant shear flow. Variational analysis is used to establish and identify the uncoupled set of homogeneous and non-homogeneous differential equations and the related solutions.

The developed semi-discretization approach to Generalized Beam Theory (GBT) is furthermore extended to include the geometrical stiffness terms for column buckling analysis based on an initial stress approach. Through variations in the potential energy a modified set of coupled homogeneous differential equations of GBT including initial stress is establish and solved. In this context instability solutions are found for simply supported columns and by solving the reduced order differential equations the cross-section displacement mode shapes and buckling load factor are given.

In order to handle arbitrary boundary conditions as well as the possibility to add concentrated loads as nodal loads the formulation of a generalized one-dimensional semi-discretized thin-walled beam element including distortional

contributions is developed. From the full assembled homogenous solution as well as the full assembled non-homogeneous solution the generalized displacements of the exact full solution along the beam are found.

This new approach is a considerable theoretical development since the obtained GBT equations including distributed loading found by discretization of the cross section are now solved analytically and the formulation is valid without special attention and approximation also for closed single or multi-cell cross sections. Furthermore, the found eigenvalues have clear mechanical meaning, since they represent the attenuation of the distortional eigenmodes and may be used in the automatic meshing of approximate distortional beam elements. The magnitude of the eigenvalues thus also gives the natural ordering of the modes.

The results are compared to results found using other computational methods taking distortion of the cross section into account. Thus, the results are compared to results found using the commercial FE program `Abaqus` as well as the free available software `GBTUL` and `CUFSM` concerning conventional GBT and the finite strip method, respectively. Reasonable matches are obtained in all cases which confirm that this new approach to GBT provides reasonable results with a very small computational cost making it a good alternative to the classical FE calculations and other available methods.

Resumé

I mange brancher såsom konstruktions-, mekanik- og rumfartsbranchen anvendes tyndvæggede konstruktioner ofte på grund af deres høje styrke og en effektiv udnyttelse af materialerne. På grund af øget anvendelse af disse konstruktioner, er der stigende fokus på optimering og mere detaljerede beregninger. Dog vil mere detaljerede beregninger være mere tidskrævende, hvis ikke umulige, på grund af det store nødvendige antal frihedsgrader. Denne afhandling omhandler en ny form-baseret formulering af den tyndvæggede bjælketeori, hvilket medfører mere detaljerede beregninger ved at medtage og inkludere tværsnitsdeformation, men samtidig også tager hensyn til tværsnitsdeformation ved brug af et begrænset antal frihedsgrader. Dette betyder, at den klassiske Vlasov bjælketeori for åbne og lukkede tværsnit generaliseres som del af en semi-diskretiserings proces ved at inkludere tværsnitsdeformation. En ny finite-element baseret formulering anvendes i kombination med en svag formulering af forskydningsbindinger og en binding af vægudvidelsen. Den svage formulering af forskydningsbindingerne gør det muligt at analysere både åbne og lukkede tværsnit ved at tillade en konstant forskydningsstrøm rundt i tværsnittet. Variationsanalyse anvendes til at identificere og etablere ukoblede sæt af homogene- og inhomogene differentialligninger og de tilhørende løsninger.

Den udviklede semi-diskretiseringsformulering til generaliseret bjælketeori (GBT) er endvidere udvidet til også at omfatte de geometriske stivhedsled for søjleudknæknings analyse baseret på en initialspændingsformulering. Gennem variationer i den potentielle energi er et modificeret sæt af de koblede homogene differentialligninger for GBT indeholdende initial spændinger opstillet og løst. I denne sammenhæng er der fundet in-stabilitets løsninger for simpelt understøttede søjler og ud fra løsningen af de fjerde ordens reducerede differentialligninger er tværsnitsdeformationsformerne og stabilitetslastfaktoren fundet.

For at kunne håndtere arbitrære randbetingelser og for at kunne påsætte

koncentrerede belastninger i form af knudelaster, er der formuleret et generaliseret en-dimensionelt semi-diskretiseret tyndvægget bjælkeelement indeholdende tværsnitsdeformation. Udfra den fuldstændige og samlede homogene løsning såvel som ud fra den fuldstændige og samlede in-homogene løsning, er de generaliserede flytninger for den eksakte, fuldstændige løsning langs bjælken fundet.

Denne nye metode udgør en betydelig teoretisk udvikling, idet de opstillede GBT ligninger, indeholdende fordelt last fundet ved semi-diskretisering af tværsnittet, nu er løst analytisk og idet formuleringen nu er gældende for lukkede og flercellede tværsnit uden specielle hensyn og approksimationer. Endvidere har de fundne egenværdier nu en klar definition, idet de repræsenter afklingningslængden af de tværsnitsdeformerede egenformer, og de kan dermed bruges i forbindelse med en automatisk inddeling af tilnærmede tværsnitsdeformerede bjælkeelementer. Endvidere angiver størrelsen af egenværdierne den naturlige hierarkiske rækkefølge af formerne.

De opnåede resultater er sammenlignet med resultater fundet vha. det kommercielle FE program `Abaqus` og det frit tilgængelige software `GBTUL` og `CUFSM`, som omhandler henholdsvis konventionel GBT og finite strip metoden. Herigennem er der opnået gode overensstemmelser i alle tilfælde, hvilket bekræfter, at denne nye formulering til GBT giver gode resultater med meget små beregningsmæssige omkostninger, hvilket gør den til et godt alternativ til de klassiske FE beregninger og andre tilgængelige metoder.

Contents

List of included papers

Included journal papers:

1. Jönsson, J., and Andreassen, M.J. (2011). Distortional eigenmodes and homogeneous solutions for semi-discretized thin-walled beams. *Thin-Walled Structures*, **49**, 691–707.

2. Andreassen, M.J., and Jönsson, J. (2012). Distortional solutions for loaded semi-discretized thin-walled beams. *Thin-Walled Structures*, **50**, 116–127.

3. Andreassen, M.J., and Jönsson, J. (2012). Distortional buckling modes of semi-discretized thin-walled columns. *Thin-Walled Structures*, **51**, 53–63.

4. Andreassen, M.J., and Jönsson, J. (2013). A distortional semi-discretized thin-walled beam element. *Thin-Walled Structures*, **62**, 142–157.

Included conference papers and abstracts:

5. Andreassen, M.J., and Jönsson, J. (2009). Distortional Modes of Thin-Walled Beams. Full conference paper published in Proceedings of the 7th EUROMECH Solid Mechanics Conference – Mini-Symposia (ISBN: 978-989-96264-2-3) (paperid: 0680), pages: 11, 2009, APMTAC – Portuguese Association for Theoretical, Applied and Computational Mechanics, Laboratório Nacional de Engenharia Civil, Av. do Brasil, 101, 1700-066 Lisboa, Portugal. Presented at ESMC2009, 7th EUROMECH Solid Mechanics Conference, 2009, Instituto Superior Técnico, Lisbon, Portugal.

6. Andreassen, M.J., and Jönsson, J. (2011). Distortional eigenmodes and solutions for thin-walled beams. Full conference paper published in Thin-Walled Structures, Recent Research Advancences and Trends (ISBN: 978-92-9147-102-7), 2011, ECCS – European Convention for Constructional

Steelwork. Presented at the International Conference on Thin-Walled Structures (ICTWS) – 6, 2011, Timisoara, Romania.

7. Jönsson, J., and Andreassen, M.J. (2012). A semi-discretization approach to generalized beam theory and analytical solutions of the generalized column equations. Full conference abstract published in Proceedings of the 8th EUROMECH Solid Mechanics Conference – Mini-Symposia, Graz, Austria.

List of Figures

List of Tables

List of Symbols

Greek

γ	Engineering shear strain
$\bar{\gamma}_d$	Shear strain in the mid plane of the wall
$\Delta\mathbf{K}_{\mathrm{FE}}$	Boundary stiffness contributions in the unconstrained FE-space
$\Delta\mathbf{R}_{\mathrm{FE}}$	Nodal loads at beam element ends and intersections in the unconstrained FE-space
δ	Virtual variation
ε	Axial strain
ε_s	Transverse strain
ζ	Axial extension
$\mathbf{\Lambda}$	Amplitude function matrix
λ	Real part of the complex eigenvalue
μ	Imaginary part of the complex eigenvalue
ν	Poisson ratio
ξ	Inverse length scale parameter which can be complex
ξ_j^2	j'th eigenvalue which can be complex
$\bar{\xi_j^2}$	Conjugated eigenvalue
Π	Energy potential
σ	Axial stress
σ_s	Transverse stress

τ	Shear stress
ϕ	Axial variation of the load
$\mathbf{\Psi}$	Axial amplitude matrix
$\widetilde{\mathbf{\Psi}}$	Axial real amplitude matrix
$\bar{\mathbf{\Psi}}$	Diagonal representation of the amplitude functions
ψ	Axial amplitude function
Ω	Axial warping displacement
Ω_0	Warping integration constant

Roman

$\mathbf{A}$	Substitute matrix
$\widetilde{\mathbf{A}}$	Real substitute matrix
$\mathbf{a}$	Real part of eigenvector
$\mathbf{B}$	Substitute matrix
B_D	Distortional bimoment
B_T	Torsional bimoment
$\mathbf{b}$	Imaginary part of eigenvector
b_e	Width of the element
C	Cross-section centerline curve
$\mathbf{C}$	Constants related to the constrain procedure or used for substitute matrix
c	Constant
$\mathbf{c}$	Vector of constants
$\widetilde{\mathbf{c}}$	Real constant vector
$\mathbf{d}_\alpha$	Vector giving the amount of each translational eigenmode to be subtracted
E	Modulus of elasticity
E_s	Plate type modulus of elasticity

G	Modulus of shear
$\mathbf{G}$	Geometrical stiffness matrix
$\mathbf{H}$	Transformation matrix
$\mathbf{I}$	Unit matrix
Im	Imaginary part index of complex number
i	Imaginary unit
K^{σ}	Total cross-section axial stiffness contribution
$\mathbf{K}$	Linear stiffness matrix
$\tilde{\mathbf{K}}$	Block stiffness matrix
$\bar{\mathbf{K}}$	Condensed stiffness matrix
$\mathbf{K}^{\sigma}$	Cross-section axial stiffness matrix
$\mathbf{K}^{\tau}$	Cross-section shear stiffness matrix
$\mathbf{K}_e$	Beam element stiffness matrix in the GBT-space
$\mathbf{K}^{s}$	Cross-section transverse stiffness matrix
$\mathbf{k}^{\sigma}$	Straight-element axial stiffness matrix
$\mathbf{k}^{\tau}$	Straight-element shear stiffness matrix
$\mathbf{k}^{s}$	Straight-element transverse stiffness matrix
L	Length of the thin-walled beam
$\mathbf{L}$	Lower triangular matrix with strictly positive diagonal used in Cholesky decomposition
$\mathbf{L}^{T}$	The conjugated transpose of L used in Cholesky decomposition
M_1	Major bending moment
M_2	Minor bending moment
N	Normal force
$\mathbf{N}$	Interpolation matrix
N_p	Load interpolation matrix
n	Local cartesian coordinate
n_c	Number of independent constraint equations

n_{dof}	Number of degrees of freedom
n_{no}	Number of nodes
$\mathbf{P}^{el}$	Nodal cross-section point load
p	Distributed cross-section load
$\mathbf{p}^{el}$	Nodal end load value of a cross-section wall element
q	Distributed load
Re	Real part index of complex number
$\mathbf{R}_e$	Beam element load vector in the GBT-space
$\mathbf{r}$	Global load vector
r^{el}	Load component of a straight cross-section element
$\mathbf{r}^e$	Extended load vector
$\mathbf{r}^{el}$	Nodal load vector of a straight cross-section element
$\tilde{\mathbf{r}}$	Load vector
$\bar{\mathbf{r}}$	Transformed load vector
s	Local cartesian coordinate
$\mathbf{T}$	Transformation matrix
$\widetilde{\mathbf{T}}$	Condensed transformation matrix
$\bar{T}_d$	Constant shear flow in the walls of the cross section
$\mathbf{T}_{\mathrm{w}}^i$	Matrix corresponding to three supplementary columns, which pick out the degrees of freedom of the first node related to v_{w}^1, v_{w}^2 and v_{w}^3
t	Wall thickness
u	Cross-section displacement component
$\mathbf{u}_\Omega$	Axial displacement vector
$\mathbf{u}_b$	Assembled boundary displacement vector
$\mathbf{u}_{\mathrm{FE}}$	Displacement vector in the unconstrained FE-space
$\mathbf{u}_{\mathrm{GBT}}$	Displacement vector in the constrained GBT-space
$\mathbf{u}_S$	Substitute vector or solution vector
$\mathbf{u}_{\mathrm{w}}$	Transverse displacement vector
$\bar{u}_z$	Centerline axial displacement

$\mathbf{V}$	Matrix of assembled modes
$\widetilde{\mathbf{V}}$	Matrix of assembled real modes
$\bar{\mathbf{V}}$	Expanded matrix of assembled modes
v	Local element degree of freedom
$\mathbf{v}$	Global displacement vector
$\mathbf{v}^e$	Extended displacement vector
v^{el}	Nodal displacement component of a straight cross-section element
$\mathbf{v}^{el}$	Nodal displacement vector of a straight cross-section element
$\mathbf{v}_S$	State vector
$\widetilde{\mathbf{v}}$	Cholesky transformed displacement vector
w	In-plane cross-section displacement component
x	Global horizontal cartesian coordinate
y	Global vertical cartesian coordinate
z	Global and local longitudinal cartesian coordinate
$\mathbf{0}$	Suitable size matrix or vector of zeroes

Superscripts and subscripts

$^{\alpha}$	Translational modes
$^{\phi}$	Rotations
$^{\Omega}$	Axial warping displacement
$^{\mathrm{a}}$	Pure axial extension
$^{ⓐ}$	Internal displacements induced by the nodal displacements without distributed loading
$^{\mathrm{axial}}$	Pure axial extension
$_{b}$	Beam modes
$^{ⓑ}$	Displacements induced by the loading on the beam with zero nodal displacements
^{c}	Constrained degrees of freedom

$_{d}$	Distortional modes
$_{ext}$	External properties
$_{g}$	Degrees of freedom in the reduced or condensed GBT space
$_{int}$	Internal properties
$_{j}$	j'th eigenvalue
$_{o}$	Other modes
$_{r}$	Remaining modes
$^{-T}$	Inverted transpose of matrix
$_{u}$	Unconstrained degrees of freedom
$_{v}$	Unconstrained displacements
$_{\mathrm{w}}$	In-plane cross-section displacement
$_{x\,\mathrm{trans}}$	Non-orthogonal translational mode in the x-direction
$_{y\,\mathrm{trans}}$	Non-orthogonal translational mode in the y-direction
$_{z\,\mathrm{rot}}$	Non-orthogonal rotational mode
$_{0}$	Contribution of the factored initial stresses
$_{1}$	Translational mode
$_{1\,\mathrm{trans}}$	Orthogonal translational mode
$_{2}$	Translational mode
$_{2\,\mathrm{trans}}$	Orthogonal translational mode
$_{3}$	Rotational mode
$_{3\,\mathrm{rot}}$	Orthogonal rotational mode

Chapter 1

Introduction

For about a century many branches of the industry have sought stronger and at the same time lighter structural solutions which optimize the effectiveness and the cost of the structures. Among them are the civil, mechanical, naval and aerospace industry. This has led to an increasing use of thin-walled structures such as cold-formed steel beams, steel and concrete box girders, ship hulls, trapezoidal steel sheeting and other structures in which one dimension is small compared to the other dimensions, see e.g. Figure 1.1. Thin-walled structures made of aluminium and composite materials are also widely used. Because of the increased slenderness of these structures, they lead to more complex structural behavior which requires the development of more comprehensive and accurate mathematical approaches. However, more detailed calculations will be very time consuming, if not impossible, due to the large amount of degrees of freedom needed.

In this thesis a novel mode-based approach is developed by extending the existing beam theory to include transverse distortion for open and closed cross

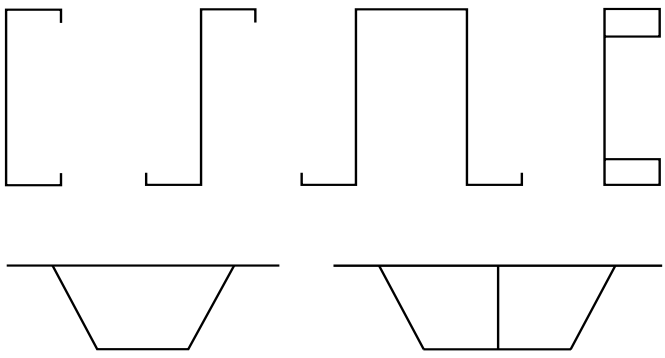

Figure 1.1: Examples of thin-walled cross sections.

sections in a new and theoretical improved context. Due to the mode (cross-section deformation multiplied by a longitudinal amplitude function) based formulation it is possible to obtain a more engineering perspective of the problem. It also implies that the physical understanding is always in focus. At the same time the novel approach model distortion by a limited number of degrees of freedom compared to the classical shell finite element method which is very time consuming, if not impossible, due to the large amount of degrees of freedom needed. In this context an advanced distortional semi-discretized thin-walled beam element has been developed. In general, this means that the thesis is a study of *distortional mechanics of thin-walled structural elements* and deals with the related kinematics and stability. The importance of research in beam theory and beam elements, which model distortion by a limited number of degrees of freedom, lies in the fast analysis of complex dynamic problems and stability related issues of distorting structures. Nowadays the studies of the dynamics of bridges are often based on a simple beam theory. An extension of these studies to include deformation of the cross section would be very interesting. It is possible to include very important contributions to the structural behavior by adding extra degrees of freedom.

To understand the importance of taking distortion into account, this chapter will start out by describing the background and history of the beam theory. Due to the research carried out in this thesis the chapter also presents the purpose and expectations, an introduction to the novel GBT approach as well as a description of the report structure.

1.1 Background and history

As far back as the 16th century the strength doctrine was founded by Galileo Galilei (1564–1642). After his death the development of the theory of elasticity was started by Robert Hooke (1635–1703) followed by Coulomb (1736–1806) developing the theory of bending of beams leading to the well known mathematical elasticity theory defining the classic beam theory, Timoshenko (1983). In the context of this foundation a brief overview of the beam theory is given in this section.

1.1.1 Classic beam theory

The classic beam theory (Euler-Bernoulli theory) is based on the assumption of Bernoulli, where plane cross sections remain plane, and it is assumed that the beam axis remain perpendicular to the cross-section in-plane (Timoshenko and Goodier, 1951). Furthermore, the physical assumption of Hooke on linear elasticity is made, which means that the strain distribution will vary linearly over the cross section. This also means that the forces can be divided into three

independent components which are (i) the normal force, (ii) bending moment related to major axis bending and (iii) bending moment related to minor axis bending. The shear forces are derived from the moment variation and the distribution of the shear stresses are found from the Grashof formula which is based on the static assumptions concerning equilibrium (Gere and Timoshenko, 1997).

The mathematical elasticity theory gives the relationship between the shear stresses and the shear strains for a 3-dimensional continuum. However, it is important to note that the simplifications of the classic beam theory lead to an inconsistency in the determination of the shear stresses. The assumptions of the cross-section deformation mean that there is no shear strains and according to the mathematical theory of elasticity consequently also no shear stresses. In the classic beam theory this problem is handled by determining the shear stresses from equilibrium considerations which are independent of the deformations. Shear forces would theoretically cause plane cross sections to not remain plane, but for relatively thick-walled cross sections the error is very small and the classic beam theory is in these cases sufficiently accurate for all practical purposes. Furthermore, the classical beam theory consider torsion to be solved based on an assumption of free torsion which means that distortion out of the plane (warping) can take place unhindered. Thereby free torsion results in warping of the cross section which contradicts the assumption of plane cross sections remaining plane. At joints between angled beam elements this leads to compatibility problems since the torsional deformations do not fit together with the flexural and axial deformations for closed cells. However, for sufficiently thick-walled beam elements the torsional deformations will usually be significantly smaller than the other deformations, which means that the incompatibility concerning most practical purposes has no significant meaning.

The relation between the cross section and the bending stiffness parameter was first made by Navier in 1820 while the formulation of the problem of homogeneous torsion of an elastic beam was made in 1855 by St. Venant (Timoshenko, 1983). Until the beginning of the 19th century this theory was state of the art. In 1921 the incorporation of shear effects into the technical theory of beam flexure was developed by Timoshenko (Timoshenko, 1983).

As mentioned above the classical technical beam theory is valid for many practical purposes. However, the validity of the theory cannot be clarified in a simple way and it depends on the cross-section design, e.g. the plate thickness in relation to the height, the length of the beam elements, and the structural application. Furthermore, with an increasing utilization of the construction material there is more beam- and frame structures, where one is compelled to incorporate the cross-section warping. Examples are frame constructions built by I-profiles. Such structures are often dimensioned based on loss of stability by

lateral torsional buckling, which necessitates a thin-walled beam theory. Bridge girders made of steel are often made as closed cross section, whereby traffic loads are able to induce torsion in the bridge girders. The stress distribution in the structure requires account for non-homogeneous torsion and thus a thin-walled beam theory.

1.1.2 Thin-walled beam theory

In 1961 a theory describing the combined effects of extension, bending, and torsion of thin-walled beams was developed by Vlasov (1961) leading to the well known theory of thin-walled beams. Often thin-walled beams are referred to as Vlasov beams as he was the first to give a systematic description of the theory of thin-walled beams. In this context Vlasov also described the warping phenomenon.

Thin-walled structures such as beams, columns, plates, shells, sheeting, pipes, among others, are frequently used in civil, naval and space constructions, see e.g. Figure 1.2 and 1.3. They are not easy to define in a precise

Figure 1.2: Examples of thin-walled structures used in civil constructions.

and quantitative way, however it seems sufficient to say that they are structures made from thin plates joined along their edges. The plate thickness is small to other cross-sectional dimensions which are in turn often small compared with the overall length of the member or substructure (Murray, 1986).

There are many reasons why thin-walled structures must be given special considerations in their analysis and design. Some of them are listed below:

- *Out-of-plane distortion.* The shear stresses and strains are relatively larger than those in a solid rectangular beam. By twisting a thin-walled structure it is easily shown that there is an out-of-plane distortion of the cross section

Figure 1.3: Examples of thin-walled structures used in offshore and aerospace constructions.

in the longitudinal beam direction (warping). Hereby the assumption of plane sections remaining plane (Bernoulli hypothesis) is violated.

- *Shear flow.* In the closed cross section the torsional moment is resisted by a shear flow around the cell. Consequently the torsional stiffness is increased considerably as compared to a similar open cross section.
- *Shear lag.* Shear lag occurs when the forces cannot be transmitted directly into the entire cross section. This means that the area that is effective in resisting the force is smaller than the total area.
- *Susceptible to local buckling.* It is well known that thin-walled structures are susceptible to local buckling when subjected to load.
- *Stress distribution.* It is well known that warping and torsion have a great influence on the stress distribution.
- *In-plane distortion.* Due to the thin walls, thin-walled beams are much susceptible to deformation of the cross section, leading to various subjects and remarks as described later in subsection 1.1.3.

In the theory of thin-walled beams the assumptions that plane cross sections remain plane are remitted. This gives a more consistent connection between torsion and bending (or normal force). The torsional problem is no longer assumed to be freely conducted, which means that so called free torsion can be obtained. This means a torsional mode where the first derivative of the torsional angle (ϕ') are no longer constant.

In contrast to the classical six degrees of freedom, the calculation of thin-walled beams also contains a warping parameter which expresses the change in

the derivative of the angle of rotation (ϕ''). This degree of freedom is associated with the bimoment which is an extra generalized force. The introduction of the warping parameter is necessary to handle lateral torsion which concerns stability. In contrast to the classical beam theory the placement of the load at the cross section is important for thin-walled beams and the torsional stiffness of a profile is highly dependent on whether the profile is open or closed. But with regards to the beam theory the solving methodology is the same.

Before the Vlasov formulation, previous works were characterized by solutions to special problems, see e.g. Timoschenko and Gere (1963) and the books Kollbrunner and Hajdin (1972) and Kollbrunner and Hajdin (1975) provide a systematic review of the theory and a number of analytical solutions for selected problems. In Murray (1986) a more practical description of the thin-walled beam theory and examples of applications are provided. Krenk (1989a;b) provides a modern description of the thin-walled beam theory based on a continuum mechanical basis and specified numerical calculations.

In thin-walled beam structures transition conditions between beam elements, that meets at non right angles, are complex. The stiffness conditions of the connections have great importance for the overall structural stiffness, and thus the buckling load. In Krenk and Damkilde (1992) this problem is handled and Petersen et al. (1991) contains a finite element formulation of both the linear problem and the stability problem.

Despite the fact that almost all the points listed above have been well researched for several years, the last and important point describing in-plane distortion still creates problems specially for closed cross sections. This subject is handled in the present thesis.

1.1.3 In-plane distortion and why it is important

As seen from the section given above concerning the classical theory of elastic thin-walled beams it is assumed that the cross sections maintain their shape in-plane and do not distort. Although the assumption is often justified, it cannot be maintained in the analysis of modern thin-walled structures. Some of the reasons to take in-plane distortion into account are listed here as

- The deformation of the cross section can give a substantial additional contribution to the deformation determined by ordinary beam theory as well as redistribution of stresses. For example cross-section deformation of box girders due to eccentric transverse load (Krenk, 1989b).

- Instability of a compressed flange caused by bending of the web. In this case the web acts essentially as a supporting spring, and thus the combined flexibility of the support and the cross-section plays a decisive role.

- Investigations by Raftoyiannis (1994), Godoy et al. (1995), Barbero (2000), and Barbero et al. (2000) show, both analytically and experimentally, that the local deformation in the cross section may strongly affect the structural buckling behavior of thin-walled composite members.

- Including distortion of the cross section gives the possibility of analyzing major bridges in the context of the overall structure instead of in a sub structural part.

- Ovalisation reduces the cross-section moment of inertia and thereby the stiffness, leading to a non-linear moment-curvature relation often called the Brazier effect. For example ovalisation of thin-walled pipes in bending (Krenk, 1989b). Note that this is a non-linear problem and that the present thesis only deals with linear problems.

The importance of taking in-plane distortion into account has been recognized as far back as 1961 in Vlasov (1961). Here Vlasov presented an approach in which each wall is treated as a beam linked to the others.

Subsequently, the subject concerning deformable cross sections have been treated by several authors. Steinle dealt with in-plane distortion of single-cell box girders (Steinle, 1967; 1970). Also Wright et al. published within this topic (Wright, 1968). Even though Steinle deals with the topic concerning deformable cross-sections he is not setting up the differential equation including the distortion. He is only dealing with an un-coupled formulation by looking at the classical beam theory to which he attaches the stresses obtained by a separated analysis of a deformed cross section. In 1979 Křístek treats the topic concerning closed cross sections (Křístek, 1979).

Inspired by others of the theory of prismatic folded structures (Faltwerke, in German) also Schardt published in 1966 a new formulation (Schardt, 1966), taking deformation of the cross section into account. The formulation was based on the theory of prismatic folded structures and the introduction of new generalized forces and cross-section deformations. The formulation was made so that the final calculation could be done by using the classical formulation of beam theory. Hereby Schardt extended the beam theory to include the deformation of the cross section. In 1975 Kollbrunner and Hajdin (1975) dealt with the topic of open and closed cross sections including warping. Schardt (1989) published a further developed formulation known as Generalized Beam Theory (GBT) or (VBT) in German. The formulation is a generalization of classical Vlasov beam theory and has been successful and fostered further research which is described in the next chapter.

A distortional theory which generalizes Vlasov beam theory by including the modified definition of the warping function and a single distortional mode was

presented in Jönsson (1998). In that work the analytical solution of coupled torsional and distortional equations was found by reduction of order and solution of the related eigenvalue problem. The single mode can here be found by equilibrium between the actual load and the shear stresses or in simple cases the mode can be estimated by intuition.

The rapid development during the last ten years within the field of distortion of thin-walled elements has prompted the publication of widespread literature on the subject which are described in chapter 2.

1.1.4 Numerical methods available

An assessment of structural performance of thin-walled beams includes linear static analysis and linear buckling analysis of the behavior which may involve global deformations, non-local in-plane distortional deformations and local in-plane distortional deformation as well as out-of-plane deformations (warping). Regarding such analyses the following main numerical analysis methods are available:

1. *Finite Element Method.* This is a method to obtain an approximate solution to a problem governed by a set of differential equations. The member is divided or discretized into smaller part (elements) in which simple expressions for the displacements are chosen, see Figure 1.4(left). Regarding thin-walled members usually shell finite elements (SFEM) are used. The displacement field is approximated by a combination of polynomial shape functions, each single one associated with a nodal displacement or rotation, see for example Zienkiewicz and Taylor (2000a;b) or Hughes (2000), perhaps with utilization of recursive substructuring (Jönsson et al., 1995). This advanced numerical technique involves a large amount of degrees of freedom.

2. *Finite Strip Method.* This method may be regarded as a special form of the finite element procedure, see for example Cheung (1976) for a comparison between finite element and finite strip methods. It is applicable for many structures having regular geometric plans and simple loading and boundary conditions. The member is discretized into strips which calls for use of simple interpolation polynomials in the transverse direction and continuously differentiable smooth series functions (e.g. Fourier series) in the longitudinal direction. The strips are rectangular finite elements spanning all the length, see Figure 1.4(right), and involves a lower number of degrees of freedom than equivalent SFEM analyses (Cheung and Tham, 1998, Williams and Wittrick, 1968, Cheung, 1976). This provides a powerful simplification to the finite element method. The method is subdivided

into the following main sub-methods, however tremendous developments of the method have been made:

- *Semi-Analytical Finite Strip Method.* This is the classical finite strip method, which is applicable only to simply supported boundary conditions and thus applicable to the buckling or vibration analysis of simply supported members subjected to longitudinally uniform internal forces and/or moments, see for example Cheung and Tham (1998). The method has been incorporated into the available free software packages `CUFSM` (Li and Schafer, 2010).
- *Spline Finite Strip Method.* This is a development of the semi-analytical finite strip method and replaces the series functions, representing the displacements in the longitudinal direction, by splines as well as handles non-standard support conditions and non-uniform internal forces and moments (Loja and Soares, 2002, Prola, 2002). The number of degrees of freedom required for a spline finite strip analysis is considerably larger than for the semi-analytical finite strip method, however it is still considerably less than that of a comparable finite element analysis (Erp and Menken, 1990).
- *Constrained Finite Strip Method (cFSM).* This method constrain the classical finite strip method to deformation fields consistent with a particular class of buckling modes. It uses conventional definitions of deformation classes such as global, distortional, local, and other deformations separated into the degrees of freedom. Thus providing both modal decomposition and modal identification to a conventional finite strip solution resulting in a better understanding of the cross-section deformation and stability (Ádány et al., 2009, Schafer and Ádány, 2006, Ádány et al., 2006). The method has been incorporated into the available free software packages `CUFSM` by Li and Schafer (2010).

3. *Conventional Generalized Beam Theory.* This is a method having the distinguishing feature of discretizing the deformed member configuration into cross-section deformation modes. The modes can either be a global, local (plate) or distortional mode (Schardt, 1989). After the determination of the modes during a cross-section analysis, the modes are, within a member analysis, multiplied by an approximated axial amplitude shape function leading to a conventional axial element interpolation and discretization. For open cross sections the method has been incorporated into the available free software packages `GBTUL` (Bebiano et al., 2008a), however the `GBTUL` cannot yet handle closed cross sections. This theory,

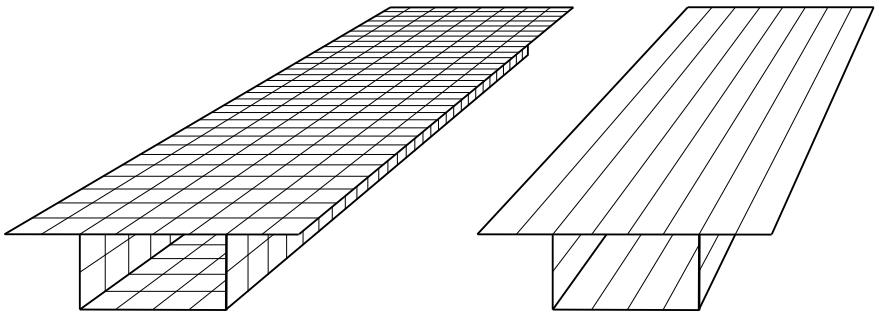

Figure 1.4: Lipped channel shell finite element discretization (left) and finite strip or GBT discretization (right).

which is less widespread than the finite element method and the finite strip method, is an extension of the classical theory by including multiple distortional modes. Thereby it is possible to perform computational analysis of advanced distortional problems with a less number of degrees of freedom than necessary for equivalent SFEM analyses, see for example Figure 1.4(right). This extension and the associated longitudinal finite element discretization using approximated axial amplitude shape function leads to a much faster analysis of complex dynamic and stability related issues. A more elaborate description of the theory is given later in section 2.2.

From the above mentioned methods, the finite element method is the most powerful and versatile tool of solution in structural analysis. The method is well known and established, and used in a wide range concerning structural analysis. However, for many structures having regular geometric plans and simple boundary conditions, a finite element analysis is often extravagant, unnecessary and at times even impossible. Therefore the finite strip method as well as the GBT approach is an alternative method, which can reduce the computational effort for the afore-mentioned class of structures.

Having described the background and history let us turn to the purpose and expectations.

1.2 Purpose and expectations

The first part of this PhD study consisted of a literature study. During this study it became clear that several formulations including transverse distortional displacements have been proposed for analysis of both open and closed cross sections. It also became clear that especially one formulation has been very successful and widespread, namely the well known formulation referred to as

GBT (Generalized Beam Theory). However, this formulation has been developed for open cross sections and still gives problems for closed cross sections. Even though GBT is an abbreviation of Generalized Beam Theory which gives the impression of covering a wide area, the abbreviation has achieved a kind of trademark related to the theory or formulation developed by Schardt (1989). As the GBT abbreviation in a word related sense also may cover a wide area it should in my opinion not be linked to a single theory or formulation. Consequently, the theory developed by Schardt will in this thesis be referred to as conventionel GBT. The conventional GBT formulation was initially proposed by Schardt (1966) as a generalization of the theory of bending (Verallgemeinerte Technische Biegetheorie, VTB in German) but was generally not so known in the international research community until Davies and Leach (1994a) presented first-order conventional GBT analysis. Conventional GBT is devoted to (first-order) distortional displacement analysis including the identification of distortional modes, as well as (second-order) linear buckling of thin-walled members, and it has fostered many research investigations as can be seen later from chapter 2.

As mentioned the conventional generalized beam theory has been studied much during the last 45 years. In general by the group at the Technical University of Darmstadt, Germany, and in the last 10 years especially and strongly intensified by the Portuguese group led by Silvestre and Camotim at the Technical University of Lisbon. Despite 45 years of research and development the theory is still limited in its distribution. This can be due to several reasons but one can be that the theory is difficult to understand and not based on the contemporary educational topics such as energy principles and the finite element method.

The hypothesis of this project, which is based on prior research performed by professor Jeppe Jönsson, has therefore and in contrast to conventional GBT been theoretical developments based on the calculus of variations and energy formulations. Formulations for the numerical analysis has been performed based on the finite element method formulations. It should be noted that the present novel approach to generalized beam theory is neither similar to conventional GBT nor an extension of the theory.

Following the arguments above has led to the following objectives and achievements for this study:

- *A literature survey on generalized beam theory.*
- *A study to enhance the understanding of the calculus of variation and energy methods.*
- *The formulation of a set of homogeneous distortional differential equations of GBT (limited number of degrees of freedom)*

in the context of a semi-discretization (modes) and a FEM formulation. This is done by using calculus of variations and an energy formulation. The formulation has to be performed so that also cross sections with closed cells can be treated without special attention.

- *The formulation and solution of a consistent eigenvalue problem that solves the full analytical homogeneous distortional differential equations of GBT and determines the distortional modes which decouple the set of differential equations.*
- *The formulation and solution of an uncoupled set of non-homogeneous distortional differential equations of GBT including the distributed loads by using the novel semi-discretization (modes) process.*
- *An extension of the formulation to include the geometrical stiffness terms, which are needed for column buckling analysis and identification of buckling modes.*
- *The development of an advanced distortional semi-discretized prismatic thin-walled element based on the objectives given above.*
- *A comparison between the novel approach to GBT and the conventional GBT.*

It is expected that the research will lead to the development of new, modern, and improved techniques for static, stability, and dynamic analysis of distorting prismatic thin-walled structural elements. It will enable static and stability analysis of distortional structural problems with very few degrees of freedom making it a good alternative to the classical finite element method which is often extravagant and unnecessary for many structures having a regular geometric plans and simple boundary conditions.

Before describing the structure of the thesis let us briefly introduce the novel GBT approach in words.

1.3 Introduction to the novel GBT approach

In this section a brief overview of the novel GBT approach is given in words before going into the detailed study. This is assumed to be worthwhile for the knowledgeable reader.

First of all, the presented novel GBT formulation for prismatic thin-walled beams with both open and closed (single or multi cell) cross sections can be regarded as an extension of classical Vlasov thin-walled beam theory to include distortional deformation modes as well as constant shear flows in the walls of

the cross section (Vlasov, 1961, Kollbrunner and Hajdin, 1972; 1975). This also means that the novel GBT approach adhere to the definition of the warping function given by Kollbrunner and Hajdin (1972) which adds the integral of the shear flow strains, see also (Jönsson, 1998; 1999a;b). Hereby the novel GBT approach is able to handle open cross sections as well as closed cross sections without special attention. It should be noticed that shear deformation accommodating Bredt's shear flow around closed cells is included in the theory through the specific definition of the warping function (Kollbrunner and Hajdin, 1972). We are dealing with a beam element adhering to generalized beam theory and not an extended weak formulation of a finite beam element that allows the addition of special (transverse extension and shear lag) modes. The approach makes it possible to analyze prismatic thin-walled members with cross-section distortion and local plate behavior in a one-dimensional formulation through the linear combination of pre-established modes of deformation. Note that a distortional theory which generalizes Vlasov beam theory by including the modified definition of the warping function and a single distortional mode is presented by Jönsson (1999a).

Furthermore, innovative theoretical developments are performed in the context of finding and solving the analytical homogeneous solution to the fourth-order differential equations of GBT to obtain the distortional displacements for a linear beam analysis. This advance enables the formulation of exact distortional beam elements with distributed load for first-order analysis using the found axial solution functions as seen from chapter 6. This is in contrast to the conventional interpolation by third-order polynomials. It also means that the novel approach finds the exact mode shapes and amplitude solutions of the reduced order GBT equations related to the discretized cross section. The formulation is performed by introducing a semi-discretization process and gives an excellent knowledge of the length scales of the modes through the magnitude of the eigenvalues found. Similar methods are used by Hanf (1989) only in his thesis and by Jönsson (1999a). In the work of Jönsson (1999a) the analytical solution of coupled torsional and distortional equations are found by reduction of order and solution of the related eigenvalue problem in the same manner as in the present work.

Introducing semi-discretization leads towards a formulation in which the rotational degrees of freedom are included, thus including local plate modes in the formulation even for the simplest discretization. The elimination of these rotational degrees of freedom could perhaps be advantageous if one wants to perform a modal decomposition of buckling displacements into distortional buckling mode and local plate buckling mode. However, we then rely on a coarse discretization. A static elimination of the rotations are performed later in order to compare with conventional GBT.

During the development of the present novel approach, the determining of the sequence of the three steps performed has been very difficult and caused much effort in order to achieve an elegant and solvable eigenvalue problem.

Having shortly introduced the novel GBT approach, the structure of the thesis is described in the next section.

1.4 Structure of the thesis

The objectives described in section 1.2 are met by an academic research containing a literature study, calculus of variation, energy methods, finite element formulations and eigenvalue problems. Hereby the analytical derivations are based on the calculus of variations, and formulations in the context of numerical analysis are based on the finite element formulations. The thesis can be read without consulting the attached papers, except from the full set of illustrative examples given. The thesis is therefore self contained and limits the repetition of basic information to a bare minimum and allows for philosophical considerations and extra clarifying informations. It is believed that this gives a much more comprehensive presentation of the work performed. Consequently, the thesis include a main part of the associated papers.

Having given an introduction including a description of the background and history of the beam theory, a presentation of the purpose and expectations, an introduction to the novel GBT approach as well as a description of the report structure the next chapter deals with a literature review.

Chapter 2

Literature Review

With the background information in section 1.1 it is clear that the theory behind thin-walled structures have been subject to extensive research, and in the recent years especially focusing on including transverse distortion of the cross section and minimizing the calculation time. As shown in subsection 1.1.4 a number of different analysis techniques involving local deformation are available. It appears, the conventional generalized beam theory known as GBT has been the most investigated technique in the recent years, due to the limited number of degrees of freedom and thereby a fast analysis of complicated problems of distorting structures.

In this chapter a statement of the distortional research will be given, even though a huge amount of research papers have become and are becoming published in these and the previous years. The chapter deals with approaches which handle in-plane distortion in the context of modal structural analysis, however the main topic in the chapter deals with the conventional GBT theory as this theory is most closely related to the novel approach developed in the present thesis. In this context, a comparison between the novel GBT approach and conventional GBT is given (later) in chapter 7. Thus, section 2.2 in the present chapter deals with an introduction of conventional GBT in general for the later comparison.

An intensive research work in the context of conventional GBT is performed by the Portuguese group lead by professor Dinar Camotim and professor Nuno Silvestre at the Technical University of Lisbon. To get insight in the expertise and knowledge of this group in the context of conventional GBT a valuable research stay in the group has been carried out by the author during a six month period. During this period the author had an invaluable opportunity to obtain an in-depth knowledge of the group, the conventional GBT approach, the research performed by the group as well as general world wide research performed in the context of conventional GBT which is reflected in this chapter.

2.1 Conventional generalized beam theory

The present section deals with a brief historical overview of the advancement and state-of-the art of the theory. Moreover, the present GBT review is divided into subsections related to the respective research groups or leaders. The hierarchical order of the subsections is related to the period of publishing.

2.1.1 Richard Schardt

The first publications by Schardt related to conventional GBT deals with first-order analysis of prismatic members with thin-walled un-branched open or cylindrical cross sections and was published in Schardt (1966; 1968). At the beginning R. Schardt and his research group at the Technical University of Darmstadt generally published only in German, which means that a wide majority of the publications were excluded for many of the international community. Even though Shardt was inspired of the theory of prismatic folded structures (Faltwerke in German), he acknowledged in Schardt (1989) that the guiding principles leading to the development of GBT were actually due to Wlassow (1958) whose premature death prevented the completion of his work towards the generalization of the classical beam theory. In that work Vlasov adopted a displacement field representation similar to the one used in conventional GBT. Please note that Wlassow and Vlassov is the same person and that the difference in spelling is due to the translation from English (Vlassov) to German (Wlassow). Since the first publication of Schardt related to conventional GBT he and his research group have published a great number of papers and dissertations as well as books concerning conventional GBT. This also includes his German book, Schardt (1989) which still constitutes the main reference within research and education in the context of conventional GBT. An overview of publications from 1966 to 2001 can be found at the website http://www.vtb.info/ controlled by Christof Schardt who is the son of Richard Schardt.

In the context of solutions to the differential equations of GBT specially the thesis by Hanf (1989) and Haakh (2004) should be mentioned. In Hanf (1989) the mathematical solution to the strong form of the semi-orthogonalized differential equations of GBT is found by solving an eigenvalue problem resulting in the axial amplitude functions and the associated solution modes. In Haakh (2004) the solutions to the strong form of the differential equations of GBT are also found. However, Haakh uses the semi-orthogonalized modes and in contrast to Hanf he finds their axial variation numerically using approximating power series.

Even though Schardt prefer to publish in German he started publishing in English on conventional GBT with the journal article Schardt (1994a). This paper deals with the conventional GBT formulation for first order analysis of

prismatic members. Note that this (English) publication was several years after the publication of his German book (Schardt, 1989).

In relation to second-order analysis in the context of conventional GBT the first application by Schardt was published in Schardt (1970) and improved by Miosga (1976). The first publication in English related to the conventional GBT formulation for second-order analysis of prismatic members was made by Schardt (1994b). A general GBT procedure to handle closed single or multi-cell cross sections was given in Möller (1982) followed by Girmscheid (1984) who improved it by adding warping in order to account for the shear lag effect. Schardt and Schrade introduced elastic constraints in the GBT member model and analyzed the stability of restrained cold-formed purlins in Schardt and Schrade (1982). Mörschardt formulated a methodology handling I-section members (Mörschardt, 1990) while Conchon used GBT to treat plates and slabs involving several support conditions and loading linearly (Conchon, 2001). More recently, R. Schardt and C. Schardt investigated the post-buckling behavior of an unstiffened plate by a GBT-based analytical approach (Schardt and Schardt, 2006).

In the context of dynamic problems, it was Saal that derived the first conventional GBT formulation for the vibration analysis of prismatic beams (Saal, 1974) and employed it to study effects of support conditions as well as local deformation on the vibration behavior of thin-walled beams. Furthermore, he also employed it to investigate the dynamic behavior of a cylindrical steel chimney under wind load. Together with Heinz, Schardt analyzed the free vibration behavior of an open-section bridge deck in Schardt and Heinz (1991), where they concluded that the frequency of the torsion mode may be significantly affected by local deformation. Furthermore, Schardt et al. (1995) and his son in Schardt (1995) employed conventional GBT to study the effect of coupling between local and global modes on the dynamic response of thin-walled members and to calculate the dynamic impact factor on prismatic bridge decks. Also working within the field of dynamic behavior is Heppner who dealt with the dynamic response of beams and plates in Heppner (1997).

More recently, the group of Schardt published several articles in Stahlbau (2010) on GBT which was as a dedication and in connection with the 80th birthday of Richard Schardt. In (Strehl, 2010) a brief history overview of the conventional GBT and the performance of the calculation method are given, while Schrade (2010) gives some interesting practical cases were the GBT is actually to be preferred in comparison to the finite element method. As examples Schrade mentions the South railway bridge in Köln (Germany) the Seidewitz valley bridge (Dohna, Germany), the Lockwitz valley bridge (Dresden, Germany) and the Dambach valley bridge (Hirschbach, Germany). In Haakh (2010) the mentioned work by Haakh (2004) and the associated software packages `VtbGui`

(http://www.ib-haakh.de/vtb) is extended by a systematic and uniform treatment and calculation of all support conditions. An extension of the GBT to include plate membrane shear lags is performed in Hanf (2010) by an approach including the implementation of kinematic shear corrections as well as additional warping degrees of freedom on secondary nodes. In contrast to the thesis by Hanf (1989) it is notable that the solution of the differential equations now adhere to the use of power series as in Haakh (2004).

2.1.2 John Michael Davies

Even though Schardt and his group also publish in English the proliferation of conventional GBT among the English speaking community was due to professor J.M. Davies from the University of Manchester. In cooperation with his PhD students P. Leach and C. Jiang, among others, Davies and his group focused mostly on the application of GBT to study the stability of cold-formed steel members. The first public contribution from the group was the PhD thesis of Leach (1989), in which the finite difference method is used to solve the GBT equations for first and second-order behavior of cold-formed members. In order to assess the accuracy of the method, the results were compared with results found using other methods and experimental tests (Davies and Leach, 1992). Later, Jiang performed elastic and inelastic analysis of cold-formed columns, purlins and decking (Jiang, 1994, Davies et al., 1994). Jiang wanted the design codes to account for distortional buckling because it is critical for the geometries of the members when they are used in practice. The two first international journal papers authored by Davies et.al. were published in 1994 as Davies and Leach (1994b;c). These publications made a presentation of the GBT formulation for first and second-order analysis. In Davies et al. (1997) GBT is used to study the buckling behavior of perforated storage rack columns, where the effect of the pertusions is indirectly considered by the members being treated as unperforated with a reduced thickness. A comparison of the design codes from the American (AISI, 1996), European (CEN, 1996), and Australian (AS/NZS, 1996) standards is presented in Davies and Jiang (1998), Kesti and Davies (1999) where also the accuracy of the calculation of the distortional buckling loads for columns and beams is treated. For an overview and his state-of-the-art review of cold-formed members of structures and design techniques see Davies (2000).

2.1.3 Janne Lepistö and Tapani Halme

A group of researchers from the Lappeenranta University of Technology in Finland used GBT to study the distortional buckling of C-sections and Hat-section columns with intermediate and end stiffeners and published in this context the paper Lepistö et al. (1996). They concluded that the GBT method suits well for

analyzing distortion of cold-formed thin walled profiles and that the mechanical behavior of the structure can be better understood by using the GBT-method than by using common numerical methods. They also concluded that the only widely used code, at the time, mentioning distortional buckling was the Eurocode 3 (CEN 1996) and that this code can give large unconservative results. Furthermore, Halme considered static, buckling, and vibration behavior of thin-walled plates in Halme (2001) and uses in Halme (2002) an alternative method for the determination of the GBT deformation modes by performing the eigenfrequency analysis of a grid with the shape of the cross section.

2.1.4 Ivan Baláž and Stanislav Rendek

The slovakian contribution to GBT was made by Baláž and Rendek from the Slovak University of Technology. They employed GBT to analyze the first order behavior of open and closed section members in Baláž (1999) and they presented an application of GBT to a cold-formed thin-walled steel cantilever beam with complex non-symmetrical open cross section (Rendek and Baláž, 2004). In order to assess the accuracy of the obtained results they performed an experimental investigation and compared with the theoretical values obtained (Rendek and Baláž, 2004). They also showed and concluded that GBT gives a very good description of the structural behavior of the thin-walled beams and therefore can be used as a good alternative to other numerical methods such as the finite element method and that GBT is a powerful tool convenient for use in pedagogical processes. In Rendek and Baláž (2002) they contributed to the GBT approach by developing a computer code which performs first-order analysis of thin-walled members with open or closed sections.

2.1.5 Luis Simões da Silva and Pedro Simão

An amazing and intensive research regarding GBT may belong to Portugal due to the two groups led by Simões da Silva and Simão as well as Camotim and Silvestre. The first group led by Simões da Silva and Simão from the University of Coimbra presents the fundamentals of GBT in Simão and da Silva (2004) also including a unified energy formulation in the framework of GBT for the non-linear analysis of both open and closed sections. They compared the buckling behavior of open and closed-section columns in Simao and da Silva (2002) where the Rayleigh-Ritz method was used to solve the equilibrium equations. Concerning hollow flange (HFB) beams and columns, the buckling behavior was investigated in Simão and da Silva (2008a). Regarding post-buckling behavior they treated cold-formed columns with open cross sections Simao and da Silva (2003b) as well as for closed cross section (Simao and da Silva, 2003a). In this context also the post-buckling behavior of hollow flange (HFB) beams

and columns was investigated in Simão and da Silva (2008b). This type of cold-formed steel sections was invented in Australia by Palmer Tube Mills Pty Ltd and is designated as "dog bone". They consist of an I-section with flanges made of triangular closed cells and thus provides high major axis moment of inertia as well as high torsional stiffness (Avery et al., 2000). Therefore, they are mainly devoted to beam elements. For a more elaborate description of the mentioned studies and developments readers are referred to the PhD thesis of Simão (Simao, 2007).

2.1.6 Dinar Camotim and Nuno Silvestre

The second Portuguese group is led by professor Dinar Camotim and Nuno Silvestre, from the Technical University of Lisbon (Portugal). The group has published a large number of papers and has in the last 10 years been on the cutting edge of research and international communication regarding GBT. They have produced more than hundred publications on the subject since the first journal articles (Silvestre and Camotim, 2002a;b). Therefore this subsection provides only a brief review of the publications and research performed by the group. Activities by this group up to 2006 can be found in Camotim et al. (2004; 2006b;a).

As a PhD student with Camotim as supervisor, Silvestre developed and implemented GBT formulations to investigate several structural problems and to enhance design provisions involving prismatic open-section members, see the highly referenced thesis (Silvestre, 2005). His investigations, in the context of cold-formed steel members, involved buckling analysis including GBT-based determination of analytical formulas to calculate the distortional buckling loads of cold-formed members with C, Z or rack-sections (Silvestre and Camotim, 2004c;a;b). Furthermore, he investigated the buckling behavior of simply supported steel tubular members with circular sections (Silvestre, 2007), elliptical sections (Silvestre, 2008a) as well as the buckling behavior of single-walled carbon nanotubes (Silvestre, 2008b). The investigations also involved post-buckling analysis (Silvestre and Camotim, 2003b; 2006b) and as mentioned in Paper I (Jönsson and Andreassen, 2011) the formulation for post-buckling analysis of GBT, which is essentially a beam theory and not a plate theory, Silvestre involved the consideration of (non-conventional) shear and transverse extension modes as well as modified constitutive relations. Additionally, he investigated vibration analysis (Silvestre and Camotim, 2006c), and the development and application of formulations for static, buckling and vibration analysis of FRP composite members (Silvestre and Camotim, 2002a;b; 2003a; 2006a). Together with Dinis and Camotim he investigated the local and global buckling behavior of angle, T-section and cruciform thin-walled steel members in the context of

GBT (Dinis et al., 2010). Recently, he revisited the Generalized Beam Theory from the kinematical assumptions to the deformation mode determination in Silvestre et al. (2011). Currently, Nanomechanics is the research field of Silvestre, and in this context he published a study concerning the buckling behavior of single-walled carbon nanotubes (CNTs) under torsion by using shell models (Silvestre, 2012).

Rodrigo Gonçalves

Gonçalves expanded the field of applicability of GBT as a PhD student with Camotim. In particular to members with non-linear elasto-plastic behavior (Gonçalves, 2007). Recently, he focused on elasto-plastic thin-walled metal members in the context of geometrically non-linear GBT (Gonçalves and Camotim, 2011; 2012). He formulated a non-linear elastic Generalized Beam Theory (GBT) and used it to investigate the buckling behavior of thin-walled columns made of aluminium and stainless steel (Gonçalves and Camotim, 2004b). In this context he analyzed the plastic bifurcation of simply supported columns with different types of cross section, used stress-strain laws of the Ramberg-Osgood type to model the uniaxial behavior as well as implemented plasticity. Later, the formulation was generalized for general loading conditions in Gonçalves and Camotim (2007). In a recent publication he developed GBT-based semi-analytical solutions for the plastic bifurcation of thin-walled members in Gonçalves et al. (2010). Together with Camotim he also developed a finite element for the elastic buckling analysis of members subjected to linear (non-uniform) internal force and moment diagrams in Gonçalves and Camotim (2004a). They used it to study the buckling behavior of C and hat-section cantilever beams. Gonçalves also presented a GBT formulation for the analysis of multi-cell closed-section members in Gonçalves et al. (2006) used within a box girder bridge analysis. The formulation has been generalized to arbitrary cross sections in Gonçalves et al. (2009). Recently, he also investigated steel-concrete composites in Goncalves and Camotim (2010).

Pedro B. Dinis

In the context of buckling Dinis developed a GBT formulation that handles arbitrary open "branched" sections (Dinis et al., 2006) and subsequently expanded to general open and closed cross sections (Dinis et al., 2008, Gonçalves et al., 2009). Together with Camotim he also investigated coupled instabilities with distortional buckling in cold-formed steel lipped channel columns (Camotim and Dinis, 2011) as well as the mechanics of thin-walled angle column instability (Dinis et al., 2012).

Cilmar Basaglia

The former PhD student at IST, Cilmar Basaglia has extended the theory to be applicable to analysis of thin-walled frames. Thus he developed a "joint element" that guarantees the compatibility of displacements between members and implemented it in the context of the GBT-based finite element analysis (Basaglia et al., 2008b). In this context he analyzed the buckling behavior of thin-walled steel frames using Generalized Beam Theory (Basaglia et al., 2007b) also subjected to arbitrary loadings (Basaglia et al., 2007a). Regarding post-buckling analysis he published Basaglia et al. (2008a) dealing with thin-walled steel members and frames and he studied the effect of non-standard support conditions on the post-buckling behavior of beams subjected to arbitrary loadings (Basaglia et al., 2009). Camotim, Basaglia and Silvestre report a state-of-art concerning GBT buckling analysis of thin-walled steel frames in Camotim et al. (2010). Recently, Basaglia also studied non-linear GBT formulation for open-section thin-walled members with arbitrary support conditions (Basaglia et al., 2011).

Nuno Silva

GBT formulations dealing with FRP (Fibre Reinforced Polymers) composites was developed by Nuno Silva. In this context he investigated the influence of material couplings on the linear and buckling behavior (Silva and Silvestre, 2007). In relation to buckling he developed a GBT formulation to analyze the buckling behavior of thin-walled FRP composite columns with open cross sections (Silva et al., 2010). Thus also taking shear deformation and cross-section deformations into account. He also investigated post-buckling behavior (Silva et al., 2008b) and studied the first-order, buckling, and post-buckling behavior of pultruded I-section GFRP (Glass Fibre Reinforced Polymers) cantilevers including comparisons with experimental results (Correia et al., 2009, Silva et al., 2009; 2011). Moreover, he developed GBT formulations that handles arbitrary cross sections (Silva et al., 2008a).

Rui Bebiano

Another of Camotim's PhD students is Bebiano. He started before his PhD studies to employ conventional GBT to study the effect of stiffeners in the buckling and post-buckling behavior of C-section columns and beams (Bebiano et al., 2005, Silvestre et al., 2005). During his PhD he investigated the stability and dynamics of thin-walled members in the context of conventional generalized beam theory (Bebiano, 2009). This PhD thesis gives a good state-of-the-art literature review valid up to 2009. In this context he derived a GBT formulation to analyze the buckling behavior of thin-walled members subjected to non-uniform bending (Bebiano et al., 2007). Furthermore, he presented a software package

GBTUL to perform buckling and vibration analyses of open cold-formed members (Bebiano et al., 2008b). This software package is used in the present thesis to compare the novel GBT approach and conventional GBT.

2.2 Conventional GBT in general

As stated above, this section is devoted to a brief overview of conventional GBT formulated in words. The overview will focus on parts also related to the novel GBT approach. From the above literature review it is clear that the conventional GBT approach has fostered a large number of publications on several different topics.

Since GBT was developed as a generalization of beam bending it leads to orthogonal warping modes. Thus the final GBT equations are decoupled with respect to normal stresses and transverse stresses, however the shear coupling terms are neglected when Schardt uses the GBT equations to find distortional deformation modes. This corresponds to modal analysis with orthogonal (Rayleigh) damping in dynamic structural analysis. Even though the conventional GBT method is an extensively investigated approach including distortion and has been very successful for open cross sections to include distortion it has involved some complications concerning the solution of the conventional GBT equations for closed (single or multi-celled hollow) thin-walled cross sections. Consequently, the shear coupling terms are given special attention in case of closed cells. The basic cross-section deformation modes of GBT are obtained by separately identifying conventional beam deformation modes and solving the eigenvalue problem defined by the warping stiffness matrix and the transverse deformation stiffness matrix. The special attention related to closed (single or multi celled hollow) thin-walled cross sections comprises that the theory needs a relaxation of the Vlasov kinematic assumption of negligible shear strain along the center lines of the cross-section walls, in order to include the warping deformation associated with the "Bredt's shear flow" around each cell (Schardt, 1989). However, it complicates the solution of the conventional GBT equations by introducing non-negligible shear coupling terms (off-diagonal) in the GBT equations as can be seen in recent GBT formulations for closed thin-walled cross sections. An analytical solution of the shear coupled GBT equations has been published only by (Hanf, 1989) while a numerical solution based on power series has been published by Haakh (2004).

Alternatively, and as a standard procedure in conventional GBT, the GBT equations have to be solved using approximate engineering methods. This means that conventional GBT finds the modes using a method similar to the well known deformation method or force method, see e.g. Silvestre (2005). After the elementary deformation modes have been determined, the components of

the tensors appearing in the equilibrium system can be calculated. Since all these tensors are fully populated, meaning that the equilibrium system is highly coupled, it is relevant to find an alternative system of coordinates in order to render the system as much uncoupled as possible. This is what in GBT is called the GBT matrices diagonalization. Note, that Both Hanf (1989) and Haakh (2004) use the original orthogonalization procedure of Schardt to establish the GBT equations, which are still coupled with respect to shear terms and perhaps transverse strains. In this diagonalization procedure some new modes are identified through a three step procedure involving subeigenvalue problems, see e.g Schardt (1989). Concerning the linear stiffness matrices, it is noted that the matrices [**C**] and [**B**] are completely diagonal, while [**D**] displays non-null terms outside the diagonal. In this matter GBT neglects these non-null terms, and in this way call [**D**] approximately diagonalized. The new modes identified are called approximated GBT modes or simply approximated deformation modes. After determination of the approximated GBT modes a GBT mode selection is performed corresponding to the problem at hand. Thus it applies that the conventional GBT approach does not involve an exact analytical solution of the classical GBT differential equations, which means that the solution is obtained by approximated longitudinal amplitude functions.

After having completed the cross-section analysis and the GBT mode selection, these found approximated modes are used as shape functions in a so called member analysis using a virtual work or potential energy formulation leading to approximated axial amplitude functions related to finite GBT beam elements. However, the discretization has to be performed without prior knowledge of the problem length scales of the individual modes. The approximated axial amplitude functions are then used in the full fourth order differential equation also containing the non-diagonalized [**D**]-matrix, which leads to a highly coupled system of modes. It should be noticed that the GBT approach finds the in-plane modes in a cross-section analysis while the axial variations are devoted to a member analysis. Thus, it should be noticed that the conventional GBT formulations do not solve the differential equations to find the distortional modes but establish a weak solution through introduction of the established approximate mode shapes (based on an orthogonal shear stiffness assumption) and use approximate modal amplitude functions. According to this procedure to identify the modes, the eigenvalue can solely be used to get the order/sequence of the modes, and not as a parameter that defines the length scale of the modes. Furthermore, there is no exact link between the in-plane modes and the axial variational function.

In these developments, the distortional modes of traditional GBT have been extended (with "other" modes) in order to encompass shear through shear modes, post-buckling through inclusion of transverse extension modes as well

special modes to accommodate shear lag. Concerning the possibility to perform post-buckling analysis with GBT, which is essentially a beam theory and not a plate theory, it was Silvestre (2005) who found it is necessary to include the additional transverse extension modes and shear modes, as well as to modify the constitutive relations. In general these kinds of modes are chosen to be referred to as "other" modes and the related method as extended conventional GBT.

In the context of stability analysis, GBT uses the modes found in the linear analysis and postulate a shape function along the axial axis. This linear part is defined as the linear stiffness matrix $\mathbf{K}$. Afterwards a non-linear part is defined as the geometrical stiffness matrix $\mathbf{G}$ including the non-linear part X^{σ} which is also non-diagonal. These definitions lead to the following linear eigensystem:

$$([\mathbf{K}] + \lambda[\mathbf{G}])\{\mathbf{a}\} = \mathbf{0} \tag{2.1}$$

The solutions to this equation are a set of buckling loads, λ (*eigenvalues*), and the associated buckling mode shapes, $\{\mathbf{a}\}$ (eigenvectors). Also the buckling modes will be highly coupled. In Silvestre (2005) it is indicated that in fact, both buckling and vibration problems always have coupled equilibrium equations.

Hereby a brief overview of the conventional GBT in general has been given and the next section deals with a brief literature review of other methods. The interested reader is referred to Silvestre (2005) and Schardt (1989) for a more elaborate description of the conventional generalized beam theory.

2.3 Other methods

Even though the conventional GBT theory is the most similar theory in relation to the present GBT approach, there are other methods representing the field of distortional mechanics of thin-walled structural elements.

As mentioned in section 1.1.4 an alternative method is the finite strip method (FSM) which have been investigated intensively by Ádány and Schäfer focusing on its relation to GBT as buckling analysis. Using GBT beam elements is an alternative to the use of finite-strip methods (FSM), see for example Zienkiewicz and Taylor (2000b). However, GBT is as its name states essentially a beam theory, whereas FSM essentially is based on plate theory. Therefore FSM does not contain a natural decomposition into basic beam, distortional, local and other modes. Since the modal decomposition may lead to advantages in design of thin-walled structures using FSM a great deal of work has been performed by Ádány and Schafer to develop a constrained finite-strip method (cFSM) and modal decomposition methods for open (single-branched) cross sections (Ádány and Schafer, 2006a;b, Schafer and Ádány, 2006, Ádány and Schafer, 2008). The modal approaches of extended conventional GBT and cFSM formulations have recently been compared in Ádány et al. (2009) and Silvestre et al. (2011).

Also a Spanish group has investigated the distortional mechanics of thin-walled structural elements within a combination of the conventional GBT theory and the finite element method, see Casafont et al. (2011).

An Italian group has presented a new approach for thin-walled member analysis in the frame work of GBT (Ranzi and Luongo, 2011), and a Romanian researcher has presented a GBT formulation to analyze the behavior of thin-walled members with variable cross section (Nedelcu, 2010).

A review of some progresses up to year 2000 in the field of cold-formed steel members can be found in Rondal (2000).

Having described some, at the time, alternative analysis methods to the shell finite element method, the next chapters will describe the new approach to generalized beam theory developed in this PhD project. In the following, the GBT approach developed by Shardt is referred to as conventional GBT. As mentioned the theoretical developments in the new approach is based on the calculus of variations, energy formulations and the formulations concerning the numerical analysis are based on finite element method formulations.

Chapter 3

Distortional homogeneous differential equations and solutions

Having described the most traditional alternative analysis methods to the shell finite element method, the next chapters will deal with the novel approach to generalized beam theory developed in this PhD project.

As mentioned, the classical thin-walled beam theory for open and closed cross sections can be generalized by including distortional displacement modes. Normally, the introduction of additional displacement modes leads to coupled differential equations, which seems to have prohibited the use of exact shape functions in the modeling of coupled torsion and distortion. However, if the distortional displacement modes are chosen as those which decouple the differential equations as in non-proportionally damped modal dynamic analysis then it may be possible to use exact shape functions and perform analysis on a reduced problem. In the recently developed generalized beam theory (GBT) the natural distortional displacement modes are determined on the basis of a quadratic eigenvalue problem. However, as in linear modal dynamic analysis of proportionally damped structures this problem has been solved approximately using linear eigenvalue analysis of modified sub problems. This seems to have worked well for open cross sections but not for closed. In this chapter it is shown that it is possible to solve the distortional quadratic eigenvalue problem and find the natural distortional displacement modes using a method equivalent to that used for non-proportionally damped (linear) dynamic modal analysis.

In this context and in view of developing an advanced beam element including distortional contributions, the distortional decoupled homogeneous differential equations and solutions are developed and solved. The chapter is related to Paper I (Jönsson and Andreassen, 2011) and Paper V (Andreassen and Jönsson, (2009).

From energy formulations, variational analysis, and a finite-element-based displacement approach the potential energy is used to establish a set of distortional homogeneous equilibrium differential equations for the generalized displacement field in a modal based formulation. Furthermore, we will adhere to the definition of the warping function given by Kollbrunner and Hajdin (1972). The innovative theoretical developments performed in this thesis lead towards a semi-discretization formulation in which the rotational degrees of freedom are included, thus including local plate modes in the formulation even for the simplest discretization. The formulation with both open and closed (single or multi-cell) cross sections can be regarded as an extension of modified classical Vlasov thin-walled beam theory to include distortional deformation modes. As we want to achieve a formulation resembling a generalization of Vlasov beam theory we also have to implement some constrains and eliminations into the differential equations. The extension of the modified classical Vlasov thin-walled beam theory also includes the introduction of constant shear flows in the walls of the cross section. Hereby, it makes it possible to analyze prismatic thin-walled members with cross-section distortion and local plate behavior in a one-dimensional formulation through the linear combination of pre-established modes of deformation.

The theories of beams are derived on the basis of assumed displacement fields which correspond to extension, flexure, torsion, warping and distortional displacements. This means that the axial stress distribution has several components representing the contributions from N, M_1, M_2, B_T and B_D, respectively. These components and their related transverse displacements are illustrated in Figure 3.1 for an open C-section. Note, that the distortional part, B_D, include more parts than the shown one, corresponding to the number of distortional modes.

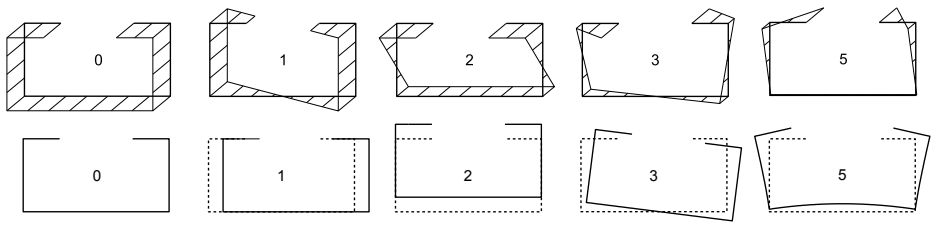

Figure 3.1: The axial stress components corresponding to N, M_1, M_2, B_T and B_D for an open C-section (upper part) and the related transverse displacements (lower part).

This corresponds to a modal separation in which each mode has a set of transverse and axial displacement fields that may be coupled. Each of these cross-section displacement fields is factorized in a displacement mode that is a

function of the in-plane coordinates, multiplied by a function of the axial coordinate, z, which describes the axial variation of the mode. In the following, we propose a method for finding these displacement modes, including global, distortional and local modes. The modes are the eigenmodes of the corresponding homogeneous set of equilibrium equations and the axial variation functions corresponds to the eigenvalues.

Even though the novel approach lead to a theoretical improvement some neglected effects should be mentioned. These are:

- The influence of curved cross-section walls in the definition of the displacements and strains is neglected. This may be deemed reasonable as it is assumed that the radius of curvature is sufficiently large.
- Local effects at corners and joints are neglected.
- Using non-coupling constitutive relations, which also means that there are no terms out of the diagonal in the constitutive matrix containing E, E_s and G. E is the modulus of elasticity, $E_s = E/(1-\nu^2)$ the plate type elasticity modulus in which ν represents the Poisson ratio and G is the shear modulus.
- No Poisson effect taking into account, however Poisson's ratio is used in the calculation of the above mentioned E_s and G.
- Only shear contributions from torsion and shear flow around cells will be allowed.

As mentioned, the formulations in this chapter only consider the first-order homogeneous linear displacements of GBT, since the goal has been to identify a theoretically sound formulation of the end effects. In other words, we find the eigensolutions for the full displacement field including the variation in the axial member direction, see the treatment of end effects in Timoshenko and Goodier (1951).

3.1 Basic kinematic assumptions of a single mode

In view of the distortional homogeneous differential equations, let us first take a look at the basic assumptions and kinematic relations for a prismatic member with an arbitrary thin-walled cross section. The entire chosen displacement field is shown in Figure 3.2. From the figure it is seen that the entire chosen displacement field is described as an in-plane displacement field multiplied by an out-of-plane axial amplitude function, ψ. In Figure 3.3 we assume a prismatic thin-walled beam described in a global Cartesian (x, y, z) coordinate system where the z-axis is in the longitudinal direction of the beam. A cross-section

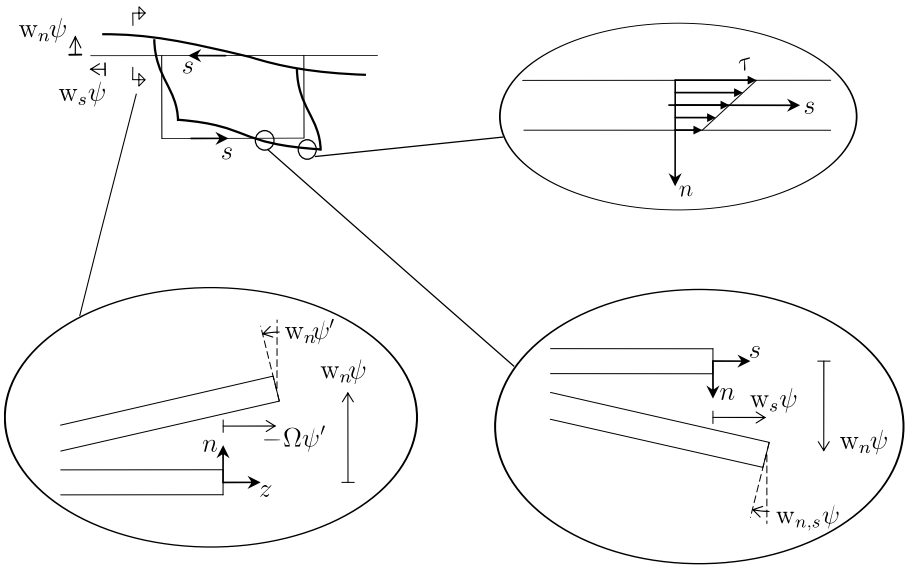

Figure 3.2: Local components of displacements and assumed shear stresses.

coordinate s is introduced as a curve parameter which runs through the entire section along the center line and the coordinate along the local normal is defined as n. Hereby the subscripts n and s are used for the components in the local coordinate system corresponding to the normal and tangential directions. As a formal standard designation, subscripts following a comma are used for derivatives, for example $u_{n,ss} = d^2u_n(s)/ds^2$ or $u_{s,n} = \partial u_s(s,n)/\partial n$. A prime, $'$, is used for the axial derivative, d/dz.

Using the stated designations the components u_n and u_s of the in-plane cross-section displacements in the local coordinate system at a point (n, s) in the cross-section, are introduced as

$$u_n(s,z) = \mathrm{w}_n(s)\psi(z) \tag{3.1}$$

$$u_s(n,s,z) = (\mathrm{w}_s(s) - n\mathrm{w}_{n,s}(s))\psi(z) \tag{3.2}$$

Here $\mathrm{w}_s(s)$ and $\mathrm{w}_n(s)$ are the local displacements of the centerline as shown in Figure 3.2, and $\psi(z)$ is the function which describes the axial variation of the in-plane distortional displacements. The axial displacements $u_z(n,s,z)$ generated by the in-plane distortional displacements are introduced as

$$u_z(n,s,z) = -(\Omega + n\mathrm{w}_n)\psi' \tag{3.3}$$

Here the axial (warping) displacement mode $\Omega(s)$ has been included with a variation corresponding to the negative axial derivative of the axial variation factor, $-\psi'$, and due consideration of local transverse variation through the term $n\mathrm{w}_n$.

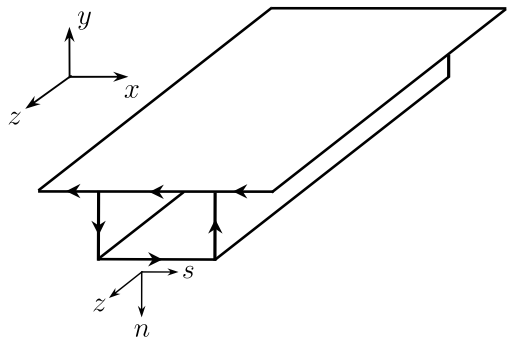

Figure 3.3: Global and local Cartesian reference frames.

Thus neglecting shear deformation contributions which are not related to St. Venant torsion and torsional shear flow around closed cells. To introduce shear deformation in the current formulation will involve the introduction of a new parameter, which is independently allocated directly to the warping function instead of the derivative of the ψ-function. This has been done in Kollbrunner and Hajdin (1972). However the change is major. Please note that shear deformation accommodating Bredt's shear flow around closed cells is included in the theory through the specific definition of the warping function (Kollbrunner and Hajdin, 1972).

The presented components represent a single displacement mode.

At this state it is important to note that pure axial extension (where $\Omega = 1$ and $\mathrm{w}_s = \mathrm{w}_n = \mathrm{w}_{n,s} = 0$) is embedded in the formulation. However, since pure extension in the present formulation does not involve transverse displacements, the axial variation $-\psi'(z)$ need not be taken as the derivative of a function, but just a function which will be introduced as $\zeta(z) = -\psi'(z)$ at a later stage.

The axial kinematic strain-displacement relation is given as

$$\varepsilon = u'_z = -(\Omega + n\mathrm{w}_n)\psi'' \tag{3.4}$$

The cross-section distortional strains are

$$\varepsilon_s = (\mathrm{w}_{s,s} - n\mathrm{w}_{n,ss})\psi \tag{3.5}$$

and the engineering shear strain in the walls of the cross section becomes

$$\gamma = \gamma_{zs} = u_{z,s} + u_{s,z} = (\mathrm{w}_s - \Omega_{,s} - 2n\mathrm{w}_{n,s})\psi' \tag{3.6}$$

To cope with the shear flow around closed cells, we introduce the shear strain in the middle of the wall as

$$\bar{\gamma}_d\psi' = (\mathrm{w}_s - \Omega_{,s})\psi' \tag{3.7}$$

Bernoulli beam theory is based on the assumption of zero shear strain and sets the shear strain equal to zero and thus determines the warping displacements (flexural modes) by the differential equation $\Omega_{,s} = \mathrm{w}_s$. This means that the formulation of Bernoulli beam theory does not include shear contributions and the axial equilibrium equation of a section cut-out is not fulfilled, which leads to the use of Grashof's method for the determination of the shear stresses. However, if we are to analyze closed cross-sections as in Vlasov beam theory, see Kollbrunner and Hajdin (1972), we have to allow for a constant shear flow around the cells and the warping of the cross-section then has to be determined by the differential equation $\Omega_{,s} = \mathrm{w}_s - \bar{\gamma}_d$ as

$$\Omega(s) = \int_0^s \mathrm{w}_s ds - \int_0^s \bar{\gamma}_d ds + \Omega_0 \tag{3.8}$$

In the current context, the warping function will be determined from a weak formulation of the assumption of a constant shear flow $\bar{T}_d$ in the walls of the cross-section, where $\bar{T}_d = Gt\bar{\gamma}_d$. Here G is the shear modulus and t the thickness of the wall. The strong formulation of the constraining assumption is that the contribution of the shear flow to the axial equilibrium equation, see Figure 3.4, of a section cut-out is zero, i.e.

$$\bar{T}_{d,s} = 0 \tag{3.9}$$

Multiplying by a virtual centerline axial displacement, $\delta\bar{u}_z$, and integrating over the cross-section centerline curve, C, we find the virtual work of the shear flow in a cross section as

$$\int_C \bar{T}_{d,s}\delta\bar{u}_z ds = 0 \tag{3.10}$$

Performing a partial integration and noting that the shear stress flow is zero at all free edges, we find the weak formulation that will be used to determine the warping function

$$\left[\bar{T}_d\delta\bar{u}_z\right]_{\text{free edges}} - \int_C \bar{T}_d\delta\bar{u}_{z,s} ds = 0 \quad \Rightarrow \int_C \bar{T}_d\delta\bar{u}_{z,s} ds = 0 \tag{3.11}$$

This is the constraint equation that we will use to enforce the assumption of zero axial work performed by the shear flow around the cells.

3.2 Internal energy assumptions

The potential energy of a single deformation mode is formulated based on the discretization of the cross section.

In the following we will adhere to simple constitutive relations, i.e. the material is assumed to be linear elastic with a modulus of elasticity E and

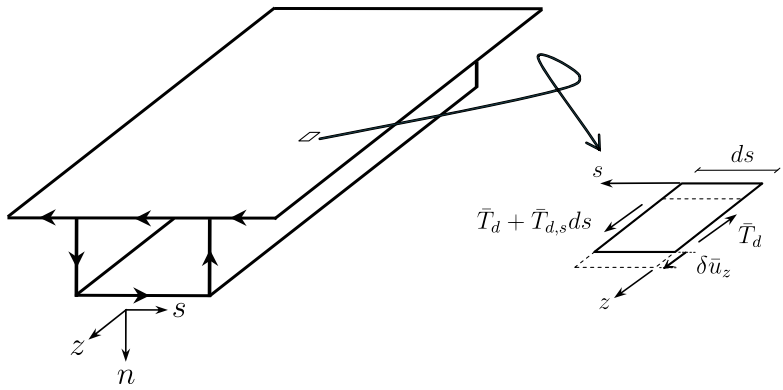

Figure 3.4: Work of shear flow through axial virtual displacement.

a shear modulus G. In the transverse direction we will assume a plate type elasticity modulus $E_s = E/(1-\nu^2)$, in which ν represents the Poisson ratio. The axial stress is determined as $\sigma = E\varepsilon$, the shear stress as $\tau = G\gamma$ and the transverse stress as $\sigma_s = E_s\varepsilon_s$. Thus the coupling of axial strain ε and transverse strain ε_s is neglected. Note that this means that we also neglect the equivalent coupling between axial and transverse curvatures in the constitutive relations for the plate moments, but with some changes it is possible to include the coupling of the curvatures. With the simple constitutive relations assumed in equation (3.12) the elastic energy potential is as given in equation (3.13). From equation (3.12) it is clear that we are using non-coupling diagonal constitutive relations or in other words there are no off-diagonal terms in the matrix containing E, E_s and G.

$$\begin{bmatrix} \sigma \\ \sigma_s \\ \tau \end{bmatrix} = \begin{bmatrix} E & 0 & 0 \\ 0 & E_s & 0 \\ 0 & 0 & G \end{bmatrix} \begin{bmatrix} \varepsilon \\ \varepsilon_s \\ \gamma \end{bmatrix} \tag{3.12}$$

$$\Pi = \int_V \left(\tfrac{1}{2} E\varepsilon^2 + \tfrac{1}{2} G\gamma^2 + \tfrac{1}{2} E_s \varepsilon_s^2 \right) dV \tag{3.13}$$

Let us introduce a thin-walled cross section assembled using straight cross-sectional elements, see Figure 3.5, and let us integrate through the thickness, t, across the widths, b_e, of the elements, and over the length, L, of the thin-walled beam. The elastic potential energy takes the following form after the

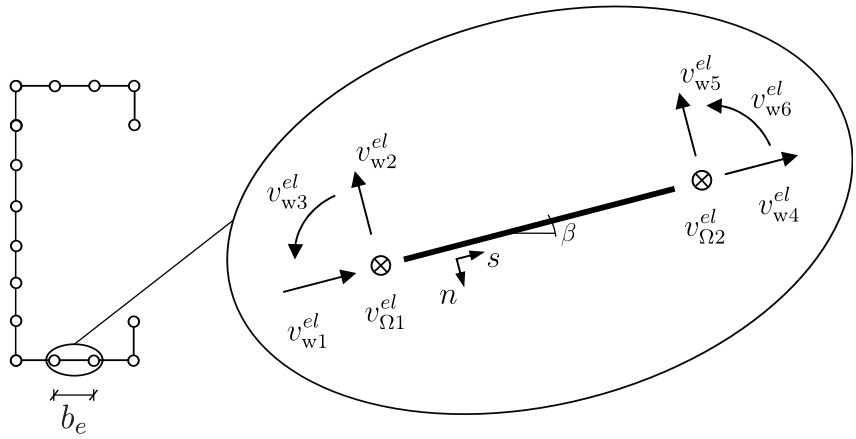

Figure 3.5: Components of the displacements vectors of a straight cross-section element.

introduction of the strains expressed by the displacement in separated form:

$$\Pi = \tfrac{1}{2}\int_0^L \Bigg[\sum_{el} \int_0^{b_e} \Big\{ \Big[\overbrace{Et(\Omega\psi'')^2}^{k^{\sigma}_{\Omega\Omega}} + \overbrace{\frac{Et^3}{12}(\mathrm{w}_n\psi'')^2}^{k^{\sigma}_{\mathrm{ww}}} \Big] + \Big[\overbrace{Gt(\mathrm{w}_s\psi')^2}^{k^{\tau}_{\mathrm{ww},1}} + \overbrace{Gt(\Omega_{,s}\,\psi')^2}^{k^{\tau}_{\Omega\Omega}} - 2\overbrace{Gt(\mathrm{w}_s\psi')(\Omega_{,s}\,\psi')}^{-k^{\tau}_{\mathrm{w}\Omega}} + \overbrace{\frac{1}{3}Gt^3(\mathrm{w}_{n,s}\psi')^2}^{k^{\tau}_{\mathrm{ww},2}} \Big] + \Big[\overbrace{E_s t(\mathrm{w}_{s,s}\psi)^2 + \frac{E_s t^3}{12}(\mathrm{w}_{n,ss}\psi)^2}^{k_s} \Big] \Big\} ds \Bigg] dz \tag{3.14}$$

In equation (3.14) it is seen that the elastic energy terms have been grouped in axial strain energy, shear energy, and transverse strain energy. Furthermore, each individual part of the equation has been overbraced and associated with the stiffness contribution as given later.

In conventional beam theory, we usually introduce rigid cross-sectional displacement modes and the elastic energy is described by a summation of the energy stored in all displacement modes. However, we have to remember the shear constraints associated with our assumption of constant shear flow, which will be introduced later. In the current work we wish to establish a set of displacement modes by using semi-discretization. To achieve this, the cross-section will be divided into discrete straight-line elements, in which we interpolate the transverse and axial displacements.

3.3 Displacement interpolations within cross-section elements

Within each straight finite cross-section element, the axial displacements, Ω, are interpolated linearly corresponding to a linear variation of the warping functions and the transverse displacement of the elements are interpolated linearly in the direction of the element and cubically (corresponding to beam elements) in the transverse direction of the element. The displacements in a straight cross-section finite element are thus interpolated as follows:

$$\begin{aligned} \Omega\psi' &= \mathbf{N}_\Omega \mathbf{v}_\Omega^{el}\psi' \\ \mathrm{w}_s\psi &= \mathbf{N}_s \mathbf{v}_\mathrm{w}^{el}\psi \\ \mathrm{w}_n\psi &= \mathbf{N}_n \mathbf{v}_\mathrm{w}^{el}\psi \end{aligned} \tag{3.15}$$

Here $\mathbf{N}_\Omega(s)$ and $\mathbf{N}_s(s)$ are linear interpolation matrices and $\mathbf{N}_n(s)$ is a cubic (beam) interpolation matrix. Furthermore, we have introduced the axial and transverse nodal displacement components of a straight cross-section element as

$$\begin{aligned} \mathbf{v}_\Omega^{el} &= \begin{bmatrix} v_{\Omega 1}^{el} & v_{\Omega 2}^{el} \end{bmatrix}^T \\ &= \begin{bmatrix} \Omega(0) & \Omega(b_e) \end{bmatrix}^T \\ \mathbf{v}_\mathrm{w}^{el} &= \begin{bmatrix} v_{\mathrm{w}1}^{el} & v_{\mathrm{w}2}^{el} & v_{\mathrm{w}3}^{el} & v_{\mathrm{w}4}^{el} & v_{\mathrm{w}5}^{el} & v_{\mathrm{w}6}^{el} \end{bmatrix}^T \\ &= \begin{bmatrix} \mathrm{w}_s(0) & -\mathrm{w}_n(0) & -\mathrm{w}_{n,s}(0) & \mathrm{w}_s(b_e) & -\mathrm{w}_n(b_e) & -\mathrm{w}_{n,s}(b_e) \end{bmatrix}^T \end{aligned} \tag{3.16}$$

Here b_e is the width of the flat element. Nodal components and the direction of the section coordinates (n, s) are shown in Figure 3.5. The element stiffness contributions to the axial strain, shear strain, and transverse strain energy can now be found using the displacement interpolations. The stiffness contributions found are seen from equation (3.14) and shown in Table 3.1, in which the first two are the axial stiffness contributions, the third is the transverse distortional stiffness term, while the last three are the shear strain stiffness contributions. These stiffness contributions can be found explicitly. Written in full the stiffness matrices takes the form

$$\mathbf{k}_{\Omega\Omega}^{\sigma} = \tfrac{tEL}{6} \begin{bmatrix} 2 & 1 \\ 1 & 2 \end{bmatrix} \tag{3.17}$$

$$
\begin{aligned}
\mathbf{k}^{\sigma}_{\Omega\Omega} &= \textstyle\int_0^{b_e} Et\mathbf{N}_{\Omega}^T\mathbf{N}_{\Omega}ds \\
\mathbf{k}^{\sigma}_{\mathrm{ww}} &= \textstyle\int_0^{b_e} \frac{Et^3}{12}\mathbf{N}_{n}^T\mathbf{N}_{n}ds \\
\mathbf{k}^{s} &= \textstyle\int_0^{b_e} \left(E_s t\mathbf{N}_{s,s}^T\mathbf{N}_{s,s} + \frac{E_s t^3}{12}\mathbf{N}_{n,ss}^T\mathbf{N}_{n,ss}\right)ds \\
\mathbf{k}^{\tau}_{\mathrm{ww}} &= \textstyle\int_0^{b_e} \left(Gt\mathbf{N}_{s}^T\mathbf{N}_{s} + \frac{Gt^3}{3}\mathbf{N}_{n,s}^T\mathbf{N}_{n,s}\right)ds \\
\mathbf{k}^{\tau}_{\Omega\Omega} &= \textstyle\int_0^{b_e} Gt\mathbf{N}_{\Omega,s}^T\mathbf{N}_{\Omega,s}ds \\
\mathbf{k}^{\tau}_{\mathrm{w}\Omega} &= [\mathbf{k}^{\tau}_{\Omega\mathrm{w}}]^T = -\textstyle\int_0^{b_e} Gt\mathbf{N}_{s}^T\mathbf{N}_{\Omega,s}ds
\end{aligned}
$$

Table 3.1: Straight-element stiffness contributions.

$$
\mathbf{k}^{\sigma}_{\mathrm{ww}} = \tfrac{Et^3L}{12\cdot 420}\begin{bmatrix}
0 & 0 & 0 & 0 & 0 & 0 \\
0 & 156 & 22L & 0 & 54 & -13L \\
0 & 22L & 4L^2 & 0 & 13L & -3L^2 \\
0 & 0 & 0 & 0 & 0 & 0 \\
0 & 54 & 13L & 0 & 156 & -22L \\
0 & -13L & -3L^2 & 0 & -22L & 4L^2
\end{bmatrix} \tag{3.18}
$$

$$
\mathbf{k}^{s} = \begin{bmatrix}
\frac{Et}{L} & 0 & 0 & \frac{-Et}{L} & 0 & 0 \\
0 & \frac{12EI}{L^3} & \frac{6EI}{L^2} & 0 & -\frac{12EI}{L^3} & \frac{6EI}{L^2} \\
0 & \frac{6EI}{L^2} & \frac{4EI}{L} & 0 & -\frac{6I}{L^2} & \frac{2EI}{L} \\
\frac{-Et}{L} & 0 & 0 & \frac{Et}{L} & 0 & 0 \\
0 & -\frac{12EI}{L^3} & -\frac{6EI}{L^2} & 0 & \frac{12EI}{L^3} & -\frac{6EI}{L^2} \\
0 & \frac{6EI}{L^2} & \frac{2EI}{L} & 0 & -\frac{6EI}{L^2} & \frac{4EI}{L}
\end{bmatrix} \tag{3.19}
$$

$$
\mathbf{k}^{\tau}_{\mathrm{ww}} = \tfrac{Gt^3}{180L}\begin{bmatrix}
60\frac{L^2}{t^2} & 0 & 0 & 30\frac{L^2}{t^2} & 0 & 0 \\
0 & 72 & 6L & 0 & -72 & 6L \\
0 & 6L & 8L^2 & 0 & -6L & -2L^2 \\
30\frac{L^2}{t^2} & 0 & 0 & 60\frac{L^2}{t^2} & 0 & 0 \\
0 & -72 & -6L & 0 & 72 & -6L \\
0 & 6L & -2L^2 & 0 & -6L & 8L^2
\end{bmatrix} \tag{3.20}
$$

$$
\mathbf{k}^{\tau}_{\Omega\Omega} = \tfrac{tG}{L}\begin{bmatrix}
1 & -1 \\
-1 & 1
\end{bmatrix} \tag{3.21}
$$

$\mathbf{K}^{\sigma}_{\Omega\Omega} = \sum_{el} \mathbf{T}^{T}_{\Omega} \mathbf{k}^{\sigma}_{\Omega\Omega} \mathbf{T}_{\Omega}$	$\mathbf{K}^{\tau}_{\mathrm{ww}} = \sum_{el} \mathbf{T}^{T}_{\mathrm{w}} \mathbf{k}^{\tau}_{\mathrm{ww}} \mathbf{T}_{\mathrm{w}}$
$\mathbf{K}^{\sigma}_{\mathrm{ww}} = \sum_{el} \mathbf{T}^{T}_{\mathrm{w}} \mathbf{k}^{\sigma}_{\mathrm{ww}} \mathbf{T}_{\mathrm{w}}$	$\mathbf{K}^{\tau}_{\Omega\Omega} = \sum_{el} \mathbf{T}^{T}_{\Omega} \mathbf{k}^{\tau}_{\Omega\Omega} \mathbf{T}_{\Omega}$
$\mathbf{K}^{s} = \sum_{el} \mathbf{T}^{T}_{\mathrm{w}} \mathbf{k}^{s} \mathbf{T}_{\mathrm{w}}$	$\mathbf{K}^{\tau}_{\mathrm{w}\Omega} = \sum_{el} \mathbf{T}^{T}_{\mathrm{w}} \mathbf{k}^{\tau}_{\mathrm{w}\Omega} \mathbf{T}_{\Omega}$

Table 3.2: Assembly into total cross-section stiffness contributions.

$$\mathbf{k}^{\tau}_{\mathrm{w}\Omega} = \tfrac{-tG}{2} \begin{bmatrix} -1 & 1 \\ 0 & 0 \\ 0 & 0 \\ -1 & 1 \\ 0 & 0 \\ 0 & 0 \end{bmatrix} \tag{3.22}$$

Note that some of the above stiffness matrices are assembled by sub contributions as also illustrated by the overbraces in equation (3.14).

To obtain a formulation of the total cross-section elastic energy we first introduce the global displacement vectors as an assembly of the local element degrees of freedom. The axial displacements and the transverse displacements are separated into two vectors as follows:

$$\begin{aligned} \mathbf{v}_{\Omega} &= [v_{\Omega 1} \;\; v_{\Omega 2} \;\; v_{\Omega 3} \;\; \ldots]^{T} \\ \mathbf{v}_{\mathrm{w}} &= [v_{x1} \;\; v_{y1} \;\; \phi_1 \;\; v_{x2} \;\; v_{y2} \;\; \phi_2 \;\; \ldots]^{T} \end{aligned} \tag{3.23}$$

Here $\mathbf{v}_{\Omega}$ holds the total local axial element degrees of freedom, and $\mathbf{v}_{\mathrm{w}}$ holds the total local element degrees of freedom, corresponding to two displacements and one rotation for each node. The number of degrees of freedom n_{dof} in the cross section is four times the number of nodes, $n_{dof} = 4n_{no}$. The transformation from local to global components is performed using a formal standard transformation of the components in the cross-section plane, i.e. $\mathbf{v}_{\Omega} = \mathbf{T}_{\Omega}\mathbf{v}^{el}_{\Omega}$ and $\mathbf{v}_{\mathrm{w}} = \mathbf{T}_{\mathrm{w}}\mathbf{v}^{el}_{\mathrm{w}}$. The global assembly of stiffness matrices is found by summation of the contribution from each element, as illustrated in Table 3.2. Introducing the described interpolation and matrix calculation scheme, the elastic potential

energy in equation (3.14) now takes the following form:

$$\Pi = \frac{1}{2}\int_0^L \left\{ \begin{bmatrix} \psi\mathbf{v}_{\mathrm{w}}^T & \psi\mathbf{v}_{\Omega}^T \end{bmatrix}'' \begin{bmatrix} \mathbf{K}_{\mathrm{ww}}^{\sigma} & \mathbf{0} \\ \mathbf{0} & \mathbf{K}_{\Omega\Omega}^{\sigma} \end{bmatrix} \begin{bmatrix} \psi\mathbf{v}_{\mathrm{w}} \\ \psi\mathbf{v}_{\Omega} \end{bmatrix}'' + \begin{bmatrix} \psi\mathbf{v}_{\mathrm{w}}^T & \psi\mathbf{v}_{\Omega}^T \end{bmatrix}' \begin{bmatrix} \mathbf{K}_{\mathrm{ww}}^{\tau} & \mathbf{K}_{\mathrm{w}\Omega}^{\tau} \\ \mathbf{K}_{\Omega\mathrm{w}}^{\tau} & \mathbf{K}_{\Omega\Omega}^{\tau} \end{bmatrix} \begin{bmatrix} \psi\mathbf{v}_{\mathrm{w}} \\ \psi\mathbf{v}_{\Omega} \end{bmatrix}' + \begin{bmatrix} \psi\mathbf{v}_{\mathrm{w}}^T & \psi\mathbf{v}_{\Omega}^T \end{bmatrix} \begin{bmatrix} \mathbf{K}^s & \mathbf{0} \\ \mathbf{0} & \mathbf{0} \end{bmatrix} \begin{bmatrix} \psi\mathbf{v}_{\mathrm{w}} \\ \psi\mathbf{v}_{\Omega} \end{bmatrix} \right\} dz \tag{3.24}$$

Here and in the following, a bold zero $\mathbf{0}$ denotes a suitable size matrix or vector of zeroes. The axial stiffness from transverse displacements sub matrix $\mathbf{K}_{\mathrm{ww}}^{\sigma}$ has a rank deficiency equal to the number of free end nodes plus the number of "intermediate" nodes between corner points of the cross section. The in-plane cross-section distortional stiffness sub matrix $\mathbf{K}^s$ has a rank deficiency of 3, corresponding to three in-plane "rigid body" or rather non-distortional displacements of the cross section. Finally the whole shear stiffness matrix has a rank deficiency of 3, corresponding to the existence of pure axial extension and two pure flexural modes without shear. It turns out that since the pure axial displacement only involves the sub matrix $\mathbf{K}_{\Omega\Omega}^{\tau}$, this matrix has a rank deficiency of one.

3.4 Formulation resembling a generalization of Vlasov beam theory

The thin-walled beam theory made by Vlasov (1961) was originally established by equilibrium equations based on equilibrium considerations. The Vlasov beam theory is derived on the basis of assumed displacement fields which correspond to extension, major and minor bending, torsion and warping. This corresponds to a modal separation in which each mode has a set of transverse and axial displacement fields that may be coupled. Even though we are here using an extended displacement field and we are using the potential energy to derive the equilibrium conditions in the form of differential equations, we want to achieve a formulation resembling a generalization of Vlasov beam theory. This means that we have to implement some constrains and eliminations into the differential equations which are:

- Elimination of the pure axial extension mode. This mode does not produce any shear and leads to a singularity in the shear stiffness matrix.
- Eliminate the two eigenmodes corresponding to transverse translation of the cross section.

- Eliminate the pure rotational eigenmode.
- Constrain the transverse displacement field so that the wall widths remain constant.

To implement these constraints and eliminations into the differential equations, three main steps need to be performed before we can solve the eigenvalue problem related to distortional displacements, including local plate type modes. Or in other words, we will introduce constraints, and identify and eliminate the basic solutions related to the conventional beam displacement modes.

3.4.1 Calculus of variation

To find the distortional differential equations of GBT the Calculus of Variation is used which is in general a field of mathematics that deals with optimizing functionals. This is in contrast to ordinary calculus that deals with functions. Functionals are often formed as definite integrals involving unknown functions and their derivatives. The aim is finding maximum or minimum conditions for a relationship between two or more variables that depend not only on the variables themselves, as in the ordinary calculus, but also on an additional arbitrary relation, or constraint, between them. This leads to an optimized functional which attains a maximum or minimum value, or stationary functions, where the rate of change of the functional is precisely zero.

The calculus of variations is one of the classical and widely used branches of mathematics and as an example among many applications geometrical problems can be solved using the calculus of variation in its general form. The topic of variational principle belongs within the calculus of variations. It develops general methods for finding functions which minimize or maximize the value of quantities that depends upon those functions. Variational principles are used for solving boundary value problems and are applicable when the given problem can be regarded as a minimization problem.

The variational methods are used in many fields, and there are more than 500 books on variational principles (Berdichevsky, 2009). Some of the principles are Fermat's principle, Euler's Calculus of Variations, Lagrange Variational Principle, and Hamilton Variational Principle.

In this thesis we will concentrate on the variational principles related to mechanics and in this context use the Hamilton variational principle which also applies to classical topics such as the electromagnetic and gravitational. It has also been extended to quantum mechanics, quantum field theory and criticality theories. The interested reader can get a description of the different principles by studying the book by Lanczos, (Lanczos, 1949), that describes the variational principles of mechanics extensively.

For beam theory, the variational method leads to generalized forces, when using so-called natural boundary conditions, which means that no conditions are imposed in advance. Therefore the generalized forces are an expression of the boundary conditions. By inserting the generalized forces into the obtained integral, we obtain the equilibrium equation and so the calculus of variation is used to obtain the equilibrium equation.

The basis of variational formulation is the principle of virtual work. However, in the principle of virtual work no change in the configuration is involved and no assumption about the constitutive laws of the material is made (Krenk, 1989a). The virtual work equation can be obtained from the first variation of the potential energy functional for an elastic material with a strain energy density function.

Having touched the calculus of variation briefly let us deal with the three main steps needed for a formulation resembling a generalization of Vlasov beam theory.

3.4.2 Step I: Pure axial extension and shear constraints

In this first step we introduce the shear constraint equations that bind axial and transverse modes together and at the same time simplify or condense equation (3.24). In this process we need to eliminate the singularity in the shear stiffness matrix related to pure axial extension. The first eigenmode that we identify is the pure axial extension; it produces no shear energy and no transverse displacement energy (due to the simple constitutive relations assumed, corresponding to beam theory and the mentioned rank deficiency).

Let us introduce the shear constraint equations using equation (3.11) as follows:

$$\begin{aligned} &\int_C \overline{T}_d \delta\overline{u}_{z,s} ds = 0 \quad \Rightarrow \\ -\ &\int_C (Gt(\mathrm{w}_s - \Omega_{,s}))\delta\Omega_{,s}\, ds = 0 \quad \Rightarrow \\ &\int_C Gt\Omega_{,s}\, \delta\Omega_{,s}\, ds = \int_C Gt\mathrm{w}_s \delta\Omega_{,s}\, ds \end{aligned} \tag{3.25}$$

Introducing the interpolation, see equation (3.15), Tables 3.1 and 3.2, and taking variations gives us the following constraint set of equations:

$$\mathbf{K}^{\tau}_{\Omega\Omega}\mathbf{v}_{\Omega} = -\mathbf{K}^{\tau}_{\Omega\mathrm{w}}\mathbf{v}_{\mathrm{w}} \tag{3.26}$$

This matrix equation is singular because pure axial extension does not produce shear. Therefore we introduce the following transformation, using superscripts a for axial and o for other:

$$\mathbf{v}_{\Omega} = \begin{bmatrix} \mathbf{T}^a_{\Omega} & \mathbf{T}^o_{\Omega} \end{bmatrix} \begin{bmatrix} v^a_{\Omega} \\ \mathbf{v}^o_{\Omega} \end{bmatrix} \tag{3.27}$$

in which $\mathbf{T}_\Omega^a = \mathbf{v}_\Omega^{\text{axial}}$ is the pure axial deformation mode (with unit value for all components). The other remaining modes are picked out by

$$\mathbf{T}_\Omega^o = \begin{bmatrix} \mathbf{0} \\ \mathbf{I}_{aa} \end{bmatrix} \begin{matrix} \} \text{ 1 d.o.f. related to the first node} \\ \} \text{ Unit diagonal matrix} \end{matrix} \tag{3.28}$$

Here $\mathbf{I}_{aa}$ is a unit diagonal matrix of dimension $n_a = n_{no} - 1$, where n_{no} is the number of nodes. Furthermore, it is worth noting that v_Ω^a is one component that corresponds to the amount of pure axial extension, while $\mathbf{v}_\Omega^o$ corresponds to all the other axial displacement degrees of freedom. Introducing the transformation in equation (3.27) into the constraint equations (3.26), we get the following by pre- and post multiplication:

$$\begin{bmatrix} 0 & \mathbf{0} \\ \mathbf{0} & \mathbf{T}_\Omega^{oT}\mathbf{K}_{\Omega\Omega}^\tau\mathbf{T}_\Omega^o \end{bmatrix} \begin{bmatrix} v_\Omega^a \\ \mathbf{v}_\Omega^o \end{bmatrix} = \begin{bmatrix} 0 \\ -\mathbf{T}_\Omega^{oT}\mathbf{K}_{\Omega\mathrm{w}}^\tau\mathbf{v}_\mathrm{w} \end{bmatrix} \quad \Rightarrow$$

$$\mathbf{v}_\Omega^o = -(\mathbf{K}_{\Omega\Omega}^{\tau oo})^{-1}\mathbf{K}_{\Omega\mathrm{w}}^{\tau o}\mathbf{v}_\mathrm{w} \tag{3.29}$$

where the matrices $\mathbf{K}_{\Omega\Omega}^{\tau oo}$ and $\mathbf{K}_{\Omega\mathrm{w}}^{\tau o}$ are given in Table 3.3. By equation (3.29) we have introduced a transformation from in-plane cross-section displacement modes to the axial displacement modes without pure axial extension as follows:

$$\mathbf{v}_\Omega^o = \mathbf{T}_{\Omega\mathrm{w}}\mathbf{v}_\mathrm{w}, \quad \text{where} \quad \mathbf{T}_{\Omega\mathrm{w}} = -(\mathbf{K}_{\Omega\Omega}^{\tau oo})^{-1}\mathbf{K}_{\Omega\mathrm{w}}^{\tau o} \tag{3.30}$$

Combining equation (3.27) and (3.29) gives

$$\mathbf{v}_\Omega = \begin{bmatrix} \mathbf{T}_\Omega^o\mathbf{T}_{\Omega\mathrm{w}} & \mathbf{T}_\Omega^a \end{bmatrix} \begin{bmatrix} \mathbf{v}_\mathrm{w} \\ v_\Omega^a \end{bmatrix} = \begin{bmatrix} \mathbf{T}_{\Omega\mathrm{w}}^r & \mathbf{T}_\Omega^a \end{bmatrix} \begin{bmatrix} \mathbf{v}_\mathrm{w} \\ v_\Omega^a \end{bmatrix} = \mathbf{T}_{\Omega\mathrm{w}}^r\mathbf{v}_\mathrm{w} + \mathbf{T}_\Omega^a v_\Omega^a \tag{3.31}$$

where $\mathbf{T}_{\Omega\mathrm{w}}^r = \mathbf{T}_\Omega^o\mathbf{T}_{\Omega\mathrm{w}}$.

The potential energy formulation (3.24) can now be modified so that the amount of axial extension is described by the separate degree of freedom v_Ω^a and the shear constraint equations are enforced. The modification of (3.24) is performed using the transformation in equation (3.31) and to clarify the variational treatment of pure axial extension we also temporally rewrite the terms pertaining to axial extension using $\zeta v_\Omega^a = -\psi' v_\Omega^a$. Introducing transformed stiffness matrices as given in Table 3.3, the elastic potential energy (for a single mode) takes the following form:

$$\Pi = \tfrac{1}{2}\int_0^L \Bigg\{ \begin{bmatrix} (\psi\mathbf{v}_\mathrm{w}^T)'' & (\zeta v_\Omega^{aT})' \end{bmatrix} \begin{bmatrix} \bar{\mathbf{K}}^\sigma & -\mathbf{K}_{\Omega\Omega}^{\sigma ra} \\ -\mathbf{K}_{\Omega\Omega}^{\sigma ar} & K_{\Omega\Omega}^{\sigma aa} \end{bmatrix} \begin{bmatrix} (\psi\mathbf{v}_\mathrm{w})'' \\ (\zeta v_\Omega^a)' \end{bmatrix} + (\psi\mathbf{v}_\mathrm{w}^T)'\mathbf{K}^\tau(\psi\mathbf{v}_\mathrm{w})' + (\psi\mathbf{v}_\mathrm{w}^T)\mathbf{K}^s(\psi\mathbf{v}_\mathrm{w}) \Bigg\} dz \tag{3.32}$$

$K^{\sigma aa}_{\Omega\Omega} = \mathbf{T}^{a\,T}_{\Omega} \mathbf{K}^{\sigma}_{\Omega\Omega} \mathbf{T}^{a}_{\Omega}$	$\mathbf{K}^{\tau rr}_{\Omega\Omega} = \mathbf{T}^{r\,T}_{\Omega\mathrm{w}} \mathbf{K}^{\tau}_{\Omega\Omega} \mathbf{T}^{r}_{\Omega\mathrm{w}}$
$\mathbf{K}^{\sigma ar}_{\Omega\Omega} = \mathbf{T}^{a\,T}_{\Omega} \mathbf{K}^{\sigma}_{\Omega\Omega} \mathbf{T}^{r}_{\Omega\mathrm{w}}$	$\mathbf{K}^{\tau r}_{\mathrm{w}\Omega} = K^{\tau}_{\mathrm{w}\Omega} \mathbf{T}^{r}_{\Omega\mathrm{w}} = \mathbf{K}^{\tau r\,T}_{\Omega\mathrm{w}}$
$\mathbf{K}^{\sigma rr}_{\Omega\Omega} = \mathbf{T}^{r\,T}_{\Omega\mathrm{w}} \mathbf{K}^{\sigma}_{\Omega\Omega} \mathbf{T}^{r}_{\Omega\mathrm{w}}$	$\mathbf{K}^{\tau oo}_{\Omega\Omega} = \mathbf{T}^{o\,T}_{\Omega} \mathbf{K}^{\tau}_{\Omega\Omega} \mathbf{T}^{o}_{\Omega}$
$\bar{\mathbf{K}}^{\sigma} = \mathbf{K}^{\sigma}_{\mathrm{ww}} + \mathbf{K}^{\sigma rr}_{\Omega\Omega}$	$\mathbf{K}^{\tau o}_{\Omega\mathrm{w}} = \mathbf{T}^{o\,T}_{\Omega} \mathbf{K}^{\tau}_{\Omega\mathrm{w}}$
$\mathbf{K}^{\sigma} = \bar{\mathbf{K}}^{\sigma} - \mathbf{K}^{\sigma ra}_{\Omega\Omega} (K^{\sigma aa}_{\Omega\Omega})^{-1} \mathbf{K}^{\sigma ar}_{\Omega\Omega}$	$\mathbf{K}^{\tau} = \mathbf{K}^{\tau}_{\mathrm{ww}} + \mathbf{K}^{\tau r}_{\mathrm{w}\Omega} + \mathbf{K}^{\tau r}_{\Omega\mathrm{w}} + \mathbf{K}^{\tau rr}_{\Omega\Omega}$

Table 3.3: Transformation of stiffness matrices related to Step I.

To find the homogeneous distortional differential equations of GBT, the first variation of the elastic potential energy is investigated by taking variations in the complete displacement field. The virtual variation of a property is denoted by a δ in front of the varied field property (displacement field), as in $\delta(v_{\mathrm{w}}\psi)'$, as the virtual variation of the first derivative of the transverse displacement field expressed by the product of the transverse displacement shape $\mathbf{v}_{\mathrm{w}}$ and the axial variation ψ'. This gives us

$$\begin{aligned}\delta\Pi = \int_0^L \Big\{ & \delta(\psi \mathbf{v}_{\mathrm{w}}^T)'' \big[\bar{\mathbf{K}}^{\sigma}(\psi \mathbf{v}_{\mathrm{w}})'' - \mathbf{K}^{\sigma ra}_{\Omega\Omega}(\zeta v^a_{\Omega})'\big] \\ & + \delta(\psi \mathbf{v}_{\mathrm{w}}^T)' \mathbf{K}^{\tau}(\psi \mathbf{v}_{\mathrm{w}})' + \delta(\psi \mathbf{v}_{\mathrm{w}}^T) \mathbf{K}^{s}(\psi \mathbf{v}_{\mathrm{w}}) \\ & + \delta(\zeta v^a_{\Omega})' [-\mathbf{K}^{\sigma ar}_{\Omega\Omega}(\psi \mathbf{v}_{\mathrm{w}})'' + K^{\sigma aa}_{\Omega\Omega}(\zeta v^a_{\Omega})'] \Big\} \, dz\end{aligned} \tag{3.33}$$

After performing up to two partial integrations on the terms and derived terms that involve axial derivatives of the (virtual) varied displacement field, $\delta(\,)'$ or $\delta(\,)''$, the first variation of the elastic potential energy takes the form:

$$\begin{aligned}\delta\Pi = \int_0^L \Big\{ & \delta(\psi \mathbf{v}_{\mathrm{w}}^T) \Big[\bar{\mathbf{K}}^{\sigma} \mathbf{v}_{\mathrm{w}} \psi'''' - \mathbf{K}^{\sigma ra}_{\Omega\Omega} v^a_{\Omega} \zeta''' - \mathbf{K}^{\tau} \mathbf{v}_{\mathrm{w}} \psi'' + \mathbf{K}^{s} \mathbf{v}_{\mathrm{w}} \psi\Big] \\ & + \delta(\zeta v^a_{\Omega}) \Big[\mathbf{K}^{\sigma ar}_{\Omega\Omega} \mathbf{v}_{\mathrm{w}} \psi''' - K^{\sigma aa}_{\Omega\Omega} v^a_{\Omega} \zeta''\Big] \Big\} \, dz \\ + \Big[& \delta(\psi \mathbf{v}_{\mathrm{w}}^T)' \Big[\bar{\mathbf{K}}^{\sigma}(\psi \mathbf{v}_{\mathrm{w}})'' - \mathbf{K}^{\sigma ra}_{\Omega\Omega}(\zeta v^a_{\Omega})'\Big] \\ & + \delta(\psi \mathbf{v}_{\mathrm{w}}^T) \Big[- \bar{\mathbf{K}}^{\sigma}(\psi \mathbf{v}_{\mathrm{w}})''' + \mathbf{K}^{\sigma ra}_{\Omega\Omega}(\zeta v^a_{\Omega})'' + \mathbf{K}^{\tau}(\psi \mathbf{v}_{\mathrm{w}})'\Big] \\ & + \delta(\zeta v^a_{\Omega}) \Big[- \mathbf{K}^{\sigma ar}_{\Omega\Omega}(\psi \mathbf{v}_{\mathrm{w}})'' - K^{\sigma aa}_{\Omega\Omega}(\zeta v^a_{\Omega})'\Big] \Big]_0^L\end{aligned} \tag{3.34}$$

For internal variation in the displacement fields $\delta(\psi \mathbf{v}_{\mathrm{w}})$ and $\delta(\zeta v_{\Omega}^{a})$, the elastic potential energy should be stationary and therefore its first variation must be equal to zero. Here the terms in the squared bracket correspond to the boundary loads and boundary conditions. Taking internal variations reveals the following coupled homogeneous differential equations of GBT in which we note that $\zeta = -\psi'$:

$$\bar{\mathbf{K}}^{\sigma}\mathbf{v}_{\mathrm{w}}\psi'''' - \mathbf{K}_{\Omega\Omega}^{\sigma ra}v_{\Omega}^{a}\zeta''' - \mathbf{K}^{\tau}\mathbf{v}_{\mathrm{w}}\psi'' + \mathbf{K}^{s}\mathbf{v}_{\mathrm{w}}\psi = \mathbf{0} \tag{3.35}$$

$$\mathbf{K}_{\Omega\Omega}^{\sigma ar}\mathbf{v}_{\mathrm{w}}\psi''' - K_{\Omega\Omega}^{\sigma aa}v_{\Omega}^{a}\zeta'' = \mathbf{0} \tag{3.36}$$

These equations establish a coupled set of homogeneous GBT differential equations that determine the displacements of a prismatic thin-walled beam for a given set of boundary conditions. To solve the boundary value problem, it is necessary to solve the related eigenvalue problem by establishing the eigenmodes/vectors and the related axial variation through the related eigenvalues. In the following, we will first consider the case where the displacement vectors do not contain transverse displacements, and then we will consider one in which they do. We start out by isolating the term $v_{\Omega}^{a}\zeta''$ in equation (3.36) as follows:

$$v_{\Omega}^{a}\zeta'' = (K_{\Omega\Omega}^{\sigma aa})^{-1}\mathbf{K}_{\Omega\Omega}^{\sigma ar}\mathbf{v}_{\mathrm{w}}\psi''' \tag{3.37}$$

We can identify pure axial extension as an eigenmode solution. For the above equations (3.35) and (3.36), it corresponds to $(\mathbf{v}_{\mathrm{w}}, v_{\Omega}^{a}) = (\mathbf{0}, 1)$, which we can see leads to a solution. In the original "global" space, the axial eigenmode is given by $(\mathbf{v}_{\mathrm{w}}, \mathbf{v}_{\Omega}) = (\mathbf{0}, \mathbf{T}_{\Omega}^{a})$. It is also clear that the axial variation of pure axial extension can be determined by double integration of equation (3.37) with $\mathbf{v}_{\mathrm{w}} = \mathbf{0}$, which gives

$$\begin{aligned}\zeta(z) &= -\psi'(z) = c_{a1} + c_{a2}z \\ &= -\boldsymbol{\Psi}_{a}{}'(z)\,\mathbf{c}_{a} = \begin{bmatrix}1 & z\end{bmatrix}\begin{bmatrix}c_{a1} \\ c_{a2}\end{bmatrix}\end{aligned} \tag{3.38}$$

Here c_{a1} and c_{a2} are constants determined by the boundary conditions of axial extension.

Having identified the "classic" eigenmode, pure axial extension, we finally turn to the solution of the transverse displacement modes. In this case, equation (3.37) determines the correction term that eliminates pure axial extension in the back substitution process. Eliminating ζ'' by using the fact that $\zeta'' = -\psi'''$ and assuming that $\psi''' \neq 0$, we find:

$$v_{\Omega}^{a} = -(K_{\Omega\Omega}^{\sigma aa})^{-1}\mathbf{K}_{\Omega\Omega}^{\sigma ar}\mathbf{v}_{\mathrm{w}} \tag{3.39}$$

Using this equation or equation (3.36), we eliminate the second term in equation (3.35) and introduce $\mathbf{K}^{\sigma}$, as given in Table 3.3. This results in the following homogeneous fourth order differential equations for determination of the transverse (global, distortional and local) distortional displacement modes of GBT:

$$\mathbf{K}^{\sigma}\mathbf{v}_{\mathrm{w}}\psi'''' - \mathbf{K}^{\tau}\mathbf{v}_{\mathrm{w}}\psi'' + \mathbf{K}^{s}\mathbf{v}_{\mathrm{w}}\psi = \mathbf{0} \tag{3.40}$$

To solve this set of equations we have to solve the related eigenvalue problem, which is of fourth order, but since only an even number of axial derivatives is involved, this reduces to a quadratic eigenvalue problem. With solutions, $\mathbf{v}_{\mathrm{w}}$, to equation (3.40), we can find $\mathbf{v}_{\Omega}^{o}$ using equation (3.30), v_{Ω}^{a} using equation (3.39), and finally $\mathbf{v}_{\Omega}$ using equation (3.27), thus revealing the full solution in global space.

3.4.3 Step II: Rigid cross-section displacements and constant wall-width constraint

In this step, we will identify and eliminate two eigenmodes corresponding to transverse translation of the cross-section, and we will identify a pure rotational eigenmode for later elimination in the next step. Furthermore, we will also constrain the transverse displacement field, so that the wall widths remain constant, i.e. we will enforce $\mathrm{w}_{s,s} \equiv 0$, see equation (3.5).

With the introduction of the shear constraints in the previous step, the flexural modes do not have shear energy and the shear stiffness matrix $\mathbf{K}^{\tau}$ is therefore singular for these modes. Since neither the pure translational modes nor the rotational mode involve any distortion of the cross-section, the transverse stiffness matrix $\mathbf{K}^{s}$ will be singular due to these modes. It turns out that the translational modes correspond to two quadruple zero eigenvalues or roots of the related characteristic equation. To orthogonalize these modes with respect to the non-singular axial stiffness matrix $\mathbf{K}^{\sigma}$, we will form the subspace spanned by the modes and orthogonalize in this subspace.

Let us first introduce two not necessarily orthogonal translational modes corresponding to a unit translation in each transverse coordinate direction, ordered in columns in the matrix $\mathbf{T}_{\mathrm{w}}^{xy} = [\mathbf{v}_{\mathrm{w}}^{\mathrm{x\ trans}}\ \ \mathbf{v}_{\mathrm{w}}^{\mathrm{y\ trans}}]$ and a rotational mode corresponding to rotation about the origin of the (initial) transverse coordinate axes $\mathbf{T}_{\mathrm{w}}^{z} = [\mathbf{v}_{\mathrm{w}}^{\mathrm{z\ rot}}]$.

In the subspace spanned by the two non-orthogonal translational modes introduced, we can find the principle flexural directions by an equivalent conventional method or by finding the eigenvectors of the following two-dimensional eigenvalue problem:

$$(\mathbf{K}_{xy}^{\sigma} - \lambda\mathbf{I})\mathbf{v}_{xy} = \mathbf{0} \quad \Rightarrow \quad \mathbf{v}_{xy} = \mathbf{v}_{xy}^{1} \text{ or } \mathbf{v}_{xy}^{2} \tag{3.41}$$

where $\mathbf{I}$ is a 2×2 diagonal unit matrix and $\mathbf{K}^{\sigma}_{xy} = \mathbf{T}^{xy\,T}_{\mathrm{w}} \mathbf{K}^{\sigma} \mathbf{T}^{xy}_{\mathrm{w}}$. The two orthogonal eigenvectors corresponding to the principle axis directions are ordered in columns in the transformation matrix

$$\mathbf{T}^{\alpha}_{xy} = \begin{bmatrix} \mathbf{v}^{1}_{xy} & \mathbf{v}^{2}_{xy} \end{bmatrix} \tag{3.42}$$

Finally, we can determine the two orthogonal translational eigenmodes in the full $\mathbf{v}_{\mathrm{w}}$-space, ordered in columns in a transformation matrix as $\mathbf{T}^{\alpha}_{\mathrm{w}} = [\mathbf{v}^{1\ \mathrm{trans}}_{\mathrm{w}} \ \ \mathbf{v}^{2\ \mathrm{trans}}_{\mathrm{w}}]$, by the following matrix multiplication:

$$\mathbf{T}^{\alpha}_{\mathrm{w}} = \mathbf{T}^{xy}_{\mathrm{w}} \mathbf{T}^{\alpha}_{xy} \tag{3.43}$$

Next, we take a look at the non-orthogonal rotational mode, and we subtract the translational part, so that the coupling term in the axial stiffness vanishes. Thus the orthogonal pure rotational mode is given by

$$\mathbf{v}^{3\ \mathrm{rot}}_{\mathrm{w}} = \mathbf{v}^{\mathrm{z\ rot}}_{\mathrm{w}} - \begin{bmatrix} \mathbf{v}^{1\ \mathrm{trans}}_{\mathrm{w}} & \mathbf{v}^{2\ \mathrm{trans}}_{\mathrm{w}} \end{bmatrix} \mathbf{d}_{\alpha} \quad \Leftrightarrow \quad \mathbf{T}^{\mathbf{3}}_{\mathrm{w}} = \mathbf{T}^{\mathbf{z}}_{\mathrm{w}} - \mathbf{T}^{\alpha}_{\mathrm{w}} \mathbf{d}_{\alpha} \tag{3.44}$$

where we have introduced the transformation "matrix" $\mathbf{T}^{3}_{\mathrm{w}} = [\mathbf{v}^{3\ \mathrm{rot}}_{\mathrm{w}}]$ and $\mathbf{d}_{\alpha}$ as a two-dimensional vector giving the amount of each translational eigenmode to be subtracted. Note that $\mathbf{d}_{\alpha}$ is related to the coordinate vector of the shear center (Jönsson, 1999a). The coupling terms in the axial stiffness between translations and rotation are found in the subspace as follows:

$$\mathbf{K}^{\sigma}_{\alpha 3} = \mathbf{T}^{\alpha\,T}_{\mathrm{w}} \mathbf{K}^{\sigma} \mathbf{T}^{3}_{\mathrm{w}} = \mathbf{T}^{\alpha\,T}_{\mathrm{w}} \mathbf{K}^{\sigma} \left(\mathbf{T}^{z}_{\mathrm{w}} - \mathbf{T}^{\alpha}_{\mathrm{w}} \mathbf{d}_{\alpha} \right) = \mathbf{K}^{\sigma}_{\alpha z} - \mathbf{K}^{\sigma}_{\alpha\alpha} \mathbf{d}_{\alpha} \tag{3.45}$$

By requiring that the coupling terms in the axial stiffness vanish, $\mathbf{K}^{\sigma}_{\alpha 3} = \mathbf{0}$, we find

$$\mathbf{d}_{\alpha} = {\mathbf{K}^{\sigma}_{\alpha\alpha}}^{-1} \mathbf{K}^{\sigma}_{\alpha \mathbf{z}} \tag{3.46}$$

Now we can finally identify the orthogonal pure rotational eigenmode by inserting equation (3.46) in (3.44) as

$$\mathbf{T}^{3}_{\mathrm{w}} = \mathbf{T}^{z}_{\mathrm{w}} - \mathbf{T}^{\alpha}_{\mathrm{w}} {\mathbf{K}^{\sigma}_{\alpha\alpha}}^{-1} \mathbf{K}^{\sigma}_{\alpha z} \tag{3.47}$$

Here the matrix transformations are given in Table 3.4.

Before performing eliminations and finding the solutions pertaining to the translational modes, we will constrain the transverse normal strains in the middle surface of the cross-section walls, i.e. we will enforce $\mathrm{w}_{s,s} \equiv 0$ or, say, enforce a constant wall-width constraint. For each wall element, this leads to a multi-point constraint equation in local degrees of freedom, $\mathbf{v}^{el}_{\mathrm{w}}$, corresponding to no centerline elongation. It takes the following form:

$$\begin{bmatrix} 1 & 0 & 0 & -1 & 0 & 0 \end{bmatrix} \mathbf{v}^{el}_{\mathrm{w}} = 0 \tag{3.48}$$

Each element constraint equation is reformulated into global degrees of freedom by a formal transformation of the form $\mathbf{v}_{\mathrm{w}}^{el} = \mathbf{T}_{\mathrm{w}}^{T}\mathbf{v}_{\mathrm{w}}$, which allows us to write n_c independent constraint equations (where n_c can be less than the number of elements due to over-constraining). The equations take the following form in the full $\mathbf{v}_{\mathrm{w}}$-space:

$$\mathbf{C}\mathbf{v}_{\mathrm{w}} = \mathbf{0} \tag{3.49}$$

The transformation method described by Cook (2001) is used to enforce the multi-point constraint equations and eliminate the related degrees of freedom. However, we must also incorporate the elimination of the translational eigenmodes and prepare for the elimination of the rotational modes.

Before any elimination of eigenmodes or constrained degrees of freedom can be performed, we must first transform the equations to a new space (with redefined degrees of freedom) in such a way that the degrees of freedom to be eliminated are clearly identified. Thus we need to choose exactly which of the constrained degrees of freedom (in each constraint equation) and which degrees of freedom related to the translational and rotational modes are to be eliminated. In our implementation, we choose to eliminate the translations and rotation of the first node, and we implement a strategic routine which chooses which of the other translational degrees of freedom related to the constraint equations are to be eliminated. The identification of the constrained degrees of freedom to be eliminated is performed by a transformation matrix $\mathbf{T}_{\mathrm{w}}^{c}$ in which each column belongs to a constraint equation and identifies the degree of freedom to be eliminated by a unit value in the corresponding row. The remaining degrees of freedom, which are not going to be separately identified (eliminated), are identified in the transformation matrix $\mathbf{T}_{\mathrm{w}}^{u}$ in which each column identifies a remaining (u for unconstrained) degree of freedom by a unit value in the corresponding row.

We are now ready to introduce the transformation to $\mathbf{v}_{\mathrm{w}}$-space from the new space. In the new space, we introduce the degrees of freedom as $\mathbf{v}_{\mathrm{w}}^{\alpha} = [v_{\mathrm{w}}^{1} \;\; v_{\mathrm{w}}^{2}]^{T}$ for the magnitudes of the two translational eigenmodes, v_{w}^{3} for the magnitude of the rotational eigenmode, $\mathbf{v}_{\mathrm{w}}^{c}$ for the degrees of freedom to be constrained, and $\mathbf{v}_{\mathrm{w}}^{u}$ for the remaining unconstrained degrees of freedom. The transformation may be written as:

$$\mathbf{v}_{\mathrm{w}} = \begin{bmatrix} \mathbf{T}_{\mathrm{w}}^{\alpha} & \mathbf{T}_{\mathrm{w}}^{3} & \mathbf{T}_{\mathrm{w}}^{c} & \mathbf{T}_{\mathrm{w}}^{u} \end{bmatrix} \begin{bmatrix} \mathbf{v}_{\mathrm{w}}^{\alpha} \\ v_{\mathrm{w}}^{3} \\ \mathbf{v}_{\mathrm{w}}^{c} \\ \mathbf{v}_{\mathrm{w}}^{u} \end{bmatrix} \tag{3.50}$$

Since we have strategically chosen the constrained degrees of freedom not to be

equal to the degrees of freedom related to the translational and rotational eigenmodes, we have a situation where $\mathbf{C}\mathbf{T}_{\mathrm{w}}^{\alpha} = \mathbf{0}$ and $\mathbf{C}\mathbf{T}_{\mathrm{w}}^{3} = 0$. So the constrain equations in (3.49) can be rewritten using equation (3.50) as

$$\mathbf{C}\mathbf{T}_{\mathrm{w}}^{c}\mathbf{v}_{\mathrm{w}}^{c} + \mathbf{C}\mathbf{T}_{\mathrm{w}}^{u}\mathbf{v}_{\mathrm{w}}^{u} = \mathbf{0} \tag{3.51}$$

This allows us to express the constrained degrees of freedom by the unconstrained as

$$\mathbf{v}_{\mathrm{w}}^{c} = -\mathbf{C}_{c}^{-1}\mathbf{C}_{u}\mathbf{v}_{\mathrm{w}}^{u} \tag{3.52}$$

in which $\mathbf{C}_c = \mathbf{C}\mathbf{T}_{\mathrm{w}}^{c}$ and $\mathbf{C}_u = \mathbf{C}\mathbf{T}_{\mathrm{w}}^{u}$. Introducing equation (3.52) in the transformation equation (3.50), we find that the total transformation is condensed as follows:

$$\mathbf{v}_{\mathrm{w}} = \begin{bmatrix}\mathbf{T}_{\mathrm{w}}^{\alpha} & \mathbf{T}_{\mathrm{w}}^{3} & \mathbf{T}_{\mathrm{w}}^{c} & \mathbf{T}_{\mathrm{w}}^{u}\end{bmatrix}\begin{bmatrix}\mathbf{v}_{\mathrm{w}}^{\alpha}\\ v_{\mathrm{w}}^{3}\\ -{\mathbf{C}_c}^{-1}\mathbf{C}_{u}\mathbf{v}_{\mathrm{w}}^{u}\\ \mathbf{v}_{\mathrm{w}}^{u}\end{bmatrix} = \begin{bmatrix}\mathbf{T}_{\mathrm{w}}^{\alpha} & \mathbf{T}_{\mathrm{w}}^{3} & \widetilde{\mathbf{T}}_{\mathrm{w}}^{u}\end{bmatrix}\begin{bmatrix}\mathbf{v}_{\mathrm{w}}^{\alpha}\\ v_{\mathrm{w}}^{3}\\ \mathbf{v}_{\mathrm{w}}^{u}\end{bmatrix} \tag{3.53}$$

Here we have defined the condensed transformation $\widetilde{\mathbf{T}}_{\mathrm{w}}^{u} = \mathbf{T}_{\mathrm{w}}^{u} - \mathbf{T}_{\mathrm{w}}^{c}{\mathbf{C}_c}^{-1}\mathbf{C}_{u}$ by using a tilde.

Introducing the transformation in (3.53) in the set of differential equations in (3.40) transforms these equations into the new space. The differential equations thereby take the following form in which we have also introduced the null terms corresponding to the rigid-body modes and zero shear strain for translational and flexural modes:

$$\begin{bmatrix}\mathbf{K}_{\alpha\alpha}^{\sigma} & \mathbf{0} & \mathbf{K}_{\alpha u}^{\sigma}\\ \mathbf{0} & K_{33}^{\sigma} & \mathbf{K}_{3u}^{\sigma}\\ \mathbf{K}_{u\alpha}^{\sigma} & \mathbf{K}_{u3}^{\sigma} & \mathbf{K}_{uu}^{\sigma}\end{bmatrix}\begin{bmatrix}\mathbf{v}_{\mathrm{w}}^{\alpha}\\ v_{\mathrm{w}}^{3}\\ \mathbf{v}_{\mathrm{w}}^{u}\end{bmatrix}\psi'''' - \begin{bmatrix}\mathbf{0} & \mathbf{0} & \mathbf{0}\\ \mathbf{0} & K_{33}^{\tau} & \mathbf{K}_{3u}^{\tau}\\ \mathbf{0} & \mathbf{K}_{u3}^{\tau} & \mathbf{K}_{uu}^{\tau}\end{bmatrix}\begin{bmatrix}\mathbf{v}_{\mathrm{w}}^{\alpha}\\ v_{\mathrm{w}}^{3}\\ \mathbf{v}_{\mathrm{w}}^{u}\end{bmatrix}\psi''$$

$$+ \begin{bmatrix}\mathbf{0} & \mathbf{0} & \mathbf{0}\\ \mathbf{0} & 0 & \mathbf{0}\\ \mathbf{0} & \mathbf{0} & \mathbf{K}_{uu}^{s}\end{bmatrix}\begin{bmatrix}\mathbf{v}_{\mathrm{w}}^{\alpha}\\ v_{\mathrm{w}}^{3}\\ \mathbf{v}_{\mathrm{w}}^{u}\end{bmatrix}\psi = \begin{bmatrix}\mathbf{0}\\ 0\\ \mathbf{0}\end{bmatrix} \tag{3.54}$$

The transformed stiffness matrices introduced in this equation are given in Table 3.4. The two-dimensional upper block matrix equation yields the translation displacements as

$$\mathbf{v}_{\mathrm{w}}^{\alpha}\psi'''' = -{\mathbf{K}_{\alpha\alpha}^{\sigma}}^{-1}\mathbf{K}_{\alpha u}^{\sigma}\mathbf{v}_{\mathrm{w}}^{u}\psi'''' \tag{3.55}$$

We can identify the two orthogonal pure translational modes, $(v_{\mathrm{w}}^{1}, v_{\mathrm{w}}^{2}, v_{\mathrm{w}}^{3}, \mathbf{v}_{\mathrm{w}}^{u}) = (1, 0, 0, \mathbf{0})$, and ,$(0, 1, 0, \mathbf{0})$, as eigenmodes or solutions to equation (3.54). For

$\mathbf{K}^{\sigma}_{\alpha\alpha} = \mathbf{T}^{\alpha\,T}_{\mathrm{w}} \mathbf{K}^{\sigma} \mathbf{T}^{\alpha}_{\mathrm{w}}$	$K^{\sigma}_{33} = \mathbf{T}^{3\,T}_{\mathrm{w}} \mathbf{K}^{\sigma} \mathbf{T}^{3}_{\mathrm{w}}$	$K^{\tau}_{33} = \mathbf{T}^{3\,T}_{\mathrm{w}} \mathbf{K}^{\tau} \mathbf{T}^{3}_{\mathrm{w}}$
$\mathbf{K}^{\sigma}_{\alpha z} = \mathbf{T}^{\alpha\,T}_{\mathrm{w}} \mathbf{K}^{\sigma} \mathbf{T}^{\mathbf{z}}_{\mathrm{w}}$	$\mathbf{K}^{\sigma}_{3u} = \mathbf{T}^{3\,T}_{\mathrm{w}} \mathbf{K}^{\sigma} \widetilde{\mathbf{T}}^{\mathbf{u}}_{\mathrm{w}}$	$\mathbf{K}^{\tau}_{3u} = \mathbf{T}^{3\,T}_{\mathrm{w}} \mathbf{K}^{\tau} \widetilde{\mathbf{T}}^{\mathbf{u}}_{\mathrm{w}}$
$\mathbf{K}^{\sigma}_{\alpha u} = \mathbf{T}^{\alpha\,T}_{\mathrm{w}} \mathbf{K}^{\sigma} \widetilde{\mathbf{T}}^{\mathbf{u}}_{\mathrm{w}}$	$\mathbf{K}^{\sigma}_{uu} = \widetilde{\mathbf{T}}^{u\,T}_{\mathrm{w}} \mathbf{K}^{\sigma} \widetilde{\mathbf{T}}^{\mathbf{u}}_{\mathrm{w}}$	$\mathbf{K}^{\tau}_{uu} = \widetilde{\mathbf{T}}^{u\,T}_{\mathrm{w}} \mathbf{K}^{\tau} \widetilde{\mathbf{T}}^{\mathbf{u}}_{\mathrm{w}}$
$\mathbf{K}^{s}_{uu} = \widetilde{\mathbf{T}}^{u\,T}_{\mathrm{w}} \mathbf{K}^{s} \widetilde{\mathbf{T}}^{u}_{\mathrm{w}}$	$\bar{\mathbf{K}}^{\sigma}_{uu} = \mathbf{K}^{\sigma}_{uu} - \mathbf{K}^{\sigma}_{u\alpha} {\mathbf{K}^{\sigma}_{\alpha\alpha}}^{-1} \mathbf{K}^{\sigma}_{\alpha u}$	

Table 3.4: Transformation of stiffness matrices related to Step II.

these pure translational modes, we find that the right-hand side of equation (3.55) vanishes and that the axial variation of the pure translational modes is therefore determined by quadruple integration, which gives:

$$\begin{aligned} \psi_1(z) &= c_{11} + c_{12} z + c_{13} z^2 + c_{14} z^3 = \mathbf{\Psi}_1(z)\, \mathbf{c}_1 \\ \psi_2(z) &= c_{21} + c_{22} z + c_{23} z^2 + c_{24} z^3 = \mathbf{\Psi}_2(z)\, \mathbf{c}_2 \end{aligned} \tag{3.56}$$

In the following we will make use of the block notation given as

$$\mathbf{\Psi}_{\alpha} \mathbf{c}_{\alpha} = \begin{bmatrix} \mathbf{\Psi}_1 & \mathbf{0} \\ \mathbf{0} & \mathbf{\Psi}_2 \end{bmatrix} \begin{bmatrix} \mathbf{c}_1 \\ \mathbf{c}_2 \end{bmatrix}, \; \mathbf{c}_1 = \begin{bmatrix} c_{11} \\ c_{12} \\ c_{13} \\ c_{14} \end{bmatrix}, \; \mathbf{c}_2 = \begin{bmatrix} c_{21} \\ c_{22} \\ c_{23} \\ c_{24} \end{bmatrix} \tag{3.57}$$

in which $\mathbf{\Psi}_1 = \mathbf{\Psi}_2 = [1 \quad z \quad z^2 \quad z^3]$. The constants in the vectors $\mathbf{c}_1$ and $\mathbf{c}_2$ are determined by the boundary conditions for pure transverse translational displacement in the two directions.

Having identified the two pure translational modes, we turn to the remaining solutions to the differential equation (3.54). In this case, equation (3.55) determines the correction term that eliminates pure transverse displacements in the back-substitution process. By dividing both sides of the equation by $\psi'''' \neq 0$ we find

$$\mathbf{v}^{\alpha}_{\mathrm{w}} = -{\mathbf{K}^{\sigma}_{\alpha\alpha}}^{-1} \mathbf{K}^{\sigma}_{\alpha u} \mathbf{v}^{u}_{\mathrm{w}} \tag{3.58}$$

Using this equation or equation (3.55), we eliminate the two pure flexural degrees of freedom and find the condensed version of the differential equation (3.54), which takes the following form:

$$\begin{bmatrix} K^{\sigma}_{33} & \mathbf{K}^{\sigma}_{3u} \\ \mathbf{K}^{\sigma}_{u3} & \bar{\mathbf{K}}^{\sigma}_{uu} \end{bmatrix} \begin{bmatrix} v^{3}_{\mathrm{w}} \\ \mathbf{v}^{u}_{\mathrm{w}} \end{bmatrix} \psi'''' - \begin{bmatrix} K^{\tau}_{33} & \mathbf{K}^{\tau}_{3u} \\ \mathbf{K}^{\tau}_{u3} & \mathbf{K}^{\tau}_{uu} \end{bmatrix} \begin{bmatrix} v^{3}_{\mathrm{w}} \\ \mathbf{v}^{u}_{\mathrm{w}} \end{bmatrix} \psi'' + \begin{bmatrix} 0 & \mathbf{0} \\ \mathbf{0} & \mathbf{K}^{s}_{uu} \end{bmatrix} \begin{bmatrix} v^{3}_{\mathrm{w}} \\ \mathbf{v}^{u}_{\mathrm{w}} \end{bmatrix} \psi = \begin{bmatrix} 0 \\ \mathbf{0} \end{bmatrix} \tag{3.59}$$

The introduced stiffness matrix $\bar{\mathbf{K}}^{\sigma}_{uu}$ is given in Table 3.4. This equation constitutes the GBT differential equations constrained by shear flow constraints and wall-width constraints after the elimination of the classical axial and two translational (flexural beam) modes.

3.4.4 Step III: Reduction of order and pure St. Venant torsion

In this step we will reduce the differential order of the coupled fourth order differential equations and the related quadratic eigenvalue problem to twice as many coupled second order differential equations with a related linear eigenvalue problem of double size. This method is equivalent to the one used for the solution of the coupled homogeneous problem of a-single-mode distortion and torsion analyzed in Jönsson (1999a). After we have changed the order of the equations, we can recognize that the pure torsional St. Venant displacement modes with a constant or a linear variation of the angle of twist are eigensolutions.

The fourth order differential equation (3.59) can be transformed into twice as many second order differential equations by introducing what is called a state vector. There are a number of different possible formulations, but we have chosen the use of the state vector $\mathbf{v}_S = [v^3_{\mathrm{w}}\psi, \mathbf{v}^u_{\mathrm{w}}\psi, v^3_{\mathrm{w}}\psi', \mathbf{v}^u_{\mathrm{w}}\psi']^T$. Introducing this state vector (and using related equality block equations) yields a reformulation of equation (3.59) as a formal second order matrix differential equation of double size, which takes the form:

$$\begin{bmatrix} 0 & \mathbf{0} & 0 & \mathbf{0} \\ \mathbf{0} & \mathbf{K}^s_{uu} & \mathbf{0} & \mathbf{0} \\ 0 & \mathbf{0} & -K^{\sigma}_{33} & -\mathbf{K}^{\sigma}_{3u} \\ \mathbf{0} & \mathbf{0} & -\mathbf{K}^{\sigma}_{u3} & -\bar{\mathbf{K}}^{\sigma}_{uu} \end{bmatrix} \begin{bmatrix} v^3_{\mathrm{w}}\psi \\ \mathbf{v}^u_{\mathrm{w}}\psi \\ v^3_{\mathrm{w}}\psi' \\ \mathbf{v}^u_{\mathrm{w}}\psi' \end{bmatrix} - \begin{bmatrix} K^{\tau}_{33} & \mathbf{K}^{\tau}_{3u} & -K^{\sigma}_{33} & -\mathbf{K}^{\sigma}_{3u} \\ \mathbf{K}^{\tau}_{u3} & \mathbf{K}^{\tau}_{uu} & -\mathbf{K}^{\sigma}_{u3} & -\bar{\mathbf{K}}^{\sigma}_{uu} \\ -K^{\sigma}_{33} & -\mathbf{K}^{\sigma}_{3u} & 0 & \mathbf{0} \\ -\mathbf{K}^{\sigma}_{u3} & -\bar{\mathbf{K}}^{\sigma}_{uu} & \mathbf{0} & \mathbf{0} \end{bmatrix} \begin{bmatrix} v^3_{\mathrm{w}}\psi \\ \mathbf{v}^u_{\mathrm{w}}\psi \\ v^3_{\mathrm{w}}\psi' \\ \mathbf{v}^u_{\mathrm{w}}\psi' \end{bmatrix}' = \begin{bmatrix} 0 \\ \mathbf{0} \\ 0 \\ \mathbf{0} \end{bmatrix} \tag{3.60}$$

Note that the matrices are symmetric about the diagonal and that the lover half of the matrices is identity equations. Seeking solutions of exponential form, $\psi(z) = e^{\xi z}$, with an eigenvector in which $v^3_{\mathrm{w}} = 1$ and $\mathbf{v}^u_w = \mathbf{0}$, we see that the first equation will lead to an eigenvalue, $\xi^2 = 0$, or a double zero root in the characteristic equation, thus giving us not exponential solutions but two linear solution terms. This corresponds to a constant or a linear variation of the first degree of freedom, which is pure twist. However, if we "persistently" seek the two classical exponential solutions for a pure twist mode with (eigen)vectors, $(1, \mathbf{0}, \xi^2, \mathbf{0})^T$, we are not able to show that this is in general a solution. In the examples section in Paper I (Jönsson and Andreassen, 2011) it is shown that for

the closed cross-section, only the linear terms of pure twist exist, whereas for the open channel section, the eigenvalue is very close to the classical result, and in the example chosen, we cannot visually see the distortion in the associated "torsional" mode with an exponential variation of twist.

To keep the matrix operations as simple as possible we introduce a new vector $\mathbf{v}_{\mathrm{w}}^{e}$ and three new block matrices, $\mathbf{K}_{ee}^{\sigma}$, $\mathbf{K}_{3e}^{\sigma}$ and $\mathbf{K}_{ue}^{\sigma}$, given by

$$\mathbf{v}_{\mathrm{w}}^{e} = \begin{bmatrix} v_{\mathrm{w}}^{3} \\ \mathbf{v}_{\mathrm{w}}^{u} \end{bmatrix} \qquad \mathbf{K}_{ee}^{\sigma} = \begin{bmatrix} \mathbf{K}_{3e}^{\sigma} \\ \mathbf{K}_{ue}^{\sigma} \end{bmatrix} = \begin{bmatrix} [\, K_{33}^{\sigma} & \mathbf{K}_{3u}^{\sigma} \,] \\ [\, \mathbf{K}_{u3}^{\sigma} & \bar{\mathbf{K}}_{uu}^{\sigma} \,] \end{bmatrix} \tag{3.61}$$

Introducing the new vector and the three block matrices defined by equation (3.61) and in Table 3.5, the second order differential equations can be written as

$$\begin{bmatrix} 0 & \mathbf{0} & \mathbf{0} \\ \mathbf{0} & \mathbf{K}_{uu}^{s} & \mathbf{0} \\ \mathbf{0} & \mathbf{0} & -\mathbf{K}_{ee}^{\sigma} \end{bmatrix} \begin{bmatrix} v_{\mathrm{w}}^{3}\psi \\ \mathbf{v}_{\mathrm{w}}^{u}\psi \\ \mathbf{v}_{\mathrm{w}}^{e}\psi'' \end{bmatrix} - \begin{bmatrix} K_{33}^{\tau} & \mathbf{K}_{3u}^{\tau} & -\mathbf{K}_{3e}^{\sigma} \\ \mathbf{K}_{u3}^{\tau} & \mathbf{K}_{uu}^{\tau} & -\mathbf{K}_{ue}^{\sigma} \\ -\mathbf{K}_{e3}^{\sigma} & -\mathbf{K}_{eu}^{\sigma} & \mathbf{0} \end{bmatrix} \begin{bmatrix} v_{\mathrm{w}}^{3}\psi \\ \mathbf{v}_{\mathrm{w}}^{u}\psi \\ \mathbf{v}_{\mathrm{w}}^{e}\psi'' \end{bmatrix}'' = \begin{bmatrix} 0 \\ \mathbf{0} \\ \mathbf{0} \end{bmatrix} \tag{3.62}$$

In the first equation we can isolate the pure rotational term resulting in the following differential equation:

$$v_{\mathrm{w}}^{3}\psi'' = -{K_{33}^{\tau}}^{-1} \left(\mathbf{K}_{3u}^{\tau}\mathbf{v}_{\mathrm{w}}^{u}\psi'' - \mathbf{K}_{3e}^{\sigma}\mathbf{v}_{\mathrm{w}}^{e}\psi''''\right) \tag{3.63}$$

It can be seen that pure St. Venant torsion (with free warping), corresponding to the solution vector, $(v_{\mathrm{w}}^{3}\psi, \mathbf{v}_{\mathrm{w}}^{u}\psi, \mathbf{v}_{\mathrm{w}}^{e}\psi'') = (c_{32}z + c_{31}, \mathbf{0}, \mathbf{0})$, is a solution of the second order differential equations in (3.62). We have thus shown that

$$\begin{aligned} \psi_3(z) &= c_{31} + c_{32}z \\ &= \mathbf{\Psi}_3(z)\mathbf{c}_3 = \begin{bmatrix} 1 & z \end{bmatrix} \begin{bmatrix} c_{31} \\ c_{32} \end{bmatrix} \end{aligned} \tag{3.64}$$

The remaining solutions to the differential equations in (3.62) are found by seeking exponential solutions of the form $\psi(z) = e^{\xi z}$. We insert the exponential solution in equation (3.63) and find the following equation, which we will use for back-substitution purposes:

$$v_{\mathrm{w}}^{3} = -{K_{33}^{\tau}}^{-1} \left(\mathbf{K}_{3u}^{\tau}\mathbf{v}_{\mathrm{w}}^{u} - \mathbf{K}_{3e}^{\sigma}(\xi^{2}\mathbf{v}_{\mathrm{w}}^{e})\right) \tag{3.65}$$

Using equation (3.63), we eliminate v_{w}^{3} from the differential equations in (3.62) and find the final distortional differential equations of GBT that determine all the distortional displacement modes as

$$\begin{bmatrix} \mathbf{K}_{uu}^{s} & \mathbf{0} \\ \mathbf{0} & -\mathbf{K}_{ee}^{\sigma} \end{bmatrix} \begin{bmatrix} \mathbf{v}_{\mathrm{w}}^{u}\psi \\ \mathbf{v}_{\mathrm{w}}^{e}\psi'' \end{bmatrix} - \begin{bmatrix} \bar{\mathbf{K}}_{uu}^{\tau} & -\bar{\mathbf{K}}_{ue}^{\sigma} \\ -\bar{\mathbf{K}}_{eu}^{\sigma} & -\bar{\mathbf{K}}_{ee}^{\sigma} \end{bmatrix} \begin{bmatrix} \mathbf{v}_{\mathrm{w}}^{u}\psi \\ \mathbf{v}_{\mathrm{w}}^{e}\psi'' \end{bmatrix}'' = \begin{bmatrix} \mathbf{0} \\ \mathbf{0} \end{bmatrix} \tag{3.66}$$

The block matrices and the transformed stiffness matrices are given in Table 3.5. In the following section we will describe the solution of these differential equations.

$\mathbf{K}^{\sigma}_{3e} = [\, K^{\sigma}_{33} \quad \mathbf{K}^{\sigma}_{3u} \,]$	$\bar{\mathbf{K}}^{\sigma}_{ee} = \mathbf{K}^{\sigma}_{e3} {K^{\tau}_{33}}^{-1} \mathbf{K}^{\sigma}_{3e}$
$\mathbf{K}^{\sigma}_{ue} = [\, \mathbf{K}^{\sigma}_{u3} \quad \bar{\mathbf{K}}^{\sigma}_{uu} \,]$	$\bar{\mathbf{K}}^{\sigma}_{ue} = \mathbf{K}^{\sigma}_{ue} - \mathbf{K}^{\tau}_{u3} {K^{\tau}_{33}}^{-1} \mathbf{K}^{\sigma}_{3e}$
${\mathbf{K}^{\sigma}_{ee}}^{T} = [\, {\mathbf{K}^{\sigma}_{3e}}^{T} \quad {\mathbf{K}^{\sigma}_{ue}}^{T} \,]$	$\bar{\mathbf{K}}^{\tau}_{uu} = \mathbf{K}^{\tau}_{uu} - \mathbf{K}^{\tau}_{u3} {K^{\tau}_{33}}^{-1} \mathbf{K}^{\tau}_{3u}$

Table 3.5: Transformation of stiffness matrices related to Step III.

3.5 The distortional eigenvalue problem and homogeneous solution functions

Now we are finally able to seek solutions to the final condensed differential matrix equation (3.66) in order to find the distortional eigenmodes, including what are called local modes. We postulate that the solutions are exponential solutions of the form

$$\psi(z) = e^{\xi z} \tag{3.67}$$

where ξ is an inverse length scale parameter which may be complex. Inserting the postulated solution leads to the following generalized linear matrix eigenvalue problem, in which the eigenvalues are ξ^2 and the eigenvectors are the distortional modes that we seek:

$$\begin{bmatrix} \mathbf{K}^{s}_{uu} & \mathbf{0} \\ \mathbf{0} & -\mathbf{K}^{\sigma}_{ee} \end{bmatrix} \begin{bmatrix} \mathbf{v}^{u}_{\mathrm{w}} \\ \xi^2 \mathbf{v}^{e}_{\mathrm{w}} \end{bmatrix} - \xi^2 \begin{bmatrix} \bar{\mathbf{K}}^{\tau}_{uu} & -\bar{\mathbf{K}}^{\sigma}_{ue} \\ -\bar{\mathbf{K}}^{\sigma}_{eu} & -\bar{\mathbf{K}}^{\sigma}_{ee} \end{bmatrix} \begin{bmatrix} \mathbf{v}^{u}_{\mathrm{w}} \\ \xi^2 \mathbf{v}^{e}_{\mathrm{w}} \end{bmatrix} = \begin{bmatrix} \mathbf{0} \\ \mathbf{0} \end{bmatrix} \tag{3.68}$$

Due to the differences in the order of magnitude of the different stiffness terms in the matrices, we have improved the numerical accuracy of the eigenvalue and eigenvector solution in our numerical implementation by introducing the following Cholesky decomposition of the block matrices in the first matrix:

$$\mathbf{K}^{s}_{uu} = \mathbf{L}_u \mathbf{L}_u^T \qquad\qquad \mathbf{K}^{\sigma}_{ee} = \mathbf{L}_e \mathbf{L}_e^T \tag{3.69}$$

We utilize the decomposition by introducing the following new intermediate vectors

$$\mathbf{v}^{u}_{\mathrm{w}} = \mathbf{L}_u^{-T} \widetilde{\mathbf{v}}^{u}_{\mathrm{w}} \qquad\qquad (\xi^2 \mathbf{v}^{e}_{\mathrm{w}}) = \mathbf{L}_e^{-T} (\xi^2 \widetilde{\mathbf{v}}^{e}_{\mathrm{w}}) \tag{3.70}$$

where the superscript $^{-T}$ corresponds to the inverted transpose of the matrix. After pre-multiplication of each block matrix equation by $\mathbf{L}_u^{-1}$ and $\mathbf{L}_e^{-1}$, the eigenvalue problem then takes the following form:

$$\begin{bmatrix} \mathbf{I}_{uu} & \mathbf{0} \\ \mathbf{0} & -\mathbf{I}_{ee} \end{bmatrix} \begin{bmatrix} \widetilde{\mathbf{v}}^{u}_{\mathrm{w}} \\ \xi^2 \widetilde{\mathbf{v}}^{e}_{\mathrm{w}} \end{bmatrix} - \xi^2 \begin{bmatrix} \mathbf{L}_u^{-1} \bar{\mathbf{K}}^{\tau}_{uu} \mathbf{L}_u^{-T} & -\mathbf{L}_u^{-1} \bar{\mathbf{K}}^{\sigma}_{ue} \mathbf{L}_e^{-T} \\ -\mathbf{L}_e^{-1} \bar{\mathbf{K}}^{\sigma}_{eu} \mathbf{L}_u^{-T} & -\mathbf{L}_e^{-1} \bar{\mathbf{K}}^{\sigma}_{ee} \mathbf{L}_e^{-T} \end{bmatrix} \begin{bmatrix} \widetilde{\mathbf{v}}^{u}_{\mathrm{w}} \\ \xi^2 \widetilde{\mathbf{v}}^{e}_{\mathrm{w}} \end{bmatrix} = \begin{bmatrix} \mathbf{0} \\ \mathbf{0} \end{bmatrix} \tag{3.71}$$

In this equation $\mathbf{I}_{uu}$ and $\mathbf{I}_{ee}$ are adequate size unit diagonal matrices. Some general eigenvalue solution routines demand that at least one of the matrices has to be symmetric as well as positive (semi-)definite. This can be achieved by a change of sign in the second block matrix equation, however the second matrix becomes asymmetric. Having found the eigenvectors, we use equation (3.70) to find $\mathbf{v}_{\mathrm{w}}^{u}$ and $(\xi^2\mathbf{v}_{\mathrm{w}}^{u})$, which can then be used for the remaining back-transformation process.

Each distortional eigenvector corresponds to a solution $\psi_{d\,i}(z)$ of the homogeneous coupled equations of distortion in equation (3.66). The solution function corresponds to our postulated function in equation (3.67), and it has now been determined by plus/minus the square root of the eigenvalues as $\pm\xi_i$. In other words, for the i'th eigenvector we find the solution

$$\begin{aligned}\psi_{d\,i}(z) &= c_{d\,2i-1}e^{\xi_i z} + c_{d\,2i}e^{-\xi_i z} \\ &= \mathbf{\Psi}_{d\,i}(z)\mathbf{c}_{d\,i} = \begin{bmatrix} e^{\xi_i z} & e^{-\xi_i z}\end{bmatrix}\begin{bmatrix} c_{d\,2i-1} \\ c_{d\,2i}\end{bmatrix}\end{aligned} \tag{3.72}$$

in which constants $c_{d\,2i-1}$ and $c_{d\,2i}$ assembled in the vector $\mathbf{c}_{d\,i}$ depend on the boundary conditions of the problem at hand. All the distortional solution functions are assembled in the distortional solution matrix Ψ_d and multiplied by the assembled vector of distortional constants $\mathbf{c}_d$ as follows:

$$\mathbf{\Psi}_d(z)\,\mathbf{c}_d = \begin{bmatrix} \mathbf{\Psi}_{d\,1}(z) & \mathbf{0} & \mathbf{0} & \cdots \\ \mathbf{0} & \mathbf{\Psi}_{d\,2}(z) & \mathbf{0} & \cdots \\ \mathbf{0} & \mathbf{0} & \mathbf{\Psi}_{d\,3}(z) & \cdots \\ \vdots & \vdots & \vdots & \ddots \end{bmatrix}\begin{bmatrix} \mathbf{c}_{d\,1} \\ \mathbf{c}_{d\,2} \\ \mathbf{c}_{d\,3} \\ \vdots \end{bmatrix} \tag{3.73}$$

This notation is used later to describe the total displacement solution.

3.6 Back substitution

Having found the distortional eigenvalues, eigenvectors and homogeneous solutions for the reduced system (3.68), we now have to perform a backward substitution through the previous steps in order to achieve the results in the original displacement vector format including all the modes. Furthermore, we also have to back-substitute all eliminated eigenvectors (multiple zero eigenvalues) and review the related homogeneous solutions.

3.6.1 Back substitution of distortional modes

In the previous sections, the formulations are related to a single displacement vector and the back substitution of the distortional modes found from solving

the eigenvalue problem in equation (3.68) is performed sequentially through equations (3.65), (3.58), (3.53), (3.39), and (3.31). In a typical modal approach, all eigenvectors are assembled column-wise in the mode matrix and the related eigenvalues ξ^2 are placed sequentially in the diagonal of the matrix $\mathbf{\Lambda}$. By introducing the capital letter $\mathbf{V}$ with related sub- and superscripts for the assembled modes, we can find the back-substituted distortional mode matrices $\mathbf{V}_{\mathrm{w}}^{d}$ and $\mathbf{V}_{\Omega}^{d}$ using the following sequence of substitutions corresponding to the sequence of equations mentioned above:

$$\mathbf{V}_{\mathrm{w}}^{3} = -{K_{33}^{\tau}}^{-1}\left(\mathbf{K}_{3u}^{\tau}\mathbf{V}_{\mathrm{w}}^{u} - \mathbf{K}_{3e}^{\sigma}(\mathbf{V}_{\mathrm{w}}^{\mathbf{e}}\mathbf{\Lambda})\right) \tag{3.74}$$

$$\mathbf{V}_{\mathrm{w}}^{\alpha} = -{\mathbf{K}_{\alpha\alpha}^{\sigma}}^{-1}\mathbf{K}_{\alpha u}^{\sigma}\mathbf{V}_{\mathrm{w}}^{u} \tag{3.75}$$

$$\mathbf{V}_{\mathrm{w}}^{d} = \mathbf{T}_{\mathrm{w}}^{\alpha}\mathbf{V}_{\mathrm{w}}^{\alpha} + \mathbf{T}_{\mathrm{w}}^{3}\mathbf{V}_{\mathrm{w}}^{3} + \widetilde{\mathbf{T}}_{\mathrm{w}}^{u}\mathbf{V}_{\mathrm{w}}^{u} \tag{3.76}$$

$$\mathbf{V}_{\Omega}^{d,a} = -(K_{\Omega\Omega}^{\sigma aa})^{-1}\mathbf{K}_{\Omega\Omega}^{\sigma ar}\mathbf{V}_{\mathrm{w}}^{d} \tag{3.77}$$

$$\mathbf{V}_{\Omega}^{d} = \mathbf{T}_{\Omega\mathrm{w}}^{r}\mathbf{V}_{\mathrm{w}}^{d} + \mathbf{T}_{\Omega}^{a}\mathbf{V}_{\Omega}^{d,a} \tag{3.78}$$

The superscript d has been introduced to distinguish the distortional modes from the total assembly of modes introduced later. The term $(\mathbf{V}_{\mathrm{w}}^{\mathbf{e}}\mathbf{\Lambda})$ is just one matrix, which is never separated into the two product terms, but just found directly as part of the eigenvectors of the reduced-order eigenvalue problem in equation (3.68).

3.6.2 Back substitution of eliminated beam displacement modes

The back substitution of eliminated beam displacement modes involves back substitution of the pure axial extension mode, the two transverse translational modes, and the pure twist mode. Using the degree-of-freedom space introduced in Step II, these modes are given by the following four transverse displacement modal vectors:

$$\begin{bmatrix} v_{\mathrm{w}}^{1} \\ v_{\mathrm{w}}^{2} \\ v_{\mathrm{w}}^{3} \\ \mathbf{v}_{\mathrm{w}}^{u} \end{bmatrix} = \begin{bmatrix} 0 \\ 0 \\ 0 \\ \mathbf{0} \end{bmatrix}, \begin{bmatrix} v_{\mathrm{w}}^{1} \\ v_{\mathrm{w}}^{2} \\ v_{\mathrm{w}}^{3} \\ \mathbf{v}_{\mathrm{w}}^{u} \end{bmatrix} = \begin{bmatrix} 1 \\ 0 \\ 0 \\ \mathbf{0} \end{bmatrix}, \begin{bmatrix} v_{\mathrm{w}}^{1} \\ v_{\mathrm{w}}^{2} \\ v_{\mathrm{w}}^{3} \\ \mathbf{v}_{\mathrm{w}}^{u} \end{bmatrix} = \begin{bmatrix} 0 \\ 1 \\ 0 \\ \mathbf{0} \end{bmatrix}, \begin{bmatrix} v_{\mathrm{w}}^{1} \\ v_{\mathrm{w}}^{2} \\ v_{\mathrm{w}}^{3} \\ \mathbf{v}_{\mathrm{w}}^{u} \end{bmatrix} = \begin{bmatrix} 0 \\ 0 \\ 1 \\ \mathbf{0} \end{bmatrix} \tag{3.79}$$

The first vector becomes the extensional eigenvector in the degree-of-freedom space introduced in Step I. The back substitution of these modes is all performed using the equation (3.53). However, we have already introduced the eigenvectors in the original transverse displacement space in the transformation matrices related to this equation, $\mathbf{T}_{\mathrm{w}}^{\alpha}$ and $\mathbf{T}_{\mathrm{w}}^{3}$ and the back transformation is obsolete for these modes. These eigenvectors are assembled in a beam mode matrix $\mathbf{V}_{\mathrm{w}}^{b}$ as follows:

$$\mathbf{V}_{\mathrm{w}}^{b} = \left[\, \mathbf{0} \;\; \mathbf{v}_{\mathrm{w}}^{1\,\mathrm{trans}} \;\; \mathbf{v}_{\mathrm{w}}^{2\,\mathrm{trans}} \;\; \mathbf{v}_{\mathrm{w}}^{3\,\mathrm{rot}} \right] \tag{3.80}$$

The back substitution of the warping displacements remains. Of course the pure axial extension warping vector is trivial and has allready been introduced as $\mathbf{T}_\Omega^{\text{axial}} = \mathbf{v}_\Omega^{\text{axial}}$, but we have to back-substitute the other modes. This is done by first calculating the axial (adjustment) component using equation (3.39) as follows:

$$\mathbf{V}_\Omega^{b,a} = \begin{bmatrix} 1 & 0 & 0 & 0 \end{bmatrix} - (K_{\Omega\Omega}^{\sigma aa})^{-1} \mathbf{K}_{\Omega\Omega}^{\sigma ar}\, \mathbf{V}_{\text{w}}^{b} \tag{3.81}$$

The beam warping vectors related to the transverse beam displacement modes can now be found using equation (3.31) as

$$\begin{aligned} \mathbf{V}_\Omega^{b} &= \begin{bmatrix} \mathbf{v}_\Omega^{\text{axial}} & \mathbf{v}_\Omega^{1\ \text{trans}} & \mathbf{v}_\Omega^{2\ \text{trans}} & \mathbf{v}_\Omega^{3\ \text{rot}} \end{bmatrix} \\ &= \mathbf{T}_{\Omega\text{w}}^{r} \mathbf{V}_{\text{w}}^{b} + \mathbf{T}_\Omega^{a} \mathbf{V}_\Omega^{b,a} \end{aligned} \tag{3.82}$$

The axial variation of the four modes has been identified in equations (3.38), (3.57), and (3.64) and can be assembled in the beam solution function matrix $\mathbf{\Psi}_b(z)$ and multiplied by the vector of beam displacement constants $\mathbf{c}_b$ as

$$\mathbf{\Psi}_b(z)\, \mathbf{c}_b = \begin{bmatrix} \mathbf{\Psi}_a(z) & \mathbf{0} & \mathbf{0} \\ \mathbf{0} & \mathbf{\Psi}_\alpha(z) & \mathbf{0} \\ \mathbf{0} & \mathbf{0} & \mathbf{\Psi}_3(z) \end{bmatrix} \begin{bmatrix} \mathbf{c}_a \\ \mathbf{c}_\alpha \\ \mathbf{c}_3 \end{bmatrix} \tag{3.83}$$

in which we have introduced the integral of the axial solution as $\mathbf{\Psi}_a = \begin{bmatrix} -z & -\frac{1}{2}z^2 \end{bmatrix}$. This matrix function does not pertain to any solution, and we might as well have set it to zero, since there are no transverse displacements, $\mathbf{v}_{\text{w}}^{\text{axial}} = \mathbf{0}$, for the pure axial deformation mode in beam theory. However, this choice allows us to use the derivative of the $\mathbf{\Psi}_a(z)$ matrix, which is the axial solution $\mathbf{\Psi}_a' = \begin{bmatrix} -1 & -z \end{bmatrix}$.

3.7 The full homogenous solution

The full homogenous solution can now be assembled from all the eigenmode vectors and the solution functions. It turns out that some of the eigenvalues and eigenvectors are complex. However, in the following we will perform a direct formulation in which we acknowledge that we are also dealing with complex quantities corresponding to related complex eigenvalues and complex axial solution functions. A transformation of the complex quantities to pairwise coupled real modes and real solution functions will be introduced in the second subsection.

3.7.1 Direct formulation

Let us assemble all the eigenvectors column-wise in a modal matrix of transverse displacement vectors $\mathbf{V}_{\text{w}}$ and a modal matrix of axial warping displacement

vectors $\mathbf{V}_\Omega$ by joining the modal matrices of the beam eigenvectors and the distortional eigenvectors in the following sequence

$$\mathbf{V}_\mathrm{w} = \left[\, \mathbf{V}_\mathrm{w}^b \;\; \mathbf{V}_\mathrm{w}^d \,\right] \qquad \mathbf{V}_\Omega = \left[\, \mathbf{V}_\Omega^b \;\; \mathbf{V}_\Omega^d \,\right] \tag{3.84}$$

The solution function matrices and the displacement constant vectors can also be assembled using the previously defined block matrices and vectors

$$\boldsymbol{\Psi}(z)\,\mathbf{c} = \begin{bmatrix} \boldsymbol{\Psi}_b(z) & \mathbf{0} \\ \mathbf{0} & \boldsymbol{\Psi}_d(z) \end{bmatrix} \begin{bmatrix} \mathbf{c}_b \\ \mathbf{c}_d \end{bmatrix} \tag{3.85}$$

The full homogeneous solution along the beam can be assembled in the nodal solution vectors $\mathbf{u}_\mathrm{w}(z)$ and $\mathbf{u}_z(z)$ as follows:

$$\begin{aligned} \mathbf{u}_\mathrm{w}(z) &= \mathbf{V}_\mathrm{w}\boldsymbol{\Psi}(z)\,\mathbf{c} \\ \mathbf{u}_z(z) &= -\mathbf{V}_\Omega\boldsymbol{\Psi}'(z)\,\mathbf{c} \end{aligned} \tag{3.86}$$

The constants have to be determined by the boundary conditions of the prismatic thin-walled beam.

To be able to present and discuss unique complex eigenmodes, all the distortional vectors in $\mathbf{V}_\mathrm{w}$ have been normalized after back substitution in such a way that the largest absolute value of all components in each vector is one and that this component is real. This has to be done to make them unique since complex eigenvectors are determined except for an arbitrary complex constant.

Following the completion and solution of the final distortional differential equations as well as the back substitution process the found mode shapes (eigenvectors) can be presented by two examples of transverse mode shapes as shown in Figures 3.6 and 3.8 and the associated primary warping mode shapes shown in Figure 3.7 and 3.9, respectively. The shown mode shapes correspond to a lipped channel and a box section used in the example section in Paper I (Jönsson and Andreassen, 2011). Note, that there is no primary warping for the local modes. The modes are scaled in such a way that the greatest displacement, being either in the horizontal or vertical direction, is equal to 10. For the complex modes consisting of both a real and an imaginary mode shape, this means that the use of a scale factor is necessary in order to be able to depict both mode shapes each having the greatest displacement equal to 10. Note that the imaginary mode shape is generally substantially smaller than the real mode shape. Also note that the modes in the present approach are ordered according to the attenuation length.

The numbers of the modes of a type (e.g., number of distortional modes) are not given but Figure 3.6 and 3.8 suggests certain numbers of modes. It is to note that e.g., the number of distortional modes of a lipped channel section seems to be more than 2, whilst conventional GBT and cFSM define 2 modes. This

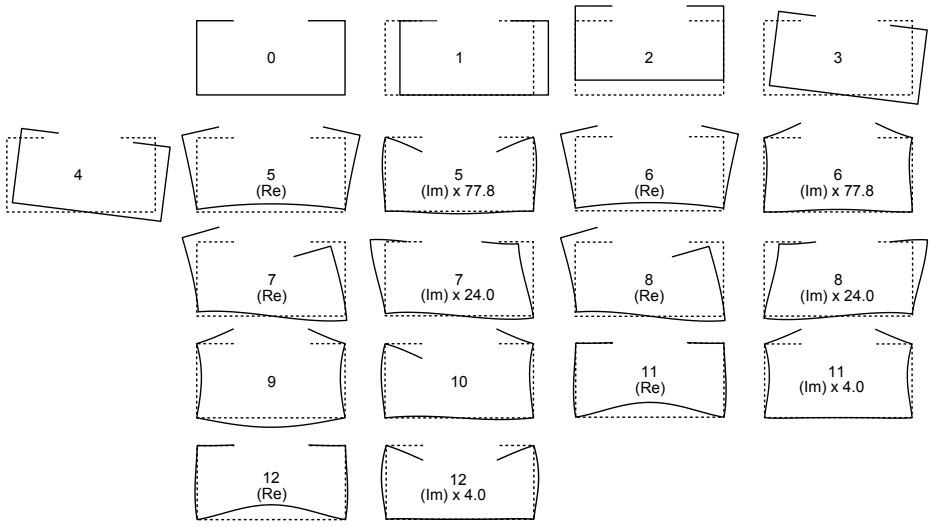

Figure 3.6: Lipped channel – 13 in-plane deformation mode shapes.

difference is because the proposed method in fact finds the exact analytical solution for the discretized cross section which involves twice as many modes (it is not an orthogonal decomposition of the space). This mode space is only orthogonal in the state space and not in the transverse displacement space. However, interesting enough, visual inspection, as in the other methods, show that we do in fact find 2 sets of paired complex and complex conjugated eigenmodes, which can be designated as non-local distortional (due to the length scale of the solution function).

The total number of modes depends on the discretization and the geometry of the cross section. This means that the number of different modes can only be defined by the illustrative examples. At the beginning of this chapter the number of dofs is four times the number of nodes. But through the steps we are changing to a GBT space with a reduced number of dofs. Moreover, we choose to solve the differential equation by reducing the differential order of the coupled fourth-order differential equations. This is done by transforming the fourth-order differential equation into twice as many second order differential equations. This means that we obtain an eigenvalue problem of double size. The number of dofs is hereby equal to the size of the eigenvalue problem but reduced through the performance of the described steps.

3.7.2 Transformation to real modes and real solution functions

Some of the distortional displacement modes found and their related eigenvalues are complex. Mathematical formulation with the use of complex numbers

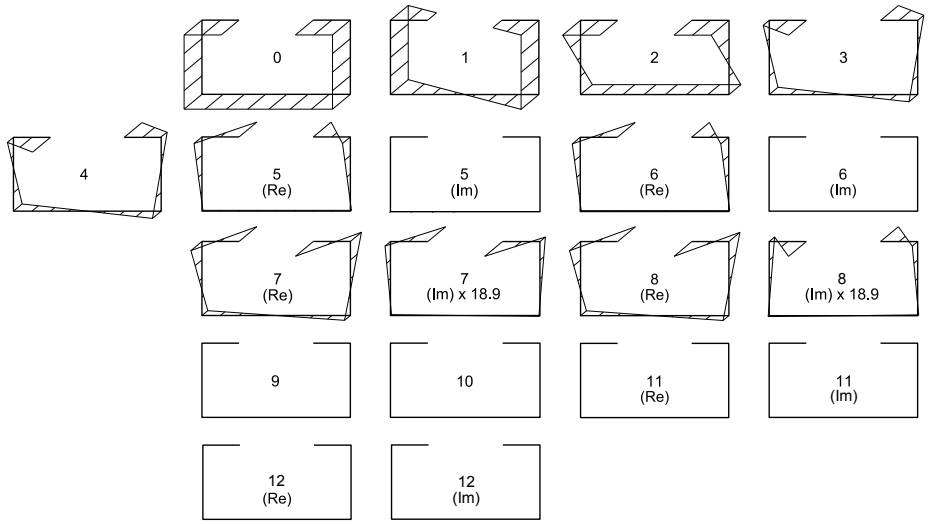

Figure 3.7: Lipped channel – 13 warping deformation mode shapes.

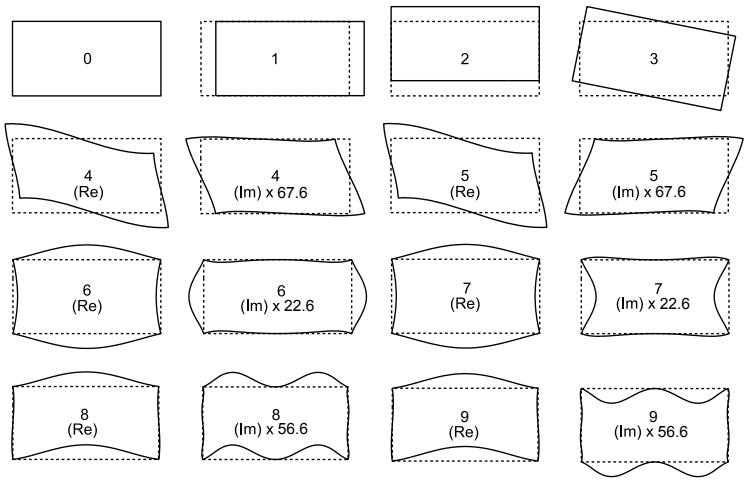

Figure 3.8: Rectangular box cross-section – 10 in-plane deformation mode shapes.

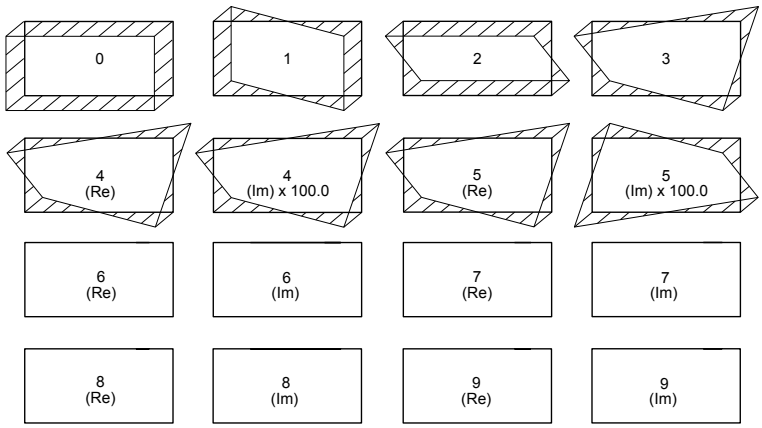

Figure 3.9: Rectangular box cross-section – 10 warping deformation mode shapes.

simplify derivations and the use of compilers, which include complex numbers with complex operations on matrices, will lead to simple algorithms. However, it may be easier to grasp the form and meaning of the solution in real quantities.

Complex eigenvalues are always found as a pair of complex conjugated eigenvalues with eigenvectors which are also complex conjugated. For the j'th complex eigenvalue, ξ_j^2, and its conjugated $j+1$'th eigenvalue, $\xi_{j+1}^2 = \overline{\xi_j^2}$, let us introduce the following notation for the positive square root values and the related eigenvector columns $\mathbf{v}_j$ and $\mathbf{v}_{j+1}$ of $\mathbf{V}_{\mathrm{w}}$:

$$\xi_j = \lambda_j + \mu_j i \quad \xi_{j+1} = \bar{\xi}_j = \lambda_j - \mu_j i \tag{3.87}$$

$$\mathbf{v}_j = \mathbf{a}_j + \mathbf{b}_j i \quad \mathbf{v}_{j+1} = \bar{\mathbf{v}}_j = \mathbf{a}_j - \mathbf{b}_j i \tag{3.88}$$

in which we have introduced the real and imaginary parts of the eigenvalues and eigenvectors. The complex eigenvectors in equation (3.88) may be conveniently written as

$$\begin{bmatrix} \mathbf{v}_j & \mathbf{v}_{j+1} \end{bmatrix} = \begin{bmatrix} \mathbf{a}_j & \mathbf{b}_j \end{bmatrix} \begin{bmatrix} 1 & 1 \\ i & -i \end{bmatrix} \tag{3.89}$$

The constants of the related parts of the homogeneous solution are also complex quantities. However we are able to assemble the two complex conjugated modal solutions into two real (but pairwise coupled) solutions by introducing the real constant vectors $\widetilde{\mathbf{c}}_j$ and $\widetilde{\mathbf{c}}_{j+1}$ as follows:

$$\begin{bmatrix} \mathbf{c}_j \\ \mathbf{c}_{j+1} \end{bmatrix} = \tfrac{1}{2} \begin{bmatrix} 1 & -i \\ 1 & i \end{bmatrix} \begin{bmatrix} \widetilde{\mathbf{c}}_j \\ \widetilde{\mathbf{c}}_{j+1} \end{bmatrix} \tag{3.90}$$

The j'th complex part of the full solution can now be rewritten using the transformations in equations (3.89) and (3.90). After multiplication and identification

of real and imaginary parts, we find the result:

$$\begin{bmatrix}\mathbf{v}_j & \mathbf{v}_{j+1}\end{bmatrix}\begin{bmatrix}\boldsymbol{\Psi}_{d_j} & \mathbf{0}\\ \mathbf{0} & \overline{\boldsymbol{\Psi}}_{d_j}\end{bmatrix}\begin{bmatrix}\mathbf{c}_j\\ \mathbf{c}_{j+1}\end{bmatrix} = \begin{bmatrix}\mathbf{a}_j & \mathbf{b}_j\end{bmatrix}\begin{bmatrix}\mathrm{Re}(\boldsymbol{\Psi}_{d\,j}) & \mathrm{Im}(\boldsymbol{\Psi}_{d\,j})\\ \mathrm{Im}(\overline{\boldsymbol{\Psi}}_{d\,j}) & \mathrm{Re}(\overline{\boldsymbol{\Psi}}_{d\,j})\end{bmatrix}\begin{bmatrix}\widetilde{\mathbf{c}}_j\\ \widetilde{\mathbf{c}}_{j+1}\end{bmatrix} \tag{3.91}$$

where the real and imaginary parts of the (in this case complex) matrix $\boldsymbol{\Psi}_{d\,j}$ introduced in (3.72) are

$$\begin{aligned}\mathrm{Re}(\boldsymbol{\Psi}_{d\,j}) = \;\; \mathrm{Re}(\overline{\boldsymbol{\Psi}}_{d\,j}) \;\; &= \begin{bmatrix} e^{\lambda_j z}\cos\mu_j z & e^{-\lambda_j z}\cos\mu_j z\end{bmatrix}\\ \mathrm{Im}(\boldsymbol{\Psi}_{d\,j}) = -\mathrm{Im}(\overline{\boldsymbol{\Psi}}_{d\,j}) &= \begin{bmatrix} e^{\lambda_j z}\sin\mu_j z & -e^{-\lambda_j z}\sin\mu_j z\end{bmatrix}\end{aligned} \tag{3.92}$$

whereby the real formulation in the right-hand side of equation (3.91) becomes

$$\begin{bmatrix}\mathbf{a}_j & \mathbf{b}_j\end{bmatrix}\begin{bmatrix} e^{\lambda_j z}\cos\mu_j z & e^{-\lambda_j z}\cos\mu_j z & e^{\lambda_j z}\sin\mu_j z & -e^{-\lambda_j z}\sin\mu_j z\\ -e^{\lambda_j z}\sin\mu_j z & e^{-\lambda_j z}\sin\mu_j z & e^{\lambda_j z}\cos\mu_j z & e^{-\lambda_j z}\cos\mu_j z\end{bmatrix}\begin{bmatrix}\widetilde{c}_{j\,1}\\ \widetilde{c}_{j\,2}\\ \widetilde{c}_{j+1\,1}\\ \widetilde{c}_{j+1\,2}\end{bmatrix} \tag{3.93}$$

This allows us to rewrite the complex quantities into real quantities. Let us modify the modal matrices $\mathbf{V}_{\mathrm{w}}$ and $\mathbf{V}_{\Omega}$ and introduce the modified modal matrices $\widetilde{\mathbf{V}}_{\mathrm{w}}$ and $\widetilde{\mathbf{V}}_{\Omega}$ by substituting the complex pairs of eigenvectors with their respective real and imaginary parts. Furthermore, let us also introduce the modified solution matrix $\widetilde{\boldsymbol{\Psi}}$ and its related modified vector of constants $\widetilde{\mathbf{c}}$ by substituting the solutions (and constants) of the complex pairs using equation (3.91), i.e. equation (3.93). This allows us to write the full homogeneous solution along the beam with real numbers as

$$\begin{aligned}\mathbf{u}_{\mathrm{w}}(z) &= \widetilde{\mathbf{V}}_{\mathrm{w}}\widetilde{\boldsymbol{\Psi}}(z)\,\widetilde{\mathbf{c}}\\ \mathbf{u}_{z}(z) &= -\widetilde{\mathbf{V}}_{\Omega}\widetilde{\boldsymbol{\Psi}}'(z)\,\widetilde{\mathbf{c}}\end{aligned} \tag{3.94}$$

We may choose to work with this real formulation or work with complex numbers using the full homogeneous solution formulated in equation (3.86).

Before elaborating on how to find the solution constants an example showing the validity of the novel approach is given.

3.8 Example

In this section an example is given showing the two eigensolutions related to the first complex distortional displacement mode of the chosen channel and box cross sections. For more examples see Paper I (Jönsson and Andreassen, 2011). We choose to illustrate the mode corresponding to the first complex distortional

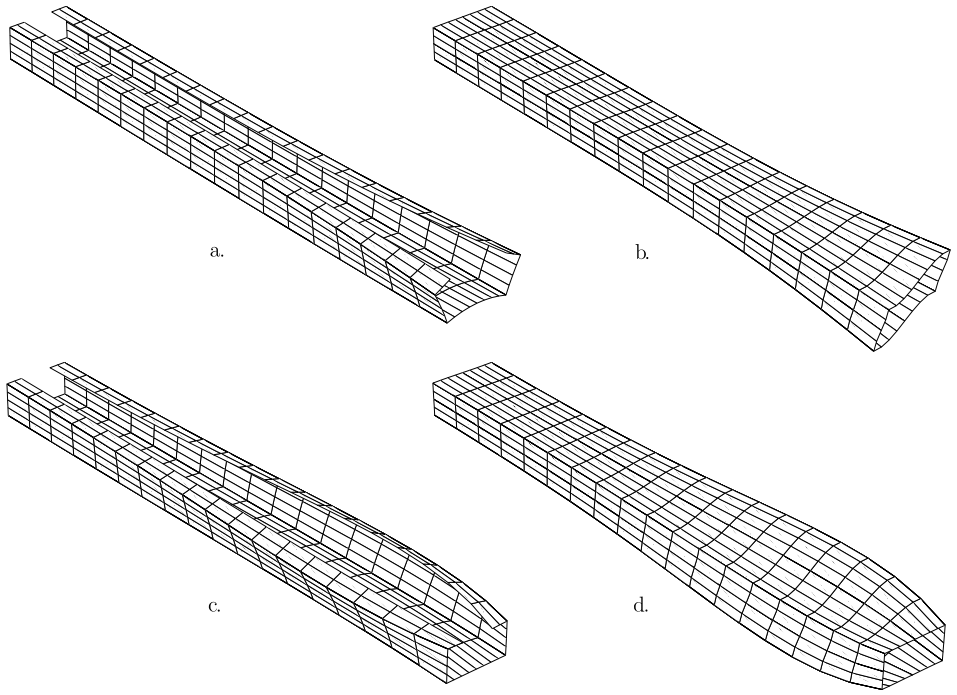

Figure 3.10: Two eigensolutions of the first complex distortional mode for a channel and a box section.

displacement mode, which are mode $j = 5$ and $j = 4$ respectively for the channel and box cross-sections. With the use of equation (3.93) in which the real part, $\mathbf{a}$, and the imaginary part, $\mathbf{b}$, of the mode are multiplied by the solution functions. We choose in Figure 3.10 to illustrate two of the four independent solution functions: one in which only $\widetilde{c}_{j\,2}$ is non-zero (shown as a. and b. in the figure), and the other (shown as c. and d.) in which only $\widetilde{c}_{j+1\,2}$ is non zero. Thus sub figure a. and b. correspond to the solution $e^{-\lambda_j z}\cos\mu_j z \cdot \mathbf{a}_j + e^{-\lambda_j z}\sin\mu_j z \cdot \mathbf{b}_j$ and sub figure c. and d. corresponds to $-e^{-\lambda_j z}\sin\mu_j z \cdot \mathbf{a}_j + e^{-\lambda_j z}\cos\mu_j z \cdot \mathbf{b}_j$. The eigensolutions shown in the figure therefore involves a coupled behavior of the real part and imaginary part of the mode.

3.9 The degree of freedom space and related transformations

To apply the present approach and make use of the solutions found in a finite element context, it is necessary to be able to relate to the different degree-of-freedom spaces in use as well as to the constraints introduced. In Step I, the introduction of shear constraints leads to a generalized beam theory (GBT) in

which only shear flow around closed cells is taken into account while all other shears are constrained. With the exception of pure axial extension, the axial displacements are determined from the axial derivative of the transverse displacements. From the boundary terms of the first variation of the potential energy given in equation (3.34), it is seen that the (virtual) generalized boundary displacements are pure axial extension (ζv_Ω^a), transverse displacements ($\psi \mathbf{v}_\mathrm{w}$), and the axial derivative of the transverse displacements $(\psi \mathbf{v}_\mathrm{w})'$. However, the transverse displacements are unconstrained, which is not compatible with classical Vlasov beam theory where the individual thin wall of the cross section is assumed to maintain its length (width) within the cross section, i.e. no cross-section centerline elongation. This is overcome in Step II where the walls are constrained using a set of multipoint constraint equations which eliminate constrained transverse displacement degrees of freedom $\mathbf{v}_\mathrm{w}^c$. The basic degrees of freedom of the GBT formulation are the pure axial extension (ζv_Ω^a), the remaining transverse displacements ($\psi \mathbf{v}_\mathrm{w}^g$), and the axial derivative hereof $(\psi \mathbf{v}_\mathrm{w}^g)'$. To be able to change degree-of-freedom space from GBT space, $\mathbf{v}_\mathrm{w}^g$, to finite element (FE) (original degree-of-freedom) space, $\mathbf{v}_\mathrm{w}$, the following transformation is introduced:

$$\mathbf{v}_\mathrm{w} = \begin{bmatrix} \mathbf{T}_\mathrm{w}^c & \mathbf{T}_\mathrm{w}^g \end{bmatrix} \begin{bmatrix} \mathbf{v}_\mathrm{w}^c \\ \mathbf{v}_\mathrm{w}^g \end{bmatrix} \quad \text{where} \quad \mathbf{T}_\mathrm{w}^g = \begin{bmatrix} \mathbf{T}_\mathrm{w}^i & \mathbf{T}_\mathrm{w}^u \end{bmatrix} \quad \text{and} \quad \mathbf{T}_\mathrm{w}^i = \begin{bmatrix} 1 & 0 & 0 \\ 0 & 1 & 0 \\ \vdots & 0 & 1 \\ & \vdots & 0 \\ & & \vdots \end{bmatrix} \tag{3.95}$$

in which $\mathbf{T}_\mathrm{w}^c$ and $\mathbf{T}_\mathrm{w}^u$ have already been introduced in Step II, and $\mathbf{T}_\mathrm{w}^i$ is a matrix corresponding to three supplementary columns, which pick out the degrees of freedom of the first node related to v_w^1, v_w^2 and v_w^3.

3.9.1 From FE displacements to GBT displacements

If the transverse displacement vector $\mathbf{v}_\mathrm{w}$ already fulfills the constraint equations, then we can find the GBT transverse displacement vector by using ${\mathbf{T}_\mathrm{w}^g}^T$, and the pure axial extension by using ${\mathbf{T}_\Omega^a}^T$ as follows:

$$\begin{bmatrix} \mathbf{v}_\mathrm{w}^g \\ v_\Omega^a \end{bmatrix} = \begin{bmatrix} {\mathbf{T}_\mathrm{w}^g}^T & \mathbf{0} \\ \mathbf{0} & {\mathbf{T}_\Omega^a}^T \end{bmatrix} \begin{bmatrix} \mathbf{v}_\mathrm{w} \\ \mathbf{v}_\Omega \end{bmatrix} \tag{3.96}$$

This is the important transformation from FE space to GBT space, which we will need to be able to find the constants of the homogeneous solution.

3.9.2 From GBT displacements to FE displacements

However, we may at some point also need the opposite transformation, which involves the constraint equations introduced in equation (3.49). Let us principally use the same method but introduce the transformation equation (3.95) whereby the multi-point constraint equations take the form

$$\mathbf{C}\mathbf{T}_{\mathrm{w}}^{c}\mathbf{v}_{\mathrm{w}}^{c}+\mathbf{C}\mathbf{T}_{\mathrm{w}}^{g}\mathbf{v}_{\mathrm{w}}^{g}=\mathbf{0}\quad\Leftrightarrow\quad\mathbf{C}_{c}\mathbf{v}_{\mathrm{w}}^{c}+\mathbf{C}_{g}\mathbf{v}_{\mathrm{w}}^{g}=\mathbf{0}\tag{3.97}$$

in which $\mathbf{C}_c = \mathbf{C}\mathbf{T}_{\mathrm{w}}^{c}$ has previously been introduced and $\mathbf{C}_g = \mathbf{C}\mathbf{T}_{\mathrm{w}}^{g}$ is introduced here. This allows us to express the constrained degrees of freedom by the GBT transverse displacement vector as:

$$\mathbf{v}_{\mathrm{w}}^{c}=-\mathbf{C}_{c}^{-1}\mathbf{C}_{g}\mathbf{v}_{\mathrm{w}}^{g}\tag{3.98}$$

Introducing the equality (3.98) in the transformation equation (3.95), we find that the total transformation condenses our problem as follows:

$$\mathbf{v}_{\mathrm{w}}=\begin{bmatrix}\mathbf{T}_{\mathrm{w}}^{c} & \mathbf{T}_{\mathrm{w}}^{g}\end{bmatrix}\begin{bmatrix}-{\mathbf{C}_{c}}^{-1}\mathbf{C}_{g}\mathbf{v}_{\mathrm{w}}^{g}\\ \mathbf{v}_{\mathrm{w}}^{g}\end{bmatrix}=\widetilde{\mathbf{T}}_{\mathrm{w}}^{g}\mathbf{v}_{\mathrm{w}}^{g}\tag{3.99}$$

where $\widetilde{\mathbf{T}}_{\mathrm{w}}^{g}=\mathbf{T}_{\mathrm{w}}^{g}-\mathbf{T}_{\mathrm{w}}^{c}{\mathbf{C}_{c}}^{-1}\mathbf{C}_{g}$ has been introduced as the condensed transformation. Using the transformation equation (3.31) that determines the warping displacements from the amount of axial extension and the transverse displacements we find

$$\mathbf{v}_{\Omega}=\begin{bmatrix}\mathbf{T}_{\Omega\mathrm{w}}^{r} & \mathbf{T}_{\Omega}^{a}\end{bmatrix}\begin{bmatrix}\mathbf{v}_{\mathrm{w}}\\ v_{\Omega}^{a}\end{bmatrix}=\begin{bmatrix}\mathbf{T}_{\Omega\mathrm{w}}^{r}\widetilde{\mathbf{T}}_{\mathrm{w}}^{g} & \mathbf{T}_{\Omega}^{a}\end{bmatrix}\begin{bmatrix}\mathbf{v}_{\mathrm{w}}^{g}\\ v_{\Omega}^{a}\end{bmatrix}\tag{3.100}$$

Using equations (3.99) and (3.100) we find the following transformation

$$\begin{bmatrix}\mathbf{v}_{\mathrm{w}}\\ \mathbf{v}_{\Omega}\end{bmatrix}=\begin{bmatrix}\widetilde{\mathbf{T}}_{\mathrm{w}}^{g} & \mathbf{0}\\ \mathbf{T}_{\Omega\mathrm{w}}^{r}\widetilde{\mathbf{T}}_{\mathrm{w}}^{g} & \mathbf{T}_{\Omega}^{a}\end{bmatrix}\begin{bmatrix}\mathbf{v}_{\mathrm{w}}^{g}\\ v_{\Omega}^{a}\end{bmatrix}\tag{3.101}$$

This transformation is used to transform from GBT space to FE space.

3.10 Displacement boundary conditions of the homogeneous solution

Having solved the eigenvalue problem and formulated solution modes in the original FE degree-of-freedom space, we would like to set up a method for determining the constants of the homogeneous solutions found. This is to be done in the GBT space. As seen from the first variation of the potential energy, the natural boundary displacements of the GBT at each boundary are the pure axial displacement u_{Ω}^{a} of the beam, the transverse displacements $\mathbf{u}_{\mathrm{w}}^{g}$, and the

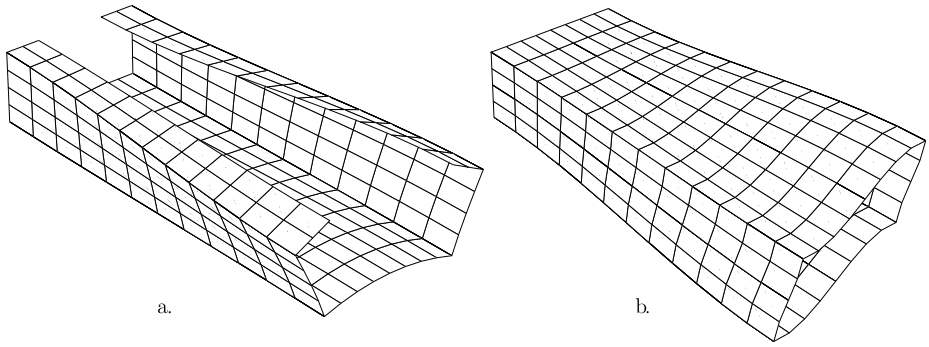

Figure 3.11: Displacement field for boundary conditions in equation (3.106).

axial derivative of the transverse displacements $\mathbf{u}_{\mathrm{w}}^{g\,\prime}$. The generalized internal displacements of the GBT beam can be expressed by using the full homogeneous solution in equation (3.86) or alternatively, as done in the following, by the real formulation in equation (3.94) and the transformation from FE to GBT displacements (3.96) as follows:

$$\begin{bmatrix} u_z^a(z) \\ \mathbf{u}_{\mathrm{w}}^g(z) \\ \mathbf{u}_{\mathrm{w}}^{g\,\prime}(z) \end{bmatrix} = \begin{bmatrix} -\mathbf{T}_{\Omega}^{a\,T}\widetilde{\mathbf{V}}_{\Omega}\widetilde{\mathbf{\Psi}}'(z) \\ \mathbf{T}_{\mathrm{w}}^{g\,T}\widetilde{\mathbf{V}}_{\mathrm{w}}\widetilde{\mathbf{\Psi}}(z) \\ \mathbf{T}_{\mathrm{w}}^{g\,T}\widetilde{\mathbf{V}}_{\mathrm{w}}\widetilde{\mathbf{\Psi}}'(z) \end{bmatrix} \widetilde{\mathbf{c}} \tag{3.102}$$

To determine the constants using displacement boundary conditions as in finite element or stiffness formulations, we need the boundary displacements at the two ends of a finite length beam, i.e. at $z = 0$ and at $z = L$ where L is the length of the beam. The assembled boundary displacement vector is denoted by $\mathbf{u}_b$. This leads to the following equation for the determination of the solution constants:

$$\mathbf{u}_b = \begin{bmatrix} u_z^a(0) \\ \mathbf{u}_{\mathrm{w}}^g(0) \\ \mathbf{u}_{\mathrm{w}}^{g\,\prime}(0) \\ u_z^a(L) \\ \mathbf{u}_{\mathrm{w}}^g(L) \\ \mathbf{u}_{\mathrm{w}}^{g\,\prime}(L) \end{bmatrix} = \begin{bmatrix} -\mathbf{T}_{\Omega}^{a\,T}\widetilde{\mathbf{V}}_{\Omega}\widetilde{\mathbf{\Psi}}'(0) \\ \mathbf{T}_{\mathrm{w}}^{g\,T}\widetilde{\mathbf{V}}_{\mathrm{w}}\widetilde{\mathbf{\Psi}}(0) \\ \mathbf{T}_{\mathrm{w}}^{g\,T}\widetilde{\mathbf{V}}_{\mathrm{w}}\widetilde{\mathbf{\Psi}}'(0) \\ -\mathbf{T}_{\Omega}^{a\,T}\widetilde{\mathbf{V}}_{\Omega}\widetilde{\mathbf{\Psi}}'(L) \\ \mathbf{T}_{\mathrm{w}}^{g\,T}\widetilde{\mathbf{V}}_{\mathrm{w}}\widetilde{\mathbf{\Psi}}(L) \\ \mathbf{T}_{\mathrm{w}}^{g\,T}\widetilde{\mathbf{V}}_{\mathrm{w}}\widetilde{\mathbf{\Psi}}'(L) \end{bmatrix} \widetilde{\mathbf{c}} = \widetilde{\mathbf{A}}\widetilde{\mathbf{c}} \tag{3.103}$$

$$\Rightarrow \quad \widetilde{\mathbf{c}} = \widetilde{\mathbf{A}}^{-1}\mathbf{u}_b \tag{3.104}$$

where we have introduced the matrix $\widetilde{\mathbf{A}}$, which is an invertible positive definite "square" matrix. However, to avoid numerical problems, the exponential solution functions in $\widetilde{\mathbf{\Psi}}(z)$ may have to be modified by replacing $\widetilde{c}_i e^{\lambda z}$ by $\hat{c}_i e^{\lambda(z-L)}$ so that the positive λz exponent is bounded.

The two solutions plotted by using equation (3.94) with only $\widetilde{c}_{j\,2}$ being non-zero in the upper half of Figure 3.10 can also be found by using the relevant boundary conditions in equation (3.104). To this end, we use the real and imaginary vectorial parts, $\mathbf{a}$, $\mathbf{b}$, of the mode shape and the modal solution functions and the derivative hereof. So in equation (3.104), we would use

$$\mathbf{u}_b = \begin{bmatrix} 0 \\ \mathbf{a} \\ -\lambda\mathbf{a} - \mu\mathbf{b} \\ 0 \\ e^{-\lambda L}(\mathbf{a}\cos\mu L + \mathbf{b}\sin\mu L) \\ -e^{-\lambda L}\left\{\mathbf{a}(\lambda\cos\mu L + \mu\sin\mu L) + \mathbf{b}(\lambda\sin\mu L - \mu\cos\mu L)\right\} \end{bmatrix} \tag{3.105}$$

and we should then find only the second constant of the j'th complex mode $\widetilde{c}_{j\,2}$ to be non zero. The two lower solutions plotted in Figure 3.10 correspond to boundary conditions in which only the fourth constant $\widetilde{c}_{j\,4}$ of the complex mode is non-zero.

It is also worth noting that just specifying the modal shape with a zero derivative (otherwise built-in support) will lead to a coupling to the remaining modes. For example, Figure 3.11 shows the displacements for the boundary displacements corresponding to the real part of the first complex distortional eigenmode at one end, but with zero axial displacements and zero displacements and axial displacement derivatives at the other end, i.e. with the following boundary condition:

$$\mathbf{u}_b^T = \begin{bmatrix} 0 & \mathbf{a}^T & \mathbf{0} & 0 & \mathbf{0} & \mathbf{0} \end{bmatrix}^T \tag{3.106}$$

With this boundary condition many modes are invoked and to achieve the zero derivative of the displacements, local distortional plate modes have also been invoked. The length scales of some of these modes are very small and will be difficult to see in an overall plot of the deformation mode.

3.11 Concluding remarks

In this chapter we have presented a new systematic method leading to the formulation of the homogeneous differential equations of a generalized beam theory (GBT) and the establishment of the full analytical solution.

Relevant deformation modes have been found by formulating and solving the distortional quadratic eigenvalue problem. Hereby it is shown that it is possible to solve the distortional quadratic eigenvalue problem and find the natural distortional displacement modes using a method equivalent to that used for non-proportionally damped (linear) dynamic modal analysis. The beam displacement field has been separated into a sum of products of the cross-section

displacement modes and their axial variation. The obtained GBT equations are now solved analytically and the formulation is valid without special attention also for closed single or multi-cell cross sections. To achieve a formulation resembling a generalization of Vlasov beam theory we have implemented some constraints and eliminations into the distortional differential equations, which has condensed the problem considerably and reduced the number of possible eigenmodes. The formulation above enables the formulation of an advanced semi-discretized prismatic thin-walled beam element developed later in chapter 6.

Having developed and solved the distortional differential equations as well as having formulated the full analytical homogeneous solution along the beam, we will in the next chapter continue with the particular solutions to the non-homogeneous set of distortional differential equations.

Chapter 4

Distortional non-homogeneous differential equations and solutions

This chapter deals with the particular solution to the non-homogeneous distortional differential equations in order to add loads on the advanced distortional beam element developed later in chapter 6. Thus, in this chapter which is related to Paper II (Andreassen and Jönsson, 2012b) and Paper VI (Andreassen and Jönsson, 2011) the distortional differential equations and solutions including distributed loads are formulated and solved. By transforming the non-homogeneous distortional differential equations into an eigenmode space, by using the distortional modal matrix found for the homogeneous system, we get the diagonalized and thus uncoupled set of differential equations including the distributed loads. Afterwards, the full solution of these uncoupled linear second-order differential equations is given. The boundary conditions considered in the example of this chapter are restricted to built in ends, which are needed for a displacement formulation of an exact first-order distortional beam element developed later in the thesis. This also means that the present approach are not yet dealing with a beam element which is part of chapter 6. Instead we are dealing with an analytical solution of the coupled differential equations. This means that we focus on boundary conditions which are displacement based, i.e. involve the displacement amplitude and the first derivative hereof. I have chosen to keep the formulation as simple as possible by not having to introduce the generalized forces and combinations of higher order derivatives. To keep the example simple with illustrative distortional deformations I have also chosen only to focus on a uniform load.

It is found necessary to follow the individual steps of the transformations and eliminations in the previous chapter 3 in order to ensure a correct formulation of the individual decoupled non-homogeneous differential equation, especially

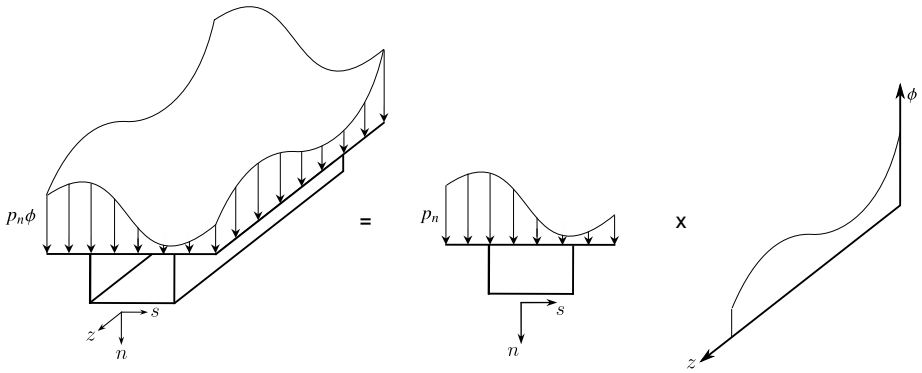

Figure 4.1: Load distribution.

for the distortional modes where we have utilized reduction of the order of the differential equations. Having done this once we may use work or energy principles to identify the individual load terms in a more direct manner.

4.1 External energy potential for distributed loads

In view of the distortional non-homogeneous differential equations and solutions, let us first introduce three types of distributed loads q_z, q_s, q_n which act on the mid plane of the individual walls in the z, s, n directions, respectively. The external load potential for these distributed loads can then for a single mode be found as

$$\Pi_{ext} = -\int_0^L\int_0^{b_e} \Big[q_z u_z + q_s u_s + q_n u_n\Big] ds\ dz \tag{4.1}$$

Using separation of variables for the distributed loads as for the displacements in chapter 3, we introduce the following load variables $q_s = p_s(s)\phi(z)$, $q_n = p_n(s)\phi(z)$, $q_z = p_z(s)\phi(z)$. In this formulation p_s, p_n, p_z represent the cross-section load distribution, and the function ϕ represents the axial variation of the loads. In the following formulation we operate with only one cross-section load distribution, which may be modified by summation of various different cross-section load distributions and axial load variation functions. The load separation is illustrated in Figure 4.1 for a distributed load $q_n = p_n(s)\phi(z)$ on the upper flange of a prismatic thin-walled beam. The local components of the loads and force vectors for a cross-section wall element is shown in Figure 4.2. Hereby the contribution to the external load potential of a single wall element takes the following form

$$\Pi_{ext,el} = -\int_0^L\int_0^{b_e} \phi\Big[p_s w_s\psi + p_n w_n\psi - p_z\Omega\psi'\Big]\ ds\ dz \tag{4.2}$$

which is suited for adequate interpolation in the following. Note that the two first load terms perform work through the transverse displacements and the last load term performs work through the axial warping displacements. Since the formulation of distortion has much in common with torsion the first two terms may be described as distortional moment loads and the last term as distortional bimoment load (Jönsson, 1999a). For the classical torsional equilibrium equation including warping of the cross section (Kollbrunner and Hajdin, 1972), these loads correspond to torsional moment load and torsional bimoment load.

4.2 Load interpolations within cross-section elements

The interpolations related to the cross section are the displacement interpolations for w_s, w_n, and Ω described in the previous chapter 3 or in Paper I (Jönsson and Andreassen, 2011), and the interpolation of the cross-section loads p_s, p_n, and p_z introduced in the following. The distributed load shown in Figure 4.1 are defined by a linear interpolation of the load on each cross-section wall element multiplied by an axial shape function $\phi(z)$, for which we introduce a specific interpolation later. The load interpolation in a cross-section wall is given by

$$p_s = \mathbf{N}_p \mathbf{p}_s^{el}, \quad p_n = \mathbf{N}_p \mathbf{p}_n^{el}, \quad p_z = \mathbf{N}_p \mathbf{p}_z^{el} \tag{4.3}$$

in which $\mathbf{N}_p(s) = [1 - s/b_e, s/b_e]$ is a linear interpolation matrix, and where the nodal end values of a cross-section wall element are given as

$$\mathbf{p}_s^{el} = \begin{bmatrix} p_{s1} \\ p_{s2} \end{bmatrix}, \quad \mathbf{p}_n^{el} = \begin{bmatrix} p_{n1} \\ p_{n2} \end{bmatrix}, \quad \mathbf{p}_z^{el} = \begin{bmatrix} p_{z1} \\ p_{z2} \end{bmatrix} \tag{4.4}$$

Using the introduced interpolations for the displacements and the loads, the external potential energy now takes the following form for a single wall element

$$\Pi_{ext,el} = -\int_0^L \int_0^{b_e} \Big[\psi \mathbf{v}_{\mathrm{w}}^{el\,T} \mathbf{N}_s{}^T \mathbf{N}_p \mathbf{p}_s^{el} + \psi \mathbf{v}_{\mathrm{w}}^{el\,T} \mathbf{N}_n{}^T \mathbf{N}_p \mathbf{p}_n^{el} - \psi' \mathbf{v}_{\Omega}^{el\,T} \mathbf{N}_\Omega{}^T \mathbf{N}_p \mathbf{p}_z^{el} \Big] \phi \, ds \, dz \tag{4.5}$$

This formulation allows us to write the element load vector in the same format as the element stiffness contributions from chapter 3. This means that we in addition to the straight-element stiffness contribution have the element load contributions as given in Table 4.1, where we have also included the nodal cross-section wall loads $\mathbf{P}_{\mathrm{w}}^{el}$ and $\mathbf{P}_{\Omega}^{el}$ corresponding to line loads also varying along the beam with ϕ. Hereby the walls of the prismatic thin-walled beam can be loaded by line loads acting at the cross-section nodes, and by surface

$\mathbf{r}_{\Omega}^{el} = \int_0^{b_e} \mathbf{N}_{\Omega}^T \mathbf{N}_p \, ds \; \mathbf{p}_z^{el} + \mathbf{P}_{\Omega}^{el}$
$\mathbf{r}_{\mathrm{w}}^{el} = \int_0^{b_e} \mathbf{N}_s^T \mathbf{N}_p \, ds \; \mathbf{p}_s^{el} + \int_0^{b_e} \mathbf{N}_n^T \mathbf{N}_p \, ds \; \mathbf{p}_n^{el} + \mathbf{P}_{\mathrm{w}}^{el}$

Table 4.1: Load contributions.

loads acting on the mid-plane of a cross-section wall. Both of these loads are distributed along the beam as given by the ϕ-function. Now, we can rewrite the external load potential of a single wall element as,

$$\Pi_{ext,el} = -\int_0^L \left[\psi \mathbf{v}_{\mathrm{w}}^{el\,T} \mathbf{r}_{\mathrm{w}}^{el} \phi - \psi' \mathbf{v}_{\Omega}^{el\,T} \mathbf{r}_{\Omega}^{el} \phi \right] dz \tag{4.6}$$

where we have introduced the axial and transverse nodal load components of a straight cross-section element as

$$\mathbf{r}_{\Omega}^{el} = \begin{bmatrix} r_{\Omega 1}^{el} & r_{\Omega 2}^{el} \end{bmatrix}^T \tag{4.7}$$

$$\mathbf{r}_{\mathrm{w}}^{el} = \begin{bmatrix} r_{\mathrm{w}1}^{el} & r_{\mathrm{w}2}^{el} & r_{\mathrm{w}3}^{el} & r_{\mathrm{w}4}^{el} & r_{\mathrm{w}5}^{el} & r_{\mathrm{w}6}^{el} \end{bmatrix}^T \tag{4.8}$$

These components are shown in Figure 4.2 along with the direction of the wall element coordinates (n, s) as well as the positive direction of the load components. We choose to assemble the single element components into two separate global vectors containing the axial load and the transverse load, respectively. These global vectors we will write as follows:

$$\mathbf{r}_{\Omega} = [r_{\Omega 1} \;\; r_{\Omega 2} \;\; r_{\Omega 3} \;\; \ldots]^T \tag{4.9}$$

$$\mathbf{r}_{\mathrm{w}} = [r_{\mathrm{w}1} \;\; r_{\mathrm{w}2} \;\; r_{\mathrm{w}3} \;\; r_{\mathrm{w}4} \;\; r_{\mathrm{w}5} \;\; r_{\mathrm{w}6} \;\; \ldots]^T \tag{4.10}$$

where the transformation from local to global components is performed using a formal standard transformation of the components in the cross-section plane, i.e.

$$\mathbf{r}_{\Omega} = \sum_{el} \mathbf{T}_{\Omega}{}^T \mathbf{r}_{\Omega}^{el} \tag{4.11}$$

$$\mathbf{r}_{\mathrm{w}} = \sum_{el} \mathbf{T}_{\mathrm{w}}{}^T \mathbf{r}_{\mathrm{w}}^{el} \tag{4.12}$$

To obtain an overview of the important transformations obtained in the previous chapter 3 and which also have to be used in the following chapters Table 4.2 has been made.

Now, we can write the total potential energy by summation of each element contribution as

$$\Pi_{tot} = \Pi_{int} + \Pi_{ext} \,, \quad \text{where} \quad \Pi_{ext} = \sum_{el} \Pi_{ext,el} \tag{4.13}$$

No.	Description	Transformations
1	Transformation from local to global axial d.o.f.	$\mathbf{v}_{\Omega} = \mathbf{T}_{\Omega}\mathbf{v}_{\Omega}^{el}$
2	Transformation from local to global transverse d.o.f.	$\mathbf{v}_{\mathrm{w}} = \mathbf{T}_{\mathrm{w}}\mathbf{v}_{\mathrm{w}}^{el}$
3	Transformation from pure axial extension and other axial d.o.f. to global axial d.o.f.	$\mathbf{v}_{\Omega} = \begin{bmatrix}\mathbf{T}_{\Omega}^{a} & \mathbf{T}_{\Omega}^{o}\end{bmatrix}\begin{bmatrix}\mathbf{v}_{\Omega}^{a}\\ \mathbf{v}_{\Omega}^{o}\end{bmatrix}$
4	Transformation from transverse d.o.f. to the other axial d.o.f. (without pure axial extension) based on the shear constrains.	$\mathbf{v}_{\Omega}^{o} = \mathbf{T}_{\Omega\mathrm{w}}\mathbf{v}_{\mathrm{w}}$
5	Transformation from transverse d.o.f. and pure axial extension d.o.f. to the global axial d.o.f.	$\mathbf{v}_{\Omega} = \begin{bmatrix}\mathbf{T}_{\Omega\mathrm{w}}^{r} & \mathbf{T}_{\Omega}^{a}\end{bmatrix}\begin{bmatrix}\mathbf{v}_{\mathrm{w}}\\ v_{\Omega}^{a}\end{bmatrix}$
6	Transformation from pure transverse translation d.o.f., pure rotation d.o.f., constant wall-width constrained d.o.f. and unconstrained d.o.f. to global transverse d.o.f. (wall-width constraints not applied).	$\mathbf{v}_{\mathrm{w}} = \begin{bmatrix}\mathbf{T}_{\mathrm{w}}^{\alpha} & \mathbf{T}_{\mathrm{w}}^{3} & \mathbf{T}_{\mathrm{w}}^{c} & \mathbf{T}_{\mathrm{w}}^{u}\end{bmatrix}\begin{bmatrix}\mathbf{v}_{\mathrm{w}}^{\alpha}\\ v_{\mathrm{w}}^{3}\\ \mathbf{v}_{\mathrm{w}}^{c}\\ \mathbf{v}_{\mathrm{w}}^{u}\end{bmatrix}$
7	Transformation from pure transverse translation d.o.f., pure rotation d.o.f. and unconstrained d.o.f. to global transverse d.o.f. (wall-width constraints applied).	$\mathbf{v}_{\mathrm{w}} = \begin{bmatrix}\mathbf{T}_{\mathrm{w}}^{\alpha} & \mathbf{T}_{\mathrm{w}}^{3} & \widetilde{\mathbf{T}}_{\mathrm{w}}^{u}\end{bmatrix}\begin{bmatrix}\mathbf{v}_{\mathrm{w}}^{\alpha}\\ v_{\mathrm{w}}^{3}\\ \mathbf{v}_{\mathrm{w}}^{u}\end{bmatrix}$
8	Transformation from constrained transverse d.o.f. and transverse GBT d.o.f. to global transverse d.o.f.	$\mathbf{v}_{\mathrm{w}} = \begin{bmatrix}\mathbf{T}_{\mathrm{w}}^{c} & \mathbf{T}_{\mathrm{w}}^{g}\end{bmatrix}\begin{bmatrix}\mathbf{v}_{\mathrm{w}}^{c}\\ \mathbf{v}_{\mathrm{w}}^{g}\end{bmatrix}$
9	Transformation from FE space to GBT space.	$\begin{bmatrix}\mathbf{v}_{\mathrm{w}}^{g}\\ v_{\Omega}^{a}\end{bmatrix} = \begin{bmatrix}\mathbf{T}_{\mathrm{w}}^{g\,T} & \mathbf{0}\\ \mathbf{0} & \mathbf{T}_{\Omega}^{a\,T}\end{bmatrix}\begin{bmatrix}\mathbf{v}_{\mathrm{w}}\\ \mathbf{v}_{\Omega}\end{bmatrix}$
10	Transformation from GBT space to FE space.	$\begin{bmatrix}\mathbf{v}_{\mathrm{w}}\\ \mathbf{v}_{\Omega}\end{bmatrix} = \begin{bmatrix}\widetilde{\mathbf{T}}_{\mathrm{w}}^{g} & \mathbf{0}\\ \mathbf{T}_{\Omega\mathrm{w}}^{r}\widetilde{\mathbf{T}}_{\mathrm{w}}^{g} & \mathbf{T}_{\Omega}^{a\,T}\end{bmatrix}\begin{bmatrix}\mathbf{v}_{\mathrm{w}}^{g}\\ v_{\Omega}^{a}\end{bmatrix}$

Table 4.2: Transformations.

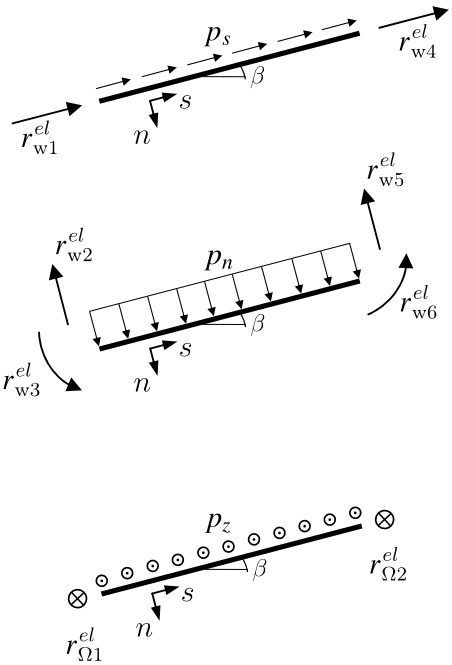

Figure 4.2: Distributed loads and the resulting load vectors.

where Π_{int} is the contribution to the potential energy from the internal properties found in chapter 3, and Π_{ext} is the contribution from the external loads. Introducing the described interpolation and matrix calculation scheme allows us to write the total potential energy as

$$\Pi_{tot} = \Pi_{int} - \int_0^L \left\{ (\psi \mathbf{v}_{\mathrm{w}}^T)\mathbf{r}_{\mathrm{w}}\phi - (\psi \mathbf{v}_{\Omega}^T)'\mathbf{r}_{\Omega}\phi \right\} dz \tag{4.14}$$

The first term corresponds to the distortional moment load which performs work through the transverse displacements and the second term corresponds to the distortional bimoment load which performs work through the axial displacements.

4.3 Modal loads and modal solutions

To obtain a formulation resembling the generalization of Vlasov beam theory including distortion, the following three main steps have to be performed again as in the previous chapter. This allows us to properly identify modal load components as well as the contributions to the individual modal differential equations.

$r^a_\Omega = \mathbf{T}^{a\,T}_\Omega \mathbf{r}_\Omega$	$\bar{\mathbf{r}}_\Omega = \mathbf{T}^{r\,T}_{\Omega\mathrm{w}} \mathbf{r}_\Omega - \mathbf{K}^{\sigma ra}_{\Omega\Omega} (K^{\sigma aa}_{\Omega\Omega})^{-1} r^a_\Omega$

Table 4.3: Transformation of load vectors related to Step I.

4.3.1 Step I: Pure axial load and shear constraints

Following the procedure which is used to identify pure axial extension as an eigenmode and to introduce shear constraints, we will identify the axial load components and separate these from the remaining equations. The potential energy formulation including the load terms in equation (4.14) have to be modified, so that the pure axial extension is described by the separate degree of freedom v^a_Ω, and so that the shear constraint equations are enforced. This modification is performed using the following transformation (No. 5 described in Table 4.2):

$$\mathbf{v}_\Omega = \mathbf{T}^r_{\Omega\mathrm{w}} \mathbf{v}_\mathrm{w} + \mathbf{T}^a_\Omega v^a_\Omega \tag{4.15}$$

To clarify the variational treatment of pure axial extension, we also temporally rewrite the terms pertaining to axial extension using $\zeta v^a_\Omega = -\psi' v^a_\Omega$. The modified elastic potential energy for a single mode takes the following form:

$$\Pi_{tot} = \Pi_{int} - \int_0^L \left\{ (\psi \mathbf{v}^T_\mathrm{w}) \mathbf{r}_\mathrm{w} \phi - (\psi \mathbf{v}^T_\mathrm{w})' \, \mathbf{T}^{r\,T}_{\Omega\mathrm{w}} \mathbf{r}_\Omega \phi + (\zeta v^a_\Omega) r^a_\Omega \phi \right\} dz \tag{4.16}$$

in which the pure axial loading is identified as r^a_Ω. It is as given in Table 4.3 identified as the product of the transpose of the pure axial deformation mode and the global axial load vector .

To obtain the differential equations of GBT, the first variation of the elastic potential energy is investigated by taking variations in the complete displacement field. This gives

$$\delta\Pi_{tot} = \delta\Pi_{int} - \int_0^L \left\{ \delta(\psi \mathbf{v}^T_\mathrm{w}) \mathbf{r}_\mathrm{w} \phi - \delta(\psi \mathbf{v}^T_\mathrm{w})' \, \mathbf{T}^{r\,T}_{\Omega\mathrm{w}} \mathbf{r}_\Omega \phi + \delta(\zeta v^a_\Omega) r^a_\Omega \phi \right\} dz \tag{4.17}$$

After performing partial integrations on the terms that involve axial derivatives of the (virtual) varied displacement field, $\delta(\,)'$, the first variation of the elastic potential energy takes the form

$$\delta\Pi_{tot} = \delta\Pi_{int} - \int_0^L \left\{ \delta(\psi \mathbf{v}^T_\mathrm{w}) \left[\mathbf{r}_\mathrm{w} \phi + \mathbf{T}^{r\,T}_{\Omega\mathrm{w}} \mathbf{r}_\Omega \phi' \right] + \delta(\zeta v^a_\Omega) r^a_\Omega \phi \right\} dz + \left[\delta(\psi \mathbf{v}^T_\mathrm{w}) \left[\mathbf{T}^{r\,T}_{\Omega\mathrm{w}} \mathbf{r}_\Omega \phi \right] \right]_0^L \tag{4.18}$$

For internal variation in the displacement fields $\delta(\psi \mathbf{v}_{\mathrm{w}})$ and $\delta(\zeta v_{\Omega}^{a})$, the elastic potential energy should be stationary and therefore its first variation must be equal to zero. Here the terms in the squared bracket correspond to the boundary loads and boundary conditions. Substituting $\delta\Pi_{int}$ from chapter 3 leads to the following coupled non-homogeneous differential equations of GBT in which we note that $\zeta = -\psi'$:

$$\bar{\mathbf{K}}^{\sigma}\mathbf{v}_{\mathrm{w}}\psi'''' - \mathbf{K}_{\Omega\Omega}^{\sigma ra}v_{\Omega}^{a}\zeta''' - \mathbf{K}^{\tau}\mathbf{v}_{\mathrm{w}}\psi'' + \mathbf{K}^{s}\mathbf{v}_{\mathrm{w}}\psi = \mathbf{r}_{\mathrm{w}}\phi + {\mathbf{T}_{\Omega\mathrm{w}}^{r}}^{T}\mathbf{r}_{\Omega}\phi' \quad (4.19)$$

$$\mathbf{K}_{\Omega\Omega}^{\sigma ar}\mathbf{v}_{\mathrm{w}}\psi''' - K_{\Omega\Omega}^{\sigma aa}v_{\Omega}^{a}\zeta'' = r_{\Omega}^{a}\phi \quad (4.20)$$

Here the left hand side of the equations corresponds to the homogeneous equations, and the right hand side are the non-homogeneous load terms.

These equations establish a coupled set of non-homogeneous GBT differential equations, that determine the displacements of a prismatic thin-walled beam for a given set of boundary conditions. The homogeneous parts of the solution have been found, and now we seek particular solutions to the modal equations. Let us start out by isolating the term $v_{\Omega}^{a}\zeta''$ in equation (4.20) as

$$v_{\Omega}^{a}\zeta'' = (K_{\Omega\Omega}^{\sigma aa})^{-1}[\mathbf{K}_{\Omega\Omega}^{\sigma ar}\mathbf{v}_{\mathrm{w}}\psi''' - r_{\Omega}^{a}\phi] \quad (4.21)$$

Let us then first consider the pure axial extension mode, which has been identified as $(\mathbf{v}_{\mathrm{w}}, v_{\Omega}^{a}) = (\mathbf{0}, 1)$, where we introduce the notation bold zero $\mathbf{0}$ for a suitable size matrix or vector of zeroes. Introducing this mode in equation (4.21) uncouples the equation (since $\mathbf{v}_{\mathrm{w}} = \mathbf{0}$). Integrating the particular solution for the axial mode, the complete solution for the axial variation is then given by adding the homogeneous part of the solution and the particular part as follows:

$$\zeta(z) = \begin{bmatrix} 1 & z \end{bmatrix} \begin{bmatrix} c_{a1} \\ c_{a2} \end{bmatrix} - (K_{\Omega\Omega}^{\sigma aa})^{-1} r_{\Omega}^{a} \iint \phi \; dzdz \quad (4.22)$$

where c_{a1} and c_{a2} are constants determined by the boundary conditions of axial extension.

In the context of the current work we will interpolate the cross-section load using a single distribution function $\phi(z)$, which varies linearly between two end values (ϕ_1 and ϕ_2) representing the values of the multiplicative function at the ends of the profile. Thus we introduce ϕ as

$$\phi = \begin{bmatrix} 1 - \frac{z}{L} & \frac{z}{L} \end{bmatrix} \boldsymbol{\phi} \quad \text{where} \quad \boldsymbol{\phi} = \begin{bmatrix} \phi_1 \\ \phi_2 \end{bmatrix} \quad (4.23)$$

Using this linear interpolation the full integrated solution of equation (4.22) takes the form

$$\zeta(z) = -\boldsymbol{\Psi}_{ah}{}'(z)\ \mathbf{c}_a - \boldsymbol{\Psi}_{ap}{}'(z)\ \phi \tag{4.24}$$

where

$$\boldsymbol{\Psi}_{ah}{}' = -\begin{bmatrix}1 & z\end{bmatrix}, \qquad \mathbf{c}_a = \begin{bmatrix}c_{a1}\\ c_{a2}\end{bmatrix}, \qquad \boldsymbol{\Psi}_{ap}{}' = \frac{L^2 r_\Omega^a}{6K_{\Omega\Omega}^{\sigma aa}}\begin{bmatrix}3(\frac{z}{L})^2 - (\frac{z}{L})^3 & (\frac{z}{L})^3\end{bmatrix} \tag{4.25}$$

The introduced subscripts h and p denote the homogeneous and the particular parts of the solution, respectively.

Let us next consider the formulation of the remaining transverse displacement modes. Inserting equation (4.21) differentiated once into equation (4.19) we eliminate pure axial extension. Introducing $\mathbf{K}^\sigma$ as in chapter 3, we obtain the following non-homogeneous fourth order differential equations for determination of the transverse (global, distortional, and local) distortional displacement modes of GBT:

$$\mathbf{K}^\sigma \mathbf{v}_{\mathrm{w}}\psi'''' - \mathbf{K}^\tau \mathbf{v}_{\mathrm{w}}\psi'' + \mathbf{K}^s \mathbf{v}_{\mathrm{w}}\psi = \mathbf{r}_{\mathrm{w}}\phi + (\mathbf{T}_{\Omega\mathrm{w}}^r{}^T \mathbf{r}_\Omega - \mathbf{K}_{\Omega\Omega}^{\sigma ra}(K_{\Omega\Omega}^{\sigma aa})^{-1} r_\Omega^a)\phi' \tag{4.26}$$

which we choose to abbreviate and write as

$$\mathbf{K}^\sigma \mathbf{v}_{\mathrm{w}}\psi'''' - \mathbf{K}^\tau \mathbf{v}_{\mathrm{w}}\psi'' + \mathbf{K}^s \mathbf{v}_{\mathrm{w}}\psi = \mathbf{r}_{\mathrm{w}}\phi + \bar{\mathbf{r}}_\Omega\phi' \tag{4.27}$$

where $\bar{\mathbf{r}}_\Omega$ is given in Table 4.3.

4.3.2 Step II: Flexural loading and constant wall width

In this step we treat two modes corresponding to transverse translations of the cross section, and one mode corresponding to pure rotation. We also constrain the transverse displacement field so that the wall widths remain constant, i.e. we enforce $\mathrm{w}_{s,s} \equiv 0$.

Let us do this by first introducing transformation No. 7 from Table 4.2 into the differential equations in (4.27), and also introduce the null terms corresponding to the rigid-body modes and zero shear strain for translational and flexural modes. Hereby the differential equations including the load terms take the following form:

$\mathbf{r}_{\mathrm{w}}^{\alpha} = \mathbf{T}_{\mathrm{w}}^{\alpha\,T}\mathbf{r}_{\mathrm{w}}$	$r_{\mathrm{w}}^{3} = \mathbf{T}_{\mathrm{w}}^{3\,T}\mathbf{r}_{\mathrm{w}}$
$\mathbf{r}_{\mathrm{w}}^{u} = \widetilde{\mathbf{T}}_{\mathrm{w}}^{u\,T}\mathbf{r}_{\mathrm{w}}$	$\mathbf{r}_{\mathrm{w}}^{u\alpha} = \mathbf{r}_{\mathrm{w}}^{u} - \mathbf{K}_{\alpha u}^{\sigma\;T}(\mathbf{K}_{\alpha\alpha}^{\sigma})^{-1}\mathbf{r}_{\mathrm{w}}^{\alpha}$
$\bar{\mathbf{r}}_{\Omega}^{\alpha} = \mathbf{T}_{\mathrm{w}}^{\alpha\,T}\bar{\mathbf{r}}_{\Omega}$	$\bar{r}_{\Omega}^{3} = \mathbf{T}_{\mathrm{w}}^{3\,T}\bar{\mathbf{r}}_{\Omega}$
$\bar{\mathbf{r}}_{\Omega}^{u} = \widetilde{\mathbf{T}}_{\mathrm{w}}^{u\,T}\bar{\mathbf{r}}_{\Omega}$	$\bar{\mathbf{r}}_{\Omega}^{u\alpha} = \bar{\mathbf{r}}_{\Omega}^{u} - \mathbf{K}_{\alpha u}^{\sigma\;T}(\mathbf{K}_{\alpha\alpha}^{\sigma})^{-1}\bar{\mathbf{r}}_{\Omega}^{\alpha}$

Table 4.4: Transformation of load vectors related to Step II.

$$\begin{bmatrix} \mathbf{K}_{\alpha\alpha}^{\sigma} & \mathbf{0} & \mathbf{K}_{\alpha u}^{\sigma} \\ \mathbf{0} & K_{33}^{\sigma} & \mathbf{K}_{3u}^{\sigma} \\ \mathbf{K}_{u\alpha}^{\sigma} & \mathbf{K}_{u3}^{\sigma} & \mathbf{K}_{uu}^{\sigma} \end{bmatrix} \begin{bmatrix} \mathbf{v}_{\mathrm{w}}^{\alpha} \\ v_{\mathrm{w}}^{3} \\ \mathbf{v}_{\mathrm{w}}^{\mathbf{u}} \end{bmatrix} \psi'''' - \begin{bmatrix} \mathbf{0} & \mathbf{0} & \mathbf{0} \\ \mathbf{0} & K_{33}^{\tau} & \mathbf{K}_{3u}^{\tau} \\ \mathbf{0} & \mathbf{K}_{u3}^{\tau} & \mathbf{K}_{uu}^{\tau} \end{bmatrix} \begin{bmatrix} \mathbf{v}_{\mathrm{w}}^{\alpha} \\ v_{\mathrm{w}}^{3} \\ \mathbf{v}_{\mathrm{w}}^{\mathbf{u}} \end{bmatrix} \psi''$$

$$+ \begin{bmatrix} \mathbf{0} & \mathbf{0} & \mathbf{0} \\ \mathbf{0} & 0 & \mathbf{0} \\ \mathbf{0} & \mathbf{0} & \mathbf{K}_{uu}^{s} \end{bmatrix} \begin{bmatrix} \mathbf{v}_{\mathrm{w}}^{\alpha} \\ v_{\mathrm{w}}^{3} \\ \mathbf{v}_{\mathrm{w}}^{\mathbf{u}} \end{bmatrix} \psi = \begin{bmatrix} \mathbf{r}_{\mathrm{w}}^{\alpha} \\ r_{\mathrm{w}}^{3} \\ \mathbf{r}_{\mathrm{w}}^{u} \end{bmatrix} \phi + \begin{bmatrix} \bar{\mathbf{r}}_{\Omega}^{\alpha} \\ \bar{r}_{\Omega}^{3} \\ \bar{\mathbf{r}}_{\Omega}^{u} \end{bmatrix} \phi' \quad (4.28)$$

where the transformed stiffness matrices are found and described in chapter 3 and the load vectors are given in Table 4.4. The two-dimensional upper block matrix equation yields the translation displacements as

$$\mathbf{v}_{\mathrm{w}}^{\alpha}\psi'''' = \mathbf{K}_{\alpha\alpha}^{\sigma\;-1}[\mathbf{r}_{\mathrm{w}}^{\alpha}\phi + \bar{\mathbf{r}}_{\Omega}^{\alpha}\phi' - \mathbf{K}_{\alpha u}^{\sigma}\mathbf{v}_{\mathrm{w}}^{u}\psi''''] \quad (4.29)$$

where $\alpha = 1$ or $\alpha = 2$. We can identify the two orthogonal pure translational modes, $(v_{\mathrm{w}}^{1}, v_{\mathrm{w}}^{2}, v_{\mathrm{w}}^{3}, \mathbf{v}_{\mathrm{w}}^{u}) = (1, 0, 0, \mathbf{0})$ and $(0, 1, 0, \mathbf{0})$, as eigenmodes or full solutions to the homogeneous part of equation (4.28). A particular solution for the axial variation of the pure translational modes is determined by quadruple integration of the non-homogeneous load terms (since $\mathbf{v}_{\mathrm{w}}^{u} = \mathbf{0}$). The complete solution is then given by summation of the full homogeneous solution and the particular solution, which we can express as

$$\psi_{\alpha}(z) = c_{\alpha 1} + c_{\alpha 2}z + c_{\alpha 3}z^{2} + c_{\alpha 4}z^{3} + \iiiint (\mathbf{K}_{\alpha\alpha}^{\sigma})^{-1}(\mathbf{r}_{\mathrm{w}}^{\alpha}\phi + \bar{\mathbf{r}}_{\Omega}^{\alpha}\phi')\; dz\; dz\; dz\; dz \quad (4.30)$$

Remembering that we in the present context introduce ϕ as one linear function as given in equation (4.23), we can perform the quadruple integration and get

$$\psi_{\alpha}(z) = \mathbf{\Psi}_{\alpha h}(z)\,\mathbf{c}_{\alpha} + \mathbf{\Psi}_{\alpha p}(z)\,\phi \quad (4.31)$$

Here $\mathbf{c}_\alpha$ is a vector containing four constants of the homogeneous part of the solution, and

$$\boldsymbol{\Psi}_{\alpha p}(z) = \boldsymbol{\Psi}^{\mathrm{w}}_{\alpha p}(z) + \boldsymbol{\Psi}^{\Omega}_{\alpha p}(z) \tag{4.32}$$

$$\boldsymbol{\Psi}_{\alpha h}(z) = \left[1 \;\; z \;\; z^2 \;\; z^3\right] \tag{4.33}$$

$$\boldsymbol{\Psi}^{\mathrm{w}}_{\alpha p}(z) = \frac{L^4}{120}\,(\mathbf{K}^{\sigma}_{\alpha\alpha})^{-1}\mathbf{r}^{\alpha}_{\mathrm{w}}\left[5(\tfrac{z}{L})^4 - (\tfrac{z}{L})^5 \;\; (\tfrac{z}{L})^5\right] \tag{4.34}$$

$$\boldsymbol{\Psi}^{\Omega}_{\alpha p}(z) = \frac{L^3}{24}\,(\mathbf{K}^{\sigma}_{\alpha\alpha})^{-1}\bar{\mathbf{r}}^{\alpha}_{\Omega}\left[4(\tfrac{z}{L})^3 - (\tfrac{z}{L})^4 \;\; (\tfrac{z}{L})^4\right] \tag{4.35}$$

Having identified the solutions related to the two pure translational modes we return to the remaining block equations of equation (4.28). Eliminating the two pure flexural degrees of freedom using equation (4.29) we obtain the condensed version of the differential equation (4.28) as

$$\begin{bmatrix} K^{\sigma}_{33} & \mathbf{K}^{\sigma}_{3u} \\ \mathbf{K}^{\sigma}_{u3} & \bar{\mathbf{K}}^{\sigma}_{uu} \end{bmatrix} \begin{bmatrix} v^3_{\mathrm{w}} \\ \mathbf{v}^u_{\mathrm{w}} \end{bmatrix} \psi'''' - \begin{bmatrix} K^{\tau}_{33} & \mathbf{K}^{\tau}_{3u} \\ \mathbf{K}^{\tau}_{u3} & \mathbf{K}^{\tau}_{uu} \end{bmatrix} \begin{bmatrix} v^3_{\mathrm{w}} \\ \mathbf{v}^u_{\mathrm{w}} \end{bmatrix} \psi'' + \begin{bmatrix} 0 & \mathbf{0} \\ \mathbf{0} & \mathbf{K}^{s}_{uu} \end{bmatrix} \begin{bmatrix} v^3_{\mathrm{w}} \\ \mathbf{v}^u_{\mathrm{w}} \end{bmatrix} \psi$$

$$= \begin{bmatrix} r^3_{\mathrm{w}} \\ \mathbf{r}^{u\alpha}_{\mathrm{w}} \end{bmatrix} \phi + \begin{bmatrix} \bar{r}^3_{\Omega} \\ \bar{\mathbf{r}}^{u\alpha}_{\Omega} \end{bmatrix} \phi' \tag{4.36}$$

The stiffness matrix $\bar{\mathbf{K}}^{\sigma}_{uu}$ is found in chapter 3 and the vectors $\mathbf{r}^{u\alpha}_{\mathrm{w}}$ and $\bar{\mathbf{r}}^{u\alpha}_{\Omega}$ are given in Table 4.4. This equation constitutes the GBT differential equations constrained by shear flow constraints and wall-width constraints after the elimination of the classical axial and two translational (flexural beam) modes.

4.3.3 Step III: Reduction of order and torsional load

The fourth order differential equation (4.36) can be transformed into twice as many second order differential equations by introducing a so-called state vector. There are a number of different possible formulations, however we choose the use of the state vector $(v^3_{\mathrm{w}}\psi, \mathbf{v}^u_{\mathrm{w}}\psi, v^3_{\mathrm{w}}\psi'', \mathbf{v}^u_{\mathrm{w}}\psi'')^T$. By introducing this state vector we obtain a reformulation of equation (4.36), leading to a formal second order matrix differential equation of double size, which takes the form

$$\begin{bmatrix} 0 & \mathbf{0} & 0 & \mathbf{0} \\ \mathbf{0} & \mathbf{K}^{s}_{uu} & \mathbf{0} & \mathbf{0} \\ 0 & \mathbf{0} & -K^{\sigma}_{33} & -\mathbf{K}^{\sigma}_{3u} \\ \mathbf{0} & \mathbf{0} & -\mathbf{K}^{\sigma}_{u3} & -\bar{\mathbf{K}}^{\sigma}_{uu} \end{bmatrix} \begin{bmatrix} v^3_{\mathrm{w}}\psi \\ \mathbf{v}^u_{\mathrm{w}}\psi \\ v^3_{\mathrm{w}}\psi'' \\ \mathbf{v}^u_{\mathrm{w}}\psi'' \end{bmatrix} - \begin{bmatrix} K^{\tau}_{33} & \mathbf{K}^{\tau}_{3u} & -K^{\sigma}_{33} & -\mathbf{K}^{\sigma}_{3u} \\ \mathbf{K}^{\tau}_{u3} & \mathbf{K}^{\tau}_{uu} & -\mathbf{K}^{\sigma}_{u3} & -\bar{\mathbf{K}}^{\sigma}_{uu} \\ -K^{\sigma}_{33} & -\mathbf{K}^{\sigma}_{3u} & 0 & \mathbf{0} \\ -\mathbf{K}^{\sigma}_{u3} & -\bar{\mathbf{K}}^{\sigma}_{uu} & \mathbf{0} & \mathbf{0} \end{bmatrix} \begin{bmatrix} v^3_{\mathrm{w}}\psi \\ \mathbf{v}^u_{\mathrm{w}}\psi \\ v^3_{\mathrm{w}}\psi'' \\ \mathbf{v}^u_{\mathrm{w}}\psi'' \end{bmatrix}''$$

$$= \begin{bmatrix} r^3_{\mathrm{w}} \\ \mathbf{r}^{u\alpha}_{\mathrm{w}} \\ 0 \\ \mathbf{0} \end{bmatrix} \phi + \begin{bmatrix} \bar{r}^3_{\Omega} \\ \bar{\mathbf{r}}^{u\alpha}_{\Omega} \\ 0 \\ \mathbf{0} \end{bmatrix} \phi' \tag{4.37}$$

To keep the matrix operations as simple as possible we introduce a new vector $\mathbf{v}_{\mathrm{w}}^{e}$, three new block matrices, $\mathbf{K}_{ee}^{\sigma}$, $\mathbf{K}_{3e}^{\sigma}$, and $\mathbf{K}_{ue}^{\sigma}$ given by

$$\mathbf{v}_{\mathrm{w}}^{e} = \begin{bmatrix} v_{\mathrm{w}}^{3} \\ \mathbf{v}_{\mathrm{w}}^{u} \end{bmatrix} \quad \mathbf{K}_{ee}^{\sigma} = \begin{bmatrix} \mathbf{K}_{3e}^{\sigma} \\ \mathbf{K}_{ue}^{\sigma} \end{bmatrix} = \begin{bmatrix} [\, K_{33}^{\sigma} \;\; \mathbf{K}_{3u}^{\sigma} \,] \\ [\, \mathbf{K}_{u3}^{\sigma} \;\; \bar{\mathbf{K}}_{uu}^{\sigma} \,] \end{bmatrix} \tag{4.38}$$

and the force vectors are given by

$$\mathbf{r}_{\mathrm{w}}^{e} = \begin{bmatrix} 0 \\ \mathbf{0} \end{bmatrix} \quad , \quad \mathbf{r}_{\Omega}^{e} = \begin{bmatrix} 0 \\ \mathbf{0} \end{bmatrix} \tag{4.39}$$

Introducing the new vectors and block matrices defined by equation (4.38) and (4.39), and the transformed loads given in Table 4.5, the second order differential equations (4.37) can be rewritten as

$$\begin{bmatrix} 0 & \mathbf{0} & \mathbf{0} \\ \mathbf{0} & \mathbf{K}_{uu}^{s} & \mathbf{0} \\ \mathbf{0} & \mathbf{0} & -\mathbf{K}_{ee}^{\sigma} \end{bmatrix} \begin{bmatrix} v_{\mathrm{w}}^{3}\psi \\ \mathbf{v}_{\mathrm{w}}^{u}\psi \\ \mathbf{v}_{\mathrm{w}}^{e}\psi'' \end{bmatrix} - \begin{bmatrix} K_{33}^{\tau} & \mathbf{K}_{3u}^{\tau} & -\mathbf{K}_{3e}^{\sigma} \\ \mathbf{K}_{u3}^{\tau} & \mathbf{K}_{uu}^{\tau} & -\mathbf{K}_{ue}^{\sigma} \\ -\mathbf{K}_{e3}^{\sigma} & -\mathbf{K}_{eu}^{\sigma} & \mathbf{0} \end{bmatrix} \begin{bmatrix} v_{\mathrm{w}}^{3}\psi \\ \mathbf{v}_{\mathrm{w}}^{u}\psi \\ \mathbf{v}_{\mathrm{w}}^{e}\psi'' \end{bmatrix}'' = \begin{bmatrix} r_{\mathrm{w}}^{3} \\ \mathbf{r}_{\mathrm{w}}^{u\alpha} \\ \mathbf{r}_{\mathrm{w}}^{e} \end{bmatrix} \phi + \begin{bmatrix} \bar{r}_{\Omega}^{3} \\ \bar{\mathbf{r}}_{\Omega}^{u\alpha} \\ \mathbf{r}_{\Omega}^{e} \end{bmatrix} \phi' \tag{4.40}$$

From the first equation we can isolate the pure rotational term resulting in the following differential equation:

$$v_{\mathrm{w}}^{3}\psi'' = -(K_{33}^{\tau})^{-1} \left(\mathbf{K}_{3u}^{\tau}\mathbf{v}_{\mathrm{w}}^{u}\psi'' - \mathbf{K}_{3e}^{\sigma}\mathbf{v}_{\mathrm{w}}^{e}\psi'''' + r_{\mathrm{w}}^{3}\phi + \bar{r}_{\Omega}^{3}\phi' \right) \tag{4.41}$$

It can be seen that pure torsion (with free warping), corresponding to the solution vector, $(v_{\mathrm{w}}^{3}\psi, \mathbf{v}_{\mathrm{w}}^{u}\psi, \mathbf{v}_{\mathrm{w}}^{e}\psi'') = (c_{32}z + c_{31}, \mathbf{0}, \mathbf{0})$, is a solution of the homogeneous second-order differential equations in (4.40). Hereby the particular solution for the axial variation of the pure torsion mode is determined by double integration of the particular part, and the full solution is found by addition of the homogeneous solution. This results in

$$\psi_3(z) = c_{31} + c_{32}z - \iint (K_{33}^{\tau})^{-1}(\bar{r}_{\mathrm{w}}^{3}\phi + \bar{r}_{\Omega}^{3}\phi')\; dz\; dz \tag{4.42}$$

Inserting the linear function ϕ from equation (4.23) we can evaluate the integrals in (4.42) and find the full solution of pure St. Venant torsion as

$$\psi_3(z) = \mathbf{\Psi}_{3h}(z)\; \mathbf{c}_3 + \mathbf{\Psi}_{3p}(z)\; \phi \tag{4.43}$$

Here $\mathbf{c}_3$ is a vector containing two constants of the homogeneous part of the solution, and

$$\boldsymbol{\Psi}_{3p}(z) = \boldsymbol{\Psi}^{\mathrm{w}}_{3p}(z) + \boldsymbol{\Psi}^{\Omega}_{3p}(z) \tag{4.44}$$

$$\boldsymbol{\Psi}_{3h}(z) = \begin{bmatrix} 1 & z \end{bmatrix} \tag{4.45}$$

$$\boldsymbol{\Psi}^{\mathrm{w}}_{3p}(z) = -\frac{L^2 r^3_{\mathrm{w}}}{6K^{\tau}_{33}} \begin{bmatrix} 3(\frac{z}{L})^2 - (\frac{z}{L})^3 & (\frac{z}{L})^3 \end{bmatrix} \tag{4.46}$$

$$\boldsymbol{\Psi}^{\Omega}_{3p}(z) = -\frac{L\bar{r}^3_{\Omega}}{2K^{\tau}_{33}} \begin{bmatrix} 2(\frac{z}{L}) - (\frac{z}{L})^2 & (\frac{z}{L})^2 \end{bmatrix} \tag{4.47}$$

Using equation (4.41) we eliminate v^3_{w} from the differential equations in (4.40) and find the final distortional non-homogeneous differential equations of GBT that determine all the distortional displacement modes as

$$\begin{bmatrix} \mathbf{K}^s_{uu} & \mathbf{0} \\ \mathbf{0} & -\mathbf{K}^{\sigma}_{ee} \end{bmatrix} \begin{bmatrix} \mathbf{v}^u_{\mathrm{w}}\psi \\ \mathbf{v}^e_{\mathrm{w}}\psi'' \end{bmatrix} - \begin{bmatrix} \bar{\mathbf{K}}^{\tau}_{uu} & -\bar{\mathbf{K}}^{\sigma}_{ue} \\ -\bar{\mathbf{K}}^{\sigma}_{eu} & -\bar{\mathbf{K}}^{\sigma}_{ee} \end{bmatrix} \begin{bmatrix} \mathbf{v}^u_{\mathrm{w}}\psi \\ \mathbf{v}^e_{\mathrm{w}}\psi'' \end{bmatrix}'' = \begin{bmatrix} \mathbf{r}^{\alpha u3}_{\mathrm{w}} \\ \mathbf{r}^{e3}_{\mathrm{w}} \end{bmatrix} \phi + \begin{bmatrix} \bar{\mathbf{r}}^{\alpha u3}_{\Omega} \\ \mathbf{r}^{e3}_{\Omega} \end{bmatrix} \phi' \tag{4.48}$$

The block matrices and the transformed stiffness matrices are found in chapter 3 and the load vectors are given in Table 4.5.

$\mathbf{r}^{\alpha u3}_{\mathrm{w}} = \mathbf{r}^{u\alpha}_{\mathrm{w}} - \mathbf{K}^{\tau}_{u3} {K^{\tau}_{33}}^{-1} r^3_{\mathrm{w}}$	$\mathbf{r}^{e3}_{\mathrm{w}} = \mathbf{r}^{e}_{\mathrm{w}} + \mathbf{K}^{\sigma}_{e3} {K^{\tau}_{33}}^{-1} r^3_{\mathrm{w}}$
$\bar{\mathbf{r}}^{\alpha u3}_{\Omega} = \bar{\mathbf{r}}^{u\alpha}_{\Omega} - \mathbf{K}^{\tau}_{u3} {K^{\tau}_{33}}^{-1} \bar{r}^3_{\Omega}$	$\mathbf{r}^{e3}_{\Omega} = \mathbf{r}^{e}_{\Omega} + \mathbf{K}^{\sigma}_{e3} {K^{\tau}_{33}}^{-1} \bar{r}^3_{\Omega}$

Table 4.5: Transformation of load vectors related to Step III.

4.4 Solution of distortional equations

The distortional eigenvalue problem for the homogeneous system of equations (4.48) was solved in chapter 3. Here the eigenvalues, $\lambda_i = \xi_i^2$, and the corresponding eigenvectors was given by

$$\begin{bmatrix} \mathbf{v}^u_{\mathrm{w}} \\ \mathbf{v}^e_{\mathrm{w}}\xi^2 \end{bmatrix}_i = \begin{bmatrix} \mathbf{v}^u_{\mathrm{w}i} \\ \mathbf{v}^e_{\mathrm{w}i}{\xi_i}^2 \end{bmatrix} \tag{4.49}$$

In the present context these eigenvectors can be used to decouple the system of equations in (4.48). The i'th decoupled equation which determines the axial variation $\psi_{di}(z)$ of the distortional eigenvector is found by inserting the i'th

eigenvector and pre-multiplying with it, which results in the following equation:

$$\begin{bmatrix} \mathbf{v}_{\mathrm{w}}^{u} \\ \mathbf{v}_{\mathrm{w}}^{e}\xi^{2} \end{bmatrix}_{i}^{T} \begin{bmatrix} \mathbf{K}_{uu}^{s} & \mathbf{0} \\ \mathbf{0} & -\mathbf{K}_{ee}^{\sigma} \end{bmatrix} \begin{bmatrix} \mathbf{v}_{\mathrm{w}}^{u} \\ \mathbf{v}_{\mathrm{w}}^{e}\xi^{2} \end{bmatrix}_{i} \psi_{di} - \begin{bmatrix} \mathbf{v}_{\mathrm{w}}^{u} \\ \mathbf{v}_{\mathrm{w}}^{e}\xi^{2} \end{bmatrix}_{i}^{T} \begin{bmatrix} \bar{\mathbf{K}}_{uu}^{\tau} & -\bar{\mathbf{K}}_{ue}^{\sigma} \\ -\bar{\mathbf{K}}_{eu}^{\sigma} & -\bar{\mathbf{K}}_{ee}^{\sigma} \end{bmatrix} \begin{bmatrix} \mathbf{v}_{\mathrm{w}}^{u} \\ \mathbf{v}_{\mathrm{w}}^{e}\xi^{2} \end{bmatrix}_{i} \psi_{di}{}'' = \begin{bmatrix} \mathbf{v}_{\mathrm{w}}^{u} \\ \mathbf{v}_{\mathrm{w}}^{e}\xi^{2} \end{bmatrix}_{i}^{T} \begin{bmatrix} \mathbf{r}_{\mathrm{w}}^{\alpha u 3} \\ \mathbf{r}_{\mathrm{w}}^{e3} \end{bmatrix} \phi + \begin{bmatrix} \mathbf{v}_{\mathrm{w}}^{u} \\ \mathbf{v}_{\mathrm{w}}^{e}\xi^{2} \end{bmatrix}_{i}^{T} \begin{bmatrix} \bar{\mathbf{r}}_{\Omega}^{\alpha u 3} \\ \mathbf{r}_{\Omega}^{e3} \end{bmatrix} \phi' \quad (4.50)$$

which we abbreviate as

$$K_{ii}^{g}\psi_{di} - K_{ii}^{d}\psi_{di}{}'' = r_{\mathrm{w}i}^{d}\phi + r_{\Omega i}^{d}\phi' \quad (4.51)$$

For the $i'th$ distortional equation, $r_{\mathrm{w}i}^{d}$ can alternatively be determined as $r_{\mathrm{w}i}^{d} = \mathbf{V}_{\mathrm{w}i}^{T}\mathbf{r}_{\mathrm{w}}$ which means the cross-section deformation mode (equation (3.84)) multiplied by the load vector $\mathbf{r}_{w}$ (equation (4.10)) in the initial degrees of freedom. Equivalent we can write $r_{\Omega i}^{d} = \mathbf{V}_{\Omega i}^{T}\mathbf{r}_{\Omega}$ which means the cross-section warping mode (equation (3.84)) multiplied by the load vector r_{ω} (equation (4.9)) in the initial degrees of freedom. This gives exactly the same values and signs as found from the transformations. This also applies to the eliminated modes. The loads in the orthogonal equations for all the modes can be determined in the same way.

Normalizing equation (4.51) and introducing that the eigenvalue ${\xi_i}^2$ is equal to K_{ii}^{g}/K_{ii}^{d}, it takes the following standard form

$$\psi_{di}{}'' - {\xi_i}^2\psi_{di} = -\frac{1}{K_{ii}^{d}}(r_{\mathrm{w}i}^{d}\phi + r_{\Omega i}^{d}\phi') \quad (4.52)$$

The above introduced distortional stiffness and load terms are given in Table 4.6. Note that $r_{\mathrm{w}i}^{d}\psi$ is the distortional moment load and $r_{\Omega i}^{d}\psi'$ is the distortional bimoment load.

$K_{ii}^{d} = \begin{bmatrix} \mathbf{v}_{\mathrm{w}}^{u} \\ \mathbf{v}_{\mathrm{w}}^{e}\xi^{2} \end{bmatrix}_{i}^{T} \begin{bmatrix} \bar{\mathbf{K}}_{uu}^{\tau} & -\bar{\mathbf{K}}_{ue}^{\sigma} \\ -\bar{\mathbf{K}}_{eu}^{\sigma} & -\bar{\mathbf{K}}_{ee}^{\sigma} \end{bmatrix} \begin{bmatrix} \mathbf{v}_{\mathrm{w}}^{u} \\ \mathbf{v}_{\mathrm{w}}^{e}\xi^{2} \end{bmatrix}_{i}$	$r_{\mathrm{w}i}^{d} = \begin{bmatrix} \mathbf{v}_{\mathrm{w}}^{u} \\ \mathbf{v}_{\mathrm{w}}^{e}\xi^{2} \end{bmatrix}_{i}^{T} \begin{bmatrix} \mathbf{r}_{\mathrm{w}}^{\alpha u 3} \\ \mathbf{r}_{\mathrm{w}}^{e3} \end{bmatrix}$
$K_{ii}^{g} = {\xi_i}^2 K_{ii}^{d} = \begin{bmatrix} \mathbf{v}_{\mathrm{w}}^{u} \\ \mathbf{v}_{\mathrm{w}}^{e}\xi^{2} \end{bmatrix}_{i}^{T} \begin{bmatrix} \mathbf{K}_{uu}^{s} & \mathbf{0} \\ \mathbf{0} & -\mathbf{K}_{ee}^{\sigma} \end{bmatrix} \begin{bmatrix} \mathbf{v}_{\mathrm{w}}^{u} \\ \mathbf{v}_{\mathrm{w}}^{e}\xi^{2} \end{bmatrix}_{i}$	$r_{\Omega i}^{d} = \begin{bmatrix} \mathbf{v}_{\mathrm{w}}^{u} \\ \mathbf{v}_{\mathrm{w}}^{e}\xi^{2} \end{bmatrix}_{i}^{T} \begin{bmatrix} \bar{\mathbf{r}}_{\Omega}^{\alpha u 3} \\ \mathbf{r}_{\Omega}^{e3} \end{bmatrix}$

Table 4.6: Modal distortional stiffness and load terms.

We find that the full solution of each of these uncoupled non-homogeneous

linear second-order differential equations is given by

$$\begin{aligned}\psi_{di}(z) = {} & c_1 e^{\xi_i z} + c_2 e^{-\xi_i z} \\ & - \frac{1}{2\xi_i} e^{\xi_i z} \int e^{-\xi_i z} \frac{1}{K_{ii}^d} (r_{\mathrm{w}i}^d \phi + r_{\Omega i}^d \phi') \, dz \\ & + \frac{1}{2\xi_i} e^{-\xi_i z} \int e^{\xi_i z} \frac{1}{K_{ii}^d} (r_{\mathrm{w}i}^d \phi + r_{\Omega i}^d \phi') \, dz\end{aligned} \tag{4.53}$$

Using that ϕ is a linear function as given in equation (4.23) and performing integration or by guessing the solution we get

$$\psi_{d\,i}(z) = \mathbf{\Psi}_{dh\,i}(z)\ \mathbf{c}_{d\,i} + \mathbf{\Psi}_{dp\,i}(z)\ \phi \tag{4.54}$$

Here $\mathbf{c}_{di}$ is a vector containing the two constants $c_{d\,2i-1}$ and $c_{d\,2i}$ of the homogeneous part of the solution, and

$$\mathbf{\Psi}_{dp\,i}(z) = \mathbf{\Psi}_{dp\,i}^{\mathrm{w}}(z) + \mathbf{\Psi}_{dp\,i}^{\Omega}(z) \tag{4.55}$$

$$\mathbf{\Psi}_{dh\,i}(z) = \begin{bmatrix} e^{\xi_i z} & e^{-\xi_i z} \end{bmatrix} \tag{4.56}$$

$$\mathbf{\Psi}_{dp\,i}^{\mathrm{w}} = \frac{r_{\mathrm{w}i}^d}{{\xi_i}^2 K_{ii}^d} \begin{bmatrix} 1 - \frac{z}{L} & \frac{z}{L} \end{bmatrix} \tag{4.57}$$

$$\mathbf{\Psi}_{dp\,i}^{\Omega} = \frac{r_{\Omega i}^d}{{\xi_i}^2 K_{ii}^d} \begin{bmatrix} \frac{-1}{L} & \frac{1}{L} \end{bmatrix} \tag{4.58}$$

This concludes the determination of all the solutions for all the displacement modes of GBT.

4.5 Assembly of the full solution

The axial variation of the four beam modes have been identified in equations (4.24), (4.30) and (4.43) and can be assembled in the beam solution function matrices $\mathbf{\Psi}_{bh}(z)$ and $\mathbf{\Psi}_{bp}(z)$ which are multiplied by the vector of beam displacement constants $\mathbf{c}_b$ and the load vector ϕ, respectively. This results in

$$\mathbf{\Psi}_{bh}(z)\,\mathbf{c}_b + \mathbf{\Psi}_{bp}(z)\,\phi \begin{bmatrix} \mathbf{\Psi}_{ah}(z) & \mathbf{0} & \mathbf{0} \\ \mathbf{0} & \mathbf{\Psi}_{\alpha h}(z) & \mathbf{0} \\ \mathbf{0} & \mathbf{0} & \mathbf{\Psi}_{3h}(z) \end{bmatrix} \begin{bmatrix} \mathbf{c}_a \\ \mathbf{c}_\alpha \\ \mathbf{c}_3 \end{bmatrix} + \begin{bmatrix} \mathbf{\Psi}_{ap}(z) \\ \mathbf{\Psi}_{\alpha p}(z) \\ \mathbf{\Psi}_{3p}(z) \end{bmatrix} \phi \tag{4.59}$$

where

$$\mathbf{\Psi}_{\alpha h}(z) = \begin{bmatrix} \mathbf{\Psi}_{1h}(z) & \mathbf{0} \\ \mathbf{0} & \mathbf{\Psi}_{2h}(z) \end{bmatrix} \tag{4.60}$$

$$\mathbf{\Psi}_{\alpha p}(z) = \begin{bmatrix} \mathbf{\Psi}_{1p}(z) \\ \mathbf{\Psi}_{2p}(z) \end{bmatrix} \tag{4.61}$$

Furthermore, the distortional solution functions can be assembled and described as

$$\boldsymbol{\Psi}_{dh}(z)\mathbf{c}_d + \boldsymbol{\Psi}_{dp}(z)\phi = \begin{bmatrix} \boldsymbol{\Psi}_{dh\,1}(z) & \mathbf{0} & \mathbf{0} & \cdots \\ \mathbf{0} & \boldsymbol{\Psi}_{dh\,2}(z) & \mathbf{0} & \cdots \\ \mathbf{0} & \mathbf{0} & \boldsymbol{\Psi}_{dh\,3}(z) & \cdots \\ \vdots & \vdots & \vdots & \ddots \end{bmatrix} \begin{bmatrix} \mathbf{c}_{d\,1} \\ \mathbf{c}_{d\,2} \\ \mathbf{c}_{d\,3} \\ \vdots \end{bmatrix} + \begin{bmatrix} \boldsymbol{\Psi}_{dp\,1}(z) \\ \boldsymbol{\Psi}_{dp\,2}(z) \\ \boldsymbol{\Psi}_{dp\,3}(z) \\ \vdots \end{bmatrix} \phi \tag{4.62}$$

Now, all the solution functions are obtained and can be assembled using the previously defined block matrices and vectors as

$$\boldsymbol{\Psi}_h(z)\mathbf{c} + \boldsymbol{\Psi}_p(z)\phi \tag{4.63}$$

in which

$$\boldsymbol{\Psi}_h(z)\,\mathbf{c} = \begin{bmatrix} \boldsymbol{\Psi}_{bh}(z) & \mathbf{0} \\ \mathbf{0} & \boldsymbol{\Psi}_{dh}(z) \end{bmatrix} \begin{bmatrix} \mathbf{c}_b \\ \mathbf{c}_d \end{bmatrix} \tag{4.64}$$

and

$$\boldsymbol{\Psi}_p(z)\,\phi = \begin{bmatrix} \boldsymbol{\Psi}_{bp}(z) \\ \boldsymbol{\Psi}_{dp}(z) \end{bmatrix} \phi \tag{4.65}$$

As we are using the in-plane modes found in chapter 3, the back-substitution process of distortional and eliminated beam displacement in-plane modes is identical to the process performed in that chapter. Hereby all the in-plane modes are assembled column-wise in a modal matrix of transverse displacement vectors $\mathbf{V}_{\mathrm{w}}$ and a modal matrix of axial warping displacement vectors $\mathbf{V}_{\Omega}$, by joining the modal matrices of the beam eigenvectors and the distortional eigenvectors as

$$\mathbf{V}_{\mathrm{w}} = \begin{bmatrix} \mathbf{V}_{\mathrm{w}}^{b} & \mathbf{V}_{\mathrm{w}}^{d} \end{bmatrix} \qquad \mathbf{V}_{\Omega} = \begin{bmatrix} \mathbf{V}_{\Omega}^{b} & \mathbf{V}_{\Omega}^{d} \end{bmatrix} \tag{4.66}$$

Having obtained and assembled all the full solution functions and in-plane modes, the full solution along the beam can be presented in the nodal solution vectors $\mathbf{u}_{\mathrm{w}}(z)$ and $\mathbf{u}_{\Omega}(z)$ as follows:

$$\begin{aligned} \mathbf{u}_{\mathrm{w}}(z) &= \mathbf{V}_{\mathrm{w}}\big[\boldsymbol{\Psi}_h(z)\,\mathbf{c} + \boldsymbol{\Psi}_p(z)\phi\big] \\ \mathbf{u}_{z}(z) &= -\mathbf{V}_{\Omega}\big[\boldsymbol{\Psi}_h'(z)\,\mathbf{c} + \boldsymbol{\Psi}_p'(z)\phi\big] \end{aligned} \tag{4.67}$$

The constants, $\mathbf{c}$, have to be determined by the boundary conditions of the prismatic thin-walled beam.

4.5.1 Transformation to real modes and real solution functions

Also from the non-homogeneous equations some of the distortional solution functions found are complex. Because these complex numbers are awkward to handle it is a matter of considerable importance to construct a more convenient complete solution when we have complex numbers. In subsection 3.7.2 we introduced the following notation for the positive square root values and the related eigenvector columns $\mathbf{v}_j$ and $\mathbf{v}_{j+1}$:

$$\xi_j = \lambda_j + \mu_j i \quad \xi_{j+1} = \bar{\xi}_j = \lambda_j - \mu_j i \tag{4.68}$$

$$\mathbf{v}_j = \mathbf{a}_j + \mathbf{b}_j i \quad \mathbf{v}_{j+1} = \bar{\mathbf{v}}_j = \mathbf{a}_j - \mathbf{b}_j i \tag{4.69}$$

in which we have introduced the real and imaginary parts of the eigenvalues and eigenvectors. The complex eigenvectors in equation (4.69) may be conveniently written as

$$\begin{bmatrix}\mathbf{v}_j & \mathbf{v}_{j+1}\end{bmatrix} = \begin{bmatrix}\mathbf{a}_j & \mathbf{b}_j\end{bmatrix} \begin{bmatrix}1 & 1\\ i & -i\end{bmatrix} \tag{4.70}$$

The constants of the related parts of the homogeneous solution are also complex quantities. However, we are able to assemble the two complex conjugated modal solutions into two real (but pairwise coupled) solutions by introducing the real constant vectors $\widetilde{\mathbf{c}}_j$ and $\widetilde{\mathbf{c}}_{j+1}$ as follows:

$$\begin{bmatrix}\mathbf{c}_j\\ \mathbf{c}_{j+1}\end{bmatrix} = \tfrac{1}{2}\begin{bmatrix}1 & -i\\ 1 & i\end{bmatrix} \begin{bmatrix}\widetilde{\mathbf{c}}_j\\ \widetilde{\mathbf{c}}_{j+1}\end{bmatrix} \tag{4.71}$$

The j'th complex part of the full solution in equation (4.67) can now be rewritten using the transformations in equations (4.70) and (4.71). After multiplication and identification of real and imaginary parts we find the following result:

$$\begin{aligned}&\begin{bmatrix}\mathbf{v}_j & \mathbf{v}_{j+1}\end{bmatrix} \left\{ \begin{bmatrix}\boldsymbol{\Psi}_{dh_j} & \mathbf{0}\\ \mathbf{0} & \overline{\boldsymbol{\Psi}}_{dh_j}\end{bmatrix} \begin{bmatrix}\mathbf{c}_j\\ \mathbf{c}_{j+1}\end{bmatrix} + \begin{bmatrix}\boldsymbol{\Psi}_{dp_j}\\ \overline{\boldsymbol{\Psi}}_{dp_j}\end{bmatrix} \begin{bmatrix}\phi_1\\ \phi_2\end{bmatrix} \right\}\\ &= \begin{bmatrix}\mathbf{a}_j & \mathbf{b}_j\end{bmatrix} \left\{ \begin{bmatrix}\mathrm{Re}(\boldsymbol{\Psi}_{dh\,j}) & \mathrm{Im}(\boldsymbol{\Psi}_{dh\,j})\\ \mathrm{Im}(\overline{\boldsymbol{\Psi}}_{dh\,j}) & \mathrm{Re}(\overline{\boldsymbol{\Psi}}_{dh\,j})\end{bmatrix} \begin{bmatrix}\widetilde{\mathbf{c}}_j\\ \widetilde{\mathbf{c}}_{j+1}\end{bmatrix} + \begin{bmatrix}2\mathrm{Re}(\boldsymbol{\Psi}_{dp\,j})\\ -2\mathrm{Im}(\overline{\boldsymbol{\Psi}}_{dp\,j})\end{bmatrix} \begin{bmatrix}\phi_1\\ \phi_2\end{bmatrix} \right\}\end{aligned} \tag{4.72}$$

Hereby it is possible to rewrite the complex quantities into real quantities. Now the modal matrices $\mathbf{V}_{\mathrm{w}}$ and $\mathbf{V}_{\Omega}$ are modified as $\widetilde{\mathbf{V}}_{\mathrm{w}}$ and $\widetilde{\mathbf{V}}_{\Omega}$ by substituting the complex pairs of eigenvectors with their respective real and imaginary parts. Furthermore, we also introduce the modified solution matrices $\widetilde{\boldsymbol{\Psi}}_{dh}$ and $\widetilde{\boldsymbol{\Psi}}_{dp}$ and the related modified vector of constants $\widetilde{\mathbf{c}}$ by substituting the solutions (and constants) of the complex pairs using equation (4.72). Now the full solution

along the beam can be written using real numbers as

$$\begin{aligned} \mathbf{u}_{\mathrm{w}}(z) &= \widetilde{\mathbf{V}}_{\mathrm{w}}\left[\widetilde{\mathbf{\Psi}}_h(z)\,\widetilde{\mathbf{c}} + \widetilde{\mathbf{\Psi}}_p(z)\,\phi\right] \\ \mathbf{u}_z(z) &= -\widetilde{\mathbf{V}}_{\Omega}\left[\widetilde{\mathbf{\Psi}}'_h(z)\,\widetilde{\mathbf{c}} + \widetilde{\mathbf{\Psi}}'_p(z)\,\phi\right] \end{aligned} \tag{4.73}$$

It is possible now to work with this real formulation or continue working with complex numbers using the full solution formulated in equation (4.67). In the following context we will use the real formulation in equation (4.73).

4.6 Displacement boundary conditions

In this section we will introduce a method for determining the constants of the non-homogeneous solutions found. This is to be done in the GBT space, which has been constrained by the relevant assumptions of the beam theory. As seen from the first variation of the potential energy, the natural boundary displacements of the GBT at each boundary are the pure axial displacement u^a_Ω of the beam, the transverse displacements $\mathbf{u}^g_{\mathrm{w}}$, and the axial derivative of the transverse displacements $\mathbf{u}^{g\,\prime}_{\mathrm{w}}$. In the following the generalized internal displacements of the GBT beam will be expressed by using the transformation from FE to GBT displacements as follows:

$$\begin{bmatrix} u^a_z(z) \\ \mathbf{u}^g_{\mathrm{w}}(z) \\ \mathbf{u}^{g\,\prime}_{\mathrm{w}}(z) \end{bmatrix} = \begin{bmatrix} -\mathbf{T}^{a\,T}_{\Omega}\widetilde{\mathbf{V}}_{\Omega}\widetilde{\mathbf{\Psi}}'_h(z) \\ \mathbf{T}^{g\,T}_{\mathrm{w}}\widetilde{\mathbf{V}}_{\mathrm{w}}\widetilde{\mathbf{\Psi}}_h(z) \\ \mathbf{T}^{g\,T}_{\mathrm{w}}\widetilde{\mathbf{V}}_{\mathrm{w}}\widetilde{\mathbf{\Psi}}'_h(z) \end{bmatrix} \widetilde{\mathbf{c}} + \begin{bmatrix} -\mathbf{T}^{a\,T}_{\Omega}\widetilde{\mathbf{V}}_{\Omega}\widetilde{\mathbf{\Psi}}'_p(z) \\ \mathbf{T}^{g\,T}_{\mathrm{w}}\widetilde{\mathbf{V}}_{\mathrm{w}}\widetilde{\mathbf{\Psi}}_p(z) \\ \mathbf{T}^{g\,T}_{\mathrm{w}}\widetilde{\mathbf{V}}_{\mathrm{w}}\widetilde{\mathbf{\Psi}}'_p(z) \end{bmatrix} \phi \tag{4.74}$$

To determine the constants using displacement boundary conditions as in finite element or stiffness formulations, the boundary displacements at the two ends of a finite length beam are needed , i.e. at $z = 0$ and at $z = L$, where L is the length of the beam. The assembled boundary displacement vector is denoted by $\mathbf{u}_b$. This leads to the following equation for the determination of the solution constants:

$$\mathbf{u}_b = \begin{bmatrix} u^a_z(0) \\ \mathbf{u}^g_{\mathrm{w}}(0) \\ \mathbf{u}^{g\,\prime}_{\mathrm{w}}(0) \\ u^a_z(L) \\ \mathbf{u}^g_{\mathrm{w}}(L) \\ \mathbf{u}^{g\,\prime}_{\mathrm{w}}(L) \end{bmatrix} = \begin{bmatrix} -\mathbf{T}^{a\,T}_{\Omega}\widetilde{\mathbf{V}}_{\Omega}\widetilde{\mathbf{\Psi}}'_h(0) \\ \mathbf{T}^{g\,T}_{\mathrm{w}}\widetilde{\mathbf{V}}_{\mathrm{w}}\widetilde{\mathbf{\Psi}}_h(0) \\ \mathbf{T}^{g\,T}_{\mathrm{w}}\widetilde{\mathbf{V}}_{\mathrm{w}}\widetilde{\mathbf{\Psi}}'_h(0) \\ -\mathbf{T}^{a\,T}_{\Omega}\widetilde{\mathbf{V}}_{\Omega}\widetilde{\mathbf{\Psi}}'_h(L) \\ \mathbf{T}^{g\,T}_{\mathrm{w}}\widetilde{\mathbf{V}}_{\mathrm{w}}\widetilde{\mathbf{\Psi}}_h(L) \\ \mathbf{T}^{g\,T}_{\mathrm{w}}\widetilde{\mathbf{V}}_{\mathrm{w}}\widetilde{\mathbf{\Psi}}'_h(L) \end{bmatrix} \widetilde{\mathbf{c}} + \begin{bmatrix} -\mathbf{T}^{a\,T}_{\Omega}\widetilde{\mathbf{V}}_{\Omega}\widetilde{\mathbf{\Psi}}'_p(0) \\ \mathbf{T}^{g\,T}_{\mathrm{w}}\widetilde{\mathbf{V}}_{\mathrm{w}}\widetilde{\mathbf{\Psi}}_p(0) \\ \mathbf{T}^{g\,T}_{\mathrm{w}}\widetilde{\mathbf{V}}_{\mathrm{w}}\widetilde{\mathbf{\Psi}}'_p(0) \\ -\mathbf{T}^{a\,T}_{\Omega}\widetilde{\mathbf{V}}_{\Omega}\widetilde{\mathbf{\Psi}}'_p(L) \\ \mathbf{T}^{g\,T}_{\mathrm{w}}\widetilde{\mathbf{V}}_{\mathrm{w}}\widetilde{\mathbf{\Psi}}_p(L) \\ \mathbf{T}^{g\,T}_{\mathrm{w}}\widetilde{\mathbf{V}}_{\mathrm{w}}\widetilde{\mathbf{\Psi}}'_p(L) \end{bmatrix} \phi = \widetilde{\mathbf{A}}\widetilde{\mathbf{c}} + \widetilde{\mathbf{B}}\phi$$

$$\Rightarrow \quad \widetilde{\mathbf{c}} = \widetilde{\mathbf{A}}^{-1}(\mathbf{u}_b - \widetilde{\mathbf{B}}\phi) \tag{4.75}$$

where we have introduced the matrix $\widetilde{\mathbf{A}}$ and $\widetilde{\mathbf{B}}$, where $\widetilde{\mathbf{A}}$ is an invertible positive definite "square" matrix. To avoid numerical problems the exponential solution functions in $\widetilde{\mathbf{\Psi}}_h(z)$ may have to be modified by replacing $\widetilde{c}_i e^{\xi_i z}$ by $\hat{c}_i e^{\xi_i (z-L)}$ so that the positive $\xi_i z$ exponent is bounded.

To see the effect of the load as it would be in a finite element context with built in edges, we choose to plot the solution by using equation (4.73), with all boundary displacements being zero (built in) as

$$\mathbf{u}_b^T = \begin{bmatrix} 0 & \mathbf{0} & \mathbf{0} & 0 & \mathbf{0} & \mathbf{0} \end{bmatrix}^T \tag{4.76}$$

This is done in the following example.

4.7 Example

In this section an example is given and nodal displacement results as well as stress distribution results of GBT are compared to those found using the commercial FE program `Abaqus`. In this example a lipped channel cross section is loaded by a distortional load as shown in Figure 4.3 and fixed at both ends. The load are uniformly distributed and thus given by a cross-section load distribution multiplied by $\phi(z) = 1$. The beam has a length of $L = 2000\ mm$, an elasticity modulus $E = 2.1 \cdot 10^5$ MPa and a Poisson ratio of $\nu = 0.3$. For more examples see the related Paper II (Andreassen and Jönsson, 2012b).

The results found using `Abaqus` are based on isotropic material and the S4 shell element with full 4 point integration. The linear elastic finite element calculations are based on a structured rectangular mesh with a side length seed of 5 mm.

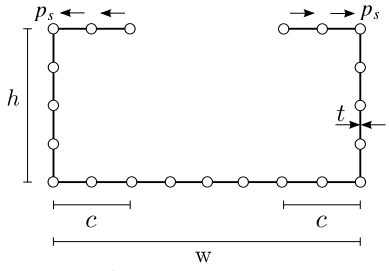

$h = 50$
w $= 100$
$c = 25$
$t = 2.0$
$p_s = 0.1\ N/mm^2$
○ Node

Figure 4.3: Geometry, parameter values and distributed distortional load for the lipped channel.

Solving the equations leads to the GBT deformation solution shown in Figure 4.4, which has displacements of the lips in both transverse coordinate directions with the maximum value at mid-span. It is seen that the distortional deformation dominates and that the boundary conditions give raise to relatively local

end effects, whereas the deformations around mid-span are relatively constant. Comparing the nodal displacements of the node marked in Figure 4.4 to the dis-

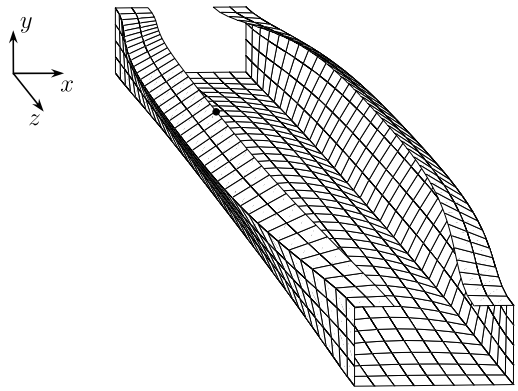

Figure 4.4: GBT plot of the lipped channel with a distortional load.

placements found using a model in the commercial FE program Abaqus gives the displacement values and the corresponding deviations shown in Table 4.7. Here the deviation according to the maximum displacement in the horizontal direction, u_x, is 0.2% and the deviation for the vertical direction, u_y, is 0.4%. We also want a comparison between the stress distributions obtained with GBT

	GBT [mm]	Abaqus [mm]	Difference [%]
u_x	−2.847	−2.841	0.2
u_y	2.093	2.084	0.4

Table 4.7: Nodal displacements of GBT and FE analysis.

and Abaqus. In order to have comparable values different from zero the results concerning the axial normal stresses are obtained from the end section. A comparison of the axial membrane stresses in the z direction are shown in Figure 4.5 and shows a maximum deviation of 7.9% as given in Table 4.8. This

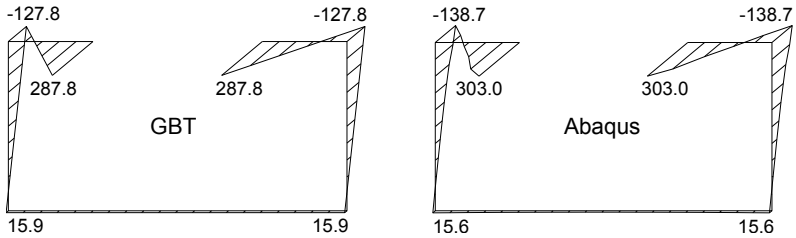

Figure 4.5: Comparison between the axial normal stress distributions obtained with GBT and Abaqus at the end of the beam. All values are in MPa.

	GBT [MPa]	Abaqus [MPa]	Difference [%]
σ_z	127.7	138.7	7.9
σ_s	197.2	196.9	0.2

Table 4.8: Stress distributions of GBT and FE analysis.

deviation can be explained by shear lag as the results are here from the end section. The transverse bending stresses at mid-span are shown in Figure 4.6. Here the maximum deviation is 0.2 % and obtained at the corner in the bottom.

The chosen examples given here and in Paper II (Andreassen and Jönsson, 2012b) show solutions which are applicable to finite element formulation of a future distortional beam element with applied loads, i.e. with fixed boundary conditions. The examples also show that shear deformation is only included for "Bredt's shear flow" around closed cells and the presented theory does not include shear lag effects. However, these and other effects may be included as extensions in approximate energy based finite element formulations which may be used to extend the capabilities of beam elements.

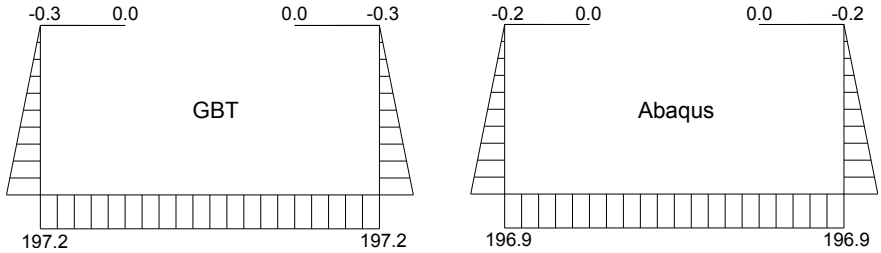

Figure 4.6: Comparison between the transverse bending stress distributions obtained with GBT and Abaqus at mid-span. All values are in MPa.

4.8 Concluding remarks

In this chapter the homogeneous differential equations as well as the full analytical solution along the beam have been extended to also hold the particular part which means that loads can be taken into account in the context of the non-homogeneous differential equations and associated full solution along the beam. By using the distortional modal matrix found for the homogeneous system we have transformed the non-homogeneous distortional differential equations into the eigenmode space, and then obtained the uncoupled set of differential equations including the distributed loads. The novel approach now gives the full analytical solution of the GBT equations with distributed loads for a given discretization of the cross section.

Having developed and solved the distortional homogeneous and non-homogeneous differential equations as well as the associated full analytical solution along the beam we will in the next chapter continue with initial stress contributions to perform linear distortional buckling analyzes.

Chapter 5

Distortional stability differential equations and solutions

An assessment of the structural performance of thin-walled beams includes linear static analyzes and linear buckling analyzes of the behavior. Linear buckling analysis is used to achieve an estimate of the load level at which certain types of structures exhibit a loss of stability through large non-linear deformations. Typically for these structures membrane strain energy is converted into flexural strain energy with very little change in externally applied load. In slender columns and thin plates or shells, the membrane stiffness is much greater than the bending stiffness, and large strain energy can be stored with very small membrane deformations. Therefore the deformations of the fundamental state are neglected and the displacements are measured from the initial perfect configuration. As the membrane stiffness is much greater than bending stiffness, comparatively large bending deformations are needed to absorb the membrane strain energy released when buckling occurs. In most buckling cases of practical interest this means that the geometric stiffness term (for compressional loading) gives a negative contribution to the total stiffness. In other words, instability may be considered at the load level at which added elastic stiffness terms are fully neutralized by a change in added negative geometric stiffness terms in the potential energy. In this chapter we therefore include initial stress contributions to the potential energy which allow us to perform linear distortional buckling analysis of semi-discretized prismatic thin-walled members.

The classical stability analysis of thin-walled columns is based on a combination of the "in-plane rigid" cross-section displacement modes (Vlasov modes, Vlasov (1961)) corresponding to: uniform axial extension, major axis bending, minor axis bending and torsion with related warping. An important feature missing here is the deformation of the cross section, which undergoes in-plane

deformations by local and distortional modes.

This chapter which is related to Paper III (Andreassen and Jönsson, 2012a) deals with the novel method based on solution of the differential initial stress equations of GBT obtained through semi-discretization and application of beam constraints. Thus, in order to take stability into account, this chapter deals with the extension of the homogeneous differential equations to also hold the geometrical stiffness (stability) terms based on the initial stress approach.

As in the previous chapters the potential energy of a single deformation mode is formulated based on the discretization of the cross section. However, through variations in the potential energy and the introduction of the well known constraints related to beam theory this leads to a modified set of coupled homogeneous differential equations of GBT with initial stress for identification of distortional buckling modes.

In this chapter we seek "simple" instability solutions using GBT initial stress equations for the classical simply supported columns with constrained transverse displacements at the end sections and a constant axial initial stress. Based on the known boundary conditions the reduced order differential equations are solved by introducing the relevant trigonometric solution function and solving the related eigenvalue problem. This directly gives us the cross-section buckling mode shape and the eigenvalue corresponding to the bifurcation load factor. It is done as in conventional FSM without the use of modal decomposition as conventionally performed in GBT.

From the previous chapters it is seen that distortional displacements can be of a local character in which the length scale is typically equal to or less than the cross-section dimension or it can be non-local in which case the length scale is typically several times the cross-section dimension or even longer. In recent buckling literature and especially in codes there is a tendency, with respect to buckling, to distinguish between these two behaviors as distortional buckling and local buckling. In chapter 3 and 4 as well as Paper V (Andreassen and Jönsson, 2009) and Paper VI (Andreassen and Jönsson, 2011) we are operating with global, distortional non-local and distortional local modes when we define first-order displacement modes. However in this chapter which concerns buckling we have chosen to distinguish between distortional buckling and local buckling as in the recent codes and literature.

5.1 Energy assumptions and initial stress

First, the internal energy potential introduced in section 3 as well as section 4 are used in this section. This is besides the new contribution to the potential energy of the initial stress terms, which are adequate for distortional buckling analysis of prismatic thin-walled members.

The elastic energy potential is given in equation (3.13) as

$$\Pi_{int} = \int_V \left(\tfrac{1}{2}E\varepsilon_z^2 + \tfrac{1}{2}G\gamma^2 + \tfrac{1}{2}E_s\varepsilon_s^2\right)dV \tag{5.1}$$

Next let us introduce the contribution to the potential energy of a constant uniform initial stress σ^0 which is adequate for column buckling analysis. Following conventional methods the initial stress σ^0 will be scaled by a factor λ. After having utilized linear equilibrium of the pre-buckling state and neglected contribution corresponding to the squared strain term $\frac{1}{2}\lambda\sigma^0 u_{z,z}^2 = \frac{1}{2}\lambda\sigma^0\varepsilon^2$ the potential energy contribution of the factored initial stress is given by

$$\Pi_0 = \int_V \left(\tfrac{1}{2}\lambda\sigma^0 u_{s,z}^2 + \tfrac{1}{2}\lambda\sigma^0 u_{n,z}^2\right)dV = \int_V \left(\tfrac{1}{2}\lambda\sigma^0 (u_s{}')^2 + \tfrac{1}{2}\lambda\sigma^0 (u_n{}')^2\right)dV \tag{5.2}$$

Let us introduce a thin-walled cross section assembled by using straight cross-sectional elements. This allows us to integrate the internal energy across the volume of the prismatic thin-walled beam. The elastic potential energy of a single mode takes the form as given in equation (3.14) after the introduction of the strains expressed by the separated displacement functions.

The factored initial stress contribution of a single mode to the potential energy takes the following form after introduction of straight cross-sectional wall elements, displacement derivatives and integration through the thickness:

$$\Pi_0 = \tfrac{1}{2}\int_0^L \left[\sum_{el}\int_0^{b_{el}} \lambda\sigma^0\Big\{t(\mathrm{w}_n\psi')^2 + t(\mathrm{w}_s\psi')^2 + \tfrac{1}{12}t^3(\mathrm{w}_{n,s}\psi')^2\Big\}ds\right]dz \tag{5.3}$$

Introducing the displacement interpolation functions into the internal elastic potential energy leads to the definition of several stiffness sub-matrices as given in chapter 3, Table 3.1. After transformation of the individual wall elements to global degrees of freedom $\mathbf{v}_\mathrm{w}$ and $\mathbf{v}_\Omega$ and assembly, the cross-section elastic potential takes the form as given in equation (3.24).

Let us also perform the same operations with the initial stress contribution to the potential energy. The introduction of the displacement interpolations leads to the definition of the geometric stiffness matrix for a single wall element as follows:

$$\mathbf{k}^0 = \int_0^{b_e} \left\{t\sigma^0\left[\mathbf{N}_n^T\mathbf{N}_n\right] + t\sigma^0\left[\mathbf{N}_s{}^T\mathbf{N}_s\right] + \tfrac{1}{12}t^3\sigma^0\left[\mathbf{N}_{n,s}{}^T\mathbf{N}_{n,s}\right]\right\}ds \tag{5.4}$$

which written out in full takes the following form:

$$\mathbf{k}^0 = \frac{\sigma^0 tL}{12\cdot 35}\begin{bmatrix} 0 & 0 & 0 & 0 & 0 & 0 \\ 0 & 156 & 22L & 0 & 54 & -13L \\ 0 & 22L & 4L^2 & 0 & 13L & -3L^2 \\ 0 & 0 & 0 & 0 & 0 & 0 \\ 0 & 54 & 13L & 0 & 156 & -22L \\ 0 & -13L & -3L^2 & 0 & -22L & 4L^2 \end{bmatrix}$$

$$+\frac{\sigma^0 t}{360}\begin{bmatrix} 120L & 0 & 0 & 60L & 0 & 0 \\ 0 & \frac{36t^2}{L} & 3t^2 & 0 & -\frac{36t^2}{L} & 3t^2 \\ 0 & 3t^2 & 4Lt^2 & 0 & -3t^2 & -Lt^2 \\ 60L & 0 & 0 & 120L & 0 & 0 \\ 0 & -\frac{36t^2}{L} & -3t^2 & 0 & \frac{36t^2}{L} & -3t^2 \\ 0 & 3t^2 & -Lt^2 & 0 & -3t^2 & 4Lt^2 \end{bmatrix} \tag{5.5}$$

Transforming from local, $\mathbf{v}_{\mathrm{w}}^{el}$, to global, $\mathbf{v}_{\mathrm{w}}$, components using a standard formal finite element transformation and assembly matrix $\mathbf{T}_{\mathrm{w}}$ we get the following global geometrical stiffness matrix:

$$\mathbf{K}^0 = \sum_{el} \mathbf{T}_{\mathrm{w}}^T \mathbf{k}^0 \mathbf{T}_{\mathrm{w}} \tag{5.6}$$

Hereby equation (5.3) in reduced form can be rewritten as

$$\Pi_0 = \frac{1}{2}\int_0^L \left\{ \begin{bmatrix} \psi \mathbf{v}_{\mathrm{w}}^T & \psi \mathbf{v}_{\Omega}^T \end{bmatrix}' \begin{bmatrix} \lambda \mathbf{K}^0 & \mathbf{0} \\ \mathbf{0} & \mathbf{0} \end{bmatrix} \begin{bmatrix} \psi \mathbf{v}_{\mathrm{w}} \\ \psi \mathbf{v}_{\Omega} \end{bmatrix}' \right\} dz \tag{5.7}$$

which is the contribution to the potential energy from the factored initial stress.

5.2 GBT differential equations with initial stress

To obtain a formulation resembling a generalization of Vlasov beam theory including distortion, we have to perform the following three main steps again:

5.2.1 Step I: Pure axial extension and influence of shear constraints

In this step, we introduce the shear constraint equations that bind axial and transverse modes together and at the same time simplify or condense equation (3.24). In this process we need to eliminate the singularity in the shear stiffness matrix related to pure axial extension. Performing step I as in section 3.4.2 the differential equations governing the stability problem can be derived by

considering the first variation of the initial stress contributions to the potential energy in the same way as the first variation of the traditional elastic potential energy provided the differential equations in chapter 3 and 4.

$$\delta\Pi_0 = \int_0^L \left\{ \delta(\psi \mathbf{v}_\mathrm{w}^T)' \lambda \mathbf{K}^0 (\psi \mathbf{v}_\mathrm{w})' \right\} dz \tag{5.8}$$

After performing partial integration the variation of the initial stress contributions to the potential energy takes the form:

$$\delta\Pi_0 = \int_0^L \left\{ \delta(\psi \mathbf{v}_\mathrm{w}^T) \Big[-(\lambda \mathbf{K}^0 \mathbf{v}_\mathrm{w} \psi')' \Big] \right\} ds + \left[\delta(\psi \mathbf{v}_\mathrm{w}^T) \Big[\lambda \mathbf{K}^0 (\psi \mathbf{v}_\mathrm{w})' \Big] \right]_0^L \tag{5.9}$$

where the term in the square bracket correspond to the boundary loads and boundary conditions. As in chapter 3 the pure axial displacement mode is identified and denoted by superscript a and the remaining axial displacement modes by superscript r. Substituting $\delta\Pi_{int}$ from chapter 3, equation (3.34) leads to the following coupled homogeneous differential equations of GBT including initial stresses in which we note that $\zeta = -\psi'$:

$$\left(\bar{\mathbf{K}}^\sigma \mathbf{v}_\mathrm{w} \psi''\right)'' - \left(\mathbf{K}_{\Omega\Omega}^{\sigma ra} v_\Omega^a \zeta'\right)'' - \left(\left[\mathbf{K}^\tau \mathbf{v}_\mathrm{w} + \lambda \mathbf{K}^0 \mathbf{v}_\mathrm{w} \right] \psi' \right)' + \mathbf{K}^s \mathbf{v}_\mathrm{w} \psi = \mathbf{0} \tag{5.10}$$

$$\left(\mathbf{K}_{\Omega\Omega}^{\sigma ar} \mathbf{v}_\mathrm{w} \psi''\right)' - \left(\mathbf{K}_{\Omega\Omega}^{\sigma aa} v_\Omega^a \zeta'\right)' = \mathbf{0} \tag{5.11}$$

These equations establish a coupled set of homogeneous GBT differential equations, that determine the displacements of a prismatic thin-walled beam for a given set of boundary conditions. Note that v_Ω^a is one component that corresponds to the amount of pure axial extension.

Now we seek solutions to the equations. As in chapter 3 we can identify pure axial extension as a solution which takes the form as given in equation (3.38).

Having identified the "trivial" displacement mode (pure axial extension) we turn to the solution of the transverse displacement modes. Eliminating ζ'' by using the fact that $\zeta'' = -\psi'''$ and assuming that $\psi''' \neq 0$, we find:

$$v_\Omega^a = -(\mathbf{K}_{\Omega\Omega}^{\sigma aa})^{-1} \mathbf{K}_{\Omega\Omega}^{\sigma ar} \mathbf{v}_\mathrm{w} \tag{5.12}$$

Using this equation or equation (5.11), we eliminate the second term in equation (5.10). This results in the following homogeneous fourth-order differential equations for determination of the transverse (global, distortional, and local) distortional displacement modes of GBT:

$$\mathbf{K}^\sigma \mathbf{v}_\mathrm{w} \psi'''' - \left(\left[\mathbf{K}^\tau + \lambda \mathbf{K}^0 \right] \mathbf{v}_\mathrm{w} \psi' \right)' + \mathbf{K}^s \mathbf{v}_\mathrm{w} \psi = \mathbf{0} \tag{5.13}$$

where $\mathbf{K}^\sigma$, $\mathbf{K}^\tau$ and $\mathbf{K}^s$ which are constants are given in Table 3.2 and 3.3. In general $\mathbf{K}^0$ is a function of the axial coordinate z corresponding to the longitudinal contribution of the initial stress. However, in the present context the

initial stress will be assumed uniformly distributed and constant whereby $\mathbf{K}^0$ is also independent of the axial coordinate z and the equation simplifies to

$$\mathbf{K}^\sigma \mathbf{v}_\mathrm{w} \psi'''' - \left[\mathbf{K}^\tau + \lambda \mathbf{K}^0\right] \mathbf{v}_\mathrm{w} \psi'' + \mathbf{K}^s \mathbf{v}_\mathrm{w} \psi = \mathbf{0} \tag{5.14}$$

This set of GBT column stability equations resemble the conventional equation for classic column stability. Now the number of degrees of freedom is $n_{dof} = 3n_{no}$, since all (n_{no}) axial dofs $\mathbf{v}_\Omega$ have been eliminated by the shear constraint equation and the pure axial deformation mode.

5.2.2 Step II: Translations and constant wall width

In this step we treat two modes corresponding to transverse translations of the cross section and one mode corresponding to pure rotation. We also constrain the transverse displacement field so that the wall widths remain constant, i.e. we enforce $\mathrm{w}_{s,s} \equiv 0$.

Let us do this by first using the transformation given in equation (3.53).

Using this transformation to transform the differential equations in (5.14), and introducing the null terms corresponding to the rigid-body modes and zero shear strain for translational and flexural modes, the differential equations take the following form:

$$\begin{bmatrix} \mathbf{K}^\sigma_{\alpha\alpha} & \mathbf{0} & \mathbf{K}^\sigma_{\alpha u} \\ \mathbf{0} & K^\sigma_{33} & \mathbf{K}^\sigma_{3u} \\ \mathbf{K}^\sigma_{u\alpha} & \mathbf{K}^\sigma_{u3} & \mathbf{K}^\sigma_{uu} \end{bmatrix} \begin{bmatrix} \mathbf{v}^\alpha_\mathrm{w} \\ v^3_\mathrm{w} \\ \mathbf{v}^\mathbf{u}_\mathrm{w} \end{bmatrix} \psi'''' - \left(\begin{bmatrix} \mathbf{0} & \mathbf{0} & \mathbf{0} \\ \mathbf{0} & K^\tau_{33} & \mathbf{K}^\tau_{3u} \\ \mathbf{0} & \mathbf{K}^\tau_{u3} & \mathbf{K}^\tau_{uu} \end{bmatrix} + \lambda \begin{bmatrix} \mathbf{K}^0_{\alpha\alpha} & \mathbf{K}^0_{\alpha 3} & \mathbf{K}^0_{\alpha u} \\ \mathbf{K}^0_{3\alpha} & K^0_{33} & \mathbf{K}^0_{3u} \\ \mathbf{K}^0_{u\alpha} & \mathbf{K}^0_{u3} & \mathbf{K}^0_{uu} \end{bmatrix} \right) \begin{bmatrix} \mathbf{v}^\alpha_\mathrm{w} \\ v^3_\mathrm{w} \\ \mathbf{v}^\mathbf{u}_\mathrm{w} \end{bmatrix} \psi'' + \begin{bmatrix} \mathbf{0} & \mathbf{0} & \mathbf{0} \\ \mathbf{0} & 0 & \mathbf{0} \\ \mathbf{0} & \mathbf{0} & \mathbf{K}^s_{uu} \end{bmatrix} \begin{bmatrix} \mathbf{v}^\alpha_\mathrm{w} \\ v^3_\mathrm{w} \\ \mathbf{v}^\mathbf{u}_\mathrm{w} \end{bmatrix} \psi = \begin{bmatrix} \mathbf{0} \\ 0 \\ \mathbf{0} \end{bmatrix} \tag{5.15}$$

Here the transformed stiffness matrices are given in Table 3.4 and the $\mathbf{K}^0$-matrices are given in Table 5.1. Now the number of degrees of freedom depends on the geometry of the cross section. We have constrained the transverse displacement field so that the wall widths remain constant, i.e. we enforce $\mathrm{w}_{s,s} \equiv 0$. This means that a single w_s-dof is eliminated for each element in the cross section. For a lipped channel cross section with $n_{el} = n_{no} - 1$ elements this means that $n_{dof} = 3n_{no} - n_{el} = 2n_{no} + 1$. For a box cross section with $n_{el} = n_{no}$ elements it means that $n_{dof} = 3n_{no} - n_{el} = 2n_{no}$.

5.2.3 Step III: Reduction of order

To solve this differential equation we choose again to reduce the differential order of the coupled fourth-order differential equations and the related quadratic

$\mathbf{K}^0_{\alpha\alpha} = \mathbf{T}^{\alpha\,T}_{\mathrm{w}}\mathbf{K}^0\mathbf{T}^{\alpha}_{\mathrm{w}}$	$\mathbf{K}^0_{\alpha 3} = \mathbf{T}^{\alpha\,T}_{\mathrm{w}}\mathbf{K}^0\mathbf{T}^{3}_{\mathrm{w}}$	$K^0_{\alpha u} = \mathbf{T}^{\alpha\,T}_{\mathrm{w}}\mathbf{K}^0\mathbf{T}^{u}_{\mathrm{w}}$
$\mathbf{K}^0_{3\alpha} = \mathbf{T}^{3\,T}_{\mathrm{w}}\mathbf{K}^0\mathbf{T}^{\alpha}_{\mathrm{w}}$	$K^0_{33} = \mathbf{T}^{3\,T}_{\mathrm{w}}\mathbf{K}^0\mathbf{T}^{\mathbf{3}}_{\mathrm{w}}$	$\mathbf{K}^0_{3u} = \mathbf{T}^{3\,T}_{\mathrm{w}}\mathbf{K}^0\widetilde{\mathbf{T}}^{\mathbf{u}}_{\mathrm{w}}$
$\mathbf{K}^0_{u\alpha} = \widetilde{\mathbf{T}}^{u\,T}_{\mathrm{w}}\mathbf{K}^0\mathbf{T}^{\alpha}_{\mathrm{w}}$	$\mathbf{K}^0_{u3} = \widetilde{\mathbf{T}}^{u\,T}_{\mathrm{w}}\mathbf{K}^0\mathbf{T}^{\mathbf{3}}_{\mathrm{w}}$	$\mathbf{K}^0_{uu} = \widetilde{\mathbf{T}}^{u\,T}_{\mathrm{w}}\mathbf{K}^0\widetilde{\mathbf{T}}^{\mathbf{u}}_{\mathrm{w}}$

Table 5.1: Transformation of K^0-stiffness matrices related to Step II.

eigenvalue problem to twice as many coupled second-order differential equations with a related linear eigenvalue problem of double size.

The fourth-order differential equation (5.15) can be transformed into twice as many second order differential equations by introducing what is called a state vector. There are a number of different possible formulations, but we have chosen the use of the state vector $\mathbf{u}_S = [\mathbf{v}^{\alpha}_{\mathrm{w}}\psi, v^{3}_{\mathrm{w}}\psi, \mathbf{v}^{u}_{\mathrm{w}}\psi, \mathbf{v}^{\alpha}_{\mathrm{w}}\psi', v^{3}_{\mathrm{w}}\psi', \mathbf{v}^{u}_{\mathrm{w}}\psi']^T$. Introducing this state vector (and using related equality block equations) yields a reformulation of equation (5.15) as a formal second order matrix differential equation of double size which takes the form:

$$
\left[\begin{array}{ccc|ccc}
\mathbf{0} & \mathbf{0} & \mathbf{0} & \mathbf{0} & \mathbf{0} & \mathbf{0} \\
\mathbf{0} & 0 & \mathbf{0} & \mathbf{0} & 0 & \mathbf{0} \\
\mathbf{0} & \mathbf{0} & \mathbf{K}^s_{uu} & \mathbf{0} & \mathbf{0} & \mathbf{0} \\
\hline
\mathbf{0} & \mathbf{0} & \mathbf{0} & -\mathbf{K}^{\sigma}_{\alpha\alpha} & \mathbf{0} & -\mathbf{K}^{\sigma}_{\alpha u} \\
\mathbf{0} & 0 & \mathbf{0} & \mathbf{0} & -K^{\sigma}_{33} & -\mathbf{K}^{\sigma}_{3u} \\
\mathbf{0} & \mathbf{0} & \mathbf{0} & -\mathbf{K}^{\sigma}_{u\alpha} & -\mathbf{K}^{\sigma}_{u3} & -\mathbf{K}^{\sigma}_{uu}
\end{array}\right]
\left[\begin{array}{c}
\mathbf{v}^{\alpha}_{\mathrm{w}}\psi \\ v^{3}_{\mathrm{w}}\psi \\ \mathbf{v}^{u}_{\mathrm{w}}\psi \\ \hline \mathbf{v}^{\alpha}_{\mathrm{w}}\psi' \\ v^{3}_{\mathrm{w}}\psi' \\ \mathbf{v}^{u}_{\mathrm{w}}\psi'
\end{array}\right] -
$$

$$
\left(\left[\begin{array}{ccc|ccc}
\mathbf{0} & \mathbf{0} & \mathbf{0} & -\mathbf{K}^{\sigma}_{\alpha\alpha} & \mathbf{0} & -\mathbf{K}^{\sigma}_{\alpha u} \\
\mathbf{0} & K^{\tau}_{33} & \mathbf{K}^{\tau}_{3u} & \mathbf{0} & -K^{\sigma}_{33} & -\mathbf{K}^{\sigma}_{3u} \\
\mathbf{0} & \mathbf{K}^{\tau}_{u3} & \mathbf{K}^{\tau}_{uu} & -\mathbf{K}^{\sigma}_{u\alpha} & -\mathbf{K}^{\sigma}_{u3} & -\mathbf{K}^{\sigma}_{uu} \\
\hline
-\mathbf{K}^{\sigma}_{\alpha\alpha} & \mathbf{0} & -\mathbf{K}^{\sigma}_{\alpha u} & \mathbf{0} & \mathbf{0} & \mathbf{0} \\
\mathbf{0} & -K^{\sigma}_{33} & -\mathbf{K}^{\sigma}_{3u} & \mathbf{0} & 0 & \mathbf{0} \\
-\mathbf{K}^{\sigma}_{u\alpha} & -\mathbf{K}^{\sigma}_{u3} & -\mathbf{K}^{\sigma}_{uu} & \mathbf{0} & \mathbf{0} & \mathbf{0}
\end{array}\right] +
\lambda
\left[\begin{array}{ccc|ccc}
\mathbf{K}^0_{\alpha\alpha} & \mathbf{K}^0_{\alpha 3} & \mathbf{K}^0_{\alpha u} & \mathbf{0} & \mathbf{0} & \mathbf{0} \\
\mathbf{K}^0_{3\alpha} & K^0_{33} & \mathbf{K}^0_{3u} & \mathbf{0} & 0 & \mathbf{0} \\
\mathbf{K}^0_{u\alpha} & \mathbf{K}^0_{u3} & \mathbf{K}^0_{uu} & \mathbf{0} & \mathbf{0} & \mathbf{0} \\
\hline
\mathbf{0} & \mathbf{0} & \mathbf{0} & \mathbf{0} & \mathbf{0} & \mathbf{0} \\
\mathbf{0} & 0 & \mathbf{0} & \mathbf{0} & 0 & \mathbf{0} \\
\mathbf{0} & \mathbf{0} & \mathbf{0} & \mathbf{0} & \mathbf{0} & \mathbf{0}
\end{array}\right]\right)
\left[\begin{array}{c}
\mathbf{v}^{\alpha}_{\mathrm{w}}\psi \\ v^{3}_{\mathrm{w}}\psi \\ \mathbf{v}^{u}_{\mathrm{w}}\psi \\ \hline \mathbf{v}^{\alpha}_{\mathrm{w}}\psi' \\ v^{3}_{\mathrm{w}}\psi' \\ \mathbf{v}^{u}_{\mathrm{w}}\psi'
\end{array}\right]'' =
\left[\begin{array}{c}
\mathbf{0} \\ 0 \\ \mathbf{0} \\ \hline \mathbf{0} \\ 0 \\ \mathbf{0}
\end{array}\right] \qquad (5.16)
$$

which we choose to abbreviate as follows using the block structure shown in equation (5.16):

$$\begin{bmatrix} \widetilde{\mathbf{K}}^{s} & \mathbf{0} \\ \mathbf{0} & -\widetilde{\mathbf{K}}^{\sigma} \end{bmatrix} \begin{bmatrix} \tilde{\mathbf{v}}_{\mathrm{w}}\psi \\ \tilde{\mathbf{v}}_{\mathrm{w}}\psi'' \end{bmatrix} - \left(\begin{bmatrix} \widetilde{\mathbf{K}}^{\tau} & -\widetilde{\mathbf{K}}^{\sigma} \\ -\widetilde{\mathbf{K}}^{\sigma} & \mathbf{0} \end{bmatrix} + \lambda \begin{bmatrix} \widetilde{\mathbf{K}}^{0} & \mathbf{0} \\ \mathbf{0} & \mathbf{0} \end{bmatrix} \right) \begin{bmatrix} \tilde{\mathbf{v}}_{\mathrm{w}}\psi \\ \tilde{\mathbf{v}}_{\mathrm{w}}\psi'' \end{bmatrix}'' = \begin{bmatrix} \mathbf{0} \\ \mathbf{0} \end{bmatrix} \quad (5.17)$$

This is the set of differential equations to which we want to find solutions.

5.3 The distortional initial stress eigenvalue problem

In the reduced order differential equations in (5.17) we substitute $\mathbf{A}$, $\mathbf{B}$, $\mathbf{C}$ and $\mathbf{u}_S$ for the respective matrices and vector in the equation. This means that $\mathbf{A}$ and $\mathbf{B}$ are linear stiffness matrices, $\mathbf{C}$ a geometrical stiffness matrix, and $\mathbf{u}_S$ a vector containing the longitudinal amplitude functions. Thus, it takes the following form:

$$\mathbf{A}\mathbf{u}_S - [\mathbf{B} + \lambda\mathbf{C}]\,\mathbf{u}_S'' = \mathbf{0} \quad (5.18)$$

This set of differential equations are homogeneous with constant coefficients and therefore lead to solution functions of exponential type.

By postulating exponential solutions of the form $\mathbf{u}_S = \mathbf{v}_S\psi(z)$, where the state space vector $\mathbf{v}_S$ is independent of the axial coordinate z and $\psi(z) = e^{\xi z}$, and inserting the solution, the following special eigenvalue problem is obtained:

$$\mathbf{A}\mathbf{v}_S - \xi^2\,[\mathbf{B} + \lambda\mathbf{C}]\,\mathbf{v}_S = \mathbf{0} \quad (5.19)$$

In the classical stability theory the solution function $\psi(z)$ is normally assumed to be a trigonometric function in order to satisfy suitable simple boundary conditions (Timoschenko and Gere, 1963). This means that $\xi = \mu i$ is a known (complex) parameter and that λ can be determined as the eigenvalue equivalent to the instability load factor, which determines the level of stress at which the structure becomes unstable. The eigenvalues and the corresponding eigenvectors $\mathbf{v}_S$ can be found by solving the eigenvalue problem.

In order to satisfy suitable simple boundary conditions let us therefore assume that the solution is of a simple trigonometric form here chosen as

$$\psi(z) = \sin \mu z \quad (5.20)$$

where $\mu = n\pi/L$ in which n is equal to the number of buckles, i.e. half-wavelengths. This solution satisfies boundary conditions corresponding to simple supports with restrained transverse cross-section displacements at $z = 0$ and $z = L$. Inserting this postulated solution in equation (5.18) and remembering the change of sign related to double differentiation of the sine function leads to the following generalized linear symmetric matrix eigenvalue problem, in which

$\mathbf{K} = \widetilde{\mathbf{K}}^s + \mu^2\widetilde{\mathbf{K}}^\tau + \mu^4\widetilde{\mathbf{K}}^\sigma$	$\mathbf{G} = \mu^2\widetilde{\mathbf{K}}^0$

Table 5.2: Definition of $\mathbf{K}$ and $\mathbf{G}$.

the eigenvalues, λ, correspond to the buckling factor and the eigenvectors are the distortional state space buckling modes:

$$\left[\mathbf{A} + \left(\frac{n\pi}{L}\right)^2 \mathbf{B}\right] \mathbf{v}_S + \lambda \left(\frac{n\pi}{L}\right)^2 \mathbf{C}\mathbf{v}_S = \mathbf{0} \tag{5.21}$$

Eliminating the second half of vector $\mathbf{v}_S$ corresponding to $\tilde{\mathbf{v}}_\mathrm{w}\psi''$ in equation (5.17) leads to the following final generalized linear symmetric matrix eigenvalue problem:

$$[\mathbf{K} + \lambda\mathbf{G}]\,\tilde{\mathbf{v}}_\mathrm{w} = \mathbf{0} \tag{5.22}$$

in which $\mathbf{K}$ and $\mathbf{G}$ are given in Table 5.2 as functions of the inverse length scale parameter μ. From the results of this eigenvalue problem we know at which load (λ) the corresponding mode has a homogeneous solution function which is sinusoidal with a number of half-waves corresponding to n, leading to conventional half wavelength buckling curves or so called cross-section signature curves. Such a signature curve is depicted in the upper left part of Figure 5.1 obtained from the example given in the following section 5.4. The signature curve is similar to the finite strip buckling curve obtained by Hancock (1985). In chapter 3 as well as in Paper I (Jönsson and Andreassen, 2011) a full decomposition of the displacement field is demonstrated (though with some complex solutions). Hereby we establish the natural analytical solution modes of the GBT differential equations for first-order analysis, while we in the present chapter establish a special set of solutions of the GBT-stability differential equations for buckling of simply supported columns. This means that we are not able to do the same full modal decomposition while the modes are not as pure as for the natural modes but a combination of several modes. The indication of the combination of natural modes for a given buckling mode is also a feature in `GBTUL` and a topic in its related papers.

The number of modes depends on the discretization and the geometry of the cross section. This means that the number of different modes can only be defined by the illustrative examples. But as mentioned we are not dealing with a modal decomposition, but with a set of buckling modes (which in conventional GBT means a combination of several first-order modes). For example, a global buckling mode is a combination of a rigid translation and some distortional local and/or non-local transverse displacement. Therefore we are not able to classify all the buckling modes in pure global, distortional, and local modes. (This also

happens in classic theory involving interaction of flexural and torsional buckling as well as in conventional GBT). At the present level the number of degrees of freedom for a lipped channel cross section is $n_{dof} = 2n_{no} + 1$, while the number of degrees of freedom for a box cross section is $n_{dof} = 2n_{no}$. The number of dofs is equal to the number of eigenvalues.

In contrast to the assumed solution function given in equations (5.20) which lead to the eigenvalue problem in equation (5.22) we could instead seek general solutions to the differential equations, see Paper VII (Jönsson and Andreassen, 2012). Thus, it is necessary to fix the initial stress level and thus perform calculations with fixed values of λ. Furthermore, it is necessary to reduce the order of the differential equations and introduce a state vector with twice the number of dofs. Through solution of the related linear eigenvalue problem of double size the state space displacement solutions are identified. The eigenvalues ξ are functions of the initial stress level and correspond to complex solution length scales (π/ξ) as plotted in the upper right part of Figure 5.1. From this part of the figure we can recognize the cross-section signature curves identical to the upper left part of the figure. Separating the cross-section signature curves the changes in the distortional solution modes and length scales are seen in the lower part of the figure.

Although we have several opportunities for investigating the problem we will here continue with the assumed trigonometric solution function and the related eigenvalue problem given in equation (5.22) leading to the following example.

5.4 Example

In this section the developed GBT approach is used to give an illustrative example of the trigonometric buckling solutions of the differential GBT equations with initial stress. The ability of the GBT approach to produce buckling curves and predict buckling is shown. The buckling of a simply supported lipped channel column in pure compression is analyzed. The chosen in-plane geometry and the discretization is shown in Figure 5.2. The end sections are constrained against transverse displacements, but otherwise free to warp (and thus also rotate).

The buckling signature curves of the cross section are developed corresponding to the buckling stress versus the buckling half-wavelength for the four lowest buckling modes. This is done by solving the GBT eigenvalue problem for consecutive values of the half-wavelength. For each buckling curve it is shown that the transverse buckling mode shape varies with the buckle half-wavelength. The buckling signature curve is used to develop the overall buckling curve including multiple buckling waves by shifting the signature curve sides ways corresponding to a number of half-wavelengths. Chosen buckling modes for given column lengths are used to illustrate local, distortional and global buckling modes. The

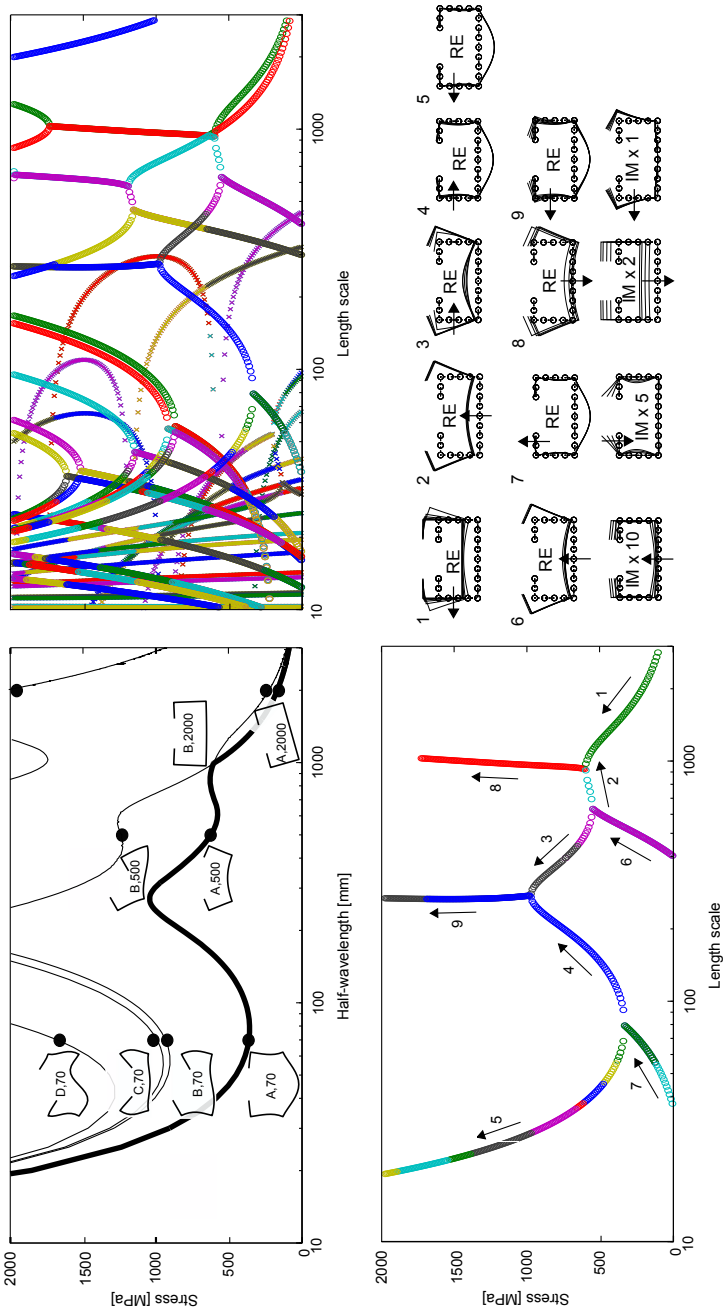

Figure 5.1: Signature curves, solution length scale curves and solution mode development.

accuracy of the results are assessed by comparison to results obtained by the use of the commercial FE program `Abaqus`.

The results found using Abaqus are based on isotropic material and the 4 node S4 shell element with full 4 point integration. The linear elastic finite element calculations are based on a structured rectangular mesh with a side length seed of 5 mm. The cross section is fixed in the transverse directions at both ends. All supports are continuous line supports. Two identical normal forces are applied as a uniform distributed shell edge load; one at each end. For further and more detailed explanations see also Abaqus (2008). This finite element model results in local transverse stress near the end supports due to the Poisson effect. These end stresses have an influence on the buckling, which is not included in the FSM or GBT models.

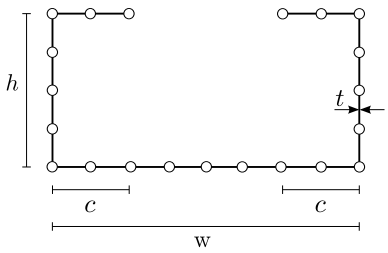

$h = 50$
w $= 100$
$c = 25$
$t = 2.0$
$E = 2.1 \times 10^5$
$G = 8.077 \times 10^4$
$\nu = 0.3$
○ Node

Figure 5.2: Geometry, discretization and parameter values of a lipped channel column.

For more examples see Paper III (Andreassen and Jönsson, 2012a). Solving the GBT initial stress eigenvalue problem given in equation (5.21) with $n = 1$ for half-wavelengths L varying from 10 mm to 3000 mm (logarithmical spaced) allows the development of the signature curve (buckling stress versus the buckle half wavelength) as shown in Figure 5.3. Thus the buckling curves shown in the figure correspond to the four lowest buckling modes with one half-wave buckle, $n = 1$.

For three different half-wavelengths the transverse buckling mode shape has been included in the figure. It is clear that the mode shape of each curve changes gradually as a function of the length. The chosen half-wavelengths correspond to the dashed lines at 70 mm, 500 mm and 2000 mm, respectively. To illuminate the changes in the deformation modes for increasing length we have chosen also to show the buckling mode shapes in 3D in Figure 5.4. The mode shapes are shown as a 3D representation even though the results are provided by a one-dimensional beam formulation.

From the figures it is seen that each developing mode represents its own curve placed in a hierarchical order according to the stress level. However, the curves are able to change place in the hierarchy at a certain column length. This phenomenon can for example be seen for buckling mode 1 and 2 (two lowest ranking graphs) at a column length of approximately 1000 mm. The

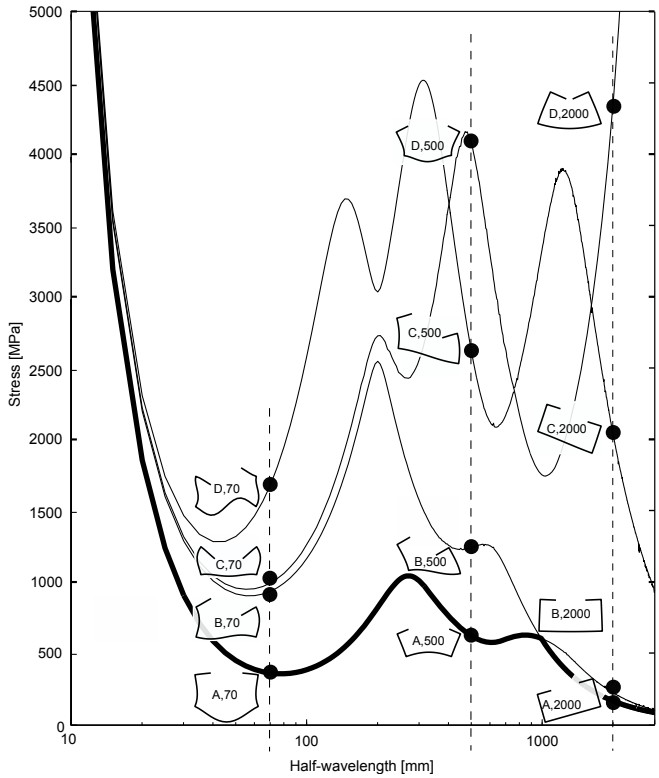

Figure 5.3: Buckling signature curve corresponding to the lowest four modes with a single half-wave buckle, $n = 1$.

signature curve, shown bold, is achieved as the very lowest of the buckling curves. For this curve short column lengths correspond to local buckling, while for increasing column lengths it corresponds to distortional buckling and finally for large column lengths it corresponds to global buckling. The signature curve is similar to the finite strip buckling curve obtained by Hancock (1985).

As mentioned Figure 5.3 is for a half-wave number $n = 1$. As the buckling loads also depend on the number of n half waves in the buckled shapes, this means that points lower than the signature curve can exist for a greater number of buckles, $n > 1$. To show this phenomenon the signature curve has been created for a varying number of n as shown in Figure 5.5. This means that the bold curve shown in Figure 5.5 represents the absolute lowest curve for the buckling stress versus column length. However, to illustrate the multitude of buckling modes for each column length, let us look at a column length of $L = 1000$ mm. In Figure 5.5 this length is represented by the vertical dashed line. For this length we can find the buckling modes $m = 1, 2, 3..$ ordered from lowest to highest critical stress, each having a different number of half waves n.

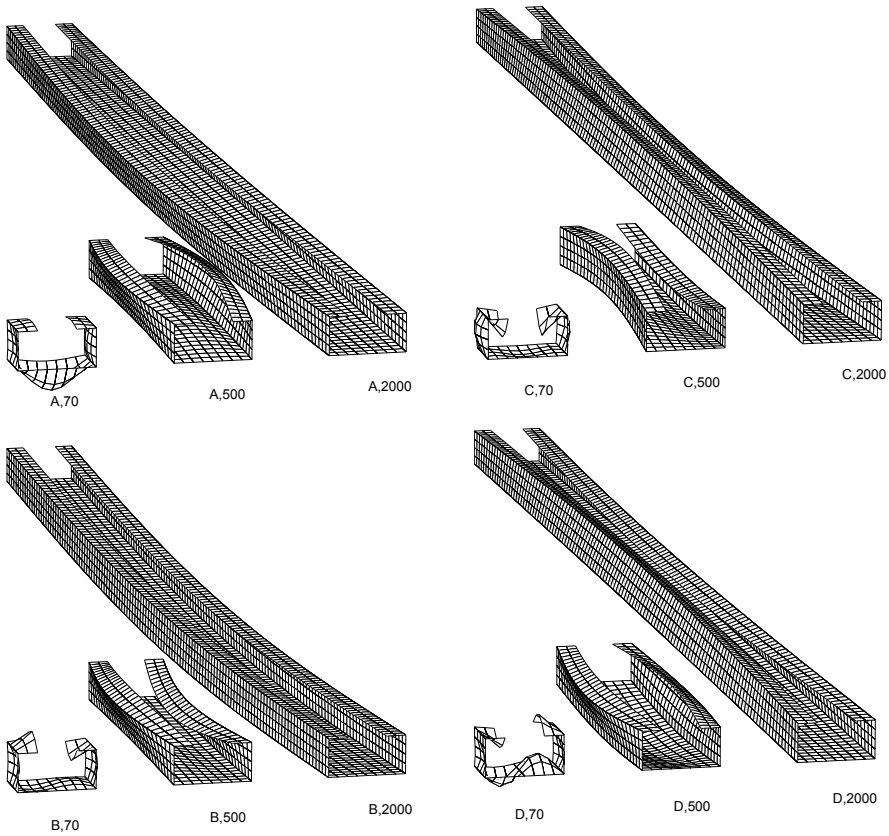

Figure 5.4: Column buckling modes associated with Figure 5.3 for single ($n = 1$) half wavelengths of 70 mm, 500 mm, and 2000 mm

In Table A.3 the buckling stresses of FE analysis using Abaqus (2008) versus the presented GBT method, conventional GBT using `GBTUL` (Bebiano et al., 2008a) and FSM using `CUFSM` (Li and Schafer, 2010) are compared. The comparison is performed for suitable mode numbers (m-values) and the associated relevant buckling modes are depicted in Figure 5.6. It shows the local buckling mode corresponding to the lowest critical stress ($m = 1$), the global beam buckling mode ($m = 20$), and a distortional mode shape ($m = 24$), respectively. The three values of m have been chosen to show the spectrum of modes represented at the given beam length.

From Table A.3 it is seen that for a column length of 1000 mm buckling will occur as local buckling consisting of thirteen sine half waves and have an associated buckling stress of 350 MPa. Furthermore, it is seen that the buckling mode shape for mode $m = 20$ is global column buckling with one buckle, $n = 1$, at a stress level of 590 MPa and finally for $m = 24$ distortional column buckling

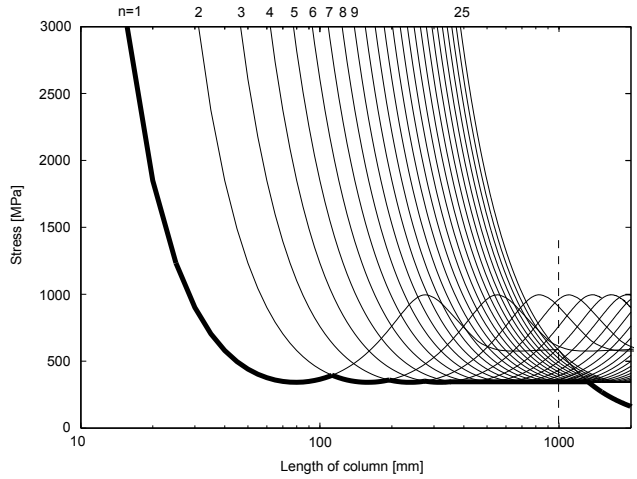

Figure 5.5: Buckling stress versus column length for the lipped channel section in compression.

m	Nr. of half waves n	Abaqus [MPa]	GBT [MPa]	Diff. %	GBTUL [MPa]	Diff. %	CUFSM [MPa]	Diff. %
1	13	404	350	13.4	412	2.0	412	2.0
20	1	580	590	1.7	589	1.6	581	0.2
24	3	903	918	1.7	933	3.3	906	0.3

Table 5.3: Comparison of buckling stresses for FE analysis versus the presented GBT method, GBTUL and CUFSM, respectively. The comparisons are related to the vertical dashed m-line in Figure 5.5.

occurs at a stress level of 918 MPa.

Comparing the GBT buckling stresses with Abaqus we obtain a deviation of 13.4% for local plate buckling, 1.7% for global buckling and 1.7% for distortional buckling. Hereby it is seen that good results are obtained for global and distortional buckling, while a rather large deviation is obtained for local buckling. The GBTUL results which are based on the conventional GBT theory shows a deviation of 2.0% for local plate buckling, 1.6% for global buckling and 3.3% for distortional buckling. In contrast to these beam theory results, Table A.3 also shows results obtained from the CUFSM program which is based on a plate theory. Here we obtain a deviation of 2.0% for local plate buckling, 0.2% for global buckling and 0.3% for distortional buckling, showing that good results are obtained in all cases. From the deviations it is obvious that GBT and GBTUL are based on beam theories while CUFSM is based on plate theory. The rather large deviation of 13.4% for the GBT results can to a certain extent

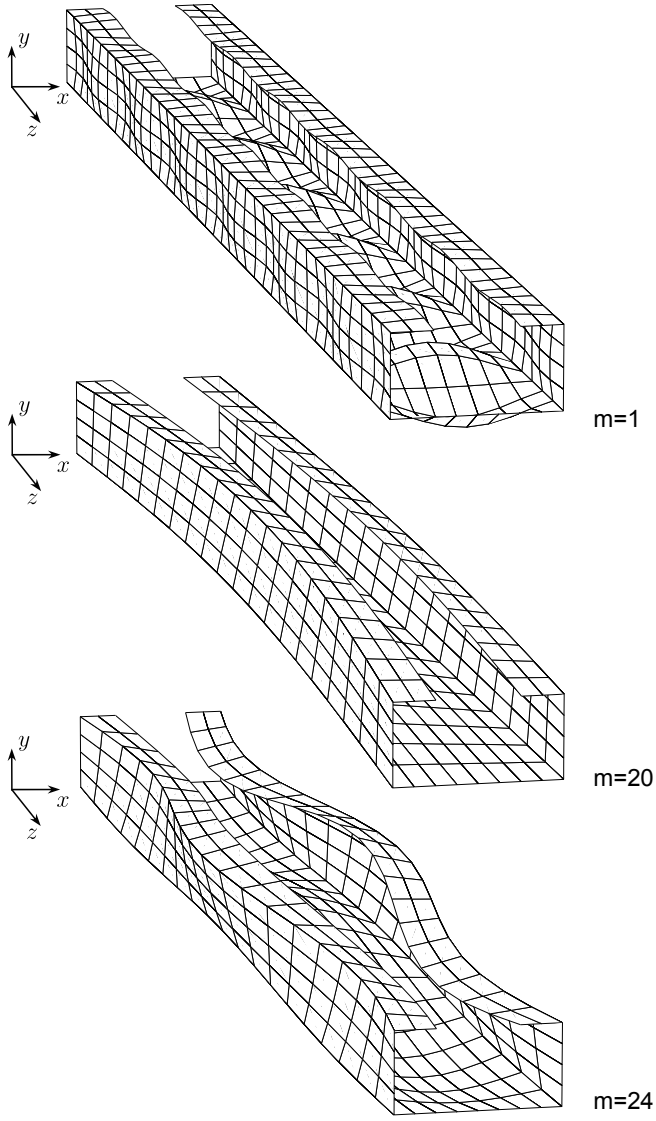

Figure 5.6: GBT column buckling mode shapes of a lipped channel column in pure compression.

be explained by the very simple constitutive relations used in the current GBT formulation where Poisson effects are not taking into account. Making a calculation in Abaqus with similar very simple non-coupling constitutive relations the deviations obtained now corresponds to (350 MPa) 0.0%, (582 MPa) 1.4% and (888 MPa) 3.4%, respectively. Hereby good matches between the two approaches are obtained, however also difference in the modeling of the boundary conditions can affect the results. Thus demonstrating that this new developed GBT approach provides reasonably accurate results with a very small computational cost, making it an alternative to the traditional and time consuming FE calculations and the other available methods. However, the constitutive relations should be modified to achieve a higher accuracy for local plate buckling.

5.5 Concluding remarks

In this chapter we have presented the extension of the novel GBT approach to include the geometrical stiffness terms which are needed for column buckling analysis. The distortional differential equations in chapter 3 are extended to a formulation including geometrical stiffness terms by using the initial stress approach to formulate the instability problem. The derived GBT differential equations with initial stress have been solved as an eigenvalue problem leading to a number of buckling modes and associated buckling stresses for simply supported columns in compression. As opposed to conventional GBT this means that we are not using a modal decomposition from a pseudo first-order analysis to establish the buckling modes as a sum of these first-order modes; we are solving the differential buckling equations of GBT directly.

Having developed and solved the distortional homogeneous and non-homogeneous differential equations and solutions along the beam as well as included the geometrical stiffness terms, we will in the next chapter finally deal with the development of an advanced distortional semi-discretized prismatic thin-walled beam element.

Chapter 6

A distortional semi-discretized prismatic thin-walled beam element

The previous chapters adhere to the solution of the developed and formulated set of distortional differential equations. Thus these chapters are not dealing with a finite element but dealing with an analytical solution of the coupled differential equations. To handle arbitrary boundary conditions as well as the possibility of adding concentrated loads as nodal loads the formulation of a finite element is needed. This chapter deals with the formulation of such a generalized one-dimensional semi-discretized prismatic thin-walled beam element including distortional contributions. It should be noticed that we are dealing with a basic generalized beam theory and not an extended finite element formulation of an approximate beam element. Furthermore, it should be noticed that the beam element developed in the present chapter do not include the geometrical stiffness terms and thus do not deal with column buckling analyzes.

6.1 Element stiffness matrix and load vector

In this section the global beam element stiffness matrix and load vector needed for the determination of the nodal element solution are found. As the load has no influence on the stiffness contributions we use the full assembled homogeneous solution along the beam found in chapter 3. We also use the homogeneous displacement modes to generate the nodal load vector. Some of the distortional displacement modes found and their related eigenvalues are complex. In contrast to the previous chapters where a transformation to real modes and real solutions are performed we will here continue working with complex numbers. This means that the use of compilers which include complex numbers with complex operations on matrices will lead to simple algorithms based directly on the

following formulations.

The homogeneous solution vectors along the beam are given by the full solution in equation (3.86) as

$$\begin{aligned} \mathbf{u}_{\mathrm{w}}(z) &= \mathbf{V}_{\mathrm{w}}\boldsymbol{\Psi}_h(z)\,\mathbf{c} \\ \mathbf{u}_z(z) &= -\mathbf{V}_{\Omega}\boldsymbol{\Psi}_h'(z)\,\mathbf{c} \end{aligned} \tag{6.1}$$

where the given constants have to be determined by the GBT-space boundary conditions of the prismatic thin-walled beam. This means that we are now considering not just a single mode but all solution modes. To establish the stiffness matrix and load vector for a single beam element the constants are viewed as temporary element degrees of freedom. The transformation between these constants and the final end displacements of the beam element will be determined by setting up the necessary GBT boundary conditions. Using the homogeneous solution vectors given in equation (6.1) the potential energy including all the homogeneous modes in equation (4.14) can be written as

$$\begin{aligned} \Pi = \tfrac{1}{2}\int_0^L \Bigg\{ & \mathbf{c}^T \begin{bmatrix} \boldsymbol{\Psi}_h^T\mathbf{V}_{\mathrm{w}}^T & \boldsymbol{\Psi}_h^T\mathbf{V}_{\Omega}^T \end{bmatrix}'' \begin{bmatrix} \mathbf{K}^{\sigma}_{\mathrm{ww}} & \mathbf{0} \\ \mathbf{0} & \mathbf{K}^{\sigma}_{\Omega\Omega} \end{bmatrix} \begin{bmatrix} \mathbf{V}_{\mathrm{w}}\boldsymbol{\Psi}_h \\ \mathbf{V}_{\Omega}\boldsymbol{\Psi}_h \end{bmatrix}'' \mathbf{c} \\ & + \mathbf{c}^T \begin{bmatrix} \boldsymbol{\Psi}_h^T\mathbf{V}_{\mathrm{w}}^T & \boldsymbol{\Psi}_h^T\mathbf{V}_{\Omega}^T \end{bmatrix}' \begin{bmatrix} \mathbf{K}^{\tau}_{\mathrm{ww}} & \mathbf{K}^{\tau}_{\mathrm{w}\Omega} \\ \mathbf{K}^{\tau}_{\Omega\mathrm{w}} & \mathbf{K}^{\tau}_{\Omega\Omega} \end{bmatrix} \begin{bmatrix} \mathbf{V}_{\mathrm{w}}\boldsymbol{\Psi}_h \\ \mathbf{V}_{\Omega}\boldsymbol{\Psi}_h \end{bmatrix}' \mathbf{c} \\ & + \mathbf{c}^T \begin{bmatrix} \boldsymbol{\Psi}_h^T\mathbf{V}_{\mathrm{w}}^T & \boldsymbol{\Psi}_h^T\mathbf{V}_{\Omega}^T \end{bmatrix} \begin{bmatrix} \mathbf{K}^{s} & \mathbf{0} \\ \mathbf{0} & \mathbf{0} \end{bmatrix} \begin{bmatrix} \mathbf{V}_{\mathrm{w}}\boldsymbol{\Psi}_h \\ \mathbf{V}_{\Omega}\boldsymbol{\Psi}_h \end{bmatrix} \mathbf{c} \\ & - \mathbf{c}^T(\boldsymbol{\Psi}_h^T\mathbf{V}_{\mathrm{w}}^T)\mathbf{r}_{\mathrm{w}}\phi - \mathbf{c}^T(\boldsymbol{\Psi}_h^T\mathbf{V}_{\Omega}^T)'\mathbf{r}_{\Omega}\phi \Bigg\} dz \end{aligned} \tag{6.2}$$

or in integrated form as

$$\Pi = \tfrac{1}{2}\mathbf{c}^T(\widetilde{\mathbf{K}}\mathbf{c} - \widetilde{\mathbf{r}}) \tag{6.3}$$

where $\widetilde{\mathbf{K}}$ is the stiffness matrix and $\widetilde{\mathbf{r}}$ the load vector related to the modal displacement constants $\mathbf{c}$. The stiffness matrix and the load vector are found by integration and addition of the individual sub matrix products in the potential energy equation (6.2) as

$$\widetilde{\mathbf{K}} = \widetilde{\mathbf{K}}^{\sigma}_{\mathrm{ww}} + \widetilde{\mathbf{K}}^{\sigma}_{\Omega\Omega} + \widetilde{\mathbf{K}}^{\tau}_{\mathrm{ww}} + \widetilde{\mathbf{K}}^{\tau}_{\mathrm{w}\Omega} + \widetilde{\mathbf{K}}^{\tau}_{\Omega\mathrm{w}} + \widetilde{\mathbf{K}}^{\tau}_{\Omega\Omega} + \widetilde{\mathbf{K}}^{s} \tag{6.4}$$

and

$$\widetilde{\mathbf{r}} = \widetilde{\mathbf{r}}_{\mathrm{w}} + \widetilde{\mathbf{r}}_{\Omega} \tag{6.5}$$

$\widetilde{\mathbf{K}}^{\sigma}_{\mathrm{ww}} = \int_0^L {\boldsymbol{\Psi}_h''}^T \mathbf{V}_{\mathrm{w}}^T \mathbf{K}^{\sigma}_{\mathrm{ww}} \mathbf{V}_{\mathrm{w}} \boldsymbol{\Psi}_h'' \, dz$	$\widetilde{\mathbf{K}}^{\sigma}_{\Omega\Omega} = \int_0^L {\boldsymbol{\Psi}_h''}^T \mathbf{V}_{\Omega}^T \mathbf{K}^{\sigma}_{\Omega\Omega} \mathbf{V}_{\Omega} \boldsymbol{\Psi}_h'' \, dz$
$\widetilde{\mathbf{K}}^{\tau}_{\mathrm{ww}} = \int_0^L {\boldsymbol{\Psi}_h'}^T \mathbf{V}_{\mathrm{w}}^T \mathbf{K}^{\tau}_{\mathrm{ww}} \mathbf{V}_{\mathrm{w}} \boldsymbol{\Psi}_h' \, dz$	$\widetilde{\mathbf{K}}^{\tau}_{\Omega\mathrm{w}} = \int_0^L {\boldsymbol{\Psi}_h'}^T \mathbf{V}_{\Omega}^T \mathbf{K}^{\tau}_{\Omega\mathrm{w}} \mathbf{V}_{\mathrm{w}} \boldsymbol{\Psi}_h' \, dz$
$\widetilde{\mathbf{K}}^{\tau}_{\mathrm{w}\Omega} = \int_0^L {\boldsymbol{\Psi}_h'}^T \mathbf{V}_{\mathrm{w}}^T \mathbf{K}^{\tau}_{\mathrm{w}\Omega} \mathbf{V}_{\Omega} \boldsymbol{\Psi}_h' \, dz$	$\widetilde{\mathbf{K}}^{\tau}_{\Omega\Omega} = \int_0^L {\boldsymbol{\Psi}_h'}^T \mathbf{V}_{\Omega}^T \mathbf{K}^{\tau}_{\Omega\Omega} \mathbf{V}_{\Omega} \boldsymbol{\Psi}_h' \, dz$
$\widetilde{\mathbf{K}}^{s} = \int_0^L {\boldsymbol{\Psi}_h}^T \mathbf{V}_{\mathrm{w}}^T \mathbf{K}^{s} \mathbf{V}_{\mathrm{w}} \boldsymbol{\Psi}_h \, dz$	

Table 6.1: Beam element stiffness contributions.

$\widetilde{\mathbf{r}}_{\mathrm{w}} = \int_0^L {\boldsymbol{\Psi}_h}^T \, \phi \, dz \, \mathbf{V}_{\mathrm{w}}^T \mathbf{r}_{\mathrm{w}}$	$\widetilde{\mathbf{r}}_{\Omega} = \int_0^L {\boldsymbol{\Psi}_h'}^T \, \phi \, dz \, \mathbf{V}_{\Omega}^T \mathbf{r}_{\Omega}$

Table 6.2: Beam element load vector contributions.

The stiffness matrix contributions are given i Table 6.1 and the two load vector contributions are given in Table 6.2. Let us now turn to a reformulation of eigenvectors and solution functions which enables clearer analytical integration.

6.1.1 Formulation enabling analytical integration

In the potential energy formulation in equation (6.2) the modal matrix of transverse displacement vectors $\mathbf{V}_{\mathrm{w}}$ and the modal matrix of axial warping displacement vectors $\mathbf{V}_{\Omega}$ contain all the found eigenmode vectors assembled column-wise. However, each eigenvector is only represented once. To ease the integration of the products of the longitudinal amplitude functions $\boldsymbol{\Psi}_h$ we will here introduce a matrix format $\overline{\boldsymbol{\Psi}}_h$ corresponding to a diagonal representation of the solution functions. This can only be done if we also introduce an expanded representation of the eigenvectors $\overline{\mathbf{V}}_{\mathrm{w}}$ and $\overline{\mathbf{V}}_{\Omega}$. By doing this each eigenvector is represented twice for double roots and four times for quadruple roots. To obtain this format we will use a transformation matrix $\mathbf{H}$ to expand the transverse displacement vectors $\mathbf{V}_{\mathrm{w}}$ and the axial warping displacement vectors $\mathbf{V}_{\Omega}$ into the full space by

$$\overline{\mathbf{V}}_{\mathrm{w}} = \mathbf{V}_{\mathrm{w}} \mathbf{H} \tag{6.6}$$

$$\overline{\mathbf{V}}_{\Omega} = \mathbf{V}_{\Omega} \mathbf{H} \tag{6.7}$$

The transformation matrix also gives a transformation from the diagonalized solution function matrix to the original format by

$$\boldsymbol{\Psi}_h = \mathbf{H} \overline{\boldsymbol{\Psi}}_h \tag{6.8}$$

The transformation matrix can be subdivided into a part $\mathbf{H}_b$ related to the transformation of the classic beam modes and a part $\mathbf{H}_d$ related to the transformation of the distortional modes by

$$\mathbf{H} = \begin{bmatrix} \mathbf{H}_b & \mathbf{0} \\ \mathbf{0} & \mathbf{H}_d \end{bmatrix} \tag{6.9}$$

Concerning the conventional beam displacements as given in equation (3.80) and (3.82) the expanding transformation matrix $\mathbf{H}_b$ takes the following form:

$$\mathbf{H}_b = \begin{bmatrix} 1 & 1 & 0 & 0 & 0 & 0 & 0 & 0 & 0 & 0 & 0 & 0 \\ 0 & 0 & 1 & 1 & 1 & 1 & 0 & 0 & 0 & 0 & 0 & 0 \\ 0 & 0 & 0 & 0 & 0 & 0 & 1 & 1 & 1 & 1 & 0 & 0 \\ 0 & 0 & 0 & 0 & 0 & 0 & 0 & 0 & 0 & 0 & 1 & 1 \end{bmatrix} \tag{6.10}$$

and for the distortional displacements the expanding transformation takes the form

$$\mathbf{H}_d = \begin{bmatrix} 1 & 1 & 0 & 0 & 0 & 0 & \cdots \\ 0 & 0 & 1 & 1 & 0 & 0 & \cdots \\ 0 & 0 & 0 & 0 & 1 & 1 & \cdots \\ \vdots & \vdots & \vdots & \vdots & \vdots & \vdots & \ddots \end{bmatrix} \tag{6.11}$$

To be clear let us repeat the formulation of the solution functions in the new diagonalized formulation. The integral of the pure axial solution in diagonalized form takes the form

$$\overline{\mathbf{\Psi}}_a(z)\ \mathbf{c}_a = \begin{bmatrix} -z & 0 \\ 0 & -\frac{1}{2}z^2 \end{bmatrix} \begin{bmatrix} c_{a1} \\ c_{a2} \end{bmatrix} \tag{6.12}$$

while the axial variation of the pure translational modes determined by quadruple integration as described in Paper I (Jönsson and Andreassen, 2011) is represented in diagonalized form as

$$\overline{\mathbf{\Psi}}_1(z)\ \mathbf{c}_1 = \begin{bmatrix} 1 & 0 & 0 & 0 \\ 0 & z & 0 & 0 \\ 0 & 0 & z^2 & 0 \\ 0 & 0 & 0 & z^3 \end{bmatrix} \begin{bmatrix} c_{11} \\ c_{12} \\ c_{13} \\ c_{14} \end{bmatrix}, \qquad \overline{\mathbf{\Psi}}_2(z)\ \mathbf{c}_2 = \begin{bmatrix} 1 & 0 & 0 & 0 \\ 0 & z & 0 & 0 \\ 0 & 0 & z^2 & 0 \\ 0 & 0 & 0 & z^3 \end{bmatrix} \begin{bmatrix} c_{21} \\ c_{22} \\ c_{23} \\ c_{24} \end{bmatrix} \tag{6.13}$$

The axial variation of the pure twist mode (St. Venant torsion) is represented by

$$\overline{\mathbf{\Psi}}_3(z)\mathbf{c}_3 = \begin{bmatrix} 1 & 0 \\ 0 & z \end{bmatrix} \begin{bmatrix} c_{31} \\ c_{32} \end{bmatrix} \tag{6.14}$$

Substituting these full diagonalized solution matrices into a diagonal block matrix formulation the assembled full diagonalized axial classical beam solution functions $\overline{\mathbf{\Psi}}_b$ are obtained.

Concerning the distortional analytical solution functions the i'th eigenvalue results in the following diagonal solution matrix representation:

$$\overline{\mathbf{\Psi}}_{d\,i}(z)\mathbf{c}_{d\,i} = \begin{bmatrix} e^{\xi_i z} & 0 \\ 0 & e^{-\xi_i z} \end{bmatrix} \begin{bmatrix} c_{d\,2i-1} \\ c_{d\,2i} \end{bmatrix} \tag{6.15}$$

The full diagonalized distortional solution functions are assembled in the (diagonal block) distortional solution matrix $\overline{\mathbf{\Psi}}_d$ and multiplied by the assembled vector of distortional constants $\mathbf{c}_d$. Finally, the longitudinal classic beam amplitude solution functions as well as the longitudinal distortional amplitude solution functions are assembled using diagonal block matrices as

$$\overline{\mathbf{\Psi}}(z)\,\mathbf{c} = \begin{bmatrix} \overline{\mathbf{\Psi}}_b(z) & \mathbf{0} \\ \mathbf{0} & \overline{\mathbf{\Psi}}_d(z) \end{bmatrix} \begin{bmatrix} \mathbf{c}_b \\ \mathbf{c}_d \end{bmatrix} \tag{6.16}$$

where $\mathbf{c}$ are the original displacement constants. Using the transformation matrix $\mathbf{H}$ as given in equation (6.9) we can obtain the original formulation of the solution function matrix by using the transformation as shown in equation (6.8).

Introducing the transformation given in equation (6.8) of the longitudinally varying amplitude solution functions in the integrals given in Table 6.1, followed by the use of equations (6.6) and (6.7) and noting that only the diagonal amplitude solution functions are dependent on z allows us to see that the product terms become simple. Thus, the individual components of the stiffness matrix only contain integrals of one product term. For example the transverse stiffness contribution is reformulated as follows:

$$\begin{aligned} \widetilde{\mathbf{K}}^s &= \int_0^L \overline{\mathbf{\Psi}}_h^T \mathbf{H}^T \mathbf{V}_{\mathrm{w}}^T \mathbf{K}^s \mathbf{V}_{\mathrm{w}} \mathbf{H} \overline{\mathbf{\Psi}}_h \, dz \\ &= \int_0^L \overline{\mathbf{\Psi}}_h \overline{\mathbf{V}}_{\mathrm{w}}^T \mathbf{K}^s \overline{\mathbf{V}}_{\mathrm{w}} \overline{\mathbf{\Psi}}_h \, dz \\ &= \overline{\mathbf{V}}_{\mathrm{w}}^T \mathbf{K}^s \overline{\mathbf{V}}_{\mathrm{w}} \circ \int_0^L \overline{\mathbf{\Psi}} \mathbf{J} \overline{\mathbf{\Psi}} \, dz \end{aligned} \tag{6.17}$$

in which $\mathbf{J}$ is a matrix of unit components (i.e. all components are equal to one) and the mathematical symbol $\circ$ represents the Hadamard product also known as the "entry-wise product" or the "Schur product". It is seen that only the diagonal matrix $\overline{\mathbf{\Psi}}$ is a function of z and that the integral of the product terms are easily solved analytically due to the simple longitudinal $\psi(z)$ solution functions. This means that the formulation of the respective beam element stiffness contributions in Table 6.1 can be reformulated as given in Table 6.3.

$$\widetilde{\mathbf{K}}^{\sigma}_{\mathrm{ww}} = \overline{\mathbf{V}}^{T}_{\mathrm{w}}\mathbf{K}^{\sigma}_{\mathrm{ww}}\overline{\mathbf{V}}_{\mathrm{w}} \circ \int_0^L \overline{\mathbf{\Psi}}''\mathbf{J}\overline{\mathbf{\Psi}}''\,dz \qquad \widetilde{\mathbf{K}}^{\sigma}_{\Omega\Omega} = \overline{\mathbf{V}}^{T}_{\Omega}\mathbf{K}^{\sigma}_{\Omega\Omega}\overline{\mathbf{V}}_{\Omega} \circ \int_0^L \overline{\mathbf{\Psi}}''\mathbf{J}\overline{\mathbf{\Psi}}''\,dz$$

$$\widetilde{\mathbf{K}}^{\tau}_{\mathrm{ww}} = \overline{\mathbf{V}}^{T}_{\mathrm{w}}\mathbf{K}^{\tau}_{\mathrm{ww}}\overline{\mathbf{V}}_{\mathrm{w}} \circ \int_0^L \overline{\mathbf{\Psi}}'\mathbf{J}\overline{\mathbf{\Psi}}'\,dz \qquad \widetilde{\mathbf{K}}^{\tau}_{\Omega\mathrm{w}} = \overline{\mathbf{V}}^{T}_{\Omega}\mathbf{K}^{\tau}_{\Omega\mathrm{w}}\overline{\mathbf{V}}_{\mathrm{w}} \circ \int_0^L \overline{\mathbf{\Psi}}'\mathbf{J}\overline{\mathbf{\Psi}}'\,dz$$

$$\widetilde{\mathbf{K}}^{\tau}_{\mathrm{w}\Omega} = \overline{\mathbf{V}}^{T}_{\mathrm{w}}\mathbf{K}^{\tau}_{\mathrm{w}\Omega}\overline{\mathbf{V}}_{\Omega} \circ \int_0^L \overline{\mathbf{\Psi}}'\mathbf{J}\overline{\mathbf{\Psi}}'\,dz \qquad \widetilde{\mathbf{K}}^{\tau}_{\Omega\Omega} = \overline{\mathbf{V}}^{T}_{\Omega}\mathbf{K}^{\tau}_{\Omega\Omega}\overline{\mathbf{V}}_{\Omega} \circ \int_0^L \overline{\mathbf{\Psi}}'\mathbf{J}\overline{\mathbf{\Psi}}'\,dz$$

$$\widetilde{\mathbf{K}}^{s} = \overline{\mathbf{V}}^{T}_{\mathrm{w}}\mathbf{K}^{s}\overline{\mathbf{V}}_{\mathrm{w}} \circ \int_0^L \overline{\mathbf{\Psi}}\mathbf{J}\overline{\mathbf{\Psi}}\,dz$$

Table 6.3: Beam element stiffness contributions enabling analytical integration.

6.1.2 Generalized displacements

The generalized displacements of the present GBT formulation are determined by the first variation of the potential energy, shear constraints and the multi point constraint equations, as described in chapter 3. This degree of freedom space is what we refer to as the GBT-space. In this space the degrees of freedom are determined as the value of the pure axial extension $u^a_z(z)$, the values of the remaining unconstrained transverse displacements $\mathbf{u}^g_{\mathrm{w}}(z)$, and their axial derivatives $\mathbf{u}^{g\,\prime}_{\mathrm{w}}(z)$ as given by the expressions involving the eigenmode vectors, solution functions and solution constants:

$$\begin{bmatrix} u^a_z(z) \\ \mathbf{u}^g_{\mathrm{w}}(z) \\ \mathbf{u}^{g\,\prime}_{\mathrm{w}}(z) \end{bmatrix} = \begin{bmatrix} -\mathbf{T}^{a\,T}_{\Omega}\mathbf{V}_{\Omega}\mathbf{\Psi}'_h(z) \\ \mathbf{T}^{g\,T}_{\mathrm{w}}\mathbf{V}_{\mathrm{w}}\mathbf{\Psi}_h(z) \\ \mathbf{T}^{g\,T}_{\mathrm{w}}\mathbf{V}_{\mathrm{w}}\mathbf{\Psi}'_h(z) \end{bmatrix} \mathbf{c} \tag{6.18}$$

Here the transformations are taken directly from chapter 3. As in a basic beam element formulation we will specify the boundary displacements at the two ends of the beam, i.e. at $z = 0$ and at $z = L$ where L is the beam length. Denoting the assembled boundary displacement vector by $\mathbf{u}_b$ we can write the following equation for the determination of the solution constants:

$$\mathbf{u}_b = \begin{bmatrix} u^a_z(0) \\ \mathbf{u}^g_{\mathrm{w}}(0) \\ \mathbf{u}^{g\,\prime}_{\mathrm{w}}(0) \\ u^a_z(L) \\ \mathbf{u}^g_{\mathrm{w}}(L) \\ \mathbf{u}^{g\,\prime}_{\mathrm{w}}(L) \end{bmatrix} = \begin{bmatrix} -\mathbf{T}^{a\,T}_{\Omega}\mathbf{V}_{\Omega}\mathbf{\Psi}'_h(0) \\ \mathbf{T}^{g\,T}_{\mathrm{w}}\mathbf{V}_{\mathrm{w}}\mathbf{\Psi}_h(0) \\ \mathbf{T}^{g\,T}_{\mathrm{w}}\mathbf{V}_{\mathrm{w}}\mathbf{\Psi}'_h(0) \\ -\mathbf{T}^{a\,T}_{\Omega}\mathbf{V}_{\Omega}\mathbf{\Psi}'_h(L) \\ \mathbf{T}^{g\,T}_{\mathrm{w}}\mathbf{V}_{\mathrm{w}}\mathbf{\Psi}_h(L) \\ \mathbf{T}^{g\,T}_{\mathrm{w}}\mathbf{V}_{\mathrm{w}}\mathbf{\Psi}'_h(L) \end{bmatrix} \mathbf{c} = \mathbf{A}\mathbf{c} \tag{6.19}$$

This equation defines the "square" invertible matrix $\mathbf{A}$ and allows the determination of the solution constants by the beam end displacements as

$$\mathbf{c} = \mathbf{A}^{-1}\mathbf{u}_b \tag{6.20}$$

The first variation of the elastic potential energy in equation (6.3) then takes the form

$$\delta\Pi = \delta\mathbf{c}^T(\widetilde{\mathbf{K}}\mathbf{c} - \widetilde{\mathbf{r}}) \tag{6.21}$$

Substituting beam boundary displacements for the solution constants using equation (6.20) we redefine the formulation to include the end displacements in GBT-space as follows:

$$\delta\Pi = \delta{\mathbf{u}_b}^T\mathbf{A}^{-T}\widetilde{\mathbf{K}}\mathbf{A}^{-1}\mathbf{u}_b - \delta{\mathbf{u}_b}^T\mathbf{A}^{-T}\widetilde{\mathbf{r}} = \delta{\mathbf{u}_b}^T\left(\mathbf{K}_e\mathbf{u}_b - \mathbf{R}_e\right) \tag{6.22}$$

where we have introduced the beam element stiffness matrix in GBT-space as

$$\mathbf{K}_e = \mathbf{A}^{-T}\widetilde{\mathbf{K}}\mathbf{A}^{-1} \tag{6.23}$$

and the beam element load vector in GBT-space as

$$\mathbf{R}_e = \mathbf{A}^{-T}\widetilde{\mathbf{r}} \tag{6.24}$$

For stationarity the first variation of the potential energy must be equal to zero whereby we can write the single element equations as

$$\mathbf{K}_e\mathbf{u}_b = \mathbf{R}_e \tag{6.25}$$

Having a prismatic structure of multiple beam elements we have to setup a global system in which the end boundary displacements (in GBT-space) are assembled. Using a standard finite element procedure to assemble the global system we obtain

$$\mathbf{K}\mathbf{u} = \mathbf{R} \quad \Leftrightarrow \quad \mathbf{u} = \mathbf{K}^{-1}\mathbf{R} \tag{6.26}$$

where $\mathbf{K}$ has to be a positive definite "square" matrix and $\mathbf{R}$ is the load vector corresponding to the chosen load. However, in order to achieve a positive definite matrix it is necessary to apply boundary conditions, for example as described in the next section. In a conventional finite element formulation the displacement field between the nodes is usually interpolated using approximated shape functions. In the present formulation we do not use approximated interpolation functions as we have found the exact shape functions as given in equation (6.18). Furthermore, we can adjust the internal displacement field to the distributed loads on the individual beam element using the particular solutions with adequate boundary conditions as described after the next section.

6.2 Boundary conditions and nodal loads

In the present formulation the global stiffness matrix $\mathbf{K}$ is related to sets of beam end degrees of freedom $\mathbf{u}_{\mathrm{GBT}}$ in the GBT-space and after assembling the

individual element matrices this global matrix will be singular corresponding to the rigid body movements. Thus we have to specify at least six conditions to keep the beam fixed in space in order to solve the equations.

Of the methods used to introduce boundary conditions in the finite element equations (6.26) I have chosen the simple method of adding stiff springs. As the present formulation is in the constrained, eliminated and transformed GBT-space it is rather difficult directly to apply the desired boundary conditions. Therefore the boundary stiffness contributions $\Delta\mathbf{K}_{\mathrm{FE}}$ are formulated in the unconstrained FE-space, $\mathbf{u}_{\mathrm{FE}}$, corresponding to all nodal degrees of freedom shown in Figure 3.5 and the axial derivatives of transverse components of these. For more clarity let us show the GBT and FE-space displacement vectors and their transformation as deduced from chapter 3:

$$\mathbf{u}_{\mathrm{GBT}} = \begin{bmatrix} u_z^a \\ \mathbf{u}_{\mathrm{w}}^g \\ \mathbf{u}_{\mathrm{w}}^{g\,\prime} \end{bmatrix} = \begin{bmatrix} \mathbf{T}_\Omega^{a\,T} & \mathbf{0} & \mathbf{0} \\ \mathbf{0} & \mathbf{T}_{\mathrm{w}}^{g\,T} & \mathbf{0} \\ \mathbf{0} & \mathbf{0} & \mathbf{T}_{\mathrm{w}}^{g\,T} \end{bmatrix} \begin{bmatrix} \mathbf{u}_z \\ \mathbf{u}_{\mathrm{w}} \\ \mathbf{u}_{\mathrm{w}}{}' \end{bmatrix} = \mathbf{T}\,\mathbf{u}_{\mathrm{FE}} \tag{6.27}$$

Thus the beam end spring stiffness contributions $\Delta\mathbf{K}_{\mathrm{FE}}$ are transformed into GBT space by

$$\Delta\mathbf{K}_{\mathrm{GBT}} = \mathbf{T}^T \Delta\mathbf{K}_{\mathrm{FE}} \mathbf{T} \tag{6.28}$$

and the nodal loads (at beam element ends and intersections) are transformed from FE-space to GBT-space by the transformation

$$\Delta\mathbf{R}_{\mathrm{GBT}} = \mathbf{T}^T \Delta\mathbf{R}_{\mathrm{FE}} \tag{6.29}$$

Using this method a wide range of situations may be analyzed. However, other methods involving coupling with traditional finite plate elements is envisioned to be possible and should be further investigated in the future.

6.3 Internal element displacements

The internal beam displacements are represented by the cross-section node displacement vectors $\mathbf{u}_z(z)$ and $\mathbf{u}_{\mathrm{w}}(z)$ as a function of the axial coordinate z. In the beam element these internal displacements are found by superposition of ⓐ the internal displacements induced by the nodal displacements without distributed loading and ⓑ the displacements induced by the loading on the beam with zero nodal displacements.

6.3.1 Nodal displacements

Adhering to this concept equation (6.30) gives us the first contribution as

$$\begin{aligned} \mathbf{u}_{\mathrm{w}}^{\textcircled{a}}(z) &= \mathbf{V}_{\mathrm{w}} \boldsymbol{\Psi}_h(z)\,\mathbf{c} \\ \mathbf{u}_z^{\textcircled{a}}(z) &= -\mathbf{V}_\Omega \boldsymbol{\Psi}_h'(z)\,\mathbf{c} \end{aligned} \tag{6.30}$$

where the constants $\mathbf{c} = \mathbf{A}^{-1}\mathbf{u}_b$ are determined by the nodal displacements, $\mathbf{u}_b$, of the element.

6.3.2 Loading induced displacements

The second contribution involves the solution of the differential equations with boundary conditions corresponding to zero nodal displacements. As the particular solution does not abide to zero displacements at the nodes, this has to be achieved by addition of a homogeneous solution. The boundary conditions for the GBT equations are formulated in chapter 4, which in the present complex formulation corresponds to:

$$\mathbf{u}_b = \begin{bmatrix} -\mathbf{T}_\Omega^{a\,T}\mathbf{V}_\Omega\boldsymbol{\Psi}_h'(0) \\ \mathbf{T}_\mathrm{w}^{g\,T}\mathbf{V}_\mathrm{w}\boldsymbol{\Psi}_h(0) \\ \mathbf{T}_\mathrm{w}^{g\,T}\mathbf{V}_\mathrm{w}\boldsymbol{\Psi}_h'(0) \\ -\mathbf{T}_\Omega^{a\,T}\mathbf{V}_\Omega\boldsymbol{\Psi}_h'(L) \\ \mathbf{T}_\mathrm{w}^{g\,T}\mathbf{V}_\mathrm{w}\boldsymbol{\Psi}_h(L) \\ \mathbf{T}_\mathrm{w}^{g\,T}\mathbf{V}_\mathrm{w}\boldsymbol{\Psi}_h'(L) \end{bmatrix} \mathbf{c}_p + \begin{bmatrix} -\mathbf{T}_\Omega^{a\,T}\mathbf{V}_\Omega\boldsymbol{\Psi}_p'(0) \\ \mathbf{T}_\mathrm{w}^{g\,T}\mathbf{V}_\mathrm{w}\boldsymbol{\Psi}_p(0) \\ \mathbf{T}_\mathrm{w}^{g\,T}\mathbf{V}_\mathrm{w}\boldsymbol{\Psi}_p'(0) \\ -\mathbf{T}_\Omega^{a\,T}\mathbf{V}_\Omega\boldsymbol{\Psi}_p'(L) \\ \mathbf{T}_\mathrm{w}^{g\,T}\mathbf{V}_\mathrm{w}\boldsymbol{\Psi}_p(L) \\ \mathbf{T}_\mathrm{w}^{g\,T}\mathbf{V}_\mathrm{w}\boldsymbol{\Psi}_p'(L) \end{bmatrix} \boldsymbol{\phi} = \mathbf{A}\mathbf{c}_p + \mathbf{B}\boldsymbol{\phi} \tag{6.31}$$

which also defines the particular solution matrix $\mathbf{B}$ that gives the displacement values of the particular solutions at the beam boundaries when multiplied by the two end load intensity values in $\boldsymbol{\phi}$. Inserting that the nodal displacements are zero we find the constants $\mathbf{c}_p$, which determine the homogeneous solutions to add to the particular solution in order to abide the boundary conditions:

$$\mathbf{u}_b = 0 \Rightarrow \mathbf{c}_p = -\mathbf{A}^{-1}\mathbf{B}\boldsymbol{\phi} \tag{6.32}$$

With this knowledge the second contribution is given by equation (4.67) as

$$\begin{aligned} \mathbf{u}_\mathrm{w}^{\textcircled{b}}(z) &= \mathbf{V}_\mathrm{w}\big[\boldsymbol{\Psi}_h(z)\,\mathbf{c}_p + \boldsymbol{\Psi}_p(z)\boldsymbol{\phi}\big] \\ \mathbf{u}_z^{\textcircled{b}}(z) &= -\mathbf{V}_\Omega\big[\boldsymbol{\Psi}_h'(z)\,\mathbf{c}_p + \boldsymbol{\Psi}_p'(z)\boldsymbol{\phi}\big] \end{aligned} \tag{6.33}$$

6.3.3 Superpositioned displacements

Finally, we can superimpose the two solutions ⓐ and ⓑ and find the semi-analytically determined internal displacement vectors as

$$\begin{aligned} \mathbf{u}_\mathrm{w}(z) &= \mathbf{V}_\mathrm{w}\big[\boldsymbol{\Psi}_h(z)\,(\mathbf{c} + \mathbf{c}_p) + \boldsymbol{\Psi}_p(z)\boldsymbol{\phi}\big] \\ \mathbf{u}_z(z) &= -\mathbf{V}_\Omega\big[\boldsymbol{\Psi}_h'(z)\,(\mathbf{c} + \mathbf{c}_p) + \boldsymbol{\Psi}_p'(z)\boldsymbol{\phi}\big] \end{aligned} \tag{6.34}$$

where $\mathbf{c} = \mathbf{A}^{-1}\mathbf{u}_b$ and $\mathbf{c}_p = -\mathbf{A}^{-1}\mathbf{B}\boldsymbol{\phi}$.

6.4 Example

In this illustrative example nodal displacement results as well as stress distribution results of GBT are compared to those found using the commercial FE program `Abaqus`. We consider a simple supported lipped channel beam loaded by two point loads symmetrically placed in the same cross section as shown in Figure 6.1. The beam have a length of 1500 mm consisting of and assembled by three single beam elements of 500 mm. The end sections are constrained against transverse displacements, but otherwise free to warp (and thus also rotate). Further, one of the ends is fixed at a single node against longitudinal translation. An elasticity modulus $E = 2.1 \cdot 10^5$ MPa and a Poisson ratio of $\nu = 0.3$ have been used. For more examples see Paper IV (Andreassen and Jönsson, 2013).

The results found using `Abaqus` are based on isotropic material and the S4 shell element with full 4 point integration. The linear elastic finite element calculations are based on a structured rectangular mesh with a side length seed of 5 mm. The cross section is fixed in the transverse directions at both ends and fixed at a single node against longitudinal translation.

All stress comparisons between the present novel approach and the commercial FE program `Abaqus` are performed in relation to the given maximum stress at the cross section.

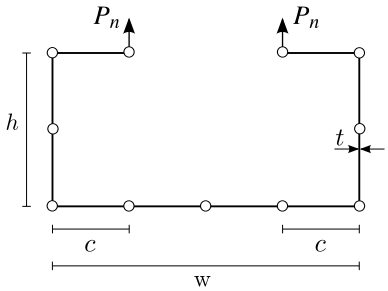

$h = 50$
w $= 100$
$c = 25$
$t = 2.0$
$P_n = 1\ kN$
○ Node

Figure 6.1: Geometry, in-plane discretization, parameter values and load for the lipped channel beam.

Using the parameters as given in Figure 6.1 and 6.2 and the full solution in equation (6.34) leads to the deformed configuration shown in Figure 6.3. Here it is seen that the global deformation is related to flexure of the beam, non-local distortional deformation of the cross section and a very local plate deformation of the lips related to the location of the point loads. Thus three length scales are represented, the global flexural beam mode as seen in Figure 6.3, the non-local distortional deformation of the lips as shown in Figure 6.4, and the local distortional plate deformation of the lip as shown in close-up in Figure 6.5. This example points out the importance of taking distortion into account in order to

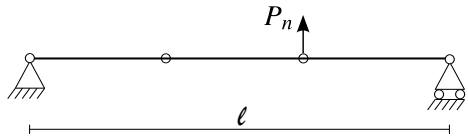

Figure 6.2: Geometry and discretization for a lipped channel beam consisting of 3 elements.

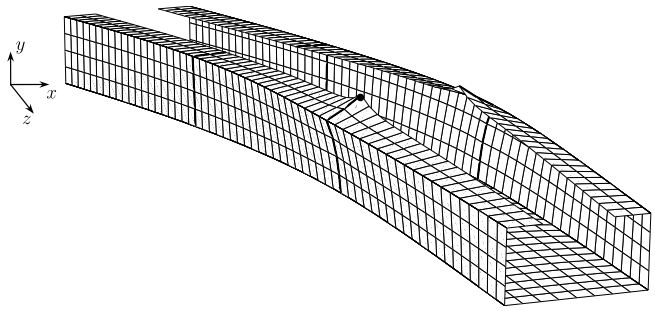

Figure 6.3: GBT plot of the lipped channel with point loads.

obtain a good approximation of the deformation shape. From Figure 6.5 it is seen that the deflection in the longitudinal z-direction decreases exponentially in the y-z-plane. It should also be noted that the deformation is so local that it is difficult to see that the surface is C^1 continuous. The decreasing non-local distortion is clear in the x-z-plot shown in Figure 6.4, which represents a part of the beam that is symmetrical about the loaded cross section. Comparing the nodal displacements of the marked node in Figure 6.3 to the displacement found using a model in the commercial FE program `Abaqus` gives the displacement values and the corresponding deviations shown in Table 6.4. From Table 6.4

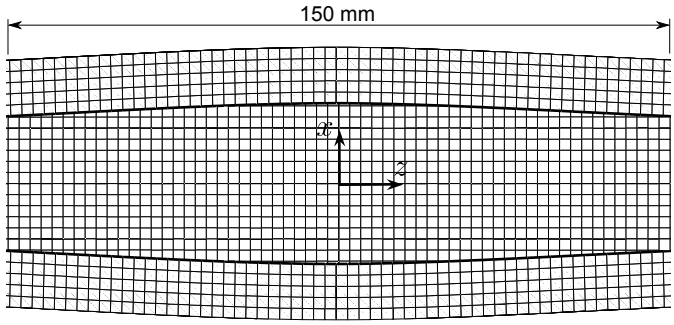

Figure 6.4: GBT plot of the lipped channel to show the exponential decrease in the x-z-plane.

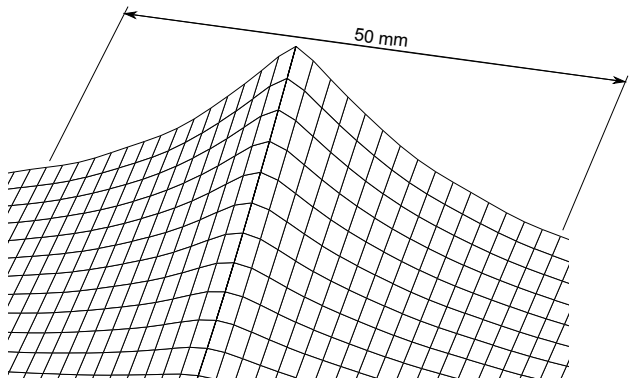

Figure 6.5: GBT plot of the lipped channel to show the exponential decrease in the y-z-plane.

	GBT [mm]	Abaqus [mm]	Difference [%]
u_x	−1.424	−1.415	0.6
u_y	4.697	4.772	1.6

Table 6.4: Nodal displacements of GBT and FE analysis.

the deviation from Abaqus results of the displacement, u_x, in the horizontal direction is 0.6% while the deviation for the vertical displacement, u_y, is 1.6%. Due to the poor discretization of the cross section and the present approach which is based on a beam theory these deviations may be expected.

Having compared the nodal displacement obtained with GBT and Abaqus we take a look at the stress distributions. A comparison of the membrane stresses in the z direction is shown in Figure 6.6. Comparing the stresses in relation to the maximum stress at the cross section a maximum deviation of 4.8% is obtained as shown in Table 6.5. This deviation level is expected as

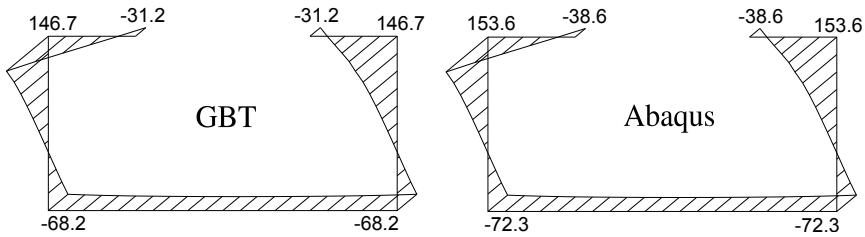

Figure 6.6: Comparison between the axial normal stress distributions obtained with GBT and Abaqus. All values are in MPa.

the chosen point is subjected to very local complex phenomena. The transverse

	GBT [MPa]	Abaqus [MPa]	Difference [%]
σ_z	−31.2	−38.6	4.8
σ_s	492.3	481.9	2.1

Table 6.5: Stress distributions of GBT and FE analysis.

bending stresses are shown in Figure 6.7. In this case a maximum deviation of

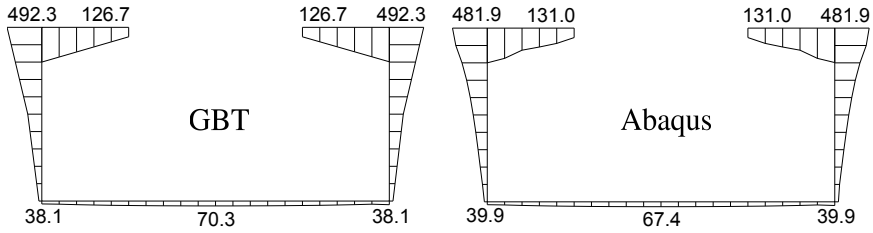

Figure 6.7: Comparison between the transverse bending stress distributions obtained with GBT and Abaqus. All values are in MPa.

2.1% is obtained.

The chosen example here and in Paper IV (Andreassen and Jönsson, 2013) show solutions which are applicable to the finite element formulation.

6.5 Concluding remarks

In this chapter the formulation of a distortional semi-discretized thin-walled beam element has been presented. Using the full assembled homogenous solution along the beam, the beam element stiffness matrices have been found. From the full assembled homogenous solution as well as the full assembled non-homogeneous solution the displacements of the full semi-analytical solution along the beam have been found in the context of a beam element.

Having finally developed a distortional semi-discretized prismatic thin-walled beam element in continuation of the distortional homogeneous and non-homogeneous differential equations and solutions, the next chapter deals with a general discussion regarding this and the previous chapters as well as a comparison of the novel approach to GBT and the conventional GBT.

Chapter 7

Discussion and comparison

Now we have developed a novel mode-based approach by extending the existing thin-walled beam theory to include transverse distortion for open and closed cross sections in a new and theoretical improved context. At the same time we have developed an approach which model distortion by a limited number of degrees of freedom. In this context also an advanced distortional semi-discretized prismatic thin-walled beam element has been developed. Based on these developments this chapter deals with a general discussion as well as a comparison of the novel approach to GBT and conventional GBT.

It should be noted that the present novel approach to generalized beam theory is neither similar to conventional GBT nor an extension of the theory.

7.1 Newsworthy

Within the area of thin-walled structures and with respect to generalized beam theory it is new and interesting that:

- A novel approach to Generalized Beam Theory (GBT) is formulated and involves a new cross-section semi-discretization process as suggested by Zienkiewicz and Taylor (2000b).

- The novel approach involves a new determination of the natural cross-section eigenmodes and related axial solution functions by exact analytical solution of the related first-order GBT equations.

- Furthermore, this thesis adheres to the definition of the warping function given in (Kollbrunner and Hajdin, 1972) which is in contrast to conventional GBT formulation that is developed as a generalization of the classic Vlasov beam theory by including the warping deformation associated with the ”Bredt’s shear flow” around each cell.

- In contrast to the available methods for identification of cross-section deformations modes developed for open cross sections, the present method is able to handle open cross sections as well as closed cross sections without special attention.

- Finding the analytical homogeneous solution to the differential GBT equations which (through the magnitude of the eigenvalues) gives a much better knowledge of the length scales of the modes.

- Discretization into finite GBT beam elements can be performed with prior knowledge of the problem length scales of the individual modes.

- The novel approach has in contrast to conventional GBT been based on the calculus of variations and energy formulations, and formulations for the numerical analysis has been performed based on the finite element method formulations.

- The novel present approach and the developed advanced one-dimensional beam element is based on and is intended to be integrated with standard FEM programs.

- The use of a displacement based finite element method is in contrast to the force method used in conventional GBT, which makes problems according to cross sections containing cells.

As mentioned in section 1.2 the conventional generalized beam theory has been subject to extensive research and is a good alternative to the classical shell finite element method which is often extravagant and unnecessary for many structures having regular geometric plans and simple boundary conditions. However, we have in this thesis and due to the arguments described in section 1.2 requested a new and improved formulation to GBT. In this context some differences between using the conventional GBT and the generalized beam formulation developed in this project are listed above, making the new formulation to an innovative theoretical development.

In the following sections the novel GBT approach and the conventional GBT theory are briefly compared. Also including accompanying illustrative examples. Even though a full comparison of the two formulations is devoted to a future publication, some of the most important differences are pointed out in the comparison.

First of all, the modes found in the present novel approach seem to be similar to the modes found in conventional GBT, see e.g. Silvestre and Camotim (2002a), as well as to the modes found by the modified GBT formulation for

closed cross sections in Gonçalves and Camotim (2004b). In this relation a comparison of the found distortional modes and the modes found by the conventional GBT formulation forms part of the following comparison.

7.2 Comparison of the novel GBT approach and conventional GBT

As mentioned in chapter 2 the novel GBT approach is, among the available distortional theories, most related to the conventional GBT. In this context, this section is devoted to a comparison of the novel GBT approach and the conventional GBT in order to define and place the novel GBT approach among the existing theories. As mentioned in chapter 2 the conventional GBT has also been compared with the cFSM modal approach in relation to the buckling analysis of un-branched thin-walled members (Ádány et al., 2009).

The present novel approach to Generalized Beam Theory (GBT) involves a cross-section semi-discretization process as well as a determination of the natural cross-section eigenmodes and related axial solution functions by exact analytical solution of the related first-order GBT differential equations of fourth order. This is done by first postulating a solution function $\psi(z) = e^{\xi z}$ to the differential equations and afterwards solving the equations as an eigenvalue problem. Consequently, the link between the in-plane modes and the axial variational function is exact. By formulating the eigenvalue problem so that the ξ parameter (which is also an inverse length scale parameter) become the eigenvalue, it is possible to use the eigenvalue as a length scale parameter. Thus the novel approach is different from the conventional GBT formulation developed in Schardt (1966) and Schardt (1989) which solves the equations using the approximate engineering methods, in which the shear coupling terms are neglected, producing orthogonal axial and transverse normal stress modes. In such a case the differential equations are not solved but a weak solution may be found through introduction of the established approximate mode shapes and use of approximate modal amplitude functions. Thus the conventional GBT formulations uses the produced approximated modes as shape functions in a virtual work or potential energy formulation leading to approximated finite GBT beam elements and the discretization has to be performed without proper prior knowledge of the problem length scales of the individual modes.

Regarding the analytical solution of the shear coupled conventional GBT equations published only by (Hanf, 1989) as well as the numerical solution based on power series published by Haakh (2004), it mentioned that both Hanf (1989) and Haakh (2004) use the original orthogonalization procedure of Schardt to establish the GBT equations. Note that these equations are still coupled with respect to shear terms and perhaps transverse strains. Hanf (1989) uses the

reduction of order of the differential equations as in the present thesis, however the description of solution modes, relations to conventional modes and treatment of complex modes is limited. In relation to this the present thesis does not rely on the pre-orthogonalization into orthogonal normal stress modes. In relations to Haakh (2004) who solves the equations numerically using approximating power series, the solutions in the present thesis are found analytically based on the numerical solution of the characteristic eigenvalue problem related to the reduced order differential equations. Note that the exponential solution functions span such a large numerical range that it is evident that the use of power series could lead to inaccuracies for the very short problem length scales of some of the local modes. Furthermore, it is interesting that Haakh (2004) formulates the GBT equations based on a two-dimensional membrane and a plate displacement field, which is independent of the formulation by Schardt (with independent notation) and not directly related to the original beam mode formulations of Schardt. Moreover, his choice of displacement field is specifically related to his choice of interpolation and does not seem consistent and he neglects some higher order (differential) terms and ends up having to use the static procedure, i.e. Grashof's method, for the final shear stress and transverse stress distribution. The work of the present thesis has been formulated as an extension of beam theory with the related shear only in closed cells, and hereby it only includes shear related to torsion and shear flow in closed cells. The beauty of the weak formulation used to allow for shear flow only around cells and to link warping and transverse displacements is profound and leads to a formulation and programming completely independent of the number of cells.

Regarding the energy formulation the novel GBT approach does not include generalized flexural Poisson's effect in contrast to conventional GBT which includes it during the linear stiffness matrix, D_{ik}^{II}, associated with wall torsion.

The novel GBT approach includes rotations as part of the degrees of freedom which is in contrast to conventional GBT which do not.

The novel GBT approach defines a mode as a combination of an in-plane deformation mode and an axial varying amplitude function which is in contrast to conventional GBT which defines a mode only as an in-plane deformation mode (found during a cross-section configuration analysis). The axial varying amplitude function is approximated with a cubic function and solved during a member analysis.

The novel GBT approach is using a FE-formulation and setting up stiffness matrices by using FE-components while the conventional GBT is using the force-method and setting up stiffness matrices by using force-method components.

Even though both methods flow into the same solution, the novel GBT approach then seems to be more elegant and a more academic approach.

Regarding the extensions with other modes as mentioned in section 2.2,

these modes are not considered in the comparison between the two approaches since they are not part of a first generation GBT and may be viewed as patches towards expanded use of a generalized beam theory.

In addition to the previous mentioned differences between the two approaches, it is also important to note that the novel GBT approach uses all the modes in the full solution, which is in contrast to conventional GBT which make a GBT mode selection and thereby only use the modes which in a visual perspective seems to be the most important.

Even though both approaches are operating with very few degrees of freedom in relation to traditional FE formulations, it should be noticed that they are also operating with rather complex and time consuming differential equations and algorithms that are difficult to devise and to implement computationally.

7.2.1 Direct comparison of results

In this subsection we will visually compare the two methods through some examples. The results obtained by the novel approach are based on the associated developed `MATLAB` code while the results obtained by the conventional GBT approach are based on the freely available software package `GBTUL`.

Like other discretized calculation methods, the results depend on the discretization of the calculated part. In the examples we will then use an identical discretization of the cross section in the two approaches. Only open cross sections are compared as `GBTUL` can not yet handle closed cross sections.

Example

As an illustrative example we compare a lipped channel cross section with the geometric parameters, discretization, and values as given i Figure 7.1.

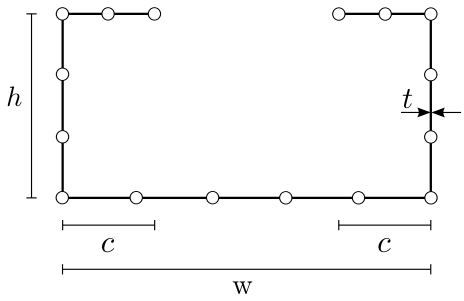

Parameter	Value
h	50
w	100
c	25
t	2.0
∘	Node

Figure 7.1: Geometric parameters and values.

As the local modes are not calculated in the same order, the comparison have to be done between the modes that visually seems to be similar, and not between the modes with the same hierarchical mode number. The visual

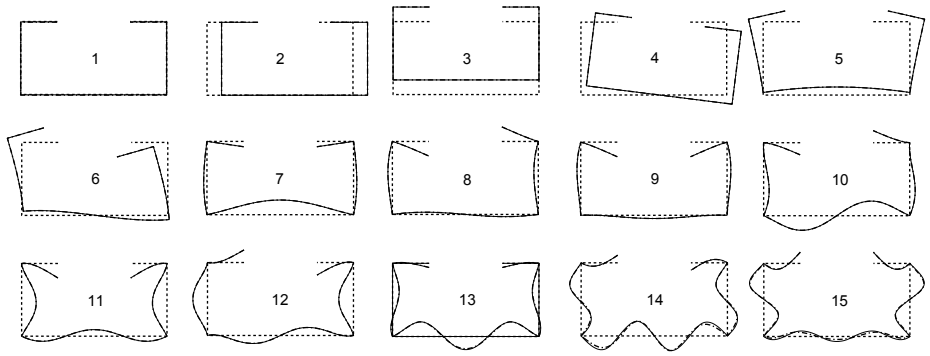

Figure 7.2: Comparison of lipped channel deformation mode in-plane shapes obtained from the novel GBT approach and conventional GBT.

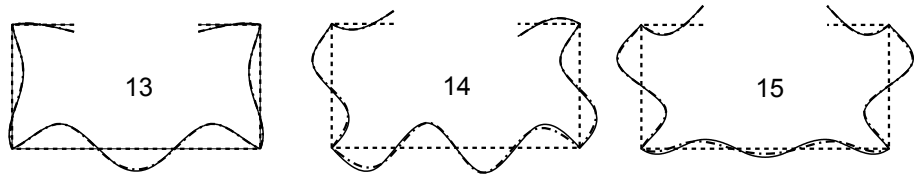

Figure 7.3: Mode shape plot to clearly show the difference between the compared in-plane mode shapes.

comparison is made by calculating the respective modes by the novel GBT approach and conventional GBT respectively, and then showing them on the same plot. All the modes are normalized in accordance with the largest node displacement in either the vertical direction or the horizontal direction. When comparing the first-order mode shapes obtained by the two approaches it is seen from Figure 7.2 and 7.3 that they are all very similar. However, the deviation for the local modes of higher order seems to increase according to an increasing mode number. On the figures, the mode shapes from the two methods are depicted in the same plot, even though they can overlap when having nearly similar mode shapes. The mode shapes obtained from the novel GBT approach are depicted by a complete solid line (–) whilst the mode shapes obtained from the conventional GBT are depicted by a dash-dotted line ($-\cdot-$). As seen from Figure 7.2 and 7.3 the modes are not exactly identical. In this context we choose to modify the novel GBT approach to be more consistent with the conventional GBT approach. Two significant differences which are easy to standardize are (i) the novel GBT approach in contrast to conventional GBT includes rotations in the degrees of freedom and (ii) the novel GBT approach does not include Poisson's effects. To show the effect on the results of these two inconsistencies we will here make another comparison when (i) making a static elimination of

the rotations in the novel GBT approach and (ii) setting the Poisson's ratio equal to 0 in both of the approaches.

7.2.2 Modified comparison of results

In this second comparison we easily set the Poisson's ratio equal to zero in the two approaches, however with respect to the rotational degrees of freedom we have to make a static elimination of the rotations in the novel GBT approach as given in the following:

Static elimination of rotations

In conventional GBT the rotational degrees of freedom are found by solving a statically indeterminate folded-plate problem by means of the force method. In the present formulation this static subproblem is not elementary but involves a reduction of the overall order of interpolation of the transverse displacements using static elimination of the rotations in the transverse stiffness matrix $\mathbf{K}^s_{uu}$. In chapter 3 we have in step II identified the unconstrained degrees of freedom as $\mathbf{v}^u_{\mathrm{w}}$ using the transformation matrix $\mathbf{T}^u_{\mathrm{w}}$ as

$$\mathbf{v}_{\mathrm{w}} = \begin{bmatrix} \mathbf{T}^\alpha_{\mathrm{w}} & \mathbf{T}^3_{\mathrm{w}} & \mathbf{T}^c_{\mathrm{w}} & \mathbf{T}^u_{\mathrm{w}} \end{bmatrix} \begin{bmatrix} \mathbf{v}^\alpha_{\mathrm{w}} \\ v^3_{\mathrm{w}} \\ \mathbf{v}^c_{\mathrm{w}} \\ \mathbf{v}^u_{\mathrm{w}} \end{bmatrix} \tag{7.1}$$

However to obtain the same degrees of freedom space as in conventional GBT we have to statically eliminate the rotations at all nodes except the one (first), which has been related to pure twist. To do this we identify the unconstrained transverse displacements $\mathbf{v}^v_{\mathrm{w}}$ and the unconstrained rotations $\mathbf{v}^\phi_{\mathrm{w}}$ in the FE degree of freedom space $\mathbf{v}_{\mathrm{w}}$ by introducing the related transformations, which pick out the relevant degrees of freedom $\mathbf{T}^v_{\mathrm{w}}$ and $\mathbf{T}^\phi_{\mathrm{w}}$. This allows us to perform the following introduction of related transformation matrices and new degree of freedom:

$$\mathbf{v}^u_{\mathrm{w}} = {\mathbf{T}^u_{\mathrm{w}}}^T \mathbf{v}_{\mathrm{w}} = {\mathbf{T}^u_{\mathrm{w}}}^T (\mathbf{T}^v_{\mathrm{w}} \mathbf{v}^v_{\mathrm{w}} + \mathbf{T}^\phi_{\mathrm{w}} \mathbf{v}^\phi_{\mathrm{w}}) = \bar{\mathbf{T}}^v_{\mathrm{w}} \mathbf{v}^v_{\mathrm{w}} + \bar{\mathbf{T}}^\phi_{\mathrm{w}} \mathbf{v}^\phi_{\mathrm{w}} \tag{7.2}$$

in which we have introduced the transformations $\bar{\mathbf{T}}^v_{\mathrm{w}} = {\mathbf{T}^u_{\mathrm{w}}}^T \mathbf{T}^v_{\mathrm{w}}$ and $\bar{\mathbf{T}}^\phi_{\mathrm{w}} = {\mathbf{T}^u_{\mathrm{w}}}^T \mathbf{T}^\phi_{\mathrm{w}}$. Using the transformation on the transverse stiffness term in the following equation (7.3) from chapter 3:

$$\begin{bmatrix} K^\sigma_{33} & \mathbf{K}^\sigma_{3u} \\ \mathbf{K}^\sigma_{u3} & \bar{\mathbf{K}}^\sigma_{uu} \end{bmatrix} \begin{bmatrix} v^3_{\mathrm{w}} \\ \mathbf{v}^u_{\mathrm{w}} \end{bmatrix} \psi'''' - \begin{bmatrix} K^\tau_{33} & \mathbf{K}^\tau_{3u} \\ \mathbf{K}^\tau_{u3} & \mathbf{K}^\tau_{uu} \end{bmatrix} \begin{bmatrix} v^3_{\mathrm{w}} \\ \mathbf{v}^u_{\mathrm{w}} \end{bmatrix} \psi'' + \begin{bmatrix} 0 & \mathbf{0} \\ \mathbf{0} & \mathbf{K}^s_{uu} \end{bmatrix} \begin{bmatrix} v^3_{\mathrm{w}} \\ \mathbf{v}^u_{\mathrm{w}} \end{bmatrix} \psi = \begin{bmatrix} 0 \\ \mathbf{0} \end{bmatrix} \tag{7.3}$$

and neglecting contributions from shear stiffness as well as warping stiffness related to the rotational degrees of freedom we find

$$\mathbf{v}^\phi_{\mathrm{w}} = -{\mathbf{K}^s_{\phi\phi}}^{-1} \mathbf{K}^s_{\phi v} \mathbf{v}^v_{\mathrm{w}} = \mathbf{T}^{\phi v}_{\mathrm{w}} \mathbf{v}^v_{\mathrm{w}} \qquad \text{where} \qquad \mathbf{T}^{\phi v}_{\mathrm{w}} = -{\mathbf{K}^s_{\phi\phi}}^{-1} \mathbf{K}^s_{\phi v} \tag{7.4}$$

$\bar{\mathbf{K}}^{\sigma}_{vv} = \mathbf{T}^{uv\,T}_{\mathrm{w}} \bar{\mathbf{K}}^{\sigma}_{uu} \mathbf{T}^{uv}_{\mathrm{w}}$	$\mathbf{K}^{\tau}_{vv} = \mathbf{T}^{uv\,T}_{\mathrm{w}} \mathbf{K}^{\tau}_{uu} \mathbf{T}^{uv}_{\mathrm{w}}$	$\bar{\mathbf{K}}^{s}_{vv} = \mathbf{T}^{uv\,T}_{\mathrm{w}} \mathbf{K}^{s}_{uu} \mathbf{T}^{uv}_{\mathrm{w}}$
$\mathbf{K}^{\sigma}_{3v} = \mathbf{K}^{\sigma}_{3u} \mathbf{T}^{uv}_{\mathrm{w}}$	$\mathbf{K}^{\tau}_{3v} = \mathbf{K}^{\tau}_{3u} \mathbf{T}^{uv}_{\mathrm{w}}$	

Table 7.1: Statically reduced stiffness matrices.

Here we have introduced the transformed matrices $\mathbf{K}^{s}_{\phi\phi} = \bar{\mathbf{T}}^{\phi\,T}_{\mathrm{w}} \mathbf{K}^{s}_{uu} \bar{\mathbf{T}}^{\phi}_{\mathrm{w}}$ and $\mathbf{K}^{s}_{\phi v} = \bar{\mathbf{T}}^{\phi\,T}_{\mathrm{w}} \mathbf{K}^{s}_{uu} \bar{\mathbf{T}}^{v}_{\mathrm{w}}$. Combining the two transformations (7.2) and (7.4) we find the following transformation from the unconstrained transverse translation d.o.f. $\mathbf{v}^{v}_{\mathrm{w}}$ to the unconstrained d.o.f. $\mathbf{v}^{u}_{\mathrm{w}}$:

$$\mathbf{v}^{u}_{\mathrm{w}} = \left(\bar{\mathbf{T}}^{v}_{\mathrm{w}} - \bar{\mathbf{T}}^{\phi}_{\mathrm{w}} \mathbf{T}^{\phi v}_{\mathrm{w}}\right) \mathbf{v}^{v}_{\mathrm{w}} = \mathbf{T}^{uv}_{\mathrm{w}} \mathbf{v}^{v}_{\mathrm{w}} \qquad \text{where} \qquad \mathbf{T}^{uv}_{\mathrm{w}} = \bar{\mathbf{T}}^{v}_{\mathrm{w}} - \bar{\mathbf{T}}^{\phi}_{\mathrm{w}} \mathbf{T}^{\phi v}_{\mathrm{w}} \tag{7.5}$$

Let us use this transformation to reduce the number of equations in (7.1) to the following:

$$\begin{bmatrix} K^{\sigma}_{33} & \mathbf{K}^{\sigma}_{3v} \\ \mathbf{K}^{\sigma}_{v3} & \bar{\mathbf{K}}^{\sigma}_{vv} \end{bmatrix} \begin{bmatrix} v^{3}_{\mathrm{w}} \\ \mathbf{v}^{v}_{\mathrm{w}} \end{bmatrix} \psi'''' - \begin{bmatrix} K^{\tau}_{33} & \mathbf{K}^{\tau}_{3v} \\ \mathbf{K}^{\tau}_{v3} & \mathbf{K}^{\tau}_{vv} \end{bmatrix} \begin{bmatrix} v^{3}_{\mathrm{w}} \\ \mathbf{v}^{v}_{\mathrm{w}} \end{bmatrix} \psi'' + \begin{bmatrix} 0 & \mathbf{0} \\ \mathbf{0} & \bar{\mathbf{K}}^{s}_{vv} \end{bmatrix} \begin{bmatrix} v^{3}_{\mathrm{w}} \\ \mathbf{v}^{v}_{\mathrm{w}} \end{bmatrix} \psi = \begin{bmatrix} 0 \\ \mathbf{0} \end{bmatrix} \tag{7.6}$$

where the new matrices have been introduced in Table 7.1. Solving this equation and using equation (7.5) for back substitution leads to a method which is more similar to conventional GBT.

The methods developed by Schardt, Silvestre, Camotim and co-workers will therefore be applicable for the presented modified (elimination of rotations) formulation.

Example

Having modified the novel GBT approach by setting Poisson's ratio equal to zero and using the presented modified (elimination of rotations) formulation we get results as shown in Figure 7.4 and 7.5 where a comparison of some relevant in-plane deformation mode shapes is depicted. Also in this example only open cross sections are compared as `GBTUL` cannot currently handle closed cross sections. In Figure 7.4 the mode shapes obtained from the modified novel GBT approach are depicted by a complete solid line (–) whilst the mode shapes obtained from the conventional GBT are depicted by a dash-dotted line ($-\cdot-$). The presence of the two mode shapes, obtained from the two methods and depicted in the same plot in Figure 7.4, are found to be close to identical. As a conclusion from Figure 7.4 it is clear that using the given discretization and modifications very similar results are obtained from the two methods.

Many of the topics given in the previous chapters point to a need for further investigations and suggestions for these are made in chapter 9 concerning recommendations for future work following after a recap with conclusions.

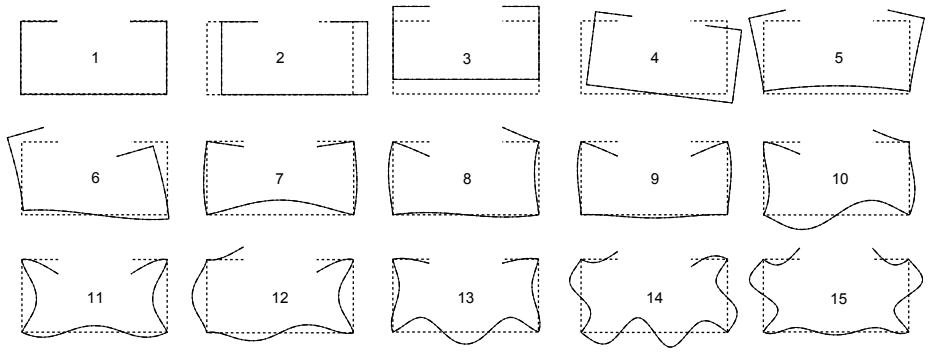

Figure 7.4: Comparison of lipped channel deformation mode in-plane shapes obtained from the novel GBT approach (Poisson's ratio equal to 0 and rotations eliminated) and conventional GBT.

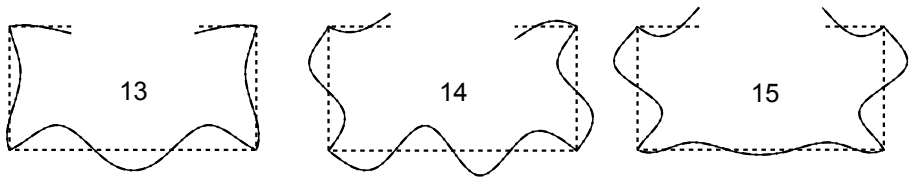

Figure 7.5: Mode shape plot to clearly show the similarity between the compared modified in-plane mode shapes.

Chapter 8
Conclusion

During this thesis we have described the importance of taking distortion of the cross section into account as well as the importance of developing a novel approach which model distortion by a limited number of degrees of freedom. Furthermore, we have presented current available analysis techniques taking in-plane distortion into account as well as presented an overview based on a literature review.

We have presented a novel GBT approach including a new systematic method accompanied by a detailed description for the full semi-discretization process from kinematic assumptions, potential energy, potential energy variation leading to the formulation of the homogeneous differential equations of a generalized beam theory (GBT) and the establishment of the full solution through identification of all eigenvalues and eigenmodes.

The beam displacement field has been separated into a sum of products of the cross-section displacement modes and their axial variation. This displacement field has been constrained to follow the shear assumptions made in Vlasov beam theory by a weak formulation of the constant shear flow assumption. Thus allowing the identical treatment of both open and closed cross sections.

The coupled homogeneous fourth-order differential equations of GBT have not been solved approximately, but by a reduction of order accompanied by a doubling of the number of equations and the introduction of a state vector, as in non-proportionally damped dynamic analysis.

It is clear that the eigenvalues of the distortional modes found are inverse length scale parameters or attenuation parameters which define the axial solution functions and allow us to predict the length of the distortional displacement field. This may be used to determine the degree of discretization in the developed distortional beam element.

We have included distributed loads in the novel semi-discretized formulation

of the distortional differential equations. By using the distortional modal matrix found for the homogeneous system we have transformed the non-homogeneous distortional differential equations into the eigenmode space, and then obtained the uncoupled set of differential equations including the distributed loads. This uncoupling is very important in GBT, since the shear stiffness contribution cannot be neglected nor approximated by the combination of axial stiffness and transverse stiffness, especially for closed cross sections. This means that conventional modal analysis (corresponding to orthogonal damping) cannot be used to solve the equations and analytical solutions must therefore be based on the eigenmodes found for the reduced order distortional differential equations.

We have presented the extension of the novel GBT approach to include the geometrical stiffness terms which are needed for column buckling analysis. The distortional differential equations are extended to a formulation including geometrical stiffness terms by using the initial stress approach to formulate the instability problem. The derived GBT differential equations with initial stress have been solved as an eigenvalue problem leading to a number of buckling modes and associated buckling stresses for simply supported columns in compression. The changes in solution modes and length scales are investigated.

We have presented the formulation of an advanced generalized one-dimensional semi-discretized prismatic thin-walled beam element including distortional contributions. Using the full assembled homogenous solution along the beam the finite beam element stiffness matrices have been found. From the full assembled homogenous solution as well as the full assembled non-homogeneous solution the generalized displacements of the exact full solution along the beam have been found.

Based on the novel approach a general discussion has been given. Furthermore, the modes found seem to be similar to the modes found in conventional GBT, see e.g. Silvestre and Camotim (2002a), as well as to the modes found by the modified GBT formulation for closed cross sections (Gonçalves and Camotim, 2004b). In this relation a comparison of the found distortional modes and the modes found by the conventional GBT formulation has been made and associated illustrative examples given.

The novel approach presented is a considerable theoretical and practical achievement, since it without approximation gives the full analytical solution along the loaded beam for a given discretization of the cross section. Furthermore, the approach is valid without special attention also for closed single or multi cell cross sections. Reasonable matches are obtained in all example cases confirming that this new developed GBT approach provides reasonable results with a very small computational cost making it an alternative to the traditional and time consuming FE calculations and the other available methods.

After having given final concluding remarks the next chapter deals with recommendations for future works.

Chapter 9

Recommendations for Future Work

There are several recommendations for future work within the presented areas of research. Directions for these are:

Extend the developed beam element also to include stability contributions. At the present state the beam element do not include the geometrical stiffness terms and thus do not deal with column buckling analyzes. The geometrical stiffness terms are only dealt with within the analytical solution of the coupled differential equations.

The GBT software developed and related to the present novel approach should be designed in a format to be released for public use. At the present state the program code is made in `MATLAB`, however it could be appropriate to do the code in traditional programming languages, such as `C/C++` or `Java` to make it more accessible to the public.

The presented theory may be extended also to include dynamical contributions and thus the possibility to perform dynamic analysis. This could lead to the determination of distortional modes of vibration and the formulation of a finite element model able to cope with dynamic problems. This will allow the development of simple solutions for many distortional problems of practical interest.

An important task such as a modeling of connections between the present advanced beam elements would be interesting. Different thin-walled structural elements are often connected using mechanical fasteners, which constrain the displacements of certain points in the structural elements. The connections must be able to handle or obtain compatible displacements of the connected elements at the points of connection. The investigation could also include the

behaviors of practical connections thus including experimental investigations.

Finally, investigation could be done in the context of performing a more elaborate comparison between the present approach and the conventional GBT approach. The objectives of such a comparison is to clarify the fundamental differences between the two methods and to provide an extensive mode-based comparison including e.g. displacement- and energy based comparisons.

Bibliography

Abaqus (2008). Abaqus, Theory manual v6.8 Simulia. 5.4, 5.4

Ádány, S. and Schafer, B. (2006a). Buckling mode decomposition of single-branched open cross-section members via finite strip method: application and examples. *Thin-Walled Structures*, 44:585–600. 2.3

Ádány, S. and Schafer, B. (2006b). Buckling mode decomposition of single-branched open cross-section members via finite strip method: derivation. *Thin-Walled Structures*, 44:563–84. 2.3

Ádány, S. and Schafer, B. (2008). A full modal decomposition of thin-walled, single-branched open cross-section members via the constrained finite strip method. *Journal of Constructional Steel Research*, 64:12–29. 2.3

Ádány, S., Silvestre, N., Schafer, B., and Camotim, D. (2009). GBT and cFSM: Two modal approaches to the buckling analysis of unbranched thin-walled members. *Advanced steel construction*, 5(2, Sp. Iss. SI):195–223. 6th International Conference on Steel and Aluminium Structures (ICSAS 07), Oxford, England, Jul 24-27, 2007. 2, 2.3, 7.2

Ádány, S., Silvestre, N., Schafer, B. W., and Camotim, D. (2006). Buckling analysis of unbranched thin-walled members using cFSM and GBT: a comparative study. Proceedings of International Colloquium on Stability and Ductility of Steel Structures (SDSS 2006 - Lisboa, 6-8/9), D. Camotim, N. Silvestre, P.B. Dinis (eds.), IST Press, 205-212. 2

Andreassen, M. J. and Jönsson, J. (2009). Distortional Modes of Thin-Walled Beams. In *Proceedings of the 7th EUROMECH Solid Mechanics Conference – Mini-Symposia (ISBN: 978-989-96264-2-3) (paperid: 0680) , pages: 11, 2009, APMTAC – Portuguese Association for Theoretical, Applied and Computational Mechanics, Laboratório Nacional de Engenharia Civil, Av. do Brasil,*

101, 1700-066 Lisboa, Portugal. ESMC2009, 7th EUROMECH Solid Mechanics Conference, 2009, Instituto Superior Técnico, Lisbon, Portugal. 3, 5

Andreassen, M. J. and Jönsson, J. (2011). Distortional eigenmodes and solutions for thin-walled beams. In *Thin-Walled Structures, Recent Research Advancences and Trends, 2011, ECCS – European Convention for Constructional Steelwork. International Conference on Thin-Walled Structures (ICTWS) – 6, 2011, Timisoara, Romania.* (ISBN: 978-92-9147-102-7). 4, 5

Andreassen, M. J. and Jönsson, J. (2012a). Distortional buckling modes of semi-discretized thin-walled columns. *Thin-Walled Structures*, 51:53–63. 5, 5.4

Andreassen, M. J. and Jönsson, J. (2012b). Distortional solutions for loaded semi-discretized thin-walled beams. *Thin-Walled Structures*, 50:116–127. 4, 4.7, 4.7

Andreassen, M. J. and Jönsson, J. (2013). A distortional semi-discretized thin-walled beam element. *Thin-Walled Structures*, 62:142–157. 6.4, 6.4

Avery, P., Mahendran, M., and Nasir, M. (2000). Flexural capacity of hollow flange beams. *Journal of Constructional Steel Research*, 53:201–223. 2.1.5

Baláž, I. (1999). Dünnwandige Stäbe mit offenem oder geschlossenem deformierbaren Querschnitt. *Stallbau*, 68, Heft 1:70–77. 2.1.4

Barbero, E. (2000). Prediction of buckling-mode interaction in composite columns. *Mech. Compos. Mater. Struct.*, 7:269–284. 1.1.3

Barbero, E., Dede, E., and Jones, S. (2000). Experimental verification of buckling-mode interaction in intermediate-length composite columns. *Int. J. Solids Struct.*, 37, 29:3919–3934. 1.1.3

Basaglia, C., Camotim, D., and Silvestre, N. (2007a). GBT-based analysis of the local and global buckling behavior of thin-walled steel frames subjected to arbitrary loadings. In *Proceedings of Fifth International Conference on Advances in Steel Structures (ICASS 2007 – Singapore, 05-07/12)*, pages 309–315. 2.1.6

Basaglia, C., Camotim, D., and Silvestre, N. (2007b). GBT-based analysis of the local-plate, distortional and global buckling behavior of thin-walled steel frames. In *Proceedings of Structural Stability Research Council 2007 Annual Stability Conference (SSRC2007 – New Orleans, 18-21/04)*, pages 391–412. 2.1.6

Basaglia, C., Camotim, D., and Silvestre, N. (2008a). GBT-based post-buckling analysis of thin-walled steel members and frames. In *Proceedings of Structural Stability Research Council 2008 Annual Stability Conference (SSRC 2008 – Nashville, 02-05/04)*, pages 215–237. 2.1.6

Basaglia, C., Camotim, D., and Silvestre, N. (2008b). Global buckling analysis of plane and space thin-walled frames in the context of GBT. *Thin-Walled Structures*, 46:79–101. 2.1.6

Basaglia, C., Camotim, D., and Silvestre, N. (2009). Non-linear Generalized Beam Theory formulation for open-section thin-walled members with arbitrary support conditions. In *Proceedings of the Twelfth International Conference on Civil, Structural and Environmental Engineering Computing (CC 2009 – Funchal, Portugal, 01-04/09)*. Civil-Comp Press. (full paper on CD-ROM proceedings). 2.1.6

Basaglia, C., Camotim, D., and Silvestre, N. (2011). Non-linear GBT formulation for open-section thin-walled members with arbitrary support conditions. *Computers and Structures*, 89:1906–1919. 2.1.6

Bebiano, R. (2009). *Stability and Dynamics of Thin-Walled Members*. PhD thesis, Technical University of Lisbon. 2.1.6

Bebiano, R., Pina, P., Silvestre, N., and Camotim, D. (2008a). GBTUL – Buckling and vibration analysis of thin-walled members. Technical report, DECivil/IST, Technical University of Lisbon, (http://www.civil.ist.utl.pt/gbt). 3, 5.4

Bebiano, R., Silvestre, N., and Camotim, D. (2005). Buckling and post-buckling behavior of stiffened cold-formed steel columns: a comparative study. In *Proceedings of the 4th European Conference on Steel and Composite Structures (EUROSTEEL 2005 – Maastricht, 08-10/06)*, pages 145–153. Druck und Verlagshaus Mainz GmbH Aachen. 2.1.6

Bebiano, R., Silvestre, N., and Camotim, D. (2007). GBT formulation to analyze the buckling behavior of thin-walled members subjected to non-uniform bending. *International Journal of Structural Stability and Dynamics*, 7(1):23–54. 2.1.6

Bebiano, R., Silvestre, N., and Camotim, D. (2008b). GBTUL – A code for the buckling analysis of cold-formed steel members. In *Proceedings of 19th International Specialty Conference on Recent Research and Developments in Cold-Formed Steel Design and Construction, R. LaBoube, W.-W. Yu (Editors), St. Louis, 14-15 October*, pages 61–79. 2.1.6

Berdichevsky, V. (2009). *Variational Principles of Continuum Mechanics-Vol 1.* Springer-Verlag. 3.4.1

Camotim, D., Basaglia, C., and Silvestre, N. (2010). GBT buckling analysis of thin-walled steel frames: A state-of-the-art report. *Thin-Walled Structures*, 48(10–11):726–43. 2.1.6

Camotim, D. and Dinis, P. (2011). Coupled instabilities with distortional buckling in cold-formed steel lipped channel columns. *Thin-Walled Structures*, 49:562–575. 2.1.6

Camotim, D., Silvestre, N., Dinis, P., Bebiano, R., and Basaglia, C. (2006a). Recent progress in the numerical analysis of thin-walled steel members and frames. In *Proceedings of International Symposium on Innovative Design of Steel Structures, B. Young (Editor), (Hong Kong, 10/11)*, pages 63–104. 2.1.6

Camotim, D., Silvestre, N., Goncalves, R., and Dinis, P. (2004). *GBT analysis of thin-walled members: new formulations and applications.* Thin-Walled Structures: Recent Advances and Future Trends in Thin-Walled Structures Technology, Canopus Publishing Ltd., Bath, 137–168. 2.1.6

Camotim, D., Silvestre, N., Goncalves, R., and Dinis, P. (2006b). GBT-Based structural analysis of thin-walled members – Overview, recent progress and future developments. In *Advances in Engineering Structures, Mechanics and Construction, Pandey M, Xie W-C, Xu L, (Editors), Waterloo: Springer (Dordrecht);*, pages 187–204. 2.1.6

Casafont, M., Marimon, F., Pastor, M., and Ferrer, M. (2011). Linear buckling analysis of thin-walled members combining the Generalised Beam Theory and the Finite Element Method. *Computers and Structures*, 89:1982–2000. 2.3

Cheung, Y. (1976). *Finite Strip Method in Structural Analysis.* Pergamon Press, Oxford. 2

Cheung, Y. K. and Tham, L. G. (1998). *The Finite Strip Method.* CRC Press, Boca Raton. 2

Conchon, R. (2001). *Berechnung von Platten mit der Verallgemeinerten Technischen Biegetheorie (Analysis of Plates in Generalised Beam Theory).* PhD thesis, Dissertation, D17, TU Darmstadt. 2.1.1

Cook, R. (2001). *Concepts and applications of finite element analysis, 4th ed.* John Wiley & Sons, Inc., United States. 3.4.3

Correia, J., Branco, F., Silva, N., Camotim, D., and Silvestre, N. (2009). First-order, buckling and post-buckling behavior of GFRP pultruded beams: Part 1

– experimental study. In *Proceedings of the Twelfth International Conference on Civil, Structural and Environmental Engineering Computing (CC 2009 – Funchal, Portugal, 01-04/09), Topping B. and Costa L. and Barros R. (Editors)*. Civil-Comp Press. Paper 31 (full paper on CD-ROM proceedings). 2.1.6

Davies, J. and Jiang, C. (1998). Design for Distortional Buckling. *Journal of Constructional Steel Research*, 46:174–175. 2.1.2

Davies, J., Jiang, C., and Leach, P. (1994). The analysis of restrained purlins using Generalised Beam Theory. In *Proceedings of the 12th International Specialty Conference on Cold-Formed Steel Structures (St. Louis, USA, 18-19/10), Yu W-W. and LaBoube R. (eds.), 109-120.* 2.1.2

Davies, J. and Leach, P. (1992). Some applications of Generalized Beam Theory. In *Proceedings of the 11th International Specialty Conference on Cold-Formed Steel Structures (St. Louis, USA, 20-21/10), Yu, W-W. and LaBoube, R. (Editors)*, pages 479–501. University of Missouri-Rolla. 2.1.2

Davies, J. and Leach, P. (1994a). First-order generalised beam theory. *Journal of Constructional Steel Research*, 31(2-3):187–220. 1.2

Davies, J. and Leach, P. (1994b). First-order Generalized Beam Theory. *Journal of Constructional Steel Research*, 31:187–220. 2.1.2

Davies, J. and Leach, P. (1994c). Second-order Generalized Beam Theory. *Journal of Constructional Steel Research*, 31:221–241. 2.1.2

Davies, J., Leach, P., and Taylor, A. (1997). The design of perforated cold-formed steel sections subject to axial load and bending. *Thin-Walled Structures*, 29(1–4):141–157. 2.1.2

Davies, J. M. (2000). Recent research advances in cold-formed steel structures. *Journal of Constructional Steel Research*, 55(1-3):267–288. 2.1.2

Dinis, P., Camotim, D., and Silvestre, N. (2006). GBT formulation to analyse the buckling behavior of thin-walled members with arbitrarily "branched" open cross-sections,. *Thin-Walled Structures*, 40:20–38. 2.1.6

Dinis, P., Camotim, D., and Silvestre, N. (2012). On the mechanics of thin-walled angle column instability. *Thin-Walled Structures*, 52:80–89. 2.1.6

Dinis, P., Gonçalves, R., and Camotim, D. (2008). On the local and global buckling behavior of cold-formed steel hollow-flange channel beams. In *Proceedings of the Fifth International Conference on Thin-Walled Structures (ICTWS 2008 – Gold Coast, Australia, 18-20/06), M. Mahendran (Editor)*, volume 1, pages 425–432. 2.1.6

Dinis, P. B., Camotim, D., and Silvestre, N. (2010). On the local and global buckling behaviour of angle, T-section and cruciform thin-walled members. *Thin-Walled Structures*, 48(10–11):786–797. 2.1.6

Erp, G. M. V. and Menken, C. M. (1990). The spline finite-strip method in the buckling analyses of thin-walled structures. *Communications in Applied Numerical Methods*, 6:477–784. 2

Gere, J. and Timoshenko, S. (1997). *Mechanics of Materials*. Pws Pub Co, 4th edition. 1.1.1

Girmscheid, G. (1984). *Ein Beitrag zur Verallgemeinerten Technischen Biegetheorie unter Berücksichtigung der Umfangsdehnungen, Schubverzerrungen und grosser Verformungen (A Contribution to Generalised Beam Theory Regarding Transverse and Shear Strain and Large Deformations)*. PhD thesis, Dissertation, D17 TU Darmstadt. 2.1.1

Godoy, L., Barbero, E., and Raftoyiannis, I. (1995). Interactive buckling analysis of fiber-reinforced thin-walled columns. *Journal of Composite Materials*, 29, 5:591–613. 1.1.3

Goncalves, R. and Camotim, D. (2010). Steel-concrete composite bridge analysis using Generalised Beam Theory. *Steel and Composite Structures*, 10(3):223–243. 2.1.6

Gonçalves, R. (2007). *Análise de Vigas de Parede Fina com Secção Deformável (Analysis of Thin-Walled Beams with Deformable Cross-Section)*. PhD thesis, IST-Technical University of Lisbon, Portugal. (in Portuguese). 2.1.6

Gonçalves, R. and Camotim, D. (2004a). Aplicação da Teoria Generalizada de Vigas (GBT) ao estudo da estabilidade local e global de vigas de aço enformadas a frio (Application of Generalized Beam Theory (GBT) to the study of local and global stability of cold-formed steel beams). In *Congresso de Métodos Computacionais em Engenharia (CMCE–Lisbon, 31/05-02/06), C.M. Soares et al. (Editors)*, number 191. (full paper in CD-ROM; in Portuguese). 2.1.6

Gonçalves, R. and Camotim, D. (2004b). GBT local and global buckling analysis of aluminium and stainless steel columns. *Computers and Structures*, 82(17–19:1473–1484. 2.1.6, 7.1, 8

Gonçalves, R. and Camotim, D. (2007). Thin-walled member plastic bifurcation analysis using Generalised Beam Theory. *Advances in Engineering Software*, 38:637–646. 2.1.6

Gonçalves, R. and Camotim, D. (2011). Generalised Beam Theory-based finite elements for elastoplastic thin-walled metal members. *Thin-Walled Structures*, 49:1237–1245. 2.1.6

Gonçalves, R. and Camotim, D. (2012). Geometrically non-linear Generalised Beam Theory for elasto-plastic thin-walled metal members. *Thin-Walled Structures*, 51:121–129. 2.1.6

Gonçalves, R., Camotim, D., and Dinis, P. (2006). Box girder bridge analysis using Generalized Beam Theory. In *Proceedings of the International Colloquium on Stability and Ductility of Steel Structures (SDSS'06 – Lisbon, 06-08/09), Camotim, D. and Silvestre, N. and Dinis, P.B. (Editors)*, pages 1027–1036. IST Press. 2.1.6

Gonçalves, R., Dinis, P., and Camotim, D. (2009). GBT formulation to analyse the first-order and buckling behaviour of thin-walled members with arbitrary cross-sections. *Thin-Walled Structures*, 47:583–600. 2.1.6, 2.1.6

Gonçalves, R., Grognec, P. L., and Camotim, D. (2010). GBT-based semi-analytical solutions for the plastic bifurcation of thin-walled members. *International Journal of Solids and Structures*, 47(1):34–50. 2.1.6

Haakh, A. (2010). Lagerungsbedingungen und Lagerkräfte in der Verallgemeinerten Technischen Biegelehre. *Stahlbau*, 79(2):144–151. 2.1.1

Haakh, A. U. (2004). *Die Erweiterung der VTB für allgemeine dünnwandige Querschnitte sowie die Lösung des Differentialgleichungssystems mit Potenzreihen.* PhD thesis, Technical University of Darmstadt, Germany. 2.1.1, 2.2, 7.2

Halme, T. (2001). Generalized Beam Theory in thin plate analysis. In *Proceedings of the 2nd European Conference on Computational Mechanics (ECCM 2001–Krakow, Poland, 26-29/06), Waszczyszyn, Z. and Pamin, J. (Editors)*, pages 1072–1073. Datacomp. (full paper in CD-ROM). 2.1.3

Halme, T. (2002). Cross-sectional property calculation in Generalized Beam Theory. In *Book of Abstracts of the Fifth World Congress on Computational Mechanics (VWCCM – Vienna, 07–12/07), Mang, H.A.,. Rammerstofer, F.G and Eberhardsteiner, J. (Editors)*, volume 2, page 450. 2.1.3

Hancock, G. J. (1985). Distortional buckling of steel storage rack columns. *Journal of Structural Engineering*, 11(12). 5.3, 5.4

Hanf, M. (1989). *Die geschlossene Lösung der linearen Differentialgleichungssysteme der Verallgemeinerten Technischen Biegetheorie mit einer Anwendung*

auf die Ermittlung plastischer Grenzlasten. PhD thesis, Technical University of Darmstadt, Germany. 1.3, 2.1.1, 2.2, 7.2

Hanf, M. (2010). Eine Erweiterung der Verallgemeinerten Technischen Biegetheorie zur Erfassung von Scheibenschubverzerrungen. *Stahlbau*, 79(2):109–125. 2.1.1

Heppner, K. (1997). *Die Berechnung von geometrisch und statisch nichtlinearen Schwingungen von vorwiegend längs beanspruchten, prismatischen Schalen mit Hilfe der VTB, (Analysis of Geometrically and Statically Nonlinear Vibrations of Mainly Axially Loaded Prismatic Shells Using GBT)*. PhD thesis, Technical University of Darmstadt, Germany. 2.1.1

Hughes, T. (2000). *The finite element method–Linear static and dynamic finite element analysis*. Prentice-Hall, Inc., Englewood Cliffs, N.J. 1

Jiang, C. (1994). *Stability analysis of light gauge steel members using the finite element mehtod and the Generalized Beam Theory*. PhD thesis, University of Salford, UK. 2.1.2

Jönsson, J. (1998). Determination of shear stresses, warping functions and section properties of thin-walled beams using finite elements. *Computers & Structures*, 68(4):393–410. 1.1.3, 1.3

Jönsson, J. (1999a). Distortional theory of thin-walled beams. *Thin-Walled Structures*, 33(4):269–303. 1.3, 3.4.3, 3.4.4, 4.1

Jönsson, J. (1999b). Distortional warping functions and shear distributions in thin-walled beams. *Thin-Walled Structures*, 33(4):245–268. 1.3

Jönsson, J. and Andreassen, M. J. (2011). Distortional eigenmodes and homogeneous solutions for semi-discretized thin-walled beams. *Thin-Walled Structures*, 49:691–707. 2.1.6, 3, 3.4.4, 3.7.1, 3.8, 4.2, 5.3, 6.1.1

Jönsson, J. and Andreassen, M. J. (2012). A semi-discretization approach to generalized beam theory and analytical solutions of the generalized column equations. In *Proceedings of the 8th EUROMECH Solid Mechanics Conference – Mini-Symposia, 2012, Graz, Austria.* 5.3

Jönsson, J., Krenk, S., and Damkilde, L. (1995). Recursive Substructuring of Finite Elements. *Computers & Structures*, 54:395–404. 1

Kesti, J. and Davies, J. (1999). Local and distorsional buckling of thin-walled short columns. *Thin-Walled Structures*, 34–2:115–134. 2.1.2

Kollbrunner, C. and Hajdin, N. (1972). *Dünnwandige Stäbe 1, Stäbe mit undeformierbaren Querschnitten.* Springer-Verlag. 1.1.2, 1.3, 3, 3.1, 3.1, 4.1, 7.1

Kollbrunner, C. and Hajdin, N. (1975). *Dünnwandige Stäbe 2, Stäbe mit deformierbaren Querschnitten, Nicht-elastisches Verhalten dünnwandiger Stäbe.* Springer-Verlag. 1.1.2, 1.1.3, 1.3

Krenk, S. (1989a). *Three-Dimensional Elastic Beam Theory, Part 1.* Technical University of Denmark, Department of Structural Engineering. 1.1.2, 3.4.1

Krenk, S. (1989b). *Three-Dimensional Elastic Beam Theory, Part 2.* Technical University of Denmark, Department of Structural Engineering. 1.1.2, 1.1.3

Krenk, S. and Damkilde, L. (1992). Torsionssteifigkeit und Deformation von Rahmenecken aus I-trägern. *Stahlbau*, 61:173–178. 1.1.2

Křístek, V. (1979). *Theory of Box Girders.* John Wiley & Sons, Czechoslovakia. 1.1.3

Lanczos, C. (1949). *The Variational Principles of Mechanics.* University of Toronto Press. 3.4.1

Leach, P. (1989). *The Generalized beam Theory with finite difference applications.* PhD thesis, University of Salford, UK. 2.1.2

Lepistö, J., Nikula, S., and Niemi, E. (1996). Optimum design of cold-formed sections using Generalized Beam Theory. In *Proceedings of the Second International Conference on Coupled Instabilities in Metal Structures (CIMS 1996–Liége, 05–07/09), Rondal, J. and Dubina, D. and Gioncu, V. (Editors)*, pages 101–108. Imperial College Press, London. 2.1.3

Li, Z. and Schafer, B. (2010). Buckling analysis of cold-formed steel members with general boundary conditions using CUFSM: conventional and constrained finite strip methods. In *Proceedings of the 20th Int. Spec. Conf. on Cold-Formed Steel Structures, St. Louis, MO.* 2, 5.4

Loja, M. and Soares, C. M. (2002). Modelling and design of adaptive structures using B-spline strip models. *Composite Structures*, 57(1-4):245–251. 2

Miosga, G. (1976). *Vorwiegend längsbeanspruchte dünnwandige prismatische stäbe und platten mit endlichen elastischen Verformungen (Mainly axially loaded thin-walled rods and plates with large deformations).* PhD thesis, Dissertation, D17 TU Darmstadt. 2.1.1

Möller, R. (1982). *Zur Berechnug Prismatischer Strukturen mit Beliebigem Nicht Formtreuem Querschnitt (Analysis of prismatic structures with arbitrary deformable sections).* PhD thesis, Bericht nr. 2, Institut für Statik, Technische Hochschule Darmstadt. 2.1.1

Mörschardt, S. (1990). Die Verallgemeinerte Technische Biegetheorie für Faltwerke mit Kragteilen (GBT for FPS with cantilever elements in the section). In *Festschrift Richard Schardt, Technische Hochschule Darmstadt, 51*, pages 259–275. 2.1.1

Murray, N. W. (1986). *Introduction to the theory of thin-walled structures.* Clarendon Press, Oxford. 1.1.2

Nedelcu, M. (2010). GBT formulation to analyse the behaviour of thin-walled members with variable cross-section. *Thin-Walled Structures*, 48(8):629–638. 2.3

Petersen, P., Krenk, S., and Damkilde, L. (1991). Stabilitet af rammer af tyndpladeprofiler. Technical report, Department of Structural Engineering, Technical University of Denmark. R 265 (in Danish). 1.1.2

Prola, L. (2002). *Estabilidade Local e Global de Elementos Estruturais de Aço Enformados a Frio (Local and global stability of cold-formed steel members).* PhD thesis, IST-Technical University of Lisbon, Portugal. (in Portuguese). 2

Raftoyiannis, I. (1994). *Buckling mode interaction in FRP columns.* PhD thesis, College of Engineering, West Virginia University, USA. 1.1.3

Ranzi, G. and Luongo, A. (2011). A new approach for thin-walled member analysis in the frame work of GBT. *Thin-Walled Structures*, 49:1404–1414. 2.3

Rendek, S. and Baláž, I. (2002). Computer program employing Generalised Beam Theory – Stability and ductility of steel structures. *Akadémiai Kiadó*, pages 809–16. Budapest. 2.1.4

Rendek, S. and Baláž, I. (2004). Distortion of thin-walled beams. *Thin-Walled Structures*, 42(2):255–277. 2.1.4

Rondal, J. (2000). Cold formed steel members and structures - General Report. *Journal of Constructional Steel Research*, 55(1-3):155–158. 2.3

Saal, G. (1974). *Ein Beitrag zur Schwingungsberechnung von Dünnwandigen, Prismatischen Schalentragwerken mit Unverzweigtem Querschnitt (A contribution to the dynamic analysis of thin-walled prismatic structures with unbranched sections).* PhD thesis, Dissertation, D17 TU Darmstadt. 2.1.1

Schafer, B. and Ádány, S. (2006). Modal decomposition for thin-walled member stability using the finite strip method. *Advances in Engineering Structures, Mechanics and Construction, Springer*, pages 411–422. 2, 2.3

Schardt, C. (1995). *Ein Beitrag zur Berechnung gekoppelter Eigenschwingungen angerissener prismatischer Stäbe unter Berücksichtigung von Querschnittsverformungen (A contribution to the analysis of coupled eigen–vibrations of prismatic rods with cracks regarding distortions)*. PhD thesis, Dissertation, D17 TU Darmstadt. 2.1.1

Schardt, R. (1966). Eine Erweiterung der technischen Biegelehre für die Berechnung biegesteifer prismatischer Faltwerke. *Stahlbau*, Heft 6:161–171. 1.1.3, 1.2, 2.1.1, 7.2

Schardt, R. (1968). Einfluss der Querschnittsverformung auf das Biegeknicken und das Biegedrillknicken (Influence of distortion on column–buckling and lateral-torsional buckling). In *8. IVBH Kongress, Schlussbericht, Wien*, pages 359–362. 2.1.1

Schardt, R. (1970). Anwendung der Erweiterten Technischen Biegetheorie auf die Berechnung prismatischer Faltwerke und Zylinderschalen nach Theorie I. und II. Ordnung (Application of Generalised Beam Theory to the analysis of prismatic folded plate structures and cylindric shells in first and second order theory). In *IASS Symposium on Folded Plates and Prismatic Structures, Vienna, 28/09–02/10*, volume 1. 2.1.1

Schardt, R. (1989). *Verallgemeinerte Technische Biegetheorie*. Springer-Verlag. 1.1.3, 3, 1.2, 2.1.1, 2.2, 2.2, 7.2

Schardt, R. (1994a). Generalized Beam Theory – An adequate method for coupled stability problems. *Thin-walled Structures*, 19:161–180. 2.1.1

Schardt, R. (1994b). Lateral torsional and distortional buckling of channel- and hat-sections. *Journal of Constructional Steel Research*, 31(2-3):243–265. 2.1.1

Schardt, R. and Heinz, D. (1991). Vibrations of thin-walled prismatic structures under simultaneous static load unsing Generalized Beam Theory. *Structural Dynamics, W.B. Krätzig et al. (eds.), Balkema, Rotterdam*, pages 921–927. 2.1.1

Schardt, R., Heppner, K., and Neujhar, M. (1995). Über die Ermittlung eines Schwingbeiwertes für prismatische Brücken mit der VTB, (Calculation of a dynamic factor for prismatic bridges using GBT). *Bauingenieur*, 70:531–539. 2.1.1

Schardt, R. and Schardt, C. (2006). Unstiffened element with torsional restraint – An analytical approach for post-buckling behaviour using GBT. In *Proceedings of the International Colloquium on Stability and Ductility of Steel Structures (SDSS 2006 – Lisbon, 06-08/09), D. Camotim and N. Silvestre and P.B. Dinis (Editors)*, pages 177–188. IST Press. 2.1.1

Schardt, R. and Schrade, W. (1982). *Kaltprofil-Pfetten (Cold-formed purlins).* PhD thesis, Bericht Nr. 1 des Instituts für Statik der TH Darmstadt. 2.1.1

Schrade, W. (2010). Anwendung der Verallgemeinerten Technischen Biegetheorie in der Ingenieurpraxis. *Stahlbau*, 79(2):127–135. 2.1.1

Silva, N., Camotim, D., and Silvestre, N. (2008a). GBT cross-section analysis of thin-walled members with arbitrary cross-sections: a novel approach. In *Proceedings of the 5th International Conference on Thin-Walled Structures (ICTWS 2008 - Gold Coast, Australia, 18-20/06), Mahendran M. (ed.), 1161-1171 (vol. II).* Fifth International Conference on Thin-Walled Structures Brisbane, Australia. 2.1.6

Silva, N., Camotim, D., Silvestre, N., Correia, J., and Branco, F. (2009). First-order, buckling and post-buckling behavior of GFRP pultruded beams: Part 2 – numerical simulation. In *Proceedings of the Twelfth International Conference on Civil, Structural and Environmental Engineering Computing (CC 2009 – Funchal, Portugal, 01-04/09), Topping B. and Costa L. and Barros R. (Editors)*. Civil-Comp Press. Paper 32 (full paper on CD-ROM proceedings). 2.1.6

Silva, N., Camotim, D., Silvestre, N., Correia, J., and Branco, F. (2011). First-order, buckling and post-buckling behaviour of GFRP pultruded beams. Part 2: Numerical simulation. *Computers and Structures*, 89:2065–2078. 2.1.6

Silva, N., Silvestre, N., and Camotim, D. (2008b). Non-linear behavior and failure analysis of laminated FRP composite thin-walled members. In *Proceedings of the 5th International Conference on Thin-Walled Structures (ICTWS 2008 – Gold Coast, Australia, 18-20/06), Mahendran, M. (Editor)*, volume 2, pages 1189–1196. 2.1.6

Silva, N., Silvestre, N., and Camotim, D. (2010). GBT formulation to analyse the buckling behaviour of FRP composite open-section thin-walled columns. *Composite Structures*, 93(1):79–92. 2.1.6

Silva, N. F. and Silvestre, N. (2007). On the influence of material couplings on the linear and buckling behaviour of I-section composite columns. *International Journal of Structural Stability and Dynamics*, 7(2):243–272. 2.1.6

Silvestre, N. (2005). *Generalised Beam Theory: New Formulations, Numerical Implementation and Applications*. PhD thesis, IST. Technical University of Lisbon. (in Portuguese). 2.1.6, 2.2, 2.2

Silvestre, N. (2007). Generalised beam theory to analyse the buckling behaviour of circular cylindrical shells and tubes. *Thin-Walled Structures*, 45:185–198. 2.1.6

Silvestre, N. (2008a). Buckling behaviour of elliptical cylindrical shells and tubes under compression. *International Journal of Solids and Structures*, 45:4427–4447. 2.1.6

Silvestre, N. (2008b). Length dependence of critical measures in single-walled carbon nanotubes. *International Journal of Solids and Structures*, 45:4902–4920. 2.1.6

Silvestre, N. (2012). On the accuracy of shell models for torsional buckling of carbon nanotubes. *European Journal of Mechanics – A/Solids*, 32:103–108. 2.1.6

Silvestre, N., Bebiano, R., and Camotim, D. (2005). On the distortional post-buckling asymmetry of cold-formed steel channel columns with different stiffener configurations. In *Proceedings of Structural Stability Research Council 2005 Annual Stability Conference (SSRC 2005 – Montréal, 06-09/04)*, pages 63–88. 2.1.6

Silvestre, N. and Camotim, D. (2002a). First-order generalised beam theory for arbitrary orthotropic materials. *Thin-Walled Structures*, 40(9):755–789. 2.1.6, 7.1, 8

Silvestre, N. and Camotim, D. (2002b). Second-order generalised beam theory for arbitrary orthotropic materials. *Thin-Walled Structures*, 40(9):791 – 820. 2.1.6

Silvestre, N. and Camotim, D. (2003a). GBT stability analysis of pultruded FRP lipped channel members. *Computers and Structures*, 81(18-19):1889–1904. 2.1.6

Silvestre, N. and Camotim, D. (2003b). Non-linear generalised beam theory for coldformed steel members. *International Journal of Structural Stability and Dynamics*, 3(4):461–490. 2.1.6

Silvestre, N. and Camotim, D. (2004a). Distortional buckling formulae for cold-formed steel C and Z-section members: Part I – Derivation. *Thin-Walled Structures*, 42(11):1567–1597. 2.1.6

Silvestre, N. and Camotim, D. (2004b). Distortional buckling formulae for cold-formed steel C and Z-section members: Part II – Validation and Application. *Thin-Walled Structures*, 42(11):1599–1629. 2.1.6

Silvestre, N. and Camotim, D. (2004c). Distortional buckling formulae for cold-formed steel rack-section members. *Steel & Composite Structures*, 4(1):49–75. 2.1.6

Silvestre, N. and Camotim, D. (2006a). GBT-based local and global vibration analysis of loaded composite thin-walled members. *International Journal of Structural Stability and Dynamics*, 6(1):1–29. 2.1.6

Silvestre, N. and Camotim, D. (2006b). Local-plate and distortional post-buckling behaviour of cold-formed steel lipped channel columns with intermediate stiffeners. *Journal of Structural Engineering (ASCE)*, 132(4):529–540. 2.1.6

Silvestre, N. and Camotim, D. (2006c). Vibration behaviour of axially compressed cold-formed steel members. *Steel & Composite Structures*, 6(3):221–236. 2.1.6

Silvestre, N., Camotim, D., and Silva, N. (2011). Generalized beam theory revisited: From the kinematical assumptions to the deformation mode determination. *International Journal of Structural Stability and Dynamics*, 11(5,SI):969–997. 2.1.6, 2.3

Simao, F. (2007). *Post-buckling bifurcational analysis of thin-walled prismatic members in the context of the Generalized Beam Theory*. PhD thesis. 2.1.5

Simao, P. and da Silva, L. S. (2002). Comparative analysis of the stability of open and closed thin-walled section members in the framework of Generalized Beam Theory. In *Proceedings of the 3rd European Conference on Steel Structures (EUROSTEEL 2002 – Coimbra, Portugal, 19-20/09), Lamas, A. and Simões da Silva, L. (Editors)*, volume 1, pages 711–721. 2.1.5

Simao, P. and da Silva, L. S. (2003a). Comportamento pós-bifurcacional de colunas metálicas enformadas a frio com secção de parede fina no contexto da GBT (Postbuckling behavior of thin-walled cold-formed steel columns in the context of GBT). In *Actas do VII Congresso de Mecânica Aplicada e Computacional (Évora, Portugal, 14–16/04), Infante Barbosa J. (Editor), (in Portuguese)*, volume 1, pages 269–278. 2.1.5

Simao, P. and da Silva, L. S. (2003b). The post-buckling behavior of open cross-section thin-walled columns in the context of Generalized Beam Theory (GBT). In *Computational Methods in Engineering and Science, Lu et al. (Editors)*, pages 891–898. Balkema Publishers, Lisse. 2.1.5

Simão, P. and da Silva, L. S. (2004). A unified energy formulation for the stability analysis of open and closed thin-walled members in the framework of the Generalized Beam Theory. *Thin-Walled Structures*, 42(10):1495–1517. 2.1.5

Simão, P. and da Silva, L. S. (2008a). GBT stability analysis of thin-walled cold-formed compact hollow-flange steel beams. In *Proceedings of the Fifth International Conference on Thin-Walled Structures (ICTWS 2008 – Gold Coast, Australia, 18-20/06), Mahendran, M. (Editor)*, volume 2, pages 1181–1188. 2.1.5

Simão, P. and da Silva, L. S. (2008b). GBT stability analysis of thin-walled cold-formed slender hollow-flange steel beams. In *Proceedings of the Fifth International Conference on Coupled Instabilities in Metal Structures (CIMS 2008 – Sydney, 23-25/06), Rasmussen, K. and Wilkinson, T. (Editors)*, volume 1, pages 257–264. 2.1.5

Stahlbau (2010). Stahlbau 79(2). *Ernst & Sohn Verlag für Architektur und technische Wissenschaften GmbH & Co. KG, Berlin, Germany.* 2.1.1

Steinle, A. (1967). *Torsion und Profilverformung – Berechnung eines in Feldmitte durch ein Torsionsmoment belasteten Trägers mit einem verformbaren biegesteifen Rechteckkastenprofil mit auskragenden Gurten.* PhD thesis, Universität (Technische Hochschule), Stuttgart. 2nd edition. 1.1.3

Steinle, A. (1970). Praktische Berechnung eines durch Verkehrslasten unsymmetrisch belasteten Kastentragers am Beispeil der Henschbachtalbrucke. *Beton- und Stahlbau*, 10:249–253. 1.1.3

Strehl, C. (2010). Verallgemeinerte Technische Biegetheorie – Einordnung in die Entwicklungsgeschichte statischer Berechnungsmethoden. *Stahlbau*, 79(2):106–108. 2.1.1

Timoschenko, S. P. and Gere, J. (1963). *Theory of elastic stability.* McGraw-Hill. 1.1.2, 5.3

Timoshenko, S. (1983). *History of Strength of Materials.* Dover Publications. 1.1, 1.1.1

Timoshenko, S. and Goodier, J. N. (1951). *Theory of Elasticity, 2nd ed.* McGraw-Hill. 1.1.1, 3

Vlasov, V. Z. (1961). *Thin-walled elastic beams.* Israel Program for scientific translations, Jerusalem, Israel, 2nd edition. 1.1.2, 1.1.3, 1.3, 3.4, 5

Williams, F. and Wittrick, W. (1968). Computational procedures for a matrix analysis of the stability and vibrations of thin flat-walled structures in compression. *Int. J. of Mechanical Sciences*, 11:979–798. 2

Wlassow, W. S. (1958). *Allgemeine Schalentheorie und ihre Anwendungen in der Technik*. Akademie verlag Berlin. 2.1.1

Wright, R. (1968). BEF analogy for analysis of box girders. *Journal of the Structural Division, Proceedings of ASCE*, 94, ST7:1719–1743. 1.1.3

Zienkiewicz, O. and Taylor, R. (2000a). *The Finite Element Method*, volume 1. Butterworth-Heinemann, Oxford, 5 edition. 1

Zienkiewicz, O. and Taylor, R. (2000b). *The Finite Element Method*, volume 2. Butterworth-Heinemann, Oxford, 5 edition. 1, 2.3, 7.1

Appendix A

Errata

List of known errors in the appended papers:

- In Paper I, the referred page number in reference [20] should be 207 instead of 308.
- Due to an error in the programmed `MATLAB` code in the form of dividing the straight-element stiffness contribution $\mathbf{k}^{\sigma}_{\mathrm{ww}}$ by the length, b_e, the following tables and figures have to be corrected: In Paper I, Table 6 and the associated Figures 6 and 7 should be corrected as given in the following as respectively Table A.1 with the associated Figures A.1 and A.2.
- In Paper I, Table 7 and the associated Figures 9 and 10 should be corrected as given in the following as respectively Table A.2 with the associated Figures A.3 and A.4.
- In Paper III, Table 4 should be corrected as given in the following as Table A.3.
- In Paper II, Figure 5, 9, 13 and 17 the unit of the distributed loads should be in N/mm^2 instead of N/mm.

Mode			Eigenvalues		Axial solution
Type		No.	$\xi^2 \times 10^6$	$\xi \times 10^3$	$\psi(z)$
Beam	**global**	0	0	0	$-c_{a1}z - c_{a2}z^2$
		1	0	0	$c_{11} + c_{12}z + c_{13}z^2 + c_{14}z^3$
		2	0	0	$c_{21} + c_{22}z + c_{23}z^2 + c_{24}z^3$
		3	0	0	$c_{31} + c_{32}z$
Distortional	**non-local**	4	0.37	0.61	$c_{d1}e^{\xi z} + c_{d2}e^{-\xi z}$
		5	$3.35 - 26.47i$	$\pm(3.87 - 3.42i)$	$c_{d3}e^{\xi z} + c_{d4}e^{-\xi z}$
		6	$3.35 + 26.47i$	$\pm(3.87 + 3.42i)$	$c_{d5}e^{\xi z} + c_{d6}e^{-\xi z}$
		7	$4.22 - 49.98i$	$\pm(5.21 - 4.79i)$	$c_{d7}e^{\xi z} + c_{d8}e^{-\xi z}$
		8	$4.22 + 49.98i$	$\pm(5.21 + 4.79i)$	$c_{d9}e^{\xi z} + c_{d10}e^{-\xi z}$
	local	9	1003.43	31.68	$c_{d11}e^{\xi z} + c_{d12}e^{-\xi z}$
		10	1088.79	33.00	$c_{d13}e^{\xi z} + c_{d14}e^{-\xi z}$
		11	$945.87 - 1390.34i$	$\pm(36.25 - 19.18i)$	$c_{d15}e^{\xi z} + c_{d16}e^{-\xi z}$
		12	$945.87 + 1390.34i$	$\pm(36.25 + 19.18i)$	$c_{d17}e^{\xi z} + c_{d18}e^{-\xi z}$

Table A.1: Eigenvalues ξ^2, the ξ value, and the related axial solutions for the lipped channel cross-section.

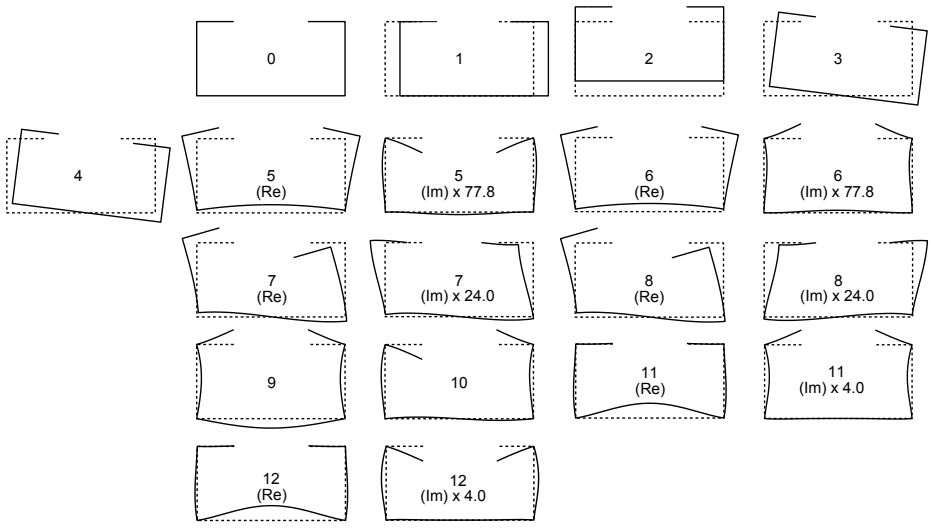

Figure A.1: Lipped channel – 13 in-plane deformation mode shapes.

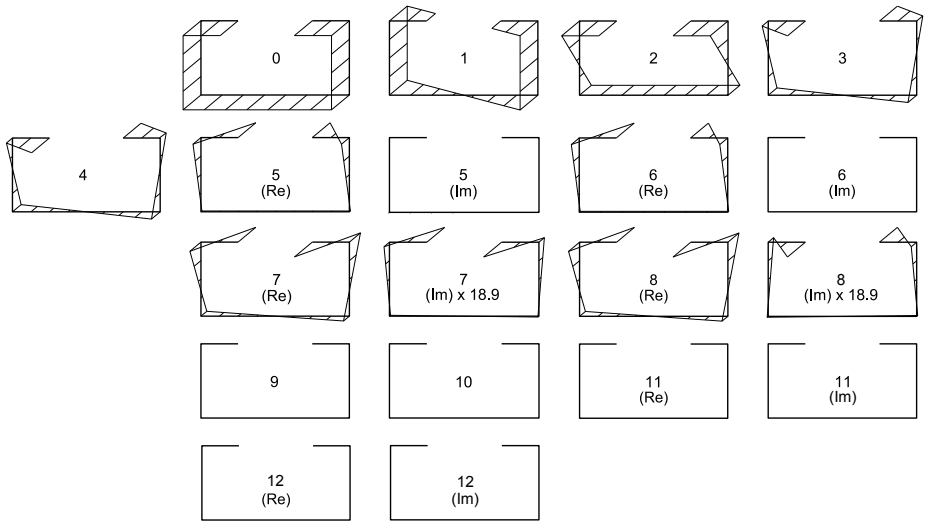

Figure A.2: Lipped channel – 13 warping deformation mode shapes.

Mode			**Eigenvalues**		**Axial solution**
Type		No.	$\xi^2 \times 10^6$	$\xi \times 10^3$	$\psi(z)$
Beam	**global**	0	0	0	$-c_{a1}z - c_{a2}z^2$
		1	0	0	$c_{11} + c_{12}z + c_{13}z^2 + c_{14}z^3$
		2	0	0	$c_{21} + c_{22}z + c_{23}z^2 + c_{24}z^3$
		3	0	0	$c_{31} + c_{32}z$
Distortional	**non-local**	4	$0.72 - 36.93i$	$\pm(4.34 - 4.26i)$	$c_{d1}e^{\xi z} + c_{d2}e^{-\xi z}$
		5	$0.72 + 36.93i$	$\pm(4.34 + 4.26i)$	$c_{d3}e^{\xi z} + c_{d4}e^{-\xi z}$
	local	6	$891.43 - 1127.00i$	$\pm(34.12 - 16.52i)$	$c_{d5}e^{\xi z} + c_{d6}e^{-\xi z}$
		7	$891.43 + 1127.00i$	$\pm(34.12 + 16.52i)$	$c_{d7}e^{\xi z} + c_{d8}e^{-\xi z}$
		8	$849.60 - 1569.79i$	$\pm(36.29 - 21.63i)$	$c_{d9}e^{\xi z} + c_{d10}e^{-\xi z}$
		9	$849.60 + 1569.79i$	$\pm(36.29 + 21.63i)$	$c_{d11}e^{\xi z} + c_{d12}e^{-\xi z}$

Table A.2: Eigenvalues ξ^2, the ξ value, and the related axial solutions for the rectangular box cross-section.

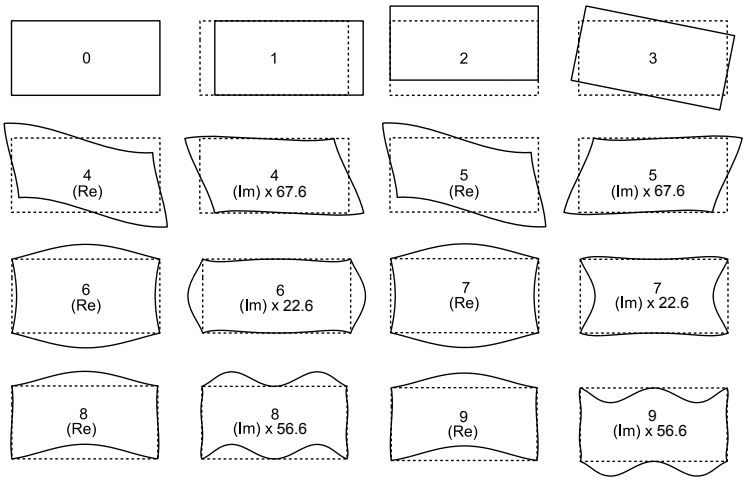

Figure A.3: Rectangular box cross-section – 10 in-plane deformation mode shapes.

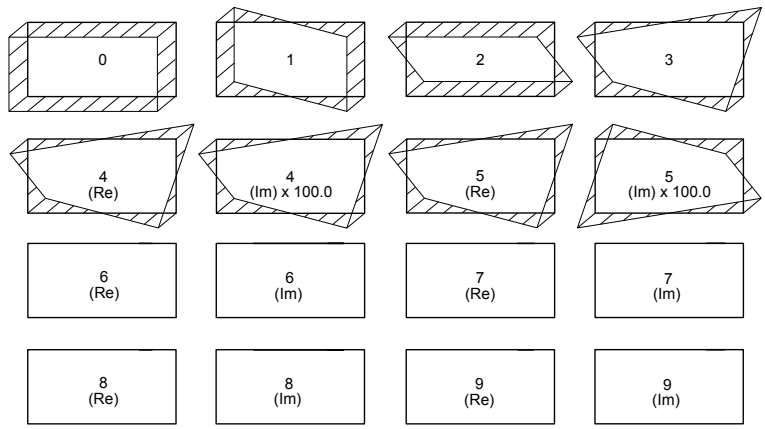

Figure A.4: Rectangular box cross-section – 10 warping deformation mode shapes.

m	Nr. of half waves n	Abaqus [MPa]	GBT [MPa]	Diff. %	GBTUL [MPa]	Diff. %	CUFSM [MPa]	Diff. %
1	13	404	350	13.4	412	2.0	412	2.0
20	1	580	590	1.7	589	1.6	581	0.2
24	3	903	918	1.7	933	3.3	906	0.3

Table A.3: Comparison of buckling stresses for FE analysis versus the presented GBT method, GBTUL and CUFSM, respectively. The comparisons are related to the vertical dashed m-line in Figure 5.5.

Appendix B

Paper I

Jönsson, J., and Andreassen, M.J. (2011).

Distortional eigenmodes and homogeneous solutions for semi-discretized thin-walled beams.

Thin-Walled Structures, **49**, 691–707.

Thin-Walled Structures 49 (2011) 691–707

Contents lists available at ScienceDirect

Thin-Walled Structures

journal homepage: www.elsevier.com/locate/tws

Distortional eigenmodes and homogeneous solutions for semi-discretized thin-walled beams

J. Jönsson *, M.J. Andreassen

Technical University of Denmark, Department of Civil Engineering, Brovej Building 118, DK-2800 Kgs. Lyngby, Denmark

ARTICLE INFO

Article history:
Received 17 May 2010
Received in revised form
16 December 2010
Accepted 25 December 2010
Available online 2 February 2011

Keywords:
Distortion
Warping
Generalized beam theory (GBT)
Thin-walled beams
Beam theory
Semi-discretization
Verallgemeinerte Technisch Biegetheorie (VTB)

ABSTRACT

The classical Vlasov theory for torsional analysis of thin-walled beams with open and closed cross-sections can be generalized by including distortional displacement fields. We show that the determination of adequate distortional displacement fields for generalized beam theory (GBT) can be found as part of a semi-discretization process. In this process the cross-section is discretized into finite cross-section elements and the axial variation of the displacement functions are solutions to the established coupled fourth order differential equations of GBT. We use a novel finite-element-based displacement approach in combination with a weak formulation of the shear constraints and constrained wall widths. The weak formulation of the shear constraints enables analysis of both open and closed cell cross-sections by allowing constant shear flow. We use variational analysis to establish and clearly identify the homogeneous differential equations, the eigenmodes, and the related homogeneous solutions. The distortional equations are solved by reduction of order and solution of the related eigenvalue problem of double size as in non-proportionally damped structural dynamic analysis. The full homogeneous solution is given as well as transformations between different degree of freedom spaces. This new approach is a considerable theoretical improvement, since the obtained GBT equations found by discretization of the cross-section are now solved analytically and the formulation is valid without special attention also for closed single or multi-cell cross-sections. Further more the found eigenvalues have clear mechanical meaning, since they represent the attenuation of the distortional eigenmodes and may be used in the automatic meshing of approximate distortional beam elements. The magnitude of the eigenvalues thus also gives the natural ordering of the modes.

1. Introduction

Thin-walled structural elements are extremely efficient due to the minimization of the thickness-to-width ratio of the cross-section walls, and the thin walls are a primary aspect in the behavior and design. The increasing slenderness leads to the insufficiency of both ordinary Euler–Bernoulli beam theory with St. Venant torsion and Vlasov beam theory for thin-walled beams [1]. An important feature missing in these theories is the distortion of the cross-sections, which do not maintain their shape, but distort and buckle. Several formulations including transverse distortional displacements have been proposed for analysis of both open and closed cross-sections. One formulation which has been very successful is the generalization of classic Vlasov beam theory for open cross-sections to include distortion. It has been based on the kinematic assumption of negligible shear strain along the center lines of the cross-section walls. This formulation is known as GBT (generalized beam theory) and it was initially proposed by Schardt [2] in 1966 as a generalization of the theory of bending (Verallgemeinerte Technisch Biegetheorie, VTB in German). For closed (single or multi-celled hollow) thin-walled cross-sections, Schardt shows in his presentation of GBT in [3] that the theory needs a relaxation of the Vlasov assumption of negligible shear strain in order to include the warping deformation associated with the "Bredt's shear flow" around each cell. However it complicates the solution of the GBT equations by introducing non negligible shear coupling terms (off diagonal) in the GBT equations as can be seen in recent GBT formulations for closed thin-walled cross-sections, e.g. [4–6]. In this paper we will therefore adhere to the definition of the warping function given by Kollbrunner and Hajdin, [7], which adds the integral of the shear flow strains, see also [8,9]. Since GBT is developed as a generalization of beam bending it leads to orthogonal warping modes. Thus the final GBT equations are decoupled with respect to normal stresses and transverse stresses, however the shear coupling terms are neglected or in case of closed cells given special attention. The basic cross-section deformation modes of

* Corresponding author. Tel.: +45 45251707.
E-mail addresses: jej@byg.dtu.dk (J. Jönsson), mican@byg.dtu.dk (M.J. Andreassen).

0263-8231/$ - see front matter © 2010 Elsevier Ltd. All rights reserved.
doi:10.1016/j.tws.2010.12.009

GBT are obtained by separately identifying conventional beam deformation modes and solving the eigenvalue problem defined by the warping stiffness matrix and the transverse deformation stiffness matrix. When solving the GBT equations the shear coupling stiffness terms are neglected. This corresponds to modal analysis with orthogonal (Rayleigh) damping in dynamic structural analysis. The solution of the shear coupled GBT equations for closed cross-sections was published by Hanf only in his thesis [10]. GBT was generally not so known in the international research community until Davies, see [11], presented first-order GBT analysis. A distortional theory which generalizes Vlasov beam theory by including the modified definition of the warping function and one distortional mode was presented by Jönsson [12]. In that work the analytical solution of coupled torsional and distortional equations was found by reduction of order and solution of the related eigenvalue problem as in the present work. GBT is devoted to (first order) distortional displacement analysis including the identification of distortional modes, as well as (second order) linear buckling of thin-walled members, and it has fostered a lot of research. Silvestre and Camotim extended the theory to include orthotropic materials, see [13,14]. Experimental verifications have also been presented, see for example Rendek and Balaz [15]. Silvestre [16] presents buckling solutions as well as non-linear post-buckling solutions. However in order to perform post-buckling analysis with GBT, which is essentially a beam theory and not a plate theory, Silvestre finds it is necessary to include additional transverse extension modes and shear modes, as well as modified constitutive relations. In the following we will refer to these kinds of modes as other modes and the related method as extended GBT. For an overview and information about the research and development of GBT see Camotim et al. [17,18].

The innovative theoretical developments performed in this paper by introducing semi-discretization lead towards a modified formulation of GBT, in which the rotational degrees of freedom are included, thus including local plate modes in the formulation even for the simplest discretization. The elimination of these rotations could perhaps be advantageous if one wants to perform a modal decomposition of buckling displacements into distortional buckling mode and local plate buckling mode, however we then rely on a coarse discretization. The methods developed by Schardt, Silvestre, Camotim and co-workers will therefore be applicable for the presented modified formulation. The presented modified GBT formulation for thin-walled beams with both open and closed (single or multi-cell) cross-sections can be regarded as an extension of classical Vlasov thin-walled beam theory to include distortional deformation modes as well as constant shear flows in the walls of the cross-section, see [1,7,19]. It makes it possible to analyze thin-walled members with cross-section distortion and local plate behavior in a one-dimensional formulation through the linear combination of pre-established modes of deformation. However in this paper we find the analytical homogeneous solution to the differential GBT equations (obtained by semi-discretization), using methods similar to Hanf [10] and Jönsson [12], this also (through the magnitude of the eigenvalues) gives a much better knowledge of the length scales of the modes. Alternatively the GBT equations may just as well have been solved using the approximate engineering methods (in which the shear coupling terms are neglected) producing orthogonal axial and transverse normal stress modes. In conventional GBT these modes are used as shape functions in a virtual work or potential energy formulation leading to finite GBT beam elements. However the discretization has to be performed without prior knowledge of the problem length scales of the individual modes. Buckling analysis using GBT beam elements is an alternative to the use of finite-strip methods (FSM), see [20]. However GBT is as its name states essentially a beam theory, whereas FSM essentially is based on plate theory. Therefore FSM does not contain a natural decomposition into basic beam, distortional, local and other modes. Further more conventional GBT does not contain other modes as mentioned above. Since the modal decomposition may lead to advantages in design of thin-walled structures using FSM a great deal of work has been performed by Ádány and Schafer to develop a constrained finite-strip method (cFSM) and modal decomposition methods for open (single-branched) cross-sections, see [21–23]. The modal approaches of extended GBT and cFSM formulations have recently been compared in [24]. The formulations in this paper only consider the (first order) homogeneous linear displacements of GBT, since the main goal has been to identify a theoretically sound formulation of the end effects or in other words find the eigensolutions for the full displacement field including the variation in the axial member direction, see the treatment of end effects by Timoshenko [25].

Let us briefly describe the contents of the following sections and illuminate the process. In the theories of beams, the displacements assumed are typically separated into a sum of (orthogonal) displacement fields. In the following sections, only one of these displacement fields is considered in the variational formulation. The basic kinematic assumptions of these displacement fields are introduced in Section 2. The displacements are separated into the product of cross-section displacement functions and the axial variation functions. The strain fields are derived, and a weak formulation of the shear constraints is described for later use. Simple constitutive energy assumptions in Section 3 lead to the formulation of the elastic energy potential. In Section 4, the cross-section is discretized by straight finite elements in which the local transverse displacements and the warping displacements are interpolated. The element interpolation functions are introduced and the elastic potential energy is formulated in a semi-discretized form. At this stage, the interpolated displacements have not yet been constrained by assumptions about shear and constant width of wall elements. Section 5 is split into three main steps leading to the final distortional differential equations in which all conventional beam modes have been eliminated and all constraints introduced. In Step I, the weak form of the shear constraint equations is introduced, and by taking adequate variations in the potential energy, the pure axial extension mode and its homogeneous solution is identified and eliminated. In Step II, the constraint equations relating to the assumption of a constant wall width are introduced, and the rigid translations and the rotational cross-section displacement eigenmodes are identified and orthogonalized. The constrained degrees of freedom and the two degrees of freedom related to the rigid translations are eliminated, leading to a condensed set of coupled fourth order differential equations. In Step III, the order of the differential equations is reduced by doubling the number of equations through the introduction of a state vector with components of different differentiation levels. The pure St. Venant torsional mode is identified as an eigenmode with its linear axial solution, St. Venant torsion is eliminated, and the final coupled differential equations are revealed. In Section 6, the distortional eigenvalue problem is solved and the solution functions are ordered in a matrix format. In Section 7, the eigenmodes and solutions are assembled in modal vectors and the back-substitution steps for the eliminated degrees of freedom are recapitulated in a matrix format. The full homogeneous solution of the GBT differential equations is formulated in Section 8 and the handling of complex eigenvectors and eigenvalues is described. Examples are given in Section 9, and in Section 10, the degree-of-freedom spaces of the finite-element formulation and the GBT formulation are treated and transformations between these are given. Finally Section 11 is devoted to the determination of solution constants using displacement boundary conditions which are relevant for the finite-element formulation of an analytical GBT beam element.

The present paper does not take distributed loads into account, but they can be incorporated in the formulation leading to the addition of inhomogeneous solution functions. In a following companion paper we will address the solution of the inhomogeneous GBT equations, since we in the development stage of the present formulation know that the eigenmodes are needed in order to decouple the reduced-order non-homogeneous differential equations as well as the conventional beam equations.

2. Basic kinematic assumptions

The prismatic thin-walled beam is described in a global Cartesian (x, y, z) coordinate system where the z-axis is in the longitudinal direction of the beam, see Fig. 1. A cross-section coordinate s is introduced as a curve parameter which runs through the section along the center line and n is the coordinate along the local normal. Subscripts n and s are used for the components in the local coordinate system corresponding to the normal and tangential directions. Subscripts following a comma are used for derivatives, for example $u_{n,ss} = d^2u_n(s)/ds^2$ or $u_{s,n} = \partial u_s(s,n)/\partial n$. A prime, $'$, is used for the axial derivative, d/dz.

The theories of beams are derived on the basis of assumed displacement fields which correspond to extension, flexure, torsion, warping and distortional displacements. This corresponds to a modal separation in which each mode has a set of transverse and axial displacement fields that may be coupled. Each of these cross-section displacement fields is factorized in a displacement mode which is a function of the in-plane coordinates, multiplied by a function of the axial coordinate, which describes the axial variation of the mode. In the following, we propose a method for finding these displacement modes, including global, distortional and local modes, as the eigenmodes of the corresponding homogeneous set of equilibrium equations and axial variation functions corresponding to the eigenvalues.

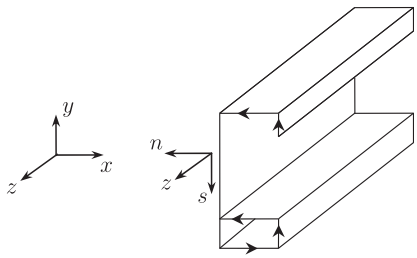

Fig. 1. Global and local Cartesian reference frames.

In the definition of the displacements and strains, the influence of curved cross-section walls is neglected and it is assumed that the radius of curvature is sufficiently large, so that curvature effects vanish. The local effects at corners and joints are also neglected. Only shear contributions from torsion and shear flow around cells will be allowed. For one displacement mode, the components u_n and u_s of the in-plane cross-section displacements in the local coordinate system at a point (n, s) in the cross-section, are introduced as

$$u_n(s,z) = w_n\psi \tag{1}$$

$$u_s(n,s,z) = (w_s - nw_{n,s})\psi \tag{2}$$

Here $w_s(s)$ and $w_n(s)$ are the local displacements of the centerline as shown in Fig. 2, and $\psi(z)$ is the function which describes the axial variation of the in-plane distortional displacements. The axial displacements $u_z(n,s,z)$ generated by the in-plane distortional displacements are introduced as

$$u_z(n,s,z) = -(\Omega + nw_n)\psi' \tag{3}$$

Here the axial (warping) displacement mode $\Omega(s)$ has been included with a variation corresponding to the negative axial derivative of the axial variation factor, $-\psi'$, and due consideration of local transverse variation through the term nw_n. Thus neglecting shear deformation contributions which are not related to St. Venant torsion and torsional shear flow around closed cells.

It is convenient at this stage to note that pure axial extension (where $\Omega = 1$ and $w_s = w_n = w_{n,s} = 0$) is embedded in this formulation. However pure extension in the present formulation, does not involve transverse displacements, the axial variation $-\psi'(z)$ need not be taken as the derivative of a function, but just a function which we will be introducing as $\zeta(z) = -\psi'(z)$ at a later stage.

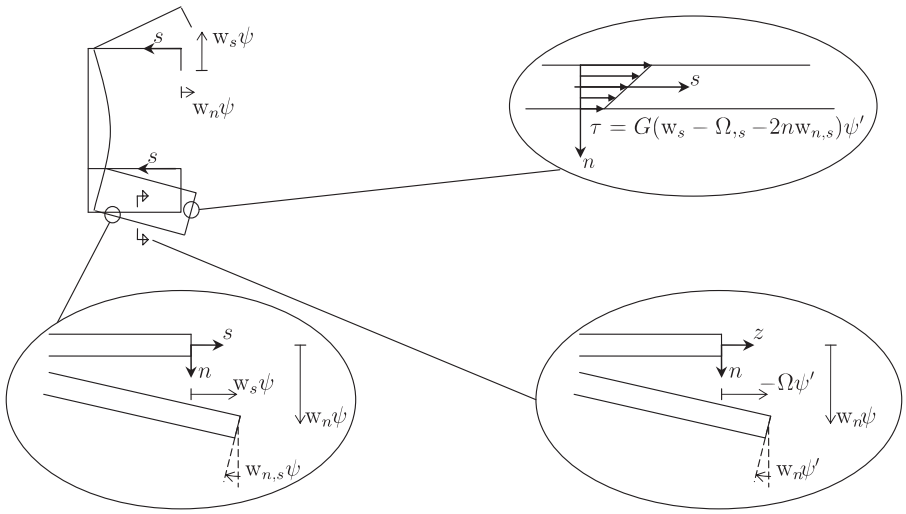

Fig. 2. Local components of displacements and assumed shear stresses.

The axial strains corresponding to the given displacements are

$$\varepsilon = u_z' = -(\Omega + nw_n)\psi'' \tag{4}$$

The cross-section distortional strains are

$$\varepsilon_s = (w_{s,s} - nw_{n,ss})\psi \tag{5}$$

The engineering shear strain in the walls of the cross-section becomes

$$\gamma = \gamma_{zs} = u_{z,s} + u_{s,z} = (w_s - \Omega_{,s} - 2nw_{n,s})\psi' \tag{6}$$

To cope with the shear flow around closed cells, we introduce the shear strain in the middle of the wall as

$$\overline{\gamma}_d\psi' = (w_s - \Omega_{,s})\psi' \tag{7}$$

Bernoulli beam theory is based on the assumption of negligible shear strain and sets the shear strain equal to zero and thus determines the warping displacements (flexural modes) by the differential equation $\Omega_{,s} = w_s$. This means that the formulation of Bernoulli beam theory does not include shear contributions and the axial equilibrium equation of a section cut-out is not fulfilled, which leads to the use of Grashof's method for the determination of the shear stresses. However, if we are to analyze closed cross-sections as in Vlasov beam theory, see [7], we have to allow for a constant shear flow around the cells and the warping of the cross-section then has to be determined by the differential equation $\Omega_{,s} = w_s - \overline{\gamma}_d$ as

$$\Omega(s) = \int_0^s w_s\, ds - \int_0^s \overline{\gamma}_d\, ds + \Omega_0 \tag{8}$$

In the current context, the warping function will be determined from a weak formulation of the assumption of a constant shear flow $\overline{T}_d$ in the walls of the cross-section (where $\overline{T}_d = Gt\overline{\gamma}_d$). The strong formulation of the constraining assumption is that the contribution of the shear flow to the axial equilibrium equation, see Fig. 3, of a section cut-out is zero, i.e.

$$\overline{T}_{d,s} = 0 \tag{9}$$

Multiplying by a virtual centerline axial displacement, $\delta\overline{u}_z$, and integrating over the cross-section we find the virtual work of the shear stresses in a cross-section as

$$\int_C \overline{T}_{d,s}\delta\overline{u}_z\, ds = 0 \tag{10}$$

Performing a partial integration and noting that the shear stress flow is zero at all free edges, we find the weak formulation that will be used to determine the warping function:

$$[\overline{T}_d\delta\overline{u}_z]_{\text{free edges}} - \int_C \overline{T}_d\delta\overline{u}_{z,s}\, ds = 0 \quad \Downarrow$$

$$\int_C \overline{T}_d\delta\overline{u}_{z,s}\, ds = 0 \tag{11}$$

This is the constraint equation that we will use to enforce the assumption of zero axial work performed by the shear flow around the cells.

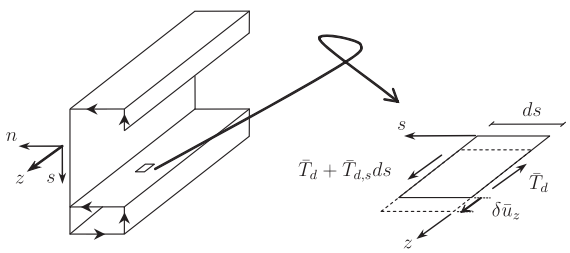

Fig. 3. Work of shear flow through axial virtual displacement.

3. Strain energy assumptions

In the following we will adhere to simple constitutive relations, i.e. the material is assumed to be linear elastic with a modulus of elasticity E and a shear modulus G. In the transverse direction we will assume a plate type elasticity modulus $E_s = E/(1-\nu^2)$, in which ν represents the Poisson ratio. The axial stress is determined as $\sigma = E\varepsilon$, the shear stress as $\tau = G\gamma$ and the transverse stress as $\sigma_s = E_s\varepsilon_s$. Thus the coupling of axial strain ε and transverse strain ε_s is neglected. Note that this means that we also neglect the equivalent coupling between axial and transverse curvatures in the constitutive relations for the plate moments, but with some changes it is possible to include the coupling of the curvatures. With the simple constitutive relations assumed, the elastic energy potential becomes

$$\Pi = \int_V \left(\frac{1}{2}E\varepsilon^2 + \frac{1}{2}G\gamma^2 + \frac{1}{2}E_s\varepsilon_s^2\right) dV \tag{12}$$

Let us introduce a thin-walled cross-section assembled using straight cross-sectional elements, see Fig. 4, and let us integrate through the thickness, t, across the widths, b_e, of the elements, and over the length, L, of the thin-walled beam. The elastic potential energy takes the following form after the introduction of the strains expressed by the displacement in separated form

$$\begin{aligned}\Pi = \frac{1}{2}\int_0^L \Bigg[\sum_{el}\int_0^{b_{el}} \Bigg\{ &\left[Et(\Omega\psi'')^2 + \frac{1}{12}Et^3(w_n\psi'')^2\right] \\ &+ \left[Gt(w_s\psi')^2 + Gt(\Omega_{,s}\psi')^2 - 2Gt(w_s\psi')(\Omega_{,s}\psi') + \frac{1}{3}Gt^3(w_{n,s}\psi')^2\right] \\ &+ \left[E_st(w_{s,s}\psi)^2 + \frac{1}{12}E_st^3(w_{n,ss}\psi)^2\right]\Bigg\}\, ds\Bigg]\, dz\end{aligned} \tag{13}$$

In Eq. (13) the elastic energy terms have been grouped in axial strain energy, shear energy, and transverse strain energy. In conventional beam theory, we usually introduce rigid cross-sectional displacement modes and the elastic energy is described by a summation of the energy stored in all displacement modes. However we have to remember the shear constraints associated with our assumption of constant shear flow, which have to be introduced later. In the current work we wish to establish a set of displacement modes by using semi-discretization. To achieve this, the cross-section will be divided into discrete straight-line elements, in which we interpolate the transverse and axial displacements.

4. Interpolation within cross-section elements

Within each straight finite cross-section element, the axial displacements, Ω, will be interpolated linearly corresponding to a linear variation of the warping functions and the transverse displacement of the elements will be interpolated linearly in the direction of the element and cubically (corresponding to beam elements) in the transverse direction of the element. The displacements in a straight cross-section finite element are thus

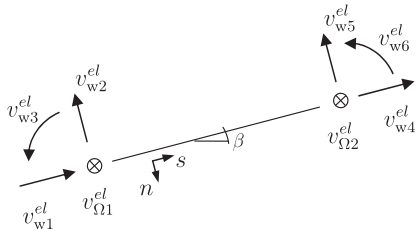

Fig. 4. Components of the displacements vectors of a straight cross-section element.

interpolated as follows:

$$\Omega\psi' = \mathbf{N}_\Omega \mathbf{v}_\Omega^{el}\psi'$$
$$w_s\psi = \mathbf{N}_s \mathbf{v}_w^{el}\psi$$
$$w_n\psi = \mathbf{N}_n \mathbf{v}_w^{el}\psi \tag{14}$$

in which $\mathbf{N}_\Omega(s)$ and $\mathbf{N}_s(s)$ are linear interpolation matrices and $\mathbf{N}_n(s)$ is a cubic (beam) interpolation matrix. Furthermore we have introduced the axial and transverse nodal displacement components of a straight cross-section element as

$$\mathbf{v}_\Omega^{el} = [v_{\Omega 1}^{el} \;\; v_{\Omega 2}^{el}]^T = [\Omega(0) \;\; \Omega(b_e)]^T$$
$$\mathbf{v}_w^{el} = [v_{w1}^{el} \;\; v_{w2}^{el} \;\; v_{w3}^{el} \;\; v_{w4}^{el} \;\; v_{w5}^{el} \;\; v_{w6}^{el}]^T$$
$$= [w_s(0) \;\; -w_n(0) \;\; -w_{n,s}(0) \;\; w_s(b_e) \;\; -w_n(b_e) \;\; -w_{n,s}(b_e)]^T \tag{15}$$

Here b_e is the width of the flat element. Nodal components and the direction of the section coordinates (n,s) are shown in Fig. 4. The element stiffness contributions to the axial strain, shear strain, and transverse strain energy can now be found using the displacement interpolations. The stiffness contributions found are shown in Table 1, in which the first two are the axial stiffness contributions, the third is the transverse distortional stiffness term, while the last three are the shear strain stiffness contributions. These stiffness contributions can be found explicitly. Let us prepare for the formulation of the total cross-section elastic energy by introducing global displacement vectors as an assembly of the local element degrees of freedom. The axial displacements and the transverse displacements are separated into two vectors as follows:

$$\mathbf{v}_\Omega = [v_{\Omega 1} \;\; v_{\Omega 2} \;\; v_{\Omega 3} \;\; \ldots]^T$$

$$\mathbf{v}_w = [v_{x1} \;\; v_{y1} \;\; \phi_1 \;\; v_{x2} \;\; v_{y2} \;\; \phi_2 \;\; \ldots]^T \tag{16}$$

In Eq. (16), $\mathbf{v}_\Omega$ holds the local axial element degrees of freedom, and $\mathbf{v}_w$ holds the local element degrees of freedom, corresponding to two displacements and one rotation for each node. The transformation from local to global components is performed using a formal standard transformation of the components in the cross-section plane, i.e. $\mathbf{v}_\Omega = \mathbf{T}_\Omega \mathbf{v}_\Omega^{el}$ and $\mathbf{v}_w = \mathbf{T}_w \mathbf{v}_w^{el}$. The global assembly of stiffness matrices is found by summation of the contribution from each element, as illustrated in Table 2. Introducing the described interpolation and matrix calculation scheme, the elastic potential energy in Eq. (13) now takes the following form:

$$\Pi = \frac{1}{2}\int_0^L \left\{ \begin{bmatrix} \psi\mathbf{v}_w^T & \psi\mathbf{v}_\Omega^T \end{bmatrix}'' \begin{bmatrix} \mathbf{K}_{ww}^\sigma & \mathbf{0} \\ \mathbf{0} & \mathbf{K}_{\Omega\Omega}^\sigma \end{bmatrix} \begin{bmatrix} \psi\mathbf{v}_w \\ \psi\mathbf{v}_\Omega \end{bmatrix}'' \right.$$
$$+ \begin{bmatrix} \psi\mathbf{v}_w^T & \psi\mathbf{v}_\Omega^T \end{bmatrix}' \begin{bmatrix} \mathbf{K}_{ww}^\tau & \mathbf{K}_{w\Omega}^\tau \\ \mathbf{K}_{\Omega w}^\tau & \mathbf{K}_{\Omega\Omega}^\tau \end{bmatrix} \begin{bmatrix} \psi\mathbf{v}_w \\ \psi\mathbf{v}_\Omega \end{bmatrix}'$$
$$\left. + \begin{bmatrix} \psi\mathbf{v}_w^T & \psi\mathbf{v}_\Omega^T \end{bmatrix} \begin{bmatrix} \mathbf{K}^s & \mathbf{0} \\ \mathbf{0} & \mathbf{0} \end{bmatrix} \begin{bmatrix} \psi\mathbf{v}_w \\ \psi\mathbf{v}_\Omega \end{bmatrix} \right\} dz \tag{17}$$

Table 1
Straight-element stiffness contributions.

$$\mathbf{k}_{\Omega\Omega}^\sigma = \int_0^{b_e} Et\mathbf{N}_\Omega^T\mathbf{N}_\Omega \, ds$$
$$\mathbf{k}_{ww}^\sigma = \int_0^{b_e} \frac{Et^3}{12}\mathbf{N}_n^T\mathbf{N}_n \, ds$$
$$\mathbf{k}^s = \int_0^{b_e} \left(E_s t\mathbf{N}_{s,s}^T\mathbf{N}_{s,s} + \frac{E_s t^3}{12}\mathbf{N}_{n,ss}^T\mathbf{N}_{n,ss} \right) ds$$
$$\mathbf{k}_{ww}^\tau = \int_0^{b_e} \left(Gt\mathbf{N}_s^T\mathbf{N}_s + \frac{Gt^3}{3}\mathbf{N}_{n,s}^T\mathbf{N}_{n,s} \right) ds$$
$$\mathbf{k}_{\Omega\Omega}^\tau = \int_0^{b_e} Gt\mathbf{N}_{\Omega,s}^T\mathbf{N}_{\Omega,s} \, ds$$
$$\mathbf{k}_{w\Omega}^\tau = [\mathbf{k}_{\Omega w}^\tau]^T = -\int_0^{b_e} Gt\mathbf{N}_s^T\mathbf{N}_{\Omega,s} \, ds$$

Table 2
Assembly into total cross-section stiffness contributions.

$$\mathbf{K}_{\Omega\Omega}^\sigma = \textstyle\sum_{el} \mathbf{T}_\Omega^T \mathbf{k}_{\Omega\Omega}^\sigma \mathbf{T}_\Omega \qquad \mathbf{K}_{ww}^\tau = \textstyle\sum_{el} \mathbf{T}_w^T \mathbf{k}_{ww}^\tau \mathbf{T}_w$$
$$\mathbf{K}_{ww}^\sigma = \textstyle\sum_{el} \mathbf{T}_w^T \mathbf{k}_{ww}^\sigma \mathbf{T}_w \qquad \mathbf{K}_{\Omega\Omega}^\tau = \textstyle\sum_{el} \mathbf{T}_\Omega^T \mathbf{k}_{\Omega\Omega}^\tau \mathbf{T}_\Omega$$
$$\mathbf{K}^s = \textstyle\sum_{el} \mathbf{T}_w^T \mathbf{k}^s \mathbf{T}_w \qquad \mathbf{K}_{w\Omega}^\tau = \textstyle\sum_{el} \mathbf{T}_w^T \mathbf{k}_{w\Omega}^\tau \mathbf{T}_\Omega$$

In Eq. (17) and in the following, a bold zero $\mathbf{0}$ denotes a suitable size matrix or vector of zeroes. The axial stiffness from transverse displacements sub-matrix $\mathbf{K}_{ww}^\sigma$ has a rank deficiency equal to the number of free end nodes plus the number of "internal" nodes between corner points of the cross-section. The in-plane cross-section distortional stiffness sub-matrix $\mathbf{K}^s$ has a rank deficiency of 3, corresponding to three in-plane "rigid body" or rather non-distortional displacements of the cross-section. Finally the whole shear stiffness matrix has a rank deficiency of 3, corresponding to the existence of pure axial extension and two pure flexural modes without shear. It turns out that since the pure axial displacement only involves the sub-matrix $\mathbf{K}_{\Omega\Omega}^\tau$, this matrix has a rank deficiency of one.

5. Constraints, eliminations, transformations and reduction of order

To achieve a formulation resembling a generalization of Vlasov beam theory including distortion, the following three main steps need to be performed, before we can solve the eigenvalue problem related to distortional displacements, including local plate type modes. In this process, we introduce constraints, and we identify and eliminate the basic solutions related to the conventional beam displacement modes.

5.1. Step I: Pure axial extension and shear constraints

In this step, we introduce the shear constraint equations that bind axial and transverse modes together and at the same time simplify or condense Eq. (17). In this process we need to eliminate the singularity in the shear stiffness matrix related to pure axial extension. The first eigenmode that we identify is the pure axial extension; it produces no shear energy and no transverse displacement energy (due to the simple constitutive relations assumed, corresponding to beam theory and the mentioned rank deficiency).

Let us introduce the shear constraint equations using Eq. (11) as follows:

$$\int_C \overline{T}_d \delta\overline{u}_{z,s} \, ds = 0 \quad \Downarrow$$

$$-\int_C Gt(w_s - \Omega_{,s})\delta\Omega_{,s} \, ds = 0 \quad \Downarrow$$

$$\int_C Gt\Omega_{,s}\delta\Omega_{,s} \, ds = \int_C Gtw_s\delta\Omega_{,s} \, ds \tag{18}$$

Introducing the interpolation, see Eq. (14), Tables 1 and 2, and taking variations gives us the constraint equations:

$$\mathbf{K}_{\Omega\Omega}^\tau \mathbf{v}_\Omega = -\mathbf{K}_{\Omega w}^\tau \mathbf{v}_w \tag{19}$$

This matrix equation is singular because pure axial extension does not produce shear. Therefore we introduce the following transformation, using superscripts a for axial and o for other:

$$\mathbf{v}_\Omega = [\mathbf{T}_\Omega^a \;\; \mathbf{T}_\Omega^o] \begin{bmatrix} v_\Omega^a \\ \mathbf{v}_\Omega^o \end{bmatrix} \tag{20}$$

in which $\mathbf{T}^a_\Omega = \mathbf{v}^{\text{axial}}_\Omega$ is the pure axial deformation mode (with unit value for all components). The other remaining modes are picked out by

$$\mathbf{T}^o_\Omega = \begin{bmatrix} \mathbf{0} \\ \mathbf{I}_{aa} \end{bmatrix} \begin{matrix} \} & \text{1 d.o.f. related to the first node} \\ \} & \text{Unit diagonal matrix} \end{matrix} \tag{21}$$

Here $\mathbf{I}_{aa}$ is a unit diagonal matrix of dimension $n_a = n_{no} - 1$, where n_{no} is the number of nodes. Furthermore, it is worth noting that v^a_Ω is one component that corresponds to the amount of pure axial extension, while $\mathbf{v}^o_\Omega$ corresponds to all the other axial displacement degrees of freedom. Introducing the transformation in Eq. (20) into the constraint Eq. (19), we get the following by pre- and post-multiplication:

$$\begin{bmatrix} 0 & \mathbf{0} \\ \mathbf{0} & \mathbf{T}^{oT}_\Omega \mathbf{K}^\tau_{\Omega\Omega} \mathbf{T}^o_\Omega \end{bmatrix} \begin{bmatrix} v^a_\Omega \\ \mathbf{v}^o_\Omega \end{bmatrix} = \begin{bmatrix} 0 \\ -\mathbf{T}^{oT}_\Omega \mathbf{K}^\tau_{\Omega w} \mathbf{v}_w \end{bmatrix} \quad \Downarrow$$

$$\mathbf{v}^o_\Omega = -(\mathbf{K}^{\tau oo}_{\Omega\Omega})^{-1} \mathbf{K}^{\tau o}_{\Omega w} \mathbf{v}_w \tag{22}$$

where the matrices $\mathbf{K}^{\tau oo}_{\Omega\Omega}$ and $\mathbf{K}^{\tau o}_{\Omega w}$ are given in Table 3. With Eq. (22) we have introduced a transformation from in-plane cross-section displacement modes to the axial displacement modes without pure axial extension as follows:

$$\mathbf{v}^o_\Omega = \mathbf{T}_{\Omega w} \mathbf{v}_w \quad \text{where } \mathbf{T}_{\Omega w} = -(\mathbf{K}^{\tau oo}_{\Omega\Omega})^{-1} \mathbf{K}^{\tau o}_{\Omega w} \tag{23}$$

Combining Eqs. (20) and (22) gives

$$\mathbf{v}_\Omega = [\mathbf{T}^o_\Omega \mathbf{T}_{\Omega w} \;\; \mathbf{T}^a_\Omega] \begin{bmatrix} \mathbf{v}_w \\ v^a_\Omega \end{bmatrix} = [\mathbf{T}^r_{\Omega w} \;\; \mathbf{T}^a_\Omega] \begin{bmatrix} \mathbf{v}_w \\ v^a_\Omega \end{bmatrix} = \mathbf{T}^r_{\Omega w} \mathbf{v}_w + \mathbf{T}^a_\Omega v^a_\Omega \tag{24}$$

where $\mathbf{T}^r_{\Omega w} = \mathbf{T}^o_\Omega \mathbf{T}_{\Omega w}$.

The potential energy formulation (17) can now be modified so that the amount of axial extension is described by the separate degree of freedom v^a_Ω and the shear constraint equations are enforced. The modification of (17) is performed using the transformation in Eq. (24) and, to clarify the variational treatment of pure axial extension, we also temporally rewrite the terms pertaining to axial extension using $\zeta v^a_\Omega = -\psi' v^a_\Omega$. Introducing transformed stiffness matrices, see Table 3, the elastic potential energy (for one mode) takes the following form

$$\begin{aligned} \Pi = \frac{1}{2} \int_0^L \Big\{ & \begin{bmatrix} (\psi \mathbf{v}^T_w)'' & (\zeta v^{aT}_\Omega)' \end{bmatrix} \begin{bmatrix} \overline{\mathbf{K}}^\sigma & -\mathbf{K}^{\sigma ra}_{\Omega\Omega} \\ -\mathbf{K}^{\sigma ar}_{\Omega\Omega} & K^{\sigma aa}_{\Omega\Omega} \end{bmatrix} \begin{bmatrix} (\psi \mathbf{v}_w)'' \\ (\zeta v^a_\Omega)' \end{bmatrix} \\ & + (\psi \mathbf{v}^T_w)' \mathbf{K}^\tau (\psi \mathbf{v}_w)' + (\psi \mathbf{v}^T_w) \mathbf{K}^s (\psi \mathbf{v}_w) \Big\} \, dz \end{aligned} \tag{25}$$

To find the homogeneous distortional differential equations of GBT, the first variation of the elastic potential energy is investigated by taking variations in the complete displacement field. The virtual variation of a property is denoted by a δ in front of the varied field property (displacement field), as in $\delta(v_w \psi)'$, as the virtual variation of the first derivative of the transverse displacement field expressed by the product of the transverse displacement shape $\mathbf{v}_w$ and the axial variation ψ'. This gives us

$$\begin{aligned} \delta\Pi = \int_0^L \Big\{ & \delta(\psi \mathbf{v}^T_w)'' [\overline{\mathbf{K}}^\sigma (\psi \mathbf{v}_w)'' - \mathbf{K}^{\sigma ra}_{\Omega\Omega} (\zeta v^a_\Omega)'] \\ & + \delta(\psi \mathbf{v}^T_w)' \mathbf{K}^\tau (\psi \mathbf{v}_w)' + \delta(\psi \mathbf{v}^T_w) \mathbf{K}^s (\psi \mathbf{v}_w) \\ & + \delta(\zeta v^a_\Omega)' [-K^{\sigma ar}_{\Omega\Omega} (\psi \mathbf{v}_w)'' + K^{\sigma aa}_{\Omega\Omega} (\zeta v^a_\Omega)'] \Big\} \, dz \end{aligned} \tag{26}$$

After performing up to two partial integrations on the terms and derived terms that involve axial derivatives of the (virtual) varied displacement field, $\delta()'$ or $\delta()''$, the first variation of the elastic potential energy takes the form:

$$\begin{aligned} \delta\Pi = \int_0^L \Big\{ & \delta(\psi \mathbf{v}^T_w) \left[\overline{\mathbf{K}}^\sigma \mathbf{v}_w \psi'''' - \mathbf{K}^{\sigma ra}_{\Omega\Omega} v^a_\Omega \zeta'''' - \mathbf{K}^\tau \mathbf{v}_w \psi'' + \mathbf{K}^s \mathbf{v}_w \psi \right] \\ & + \delta(\zeta v^a_\Omega) [\mathbf{K}^{\sigma ar}_{\Omega\Omega} \mathbf{v}_w \psi''' - K^{\sigma aa}_{\Omega\Omega} v^a_\Omega \zeta''] \Big\} dz \\ & + \Big[\delta(\psi \mathbf{v}^T_w)' [\overline{\mathbf{K}}^\sigma (\psi \mathbf{v}_w)'' - \mathbf{K}^{\sigma ra}_{\Omega\Omega} (\zeta v^a_\Omega)'] \\ & + \delta(\psi \mathbf{v}^T_w) [-\overline{\mathbf{K}}^\sigma (\psi \mathbf{v}_w)''' + \mathbf{K}^{\sigma ra}_{\Omega\Omega} (\zeta v^a_\Omega)'' + \mathbf{K}^\tau (\psi \mathbf{v}_w)'] \\ & + \delta(\zeta v^a_\Omega) [-\mathbf{K}^{\sigma ar}_{\Omega\Omega} (\psi \mathbf{v}_w)'' - K^{\sigma aa}_{\Omega\Omega} (\zeta v^a_\Omega)'] \Big]_0^L \end{aligned} \tag{27}$$

For internal variation in the displacement fields $\delta(\psi \mathbf{v}_w)$ and $\delta(\zeta v^a_\Omega)$, the elastic potential energy should be stationary and therefore its first variation must be equal to zero. Here the terms in the squared bracket correspond to the boundary loads and boundary conditions. Taking internal variations reveals the following coupled homogeneous differential equations of GBT in which we note that $\zeta = -\psi'$:

$$\overline{\mathbf{K}}^\sigma \mathbf{v}_w \psi'''' - \mathbf{K}^{\sigma ra}_{\Omega\Omega} v^a_\Omega \zeta'''' - \mathbf{K}^\tau \mathbf{v}_w \psi'' + \mathbf{K}^s \mathbf{v}_w \psi = \mathbf{0} \tag{28}$$

$$\mathbf{K}^{\sigma ar}_{\Omega\Omega} \mathbf{v}_w \psi''' - K^{\sigma aa}_{\Omega\Omega} v^a_\Omega \zeta'' = \mathbf{0} \tag{29}$$

These equations establish a coupled set of homogeneous GBT differential equations that determine the displacements of a thin-walled beam for a given set of boundary conditions. To solve the boundary value problem, it is necessary to solve the related eigenvalue problem by establishing the eigenmodes/vectors and the related axial variation through the related eigenvalues. In the following, we will first consider the case where the displacement vectors do not contain transverse displacements, and then we will consider one in which they do. We start out by isolating the term $v^a_\Omega \zeta''$ in Eq. (29) as follows:

$$v^a_\Omega \zeta'' = (K^{\sigma aa}_{\Omega\Omega})^{-1} \mathbf{K}^{\sigma ar}_{\Omega\Omega} \mathbf{v}_w \psi''' \tag{30}$$

We can identify pure axial extension as an eigenmode solution. For the above Eqs. (28) and (29), it corresponds to $(\mathbf{v}_w, v^a_\Omega) = (\mathbf{0}, 1)$, which we can see leads to a solution. In the original "global" space, the axial eigenmode is given by $(\mathbf{v}_w, \mathbf{v}_\Omega) = (\mathbf{0}, \mathbf{T}^a_\Omega)$. It is also clear that the axial variation of pure axial extension can be determined by double integration of Eq. (30) with $\mathbf{v}_w = \mathbf{0}$, which results in

$$\zeta(z) = -\psi'(z) = c_{a1} + c_{a2} z = -\mathbf{\Psi}_a'(z) \mathbf{c}_a = [1 \quad z] \begin{bmatrix} c_{a1} \\ c_{a2} \end{bmatrix} \tag{31}$$

where c_{a1} and c_{a2} are constants determined by the boundary conditions of axial extension.

Having identified the "trivial" eigenmode, pure axial extension, we finally turn to the solution of the transverse displacement modes. In this case, Eq. (30) determines the correction term that eliminates pure axial extension in the back-substitution process. Eliminating ζ'' by using the fact that $\zeta'' = -\psi'''$ and assuming that $\psi''' \neq 0$, we find

$$v^a_\Omega = -(K^{\sigma aa}_{\Omega\Omega})^{-1} \mathbf{K}^{\sigma ar}_{\Omega\Omega} \mathbf{v}_w \tag{32}$$

Using this equation or Eq. (29), we eliminate the second term in Eq. (28) and introduce $\mathbf{K}^\sigma$, as given in Table 3. This results in the following homogeneous fourth order differential equations for determination of the transverse (global, distortional and local)

Table 3
Transformation of stiffness matrices related to Step I.

$K^{\sigma aa}_{\Omega\Omega} = \mathbf{T}^{aT}_\Omega \mathbf{K}^\sigma_{\Omega\Omega} \mathbf{T}^a_\Omega$	$\mathbf{K}^{\tau rr}_{\Omega\Omega} = \mathbf{T}^{rT}_{\Omega w} \mathbf{K}^\tau_{\Omega\Omega} \mathbf{T}^r_{\Omega w}$
$\mathbf{K}^{\sigma ar}_{\Omega\Omega} = \mathbf{T}^{aT}_\Omega \mathbf{K}^\sigma_{\Omega\Omega} \mathbf{T}^r_{\Omega w}$	$\mathbf{K}^{\tau r}_{w\Omega} = \mathbf{K}^\tau_{w\Omega} \mathbf{T}^r_{\Omega w} = \mathbf{K}^{\tau r\,T}_{\Omega w}$
$\mathbf{K}^{\sigma rr}_{\Omega\Omega} = \mathbf{T}^{rT}_{\Omega w} \mathbf{K}^\sigma_{\Omega\Omega} \mathbf{T}^r_{\Omega w}$	$\mathbf{K}^{\tau oo}_{\Omega\Omega} = \mathbf{T}^{oT}_\Omega \mathbf{K}^\tau_{\Omega\Omega} \mathbf{T}^o_\Omega$
$\overline{\mathbf{K}}^\sigma = \mathbf{K}^\sigma_{ww} + \mathbf{K}^{\sigma rr}_{\Omega\Omega}$	$\mathbf{K}^{\tau o}_{\Omega w} = \mathbf{T}^{oT}_\Omega \mathbf{K}^\tau_{\Omega w}$
$\mathbf{K}^\sigma = \overline{\mathbf{K}}^\sigma - \mathbf{K}^{\sigma ra}_{\Omega\Omega} (K^{\sigma aa}_{\Omega\Omega})^{-1} \mathbf{K}^{\sigma ar}_{\Omega\Omega}$	$\mathbf{K}^\tau = \mathbf{K}^\tau_{ww} + \mathbf{K}^{\tau r}_{w\Omega} + \mathbf{K}^{\tau rr}_{\Omega w} + \mathbf{K}^{\tau rr}_{\Omega\Omega}$

distortional displacement modes of GBT:

$$\mathbf{K}^{\sigma}\mathbf{v}_w\psi''''-\mathbf{K}^{\tau}\mathbf{v}_w\psi''+\mathbf{K}^{s}\mathbf{v}_w\psi=\mathbf{0} \tag{33}$$

To solve this set of equations we have to solve the related eigenvalue problem, which is of fourth order, but since only an even number of axial derivatives is involved, this reduces to a quadratic eigenvalue problem. With solutions, $\mathbf{v}_w$, to Eq. (33), we can find $\mathbf{v}_{\Omega}^{o}$ using Eq. (23), v_{Ω}^{a} using Eq. (32), and finally $\mathbf{v}_{\Omega}$ using Eq. (20), thus revealing the full solution (in global space).

5.2. Step II: Rigid cross-section displacements and constant wall-width constraint

In this step, we will identify and eliminate two eigenmodes corresponding to transverse translation of the cross-section, and we will identify a pure rotational eigenmode for later elimination in the next step. Furthermore, we will also constrain the transverse displacement field, so that the wall widths remain constant, i.e. we will enforce $w_{s,s}\equiv 0$, see Eq. (5).

With the introduction of the shear constraints in the previous step, the flexural modes do not have shear energy and the shear stiffness matrix $\mathbf{K}^{\tau}$ is therefore singular for these modes. Since neither the pure translational modes nor the rotational mode involve any distortion of the cross-section, the transverse stiffness matrix $\mathbf{K}^{s}$ will be singular for these modes. It turns out that the translational modes correspond to two quadruple zero eigenvalues or roots of the related characteristic equation. To orthogonalize these modes with respect to the non-singular axial stiffness matrix $\mathbf{K}^{\sigma}$, we will form the subspace spanned by the modes and orthogonalize in this subspace.

Let us first introduce two not necessarily orthogonal translational modes corresponding to a unit translation in each transverse coordinate direction, ordered in columns in the matrix $\mathbf{T}_w^{xy}=[\mathbf{v}_w^{x\ \mathrm{trans}}\ \mathbf{v}_w^{y\ \mathrm{trans}}]$ and a rotational mode corresponding to rotation about the origin of the (initial) transverse coordinate axes $\mathbf{T}_w^{z}=[\mathbf{v}_w^{z\ \mathrm{rot}}]$.

In the subspace spanned by the two non-orthogonal translational modes introduced, we can find the principle flexural directions by an equivalent conventional method or by finding the eigenvectors of the following two-dimensional eigenvalue problem:

$$(\mathbf{K}_{xy}^{\sigma}-\lambda\mathbf{I})\mathbf{v}_{xy}=\mathbf{0}\quad\Rightarrow\quad\mathbf{v}_{xy}=\mathbf{v}_{xy}^{1}\quad\text{or}\quad\mathbf{v}_{xy}^{2} \tag{34}$$

where $\mathbf{I}$ is a 2×2 diagonal unit matrix and $\mathbf{K}_{xy}^{\sigma}=\mathbf{T}_w^{xy\,T}\mathbf{K}^{\sigma}\mathbf{T}_w^{xy}$. The two orthogonal eigenvectors corresponding to the principle axis directions are ordered in columns in the transformation matrix

$$\mathbf{T}_{xy}^{\alpha}=[\mathbf{v}_{xy}^{1}\ \ \mathbf{v}_{xy}^{2}] \tag{35}$$

Finally we can determine the two orthogonal translational eigenmodes in the full $\mathbf{v}_w$ space, ordered in columns in a transformation matrix as $\mathbf{T}_w^{\alpha}=[\mathbf{v}_w^{1\ \mathrm{trans}}\ \mathbf{v}_w^{2\ \mathrm{trans}}]$, by the simple matrix multiplication

$$\mathbf{T}_w^{\alpha}=\mathbf{T}_w^{xy}\mathbf{T}_{xy}^{\alpha} \tag{36}$$

Next we turn to the non-orthogonal rotational mode, and we subtract the translational part, so that the coupling term in the axial stiffness vanishes. Thus the orthogonal pure rotational mode is given by

$$\mathbf{v}_w^{3\ \mathrm{rot}}=\mathbf{v}_w^{z\ \mathrm{rot}}-[\mathbf{v}_w^{1\ \mathrm{trans}}\ \mathbf{v}_w^{2\ \mathrm{trans}}]\mathbf{d}_{\alpha}\quad\Updownarrow$$

$$\mathbf{T}_w^{3}=\mathbf{T}_w^{z}-\mathbf{T}_w^{\alpha}\mathbf{d}_{\alpha} \tag{37}$$

where we have introduced the transformation "matrix" $\mathbf{T}_w^{3}=[\mathbf{v}_w^{3\ \mathrm{rot}}]$ and $\mathbf{d}_{\alpha}$ as a two-dimensional vector giving the amount of each translational eigenmode to be subtracted. Note that $\mathbf{d}_{\alpha}$ is related to the coordinate vector of the shear center, see [12]. The coupling terms in the axial stiffness between translations and rotation are found as follows (in the subspace):

$$\mathbf{K}_{\alpha 3}^{\sigma}=\mathbf{T}_w^{\alpha\,T}\mathbf{K}^{\sigma}\mathbf{T}_w^{3}=\mathbf{T}_w^{\alpha\,T}\mathbf{K}^{\sigma}(\mathbf{T}_w^{z}-\mathbf{T}_w^{\alpha}\mathbf{d}_{\alpha})=\mathbf{K}_{\alpha z}^{\sigma}-\mathbf{K}_{\alpha\alpha}^{\sigma}\mathbf{d}_{\alpha} \tag{38}$$

By requiring that the coupling terms in the axial stiffness vanish $\mathbf{K}_{\alpha 3}^{\sigma}=\mathbf{0}$, we find

$$\mathbf{d}_{\alpha}=\mathbf{K}_{\alpha\alpha}^{\sigma\ -1}\mathbf{K}_{\alpha z}^{\sigma} \tag{39}$$

Now we can completely identify the orthogonal pure rotational eigenmode by inserting Eq. (39) in Eq. (37) as

$$\mathbf{T}_w^{3}=\mathbf{T}_w^{z}-\mathbf{T}_w^{\alpha}\mathbf{K}_{\alpha\alpha}^{\sigma\ -1}\mathbf{K}_{\alpha z}^{\sigma} \tag{40}$$

Here the matrix transformations are given in Table 4.

Before performing eliminations and finding the solutions pertaining to the translational modes, we will constrain the transverse normal strains in the middle surface of the cross-section walls, i.e. we will enforce $w_{s,s}\equiv 0$ or, say, enforce a constant wall-width constraint. For each wall element, this leads to a multi-point constraint equation in local degrees of freedom, $\mathbf{v}_w^{el}$, corresponding to no centerline elongation. It takes the following form:

$$[1\ \ 0\ \ 0\ \ -1\ \ 0\ \ 0]\mathbf{v}_w^{el}=0 \tag{41}$$

Each element constraint equation is reformulated into global degrees of freedom by a formal transformation of the form $\mathbf{v}_w^{el}=\mathbf{T}_w^{T}\mathbf{v}_w$, which allows us to write n_c independent constraint equations (where n_c can be less than the number of elements due to over-constraining). The equations take the following form in the full $\mathbf{v}_w$-space:

$$\mathbf{C}\mathbf{v}_w=\mathbf{0} \tag{42}$$

The transformation method described by Cook et al. [26] will be used to enforce the multi-point constraint equations and eliminate the related degrees of freedom. However, we must also incorporate the elimination of the translational eigenmodes and prepare for the elimination of the rotational modes.

Before any elimination of eigenmodes or constrained degrees of freedom can be performed, we must first transform the equations to a new space (with redefined degrees of freedom) in such a way that the degrees of freedom to be eliminated are clearly identified. Thus we need to choose exactly which of the constrained degrees of freedom (in each constraint equation) and which degrees of freedom related to the translational and rotational modes are to be eliminated. In our implementation, we choose to eliminate the translations and rotation of the first node, and we implement a strategic routine which chooses which of the other translational degrees of freedom related to the constraint equations are to be eliminated. The identification of the constrained degrees of freedom to be eliminated is performed by a transformation matrix $\mathbf{T}_w^{c}$ in which each column belongs to a constraint equation and identifies the degree of freedom to be eliminated by a unit value in the corresponding row. The remaining degrees of freedom, which are not going to be separately identified (eliminated), are identified in the transformation matrix $\mathbf{T}_w^{u}$ in which each column identifies a remaining (u for unconstrained) degree of freedom by a unit value in the corresponding row.

We are now ready to introduce the transformation to $\mathbf{v}_w$-space from the new space. In the new space, we introduce the degrees

Table 4
Transformation of stiffness matrices related to Step II.

$\mathbf{K}_{\alpha\alpha}^{\sigma}=\mathbf{T}_w^{\alpha\,T}\mathbf{K}^{\sigma}\mathbf{T}_w^{\alpha}$	$K_{33}^{\sigma}=\mathbf{T}_w^{3\ T}\mathbf{K}^{\sigma}\mathbf{T}_w^{3}$	$K_{33}^{\tau}=\mathbf{T}_w^{3\ T}\mathbf{K}^{\tau}\mathbf{T}_w^{3}$
$\mathbf{K}_{\alpha z}^{\sigma}=\mathbf{T}_w^{\alpha\,T}\mathbf{K}^{\sigma}\mathbf{T}_w^{z}$	$\mathbf{K}_{3u}^{\sigma}=\mathbf{T}_w^{3\ T}\mathbf{K}^{\sigma}\bar{\mathbf{T}}_w^{u}$	$\mathbf{K}_{3u}^{\tau}=\mathbf{T}_w^{3\ T}\mathbf{K}^{\tau}\bar{\mathbf{T}}_w^{u}$
$\mathbf{K}_{\alpha u}^{\sigma}=\mathbf{T}_w^{\alpha\,T}\mathbf{K}^{\sigma}\bar{\mathbf{T}}_w^{u}$	$\mathbf{K}_{uu}^{\sigma}=\bar{\mathbf{T}}_w^{u\ T}\mathbf{K}^{\sigma}\bar{\mathbf{T}}_w^{u}$	$\mathbf{K}_{uu}^{\tau}=\bar{\mathbf{T}}_w^{u\ T}\mathbf{K}^{\tau}\bar{\mathbf{T}}_w^{u}$
$\mathbf{K}_{uu}^{s}=\bar{\mathbf{T}}_w^{u\ T}\mathbf{K}^{s}\bar{\mathbf{T}}_w^{u}$	$\bar{\mathbf{K}}_{uu}^{\sigma}=\mathbf{K}_{uu}^{\sigma}-\mathbf{K}_{u\alpha}^{\sigma}\mathbf{K}_{\alpha\alpha}^{\sigma\ -1}\mathbf{K}_{\alpha u}^{\sigma}$	

of freedom as, $\mathbf{v}_w^\alpha = [v_w^1\ v_w^2]^T$ for the magnitudes of the two translational eigenmodes, v_w^3 for the magnitude of the rotational eigenmode, $\mathbf{v}_w^c$ for the degrees of freedom to be constrained, and $\mathbf{v}_w^u$ for the remaining unconstrained degrees of freedom. The transformation may be written as:

$$\mathbf{v}_w = [\mathbf{T}_w^\alpha\ \ \mathbf{T}_w^3\ \ \mathbf{T}_w^c\ \ \mathbf{T}_w^u]\begin{bmatrix}\mathbf{v}_w^\alpha\\ v_w^3\\ \mathbf{v}_w^c\\ \mathbf{v}_w^u\end{bmatrix} \tag{43}$$

Since we have strategically chosen the constrained degrees of freedom not to be equal to the degrees of freedom related to the translational and rotational eigenmodes, we have a situation where $\mathbf{CT}_w^\alpha = \mathbf{0}$ and $\mathbf{CT}_w^3 = 0$. So the constrain equations in (42) can be rewritten using Eq. (43) as

$$\mathbf{CT}_w^c\mathbf{v}_w^c + \mathbf{CT}_w^u\mathbf{v}_w^u = \mathbf{0} \tag{44}$$

This allows us to express the constrained degrees of freedom by the unconstrained as

$$\mathbf{v}_w^c = -\mathbf{C}_c^{-1}\mathbf{C}_u\mathbf{v}_w^u \tag{45}$$

in which $\mathbf{C}_c = \mathbf{CT}_w^c$ and $\mathbf{C}_u = \mathbf{CT}_w^u$. Introducing (45) in the transformation Eq. (43), we find that the total transformation is condensed as follows:

$$\mathbf{v}_w = [\mathbf{T}_w^\alpha\ \ \mathbf{T}_w^3\ \ \mathbf{T}_w^c\ \ \mathbf{T}_w^u]\begin{bmatrix}\mathbf{v}_w^\alpha\\ v_w^3\\ -\mathbf{C}_c^{-1}\mathbf{C}_u\mathbf{v}_w^u\\ \mathbf{v}_w^u\end{bmatrix} = [\mathbf{T}_w^\alpha\ \ \mathbf{T}_w^3\ \ \widetilde{\mathbf{T}}_w^u]\begin{bmatrix}\mathbf{v}_w^\alpha\\ v_w^3\\ \mathbf{v}_w^u\end{bmatrix} \tag{46}$$

where $\widetilde{\mathbf{T}}_w^u = \mathbf{T}_w^u - \mathbf{T}_w^c\mathbf{C}_c^{-1}\mathbf{C}_u$ has been introduced as the condensed transformation by using a tilde.

Introducing the transformation in (46) in the differential equations in (33) transforms these equations into the new space. The differential equations thereby take the following form in which we have also introduced the null terms corresponding to the rigid-body modes and zero shear strain for translational and flexural modes:

$$\begin{bmatrix}\mathbf{K}_{\alpha\alpha}^\sigma & \mathbf{0} & \mathbf{K}_{\alpha u}^\sigma\\ \mathbf{0} & K_{33}^\sigma & \mathbf{K}_{3u}^\sigma\\ \mathbf{K}_{u\alpha}^\sigma & \mathbf{K}_{u3}^\sigma & \mathbf{K}_{uu}^\sigma\end{bmatrix}\begin{bmatrix}\mathbf{v}_w^\alpha\\ v_w^3\\ \mathbf{v}_w^u\end{bmatrix}\psi'''' - \begin{bmatrix}\mathbf{0} & \mathbf{0} & \mathbf{0}\\ \mathbf{0} & K_{33}^\tau & \mathbf{K}_{3u}^\tau\\ \mathbf{0} & \mathbf{K}_{u3}^\tau & \mathbf{K}_{uu}^\tau\end{bmatrix}\begin{bmatrix}\mathbf{v}_w^\alpha\\ v_w^3\\ \mathbf{v}_w^u\end{bmatrix}\psi'' + \begin{bmatrix}\mathbf{0} & \mathbf{0} & \mathbf{0}\\ \mathbf{0} & 0 & \mathbf{0}\\ \mathbf{0} & \mathbf{0} & \mathbf{K}_{uu}^s\end{bmatrix}\begin{bmatrix}\mathbf{v}_w^\alpha\\ v_w^3\\ \mathbf{v}_w^u\end{bmatrix}\psi = \begin{bmatrix}\mathbf{0}\\ 0\\ \mathbf{0}\end{bmatrix} \tag{47}$$

The transformed stiffness matrices introduced in this equation are given in Table 4. The two-dimensional upper block matrix equation yields the translation displacements as

$$\mathbf{v}_w^\alpha\psi'''' = -\mathbf{K}_{\alpha\alpha}^{\sigma\ -1}\mathbf{K}_{\alpha u}^\sigma\mathbf{v}_w^u\psi'''' \tag{48}$$

We can identify the two orthogonal pure translational modes, (v_w^1, v_w^2, v_w^3, $\mathbf{v}_w^u$) = (1, 0, 0, $\mathbf{0}$) and (0, 1, 0, $\mathbf{0}$), as eigenmodes or solutions to Eq. (47). For these pure translational modes, we find that the right-hand side of Eq. (48) vanishes and that the axial variation of the pure translational modes is therefore determined by quadruple integration, which gives:

$$\psi_1(z) = c_{11} + c_{12}z + c_{13}z^2 + c_{14}z^3 = \mathbf{\Psi}_1(z)\mathbf{c}_1$$

$$\psi_2(z) = c_{21} + c_{22}z + c_{23}z^2 + c_{24}z^3 = \mathbf{\Psi}_2(z)\mathbf{c}_2 \tag{49}$$

We will make use of the following block notation:

$$\mathbf{\Psi}_\alpha\mathbf{c}_\alpha = \begin{bmatrix}\mathbf{\Psi}_1 & \mathbf{0}\\ \mathbf{0} & \mathbf{\Psi}_2\end{bmatrix}\begin{bmatrix}\mathbf{c}_1\\ \mathbf{c}_2\end{bmatrix},\quad \mathbf{c}_1 = \begin{bmatrix}c_{11}\\ c_{12}\\ c_{13}\\ c_{14}\end{bmatrix},\quad \mathbf{c}_2 = \begin{bmatrix}c_{21}\\ c_{22}\\ c_{23}\\ c_{24}\end{bmatrix} \tag{50}$$

in which $\mathbf{\Psi}_1 = \mathbf{\Psi}_2 = [1\ \ z\ \ z^2\ \ z^3]$. The constants in the vectors $\mathbf{c}_1$ and $\mathbf{c}_2$ are determined by the boundary conditions for pure transverse translational displacement in the two directions.

Having identified the two pure translational modes, we turn to the remaining solutions to the differential Eq. (47). In this case, Eq. (48) determines the correction term that eliminates pure transverse displacements in the back-substitution process. By dividing both sides of the equation by $\psi'''' \neq 0$ we find

$$\mathbf{v}_w^\alpha = -\mathbf{K}_{\alpha\alpha}^{\sigma\ -1}\mathbf{K}_{\alpha u}^\sigma\mathbf{v}_w^u \tag{51}$$

Using this equation or Eq. (48), we eliminate the two pure flexural degrees of freedom and find the condensed version of the differential Eq. (47), which takes the following form:

$$\begin{bmatrix}K_{33}^\sigma & \mathbf{K}_{3u}^\sigma\\ \mathbf{K}_{u3}^\sigma & \overline{\mathbf{K}}_{uu}^\sigma\end{bmatrix}\begin{bmatrix}v_w^3\\ \mathbf{v}_w^u\end{bmatrix}\psi'''' - \begin{bmatrix}K_{33}^\tau & \mathbf{K}_{3u}^\tau\\ \mathbf{K}_{u3}^\tau & \mathbf{K}_{uu}^\tau\end{bmatrix}\begin{bmatrix}v_w^3\\ \mathbf{v}_w^u\end{bmatrix}\psi'' + \begin{bmatrix}0 & \mathbf{0}\\ \mathbf{0} & \mathbf{K}_{uu}^s\end{bmatrix}\begin{bmatrix}v_w^3\\ \mathbf{v}_w^u\end{bmatrix}\psi = \begin{bmatrix}0\\ \mathbf{0}\end{bmatrix} \tag{52}$$

The introduced stiffness matrix $\overline{\mathbf{K}}_{uu}^\sigma$ is given in Table 4. This equation constitutes the GBT differential equations constrained by shear flow constraints and wall-width constraints after the elimination of the classical axial and two translational (flexural beam) modes.

5.3. Step III: Reduction of order and pure st. venant torsion

In the following, we will reduce the differential order of the coupled fourth order differential equations and the related quadratic eigenvalue problem to twice as many coupled second order differential equations with a related linear eigenvalue problem of double size. This method is equivalent to the one used for the solution of the coupled homogeneous problem of one-mode distortion and torsion analyzed in [12]. After we have changed the order of the equations, we can recognize that the pure torsional St. Venant displacement modes with a constant or a linear variation of the angle of twist are eigensolutions.

The fourth order differential Eq. (52) can be transformed into twice as many second order differential equations by introducing what is called a state vector. There are a number of different possible formulations, but we have chosen the use of the state vector $\mathbf{v}_S = [v_w^3\psi, \mathbf{v}_w^u\psi, v_w^3\psi'', \mathbf{v}_w^u\psi'']^T$. Introducing this state vector (and using related equality block equations) yields a reformulation of Eq. (52) as a formal second order matrix differential equation of double size, which takes the form:

$$\begin{bmatrix}0 & \mathbf{0} & 0 & \mathbf{0}\\ \mathbf{0} & \mathbf{K}_{uu}^s & \mathbf{0} & \mathbf{0}\\ 0 & \mathbf{0} & -K_{33}^\sigma & -\mathbf{K}_{3u}^\sigma\\ \mathbf{0} & \mathbf{0} & -\mathbf{K}_{u3}^\sigma & -\overline{\mathbf{K}}_{uu}^\sigma\end{bmatrix}\begin{bmatrix}v_w^3\psi\\ \mathbf{v}_w^u\psi\\ v_w^3\psi''\\ \mathbf{v}_w^u\psi''\end{bmatrix} - \begin{bmatrix}K_{33}^\tau & \mathbf{K}_{3u}^\tau & -K_{33}^\sigma & -\mathbf{K}_{3u}^\sigma\\ \mathbf{K}_{u3}^\tau & \mathbf{K}_{uu}^\tau & -\mathbf{K}_{u3}^\sigma & -\overline{\mathbf{K}}_{uu}^\sigma\\ -K_{33}^\sigma & -\mathbf{K}_{3u}^\sigma & 0 & \mathbf{0}\\ -\mathbf{K}_{u3}^\sigma & -\overline{\mathbf{K}}_{uu}^\sigma & \mathbf{0} & \mathbf{0}\end{bmatrix}\begin{bmatrix}v_w^3\psi\\ \mathbf{v}_w^u\psi\\ v_w^3\psi''\\ \mathbf{v}_w^u\psi''\end{bmatrix}'' = \begin{bmatrix}0\\ \mathbf{0}\\ 0\\ \mathbf{0}\end{bmatrix} \tag{53}$$

Seeking solutions of exponential form, $\psi(z) = e^{\xi z}$, with an eigenvector in which $v_w^3 = 1$ and $\mathbf{v}_w^u = \mathbf{0}$, we see that the first equation will lead to an eigenvalue, $\xi^2 = 0$, or a double zero root (in the characteristic equation), thus giving us not exponential solutions but two linear solution terms. This corresponds to a constant or a

Table 5
Transformation of stiffness matrices related to Step III.

$\mathbf{K}^{\sigma}_{3e}=[K^{\sigma}_{33}\ \ \mathbf{K}^{\sigma}_{3u}]$	$\mathbf{K}^{\sigma}_{ue}=[\mathbf{K}^{\sigma}_{u3}\ \ \overline{\mathbf{K}}^{\sigma}_{uu}]$	$\mathbf{K}^{\sigma\ T}_{ee}=[\mathbf{K}^{\sigma\ T}_{3e}\ \ \mathbf{K}^{\sigma\ T}_{ue}]$
$\overline{\mathbf{K}}^{\sigma}_{ee}=\mathbf{K}^{\sigma}_{e3}{K^{\tau}_{33}}^{-1}\mathbf{K}^{\sigma}_{3e}$	$\overline{\mathbf{K}}^{\sigma}_{ue}=\mathbf{K}^{\sigma}_{ue}-\mathbf{K}^{\tau}_{u3}{K^{\tau}_{33}}^{-1}\mathbf{K}^{\sigma}_{3e}$	$\overline{\mathbf{K}}^{\tau}_{uu}=\mathbf{K}^{\tau}_{uu}-\mathbf{K}^{\tau}_{u3}{K^{\tau}_{33}}^{-1}\mathbf{K}^{\tau}_{3u}$

linear variation of the first degree of freedom, which is pure twist. However if we "persistently" seek the two classical exponential solutions for a pure twist mode with (eigen)vectors, $(1,\mathbf{0},\xi^2,\mathbf{0})^T$, we are not able to show that this is in general a solution. In the examples section, we will see that for the closed cross-section, only the linear terms of pure twist exist, whereas for the open channel section, the eigenvalue is very close to the classical result, and in the example chosen, we cannot visually see the distortion in the associated "torsional" mode with an exponential variation of twist.

To keep the matrix operations as simple as possible we introduce a new vector $\mathbf{v}^e_w$ and three new block matrices, $\mathbf{K}^{\sigma}_{ee}$, $\mathbf{K}^{\sigma}_{3e}$ and $\mathbf{K}^{\sigma}_{ue}$, given by

$$\mathbf{v}^e_w=\begin{bmatrix}v^3_w\\ \mathbf{v}^u_w\end{bmatrix},\quad \mathbf{K}^{\sigma}_{ee}=\begin{bmatrix}\mathbf{K}^{\sigma}_{3e}\\ \mathbf{K}^{\sigma}_{ue}\end{bmatrix}=\begin{bmatrix}[K^{\sigma}_{33}\ \ \mathbf{K}^{\sigma}_{3u}]\\ [\mathbf{K}^{\sigma}_{u3}\ \ \overline{\mathbf{K}}^{\sigma}_{uu}]\end{bmatrix} \tag{54}$$

When we introduce the new vector and the three block matrices defined by Eq. (54) and in Table 5, the second order differential equations can be written as

$$\begin{bmatrix}0&\mathbf{0}&\mathbf{0}\\ \mathbf{0}&\mathbf{K}^{s}_{uu}&\mathbf{0}\\ \mathbf{0}&\mathbf{0}&-\mathbf{K}^{\sigma}_{ee}\end{bmatrix}\begin{bmatrix}v^3_w\psi\\ \mathbf{v}^u_w\psi\\ \mathbf{v}^e_w\psi''\end{bmatrix}-\begin{bmatrix}K^{\tau}_{33}&\mathbf{K}^{\tau}_{3u}&-\mathbf{K}^{\sigma}_{3e}\\ \mathbf{K}^{\tau}_{u3}&\mathbf{K}^{\tau}_{uu}&-\mathbf{K}^{\sigma}_{ue}\\ -\mathbf{K}^{\sigma}_{e3}&-\mathbf{K}^{\sigma}_{eu}&\mathbf{0}\end{bmatrix}\begin{bmatrix}v^3_w\psi\\ \mathbf{v}^u_w\psi\\ \mathbf{v}^e_w\psi''\end{bmatrix}''=\begin{bmatrix}0\\ \mathbf{0}\\ \mathbf{0}\end{bmatrix} \tag{55}$$

In the first equation we can isolate the pure rotational term resulting in the following differential equation:

$$v^3_w\psi''=-{K^{\tau}_{33}}^{-1}(\mathbf{K}^{\tau}_{3u}\mathbf{v}^u_w\psi''-\mathbf{K}^{\sigma}_{3e}\mathbf{v}^e_w\psi'''') \tag{56}$$

It can be seen that pure St. Venant torsion (with free warping), corresponding to the solution vector, $(v^3_w\psi,\mathbf{v}^u_w\psi,\mathbf{v}^e_w\psi'')=(c_{32}z+c_{31},\mathbf{0},\mathbf{0})$, is a solution of the second order differential equations in (55). We have thus shown that

$$\psi_3(z)=c_{31}+c_{32}z=\mathbf{\Psi}_3(z)\mathbf{c}_3=[1\ \ z]\begin{bmatrix}c_{31}\\ c_{32}\end{bmatrix} \tag{57}$$

The remaining solutions to the differential equations in (55) are found by seeking exponential solutions of the form $\psi(z)=e^{\xi z}$. We insert the exponential solution in Eq. (56) and find the following equation, which we will use for back-substitution purposes:

$$v^3_w=-{K^{\tau}_{33}}^{-1}(\mathbf{K}^{\tau}_{3u}\mathbf{v}^u_w-\mathbf{K}^{\sigma}_{3e}(\xi^2\mathbf{v}^e_w)) \tag{58}$$

Using Eq. (56), we eliminate v^3_w from the differential equations in (55) and find the final distortional differential equations of GBT that determine all the distortional displacement modes as

$$\begin{bmatrix}\mathbf{K}^{s}_{uu}&\mathbf{0}\\ \mathbf{0}&-\mathbf{K}^{\sigma}_{ee}\end{bmatrix}\begin{bmatrix}\mathbf{v}^u_w\psi\\ \mathbf{v}^e_w\psi''\end{bmatrix}-\begin{bmatrix}\overline{\mathbf{K}}^{\tau}_{uu}&-\overline{\mathbf{K}}^{\sigma}_{ue}\\ -\overline{\mathbf{K}}^{\sigma}_{eu}&-\overline{\mathbf{K}}^{\sigma}_{ee}\end{bmatrix}\begin{bmatrix}\mathbf{v}^u_w\psi\\ \mathbf{v}^e_w\psi''\end{bmatrix}''=\begin{bmatrix}\mathbf{0}\\ \mathbf{0}\end{bmatrix} \tag{59}$$

The block matrices and the transformed stiffness matrices are given in Table 5. In the following section we will describe the solution of these differential equations.

6. The distortional eigenvalue problem and homogeneous solution functions

To find the distortional eigenmodes, including what are called local modes, we are finally able to seek solutions to the final condensed differential matrix Eq. (59). We postulate that the solutions are exponential solutions of the form

$$\psi(z)=e^{\xi z} \tag{60}$$

where ξ is an inverse length scale parameter which may be complex. Inserting the postulated solution leads to the following generalized linear matrix eigenvalue problem, in which the eigenvalues are ξ^2 and the eigenvectors are the distortional modes that we seek:

$$\begin{bmatrix}\mathbf{K}^{s}_{uu}&\mathbf{0}\\ \mathbf{0}&-\mathbf{K}^{\sigma}_{ee}\end{bmatrix}\begin{bmatrix}\mathbf{v}^u_w\\ \xi^2\mathbf{v}^e_w\end{bmatrix}-\xi^2\begin{bmatrix}\overline{\mathbf{K}}^{\tau}_{uu}&-\overline{\mathbf{K}}^{\sigma}_{ue}\\ -\overline{\mathbf{K}}^{\sigma}_{eu}&-\overline{\mathbf{K}}^{\sigma}_{ee}\end{bmatrix}\begin{bmatrix}\mathbf{v}^u_w\\ \xi^2\mathbf{v}^e_w\end{bmatrix}=\begin{bmatrix}\mathbf{0}\\ \mathbf{0}\end{bmatrix} \tag{61}$$

Due to the differences in the order of magnitude of the different stiffness terms in the matrices, we have chosen to improve the numerical accuracy of the eigenvalue and eigenvector solution in our numerical implementation by introducing the following Cholesky decomposition of the block matrices in the first matrix:

$$\mathbf{K}^{s}_{uu}=\mathbf{L}_u\mathbf{L}^T_u,\quad \mathbf{K}^{\sigma}_{ee}=\mathbf{L}_e\mathbf{L}^T_e \tag{62}$$

We utilize the decomposition by introducing the following new intermediate vectors

$$\mathbf{v}^u_w=\mathbf{L}^{-T}_u\tilde{\mathbf{v}}^u_w,\quad (\xi^2\mathbf{v}^e_w)=\mathbf{L}^{-T}_e(\xi^2\tilde{\mathbf{v}}^e_w) \tag{63}$$

where the superscript $^{-T}$ corresponds to the inverted transpose of the matrix. After pre-multiplication of each block matrix equation by $\mathbf{L}_u^{-1}$ and $\mathbf{L}_e^{-1}$, the eigenvalue problem then takes the following form:

$$\begin{bmatrix}\mathbf{I}_{uu}&\mathbf{0}\\ \mathbf{0}&-\mathbf{I}_{ee}\end{bmatrix}\begin{bmatrix}\tilde{\mathbf{v}}^u_w\\ \xi^2\tilde{\mathbf{v}}^e_w\end{bmatrix}-\xi^2\begin{bmatrix}\mathbf{L}^{-1}_u\overline{\mathbf{K}}^{\tau}_{uu}\mathbf{L}^{-T}_u&-\mathbf{L}^{-1}_u\overline{\mathbf{K}}^{\sigma}_{ue}\mathbf{L}^{-T}_e\\ -\mathbf{L}^{-1}_e\overline{\mathbf{K}}^{\sigma}_{eu}\mathbf{L}^{-T}_u&-\mathbf{L}^{-1}_e\overline{\mathbf{K}}^{\sigma}_{ee}\mathbf{L}^{-T}_e\end{bmatrix}\begin{bmatrix}\tilde{\mathbf{v}}^u_w\\ \xi^2\tilde{\mathbf{v}}^e_w\end{bmatrix}=\begin{bmatrix}\mathbf{0}\\ \mathbf{0}\end{bmatrix} \tag{64}$$

In this equation $\mathbf{I}_{uu}$ and $\mathbf{I}_{ee}$ are adequate size unit diagonal matrices. Some general eigenvalue solution routines demand that at least one of the matrices has to be symmetric as well as positive (semi-)definite. This can be achieved by a change of sign in the second block matrix equation, however the second matrix becomes asymmetric. Having found the eigenvectors, we use Eq. (63) to find $\mathbf{v}^u_w$ and $(\xi^2\mathbf{v}^u_w)$, which can then be used for the remaining back-transformation process.

Each distortional eigenvector corresponds to a solution $\psi_{d_i}(z)$ of the homogeneous coupled equations of distortion in Eq. (59). The solution function corresponds to our trial function in Eq. (60), and it has now been determined by plus/minus the square root of the eigenvalues as $\pm\xi_i$. In other words, for the ith eigenvector we find the solution

$$\psi_{d_i}(z)=c_{d_{2i-1}}e^{\xi_i z}+c_{d_{2i}}e^{-\xi_i z}=\mathbf{\Psi}_{d_i}(z)\mathbf{c}_{d_i}=[e^{\xi_i z}\ \ e^{-\xi_i z}]\begin{bmatrix}c_{d_{2i-1}}\\ c_{d_{2i}}\end{bmatrix} \tag{65}$$

in which constants $c_{d_{2i-1}}$ and $c_{d_{2i}}$ assembled in the vector $\mathbf{c}_{d_i}$ depend on the boundary conditions of the problem at hand. All the distortional solution functions are assembled in the distortional solution matrix Ψ_d and multiplied by the assembled vector of distortional constants $\mathbf{c}_d$ as follows:

$$\mathbf{\Psi}_d(z)\mathbf{c}_d=\begin{bmatrix}\mathbf{\Psi}_{d_1}(z)&\mathbf{0}&\mathbf{0}&\cdots\\ \mathbf{0}&\mathbf{\Psi}_{d_2}(z)&\mathbf{0}&\cdots\\ \mathbf{0}&\mathbf{0}&\mathbf{\Psi}_{d_3}(z)&\cdots\\ \vdots&\vdots&\vdots&\ddots\end{bmatrix}\begin{bmatrix}\mathbf{c}_{d_1}\\ \mathbf{c}_{d_2}\\ \mathbf{c}_{d_3}\\ \vdots\end{bmatrix} \tag{66}$$

This notation is used later to describe the total displacement solution.

7. Back substitution

Having found the distortional eigenvalues, eigenvectors and homogeneous solutions for the reduced system (61), we now have to perform a backward substitution through the previous steps in order to achieve the results in the original displacement vector format. Furthermore, we also have to back-substitute all eliminated eigenvectors (multiple zero eigenvalues) and review the related homogeneous solutions.

7.1. Back substitution of distortional modes

In the previous sections, the formulations are related to a single displacement vector and the back substitution of the distortional modes found from solving the eigenvalue problem in Eq. (61) is performed sequentially through Eqs. (58), (51), (46), (32) and (24). In a typical modal approach, all eigenvectors are assembled column-wise in the mode matrix and the related eigenvalues ξ^2 are placed sequentially in the diagonal of the matrix $\mathbf{\Lambda}$. By introducing the capital letter $\mathbf{V}$ with related sub- and superscripts for the assembled modes, we can find the back-substituted distortional mode matrices $\mathbf{V}_w^d$ and $\mathbf{V}_\Omega^d$ using the following sequence of substitutions corresponding to the sequence of equations mentioned above:

$$\mathbf{V}_w^3 = -K_{33}^{\tau\,-1}(\mathbf{K}_{3u}^{\tau}\mathbf{V}_w^u - \mathbf{K}_{3e}^{\sigma}(\mathbf{V}_w^e\mathbf{\Lambda})) \tag{67}$$

$$\mathbf{V}_w^\alpha = -\mathbf{K}_{\alpha\alpha}^{\sigma\,-1}\mathbf{K}_{\alpha u}^{\sigma}\mathbf{V}_w^u \tag{68}$$

$$\mathbf{V}_w^d = \mathbf{T}_w^\alpha\mathbf{V}_w^\alpha + \mathbf{T}_w^3\mathbf{V}_w^3 + \widetilde{\mathbf{T}}_w^u\mathbf{V}_w^u \tag{69}$$

$$\mathbf{V}_\Omega^{d,a} = -(K_{\Omega\Omega}^{\sigma aa})^{-1}\mathbf{K}_{\Omega\Omega}^{\sigma ar}\mathbf{V}_w^d \tag{70}$$

$$\mathbf{V}_\Omega^d = \mathbf{T}_{\Omega w}^r\mathbf{V}_w^d + \mathbf{T}_\Omega^a\mathbf{V}_\Omega^{d,a} \tag{71}$$

The superscript d has been introduced to distinguish the distortional modes from the total assembly of modes introduced later. The term $(\mathbf{V}_w^e\mathbf{\Lambda})$ is just one matrix, which is never separated into the two product terms, but just found directly as part of the eigenvectors of the reduced-order eigenvalue problem in Eq. (61).

7.2. Back substitution of eliminated beam displacement modes

The back substitution of eliminated beam displacement modes involves back substitution of the pure axial extension mode, the two transverse translational modes, and the pure twist mode. Using the degree-of-freedom space introduced in Step II, these modes are given by the following four transverse displacement modal vectors:

$$\begin{bmatrix} v_w^1 \\ v_w^2 \\ v_w^3 \\ \mathbf{v}_w^u \end{bmatrix} = \begin{bmatrix} 0 \\ 0 \\ 0 \\ \mathbf{0} \end{bmatrix}, \quad \begin{bmatrix} v_w^1 \\ v_w^2 \\ v_w^3 \\ \mathbf{v}_w^u \end{bmatrix} = \begin{bmatrix} 1 \\ 0 \\ 0 \\ \mathbf{0} \end{bmatrix}, \quad \begin{bmatrix} v_w^1 \\ v_w^2 \\ v_w^3 \\ \mathbf{v}_w^u \end{bmatrix} = \begin{bmatrix} 0 \\ 1 \\ 0 \\ \mathbf{0} \end{bmatrix}, \quad \begin{bmatrix} v_w^1 \\ v_w^2 \\ v_w^3 \\ \mathbf{v}_w^u \end{bmatrix} = \begin{bmatrix} 0 \\ 0 \\ 1 \\ \mathbf{0} \end{bmatrix} \tag{72}$$

The first vector becomes the extensional eigenvector in the degree-of-freedom space introduced in Step I. The back substitution of these modes is all performed using Eq. (46). However, we have already introduced the eigenvectors in the original transverse displacement space in the transformation matrices related to this equation, $\mathbf{T}_w^\alpha$ and $\mathbf{T}_w^3$ and the back transformation is obsolete for these modes. These eigenvectors are assembled in a beam mode matrix $\mathbf{V}_w^b$ as follows:

$$\mathbf{V}_w^b = [\mathbf{0} \;\; \mathbf{v}_w^{1\ \mathrm{trans}} \;\; \mathbf{v}_w^{2\ \mathrm{trans}} \;\; \mathbf{v}_w^{3\ \mathrm{rot}}] \tag{73}$$

The back substitution of the warping displacements remains. Of course the pure axial extension warping vector is trivial and has already been introduced as $\mathbf{T}_\Omega^{\mathrm{axial}} = \mathbf{v}_\Omega^{\mathrm{axial}}$, but we have to back-substitute the other modes. This is done by first calculating the axial (adjustment) component using Eq. (32) as follows:

$$\mathbf{V}_\Omega^{b,a} = [1\ 0\ 0\ 0] - (K_{\Omega\Omega}^{\sigma aa})^{-1}\mathbf{K}_{\Omega\Omega}^{\sigma ar}\mathbf{V}_w^b \tag{74}$$

The beam warping vectors related to the transverse beam displacement modes can now be found using Eq. (24) as

$$\mathbf{V}_\Omega^b = [\mathbf{v}_\Omega^{\mathrm{axial}} \;\; \mathbf{v}_\Omega^{1\ \mathrm{trans}} \;\; \mathbf{v}_\Omega^{2\ \mathrm{trans}} \;\; \mathbf{v}_\Omega^{3\ \mathrm{rot}}] = \mathbf{T}_{\Omega w}^r\mathbf{V}_w^b + \mathbf{T}_\Omega^a\mathbf{V}_\Omega^{b,a} \tag{75}$$

The axial variation of the four modes has been identified in Eqs. (31), (50) and (57) and can be assembled in the beam solution function matrix $\mathbf{\Psi}_b(z)$ and multiplied by the vector of beam displacement constants $\mathbf{c}_b$ as

$$\mathbf{\Psi}_b(z)\mathbf{c}_b = \begin{bmatrix} \mathbf{\Psi}_a(z) & \mathbf{0} & \mathbf{0} \\ \mathbf{0} & \mathbf{\Psi}_\alpha(z) & \mathbf{0} \\ \mathbf{0} & \mathbf{0} & \mathbf{\Psi}_3(z) \end{bmatrix} \begin{bmatrix} \mathbf{c}_a \\ \mathbf{c}_\alpha \\ \mathbf{c}_3 \end{bmatrix} \tag{76}$$

in which we have introduced the integral of the axial solution as $\mathbf{\Psi}_a = [-z \;\; -\frac{1}{2}z^2]$. This matrix function does not pertain to any solution, and we might as well have set it to zero, since there are no transverse displacements, $\mathbf{v}_w^{\mathrm{axial}} = \mathbf{0}$, for the pure axial deformation mode in beam theory. However, this choice allows us to use the derivative of the $\mathbf{\Psi}_a(z)$ matrix, which is the axial solution $\mathbf{\Psi}'_a = [-1 \;\; -z]$.

8. The full homogenous solution

The full homogenous solution can now be assembled from all the eigenmode vectors and the solution functions. It turns out that some of the eigenvalues and eigenvectors are complex. However in the following we will just perform a direct formulation in which we acknowledge that we are also dealing with complex quantities corresponding to related complex eigenvalues and complex axial solution functions. A transformation of the complex quantities to pairwise coupled real modes and real solution functions will be introduced in the second subsection.

8.1. Direct formulation

Let us assemble all the eigenvectors column-wise in a modal matrix of transverse displacement vectors $\mathbf{V}_w$ and a modal matrix of axial warping displacement vectors $\mathbf{V}_\Omega$ by joining the modal matrices of the beam eigenvectors and the distortional eigenvectors in the following sequence:

$$\mathbf{V}_w = [\mathbf{V}_w^b \;\; \mathbf{V}_w^d], \quad \mathbf{V}_\Omega = [\mathbf{V}_\Omega^b \;\; \mathbf{V}_\Omega^d] \tag{77}$$

The solution function matrices and the displacement constant vectors can also be assembled using the previously defined block matrices and vectors

$$\mathbf{\Psi}(z)\mathbf{c} = \begin{bmatrix} \mathbf{\Psi}_b(z) & \mathbf{0} \\ \mathbf{0} & \mathbf{\Psi}_d(z) \end{bmatrix} \begin{bmatrix} \mathbf{c}_b \\ \mathbf{c}_d \end{bmatrix} \tag{78}$$

The full homogeneous solution along the beam can be assembled in the nodal solution vectors $\mathbf{u}_w(z)$ and $\mathbf{u}_z(z)$ as follows:

$$\mathbf{u}_w(z) = \mathbf{V}_w\mathbf{\Psi}(z)\mathbf{c}$$

$$\mathbf{u}_z(z) = -\mathbf{V}_\Omega\mathbf{\Psi}'(z)\mathbf{c} \tag{79}$$

The constants have to be determined by the boundary conditions of the thin-walled beam.

To be able to present and discuss unique complex eigenmodes, all the distortional vectors in $\mathbf{V}_w$ have been normalized after back substitution in such a way that the largest absolute value of all

components in each vector is one and that this component is real. This has to be done to make them unique since complex eigenvectors are determined except for an arbitrary complex constant.

8.2. Transformation to real modes and real solution functions

Some of the distortional displacement modes found and their related eigenvalues are complex. Mathematical formulation with the use of complex numbers simplify derivations and the use of compilers, which include complex numbers with complex operations on matrices, will lead to simple algorithms. However it may be easier to grasp the form and meaning of the solution in real quantities.

Complex eigenvalues are always found as a pair of complex conjugated eigenvalues with eigenvectors which are also complex conjugated. For the jth complex eigenvalue, ξ_j^2, and its conjugated $j+1$th eigenvalue, $\xi_{j+1}^2=\overline{\xi}_j^2$, let us introduce the following notation for the positive square root values and the related eigenvector columns $\mathbf{v}_j$ and $\mathbf{v}_{j+1}$ of $\mathbf{V}_w$:

$$\xi_j=\lambda_j+\mu_j i,\quad \xi_{j+1}=\overline{\xi}_j=\lambda_j-\mu_j i \tag{80}$$

$$\mathbf{v}_j=\mathbf{a}_j+\mathbf{b}_j i,\quad \mathbf{v}_{j+1}=\overline{\mathbf{v}}_j=\mathbf{a}_j-\mathbf{b}_j i \tag{81}$$

in which we have introduced the real and imaginary parts of the eigenvalues and eigenvectors. The complex eigenvectors in Eq. (81) may be conveniently written as

$$[\mathbf{v}_j\quad \mathbf{v}_{j+1}]=[\mathbf{a}_j\ \ \mathbf{b}_j]\begin{bmatrix}1 & 1\\ i & -i\end{bmatrix} \tag{82}$$

The constants of the related parts of the homogeneous solution are also complex quantities. However we are able to assemble the two complex conjugated modal solutions into two real (but pairwise coupled) solutions by introducing the real constant vectors $\widetilde{\mathbf{c}}_j$ and $\widetilde{\mathbf{c}}_{j+1}$ as follows:

$$\begin{bmatrix}\mathbf{c}_j\\ \mathbf{c}_{j+1}\end{bmatrix}=\frac{1}{2}\begin{bmatrix}1 & -i\\ 1 & i\end{bmatrix}\begin{bmatrix}\widetilde{\mathbf{c}}_j\\ \widetilde{\mathbf{c}}_{j+1}\end{bmatrix} \tag{83}$$

The jth complex part of the full solution can now be rewritten using the transformations in Eqs. (82) and (83). After multiplication and identification of real and imaginary parts, we find the following result:

$$[\mathbf{v}_j\ \ \mathbf{v}_{j+1}]\begin{bmatrix}\boldsymbol{\Psi}_{d_j} & \mathbf{0}\\ \mathbf{0} & \overline{\boldsymbol{\Psi}}_{d_j}\end{bmatrix}\begin{bmatrix}\mathbf{c}_j\\ \mathbf{c}_{j+1}\end{bmatrix}=[\mathbf{a}_j\ \ \mathbf{b}_j]\begin{bmatrix}\mathrm{Re}(\boldsymbol{\Psi}_{d_j}) & \mathrm{Im}(\boldsymbol{\Psi}_{d_j})\\ \mathrm{Im}(\overline{\boldsymbol{\Psi}}_{d_j}) & \mathrm{Re}(\overline{\boldsymbol{\Psi}}_{d_j})\end{bmatrix}\begin{bmatrix}\widetilde{\mathbf{c}}_j\\ \widetilde{\mathbf{c}}_{j+1}\end{bmatrix} \tag{84}$$

where the real and imaginary parts of the (in this case complex) matrix $\boldsymbol{\Psi}_{d_j}$ introduced in (65) are

$$\mathrm{Re}(\boldsymbol{\Psi}_{d_j})=\mathrm{Re}(\overline{\boldsymbol{\Psi}}_{d_j})=[e^{\lambda_j z}\cos\mu_j z\quad e^{-\lambda_j z}\cos\mu_j z]$$

$$\mathrm{Im}(\boldsymbol{\Psi}_{d_j})=-\mathrm{Im}(\overline{\boldsymbol{\Psi}}_{d_j})=[e^{\lambda_j z}\sin\mu_j z\quad -e^{-\lambda_j z}\sin\mu_j z] \tag{85}$$

whereby the real formulation in the right-hand side of Eq. (84) becomes

$$[\mathbf{a}_j\ \ \mathbf{b}_j]\begin{bmatrix}e^{\lambda_j z}\cos\mu_j z & e^{-\lambda_j z}\cos\mu_j z & e^{\lambda_j z}\sin\mu_j z & -e^{-\lambda_j z}\sin\mu_j z\\ -e^{\lambda_j z}\sin\mu_j z & e^{-\lambda_j z}\sin\mu_j z & e^{\lambda_j z}\cos\mu_j z & e^{-\lambda_j z}\cos\mu_j z\end{bmatrix}\begin{bmatrix}\widetilde{c}_{j_1}\\ \widetilde{c}_{j_2}\\ \widetilde{c}_{j+1_1}\\ \widetilde{c}_{j+1_2}\end{bmatrix} \tag{86}$$

This allows us to rewrite the complex quantities into real quantities. Let us modify the modal matrices $\mathbf{V}_w$ and $\mathbf{V}_\Omega$ and introduce the modified modal matrices $\widetilde{\mathbf{V}}_w$ and $\widetilde{\mathbf{V}}_\Omega$ by substituting the complex pairs of eigenvectors with their respective real and imaginary parts. Further more let us also introduce the modified solution matrix $\widetilde{\boldsymbol{\Psi}}$ and its related modified vector of constants $\widetilde{\mathbf{c}}$ by substituting the solutions (and constants) of the complex pairs using Eq. (84), i.e. Eq. (86). This allows us to write the full homogeneous solution along the beam with real numbers as

$$\mathbf{u}_w(z)=\widetilde{\mathbf{V}}_w\widetilde{\boldsymbol{\Psi}}(z)\widetilde{\mathbf{c}}$$

$$\mathbf{u}_z(z)=-\widetilde{\mathbf{V}}_\Omega\widetilde{\boldsymbol{\Psi}}'(z)\widetilde{\mathbf{c}} \tag{87}$$

We may choose to work with this real formulation or continue working with complex numbers using the full homogeneous solution formulated in Eq. (79). Before elaborating on how to find the solution constants, we will look at a couple of examples, showing the different modes and eigenvalues.

9. Examples of transverse and axial displacement modes

Using the approach described, it is possible to identify all the eigenvectors of the current GBT formulation, which is based on simple constitutive relations, discretization of the cross-section displacements in combination with a weak formulation of the shear constraints and constrained wall width. The approach allows direct analysis of both open and closed thin-walled cross-sections without special considerations. Furthermore, the mathematical solution of the problem is not approximate, but performed as in non-proportionally damped modal analysis.

The following three examples illustrate the eigenmodes related to the lowest eigenvalues of the formulated eigenvalue problem for generalized thin-walled beams. The first example relates to an open channel cross-section and the second relates to a closed rectangular box cross-section. The third example illustrates the 3D behavior of distortional eigensolutions. The examples show that some of the important distortional modes and related eigenvalues are complex. We have chosen to show both real and imaginary parts of all the eigenmodes in order to illustrate that they come in pairs and that the imaginary part of the conjugated mode changes sign. However as we have seen in Section 8.2 the conjugated pair can be replaced by two real modes corresponding to the real and the imaginary part of one of the pair bearing in mind that these two are then coupled and interact along the beam. Even though we in our examples only show results for real local distortional modes we have to state that a few of the higher modes become complex, therefor we are not, on the basis of these examples, able to draw conclusions on this.

The examples also illustrate that the pure St. Venant twist mode is included with a linear axial solution for both closed and open sections, while the exponential solution with pure rigid cross-section twist does not seem to exist for the closed rectangular cross-section, and an investigation of the mode found for the open cross-section shows that it contains very small distortions.

9.1. Example 1: Eigenmodes of a lipped channel cross-section

Solving the generalized eigenvalue problem in Eq. (61) using geometric parameters and values as given in Fig. 5 leads to a number of modes corresponding to the number of degrees of freedom. The first 13 eigenvalues are shown in Table 6. For this lipped channel cross-section, modes 0, 1, 2, 3 are beam modes, modes 4, 5, 6, 7, 8 are non-local distortional, and the remaining modes 9–84 are local distortional modes. The designation of local and non-local distortional modes is made on the basis of the difference in the attenuation of the modes (difference in problem length scales) seen in relation to the typical dimensions of the cross-section. Mode 4 is the exponentially varying counterpart to pure St. Venant twist, but it also contains wall distortions, which in this example are in the order of

magnitude 10^{-3} of the twist displacements, and in this formulation it is therefore an independent mode. The in-plane mode shapes corresponding to the eigenvalues in Table 6 are shown in Fig. 6, while the corresponding warping mode shapes are shown in Fig. 7. Note that the imaginary part of the mode vector is about 10–100 times smaller than the real counterpart. The modes found seem very similar to the most important modes found by Silvestre in [13]. Note that Silvestre does not comment on the choice of numbering order, where the modes in this paper are ordered according to the attenuation length.

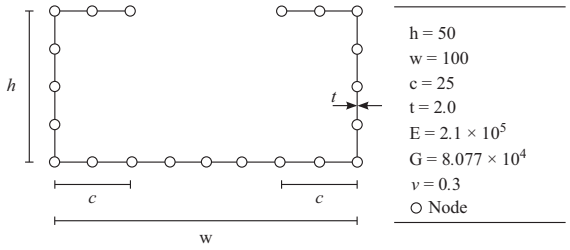

Fig. 5. Geometry and parameter values of a lipped channel.

9.2. Example 3: Eigenmodes of a rectangular box cross-section

Using the geometric parameters and values as given in Fig. 8 leads to a number of modes corresponding to the number of degrees of freedom. The first ten calculated eigenvalues are shown in Table 7. For this channel cross-section, modes 0, 1, 2, 3 are beam modes, modes 4, 5 are non-local distortional modes, and the remaining modes 6–94 are local distortional modes. Note that there is no exponentially varying counterpart to pure St. Venant twist. The in-plane mode shapes corresponding to the eigenvalues in Table 7 are shown in Fig. 9, while the corresponding warping mode shapes are shown in Fig. 10. Also note that for the closed section the imaginary part of the mode vector is 10–100 times smaller than its real counterpart. The modes found seem very similar to the modes found by Gonçalves and Camotim in [4] and seem to span the same deformation space.

9.3. Example 3: Two distortional eigensolutions for both channel and box beams

In this example we show the two eigensolutions related to the first complex distortional displacement mode of the channel and box cross-sections. We choose to illustrate the mode corresponding

Table 6
Eigenvalues ξ^2, the ξ value and the related axial solutions for the lipped channel cross-section.

Mode			Eigenvalues		Axial solution
Type	Scale	No.	$\xi^2 \times 10^6$	$\xi \times 10^3$	$\psi(z)$
Beam	**Global**	0	0	0	$-c_{a1}z-c_{a2}z^2$
		1	0	0	$c_{11}+c_{12}z+c_{13}\,z^2+c_{14}z^3$
		2	0	0	$c_{21}+c_{22}z+c_{23}z^2+c_{24}z^3$
		3	0	0	$c_{31}+c_{32}z$
Distortional	**Non-local**	4	0.37	0.61	$c_{d1}e^{\xi z}+c_{d2}e^{-\xi z}$
		5	3.36-26.52i	$\pm$(3.88−3.42i)	$c_{d3}e^{\xi z}+c_{d4}e^{-\xi z}$
		6	3.36+26.52i	$\pm$(3.88+3.42i)	$c_{d5}e^{\xi z}+c_{d6}e^{-\xi z}$
		7	4.23−50.04i	$\pm$(5.22−4.80i)	$c_{d7}e^{\xi z}+c_{d8}e^{-\xi z}$
		8	4.23+50.04i	$\pm$(5.22+4.80i)	$c_{d9}e^{\xi z}+c_{d10}e^{-\xi z}$
	Local	9	825.6	28.7	$c_{d11}e^{\xi z}+c_{d12}e^{-\xi z}$
		10	951.1	30.8	$c_{d13}e^{\xi z}+c_{d14}e^{-\xi z}$
		11	1823	42.7	$c_{d15}e^{\xi z}+c_{d16}e^{-\xi z}$
		12	3359	58.0	$c_{d17}e^{\xi z}+c_{d18}e^{-\xi z}$

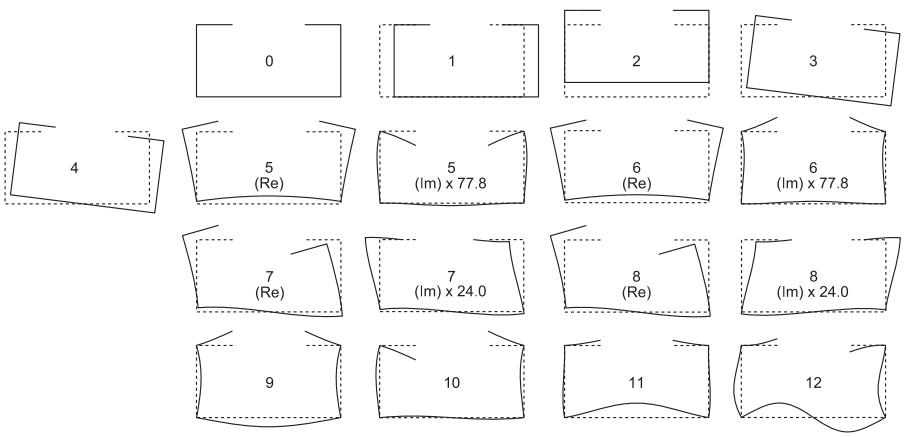

Fig. 6. Lipped channel – 13 in-plane deformation mode shapes.

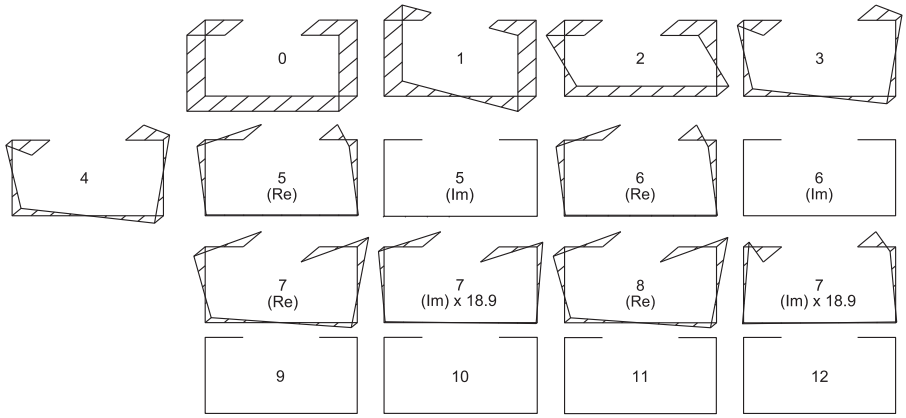

Fig. 7. Lipped channel – 13 warping deformation mode shapes.

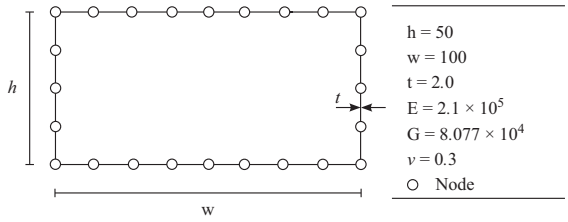

Fig. 8. Geometry and parameter values of a rectangular section.

to the first complex distortional displacement mode, which are mode $j=5$ and $j=4$ respectively for the channel and box cross-sections. With the use of Eq. (86) in which the real part, **a**, and the imaginary part, **b**, of the mode are multiplied by the solution functions. We choose in Fig. 11 to illustrate two of the four independent solution functions: one in which only $\widetilde{c}_{j_2}$ is non-zero (shown as a and b in the figure), and the other (shown as c and d) in which only $\widetilde{c}_{j+1_2}$ is non-zero. Thus sub-figures a and b correspond to the solution $e^{-\lambda_j z}\cos\mu_j z \cdot \mathbf{a}_j + e^{-\lambda_j z}\sin\mu_j z \cdot \mathbf{b}_j$ and sub-figures c and d correspond to $-e^{-\lambda_j z}\sin\mu_j z \cdot \mathbf{a}_j + e^{-\lambda_j z}\cos\mu_j z \cdot \mathbf{b}_j$. The eigensolutions shown in the figure therefore involves a coupled behavior of the real part and imaginary part of the mode.

10. The degree of freedom space and related transformations

To apply the present work and make use of the solutions found in a finite-element context, it is necessary to be able to relate to the different degree-of-freedom spaces in use as well as to the constraints introduced. In Step I, the introduction of shear constraints leads to a generalized beam theory (GBT) in which only shear flow around closed cells is taken into account while all other shears are constrained. With the exception of pure axial extension, the axial displacements are determined from the axial derivative of the transverse displacements. From the boundary terms of the first variation of the potential energy given in Eq. (27), it is seen that the (virtual) generalized boundary displacements are pure axial extension (ζv_Ω^a), transverse displacements ($\psi \mathbf{v}_w$), and the axial derivative of the transverse displacements $(\psi \mathbf{v}_w)'$. However the transverse displacements are unconstrained, which is not compatible with classical Vlasov beam theory where the individual thin wall of the cross-section is assumed to maintain its length (width) within the cross-section, i.e. no cross-section centerline elongation. This is overcome in Step II where the walls are constrained using a set of multi-point constraint equations which eliminate constrained transverse displacement degrees of freedom $\mathbf{v}_w^c$. The basic degrees of freedom of the GBT formulation are the pure axial extension (ζv_Ω^a), the remaining transverse displacements ($\psi \mathbf{v}_w^g$), and the axial derivative hereof $(\psi \mathbf{v}_w^g)'$. To be able to change degree-of-freedom space from GBT space $\mathbf{v}_w^g$ to finite element (FE) (original degree-of-freedom) space $\mathbf{v}_w$, the following transformation is introduced:

$$\mathbf{v}_w = [\mathbf{T}_w^c \;\; \mathbf{T}_w^g] \begin{bmatrix} \mathbf{v}_w^c \\ \mathbf{v}_w^g \end{bmatrix} \tag{88}$$

where

$$\mathbf{T}_w^g = [\mathbf{T}_w^i \;\; \mathbf{T}_w^u] \quad \text{and} \quad \mathbf{T}_w^i = \begin{bmatrix} 1 & 0 & 0 \\ 0 & 1 & 0 \\ \vdots & 0 & 1 \\ & \vdots & 0 \\ & & \vdots \end{bmatrix}$$

in which $\mathbf{T}_w^c$ and $\mathbf{T}_w^u$ have already been introduced in Step II, and $\mathbf{T}_w^i$ is a matrix corresponding to three supplementary columns, which pick out the degrees of freedom of the first node related to v_w^1, v_w^2 and v_w^3.

10.1. From FE displacements to GBT displacements

If the transverse displacement vector $\mathbf{v}_w$ already fulfills the constraint equations, then we can find the GBT transverse displacement vector by using $\mathbf{T}_w^{g\,T}$, and the pure axial extension by using $\mathbf{T}_\Omega^{a\,T}$ as follows:

$$\begin{bmatrix} \mathbf{v}_w^g \\ v_\Omega^a \end{bmatrix} = \begin{bmatrix} \mathbf{T}_w^{g\,T} & \mathbf{0} \\ \mathbf{0} & \mathbf{T}_\Omega^{a\,T} \end{bmatrix} \begin{bmatrix} \mathbf{v}_w \\ \mathbf{v}_\Omega \end{bmatrix} \tag{89}$$

This is the important transformation from FE space to GBT space, which we will need to be able to find the constants of the homogeneous solution.

10.2. From GBT displacements to FE displacements

However we may at some point also need the opposite transformation, which involves the constraint equations introduced in Eq. (42). Let us principally use the same method but introduce the transformation Eq. (88) whereby the multi-point

Table 7
Eigenvalues ξ^2, the ξ value and the related axial solutions for the rectangular box cross-section.

Mode			**Eigenvalues**		**Axial solution**
Type	Scale	No.	$\xi^2 \times 10^6$	$\xi \times 10^3$	$\psi(z)$
Beam	**Global**	0	0	0	$-c_{a1}z-c_{a2}z^2$
		1	0	0	$c_{11}+c_{12}z+c_{13}z^2+c_{14}z^3$
		2	0	0	$c_{21}+c_{22}z+c_{23}z^2+c_{24}z^3$
		3	0	0	$c_{31}+c_{32}z$
Distortional	**Non-local**	4	$0.72-36.95i$	$\pm(4.34-4.26i)$	$c_{d1}e^{\xi z}+c_{d2}e^{-\xi z}$
		5	$0.72+36.95i$	$\pm(4.34+4.26i)$	$c_{d3}e^{\xi z}+c_{d4}e^{-\xi z}$
	Local	6	1205	34.7	$c_{d5}e^{\xi z}+c_{d6}e^{-\xi z}$
		7	2661	51.6	$c_{d7}e^{\xi z}+c_{d8}e^{-\xi z}$
		8	2050	45.3	$c_{d9}e^{\xi z}+c_{d10}e^{-\xi z}$
		9	4837	69.6	$c_{d11}e^{\xi z}+c_{d12}e^{-\xi z}$

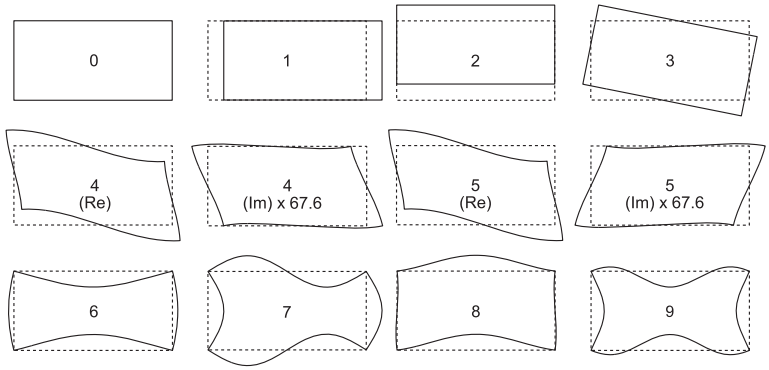

Fig. 9. Rectangular box cross-section – 10 in-plane deformation mode shapes.

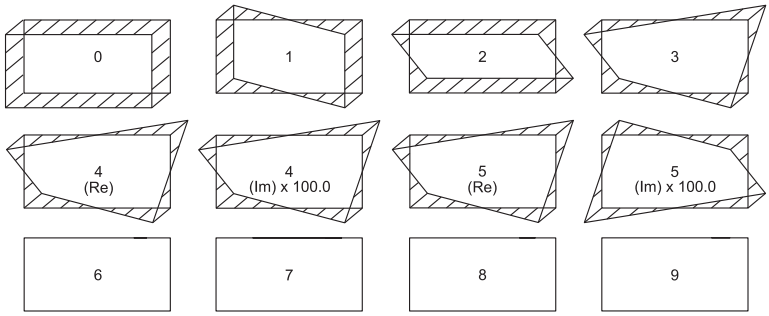

Fig. 10. Rectangular box cross-section – 10 warping deformation mode shapes.

constraint equations take the form

$$\mathbf{C}\mathbf{T}_w^c\mathbf{v}_w^c+\mathbf{C}\mathbf{T}_w^g\mathbf{v}_w^g=\mathbf{0} \quad \Leftrightarrow \quad \mathbf{C}_c\mathbf{v}_w^c+\mathbf{C}_g\mathbf{v}_w^g=\mathbf{0} \tag{90}$$

in which $\mathbf{C}_c = \mathbf{C}\mathbf{T}_w^c$ has previously been introduced and $\mathbf{C}_g = \mathbf{C}\mathbf{T}_w^g$ is introduced here. This allows us to express the constrained degrees of freedom by the GBT transverse displacement vector as

$$\mathbf{v}_w^c=-\mathbf{C}_c^{-1}\mathbf{C}_g\mathbf{v}_w^g \tag{91}$$

Introducing the equality (91) in the transformation Eq. (88), we find that the total transformation condenses our problem as follows:

$$\mathbf{v}_w=[\mathbf{T}_w^c \;\; \mathbf{T}_w^g]\begin{bmatrix}-\mathbf{C}_c^{-1}\mathbf{C}_g\mathbf{v}_w^g\\ \mathbf{v}_w^g\end{bmatrix}=\tilde{\mathbf{T}}_w^g\mathbf{v}_w^g \tag{92}$$

where $\tilde{\mathbf{T}}_w^g=\mathbf{T}_w^g-\mathbf{T}_w^c\mathbf{C}_c^{-1}\mathbf{C}_g$ has been introduced as the condensed transformation. Using the transformation Eq. (24) that determines the warping displacements from the amount of axial extension and the transverse displacements we find

$$\mathbf{v}_\Omega=[\mathbf{T}_{\Omega w}^r \;\; \mathbf{T}_\Omega^a]\begin{bmatrix}\mathbf{v}_w\\ \mathbf{v}_\Omega^a\end{bmatrix}=[\mathbf{T}_{\Omega w}^r\tilde{\mathbf{T}}_w^g \quad \mathbf{T}_\Omega^a]\begin{bmatrix}\mathbf{v}_w^g\\ \mathbf{v}_\Omega^a\end{bmatrix} \tag{93}$$

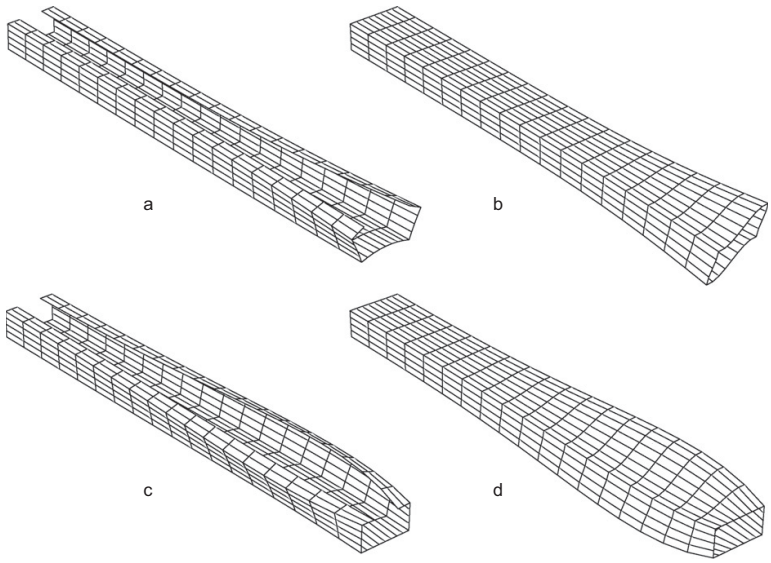

Fig. 11. Two eigensolutions of the first complex distortional mode for a channel and a box section.

Using Eqs. (92) and (93) we find the following transformation

$$\begin{bmatrix} \mathbf{v}_w \\ \mathbf{v}_\Omega \end{bmatrix} = \begin{bmatrix} \widetilde{\mathbf{T}}_w^g & \mathbf{0} \\ \mathbf{T}_{\Omega w}^r \widetilde{\mathbf{T}}_w^g & \mathbf{T}_\Omega^a \end{bmatrix} \begin{bmatrix} \mathbf{v}_w^g \\ v_\Omega^a \end{bmatrix} \tag{94}$$

This transformation is used to transform from GBT space to FE space.

11. Displacement boundary conditions of the homogeneous solution

Having solved the eigenvalue problem and formulated solution modes in the original FE degree-of-freedom space, we would like to set up a method for determining the constants of the homogeneous solutions found. This is to be done in the GBT space. As seen from the first variation of the potential energy, the natural boundary displacements of the GBT at each boundary are the pure axial displacement u_Ω^a of the beam, the transverse displacements $\mathbf{u}_w^g$, and the axial derivative of the transverse displacements $\mathbf{u}_w^{g\prime}$. The generalized internal displacements of the GBT beam can be expressed by using the full homogeneous solution in Eq. (79) or alternatively, as done in the following, by the real formulation in Eq. (87) and the transformation from FE to GBT displacements (89) as follows:

$$\begin{bmatrix} u_z^a(z) \\ \mathbf{u}_w^g(z) \\ \mathbf{u}_w^{g\prime}(z) \end{bmatrix} = \begin{bmatrix} -\mathbf{T}_\Omega^{a\,T} \widetilde{\mathbf{V}}_\Omega \widetilde{\mathbf{\Psi}}'(z) \\ \mathbf{T}_w^{g\,T} \widetilde{\mathbf{V}}_w \widetilde{\mathbf{\Psi}}(z) \\ \mathbf{T}_w^{g\,T} \widetilde{\mathbf{V}}_w \widetilde{\mathbf{\Psi}}'(z) \end{bmatrix} \widetilde{\mathbf{c}} \tag{95}$$

To determine the constants using displacement boundary conditions as in finite element or stiffness formulations, we need the boundary displacements at the two ends of a finite length beam, i.e. at $z=0$ and L where L is the length of the beam. The assembled boundary displacement vector is denoted by $\mathbf{u}_b$. This leads to the following equation for the determination of the solution constants:

$$\mathbf{u}_b = \begin{bmatrix} u_z^a(0) \\ \mathbf{u}_w^g(0) \\ \mathbf{u}_w^{g\prime}(0) \\ u_z^a(L) \\ \mathbf{u}_w^g(L) \\ \mathbf{u}_w^{g\prime}(L) \end{bmatrix} = \begin{bmatrix} -\mathbf{T}_\Omega^{a\,T} \widetilde{\mathbf{V}}_\Omega \widetilde{\mathbf{\Psi}}'(0) \\ \mathbf{T}_w^{g\,T} \widetilde{\mathbf{V}}_w \widetilde{\mathbf{\Psi}}(0) \\ \mathbf{T}_w^{g\,T} \widetilde{\mathbf{V}}_w \widetilde{\mathbf{\Psi}}'(0) \\ -\mathbf{T}_\Omega^{a\,T} \widetilde{\mathbf{V}}_\Omega \widetilde{\mathbf{\Psi}}'(L) \\ \mathbf{T}_w^{g\,T} \widetilde{\mathbf{V}}_w \widetilde{\mathbf{\Psi}}(L) \\ \mathbf{T}_w^{g\,T} \widetilde{\mathbf{V}}_w \widetilde{\mathbf{\Psi}}'(L) \end{bmatrix} \widetilde{\mathbf{c}} = \widetilde{\mathbf{A}} \widetilde{\mathbf{c}} \tag{96}$$

$$\Rightarrow \quad \widetilde{\mathbf{c}} = \widetilde{\mathbf{A}}^{-1} \mathbf{u}_b \tag{97}$$

where we have introduced the matrix $\widetilde{\mathbf{A}}$, which is an invertible positive definite "square" matrix. However to avoid numerical problems, the exponential solution functions in $\widetilde{\mathbf{\Psi}}(z)$ may have to be modified by replacing $\widetilde{c}_i e^{\lambda z}$ by $\hat{c}_i e^{\lambda(z-L)}$ so that the positive λz exponent is bounded.

The two solutions plotted by using Eq. (87) with only $\widetilde{c}_{j_2}$ being non-zero in the upper half of Fig. 11 can also be found by using the relevant boundary conditions in Eq. (97). To this end, we use the real and imaginary vectorial parts, **a** and **b**, of the mode shape and the modal solution functions and the derivative hereof. So in Eq. (97), we would use

$$\mathbf{u}_b = \begin{bmatrix} 0 \\ \mathbf{a} \\ -\lambda\mathbf{a} - \mu\mathbf{b} \\ 0 \\ e^{-\lambda L}(\mathbf{a}\cos\mu L + \mathbf{b}\sin\mu L) \\ -e^{-\lambda L}\{\mathbf{a}(\lambda\cos\mu L + \mu\sin\mu L) + \mathbf{b}(\lambda\sin\mu L - \mu\cos\mu L)\} \end{bmatrix} \tag{98}$$

and we should then find only the second constant of the jth complex mode $\widetilde{c}_{j_2}$ to be non-zero. The two lower solutions plotted in Fig. 11 correspond to boundary conditions in which only the fourth constant $\widetilde{c}_{j_4}$ of the complex mode is non-zero.

It is also worth noting that just specifying the modal shape with a zero derivative (otherwise built-in support) will lead to a coupling to the remaining modes. For example, Fig. 12 shows the

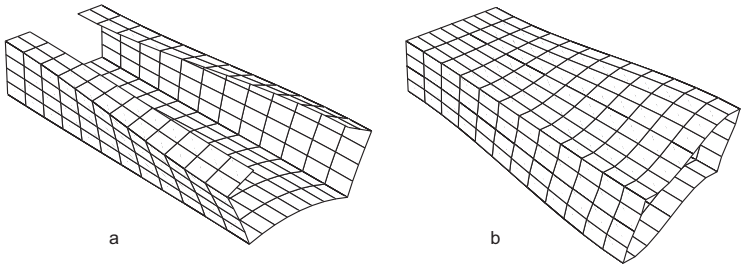

Fig. 12. Displacement field for boundary conditions in Eq. (99).

displacements for the boundary displacements corresponding to the real part of the first complex distortional eigenmode at one end, but with zero axial displacements and zero displacements and axial displacement derivatives at the other end, i.e. with the following boundary condition:

$$\mathbf{u}_b^T = [0\ \ \mathbf{a}^T\ \ \mathbf{0}\ \ 0\ \ \mathbf{0}\ \ \mathbf{0}]^T \tag{99}$$

With this boundary condition many modes are invoked and to achieve the zero derivative of the displacements, local distortional plate modes have also been invoked. The problem length scales of some of these modes are very small and will be difficult to see in an overall plot of the deformation mode. The formulation above enables finite-element formulation of advanced semi-discretized thin-walled beam elements.

12. Conclusion

We have presented a new systematic method accompanied by a detailed description for the whole semi-discretization process from kinematic assumptions, potential energy, potential energy variation leading to the formulation of the homogeneous differential equations of a generalized beam theory (GBT) and the establishment of the full solution through identification of all eigenvalues and eigenmodes. This new approach is a considerable theoretical and practical development, since the obtained GBT equations are now solved analytically and the formulation is valid without special attention also for closed single or multi-cell cross-sections.

The beam displacement field was separated into a sum of products of the cross-section displacement modes and their axial variation. This displacement field was constrained to follow the shear assumptions made in Vlasov beam theory by a weak formulation of the constant shear flow assumption. This allows the identical treatment of both open and closed cross-sections.

The coupled homogeneous fourth order differential equations of GBT have not been solved approximately, but by a reduction of order accompanied by a doubling of the number of equations and the introduction of a state vector, as in non-proportionally damped dynamic analysis. In traditional GBT analysis, the eigenvalue problem, which defines the distortional modes corresponds to the solution of the undamped eigenvalue problem solved in proportionally damped dynamic structural analysis (i.e. by neglecting the shear stiffness matrix related to torsion). However the related eigenvalues have not been used for assessment of the attenuation behavior.

It is clear that the eigenvalues of the distortional modes found are inverse length scale parameters or attenuation parameters which define the axial solution functions and allow us to predict the length of the distortional displacement field. This may be used to determine the degree of discretization if the eigenmodes found are to be used in a traditional type GBT finite-element formulation with a reduced number of modes and with approximate shape functions for the axial variation. Alternatively future formulation of distortional beam elements may be based on the found distortional modes with axial variations based on the analytical solution functions. In a following paper we will address the solution of the inhomogeneous GBT equations using the eigenmodes found in this paper in order to decouple the non-homogeneous differential equations.

The modes found in this paper seem to be similar to the modes found in traditional GBT, see e.g. [13], as well as to the modes found by the modified GBT formulation for closed cross-sections, see [4]. In this relation it will be of interest to perform a proper comparison of the found distortional modes and the modes found by the conventional GBT formulation.

References

[1] Vlasov VZ. Thin-walled elastic beams, 2nd ed. Jerusalem, Israel: Israel Program for Scientific Translations; 1961.
[2] Schardt R. Eine Erweiterung der technischen Biegelehre für die Berechnung biegesteifer prismatischer Faltwerke. Der Stahlbau 1966;35:161–71.
[3] Schardt R. Verallgemeinerte Technische Biegetheorie. Germany: Springer-Verlag; 1989.
[4] Gonçalves R, Camotim D. GBT local and global buckling analysis of aluminium and stainless steel columns. Computers and Structures 2004;82:1473–84.
[5] Gonçalves R, Dinis PB, Camotim D. GBT formulation to analyse the first-order and buckling behaviour of thin-walled members with arbitrary cross-sections. Thin-Walled Structures 2009;47:583–600.
[6] Gonçalves R, Ritto-Corrêa M, Camotim D. A new approach to the calculation of cross-section deformation modes in the framework of generalized beam theory. Computational Mechanics 2010;46:759–81.
[7] Kollbrunner CF, Hajdin N. Dünnwandige Stäbe 1, Stäbe mit undeformierbaren Querschnitten. Berlin: Springer-Verlag; 1972, 1975.
[8] Jönsson J. Determination of shear stresses, warping functions and section properties of thin-walled beams using finite elements. Computers and Structures 1998;68:393–410.
[9] Jönsson J. Distortional warping functions and shear distributions in thin-walled beams. Thin-Walled Structures 1999;33:245–68.
[10] Hanf M. Die geschlossene Lösung der linearen Differentialgleichungssysteme der Verallgemeinerten Technischen Biegetheorie mit einer Anwendung auf die Ermittlung plastischer Grenzlasten. Instituts für Werkstoffe und Mechanik im Bauwesen der TU Darmstadt 1989;9.
[11] Davies JM, Leach P. First-order generalised beam theory. Journal of Constructional Steel Research 1994;31(2–3):187–220.
[12] Jönsson J. Distortional theory of thin-walled beams. Thin-Walled Structures 1999;33:269–303.
[13] Silvestre N, Camotim D. First-order generalised beam theory for arbitrary orthotropic materials. Thin-Walled Structures 2002;40:755–89.
[14] Silvestre N, Camotim D. Second-order generalised beam theory for arbitrary orthotropic materials. Thin-Walled Structures 2002;40:791–820.
[15] Rendek S, Baláž I. Distortion of thin-walled beams. Thin-Walled Structures 2004;42:255–77.
[16] Silvestre N. Generalized beam theory: new formulations, numerical implementation and applications. PhD thesis, IST–Technical University of Lisbon, Portugal; 2005 (in Portuguese).
[17] Camotim D, Silvestre N, Gonçalves R, Dinis PB. GBT analysis of thin-walled members: new formulations and applications. In: Loughlan J, editor. Thin-walled structures: recent advances and future trends in thin-walled structures technology. Bath: Canopus Publishing Ltd.; 2004. p. 137–68.

[18] Camotim D, Silvestre N, Gonçalves R, Dinis PB. GBT-based structural analysis of thin-walled members: overview, recent progress and future developments. In: Pandey M, Xie W-C, Xu L, editors. Advances in engineering structures, mechanics and construction. Waterloo: Springer (Dordrecht); 2006. p. 187–204.
[19] Kollbrunner CF, Hajdin N. Dünnwandige Stäbe 2, Stäbe mit deformierbaren Querschnitten, Nicht-elastisches Verhalten dünnwandiger Stäbe. Berlin: Springer-Verlag; 1972, 1975.
[20] Zienkiewicz OC, Taylor RL. Finite element method, Solid mechanics, vol. 2, 5th ed., Elsevier; 2000. p. 308.
[21] Ádány S, Schafer BW. Buckling mode decomposition of single-branched open cross-section members via finite strip method: derivation. Thin-Walled Structures 2006;44:563–84.
[22] Ádány S, Schafer BW. Buckling mode decomposition of single-branched open cross-section members via finite strip method: application and examples. Thin-Walled Structures 2006;44:585–600.
[23] Ádány S, Schafer BW. A full modal decomposition of thin-walled, signle-branched open cross-section members via the constrained finite strip method. Journal of Constructional Steel Research 2008;64:12–29.
[24] Ádány S, Silvestre N, Schafer BW, Camotim D. GBT and cFSM: two modal approaches to the buckling analysis of unbranched thin-walled members. International Journal of Advanced Steel Construction 2009;5:195–223.
[25] Timoshenko SP, Goodier JN. Theory of elasticity. 3rd International ed. Singapore: McGraw Hill Book Company; 1970. p. 61.
[26] Cook RD, et al. Concepts and applications of finite element analysis. 4th ed. United States: John Wiley & Sons, Inc.; 2001. p. 489.

Appendix C

Paper II

Andreassen, M.J., and Jönsson, J. (2012).

Distortional solutions for loaded semi-discretized thin-walled beams.

Thin-Walled Structures, **50**, 116–127.

Thin-Walled Structures 50 (2012) 116–127

Contents lists available at SciVerse ScienceDirect

Thin-Walled Structures

journal homepage: www.elsevier.com/locate/tws

Distortional solutions for loaded semi-discretized thin-walled beams

M.J. Andreassen, J. Jönsson *

Technical University of Denmark, Department of Civil Engineering, Brovej Building 118, DK-2800 Kgs. Lyngby, Denmark

ARTICLE INFO

Article history:
Received 30 November 2010
Received in revised form
23 August 2011
Accepted 23 August 2011
Available online 27 October 2011

Keywords:
Distortion
Warping
Distortional beam theory
Generalized beam theory (GBT)
Thin-walled beams
Beam theory
Semi-discretization
Non-homogeneous
Load

ABSTRACT

For thin-walled beams, the classic theory for flexural and torsional analysis of open and closed cross-sections can be generalized by including distortional displacements. In a companion paper it is shown that using a novel semi-discretization process, it is possible to determine specific distortional displacement fields which decouple the reduced order differential equations. In this process the cross section is discretized into finite cross-section elements, and the natural distortional modes as well as the related axial variations are found as solutions to the established coupled fourth order homogeneous differential equations of GBT.

In this paper the non-homogeneous distortional differential equations of GBT are formulated using this novel semi-discretization process. Transforming these non-homogeneous distortional differential equations into the natural eigenmode space by using the distortional modal matrix found for the homogeneous system, we get the uncoupled set of differential equations including the distributed loads. This uncoupling is very important in GBT, since the shear stiffness contribution from St. Venant torsional shear stress as well as "Bredt's shear flow" cannot be neglected nor approximated by the combination of axial stiffness and transverse stiffness, especially for closed cross sections. The full analytical solutions of these linear non-homogeneous differential equations are given, including four illustrative examples, which illustrate the strength of this novel approach to GBT. This new approach is a considerable theoretical achievement, since it without approximation gives the full analytical solution for a given discretization of the cross section including distributed loading. The boundary conditions considered in the examples of this paper are restricted to built in ends, which are needed for future displacement formulation of an exact first-order distortional beam element.

1. Introduction

Thin-walled members are often used in the civil, mechanical and aerospace industry because of the high strength and the effective use of material. Due to the increased consumption of thin-walled structural elements there has been increasing focus and need for more detailed calculations. Thus, it has been necessary to extend the classic beam theory to include the distortion of the cross section. Such an extension of the theory is considered in this paper and in the companion paper [1] where a novel approach to the determination of distortional displacement modes of Generalized Beam Theory (GBT) is formulated. This novel approach involves a new cross-section semi-discretization process as well as a novel determination of the natural cross-section eigenmodes and related axial solution functions by exact analytical solution of the related first-order GBT equations. A variety of other formulations including distortional displacements have been proposed for analysis of both open and closed cross sections. Specially, the traditional first generation of generalized beam theory, known as GBT, initially proposed by Schardt in 1966 [2], has been very popular and fostered a lot of research and developments, mostly undertaken by a few independently working European groups, among others by Schardt [3], Davies [4], Lepistö [5], Baláž and Rendek [6], Simões da Silva and Simão [7], Gonçalves et al. [8], Gonçalves and Camotim [9] and Camotim and Silvestre [10,11]. In these developments the distortional modes of traditional GBT have been extended (with "other" modes) in order to encompass shear through shear modes, post buckling through inclusion of transverse extension modes as well special modes to accommodate shear lag. However, these extensions with other modes are not considered in the present paper, since they are not part of a first generation GBT and may be viewed as patches toward expanded use of a generalized beam theory in a finite element context. For a more elaborate introduction see the companion paper [1]. Particularly relevant in relation to our research is the closely related work of Hanf [12] as well as the work on distortional theory of thin-walled beams by Jönsson [13]. In contrast to and as a considerable advance on the traditional GBT formulation this novel GBT approach solves the fourth-order differential equations to obtain the distortional

* Corresponding author. Tel.: +45 45251707.
E-mail addresses: mican@byg.dtu.dk (M.J. Andreassen), jej@byg.dtu.dk (J. Jönsson).

0263-8231/$ - see front matter © 2011 Elsevier Ltd. All rights reserved.
doi:10.1016/j.tws.2011.08.013

displacements for a linear beam analysis. This advance will enable future formulation of exact distortional beam elements with distributed load for first-order analysis using the found axial solution-functions (solutions of the GBT equations) instead of conventional interpolation by third-order polynomials.

Thus, in this paper the distortional differential equations including distributed loads are formulated. Transforming the non-homogeneous distortional differential equations into an eigenmode space, by using the distortional modal matrix found for the homogeneous system, we get the diagonalized and thus uncoupled set of differential equations including the distributed loads. The full solution of these uncoupled linear differential equations is given and followed by four illustrative examples. The boundary conditions considered in the examples of this paper are restricted to built in ends, which are needed for future displacement formulation of an exact first-order distortional beam element. It should be mentioned that the theory and formulations in paper [1] remain valid, which implies that mainly the development of the particular part and the following final general solution will be presented in this paper. It was found necessary to follow the individual steps of the transformations and eliminations in the companion paper [1], in order to ensure a correct formulation of the individual decoupled non-homogeneous differential equation, especially for the distortional modes where we have utilized reduction of the order of the differential equations. Having done this once we may use work or energy principles to identify the individual load terms in a more direct manner.

2. Basic kinematic assumptions

The theories of beams are derived on the basis of assumed displacement fields which correspond to extension, flexure, torsion, warping and distortional displacements. This corresponds to a modal separation in which each mode has a set of transverse and axial displacement fields that may be coupled. Each of these cross-section displacement fields is factorized in a displacement mode which is a function of the in-plane coordinates, multiplied by a function of the axial coordinate, which describes the axial variation of the mode.

In the following the prismatic beam is described in a global Cartesian (x,y,z) coordinate system as shown in Fig. 1. The figure introduces and shows the local coordinates (z,n,s) corresponding to the axial, normal and tangential directions. In the local coordinate system the displacement components of one displacement mode u_n, u_s and u_z are given by the separated displacement functions as follows

$$u_n(s,z) = \mathrm{w}_n(s)\psi(z) \tag{1}$$

$$u_s(n,s,z) = \big(\mathrm{w}_s(s) - n\mathrm{w}_{n,s}(s)\big)\psi(z) \tag{2}$$

$$u_z(n,s,z) = -\big(\Omega(s) + n\mathrm{w}_n(s)\big)\psi'(z) \tag{3}$$

where the local components are shown in Fig. 2.

The corresponding strains become

$$\varepsilon_z = -(\Omega + n\mathrm{w}_n)\psi'' \tag{4}$$

$$\varepsilon_s = (\mathrm{w}_{s,s} - n\mathrm{w}_{n,ss})\psi \tag{5}$$

$$\gamma = \gamma_{zs} = u_{z,s} + u_{s,z} = (\mathrm{w}_s - \Omega_{,s} - 2n\mathrm{w}_{n,s})\psi' \tag{6}$$

These are described in greater detail in the companion paper [1].

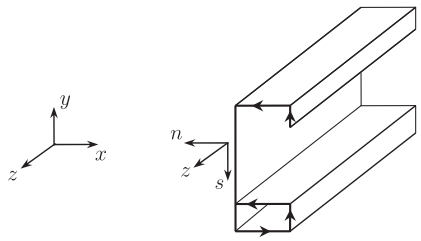

Fig. 1. Global and local Cartesian reference frames.

3. Energy assumptions

The internal energy potential introduced in paper [1] will be briefly presented in this section followed by a separate introduction of the external energy potential for distributed loads.

3.1. Internal energy potential

In the classic beam theory simple constitutive relations are used, which means that the material is assumed to be linear elastic with a modulus of elasticity E and shear modulus G. In this paper also a plate elasticity modulus $E_s = E/(1-\nu^2)$ in the transverse direction will be utilized. The axial stress is determined as $\sigma_z = E\varepsilon_z$, the shear stress as $\tau = G\gamma$ and finally the transverse stress as $\sigma_s = E_s\varepsilon_s$. Thus taking the transverse plate bending effect into account but neglecting the coupling of axial strain ε_z and transverse strain ε_s. With the constitutive relations assumed the

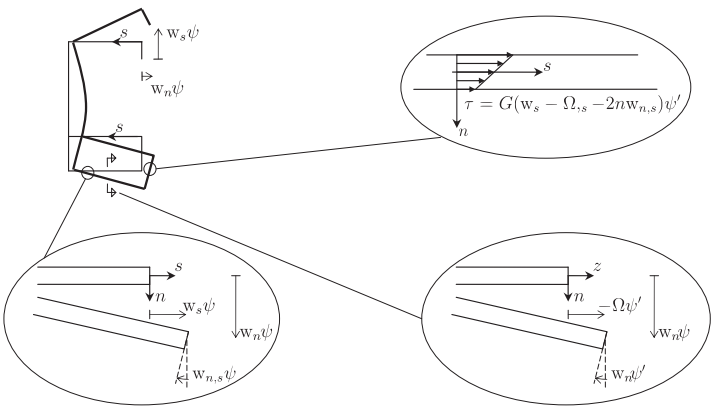

Fig. 2. Local components of displacements and assumed shear stresses.

elastic energy potential becomes

$$\Pi_{int} = \int_V \left(\frac{1}{2} E\varepsilon_z^2 + \frac{1}{2} G\gamma^2 + \frac{1}{2} E_s \varepsilon_s^2 \right) dV \tag{7}$$

Let us introduce a thin-walled cross section assembled by using straight cross sectional elements. This allows us to integrate the internal energy across the volume of the thin-walled beam. In the following we will denote the thickness of the individual plane cross section elements by t and the width by b_{el}. The elastic potential energy of one mode takes the following form after the introduction of the strains expressed by the separated displacement functions:

$$\begin{aligned}\Pi_{int} = \frac{1}{2}\int_0^L \Bigg[\sum_{el} \int_0^{b_{el}} \Bigg\{ & \left[Et(\Omega\psi'')^2 + \frac{1}{12} Et^3 (\mathrm{w}_n \psi'')^2 \right] \\ & + \Big[Gt(\mathrm{w}_s \psi')^2 + Gt(\Omega_{,s}\psi')^2 \\ & - 2Gt(\mathrm{w}_s\psi')(\Omega_{,s}\psi') + \frac{1}{3} Gt^3 (\mathrm{w}_{n,s}\psi')^2 \Big] \\ & + \left[E_s t(\mathrm{w}_{s,s}\psi)^2 + \frac{1}{12} E_s t^3 (\mathrm{w}_{n,ss}\psi)^2 \right] \Bigg\} ds \Bigg] dz \end{aligned} \tag{8}$$

The elastic energy terms have been grouped in axial strain energy, shear energy, and transverse strain energy. Introducing the displacement interpolation functions leads to the definition of several stiffness sub-matrices as given in Table 1. The superscripts σ, τ and s correspond to components of the axial stiffness, shear stiffness and transverse stiffness, respectively.

3.2. External energy potential for distributed loads

Let us now introduce three types of distributed loads q_z, q_s, q_n which act on the mid plane of the individual walls in the z,s,n directions, respectively. The external load potential for these distributed loads can then for one mode be found as

$$\Pi_{ext} = -\int_0^L \int_0^{b_{el}} \left[q_z u_z + q_s u_s + q_n u_n \right] ds\, dz \tag{9}$$

Using separation of variables for the distributed loads as for the displacements, we introduce the following load variables $q_s = p_s(s)\phi(z)$, $q_n = p_n(s)\phi(z)$, $q_z = p_z(s)\phi(z)$. In this formulation p_s, p_n, p_z represent the cross-section load distribution, and the function ϕ represents the axial variation of the loads. In the following formulation we operate with only one cross-section load distribution, which may be modified by summation of various different cross section load distributions and axial load variation functions. The load separation is illustrated in Fig. 3 for a distributed load $q_n = p_n(s)\phi(z)$ on the upper flange of a thin-walled beam. The local components of the loads and force vectors for a cross section wall element are shown in Fig. 4. Hereby the contribution to the external load potential of a single wall element takes the following form:

$$\Pi_{ext,el} = -\int_0^L \int_0^{b_{el}} \phi \left[p_s w_s \psi + p_n w_n \psi - p_z \Omega \psi' \right] ds\, dz \tag{10}$$

which is suited for adequate interpolation in the following. Note that the two first load terms perform work through the transverse displacements and the last load term performs work through the axial warping displacements. Since the formulation of distortion

Table 1
Straight-element stiffness and load contributions.

$$\mathbf{k}^{\sigma}_{\Omega\Omega} = \int_0^{b_e} Et \mathbf{N}_{\Omega}^T \mathbf{N}_{\Omega}\, ds$$
$$\mathbf{k}^{\sigma}_{\mathrm{ww}} = \int_0^{b_e} \frac{Et^3}{12} \mathbf{N}_n^T \mathbf{N}_n\, ds$$
$$\mathbf{k}^{s} = \int_0^{b_e} \left(E_s t \mathbf{N}_{s,s}^T \mathbf{N}_{s,s} + \frac{E_s t^3}{12} \mathbf{N}_{n,ss}^T \mathbf{N}_{n,ss} \right) ds$$
$$\mathbf{k}^{\tau}_{\mathrm{ww}} = \int_0^{b_e} \left(Gt \mathbf{N}_s^T \mathbf{N}_s + \frac{Gt^3}{3} \mathbf{N}_{n,s}^T \mathbf{N}_{n,s} \right) ds$$
$$\mathbf{k}^{\tau}_{\Omega\Omega} = \int_0^{b_e} Gt \mathbf{N}_{\Omega,s}^T \mathbf{N}_{\Omega,s}\, ds$$
$$\mathbf{k}^{\tau}_{\mathrm{w}\Omega} = [\mathbf{k}^{\tau}_{\Omega\mathrm{w}}]^T = -\int_0^{b_e} Gt \mathbf{N}_s^T \mathbf{N}_{\Omega,s}\, ds$$
$$\mathbf{r}^{el}_{\Omega} = \int_0^{b_e} \mathbf{N}_{\Omega}^T \mathbf{N}_p\, ds\, \mathbf{p}_z^{el} + \mathbf{P}_{\Omega}^{el}$$
$$\mathbf{r}^{el}_{\mathrm{w}} = \int_0^{b_e} \mathbf{N}_s^T \mathbf{N}_p\, ds\, \mathbf{p}_s^{el} + \int_0^{b_e} \mathbf{N}_n^T \mathbf{N}_p\, ds\, \mathbf{p}_n^{el} + \mathbf{P}_{\mathrm{w}}^{el}$$

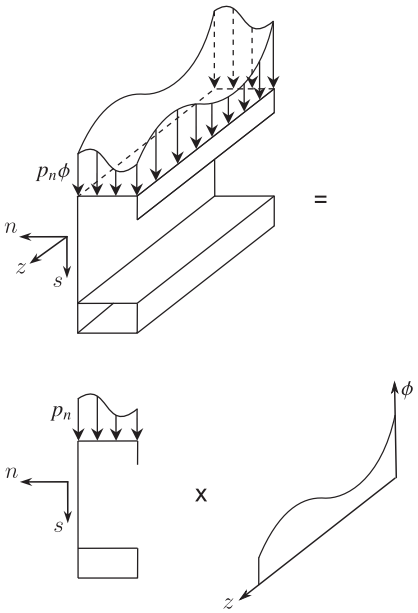

Fig. 3. Load distribution.

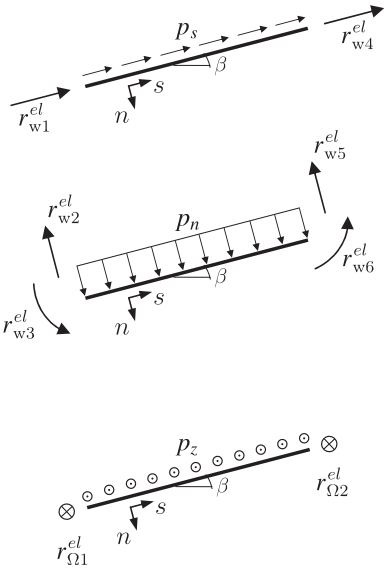

Fig. 4. Distributed loads and the resulting load vectors.

has much in common with torsion the first two terms may be described as distortional moment loads and the last term as distortional bimoment load, see [13]. For the classic torsional equilibrium equation including warping of the cross section, see [14], these loads correspond to torsional moment load and torsional bimoment load.

4. Interpolation within cross-section elements

The interpolations related to the cross section are the displacement interpolations for w_s, w_n and Ω described in the companion paper [1], and the interpolation of the cross section loads p_s, p_n and p_z introduced in the following. The distributed load shown in Fig. 3 will be defined by a linear interpolation of the load on each cross section wall element multiplied by an axial shape function $\phi(z)$, for which we will introduce a specific interpolation later in a following section. The load interpolation in a cross-section wall is given by

$$p_s = \mathbf{N}_p \mathbf{p}_s^{el}, \quad p_n = \mathbf{N}_p \mathbf{p}_n^{el}, \quad p_z = \mathbf{N}_p \mathbf{p}_z^{el} \tag{11}$$

in which $\mathbf{N}_p(s) = [1 - s/b_{el}, s/b_{el}]$ is the linear interpolation matrix, and where the nodal end values of a cross-section wall element are given as

$$\mathbf{p}_s^{el} = \begin{bmatrix} p_{s1} \\ p_{s2} \end{bmatrix}, \quad \mathbf{p}_n^{el} = \begin{bmatrix} p_{n1} \\ p_{n2} \end{bmatrix}, \quad \mathbf{p}_z^{el} = \begin{bmatrix} p_{z1} \\ p_{z2} \end{bmatrix} \tag{12}$$

Using the introduced interpolations for the displacements and the loads, the external potential energy now takes the following form for a single wall element:

$$\Pi_{ext,el} = -\int_0^L \int_0^{b_{el}} \left[\psi \mathbf{v}_w^{el^T} \mathbf{N}_s^T \mathbf{N}_p \mathbf{p}_s^{el} + \psi \mathbf{v}_w^{el^T} \mathbf{N}_n^T \mathbf{N}_p \mathbf{p}_n^{el} - \psi' \mathbf{v}_\Omega^{el^T} \mathbf{N}_\Omega^T \mathbf{N}_p \mathbf{p}_z^{el} \right] \phi \, ds \, dz \tag{13}$$

This formulation allows us to write the element load vector in the same format as the element stiffness contributions from paper [1]. These are shown in Table 1, where we have also included the nodal cross section wall loads $\mathbf{P}_w^{el}$ and $\mathbf{P}_\Omega^{el}$ corresponding to line loads also varying along the beam with ϕ. Hereby the walls of the thin-walled beam can be loaded by line loads acting at the cross section nodes, and by surface loads acting on the mid-plane of a cross section wall. Both of these loads are distributed along the beam as given by the ϕ-function. Now we can rewrite the external load potential of a single wall element as

$$\Pi_{ext,el} = -\int_0^L [\psi \mathbf{v}_w^{el^T} \mathbf{r}_w^{el} \phi - \psi' \mathbf{v}_\Omega^{el^T} \mathbf{r}_\Omega^{el} \phi] \, dz \tag{14}$$

where we have introduced the axial and transverse nodal load components of a straight cross-section element as

$$\mathbf{r}_\Omega^{el} = [r_{\Omega 1}^{el} \;\; r_{\Omega 2}^{el}]^T \tag{15}$$

$$\mathbf{r}_w^{el} = [r_{w1}^{el} \;\; r_{w2}^{el} \;\; r_{w3}^{el} \;\; r_{w4}^{el} \;\; r_{w5}^{el} \;\; r_{w6}^{el}]^T \tag{16}$$

These components are shown in Fig. 4 along with the direction of the wall element coordinates (n,s) as well as the positive direction of the load components. We choose to assemble the single element components into two separate global vectors containing the axial load and the transverse load, respectively. These global vectors we will write as follows:

$$\mathbf{r}_\Omega = [r_{\Omega 1} \;\; r_{\Omega 2} \;\; r_{\Omega 3} \;\; \ldots]^T \tag{17}$$

$$\mathbf{r}_w = [r_{w1} \;\; r_{w2} \;\; r_{w3} \;\; r_{w4} \;\; r_{w5} \;\; r_{w6} \;\; \ldots]^T \tag{18}$$

where the transformation from local to global components is performed using a formal standard transformation of the components in the cross-section plane, i.e.

$$\mathbf{r}_\Omega = \sum_{el} \mathbf{T}_\Omega^T \mathbf{r}_\Omega^{el} \tag{19}$$

$$\mathbf{r}_w = \sum_{el} \mathbf{T}_w^T \mathbf{r}_w^{el} \tag{20}$$

See Table 2 for a overview of the important transformations used in this and in the companion paper [1]. Now we can write the total potential energy by summation of each element contribution as

$$\Pi_{tot} = \Pi_{int} + \Pi_{ext} \quad \text{where } \Pi_{ext} = \sum_{el} \Pi_{ext,el} \tag{21}$$

where Π_{int} is the contribution to the potential energy from the internal properties found in paper [1], and Π_{ext} is the contribution from the external loads. Introducing the described interpolation and

Table 2
Transformations.

No.	Description	Transformations
1	Transformation from local to global axial d.o.f.	$\mathbf{v}_\Omega = \mathbf{T}_\Omega \mathbf{v}_\Omega^{el}$
2	Transformation from local to global transverse d.o.f.	$\mathbf{v}_w = \mathbf{T}_w \mathbf{v}_w^{el}$
3	Transformation from pure axial extension and other axial d.o.f. to global axial d.o.f.	$\mathbf{v}_\Omega = [\mathbf{T}_\Omega^o \;\; \mathbf{T}_\Omega^a] \begin{bmatrix} \mathbf{v}_\Omega^o \\ \mathbf{v}_\Omega^a \end{bmatrix}$
4	Transformation from transverse d.o.f. to the other axial d.o.f. (without pure axial extension) based on the shear constrains	$\mathbf{v}_\Omega^o = \mathbf{T}_{\Omega w} \mathbf{v}_w$
5	Transformation from transverse d.o.f. and pure axial extension d.o.f. to the global axial d.o.f.	$\mathbf{v}_\Omega = [\mathbf{T}_{\Omega w}^r \;\; \mathbf{T}_\Omega^a] \begin{bmatrix} \mathbf{v}_w \\ v_\Omega^a \end{bmatrix}$
6	Transformation from pure transverse translation d.o.f., pure rotation d.o.f., constant wall-width constrained d.o.f. and unconstrained d.o.f. to global transverse d.o.f. (wall-width constraints not applied)	$\mathbf{v}_w = [\mathbf{T}_w^\alpha \;\; \mathbf{T}_w^3 \;\; \mathbf{T}_w^c \;\; \mathbf{T}_w^u] \begin{bmatrix} \mathbf{v}_w^\alpha \\ v_w^3 \\ \mathbf{v}_w^c \\ \mathbf{v}_w^u \end{bmatrix}$
7	Transformation from pure transverse translation d.o.f., pure rotation d.o.f. and unconstrainedd.o.f. to global transverse d.o.f. (wall-width constraints applied)	$\mathbf{v}_w = [\mathbf{T}_w^\alpha \;\; \mathbf{T}_w^3 \;\; \tilde{\mathbf{T}}_w^u] \begin{bmatrix} \mathbf{v}_w^\alpha \\ v_w^3 \\ \mathbf{v}_w^u \end{bmatrix}$
8	Transformation from constrained transverse d.o.f. and transverse GBT d.o.f. to global transverse d.o.f.	$\mathbf{v}_w = [\mathbf{T}_w^c \;\; \mathbf{T}_w^g] \begin{bmatrix} \mathbf{v}_w^c \\ \mathbf{v}_w^g \end{bmatrix}$
9	Transformation from FE space to GBT space	$\begin{bmatrix} \mathbf{v}_w^g \\ v_\Omega^a \end{bmatrix} = \begin{bmatrix} \mathbf{T}_w^{g^T} & \mathbf{0} \\ \mathbf{0} & \mathbf{T}_\Omega^{a^T} \end{bmatrix} \begin{bmatrix} \mathbf{v}_w \\ \mathbf{v}_\Omega \end{bmatrix}$
10	Transformation from GBT space to FE space	$\begin{bmatrix} \mathbf{v}_w \\ \mathbf{v}_\Omega \end{bmatrix} = \begin{bmatrix} \tilde{\mathbf{T}}_w^g & \mathbf{0} \\ \mathbf{T}_{\Omega w}^r \tilde{\mathbf{T}}_w^g & \mathbf{T}_\Omega^{a^T} \end{bmatrix} \begin{bmatrix} \mathbf{v}_w^g \\ v_\Omega^a \end{bmatrix}$

matrix calculation scheme allows us to write the total potential energy as

$$\Pi_{tot} = \Pi_{int} - \int_0^L \left\{ (\psi \mathbf{v}_w^T)\mathbf{r}_w\phi - (\psi \mathbf{v}_\Omega^T)'\mathbf{r}_\Omega\phi \right\} dz \tag{22}$$

The first term corresponds to the distortional moment load which performs work through the transverse displacements. The second term corresponds to the distortional bimoment load which performs work through the axial displacements.

5. Modal loads and modal solutions

To obtain a formulation resembling the generalization of Vlasov beam theory including distortion, the following three main steps are performed as in the companion paper [1]. This allows us to properly identify modal load components as well as the contributions to the individual modal differential equations.

5.1. Step I–Pure axial load and shear constraints

Following the procedure which is used to identify pure axial extension as an eigenmode and to introduce shear constraints, we will identify the axial load components and separate these from the remaining equations. The potential energy formulation including the load terms in Eq. (22) have to be modified, so that the pure axial extension is described by the separate degree of freedom v_Ω^a, and so that the shear constraint equations are enforced. This modification is performed using the following transformation No. 5 described in Table 2:

$$\mathbf{v}_\Omega = \mathbf{T}_{\Omega w}^r \mathbf{v}_w + \mathbf{T}_\Omega^a v_\Omega^a \tag{23}$$

To clarify the variational treatment of pure axial extension, we also temporally rewrite the terms pertaining to axial extension using $\zeta v_\Omega^a = -\psi' v_\Omega^a$. The modified elastic potential energy (for a single mode) takes the following form:

$$\Pi_{tot} = \Pi_{int} - \int_0^L \left\{ (\psi \mathbf{v}_w^T)\mathbf{r}_w\phi - (\psi \mathbf{v}_w^T)'\ \mathbf{T}_{\Omega w}^{r^T}\mathbf{r}_\Omega\phi + (\zeta v_\Omega^a) r_\Omega^a \phi \right\} dz \tag{24}$$

in which the pure axial loading is identified as r_Ω^a. It is as given in Table 3 identified as the product of the transpose of the pure axial deformation mode and the global axial load vector.

To obtain the differential equations of GBT, the first variation of the elastic potential energy is investigated by taking variations in the complete displacement field. This gives

$$\delta\Pi_{tot} = \delta\Pi_{int} - \int_0^L \left\{ \delta(\psi \mathbf{v}_w^T)\mathbf{r}_w\phi - \delta(\psi \mathbf{v}_w^T)'\ \mathbf{T}_{\Omega w}^{r^T}\mathbf{r}_\Omega\phi + \delta(\zeta v_\Omega^a) r_\Omega^a \phi \right\} dz \tag{25}$$

After performing partial integrations on the terms that involve axial derivatives of the (virtual) varied displacement field, $\delta(\,)'$, the first variation of the elastic potential energy takes the form

$$\delta\Pi_{tot} = \delta\Pi_{int} - \int_0^L \left\{ \delta(\psi \mathbf{v}_w^T)[\mathbf{r}_w\phi + \mathbf{T}_{\Omega w}^{r^T}\mathbf{r}_\Omega\phi'] + \delta(\zeta v_\Omega^a) r_\Omega^a \phi \right\} ds + \left[\delta(\psi \mathbf{v}_w^T)[\mathbf{T}_{\Omega w}^{r^T}\mathbf{r}_\Omega\phi] \right]_0^L \tag{26}$$

For internal variation in the displacement fields $\delta(\psi \mathbf{v}_w)$ and $\delta(\zeta v_\Omega^a)$, the elastic potential energy should be stationary and therefore its first variation must be equal to zero. Here the terms in the squared bracket correspond to the boundary loads and boundary conditions. Substituting $\delta\Pi_{int}$ from the companion paper [1] leads to the following coupled non-homogeneous differential equations of GBT in which we note that $\zeta = -\psi'$:

$$\overline{\mathbf{K}}^\sigma \mathbf{v}_w\psi'''' - \mathbf{K}_{\Omega\Omega}^{\sigma ra} v_\Omega^a \zeta'''' - \mathbf{K}^\tau \mathbf{v}_w\psi'' + \mathbf{K}^s \mathbf{v}_w\psi = \mathbf{r}_w\phi + \mathbf{T}_{\Omega w}^{r^T}\mathbf{r}_\Omega\phi' \tag{27}$$

$$\mathbf{K}_{\Omega\Omega}^{\sigma ar}\mathbf{v}_w\psi''' - K_{\Omega\Omega}^{\sigma aa} v_\Omega^a \zeta'' = r_\Omega^a\phi \tag{28}$$

Here the left hand side of the equations corresponds to the homogeneous equations, and the right hand side are the non homogeneous (load) terms. The stiffness matrices, $\mathbf{K}$, are found and described in paper [1].

These equations establish a coupled set of non-homogeneous GBT differential equations that determine the displacements of a thin-walled beam for a given set of boundary conditions. The homogeneous parts of the solution have been found, and now we seek particular solutions to the modal equations. Let us start out by isolating the term $v_\Omega^a\zeta''$ in Eq. (28) as

$$v_\Omega^a\zeta'' = (K_{\Omega\Omega}^{\sigma aa})^{-1}[\mathbf{K}_{\Omega\Omega}^{\sigma ar}\mathbf{v}_w\psi''' - r_\Omega^a\phi] \tag{29}$$

Let us then first consider the pure axial extension mode, which has been identified as $(\mathbf{v}_w, v_\Omega^a) = (\mathbf{0}, 1)$, where we introduce the notation bold zero $\mathbf{0}$ for a suitable size matrix or vector of zeroes. Introducing this mode in Eq. (29) uncouples the equation (since $\mathbf{v}_w = \mathbf{0}$). Integrating the particular solution for the axial mode, the complete solution for the axial variation is then given by adding the homogeneous part of the solution and the particular part as follows:

$$\zeta(z) = [1\ \ z]\begin{bmatrix} c_{a1} \\ c_{a2} \end{bmatrix} - (K_{\Omega\Omega}^{\sigma aa})^{-1} r_\Omega^a \iint \phi\ dz\ dz \tag{30}$$

where c_{a1} and c_{a2} are constants determined by the boundary conditions of axial extension.

In the context of the current work we will interpolate the cross section load using one distribution function $\phi(z)$, which varies linearly between two end values (ϕ_1 and ϕ_2) representing the values of the multiplicative function at the ends of the profile. Thus we introduce ϕ as

$$\phi = \begin{bmatrix} 1 - \frac{z}{L} & \frac{z}{L} \end{bmatrix}\boldsymbol{\phi} \quad \text{where } \boldsymbol{\phi} = \begin{bmatrix} \phi_1 \\ \phi_2 \end{bmatrix} \tag{31}$$

Using this linear interpolation the full integrated solution of Eq. (30) takes the form

$$\zeta(z) = -\boldsymbol{\Psi}'_{ah}(z)\mathbf{c}_a - \boldsymbol{\Psi}'_{ap}(z)\boldsymbol{\phi} \tag{32}$$

where

$$\boldsymbol{\Psi}'_{ah} = -[1\ \ z] \quad \mathbf{c}_a = \begin{bmatrix} c_{a1} \\ c_{a2} \end{bmatrix}$$

$$\boldsymbol{\Psi}'_{ap} = \frac{L^2 r_\Omega^a}{6K_{\Omega\Omega}^{\sigma aa}} \begin{bmatrix} 3\left(\frac{z}{L}\right)^2 - \left(\frac{z}{L}\right)^3 & \left(\frac{z}{L}\right)^3 \end{bmatrix}$$

The introduced subscripts h and p denote the homogeneous and the particular parts of the solution, respectively.

Next let us consider the formulation of the remaining transverse displacement modes. Inserting Eq. (29) differentiated once into Eq. (27) we eliminate pure axial extension. Introducing $\mathbf{K}^\sigma$ as in paper [1], we obtain the following non-homogeneous fourth order differential equations for determination of the transverse (global, distortional and local) distortional displacement modes of GBT:

$$\mathbf{K}^\sigma \mathbf{v}_w\psi'''' - \mathbf{K}^\tau \mathbf{v}_w\psi'' + \mathbf{K}^s \mathbf{v}_w\psi = \mathbf{r}_w\phi + (\mathbf{T}_{\Omega w}^{r^T}\mathbf{r}_\Omega - \mathbf{K}_{\Omega\Omega}^{\sigma ra}(K_{\Omega\Omega}^{\sigma aa})^{-1} r_\Omega^a)\phi' \tag{33}$$

Table 3
Transformation of load vectors related to Step I.

$r_\Omega^a = \mathbf{T}_\Omega^{a^T}\mathbf{r}_\Omega$	$\bar{\mathbf{r}}_\Omega = \mathbf{T}_{\Omega w}^{r^T}\mathbf{r}_\Omega - \mathbf{K}_{\Omega\Omega}^{\sigma ra}(K_{\Omega\Omega}^{\sigma aa})^{-1} r_\Omega^a$

which we choose to abbreviate and write as

$$\mathbf{K}^{\sigma}\mathbf{v}_{\mathrm{w}}\psi''''-\mathbf{K}^{\tau}\mathbf{v}_{\mathrm{w}}\psi''+\mathbf{K}^{s}\mathbf{v}_{\mathrm{w}}\psi=\mathbf{r}_{\mathrm{w}}\phi+\overline{\mathbf{r}}_{\Omega}\phi' \tag{34}$$

where $\overline{\mathbf{r}}_{\Omega}$ is given in Table 3.

5.2. Step II—flexural loading and constant wall width

In this step we treat two modes corresponding to transverse translations of the cross section, and one mode corresponding to pure rotation. We also constrain the transverse displacement field so that the wall widths remain constant, i.e. we enforce $\mathrm{w}_{s,s}\equiv 0$.

Let us do this by first introducing transformation No. 7 from Table 2 into the differential equations in (34), and also introduce the null terms corresponding to the rigid-body modes and zero shear strain for translational and flexural modes. Hereby the differential equations including the load terms take the following form:

$$\begin{bmatrix}\mathbf{K}^{\sigma}_{\alpha\alpha} & \mathbf{0} & \mathbf{K}^{\sigma}_{\alpha u}\\ \mathbf{0} & K^{\sigma}_{33} & \mathbf{K}^{\sigma}_{3u}\\ \mathbf{K}^{\sigma}_{u\alpha} & \mathbf{K}^{\sigma}_{u3} & \mathbf{K}^{\sigma}_{uu}\end{bmatrix}\begin{bmatrix}\mathbf{v}^{\alpha}_{\mathrm{w}}\\ v^{3}_{\mathrm{w}}\\ \mathbf{v}^{u}_{\mathrm{w}}\end{bmatrix}\psi''''-\begin{bmatrix}\mathbf{0} & \mathbf{0} & \mathbf{0}\\ \mathbf{0} & K^{\tau}_{33} & \mathbf{K}^{\tau}_{3u}\\ \mathbf{0} & \mathbf{K}^{\tau}_{u3} & \mathbf{K}^{\tau}_{uu}\end{bmatrix}\begin{bmatrix}\mathbf{v}^{\alpha}_{\mathrm{w}}\\ v^{3}_{\mathrm{w}}\\ \mathbf{v}^{u}_{\mathrm{w}}\end{bmatrix}\psi''$$
$$+\begin{bmatrix}\mathbf{0} & \mathbf{0} & \mathbf{0}\\ \mathbf{0} & 0 & \mathbf{0}\\ \mathbf{0} & \mathbf{0} & \mathbf{K}^{s}_{uu}\end{bmatrix}\begin{bmatrix}\mathbf{v}^{\alpha}_{\mathrm{w}}\\ v^{3}_{\mathrm{w}}\\ \mathbf{v}^{u}_{\mathrm{w}}\end{bmatrix}\psi=\begin{bmatrix}\mathbf{r}^{\alpha}_{\mathrm{w}}\\ r^{3}_{\mathrm{w}}\\ \mathbf{r}^{u}_{\mathrm{w}}\end{bmatrix}\phi+\begin{bmatrix}\overline{\mathbf{r}}^{\alpha}_{\Omega}\\ \overline{r}^{3}_{\Omega}\\ \overline{\mathbf{r}}^{u}_{\Omega}\end{bmatrix}\phi' \tag{35}$$

where the transformed stiffness matrices are found and described in paper [1] and the load vectors are given in Table 4. The two-dimensional upper block matrix equation yields the translation displacements as

$$\mathbf{v}^{\alpha}_{\mathrm{w}}\psi''''=\mathbf{K}^{\sigma-1}_{\alpha\alpha}[\mathbf{r}^{\alpha}_{\mathrm{w}}\phi+\overline{\mathbf{r}}^{\alpha}_{\Omega}\phi'-\mathbf{K}^{\sigma}_{\alpha u}\mathbf{v}^{u}_{\mathrm{w}}\psi''''] \tag{36}$$

where $\alpha=1$ or $\alpha=2$. We can identify the two orthogonal pure translational modes, $(v^{1}_{\mathrm{w}},\mathbf{v}^{2}_{\mathrm{w}},v^{3}_{\mathrm{w}},\mathbf{v}^{u}_{\mathrm{w}})=(1,0,0,\mathbf{0})$ and $(0,1,0,\mathbf{0})$, as eigenmodes or full solutions to the homogeneous part of Eq. (35). A particular solution for the axial variation of the pure translational modes is determined by quadruple integration of the non-homogeneous load terms (since $\mathbf{v}^{u}_{\mathrm{w}}=\mathbf{0}$). The complete solution is then given by summation of the full homogeneous solution and the particular solution, which we can express as

$$\psi_{\alpha}(z)=c_{\alpha 1}+c_{\alpha 2}z+c_{\alpha 3}z^{2}+c_{\alpha 4}z^{3}+\iiiint(\mathbf{K}^{\sigma}_{\alpha\alpha})^{-1}(\mathbf{r}^{\alpha}_{\mathrm{w}}\phi+\overline{\mathbf{r}}^{\alpha}_{\Omega}\phi')\,dz\,dz\,dz\,dz \tag{37}$$

Remembering that we in the present context introduce ϕ as one linear function as given in Eq. (31), we can perform the quadruple integration and get

$$\psi_{\alpha}(z)=\mathbf{\Psi}_{\alpha h}(z)\mathbf{c}_{\alpha}+\mathbf{\Psi}_{\alpha p}(z)\boldsymbol{\phi} \tag{38}$$

Here $\mathbf{c}_{\alpha}$ is a vector containing four constants of the homogeneous part of the solution, and

$$\mathbf{\Psi}_{\alpha p}(z)=\mathbf{\Psi}^{\mathrm{w}}_{\alpha p}(z)+\mathbf{\Psi}^{\Omega}_{\alpha p}(z) \tag{39}$$

$$\mathbf{\Psi}_{\alpha h}(z)=[1\;\; z\;\; z^{2}\;\; z^{3}] \tag{40}$$

$$\mathbf{\Psi}^{\mathrm{w}}_{\alpha p}(z)=\frac{L^{4}}{120}\,(\mathbf{K}^{\sigma}_{\alpha\alpha})^{-1}\mathbf{r}^{\alpha}_{\mathrm{w}}\left[5\left(\frac{z}{L}\right)^{4}-\left(\frac{z}{L}\right)^{5}\;\;\left(\frac{z}{L}\right)^{5}\right] \tag{41}$$

Table 4
Transformation of load vectors related to Step II.

$\mathbf{r}^{\alpha}_{\mathrm{w}}=\mathbf{T}^{\alpha T}_{\mathrm{w}}\mathbf{r}_{\mathrm{w}}$	$r^{3}_{\mathrm{w}}=\mathbf{T}^{3T}_{\mathrm{w}}\mathbf{r}_{\mathrm{w}}$
$\mathbf{r}^{u}_{\mathrm{w}}=\mathbf{T}^{uT}_{\mathrm{w}}\mathbf{r}_{\mathrm{w}}$	$\mathbf{r}^{u\alpha}_{\mathrm{w}}=\mathbf{r}^{u}_{\mathrm{w}}-\mathbf{K}^{\sigma T}_{\alpha u}(\mathbf{K}^{\sigma}_{\alpha\alpha})^{-1}\mathbf{r}^{\alpha}_{\mathrm{w}}$
$\overline{\mathbf{r}}^{\alpha}_{\Omega}=\mathbf{T}^{\alpha T}_{\mathrm{w}}\overline{\mathbf{r}}_{\Omega}$	$\overline{r}^{3}_{\Omega}=\mathbf{T}^{3T}_{\mathrm{w}}\overline{\mathbf{r}}_{\Omega}$
$\overline{\mathbf{r}}^{u}_{\Omega}=\overline{\mathbf{T}}^{uT}_{\mathrm{w}}\overline{\mathbf{r}}_{\Omega}$	$\overline{\mathbf{r}}^{u\alpha}_{\Omega}=\overline{\mathbf{r}}^{u}_{\Omega}-\mathbf{K}^{\sigma T}_{\alpha u}(\mathbf{K}^{\sigma}_{\alpha\alpha})^{-1}\overline{\mathbf{r}}^{\alpha}_{\Omega}$

$$\mathbf{\Psi}^{\Omega}_{\alpha p}(z)=\frac{L^{3}}{24}(\mathbf{K}^{\sigma}_{\alpha\alpha})^{-1}\overline{\mathbf{r}}^{\alpha}_{\Omega}\left[4\left(\frac{z}{L}\right)^{3}-\left(\frac{z}{L}\right)^{4}\;\;\left(\frac{z}{L}\right)^{4}\right] \tag{42}$$

Having identified the solutions related to the two pure translational modes we return to the remaining block equations of Eq. (35). Eliminating the two pure flexural degrees of freedom using Eq. (36) we obtain the condensed version of the differential Eq. (35) as

$$\begin{bmatrix}K^{\sigma}_{33} & \mathbf{K}^{\sigma}_{3u}\\ \mathbf{K}^{\sigma}_{u3} & \overline{\mathbf{K}}^{\sigma}_{uu}\end{bmatrix}\begin{bmatrix}v^{3}_{\mathrm{w}}\\ \mathbf{v}^{u}_{\mathrm{w}}\end{bmatrix}\psi''''-\begin{bmatrix}K^{\tau}_{33} & \mathbf{K}^{\tau}_{3u}\\ \mathbf{K}^{\tau}_{u3} & \mathbf{K}^{\tau}_{uu}\end{bmatrix}\begin{bmatrix}v^{3}_{\mathrm{w}}\\ \mathbf{v}^{u}_{\mathrm{w}}\end{bmatrix}\psi''$$
$$+\begin{bmatrix}0 & \mathbf{0}\\ \mathbf{0} & \mathbf{K}^{s}_{uu}\end{bmatrix}\begin{bmatrix}v^{3}_{\mathrm{w}}\\ \mathbf{v}^{u}_{\mathrm{w}}\end{bmatrix}\psi=\begin{bmatrix}r^{3}_{\mathrm{w}}\\ \mathbf{r}^{u\alpha}_{\mathrm{w}}\end{bmatrix}\phi+\begin{bmatrix}\overline{r}^{3}_{\Omega}\\ \overline{\mathbf{r}}^{u\alpha}_{\Omega}\end{bmatrix}\phi' \tag{43}$$

The stiffness matrix $\overline{\mathbf{K}}^{\sigma}_{uu}$ is found in the companion paper [1] and the vectors $\mathbf{r}^{u\alpha}_{\mathrm{w}}$ and $\overline{\mathbf{r}}^{u\alpha}_{\Omega}$ are given in Table 4. This equation constitutes the GBT differential equations constrained by shear flow constraints and wall-width constraints after the elimination of the classical axial and two translational (flexural beam) modes.

5.3. Step III—reduction of order and torsional load

The fourth order differential Eq. (43) can be transformed into twice as many second order differential equations by introducing a so called state vector. There are a number of different possible formulations, however we choose the use of the state vector $(v^{3}_{\mathrm{w}}\psi,\mathbf{v}^{u}_{\mathrm{w}}\psi,v^{3}_{\mathrm{w}}\psi'',\mathbf{v}^{u}_{\mathrm{w}}\psi'')^{T}$. By introducing this state vector we obtain a reformulation of Eq. (43), leading to a formal second order matrix differential equation of double size, which takes the form

$$\begin{bmatrix}0 & \mathbf{0} & 0 & \mathbf{0}\\ \mathbf{0} & \mathbf{K}^{s}_{uu} & \mathbf{0} & \mathbf{0}\\ 0 & \mathbf{0} & -K^{\sigma}_{33} & -\mathbf{K}^{\sigma}_{3u}\\ \mathbf{0} & \mathbf{0} & -\mathbf{K}^{\sigma}_{u3} & -\overline{\mathbf{K}}^{\sigma}_{uu}\end{bmatrix}\begin{bmatrix}v^{3}_{\mathrm{w}}\psi\\ \mathbf{v}^{u}_{\mathrm{w}}\psi\\ v^{3}_{\mathrm{w}}\psi''\\ \mathbf{v}^{u}_{\mathrm{w}}\psi''\end{bmatrix}$$
$$-\begin{bmatrix}K^{\tau}_{33} & \mathbf{K}^{\tau}_{3u} & -K^{\sigma}_{33} & -\mathbf{K}^{\sigma}_{3u}\\ \mathbf{K}^{\tau}_{u3} & \mathbf{K}^{\tau}_{uu} & -\mathbf{K}^{\sigma}_{u3} & -\overline{\mathbf{K}}^{\sigma}_{uu}\\ -K^{\sigma}_{33} & -\mathbf{K}^{\sigma}_{3u} & 0 & \mathbf{0}\\ -\mathbf{K}^{\sigma}_{u3} & -\overline{\mathbf{K}}^{\sigma}_{uu} & \mathbf{0} & \mathbf{0}\end{bmatrix}\begin{bmatrix}v^{3}_{\mathrm{w}}\psi\\ \mathbf{v}^{u}_{\mathrm{w}}\psi\\ v^{3}_{\mathrm{w}}\psi''\\ \mathbf{v}^{u}_{\mathrm{w}}\psi''\end{bmatrix}''$$
$$=\begin{bmatrix}r^{3}_{\mathrm{w}}\\ \mathbf{r}^{u\alpha}_{\mathrm{w}}\\ 0\\ \mathbf{0}\end{bmatrix}\phi+\begin{bmatrix}\overline{r}^{3}_{\Omega}\\ \overline{\mathbf{r}}^{u\alpha}_{\Omega}\\ 0\\ \mathbf{0}\end{bmatrix}\phi' \tag{44}$$

To keep the matrix operations as simple as possible we introduce a new vector $\mathbf{v}^{e}_{\mathrm{w}}$, three new block matrices, $\mathbf{K}^{\sigma}_{ee}$, $\mathbf{K}^{\sigma}_{3e}$, and $\mathbf{K}^{\sigma}_{ue}$ given by

$$\mathbf{v}^{e}_{\mathrm{w}}=\begin{bmatrix}v^{3}_{\mathrm{w}}\\ \mathbf{v}^{u}_{\mathrm{w}}\end{bmatrix},\quad \mathbf{K}^{\sigma}_{ee}=\begin{bmatrix}\mathbf{K}^{\sigma}_{3e}\\ \mathbf{K}^{\sigma}_{ue}\end{bmatrix}=\begin{bmatrix}[K^{\sigma}_{33} & \mathbf{K}^{\sigma}_{3u}]\\ [\mathbf{K}^{\sigma}_{u3} & \overline{\mathbf{K}}^{\sigma}_{uu}]\end{bmatrix} \tag{45}$$

and the force vectors are given by

$$\mathbf{r}^{e}_{\mathrm{w}}=\begin{bmatrix}0\\ \mathbf{0}\end{bmatrix},\quad \mathbf{r}^{e}_{\Omega}=\begin{bmatrix}0\\ \mathbf{0}\end{bmatrix} \tag{46}$$

Introducing the new vectors and block matrices defined by Eq. (45) and (46), and the transformed loads given in Table 5, the

Table 5
Transformation of load vectors related to Step III.

$\mathbf{r}^{u3}_{\mathrm{w}}=\mathbf{r}^{u\alpha}_{\mathrm{w}}-\mathbf{K}^{\tau}_{u3}K^{\tau-1}_{33}r^{3}_{\mathrm{w}}$	$\mathbf{r}^{e3}_{\mathrm{w}}=\mathbf{r}^{e}_{\mathrm{w}}+\mathbf{K}^{\sigma}_{e3}K^{\tau-1}_{33}r^{3}_{\mathrm{w}}$
$\overline{\mathbf{r}}^{u3}_{\Omega}=\overline{\mathbf{r}}^{u\alpha}_{\Omega}-\mathbf{K}^{\tau}_{u3}K^{\tau-1}_{33}\overline{r}^{3}_{\Omega}$	$\mathbf{r}^{e3}_{\Omega}=\mathbf{r}^{e}_{\Omega}+\mathbf{K}^{\sigma}_{e3}K^{\tau-1}_{33}\overline{r}^{3}_{\Omega}$

second order differential equations (44) can be rewritten as

$$\begin{bmatrix} 0 & \mathbf{0} & \mathbf{0} \\ \mathbf{0} & \mathbf{K}^s_{uu} & \mathbf{0} \\ \mathbf{0} & \mathbf{0} & -\mathbf{K}^\sigma_{ee} \end{bmatrix} \begin{bmatrix} v^3_w\psi \\ \mathbf{v}^u_w\psi \\ \mathbf{v}^e_w\psi'' \end{bmatrix} - \begin{bmatrix} K^\tau_{33} & \mathbf{K}^\tau_{3u} & -\mathbf{K}^\sigma_{3e} \\ \mathbf{K}^\tau_{u3} & \mathbf{K}^\tau_{uu} & -\mathbf{K}^\sigma_{ue} \\ -\mathbf{K}^\sigma_{e3} & -\mathbf{K}^\sigma_{eu} & \mathbf{0} \end{bmatrix} \begin{bmatrix} v^3_w\psi \\ \mathbf{v}^u_w\psi \\ \mathbf{v}^e_w\psi'' \end{bmatrix}'' = \begin{bmatrix} r^3_w \\ \mathbf{r}^{u\alpha}_w \\ \mathbf{r}^e_w \end{bmatrix}\phi + \begin{bmatrix} \overline{r}^3_\Omega \\ \overline{\mathbf{r}}^{u\alpha}_\Omega \\ \mathbf{r}^e_\Omega \end{bmatrix}\phi' \tag{47}$$

From the first equation we can isolate the pure rotational term resulting in the following differential equation:

$$v^3_w\psi'' = -(K^\tau_{33})^{-1}(\mathbf{K}^\tau_{3u}\mathbf{v}^u_w\psi'' - \mathbf{K}^\sigma_{3e}\mathbf{v}^e_w\psi'''' + r^3_w\phi + \overline{r}^3_\Omega\phi') \tag{48}$$

It can be seen that pure torsion (with free warping), corresponding to the solution vector, $(v^3_w\psi, \mathbf{v}^u_w\psi, \mathbf{v}^e_w\psi'') = (c_{32}z + c_{31}, \mathbf{0}, \mathbf{0})$, is a solution of the homogeneous second order differential equations in (47). Hereby the particular solution for the axial variation of the pure torsion mode is determined by double integration of particular part, and the full solution is found by addition of the homogeneous solution. This results in

$$\psi_3(z) = c_{31} + c_{32}z - \iint (K^\tau_{33})^{-1}(\overline{r}^3_w\phi + \overline{r}^3_\Omega\phi')\,dz\,dz \tag{49}$$

Inserting the linear function ϕ from Eq. (31) we can evaluate the integrals in (49) and find the full solution of pure St. Venant torsion as

$$\psi_3(z) = \mathbf{\Psi}_{3h}(z)\mathbf{c}_3 + \mathbf{\Psi}_{3p}(z)\boldsymbol{\phi} \tag{50}$$

Here $\mathbf{c}_3$ is a vector containing two constants of the homogeneous part of the solution, and

$$\mathbf{\Psi}_{3p}(z) = \mathbf{\Psi}^w_{3p}(z) + \mathbf{\Psi}^\Omega_{3p}(z) \tag{51}$$

$$\mathbf{\Psi}_{3h}(z) = [1 \;\; z] \tag{52}$$

$$\mathbf{\Psi}^w_{3p}(z) = -\frac{L^2 r^3_w}{6K^\tau_{33}}\left[3\left(\frac{z}{L}\right)^2 - \left(\frac{z}{L}\right)^3 \;\; \left(\frac{z}{L}\right)^3\right] \tag{53}$$

$$\mathbf{\Psi}^\Omega_{3p}(z) = -\frac{L\overline{r}^3_\Omega}{2K^\tau_{33}}\left[2\left(\frac{z}{L}\right) - \left(\frac{z}{L}\right)^2 \;\; \left(\frac{z}{L}\right)^2\right] \tag{54}$$

Using Eq. (48) we eliminate v^3_w from the differential equations in (47) and find the final distortional non-homogeneous differential equations of GBT that determine all the distortional displacement modes as

$$\begin{bmatrix} \mathbf{K}^s_{uu} & \mathbf{0} \\ \mathbf{0} & -\mathbf{K}^\sigma_{ee} \end{bmatrix} \begin{bmatrix} \mathbf{v}^u_w\psi \\ \mathbf{v}^e_w\psi'' \end{bmatrix} - \begin{bmatrix} \overline{\mathbf{K}}^\tau_{uu} - \overline{\mathbf{K}}^\sigma_{ue} \\ -\overline{\mathbf{K}}^\sigma_{eu} - \overline{\mathbf{K}}^\sigma_{ee} \end{bmatrix} \begin{bmatrix} \mathbf{v}^u_w\psi \\ \mathbf{v}^e_w\psi'' \end{bmatrix}'' = \begin{bmatrix} \mathbf{r}^{\alpha u3}_w \\ \mathbf{r}^{e3}_w \end{bmatrix}\phi + \begin{bmatrix} \overline{\mathbf{r}}^{\alpha u3}_\Omega \\ \mathbf{r}^{e3}_\Omega \end{bmatrix}\phi' \tag{55}$$

The block matrices and the transformed stiffness matrices are introduced in the companion paper [1] and the load vectors are given in Table 5.

6. Solution of distortional equations

The distortional eigenvalue problem for the homogeneous system of equations (55) was solved in the companion paper [1]. Here the eigenvalues, $\lambda_i = \xi^2_i$, and the corresponding eigenvectors was given by

$$\begin{bmatrix} \mathbf{v}^u_w \\ \mathbf{v}^e_w\xi^2 \end{bmatrix}_i = \begin{bmatrix} \mathbf{v}^u_{wi} \\ \mathbf{v}^e_{wi}\xi^2_i \end{bmatrix} \tag{56}$$

In the presents context these eigenvectors can be used to decouple the system of equations in (55). The i'th decoupled equation which determines the axial variation $\psi_{di}(z)$ of the distortional eigenvector is found by inserting the i'th eigenvector and pre multiplying by it, which results in the following equation:

$$\begin{bmatrix} \mathbf{v}^u_w \\ \mathbf{v}^e_w\xi^2 \end{bmatrix}^T_i \begin{bmatrix} \mathbf{K}^s_{uu} & \mathbf{0} \\ \mathbf{0} & -\mathbf{K}^\sigma_{ee} \end{bmatrix} \begin{bmatrix} \mathbf{v}^u_w \\ \mathbf{v}^e_w\xi^2 \end{bmatrix}_i \psi_{di} - \begin{bmatrix} \mathbf{v}^u_w \\ \mathbf{v}^e_w\xi^2 \end{bmatrix}^T_i \begin{bmatrix} \overline{\mathbf{K}}^\tau_{uu} - \overline{\mathbf{K}}^\sigma_{ue} \\ -\overline{\mathbf{K}}^\sigma_{eu} - \overline{\mathbf{K}}^\sigma_{ee} \end{bmatrix} \begin{bmatrix} \mathbf{v}^u_w \\ \mathbf{v}^e_w\xi^2 \end{bmatrix}_i \psi''_{di} = \begin{bmatrix} \mathbf{v}^u_w \\ \mathbf{v}^e_w\xi^2 \end{bmatrix}^T_i \begin{bmatrix} \mathbf{r}^{\alpha u3}_w \\ \mathbf{r}^{e3}_w \end{bmatrix}\phi + \begin{bmatrix} \mathbf{v}^u_w \\ \mathbf{v}^e_w\xi^2 \end{bmatrix}^T_i \begin{bmatrix} \overline{\mathbf{r}}^{\alpha u3}_\Omega \\ \mathbf{r}^{e3}_\Omega \end{bmatrix}\phi' \tag{57}$$

which we abbreviate as

$$K^g_{ii}\psi_{di} - K^d_{ii}\psi''_{di} = r_{w_i}{}^d\phi + r_{\Omega_i}{}^d\phi' \tag{58}$$

Normalizing this equation and introducing that the eigenvalue ξ^2_i is equal to K^g_{ii}/K^d_{ii}, it takes the following standard form:

$$\psi''_{di} - \xi^2_i\psi_{di} = -\frac{1}{K^d_{ii}}(r_{w_i}{}^d\phi + r_{\Omega_i}{}^d\phi') \tag{59}$$

The above introduced distortional stiffness and load terms are given in Table 6. Note that $r_{w_i}{}^d\psi$ is the distortional moment load and $r_{\Omega_i}{}^d\psi'$ is the distortional bimoment load.

We find that the full solution of each of these uncoupled non-homogeneous linear 2 order differential equations is given by

$$\psi_{di}(z) = c_1e^{\xi_iz} + c_2e^{-\xi_iz} - \frac{1}{2\xi_i}e^{-\xi_iz}\int e^{-\xi_iz}\frac{1}{K^d_{ii}}(r_{w_i}{}^d\phi + r_{\Omega_i}{}^d\phi')\,dz + \frac{1}{2\xi_i}e^{-\xi_iz}\int e^{\xi_iz}\frac{1}{K^d_{ii}}(r_{w_i}{}^d\phi + r_{\Omega_i}{}^d\phi')\,dz \tag{60}$$

Using that ϕ is a linear function as given in Eq. (31) and performing integration or by guessing the solution we get

$$\psi_{d_i}(z) = \mathbf{\Psi}_{dh_i}(z)\mathbf{c}_{d_i} + \mathbf{\Psi}_{dp_i}(z)\boldsymbol{\phi} \tag{61}$$

Here $\mathbf{c}_{di}$ is a vector containing the two constants $c_{d_{2i-1}}$ and $c_{d_{2i}}$ of the homogeneous part of the solution, and

$$\mathbf{\Psi}_{dp_i}(z) = \mathbf{\Psi}^w_{dp_i}(z) + \mathbf{\Psi}^\Omega_{dp_i}(z) \tag{62}$$

$$\mathbf{\Psi}_{dh_i}(z) = [e^{\xi_iz} \;\; e^{-\xi_iz}] \tag{63}$$

$$\mathbf{\Psi}^w_{dp_i} = \frac{r_{w_i}{}^d}{\xi^2_iK^d_{ii}}\left[1 - \frac{z}{L} \;\; \frac{z}{L}\right] \tag{64}$$

$$\mathbf{\Psi}^\Omega_{dp_i} = \frac{r_{\Omega_i}{}^d}{\xi^2_iK^d_{ii}}\left[\frac{-1}{L} \;\; \frac{1}{L}\right] \tag{65}$$

This concludes the determination of all the solutions for all the displacement modes of GBT.

Table 6
Modal distortional stiffness and load terms.

$$K^d_{ii} = \begin{bmatrix} \mathbf{v}^u_w \\ \mathbf{v}^e_w\xi^2 \end{bmatrix}^T_i \begin{bmatrix} \overline{\mathbf{K}}^\tau_{uu} & -\overline{\mathbf{K}}^\sigma_{ue} \\ -\overline{\mathbf{K}}^\sigma_{eu} & -\overline{\mathbf{K}}^\sigma_{ee} \end{bmatrix} \begin{bmatrix} \mathbf{v}^u_w \\ \mathbf{v}^e_w\xi^2 \end{bmatrix}_i \qquad r^d_{w_i} = \begin{bmatrix} \mathbf{v}^u_w \\ \mathbf{v}^e_w\xi^2 \end{bmatrix}^T_i \begin{bmatrix} \mathbf{r}^{\alpha u3}_w \\ \mathbf{r}^{e3}_w \end{bmatrix}$$

$$K^g_{ii} = \xi^2_iK^d_{ii} = \begin{bmatrix} \mathbf{v}^u_w \\ \mathbf{v}^e_w\xi^2 \end{bmatrix}^T_i \begin{bmatrix} \mathbf{K}^s_{uu} & \mathbf{0} \\ \mathbf{0} & -\mathbf{K}^\sigma_{ee} \end{bmatrix} \begin{bmatrix} \mathbf{v}^u_w \\ \mathbf{v}^e_w\xi^2 \end{bmatrix}_i \qquad r^d_{\Omega_i} = \begin{bmatrix} \mathbf{v}^u_w \\ \mathbf{v}^e_w\xi^2 \end{bmatrix}^T_i \begin{bmatrix} \overline{\mathbf{r}}^{\alpha u3}_\Omega \\ \mathbf{r}^{e3}_\Omega \end{bmatrix}$$

7. Assembly of the full solution

The axial variation of the four beam modes have been identified in Eqs. (32), (37) and (50) and can be assembled in the beam solution function matrices $\mathbf{\Psi}_{bh}(z)$ and $\mathbf{\Psi}_{bp}(z)$ which are multiplied by the vector of beam displacement constants $\mathbf{c}_b$ and the load vector

$\boldsymbol{\phi}$ respectively. This results in

$$\boldsymbol{\Psi}_{bh}(z)\mathbf{c}_b+\boldsymbol{\Psi}_{bp}(z)\boldsymbol{\phi}= \begin{bmatrix} \boldsymbol{\Psi}_{ah}(z) & \mathbf{0} & \mathbf{0} \\ \mathbf{0} & \boldsymbol{\Psi}_{\alpha h}(z) & \mathbf{0} \\ \mathbf{0} & \mathbf{0} & \boldsymbol{\Psi}_{3h}(z) \end{bmatrix} \begin{bmatrix} \mathbf{c}_a \\ \mathbf{c}_\alpha \\ \mathbf{c}_3 \end{bmatrix} + \begin{bmatrix} \boldsymbol{\Psi}_{ap}(z) \\ \boldsymbol{\Psi}_{\alpha p}(z) \\ \boldsymbol{\Psi}_{3p}(z) \end{bmatrix} \boldsymbol{\phi} \tag{66}$$

where

$$\boldsymbol{\Psi}_{\alpha h}(z)= \begin{bmatrix} \boldsymbol{\Psi}_{1h}(z) & \mathbf{0} \\ \mathbf{0} & \boldsymbol{\Psi}_{2h}(z) \end{bmatrix} \tag{67}$$

$$\boldsymbol{\Psi}_{\alpha p}(z)= \begin{bmatrix} \boldsymbol{\Psi}_{1p}(z) \\ \boldsymbol{\Psi}_{2p}(z) \end{bmatrix} \tag{68}$$

Furthermore the distortional solution functions can be assembled and described as

$$\boldsymbol{\Psi}_{dh}(z)\mathbf{c}_d+\boldsymbol{\Psi}_{dp}(z)\boldsymbol{\phi}= \begin{bmatrix} \boldsymbol{\Psi}_{dh_1}(z) & \mathbf{0} & \mathbf{0} & \cdots \\ \mathbf{0} & \boldsymbol{\Psi}_{dh_2}(z) & \mathbf{0} & \cdots \\ \mathbf{0} & \mathbf{0} & \boldsymbol{\Psi}_{dh_3}(z) & \cdots \\ \vdots & \vdots & \vdots & \ddots \end{bmatrix} \begin{bmatrix} \mathbf{c}_{d_1} \\ \mathbf{c}_{d_2} \\ \mathbf{c}_{d_3} \\ \vdots \end{bmatrix} + \begin{bmatrix} \boldsymbol{\Psi}_{dp_1}(z) \\ \boldsymbol{\Psi}_{dp_2}(z) \\ \boldsymbol{\Psi}_{dp_3}(z) \\ \vdots \end{bmatrix} \boldsymbol{\phi} \tag{69}$$

Now all the solution functions are obtained and can be assembled using the previously defined block matrices and vectors as

$$\boldsymbol{\Psi}_h(z)\mathbf{c}+\boldsymbol{\Psi}_p(z)\boldsymbol{\phi} \tag{70}$$

in which

$$\boldsymbol{\Psi}_h(z)\mathbf{c}= \begin{bmatrix} \boldsymbol{\Psi}_{bh}(z) & \mathbf{0} \\ \mathbf{0} & \boldsymbol{\Psi}_{dh}(z) \end{bmatrix} \begin{bmatrix} \mathbf{c}_b \\ \mathbf{c}_d \end{bmatrix} \tag{71}$$

and

$$\boldsymbol{\Psi}_p(z)\boldsymbol{\phi}= \begin{bmatrix} \boldsymbol{\Psi}_{bp}(z) \\ \boldsymbol{\Psi}_{dp}(z) \end{bmatrix} \boldsymbol{\phi} \tag{72}$$

As we are using the in-plane modes found in the companion paper [1], the back substitution process of distortional and eliminated beam displacement in-plane modes is identical to the process performed in the companion paper. Hereby all the in-plane modes are assembled column-wise in a modal matrix of transverse displacement vectors $\mathbf{V}_{\mathrm{w}}$ and a modal matrix of axial warping displacement vectors $\mathbf{V}_{\Omega}$, by joining the modal matrices of the beam eigenvectors and the distortional eigenvectors as

$$\mathbf{V}_{\mathrm{w}}=[\mathbf{V}_{\mathrm{w}}^{b}\ \ \mathbf{V}_{\mathrm{w}}^{d}] \quad \mathbf{V}_{\Omega}=[\mathbf{V}_{\Omega}^{b}\ \ \mathbf{V}_{\Omega}^{d}] \tag{73}$$

Having obtained and assembled all the full solution functions and in-plane modes, the full solution along the beam can be presented in the nodal solution vectors $\mathbf{u}_{\mathrm{w}}(z)$ and $\mathbf{u}_{\Omega}(z)$ as follows:

$$\mathbf{u}_{\mathrm{w}}(z)=\mathbf{V}_{\mathrm{w}}[\boldsymbol{\Psi}_h(z)\mathbf{c}+\boldsymbol{\Psi}_p(z)\boldsymbol{\phi}]$$

$$\mathbf{u}_{z}(z)=-\mathbf{V}_{\Omega}[\boldsymbol{\Psi}'_h(z)\mathbf{c}+\boldsymbol{\Psi}'_p(z)\boldsymbol{\phi}] \tag{74}$$

The constants, $\mathbf{c}$, have to be determined by the boundary conditions of the thin-walled beam.

7.1. Transformation to real modes and real solution functions

Some of the distortional solution functions found are complex. Because these complex numbers are awkward to handle it is a matter of considerable importance to construct a more convenient complete solution when we have complex numbers. In [1] we introduce the following notation for the positive square root values and the related eigenvector columns $\mathbf{v}_j$ and $\mathbf{v}_{j+1}$:

$$\xi_j=\lambda_j+\mu_j\mathbf{i}, \quad \xi_{j+1}=\overline{\xi}_j=\lambda_j-\mu_j\mathbf{i} \tag{75}$$

$$\mathbf{v}_j=\mathbf{a}_j+\mathbf{b}_j\mathbf{i}, \quad \mathbf{v}_{j+1}=\overline{\mathbf{v}}_j=\mathbf{a}_j-\mathbf{b}_j\mathbf{i} \tag{76}$$

in which we have introduced the real and imaginary parts of the eigenvalues and eigenvectors. The complex eigenvectors in Eq. (76) may be conveniently written as

$$[\mathbf{v}_j\ \ \mathbf{v}_{j+1}]=[\mathbf{a}_j\ \ \mathbf{b}_j] \begin{bmatrix} 1 & 1 \\ i & -i \end{bmatrix} \tag{77}$$

The constants of the related parts of the homogeneous solution are also complex quantities. However we are able to assemble the two complex conjugated modal solutions into two real (but pairwise coupled) solutions by introducing the real constant vectors $\tilde{\mathbf{c}}_j$ and $\tilde{\mathbf{c}}_{j+1}$ as follows:

$$\begin{bmatrix} \mathbf{c}_j \\ \mathbf{c}_{j+1} \end{bmatrix} = \frac{1}{2} \begin{bmatrix} 1 & -i \\ 1 & i \end{bmatrix} \begin{bmatrix} \tilde{\mathbf{c}}_j \\ \tilde{\mathbf{c}}_{j+1} \end{bmatrix} \tag{78}$$

The j'th complex part of the full solution in Eq. (74) can now be rewritten using the transformations in Eqs. (77) and (78). After multiplication and identification of real and imaginary parts we find the following result:

$$\begin{aligned} &[\mathbf{v}_j\ \ \mathbf{v}_{j+1}] \left\{ \begin{bmatrix} \boldsymbol{\Psi}_{dh_j} & \mathbf{0} \\ \mathbf{0} & \overline{\boldsymbol{\Psi}}_{dh_j} \end{bmatrix} \begin{bmatrix} \mathbf{c}_j \\ \mathbf{c}_{j+1} \end{bmatrix} + \begin{bmatrix} \boldsymbol{\Psi}_{dp_j} \\ \overline{\boldsymbol{\Psi}}_{dp_j} \end{bmatrix} \begin{bmatrix} \phi_1 \\ \phi_2 \end{bmatrix} \right\} \\ &\quad =[\mathbf{a}_j\ \ \mathbf{b}_j] \left\{ \begin{bmatrix} \mathrm{Re}(\boldsymbol{\Psi}_{dh_j}) & \mathrm{Im}(\boldsymbol{\Psi}_{dh_j}) \\ \mathrm{Im}(\overline{\boldsymbol{\Psi}}_{dh_j}) & \mathrm{Re}(\overline{\boldsymbol{\Psi}}_{dh_j}) \end{bmatrix} \begin{bmatrix} \tilde{\mathbf{c}}_j \\ \tilde{\mathbf{c}}_{j+1} \end{bmatrix} \right. \\ &\qquad \left. + \begin{bmatrix} 2\mathrm{Re}(\boldsymbol{\Psi}_{dp_j}) \\ -2\mathrm{Im}(\overline{\boldsymbol{\Psi}}_{dp_j}) \end{bmatrix} \begin{bmatrix} \phi_1 \\ \phi_2 \end{bmatrix} \right\} \end{aligned} \tag{79}$$

Hereby it is possible to rewrite the complex quantities into real quantities. Now the modal matrices $\mathbf{V}_{\mathrm{w}}$ and $\mathbf{V}_{\Omega}$ are modified as $\tilde{\mathbf{V}}_{\mathrm{w}}$ and $\tilde{\mathbf{V}}_{\Omega}$ by substituting the complex pairs of eigenvectors with their respective real and imaginary parts. Furthermore we also introduce the modified solution matrices $\tilde{\boldsymbol{\Psi}}_{dh}$ and $\tilde{\boldsymbol{\Psi}}_{dp}$ and the related modified vector of constants $\tilde{\mathbf{c}}$ by substituting the solutions (and constants) of the complex pairs using Eq. (79). Now the full solution along the beam can be written using real numbers as

$$\mathbf{u}_{\mathrm{w}}(z)=\tilde{\mathbf{V}}_{\mathrm{w}}[\tilde{\boldsymbol{\Psi}}_h(z)\tilde{\mathbf{c}}+\tilde{\boldsymbol{\Psi}}_p(z)\boldsymbol{\phi}]$$

$$\mathbf{u}_{z}(z)=-\tilde{\mathbf{V}}_{\Omega}[\tilde{\boldsymbol{\Psi}}'_h(z)\tilde{\mathbf{c}}+\tilde{\boldsymbol{\Psi}}'_p(z)\boldsymbol{\phi}] \tag{80}$$

Hereby it is possible to work with this real formulation or continue working with complex numbers using the full solution formulated in Eq. (74). In the following context we will use the real formulation in Eq. (80).

8. Displacement boundary conditions

In this section we will introduce a method for determining the constants of the non-homogeneous solutions found. This is to be done in the GBT space, which has been constrained by the relevant assumptions of the beam theory. As seen from the first variation of the potential energy, the natural boundary displacements of the GBT at each boundary are the pure axial displacement u_{Ω}^{g} of the beam, the transverse displacements $\mathbf{u}_{\mathrm{w}}^{g}$, and the axial derivative of the transverse displacements $\mathbf{u}_{\mathrm{w}}^{g'}$. In the following the generalized internal displacements of the GBT beam will be expressed by using the transformation from FE to GBT displacements as follows:

$$\begin{bmatrix} u_z(z) \\ \mathbf{u}_{\mathrm{w}}^{g}(z) \\ \mathbf{u}_{\mathrm{w}}^{g'}(z) \end{bmatrix} = \begin{bmatrix} -\mathbf{T}_{\Omega}^{g^T}\tilde{\mathbf{V}}_{\Omega}\tilde{\boldsymbol{\Psi}}'_h(z) \\ \mathbf{T}_{\mathrm{w}}^{g^T}\tilde{\mathbf{V}}_{\mathrm{w}}\tilde{\boldsymbol{\Psi}}_h(z) \\ \mathbf{T}_{\mathrm{w}}^{g^T}\tilde{\mathbf{V}}_{\mathrm{w}}\tilde{\boldsymbol{\Psi}}'_h(z) \end{bmatrix} \tilde{\mathbf{c}} + \begin{bmatrix} -\mathbf{T}_{\Omega}^{g^T}\tilde{\mathbf{V}}_{\Omega}\tilde{\boldsymbol{\Psi}}'_p(z) \\ \mathbf{T}_{\mathrm{w}}^{g^T}\tilde{\mathbf{V}}_{\mathrm{w}}\tilde{\boldsymbol{\Psi}}_p(z) \\ \mathbf{T}_{\mathrm{w}}^{g^T}\tilde{\mathbf{V}}_{\mathrm{w}}\tilde{\boldsymbol{\Psi}}'_p(z) \end{bmatrix} \boldsymbol{\phi} \tag{81}$$

To determine the constants using displacement boundary conditions as in finite element or stiffness formulations, the boundary displacements at the two ends of a finite length beam are needed, i.e. at $z=0$ and at $z=L$, where L is the length of the beam. The assembled boundary displacement vector is denoted by $\mathbf{u}_b$. This leads to the following equation for the determination of the solution constants:

$$\mathbf{u}_b = \begin{bmatrix} u_z^a(0) \\ \mathbf{u}_w^g(0) \\ \mathbf{u}_w^{g\prime}(0) \\ u_z^a(L) \\ \mathbf{u}_w^g(L) \\ \mathbf{u}_w^{g\prime}(L) \end{bmatrix} \tag{82}$$

$$= \begin{bmatrix} -\mathbf{T}_\Omega^{a^T}\tilde{\mathbf{V}}_\Omega\tilde{\mathbf{\Psi}}_h'(0) \\ \mathbf{T}_w^{g^T}\tilde{\mathbf{V}}_w\tilde{\mathbf{\Psi}}_h(0) \\ \mathbf{T}_w^{g^T}\tilde{\mathbf{V}}_w\tilde{\mathbf{\Psi}}_h'(0) \\ -\mathbf{T}_\Omega^{a^T}\tilde{\mathbf{V}}_\Omega\tilde{\mathbf{\Psi}}_h'(L) \\ \mathbf{T}_w^{g^T}\tilde{\mathbf{V}}_w\tilde{\mathbf{\Psi}}_h(L) \\ \mathbf{T}_w^{g^T}\tilde{\mathbf{V}}_w\tilde{\mathbf{\Psi}}_h'(L) \end{bmatrix} \tilde{\mathbf{c}} + \begin{bmatrix} -\mathbf{T}_\Omega^{a^T}\tilde{\mathbf{V}}_\Omega\tilde{\mathbf{\Psi}}_p'(0) \\ \mathbf{T}_w^{g^T}\tilde{\mathbf{V}}_w\tilde{\mathbf{\Psi}}_p(0) \\ \mathbf{T}_w^{g^T}\tilde{\mathbf{V}}_w\tilde{\mathbf{\Psi}}_p'(0) \\ -\mathbf{T}_\Omega^{a^T}\tilde{\mathbf{V}}_\Omega\tilde{\mathbf{\Psi}}_p'(L) \\ \mathbf{T}_w^{g^T}\tilde{\mathbf{V}}_w\tilde{\mathbf{\Psi}}_p(L) \\ \mathbf{T}_w^{g^T}\tilde{\mathbf{V}}_w\tilde{\mathbf{\Psi}}_p'(L) \end{bmatrix} \boldsymbol{\phi} \tag{83}$$

$$= \tilde{\mathbf{A}}\tilde{\mathbf{c}} + \tilde{\mathbf{B}}\boldsymbol{\phi} \tag{84}$$

$$\Rightarrow \quad \tilde{\mathbf{c}} = \tilde{\mathbf{A}}^{-1}(\mathbf{u}_b - \tilde{\mathbf{B}}\boldsymbol{\phi}) \tag{85}$$

where we have introduced the matrix $\tilde{\mathbf{A}}$ and $\tilde{\mathbf{B}}$, where $\tilde{\mathbf{A}}$ is an invertible positive definite "square" matrix. To avoid numerical problems the exponential solution functions in $\tilde{\mathbf{\Psi}}_h(z)$ may have to be modified by replacing $\tilde{c}_i e^{\xi_i z}$ by $\hat{c}_i e^{\xi_i(z-L)}$ so that the positive $\xi_i z$ exponent is bounded.

To see the effect of the load as it would be in a finite element context with built in edges, we choose to plot the solution by using Eq. (80), with all boundary displacements being zero (built in) as

$$\mathbf{u}_b^T = [0\ \mathbf{0}\ \mathbf{0}\ 0\ \mathbf{0}\ \mathbf{0}]^T \tag{86}$$

This is done in the following examples.

9. Examples

In this section four examples will be given and nodal displacement results as well as stress distribution results of GBT will be compared to those found using the commercial FE program Abaqus. In the examples we consider a lipped channel and a box beam, both for two different load cases. For all load cases the loads are uniformly distributed and thus given by a cross-section load distribution multiplied by $\phi(z)=1$. In all four examples the beams have a length of $L=2000$ mm, an elasticity modulus $E=2.1\times10^5$ MPa and a Poisson ratio of $v=0.3$.

The results found using Abaqus are based on isotropic material and the S4 shell element with full 4 point integration. The linear elastic finite element calculations are based on a structured rectangular mesh with a side length seed of 5 mm.

9.1. Example 1—flexural load on lipped channel

Using the full solution in Eq. (80) with parameters, discretization and distributed cross-section load as given and shown in Fig. 5 leads to the deformations shown in Fig. 6. Here it is seen that the main deformation is related to flexure, however also an in-plane deformation of the cross section becomes clear. This points out the importance of taking distortion into account in order to obtain a good approximation of the deformation shape even in simple load cases.

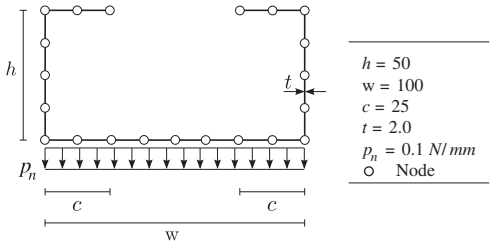

Fig. 5. Geometry, parameter values and load for the lipped channel.

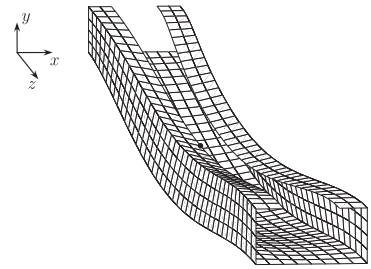

Fig. 6. GBT plot of the lipped channel with a flexural load.

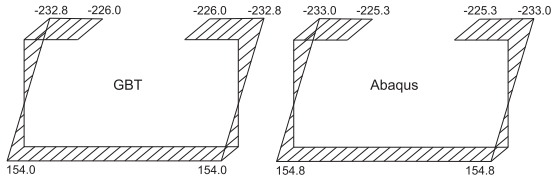

Fig. 7. Comparison between the axial normal stress distributions obtained with GBT and Abaqus at mid-span. All values are in MPa.

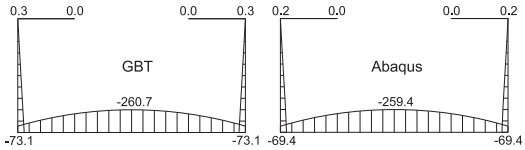

Fig. 8. Comparison between the transverse bending stress distributions obtained with GBT and Abaqus at mid-span. All values are in MPa.

Comparing a nodal displacement of GBT to the one found from a model in the commercial FE program Abaqus gives the values and the corresponding deviations shown in Table 7. The values correspond to the node marked on the deformed plot of the GBT solution in Fig. 6 at mid-span of the beam. From Table 8 the deviation from Abaqus results of the displacement, u_x, in the horizontal direction is 0.6%. As the present approach is based on a beam theory this deviation may be expected. In contrast, the deviation for the vertical displacement, u_y, is as large as 3.3%, however this can be explained by the formulation of the present theory, which is based on a beam theory where the shear deformations are neglected. In our Abaqus model we are using shell elements which include in-plane shear deformation. Calculating the contribution of shear deformations to the displacement

Table 7
Example 1: nodal displacements of GBT and FE analysis.

	GBT (mm)	Abaqus (mm)	Difference (%)
u_x	2.409	2.395	0.6
u_y	−10.844	−11.213	3.3

Table 8
Example 1: stress comparison of GBT and FE analysis.

	GBT (MPa)	Abaqus (MPa)	Difference (%)
σ_z	154.0	154.8	0.5
σ_s	−73.1	−69.4	5.3

Table 9
Example 2: nodal displacements of GBT and FE analysis.

	GBT (mm)	Abaqus (mm)	Difference (%)
u_x	−2.847	−2.841	0.2
u_y	2.093	2.084	0.4

as follows gives

$$\Delta u_y(z) = \frac{1}{8}\frac{pL^2}{A_{web}G} = 0.31 \text{ mm} \quad (87)$$

which is based on a web area of $A_{web} = 2ht$ and a load of $p = p_n$w in which h is the height of one of the two webs and w is the width of the loaded flange. Adding this contribution to the vertical GBT displacement value in Table 7 gives $u_y = 10.844$ mm + 0.3 mm = 11.144 mm, which then corresponds to a deviation of 0.6%. Having compared the nodal displacement obtained with GBT and Abaqus we will now take a look at the stress distributions. A comparison of the membrane stresses in the z direction at mid-span is shown in Fig. 7 which gives a maximum deviation of 0.5% as shown in Table 8. As the present approach is based on a beam theory this deviation may be expected. The transverse bending stresses at mid-span are shown in Fig. 8 and show a maximum deviation in the corner at the bottom of 5.3% which is caused by the approach based on a beam theory and by the chosen mesh size. Reducing the mesh side length seed to 3 mm the maximum deviation is reduced to 3.1%.

9.2. Example 2—distortional load on lipped channel

In this example the same lipped channel cross section as in the first example is now loaded by a distortional load as shown in Fig. 9. Solving the equations leads to the GBT deformation solution shown in Fig. 10, which has displacements of the lips in both transverse coordinate directions with the maximum value at mid-span. It is seen that the distortional deformation dominates and that the boundary conditions give raise to relatively local end effects, whereas the deformations around mid span are relatively constant. Comparing the nodal displacements of the node marked in Fig. 10 to the displacements found using a model in the commercial FE program Abaqus gives the displacement values and the corresponding deviations shown in Table 9. Here the deviation according to the maximum displacement in the horizontal direction, u_x, is 0.2% and the deviation for the vertical direction, u_y, is 0.4%. Again we also want a comparison between the stress distributions obtained with GBT and Abaqus. In order to have comparable values different from zero the results concerning the axial normal stresses are obtained from the end section.

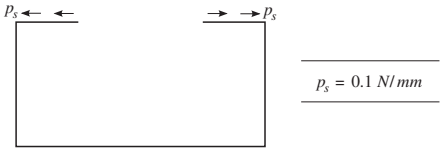

Fig. 9. Distributed distortional load.

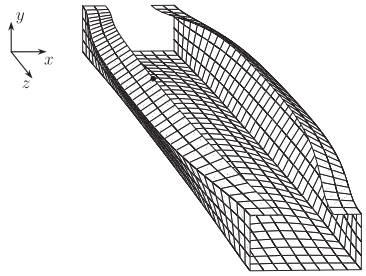

Fig. 10. GBT plot of the lipped channel with a distortional load.

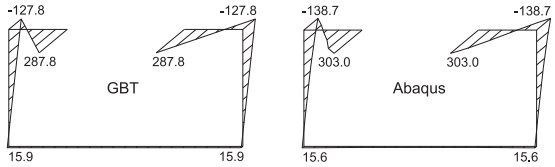

Fig. 11. Comparison between the axial normal stress distributions obtained with GBT and Abaqus at the end of the beam. All values are in MPa.

Table 10
Example 2: stress comparison of GBT and FE analysis.

	GBT (MPa)	Abaqus (MPa)	Difference (%)
σ_z	127.7	138.7	7.9
σ_s	197.2	196.9	0.2

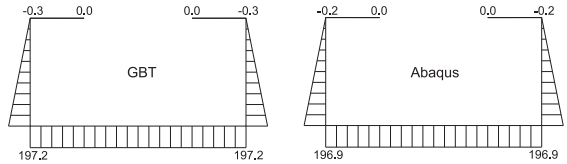

Fig. 12. Comparison between the transverse bending stress distributions obtained with GBT and Abaqus at mid-span. All values are in MPa.

A comparison of the axial membrane stresses in the z direction is shown in Fig. 11 and show a maximum deviation of 7.9% as given in Table 10. This deviation can be explained by shear lag as the results are here from the end section. The transverse bending stresses at mid-span are shown in Fig. 12. Here the maximum deviation is 0.2% and obtained at the corner in the bottom.

9.3. Example 3—flexural load on box section

In this third example a box beam is loaded by a flexural load. The geometry, parameters values, discretization of the cross section and the distributed vertical load are as given and shown

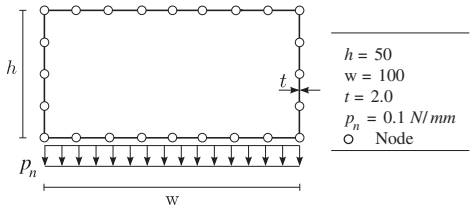

Fig. 13. Geometry, parameter values and load for the box beam.

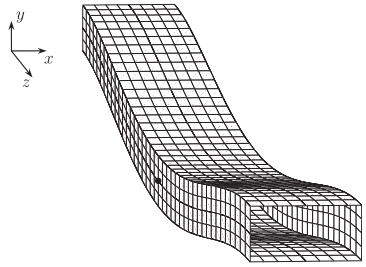

Fig. 14. GBT plot of the box beam with a flexural load.

Table 11
Example 3: nodal displacements of GBT and FE analysis.

	GBT (mm)	Abaqus (mm)	Difference (%)
u_x	0.056	0.056	0.0
u_y	−6.802	−7.200	5.5

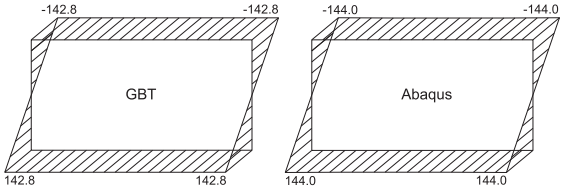

Fig. 15. Comparison between the axial membrane stress distributions obtained with GBT and Abaqus for at mid-span. All values are in MPa.

Table 12
Example 3: stress comparison of GBT and FE analysis.

	GBT (MPa)	Abaqus (MPa)	Difference (%)
σ_z	142.8	144.0	0.8
σ_s	−11.9	−11.7	1.7

in Fig. 13. This leads to the deformation shown in Fig. 14. As seen for the lipped channel in example 1, the main deformation is also here related to flexure of the beam. A comparison of the displacement values found using GBT to the FE results found using a Abaqus model is given in Table 11. Here it is seen that the deviation of the maximum displacement in the horizontal direction, u_x, is 0.0% and the deviation for the vertical direction, u_y, is 5.5%. Again the large deviation can be explained by the neglected shear deformations. Calculating the effect of shear deformations as in Eq. (87) gives a contribution to the displacement of $\Delta u_y(z) = 0.31$ mm and thus a total displacement of $u_y = 6.802$ mm + 0.31 mm = 7.112 mm. Hereby the deviation is reduced to 1.2%.

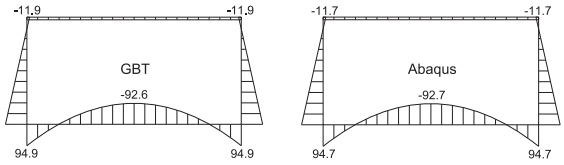

Fig. 16. Comparison between the transverse bending stress distributions obtained with GBT and Abaqus at mid-span. All values are in MPa.

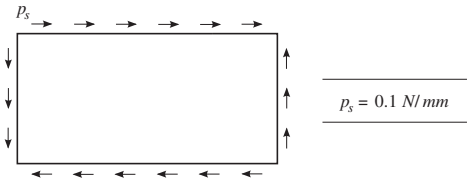

Fig. 17. Distributed distortional load.

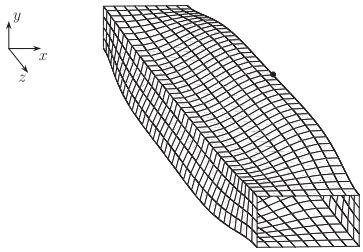

Fig. 18. GBT plot of the box beam with a distortional load.

Table 13
Example 4: nodal displacements of GBT and FE analysis.

	GBT (mm)	Abaqus (mm)	Difference (%)
u_x	0.266	0.262	1.5
u_y	0.515	0.509	1.2

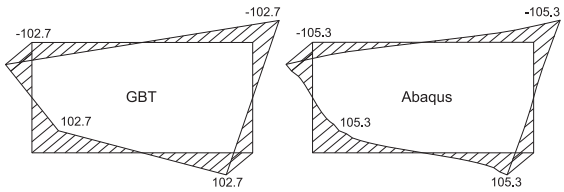

Fig. 19. Comparison between the axial normal stress distributions obtained with GBT and Abaqus at mid-span of the beam. All values are in MPa.

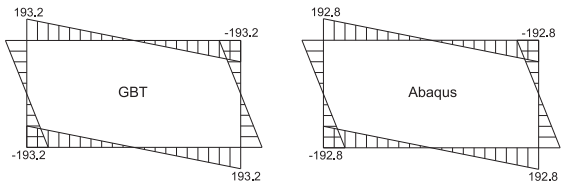

Fig. 20. Comparison between the transverse bending stress distributions obtained with GBT and Abaqus at mid-span. All values are in MPa.

Table 14
Example 4: stress comparison of GBT and FE analysis.

	GBT (MPa)	Abaqus (MPa)	Difference (%)
σ_z	102.7	105.3	2.5
σ_s	193.2	192.8	0.2

Making a comparison between the stress distributions obtained with GBT and Abaqus we obtain the following results. Concerning the axial membrane stresses in the z direction at mid-span we obtain the values and distribution presented in Fig. 15. In this case a maximum deviation of 0.8% is obtained as given in Table 12. The transverse bending stresses at mid-span are shown in Fig. 16 and show a maximum deviation of 1.7%.

9.4. Example 4—distortional load on box section

In this last example the same box beam as in the previous third example is now loaded by a distortional load as shown in Fig. 17. Solving the differential equations of GBT leads to deformations shown in Fig. 18. A comparison of the GBT displacements of the node marked in the figure to those found using the Abaqus finite element model, the values is given in Table 13. Here it is seen that the deviation of the maximum displacement in the horizontal direction, u_x, is 1.5% and the deviation for the vertical direction is 1.2%. Having compared the nodal displacement obtained with GBT and Abaqus we take a look at the stress distributions. A comparison of the membrane stresses in the z direction at mid-span are shown in Fig. 19 which gives a maximum deviation of 2.5% as shown in Table 14. The transverse bending stresses at mid-span are shown in Fig. 20. In this case a maximum deviation of 0.2% is obtained.

10. Conclusion

In this paper we have included distributed loads in a novel semi-discretized formulation of the distortional differential equations. By using the distortional modal matrix found for the homogeneous system we have transformed the non-homogeneous distortional differential equations into the eigenmode space, and then obtained the uncoupled set of differential equations including the distributed loads. This uncoupling is very important in GBT, since the shear stiffness contribution cannot be neglected nor approximated by the combination of axial stiffness and transverse stiffness, especially for closed cross sections. This means that conventional modal analysis (corresponding to orthogonal damping) cannot be used to solve the equations and analytical solutions must therefore be based on the eigenmodes found for the reduced order distortional differential equations. Examples have been given for thin-walled beams with distributed uniform loads. The chosen examples show solutions which are applicable to finite element formulation of a future distortional beam element with applied loads, i.e. with fixed boundary conditions. The boundary conditions will be handled by the eigenmodes of the homogeneous solution. The examples also show that shear deformation is only included for "Bredt's shear flow" around closed cells. The examples also show that the presented theory does not include shear lag effects. However these and other effects may be included as extensions in approximate energy based finite element formulations which may be used to extend the capabilities of beam elements. The novel approach presented in this paper is a considerable theoretical achievement, since it without approximation gives the full analytical solution of the GBT equations with distributed loads for a given discretization of the cross section.

References

[1] Jönsson J, Andreassen MJ. Distortional eigenmodes and homogeneous solutions of semi-discretized thin-walled beams. Thin-Walled Structures 2011;49:691–707.
[2] Schardt R. Eine Erweiterung der technischen Biegelehre für die Berechnung biegesteifer prismatischer Faltwerke. Der Stahlbau 1966;35:161–71.
[3] Schardt R. Verallgemeinerte Technische Biegetheorie. Germany: Springer-Verlag; 1989.
[4] Davies JM, Leach P. First-order generalised beam theory. Journal of Constructional Steel Research 1994;31(2-3):187–220.
[5] Lepistö J, Nikula S, Niemi E. Optimum design of cold-formed sections using Generalized Beam Theory. In: Rondal J, Dubina D, Gioncu V, editors. Proceedings of the second international conference on coupled instabilities in metal structures (CIMS 1996—Liége, 05-07/09). London: Imperial College Press; 1996. p. 101–8.
[6] Rendek S, Baláž I. Distortion of thin-walled beams. Thin-Walled Structures 2004;42:255–77.
[7] Simão P, Simões da Silva, L. Comparative analysis of the stability of open and closed thin-walled section members in the framework of generalized beam theory. In: Lamas A, Simões da Silva L, editors. Proceedings of the 3rd European conference on steel structures (EUROSTEEL 2002—Coimbra, Portugal, 19-20/09), vol. 1. p. 711–21.
[8] Gonçalves R, Dinis PB, Camotim D. GBT formulation to analyse the first-order and buckling behaviour of thin-walled members with arbitrary cross-sections. Thin-Walled Structures 2009;47:583–600.
[9] Gonçalves R, Camotim D. Steel-concrete composite bridge analysis using generalised beam theory. Steel and Composite Structures 2010;10:223–43.
[10] Silvestre N, Camotim D. First-order generalised beam theory for arbitrary orthotropic materials. Thin-Walled Structures 2002;40:755–89.
[11] Silvestre N. Generalized beam theory: new formulations, numerical implementation and applications. PhD thesis. Portugal: IST—Technical University of Lisbon; 2005 (in Portuguese).
[12] Hanf M. Die geschlossene Lösung der linearen Differentialgleichungssysteme der Verallgemeinerten Technischen Biegetheorie mit einer Anwendung auf die Ermittlung plastischer Grenzlasten. Instituts für Werkstoffe und Mechanik im Bauwesen der TU Darmstadt 1989;9.
[13] Jönsson J. Distortional theory of thin-walled beams. Thin-Walled Structures 1999;33:269–303.
[14] Kollbrunner CF, Hajdin N. Dünnwandige Stäbe 1, Stäbe mit undeformierbaren Querschnitten. Berlin: Springer-Verlag; 1972. 1975.

Appendix D

Paper III

Michael Joachim Andreassen and Jeppe Jönsson, (2012).

Distortional buckling modes of semi-discretized thin-walled columns.

Thin-Walled Structures, **51**, 53–63.

Thin-Walled Structures 51 (2012) 53–63

Contents lists available at SciVerse ScienceDirect

Thin-Walled Structures

journal homepage: www.elsevier.com/locate/tws

Distortional buckling modes of semi-discretized thin-walled columns

Michael Joachim Andreassen, Jeppe Jönsson*

Technical University of Denmark, Department of Civil Engineering, Brovej Building 118, DK-2800 Kgs. Lyngby, Denmark

ARTICLE INFO

Article history:
Received 21 September 2011
Received in revised form
2 November 2011
Accepted 2 November 2011

Keywords:
Thin-walled beams
Beam theory
Stability
Distortion
Warping
Distortional beam theory
Generalized beam theory
Semi-discretization
Bifurcation
Buckling
Columns

ABSTRACT

This paper presents distorting buckling solutions for semi-discretized thin-walled columns using the coupled differential equations of a generalized beam theory (GBT). In two related papers recently published by the authors a novel semi-discretization approach to GBT has been presented. The cross section is discretized and analytical solutions are sought for the variation along the beam. With this new approach the general GBT equations for identification of a full set of deformation modes corresponding to both homogeneous and non-homogenous equations are formulated and solved. Thereby giving the (complex) deformation modes of GBT which decouple the state space equations corresponding to the reduced order differential equations.

In this paper the developed semi-discretization approach to generalized beam theory (GBT) is extended to include the geometrical stiffness terms, which are needed for column buckling analysis and identification of buckling modes. The extension is based on an initial stress approach by addition of the related potential energy terms. The potential energy of a single deformation mode is formulated based on a discretization of the cross section. Through variations in the potential energy and the introduction of the constraints related to beam theory this leads to a modified set of coupled homogeneous differential equations of GBT with initial stress for identification of distortional displacement modes. In this paper we seek instability solutions using these GBT initial stress equations for simply supported columns with constrained transverse displacements at the end sections and a constant axial initial stress. Based on the known boundary conditions the reduced order differential equations are solved by using the trigonometric solution functions and solving the related eigenvalue problem. This gives the buckling mode shapes and the associated eigenvalues corresponding to the bifurcation load factors. Thus the buckling modes are found directly by the analytical solution of the coupled GBT-equations without modal decomposition. Illustrative examples showing global column buckling, distortional buckling and local buckling are given and it is shown how the novel approach may be used to develop signature curves and elastic buckling curves. In order to assess the accuracy of the method some of the results are compared to results found using the commercial FE program Abaqus as well as the conventional GBT and FSM methods using the software packages GBTUL and CUFSM.

1. Introduction

An assessment of the structural performance of thin-walled beams includes linear static analysis and linear buckling analysis of the behavior. Linear buckling analysis is used to achieve an estimate of the load level at which certain types of structures exhibit a loss of stability through large non-linear deformations. Typically for these structures membrane strain energy is converted into flexural strain energy with very little change in externally applied load. In slender columns and thin plates or shells, the membrane stiffness is much greater than the bending stiffness, and large strain energy can be stored with very small membrane deformations. Therefore, the deformations of the fundamental state are neglected and the displacements are measured from the initial perfect configuration. As the membrane stiffness is much greater than bending stiffness, comparatively large bending deformations are needed to absorb the membrane strain energy released when buckling occurs. In most buckling cases of practical interest this means that the geometric stiffness term (for compressional loading) gives a negative contribution to the total stiffness. In other words, instability may be considered as the load level at which added elastic stiffness terms are fully neutralized by a change in added negative geometric stiffness terms in the potential energy. In this paper we therefore include initial stress contributions to the potential energy which allow us to perform linear distortional buckling analysis of semi-discretized thin-walled members.

* Corresponding author. Tel.: +45 45251707.
E-mail addresses: mican@byg.dtu.dk (M.J. Andreassen), jej@byg.dtu.dk (J. Jönsson).

0263-8231/$ - see front matter © 2011 Elsevier Ltd. All rights reserved.
doi:10.1016/j.tws.2011.11.002

The classic stability analysis of thin-walled columns is based on a combination of the "in-plane rigid" cross-section displacement modes (Vlasov modes, [1]) corresponding to: Uniform axial extension, major axis bending, minor axis bending and torsion with related warping. An important feature missing here is the deformation of the cross section, which undergoes in-plane deformations by local and distortional modes. Concerning analysis of thin-walled members including distortion of the cross section there are a number of methods available among which are: (i) The use of shell finite elements in the finite element method (FEM), [2,3], perhaps with utilization of recursive substructuring, [4], (ii) the finite strip method (FSM), [5–9], and (iii) the use of approximate GBT-finite beam elements. In this context the first application of the first generation of GBT to buckling analysis was published in 1970 by Schardt [10]. Among others also Davies [11], Lepistö [12], Simão [13] and Camotim [14] has investigated the area. This paper deals with a novel method based on solution of the differential initial stress equations of GBT obtained through semi-discretization and application of beam constraints. In the two related papers by the authors [15,16] a novel finite element based semi-discretization approach to generalized beam theory (GBT) is presented. In contrast to the traditional GBT formulations which do not solve the differential equations but establish a weak solution through introduction of mode shapes (based on an orthogonal shear stiffness assumption) and use approximate modal amplitude functions, the novel approach in [15,16] finds the exact modes shapes and amplitude solutions of the reduced order GBT equations related to the discretized cross section. In the same context the novel approach in [15,16] adhere to the definition of the warping function given by Kollbrunner and Hajdin, [17], which adds the integral of the shear flow strains, see also [18,19]. For a more elaborate description see the companion paper, [15].

In this paper the developed semi-discretization formulation is extended by including the initial stress terms. The potential energy of a single deformation mode is formulated based on the discretization of the cross section. Through variations in the potential energy and the introduction of the constraints related to beam theory this leads to a modified set of coupled homogeneous differential equations of GBT with initial stress for identification of distortional buckling modes. In this paper we seek "simple" instability solutions using these GBT initial stress equations for the classical simply supported columns with constrained transverse displacements at the end sections and a constant axial initial stress. Based on the known boundary conditions the reduced order differential equations are solved by introducing the relevant trigonometric solution function and solving the related eigenvalue problem. This directly gives us the cross-section buckling mode shape and the eigenvalue corresponding to the bifurcation load factor. This is done as in conventional FSM without the use of modal decomposition as conventionally performed in GBT.

Let us shortly make an outline of this paper. We will start out by introducing the basic assumptions and kinematic relations in Section 2. The displacements of a single mode are separated into the products of cross-section displacement functions and the axial variation functions. Furthermore the expressions for the strains are derived and the element interpolation functions as well as the nodal displacement components of a straight cross-section element are described. Based on simple constitutive relations the potential elastic energy as well as the potential energy contribution of the factored initial stress is formulated in Section 3. Furthermore the global geometrical stiffness matrix is formulated and the load parameter λ is introduced. Section 4 is split into two main steps leading to the final distortional differential equations of double size to which we want to find solutions. In step I we perform variations in the potential energy whereby the pure axial extension mode and its homogeneous solution is identified and eliminated. In Step II the constraint equations relating to the assumption of a constant wall width are introduced, and the rigid translations and the rigid rotational cross-section displacement eigenmodes are identified and orthogonalized. As in classic beam theory the elimination or separate formulation of the flexural and torsional buckling equations (including initial stress terms) are not possible since they now couple with each other and with the remaining distortional equations. This results in global modes which always include distortion of the cross section to a certain degree. The order of the differential equations is reduced by doubling the number of equations through the introduction of a state vector with components of different differentiation levels. From the final differential equations the eigenvalue problem is formulated. In Section 5 trigonometric solutions of the eigenvalue problem are considered. Finally Section 6 is devoted to illustrative examples including development of classic buckling curves and comparison of results with finite element results found using Abaqus, [20], as well as with FSM and conventional GBT results found using the freely available software packages CUFSM and GBTUL, see [21,22].

2. Basic assumptions and kinematic relations

The prismatic beam is described in a global Cartesian (x,y,z) coordinate system as shown in Fig. 1. From the figure it is seen that a local coordinate system (z,n,s) corresponding to the normal and tangential directions is introduced. In the local coordinate system the displacements u_n, u_s and u_z are introduced as

$$u_n(s,z) = \mathrm{w}_n(s)\psi(z) \tag{1}$$

$$u_s(n,s,z) = \big(\mathrm{w}_s(s) - n\mathrm{w}_{n,s}(s)\big)\psi(z) \tag{2}$$

$$u_z(n,s,z) = -\big(\Omega(s) + n\mathrm{w}_n(s)\big)\psi'(z) \tag{3}$$

For the local transverse displacements $u_n(s,z)$ and $u_s(n,s,z)$, the components $\mathrm{w}_s(s)$ and $\mathrm{w}_n(s)$ are the local displacements of the centerline and $\psi(z)$ is the function which describes the axial variation of the in-plane distortional displacements. For the axial displacements $u_z(n,s,z)$ generated by the out-of-plane distortional cross-sectional displacements, the axial (warping) displacement mode $\Omega(s)$ has been included with a variation corresponding to the negative axial derivative of the axial variation factor, $-\psi'$, and due consideration of local transverse variation through the term $n\mathrm{w}_n$. The local components are shown in Fig. 2.

The corresponding strains referred to as axial strains, transverse strains and engineering shear strains, respectively, are introduced as

$$\varepsilon_z = -(\Omega + n\mathrm{w}_n)\psi'' \tag{4}$$

$$\varepsilon_s = (\mathrm{w}_{s,s} - n\mathrm{w}_{n,ss})\psi \tag{5}$$

$$\gamma_{zs} = (\mathrm{w}_s - \Omega_{,s} - 2n\mathrm{w}_{n,s})\psi' \tag{6}$$

In this approach the thin-walled cross section is discretized in straight cross-sectional elements. The thickness of the individual

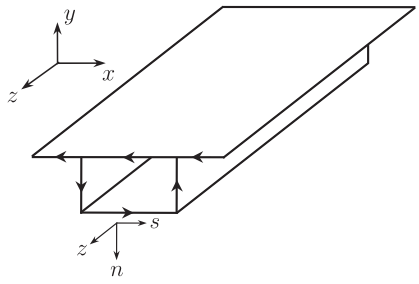

Fig. 1. Global and local Cartesian reference frames.

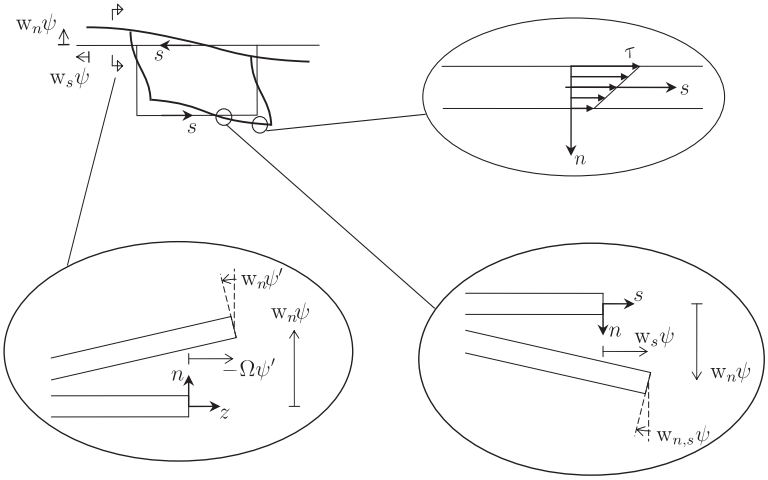

Fig. 2. Local components of the displacement field and assumed shear stresses.

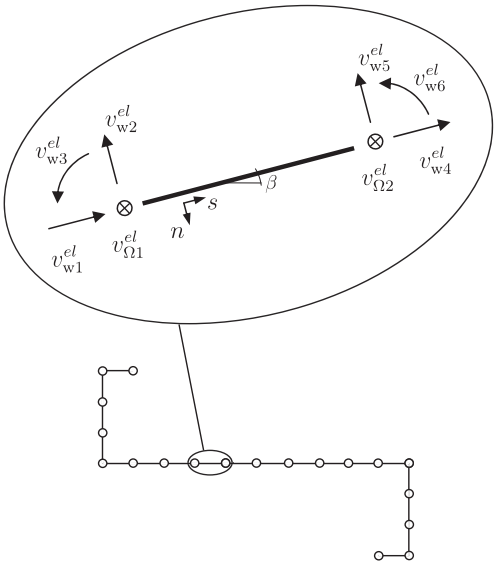

Fig. 3. Nodal components of a straight single flat element.

plane cross-section element is denoted by t and the width of the wall element by b_{el}. The modal displacements of the individual wall element is interpolated using the following interpolation functions:

$$\Omega\psi' = \mathbf{N}_\Omega \mathbf{v}^{el}_\Omega \psi' \tag{7}$$

$$w_s\psi = \mathbf{N}_s \mathbf{v}^{el}_w \psi \tag{8}$$

$$w_n\psi = \mathbf{N}_n \mathbf{v}^{el}_w \psi \tag{9}$$

in which $\mathbf{N}_\Omega(s)$ and $\mathbf{N}_s(s)$ are linear interpolation matrices and $\mathbf{N}_n(s)$ is a cubic (beam) interpolation matrix. Furthermore we have introduced the axial and transverse nodal displacement components of a straight cross-section element as

$$\mathbf{v}^{el}_\Omega = [v^{el}_{\Omega1} \;\; v^{el}_{\Omega2}]^T$$

$$\mathbf{v}^{el}_w = [v^{el}_{w1} \;\; v^{el}_{w2} \;\; v^{el}_{w3} \;\; v^{el}_{w4} \;\; v^{el}_{w5} \;\; v^{el}_{w6}]^T \tag{10}$$

The nodal components and the direction of the section coordinates (n,s) are shown in Fig. 3. Assembling the local element degrees of freedom, the global displacement vectors for the total cross section are given as

$$\mathbf{v}_\Omega = [v_{\Omega1} \;\; v_{\Omega2} \;\; v_{\Omega3} \;\; \ldots]^T$$

$$\mathbf{v}_w = [v_{x1} \;\; v_{y1} \;\; \phi_1 \;\; v_{x2} \;\; v_{y2} \;\; \phi_2 \;\; \ldots]^T \tag{11}$$

where the axial displacements and the transverse displacements are separated into two vectors. The number of degrees of freedom n_{dof} in the cross section is four times the number of nodes, $n_{dof} = 4n_{no}$.

3. Energy assumptions and initial stress

The internal energy potential introduced in paper [15,16] will be briefly presented in this section as well as the new contribution to the potential energy of the initial stress terms, which are adequate for distortional buckling analysis of thin-walled members.

In the classic beam theory simple constitutive relations are used, which means that the material is assumed to be linear elastic with a modulus of elasticity E and shear modulus G. In this paper also a plate elasticity modulus $E_s = E/(1-\nu^2)$ in the transverse direction is utilized. The axial stress is determined as $\sigma_z = E\varepsilon_z$, the shear stress as $\tau = G\gamma$ and finally the transverse stress as $\sigma_s = E_s\varepsilon_s$. Thus taking the transverse plate bending effect into account but neglecting the coupling of axial strain ε_z and transverse strain ε_s. With the constitutive relations assumed the basic elastic energy potential becomes

$$\Pi_{int} = \int_V \left(\frac{1}{2}E\varepsilon_z^2 + \frac{1}{2}G\gamma^2 + \frac{1}{2}E_s\varepsilon_s^2\right) dV \tag{12}$$

Let us next introduce the contribution to the potential energy of a constant uniform initial stress σ^0 which is adequate for column buckling analysis. Following conventional methods the initial stress σ^0 will be scaled by a factor λ. After having utilized linear equilibrium of the pre-buckling state and neglected contribution corresponding to the squared strain term $\frac{1}{2}\lambda\sigma^0 u^2_{z,z} = \frac{1}{2}\lambda\sigma^0\varepsilon^2$ the potential energy contribution of the factored initial stress is given by

$$\Pi_0 = \int_V \left(\frac{1}{2}\lambda\sigma^0 u^2_{s,z} + \frac{1}{2}\lambda\sigma^0 u^2_{n,z}\right) dV$$

$$= \int_V \left(\frac{1}{2}\lambda\sigma^0 (u'_s)^2 + \frac{1}{2}\lambda\sigma^0 (u'_n)^2\right) dV \tag{13}$$

Let us introduce a thin-walled cross section assembled by using straight cross-sectional elements. This allows us to integrate the internal energy across the volume of the thin-walled beam. The elastic potential energy of a single mode takes the following form after the introduction of the strains expressed by the separated displacement functions:

$$\Pi_{int} = \frac{1}{2}\int_0^L \left[\sum_{el} \int_0^{b_{el}} \left\{ \left[Et(\Omega\psi'')^2 + \frac{1}{12}Et^3(\mathrm{w}_n\psi'')^2 \right] + \left[Gt(\mathrm{w}_s\psi')^2 + Gt(\Omega_{,s}\psi')^2 - 2Gt(\mathrm{w}_s\psi')(\Omega_{,s}\psi') + \frac{1}{3}Gt^3(\mathrm{w}_{n,s}\psi')^2 \right] + \left[E_s t(\mathrm{w}_{s,s}\psi)^2 + \frac{1}{12}E_s t^3(\mathrm{w}_{n,ss}\psi)^2 \right] \right\} ds \right] dz \tag{14}$$

The elastic energy terms have been grouped in axial strain energy, shear energy, and transverse strain energy.

The factored initial stress contribution of a single mode to the potential energy takes the following form after introduction of straight cross-sectional wall elements, displacement derivatives and integration through the thickness:

$$\Pi_0 = \frac{1}{2}\int_0^L \left[\sum_{el} \int_0^{b_{el}} \lambda\sigma^0 \left\{ t(\mathrm{w}_n\psi')^2 + t(\mathrm{w}_s\psi')^2 + \frac{1}{12}t^3(\mathrm{w}_{n,s}\psi')^2 \right\} ds \right] dz \tag{15}$$

Introducing the displacement interpolation functions into the internal elastic potential energy leads to the definition of several stiffness sub-matrices as given in Table 1. The superscripts σ, τ and s correspond to components of the axial stiffness, shear stiffness and transverse stiffness, respectively. After transformation of the individual wall elements to global degrees of freedom $\mathbf{v}_\mathrm{w}$ and $\mathbf{v}_\Omega$ and assembly, the cross-section elastic potential as introduced in [15] takes the form

$$\Pi_{int} = \frac{1}{2}\int_0^L \left\{ \begin{bmatrix} \psi\mathbf{v}_\mathrm{w}^T & \psi\mathbf{v}_\Omega^T \end{bmatrix}'' \begin{bmatrix} \mathbf{K}^\sigma_{\mathrm{ww}} & \mathbf{0} \\ \mathbf{0} & \mathbf{K}^\sigma_{\Omega\Omega} \end{bmatrix} \begin{bmatrix} \psi\mathbf{v}_\mathrm{w} \\ \psi\mathbf{v}_\Omega \end{bmatrix}'' + \begin{bmatrix} \psi\mathbf{v}_\mathrm{w}^T & \psi\mathbf{v}_\Omega^T \end{bmatrix}' \begin{bmatrix} \mathbf{K}^\tau_{\mathrm{ww}} & \mathbf{K}^\tau_{\mathrm{w}\Omega} \\ \mathbf{K}^\tau_{\Omega\mathrm{w}} & \mathbf{K}^\tau_{\Omega\Omega} \end{bmatrix} \begin{bmatrix} \psi\mathbf{v}_\mathrm{w} \\ \psi\mathbf{v}_\Omega \end{bmatrix}' + \begin{bmatrix} \psi\mathbf{v}_\mathrm{w}^T & \psi\mathbf{v}_\Omega^T \end{bmatrix} \begin{bmatrix} \mathbf{K}^s & \mathbf{0} \\ \mathbf{0} & \mathbf{0} \end{bmatrix} \begin{bmatrix} \psi\mathbf{v}_\mathrm{w} \\ \psi\mathbf{v}_\Omega \end{bmatrix} \right\} dz \tag{16}$$

Besides the global stiffness matrices $\mathbf{K}$ in Eq. (16), a bold zero $\mathbf{0}$ denotes here and in the following a suitable size matrix or vector of zeroes.

Let us also perform the same operations with the initial stress contribution to the potential energy. The introduction of the displacement interpolations leads to the definition of the geometric stiffness matrix for a single wall element as follows:

$$\mathbf{k}^0 = \int_0^{b_e} \left\{ t\sigma^0[\mathbf{N}_n^T\mathbf{N}_n] + t\sigma^0[\mathbf{N}_s^T\mathbf{N}_s] + \frac{1}{12}t^3\sigma^0[\mathbf{N}_{n,s}^T\mathbf{N}_{n,s}] \right\} ds \tag{17}$$

Transforming from local, $\mathbf{v}_\mathrm{w}^{el}$, to global, $\mathbf{v}_\mathrm{w}$, components using a standard formal finite element transformation and assembly matrix $\mathbf{T}_\mathrm{w}$ we get the following global geometrical stiffness matrix:

$$\mathbf{K}^0 = \sum_{el} \mathbf{T}_\mathrm{w}^T\mathbf{k}^0\mathbf{T}_\mathrm{w} \tag{18}$$

Hereby Eq. (15) in reduced form can be rewritten as

$$\Pi_0 = \frac{1}{2}\int_0^L \left\{ \begin{bmatrix} \psi\mathbf{v}_\mathrm{w}^T & \psi\mathbf{v}_\Omega^T \end{bmatrix}' \begin{bmatrix} \lambda\mathbf{K}^0 & \mathbf{0} \\ \mathbf{0} & \mathbf{0} \end{bmatrix} \begin{bmatrix} \psi\mathbf{v}_\mathrm{w} \\ \psi\mathbf{v}_\Omega \end{bmatrix}' \right\} dz \tag{19}$$

which is the contribution to the potential energy from the factored initial stress.

Table 1
Elastic stiffness contributions of one wall element.

$$\mathbf{k}^\sigma_{\Omega\Omega} = \int_0^{b_e} Et\mathbf{N}_\Omega^T\mathbf{N}_\Omega \, ds$$

$$\mathbf{k}^\sigma_{\mathrm{ww}} = \int_0^{b_e} \frac{Et^3}{12}\mathbf{N}_n^T\mathbf{N}_n \, ds$$

$$\mathbf{k}^s = \int_0^{b_e} \left(E_s t\mathbf{N}_{s,s}^T\mathbf{N}_{s,s} + \frac{E_s t^3}{12}\mathbf{N}_{n,ss}^T\mathbf{N}_{n,ss} \right) ds$$

$$\mathbf{k}^\tau_{\mathrm{ww}} = \int_0^{b_e} \left(Gt\mathbf{N}_s^T\mathbf{N}_s + \frac{Gt^3}{3}\mathbf{N}_{n,s}^T\mathbf{N}_{n,s} \right) ds$$

$$\mathbf{k}^\tau_{\Omega\Omega} = \int_0^{b_e} Gt\mathbf{N}_{\Omega,s}^T\mathbf{N}_{\Omega,s} \, ds$$

$$\mathbf{k}^\tau_{\mathrm{w}\Omega} = [\mathbf{k}^\tau_{\Omega\mathrm{w}}]^T = -\int_0^{b_e} Gt\mathbf{N}_s^T\mathbf{N}_{\Omega,s} \, ds$$

4. GBT differential equations with initial stress

To obtain a formulation resembling a generalization of Vlasov beam theory including distortion, the following main steps need to be performed as in the related papers [15,16].

4.1. Step I: pure axial extension and influence of shear constraints

In this step, we introduce the shear constraint equations that bind axial and transverse modes together and at the same time simplify or condense Eq. (16). In this process we need to eliminate the singularity in the shear stiffness matrix related to pure axial extension. Performing step I as in the related papers the differential equations governing the stability problem can be derived by considering the first variation of the initial stress contributions to the potential energy in the same way as the first variation of the traditional elastic potential energy provided the differential equations in the related papers [15,16]:

$$\delta\Pi_0 = \int_0^L \left\{ \delta(\psi\mathbf{v}_\mathrm{w}^T)'\lambda\mathbf{K}^0(\psi\mathbf{v}_\mathrm{w})' \right\} dz \tag{20}$$

After performing partial integration the variation of the initial stress contributions to the potential energy take the form:

$$\delta\Pi_0 = \int_0^L \left\{ \delta(\psi\mathbf{v}_\mathrm{w}^T)[-(\lambda\mathbf{K}^0\mathbf{v}_\mathrm{w}\psi')'] \right\} ds + \left[\delta(\psi\mathbf{v}_\mathrm{w}^T)[\lambda\mathbf{K}^0(\psi\mathbf{v}_\mathrm{w})'] \right]_0^L \tag{21}$$

where the term in the square bracket correspond to the boundary loads and boundary conditions. As in the related paper [15] the pure axial displacement mode is identified and denoted by superscript a and the remaining axial displacement modes by superscript r. Substituting $\delta\Pi_{int}$ from the related paper leads to the following coupled homogeneous differential equations of GBT including initial stresses in which we note that $\zeta = -\psi'$:

$$(\overline{\mathbf{K}}^\sigma\mathbf{v}_\mathrm{w}\psi'')'' - (\mathbf{K}^{\sigma ra}_{\Omega\Omega}\nu^a_\Omega\zeta')'' - ([\mathbf{K}^\tau\mathbf{v}_\mathrm{w} + \lambda\mathbf{K}^0\mathbf{v}_\mathrm{w}]\psi')' + \mathbf{K}^s\mathbf{v}_\mathrm{w}\psi = \mathbf{0} \tag{22}$$

$$(\mathbf{K}^{\sigma ar}_{\Omega\Omega}\mathbf{v}_\mathrm{w}\psi'')' - (\mathbf{K}^{\sigma aa}_{\Omega\Omega}\nu^a_\Omega\zeta')' = \mathbf{0} \tag{23}$$

These equations establish a coupled set of homogeneous GBT differential equations, that determine the displacements of a thin-walled beam for a given set of boundary conditions. Note that ν^a_Ω is one component that corresponds to the amount of pure axial extension.

Now we seek solutions to the equations. As in paper [15] we can identify pure axial extension as a solution which takes the form

$$\zeta(z) = -\psi'(z) = c_{a1} + c_{a2}z = -\mathbf{\Psi}'_a(z)\,\mathbf{c}_a = [1 \;\; z]\begin{bmatrix} c_{a1} \\ c_{a2} \end{bmatrix} \tag{24}$$

where c_{a1} and c_{a2} are constants determined by the boundary conditions of axial extension.

Having identified the "trivial" displacement mode, pure axial extension, we turn to the solution of the transverse displacement modes. Eliminating ζ'' by using the fact that $\zeta''=-\psi'''$ and assuming that $\psi'''\neq 0$, we find:

$$v_{\Omega}^{a}=-(\mathbf{K}_{\Omega\Omega}^{\sigma a a})^{-1}\mathbf{K}_{\Omega\Omega}^{\sigma a r}\mathbf{v}_{\mathrm{w}} \tag{25}$$

Using this equation or Eq. (23), we eliminate the second term in Eq. (22). This results in the following homogeneous fourth order differential equations for determination of the transverse (global, distortional and local) distortional displacement modes of GBT:

$$\mathbf{K}^{\sigma}\mathbf{v}_{\mathrm{w}}\psi''''-\left([\mathbf{K}^{\tau}+\lambda\mathbf{K}^{0}]\mathbf{v}_{\mathrm{w}}\psi'\right)'+\mathbf{K}^{s}\mathbf{v}_{\mathrm{w}}\psi=\mathbf{0} \tag{26}$$

where $\mathbf{K}^{\sigma}$, $\mathbf{K}^{\tau}$ and $\mathbf{K}^{s}$ which are constants are given in the related paper [15]. In general $\mathbf{K}^{0}$ is a function of the axial coordinate z corresponding to the longitudinal contribution of the initial stress. However, in the present context the initial stress will be assumed uniformly distributed and constant whereby $\mathbf{K}^{0}$ is also independent of the axial coordinate z and the equation simplifies to

$$\mathbf{K}^{\sigma}\mathbf{v}_{\mathrm{w}}\psi''''-[\mathbf{K}^{\tau}+\lambda\mathbf{K}^{0}]\mathbf{v}_{\mathrm{w}}\psi''+\mathbf{K}^{s}\mathbf{v}_{\mathrm{w}}\psi=\mathbf{0} \tag{27}$$

This set of GBT column stability equations resemble the conventional equation for classic column stability. Now the number of degrees of freedom is $n_{dof}=3n_{no}$, since all (n_{no}) axial dofs $\mathbf{v}_{\Omega}$ have been eliminated by the shear constraint equation and the pure axial deformation mode.

4.2. Step II: translations, constant wall width and reduction of order

In this step we treat two modes corresponding to transverse translations of the cross section and one mode corresponding to pure rotation. We also constrain the transverse displacement field so that the wall widths remain constant, i.e. we enforce $\mathrm{w}_{s,s}\equiv 0$.

Let us do this by first using the following transformation fully described in [15]:

$$\mathbf{v}_{\mathrm{w}}=[\mathbf{T}_{\mathrm{w}}^{\alpha}\ \ \mathbf{T}_{\mathrm{w}}^{3}\ \ \tilde{\mathbf{T}}_{\mathrm{w}}^{u}]\begin{bmatrix}\mathbf{v}_{\mathrm{w}}^{\alpha}\\ v_{\mathrm{w}}^{3}\\ \mathbf{v}_{\mathrm{w}}^{u}\end{bmatrix} \tag{28}$$

Here the two orthogonal translational eigenmodes are ordered in the transformation matrix $\mathbf{T}_{\mathrm{w}}^{\alpha}$ and the orthogonal pure rotational eigenmode in $\mathbf{T}_{\mathrm{w}}^{3}$. The identification of the constrained degrees of freedom to be eliminated is performed by a transformation matrix $\mathbf{T}_{\mathrm{w}}^{c}$ while the remaining unconstrained degrees of freedom are identified in the transformation matrix $\mathbf{T}_{\mathrm{w}}^{u}$. By expressing the constrained degrees of freedom by the unconstrained we find the total condensed transformation introduced as $\tilde{\mathbf{T}}_{\mathrm{w}}^{u}$, as derived in [15].

Using this transformation to transform the differential equations in (27), and introducing the null terms corresponding to the rigid-body modes and zero shear strain for translational and flexural modes, the differential equations take the following form:

$$\begin{bmatrix}\mathbf{K}_{\alpha\alpha}^{\sigma} & \mathbf{0} & \mathbf{K}_{\alpha u}^{\sigma}\\ \mathbf{0} & K_{33}^{\sigma} & \mathbf{K}_{3u}^{\sigma}\\ \mathbf{K}_{u\alpha}^{\sigma} & \mathbf{K}_{u3}^{\sigma} & \mathbf{K}_{uu}^{\sigma}\end{bmatrix}\begin{bmatrix}\mathbf{v}_{\mathrm{w}}^{\alpha}\\ v_{\mathrm{w}}^{3}\\ \mathbf{v}_{\mathrm{w}}^{u}\end{bmatrix}\psi''''-\left(\begin{bmatrix}\mathbf{0} & \mathbf{0} & \mathbf{0}\\ \mathbf{0} & K_{33}^{\tau} & \mathbf{K}_{3u}^{\tau}\\ \mathbf{0} & \mathbf{K}_{u3}^{\tau} & \mathbf{K}_{uu}^{\tau}\end{bmatrix}+\lambda\begin{bmatrix}\mathbf{K}_{\alpha\alpha}^{0} & \mathbf{K}_{\alpha 3}^{0} & \mathbf{K}_{\alpha u}^{0}\\ \mathbf{K}_{3\alpha}^{0} & K_{33}^{0} & \mathbf{K}_{3u}^{0}\\ \mathbf{K}_{u\alpha}^{0} & \mathbf{K}_{u3}^{0} & \mathbf{K}_{uu}^{0}\end{bmatrix}\right)\begin{bmatrix}\mathbf{v}_{\mathrm{w}}^{\alpha}\\ v_{\mathrm{w}}^{3}\\ \mathbf{v}_{\mathrm{w}}^{u}\end{bmatrix}\psi''+\begin{bmatrix}\mathbf{0} & \mathbf{0} & \mathbf{0}\\ \mathbf{0} & 0 & \mathbf{0}\\ \mathbf{0} & \mathbf{0} & \mathbf{K}_{uu}^{s}\end{bmatrix}\begin{bmatrix}\mathbf{v}_{\mathrm{w}}^{\alpha}\\ v_{\mathrm{w}}^{3}\\ \mathbf{v}_{\mathrm{w}}^{u}\end{bmatrix}\psi=\begin{bmatrix}\mathbf{0}\\ 0\\ \mathbf{0}\end{bmatrix} \tag{29}$$

The transformed stiffness matrices are found and described in paper [15] and the $\mathbf{K}^{0}$-matrices are given in Table 2. Now the number of degrees of freedom depends on the geometry of the cross section. We have constrained the transverse displacement field so that the wall widths remain constant, i.e. we enforce $\mathrm{w}_{s,s}\equiv 0$. This means that a single w_{s}−dof is eliminated for each element in the cross section. For a lipped channel cross section with $n_{el}=n_{no}-1$ elements this means that $n_{dof}=3n_{no}-n_{el}=2n_{no}+1$. For a box cross section with $n_{el}=n_{no}$ elements it means that $n_{dof}=3n_{no}-n_{el}=2n_{no}$.

Table 2
Transformation of K^{0}-stiffness matrices related to Step II.

$\mathbf{K}_{\alpha\alpha}^{0}=\mathbf{T}_{\mathrm{w}}^{\alpha\ T}\mathbf{K}^{0}\mathbf{T}_{\mathrm{w}}^{\alpha}$	$\mathbf{K}_{\alpha 3}^{0}=\mathbf{T}_{\mathrm{w}}^{\alpha\ T}\mathbf{K}^{0}\mathbf{T}_{\mathrm{w}}^{3}$	$K_{\alpha u}^{0}=\mathbf{T}_{\mathrm{w}}^{\alpha\ T}\mathbf{K}^{0}\mathbf{T}_{\mathrm{w}}^{u}$
$\mathbf{K}_{3\alpha}^{0}=\mathbf{T}_{\mathrm{w}}^{3\ T}\mathbf{K}^{0}\mathbf{T}_{\mathrm{w}}^{\alpha}$	$K_{33}^{0}=\mathbf{T}_{\mathrm{w}}^{3\ T}\mathbf{K}^{0}\mathbf{T}_{\mathrm{w}}^{3}$	$\mathbf{K}_{3u}^{0}=\mathbf{T}_{\mathrm{w}}^{3\ T}\mathbf{K}^{0}\tilde{\mathbf{T}}_{\mathrm{w}}^{u}$
$\mathbf{K}_{u\alpha}^{0}=\tilde{\mathbf{T}}_{\mathrm{w}}^{u\ T}\mathbf{K}^{0}\mathbf{T}_{\mathrm{w}}^{\alpha}$	$\mathbf{K}_{u3}^{0}=\tilde{\mathbf{T}}_{\mathrm{w}}^{u\ T}\mathbf{K}^{0}\mathbf{T}_{\mathrm{w}}^{3}$	$\mathbf{K}_{uu}^{0}=\tilde{\mathbf{T}}_{\mathrm{w}}^{u\ T}\mathbf{K}^{0}\tilde{\mathbf{T}}_{\mathrm{w}}^{u}$

To solve this differential equation we choose to reduce the differential order of the coupled fourth-order differential equations and the related quadratic eigenvalue problem to twice as many coupled second-order differential equations with a related linear eigenvalue problem of double size. This is done in the following. This method is equivalent to the one used for the solution of the coupled homogeneous problem of one-mode distortion and torsion analyzed in [23].

The fourth order differential Eq. (29) can be transformed into twice as many second order differential equations by introducing what is called a state vector. There are a number of different possible formulations, but we have chosen the use of the state vector $\mathbf{u}_{S}=[\mathbf{v}_{\mathrm{w}}^{\alpha}\psi,v_{\mathrm{w}}^{3}\psi,\mathbf{v}_{\mathrm{w}}^{u}\psi,\mathbf{v}_{\mathrm{w}}^{\alpha}\psi'',v_{\mathrm{w}}^{3}\psi'',\mathbf{v}_{\mathrm{w}}^{u}\psi'']^{T}$. Introducing this state vector (and using related equality block equations) yields a reformulation of Eq. (29) as a formal second order matrix differential equation of double size which takes the form:

$$\left[\begin{array}{ccc|ccc}\mathbf{0} & \mathbf{0} & \mathbf{0} & \mathbf{0} & \mathbf{0} & \mathbf{0}\\ \mathbf{0} & 0 & \mathbf{0} & \mathbf{0} & 0 & \mathbf{0}\\ \mathbf{0} & \mathbf{0} & \mathbf{K}_{uu}^{s} & \mathbf{0} & \mathbf{0} & \mathbf{0}\\ \hline \mathbf{0} & \mathbf{0} & \mathbf{0} & -\mathbf{K}_{\alpha\alpha}^{\sigma} & \mathbf{0} & -\mathbf{K}_{\alpha u}^{\sigma}\\ \mathbf{0} & 0 & \mathbf{0} & \mathbf{0} & -K_{33}^{\sigma} & -\mathbf{K}_{3u}^{\sigma}\\ \mathbf{0} & \mathbf{0} & \mathbf{0} & -\mathbf{K}_{u\alpha}^{\sigma} & -\mathbf{K}_{u3}^{\sigma} & -\mathbf{K}_{uu}^{\sigma}\end{array}\right]\left[\begin{array}{c}\mathbf{v}_{\mathrm{w}}^{\alpha}\psi\\ v_{\mathrm{w}}^{3}\psi\\ \mathbf{v}_{\mathrm{w}}^{u}\psi\\ \hline \mathbf{v}_{\mathrm{w}}^{\alpha}\psi''\\ v_{\mathrm{w}}^{3}\psi''\\ \mathbf{v}_{\mathrm{w}}^{u}\psi''\end{array}\right]$$
$$-\left(\left[\begin{array}{ccc|ccc}\mathbf{0} & \mathbf{0} & \mathbf{0} & -\mathbf{K}_{\alpha\alpha}^{\sigma} & \mathbf{0} & -\mathbf{K}_{\alpha u}^{\sigma}\\ \mathbf{0} & K_{33}^{\tau} & \mathbf{K}_{3u}^{\tau} & \mathbf{0} & -K_{33}^{\sigma} & -\mathbf{K}_{3u}^{\sigma}\\ \mathbf{0} & \mathbf{K}_{u3}^{\tau} & \mathbf{K}_{uu}^{\tau} & -\mathbf{K}_{u\alpha}^{\sigma} & -\mathbf{K}_{u3}^{\sigma} & -\mathbf{K}_{uu}^{\sigma}\\ \hline -\mathbf{K}_{\alpha\alpha}^{\sigma} & \mathbf{0} & -\mathbf{K}_{\alpha u}^{\sigma} & \mathbf{0} & \mathbf{0} & \mathbf{0}\\ \mathbf{0} & -K_{33}^{\sigma} & -\mathbf{K}_{3u}^{\sigma} & \mathbf{0} & 0 & \mathbf{0}\\ -\mathbf{K}_{u\alpha}^{\sigma} & -\mathbf{K}_{u3}^{\sigma} & -\mathbf{K}_{uu}^{\sigma} & \mathbf{0} & \mathbf{0} & \mathbf{0}\end{array}\right]+\lambda\left[\begin{array}{ccc|ccc}\mathbf{K}_{\alpha\alpha}^{0} & \mathbf{K}_{\alpha 3}^{0} & \mathbf{K}_{\alpha u}^{0} & \mathbf{0} & \mathbf{0} & \mathbf{0}\\ \mathbf{K}_{3\alpha}^{0} & K_{33}^{0} & \mathbf{K}_{3u}^{0} & \mathbf{0} & 0 & \mathbf{0}\\ \mathbf{K}_{u\alpha}^{0} & \mathbf{K}_{u3}^{0} & \mathbf{K}_{uu}^{0} & \mathbf{0} & \mathbf{0} & \mathbf{0}\\ \hline \mathbf{0} & \mathbf{0} & \mathbf{0} & \mathbf{0} & \mathbf{0} & \mathbf{0}\\ \mathbf{0} & 0 & \mathbf{0} & \mathbf{0} & 0 & \mathbf{0}\\ \mathbf{0} & \mathbf{0} & \mathbf{0} & \mathbf{0} & \mathbf{0} & \mathbf{0}\end{array}\right]\right)\left[\begin{array}{c}\mathbf{v}_{\mathrm{w}}^{\alpha}\psi\\ v_{\mathrm{w}}^{3}\psi\\ \mathbf{v}_{\mathrm{w}}^{u}\psi\\ \hline \mathbf{v}_{\mathrm{w}}^{\alpha}\psi''\\ v_{\mathrm{w}}^{3}\psi''\\ \mathbf{v}_{\mathrm{w}}^{u}\psi''\end{array}\right]''=\left[\begin{array}{c}\mathbf{0}\\ 0\\ \mathbf{0}\\ \hline \mathbf{0}\\ 0\\ \mathbf{0}\end{array}\right] \tag{30}$$

which we choose to abbreviate as follows using the block structure shown in Eq. (30):

$$\begin{bmatrix}\tilde{\mathbf{K}}^{s} & \mathbf{0}\\ \mathbf{0} & -\tilde{\mathbf{K}}^{\sigma}\end{bmatrix}\begin{bmatrix}\tilde{\mathbf{v}}_{\mathrm{w}}\psi\\ \tilde{\mathbf{v}}_{\mathrm{w}}\psi''\end{bmatrix}-\left(\begin{bmatrix}\tilde{\mathbf{K}}^{\tau} & -\tilde{\mathbf{K}}^{\sigma}\\ -\tilde{\mathbf{K}}^{\sigma} & \mathbf{0}\end{bmatrix}+\lambda\begin{bmatrix}\tilde{\mathbf{K}}^{0} & \mathbf{0}\\ \mathbf{0} & \mathbf{0}\end{bmatrix}\right)\begin{bmatrix}\tilde{\mathbf{v}}_{\mathrm{w}}\psi\\ \tilde{\mathbf{v}}_{\mathrm{w}}\psi''\end{bmatrix}''=\begin{bmatrix}\mathbf{0}\\ \mathbf{0}\end{bmatrix} \tag{31}$$

This is the set of differential equations to which we want to find solutions.

5. The distortional initial stress eigenvalue problem

In the reduced order differential equations in (31) we substitute **A**, **B**, **C** and $\mathbf{u}_S$ for the respective matrices and vector in the equation. This means that **A** and **B** are linear stiffness matrices, **C** a geometrical stiffness matrix and $\mathbf{u}_S$ a vector containing the longitudinal amplitude functions. Thus it takes the following form:

$$\mathbf{A}\mathbf{u}_S - [\mathbf{B}+\lambda\mathbf{C}]\mathbf{u}_S'' = \mathbf{0} \tag{32}$$

This set of differential equations are homogeneous with constant coefficients and therefore lead to solution functions of exponential type.

By postulating exponential solutions of the form $\mathbf{u}_S = \mathbf{v}_S\psi(z)$, where the state space vector $\mathbf{v}_S$ is independent of the axial coordinate z and $\psi(z) = e^{\xi z}$, and inserting the solution the following special eigenvalue problem is obtained:

$$\mathbf{A}\mathbf{v}_S - \xi^2[\mathbf{B}+\lambda\mathbf{C}]\mathbf{v}_S = \mathbf{0} \tag{33}$$

In the classic stability theory the solution function $\psi(z)$ is normally assumed to be a trigonometric function in order to satisfy suitable simple boundary conditions, see [24]. This means that $\xi = \mu i$ is a known (complex) parameter and that λ can be determined as the eigenvalue equivalent to the instability load factor, which determines the level of stress at which the structure becomes unstable. The eigenvalues and the corresponding eigenvectors $\mathbf{v}_S$ can be found by solving the eigenvalue problem.

In order to satisfy suitable simple boundary conditions let us therefore assume that the solution is of a simple trigonometric form here chosen as

$$\psi(z) = \sin \mu z \tag{34}$$

where $\mu = n\pi/L$ in which n is equal to the number of buckles, i.e. half-wavelengths. This solution satisfies boundary conditions corresponding to simple supports with restrained transverse cross-section displacements at $z=0$ and $z=L$. Inserting this postulated solution in Eq. (32) and remembering the change of sign related to double differentiation of the sine function leads to the following generalized linear symmetric matrix eigenvalue problem, in which the eigenvalues, λ, correspond to the buckling factor and the eigenvectors are the distortional state space buckling modes:

$$\left[\mathbf{A} + \left(\frac{n\pi}{L}\right)^2\mathbf{B}\right]\mathbf{v}_S + \lambda\left(\frac{n\pi}{L}\right)^2\mathbf{C}\mathbf{v}_S = \mathbf{0} \tag{35}$$

Eliminating the second half of vector $\mathbf{v}_S$ corresponding to $\tilde{\mathbf{v}}_w\psi''$ in Eq. (31) leads to the following final generalized linear symmetric matrix eigenvalue problem:

$$[\mathbf{K}+\lambda\mathbf{G}]\tilde{\mathbf{v}}_w = \mathbf{0} \tag{36}$$

in which **K** and **G** are given in Table 3 as functions of the inverse length scale parameter μ.

From the results of this eigenvalue problem we know at which load (λ) the corresponding mode has a homogeneous solution function which is sinusoidal with a number of half-waves corresponding to n. Here the number of degrees of freedom for a lipped channel cross section is $n_{dof} = 2n_{no}+1$, while the number of degrees of freedom for a box cross section is $n_{dof} = 2n_{no}$. The number of dofs is equal to the number of eigenvalues. In the following we will see this applied in the examples.

Table 3
Definition of **K** and **G**.

$\mathbf{K} = \tilde{\mathbf{K}}^s + \mu^2\tilde{\mathbf{K}}^\tau + \mu^4\tilde{\mathbf{K}}^\sigma$	$\mathbf{G} = \mu^2\tilde{\mathbf{K}}^0$

6. Examples

In this section the developed GBT approach is used to give illustrative examples of the trigonometric buckling solutions of the differential GBT equations with initial stress. The ability of the GBT approach to produce buckling curves and predict buckling is shown. The examples consider simply supported columns in uniform compression. The end sections are constrained against transverse displacements, but otherwise free to warp (and thus also rotate). The two examples are based on a lipped channel section and a rectangular hollow section, respectively.

In each example the buckling signature curves of the cross section are developed corresponding to the buckling stress versus the buckling half-wavelength for the four lowest buckling modes. This is done by solving the GBT eigenvalue problem for consecutive values of the half-wavelength. For each buckling curve it is shown that the transverse buckling mode shape varies with the buckle half-wavelength. The buckling signature curve is used to develop the overall buckling curve including multiple buckling waves by shifting the signature curve sides ways corresponding to a number of half-wavelengths. Chosen buckling modes for given column lengths are used to illustrate local, distortional and global buckling modes. The accuracy of the results are assessed by comparison to results obtained by the use of the commercial FE program Abaqus.

The results found using Abaqus are based on isotropic material and the 4 node S4 shell element with full 4 point integration. The linear elastic finite element calculations are based on a structured rectangular mesh with a side length seed of 5 mm. The cross section is fixed in the transverse directions at both ends and fixed at one node against longitudinal translation. All supports are continuous line supports. Two identical normal forces are applied as a uniform distributed shell edge load; one at each end. For further and more detailed explanations see also [20]. This finite element model results in local transverse stress near the end supports due to the Poisson effect. These end stresses have an influence on the buckling, which is not included in the FSM or GBT models.

6.1. Example 1: buckling of a lipped channel column

In this example the buckling of a simply supported lipped channel column in pure compression is analyzed. The chosen in-plane geometry and the discretization is shown in Fig. 4.

Solving the GBT initial stress eigenvalue problem given in Eq. (35) with n=1 for half-wavelengths L varying from 10 mm to 3000 mm (logarithmical spaced) allows the development of the signature curve (buckling stress versus the buckle half wavelength) as shown in Fig. 5. Thus the buckling curves shown in the figure correspond to the four lowest buckling modes with one half-wave buckle, $n=1$. For three different half-wavelengths the transverse buckling mode shape has been included in the figure. It is clear that the mode shape of each curve changes gradually as a function of the length. The chosen half-wavelengths correspond to the dashed lines at 70 mm, 500 mm and 2000 mm, respectively. To illuminate the changes in the deformation modes for increasing length we have chosen also to show the buckling mode shapes in 3D in Fig. 6. The mode shapes are shown as a 3D representation even though the results are provided by a one-dimensional beam formulation.

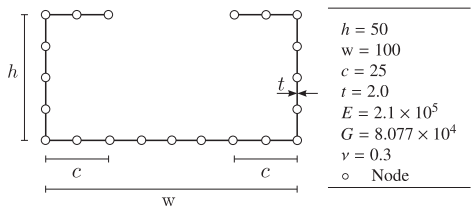

Fig. 4. Geometry, discretization and parameter values of a lipped channel column.

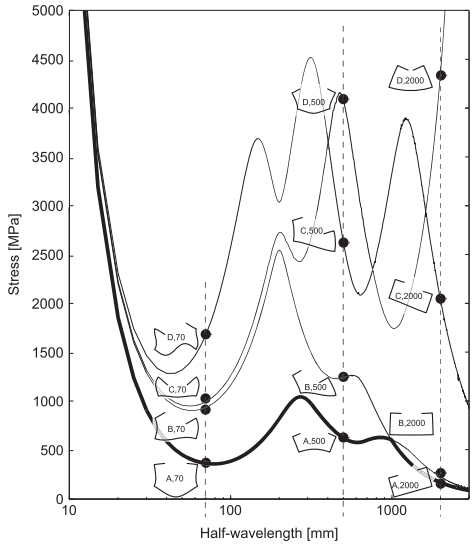

Fig. 5. Buckling signature curve corresponding to the lowest four modes with a single half-wave buckle, $n=1$.

From the figures it is seen that each developing mode represents its own curve placed in a hierarchical order according to the stress level. However, the curves are able to change place in the hierarchy at a certain column length. This phenomenon can for example be seen for buckling mode 1 and 2 (two lowest ranking graphs) at a column length of approximately 1000 mm. The signature curve, shown bold, is achieved as the very lowest of the buckling curves. For this curve a short column lengths correspond to local buckling, while for increasing column lengths it corresponds to distortional buckling and finally for large column lengths it corresponds to global buckling. The signature curve is similar to the finite strip buckling curve obtained by Hancock [25].

As mentioned Fig. 5 is for a half-wave number $n=1$. As the buckling loads also depend on the number of n half waves in the buckled shapes, this means that points lower than the signature curve can exist for a greater number of buckles, $n>1$. To show this phenomenon the signature curve has been created for a varying number of n as shown in Fig. 7.

This means that the bold curve shown in Fig. 7 represents the absolute lowest curve for the buckling stress versus column length. However, to illustrate the multitude of buckling modes for each column length, let us look at a column length of $L=1000$ mm. In Fig. 7 this length is represented by the vertical dashed line. For this length we can find the buckling modes $m=1,2,3..$ ordered from lowest to highest critical stress, each having a different number of half waves n.

In Table 4 the buckling stresses of FE analysis using Abaqus [20] versus the presented GBT method, conventional GBT using GBTUL [22] and FSM using CUFSM [21] are compared. The comparison is performed for suitable mode numbers (m-values) and the associated relevant buckling modes are depicted in Fig. 8, which shows the local buckling mode corresponding to the lowest critical stress ($m=1$), the global beam buckling mode ($m=20$) and a distortional mode shape ($m=24$), respectively. The three values of m have been chosen to show the spectrum of modes represented at the given beam length.

From Table 4 it is seen that for a column length of 1000 mm buckling will occur as local buckling consisting of thirteen sine half waves and have an associated buckling stress of 350 MPa. Further more it is seen that the buckling mode shape for mode $m=20$ is global column buckling with one buckle, $n=1$, at a stress level of 590 Mpa and finally for $m=24$ distortional column buckling occurs at a stress level of 918 Mpa.

Comparing the GBT buckling stresses with Abaqus we obtain a deviation of 13.4% for local plate buckling, 1.7% for global buckling and 1.7% for distortional buckling. Hereby it is seen that good results are obtained for global and distortional buckling, while a rather large deviation is obtained for local buckling. The same phenomenon is seen from the GBTUL results which are based on the classic GBT theory. Here a deviation of 7.9% is obtained for local plate buckling and 1.6% for global buckling. In contrast to these beam theory results, Table 4 also shows results obtained from the CUFSM program which is based on a plate theory. Here we obtain a deviation of 2.0% for local plate buckling, 0.2% for global buckling and 0.3% for distortional buckling, showing that good results are obtained in all cases. From the deviations it is obvious that GBT and GBTUL are based on beam theories while CUFSM is based on plate theory. The rather large deviation of 13.4% for the GBT results compared with the deviation of 7.9% obtained with GBTUL, can to a certain extent be explained by the very simple constitutive relations used in the current GBT formulation. Making a calculation in Abaqus with similar very simple non-coupling constitutive relations the deviations obtained now corresponds to (350 MPa) 0.0%, (582 MPa) 1.4% and (888 MPa) 3.4%, respectively. Hereby good matches between the two approaches are obtained, however, also difference in the modeling of the boundary conditions can affect the results. Thus demonstrating that this new developed GBT approach provides reasonably accurate results with a very small computational cost, making it an alternative to the traditional and time consuming FE calculations and the other available methods. However, the constitutive relations should be modified to achieve a higher accuracy for local plate buckling.

6.2. Example 2: buckling of a rectangular hollow section column

In this example a simply supported rectangular hollow section (RHS) column is analyzed. The discretization of the cross section and the used parameters are as given in Fig. 9. Considering the given cross section and solving the eigenvalue problem in Eq. (35) the buckling signature curves can be established as depicted in Fig. 10. The buckling curves depicted corresponds to the lowest four buckling modes with a single half-wave buckle, $n=1$. In this example we have chosen to show the buckling mode shapes of the four lowest curves. The mode shapes are shown for two values of the half-wave buckling length corresponding to 200 mm and 900 mm, respectively. The corresponding 3D plots of the column buckling mode shapes are shown in Fig. 11.

From the figures it is seen that each developing mode represents its own curve placed in a hierarchical order according to the stress level. Also here it is seen that the curves are able to change place in the hierarchy. Looking at the very lowest curve

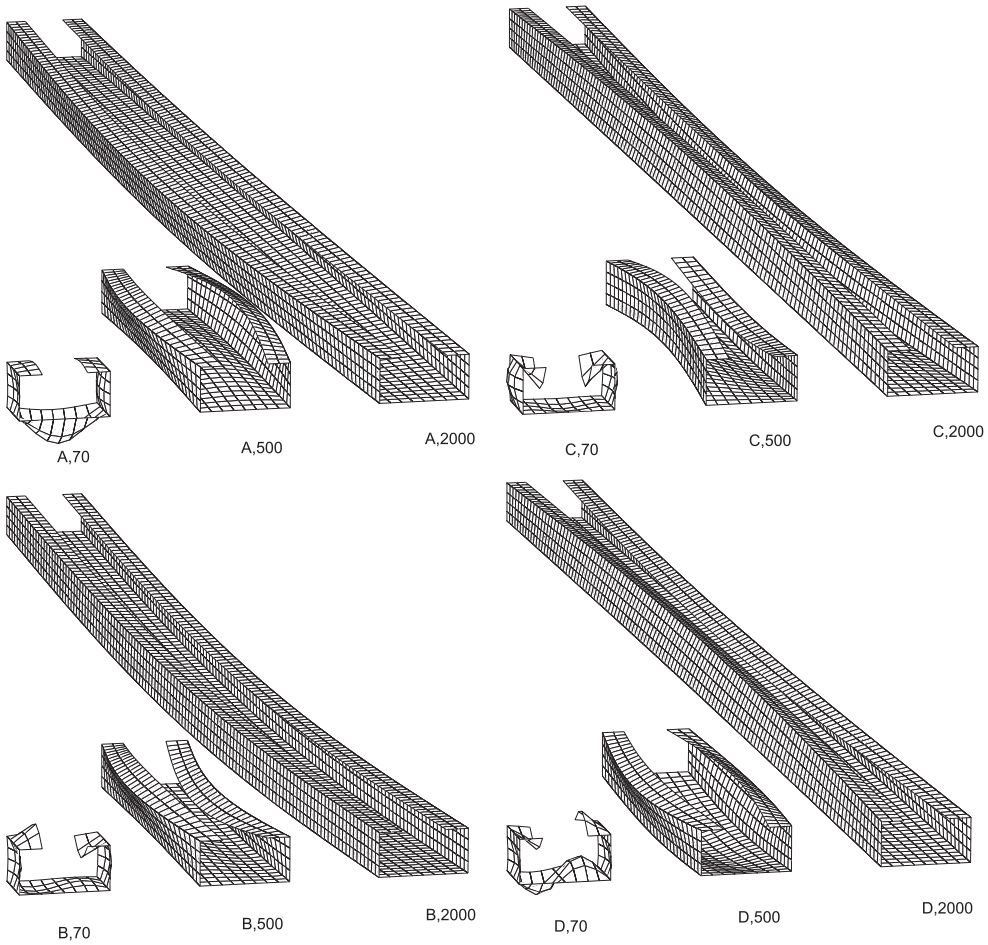

Fig. 6. Column buckling modes associated with Fig. 5 for single ($n=1$) half wavelengths of 70 mm, 500 mm and 2000 mm.

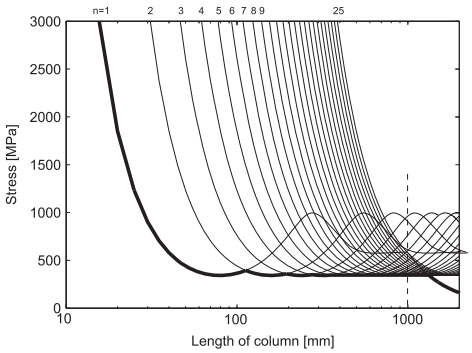

Fig. 7. Buckling stress versus column length for the lipped channel section in compression.

(the signature curve) shown as the bolded curve it is seen that short column length corresponds to local buckling, while larger column lengths correspond to global buckling.

As mentioned Fig. 10 is for a half-wave number of $n=1$. To show the signature curve for a varying number of n half waves in the buckled shapes Fig. 13 has been created. This means that Fig. 13 represent the absolute lowest curve for the buckling stress versus column length for the section given in Fig. 9. To illustrate the multitude of buckling modes for a given column length let us look at a column length of $L=1000$ mm. For this length we look at the ordered buckling modes, $m=1,2,3..$ each having a different number of half-wave buckles. In Fig. 13 this length is represented by the vertical dashed line.

In Table 5 the buckling stresses of FE analysis [20] versus the presented GBT method and FSM using CUFSM [21] are compared for suitable m-values. Further more the associated relevant

Table 4
Comparison of buckling stresses for FE analysis versus the presented GBT method, GBTUL and CUFSM, respectively. The comparisons are related to the vertical dashed m-line in Fig. 7.

m	Nr. of half waves n	Abaqus (MPa)	GBT (MPa)	Diff. (%)	GBTUL (MPa)	Diff. (%)	CUFSM (MPa)	Diff. (%)
1	13	404	350	13.4	436	7.9	412	2.0
20	1	580	590	1.7	589	1.6	581	0.2
24	3	903	918	1.7	–	–	906	0.3

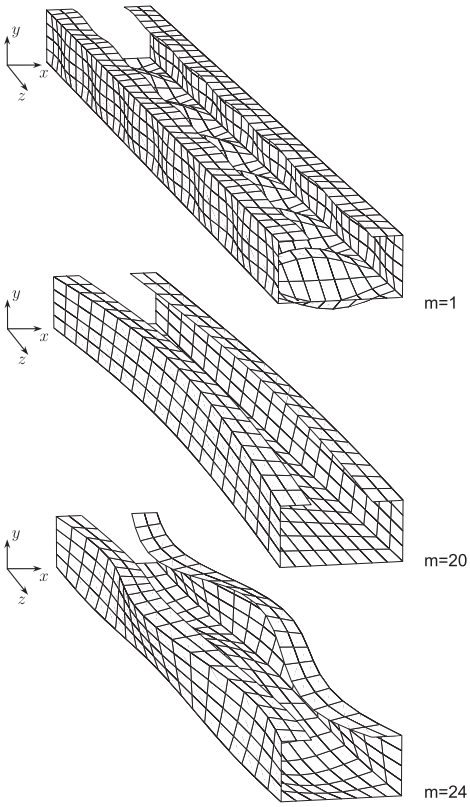

Fig. 8. GBT column buckling mode shapes of a lipped channel column in pure compression.

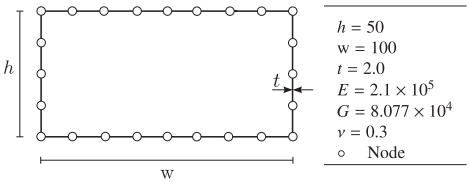

Fig. 9. Geometry and parameter values of a rectangular hollow section column.

buckling configurations are depicted in Fig. 12 representing a local buckling at the lowest critical stress ($m=1$) and a global buckling ($m=22$). The two values of m have been chosen to show the spectrum of modes represented at a given column length.

Comparing the buckling stresses corresponding to the figures in Fig. 12 with the commercial FE program Abaqus a maximum deviation of 14.1% is obtained for the first buckling mode ($m=1$) corresponding to local plate buckling while a deviation of 4.2% is obtained for m equal to 22 corresponding to global column buckling with some distortion included. Also here it is seen that good results are obtained for global buckling while a rather large deviation is obtained for local buckling. Using the CUFSM software we obtain FSM results with a deviation of 1.8% for local plate buckling and 0.7% for global buckling which confirms good results in both cases. From the given deviations it is clear that GBT results are based on a beam theory while FSM results are based on a plate theory. In contrast to Example 1 a comparison using the GBTUL

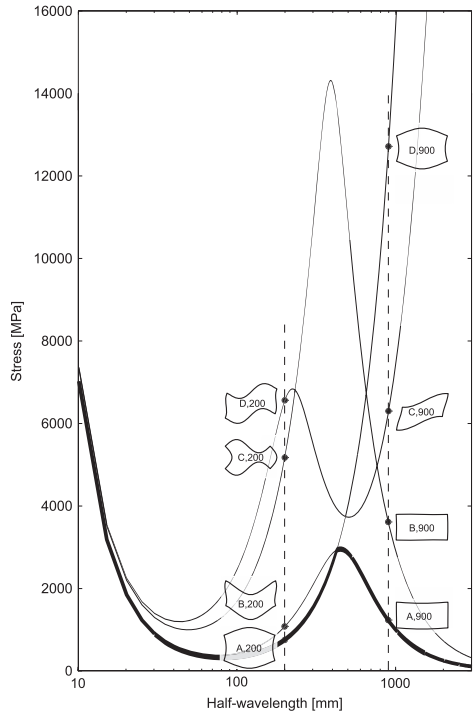

Fig. 10. Buckling signature curve corresponding to the lowest four modes with a single half-wave buckle, $n=1$.

software is not performed in this example as GBTUL cannot currently handle closed cross sections. The large deviation of 14.1% obtained by the presented GBT method can to a great extent be explained by the chosen constitutive relations in the current approach. Using identical simple non-coupling constitutive relations in the Abaqus finite element model the deviations now corresponds to (330 MPa) 0.0% and (941 MPa) 4.9%, respectively. Hereby reasonable matches between the two approaches are obtained for a rectangular hollow section, thus confirming that this new developed GBT approach provides adequate results with a very small computational cost, making it an alternative to the traditional and time consuming FE calculations and the other available methods. However, there is a need to improve the constitutive assumptions related to the local plate behavior.

7. Conclusion

This paper presented the extension of the novel GBT approach developed by the authors in [15,16] to include the geometrical stiffness terms which are need for column buckling analysis. The distortional differential equations developed in papers [15,16] are extended to a formulation including geometrical stiffness terms by using the initial stress approach to formulate the instability problem. The derived GBT differential equations with initial stress have been solved as an eigenvalue problem leading to a number of buckling modes and associated buckling stresses for simply supported columns in compression. Illustrative examples have been given dealing with a lipped channel column section and a rectangular hollow column section, respectively. In order to illustrate the application and validity of the approach the results have been compared with FE results obtained using the

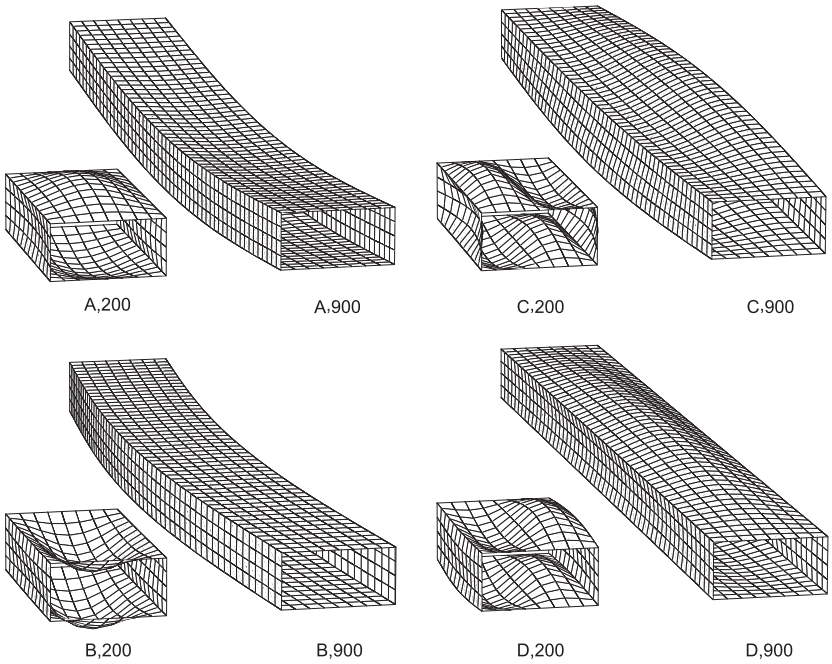

Fig. 11. Column buckling modes associated with Fig. 10 for single ($n=1$) half wavelengths of 200 mm and 900 mm.

Table 5
Comparison of buckling stresses for FE analysis versus the presented GBT method and CUFSM, respectively. The comparisons are related to the vertical dashed m-line in Fig. 13.

m	Nr. of half waves n	Abaqus (MPa)	GBT (MPa)	Diff. (%)	CUFSM (MPa)	Diff. (%)
1	12	384	330	14.1	391	1.8
22	1	947	987	4.2	940	0.7

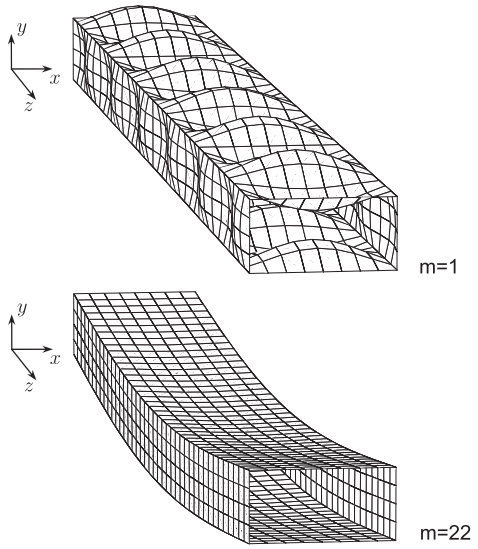

Fig. 12. GBT column buckling mode shapes of a rectangular hollow section column in pure compression.

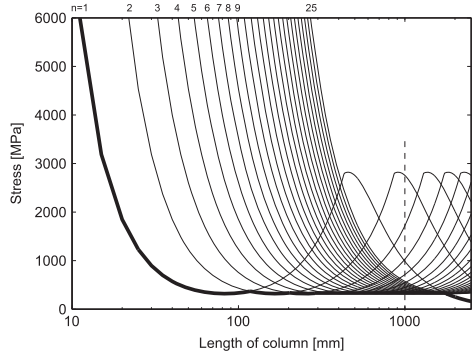

Fig. 13. Buckling stress versus column length for the rectangular hollow section in compression.

commercial program Abaqus as well as with FSM and conventional GBT results found using the freely available software packages CUFSM and GBTUL, respectively. For both sections reasonable matches are obtained confirming that this new developed GBT approach including geometrical stiffness terms provides reasonable results with a very small computational cost making it an alternative to the traditional and time consuming FE calculations and the other available methods. However, the constitutive relations may have to be modified in order to achieve higher accuracy for local plate buckling.

References

[1] Vlasov VZ. Thin-walled elastic beams. 2nd ed. Jerusalem, Israel: Israel Program for Scientific Translations; 1961.
[2] Zienkiewicz OC, Taylor RL. The finite element method. In: Basic formulations and linear problems, vol. 1, 4th ed. UK: McGraw-Hill Book Company; 1989.

[3] Hughes TJR. The finite element method: linear static and dynamic finite element analysis. Englewood Cliffs, NJ: Prentice-Hall, Inc.; 2000.
[4] Jönsson J, Krenk S, Damkilde L. Recursive substructuring of finite elements. Computers & Structures 1995;54:395–404.
[5] Cheung YK. Finite strip method in structural analysis. Oxford: Pergamon Press; 1976.
[6] Cheung YK, Tham LG. The finite strip method. Boca Raton: CRC Press; 1998.
[7] Williams FW, Wittrick WH. Computational procedures for a matrix analysis of the stability and vibrations of thin flat-walled structures in compression. International Journal of Mechanical Sciences 1968;11:798–979.
[8] Loja M, Mota Soares CM, Mota Soares CA. Modelling and design of adaptive structures using B-spline strip models. Composite Structures 2002;57(1–4) 245–51.
[9] Schafer BW, Ádány S. Modal decomposition for thin-walled member stability using the finite strip method. Advances in engineering structures, mechanics and construction.Springer; 2006. p. 411–22.
[10] Schardt R. Anwendung der erweiterten technischen biegetheorie auf die berechnung prismatischer faltwerke und zylinderschalen nach theorie I. und II. ordnung. ordnung. In: IASS—symposium on folded plates and prismatic structures, vol. 1, Wien, 1970.
[11] Davies JM, Leach P. Second-order generalised beam theory. Journal of Constructional Steel Research 1994;31:221–41.
[12] Lepistö J, Nikula S, Niemi E. Optimum design of cold-formed sections using generalized beam theory. In: Rondal J, Dubina D, Gioncu V, editors. Proceedings of the second international conference on coupled instabilities in metal structures (CIMS 1996—Liège, 05-07/09). London: Imperial College Press; 1996. p. 101–8.
[13] Simão P, Simões da Silva L. Comparative analysis of the stability of open and closed thin-walled section members in the framework of generalized beam theory. In: EUROSTEEL—proceedings of the third European conference on steel structures, vol. 1, Portugal, 2002.
[14] Camotim D, Silvestre N, Basaglia C, Bebiano R. GBT-based buckling analysis of thin-walled members with non-standard support conditions. Thin-Walled Structures 2008;46:800–15.
[15] Jönsson J, Andreassen MJ. Distortional eigenmodes and homogeneous solutions of semi-discretized thin-walled beams. Thin-Walled Structures 2011; 49:691–707.
[16] Andreassen MJ, Jönsson J. Distortional solutions for loaded semi-discretized thin-walled beams. Thin-Walled Structures 2012;50:116–27.
[17] Kollbrunner CF, Hajdin N. Dünnwandige stäbe 1, stäbe mit undeformierbaren querschnitten. Berlin: Springer-Verlag; 1972. p. 1975.
[18] Jönsson J. Determination of shear stresses warping functions and section properties of thin-walled beams using finite elements. Computers & Structures 1998;68:393–410.
[19] Jönsson J. Distortional warping functions and shear distributions in thin-walled beams. Thin-Walled Structures 1999;33:245–68.
[20] ABAQUS. Theory manual v6.8 Simulia, 2008.
[21] Li Z, Schafer BW. Buckling analysis of cold-formed steel members with general boundary conditions using CUFSM: conventional and constrained finite strip methods. In: Proceedings of the 20th international special conference on cold-formed steel structures, St. Louis, MO, November 2010.
[22] Bebiano R, Pina P, Silvestre N, Camotim D. GBTUL—buckling and vibration analysis of thin-walled members. DECivil/IST, Technical University of Lisbon 〈http://www.civil.ist.utl.pt/gbt〉; 2008.
[23] Jönsson J. Distortional theory of thin-walled beams. Thin-Walled Structures 1999;33:269–303.
[24] Timoshenko SP, Gere JM. Theory of elastic stability. New York: McGraw-Hill; 1961.
[25] Hancock GJ. Distortional buckling of steel storage rack column. Journal of Structural Engineering 1985;111(12).

Appendix E

Paper IV

Michael Joachim Andreassen and Jeppe Jönsson, (2013).

A distortional semi-discretized thin-walled beam element.

Thin-Walled Structures, **62**, 142–157.

Thin-Walled Structures 62 (2013) 142–157

Contents lists available at SciVerse ScienceDirect

Thin-Walled Structures

journal homepage: www.elsevier.com/locate/tws

A distortional semi-discretized thin-walled beam element

Michael Joachim Andreassen, Jeppe Jönsson*

Technical University of Denmark, Department of Civil Engineering, Brovej Building 118, DK-2800 Kgs. Lyngby, Denmark

ARTICLE INFO

Article history:
Received 16 March 2012
Accepted 10 July 2012

Keywords:
Thin-walled beams
Beam theory
Distortion
Warping
Distortional beam theory
Generalized beam theory
Semi-discretization
Beam element
One-dimensional

ABSTRACT

Due to the increased consumption of thin-walled structural elements there has been increasing focus and need for more detailed calculations as well as development of new approaches. In this paper a thin-walled beam element including distortion of the cross section is formulated. The formulation is based on a generalized beam theory (GBT), in which the classic Vlasov beam theory for analysis of open and closed thin-walled cross sections is generalized by including distortional displacements. The beam element formulation utilizes a semi-discretization approach in which the cross section is discretized into wall elements and the analytical solutions of the related GBT beam equations are used as displacement functions in the axial direction. Thus the beam element contains the semi-analytical solutions. In three related papers the authors have recently presented the semi-discretization approach and the analytical solution of the beam equations of GBT. In this approach a full set of deformation modes corresponding to the homogeneous GBT equations are found. The deformation modes of which some are complex decouple the state space equations corresponding to the reduced order differential equations of GBT and allow the determination of the analytical solutions. Solutions of the non-homogeneous GBT differential equations and the distortional buckling equations have also been found and analyzed. Thus, these related papers are not dealing with an element but dealing with analytical solutions to the coupled differential equations.

To handle arbitrary boundary conditions as well as the possibility of adding concentrated loads as nodal loads the formulation of a beam element is needed. This paper presents the formulation of such a generalized one-dimensional semi-discretized thin-walled beam element including distortional contributions. It should be noticed that we are only dealing with a basic generalized beam theory and not an extended finite element formulation of an approximate beam element, which allows the addition of special (transverse extension and shear lag) modes. Illustrative examples showing the validity and the accuracy of the developed distortional semi-discretized thin-walled beam element are given and it is shown how the novel approach provides accurate results making it a good alternative to the traditional and time consuming FE calculations.

1. Introduction

In the civil, mechanical and aerospace industry thin-walled members are often used because of the high strength and the effective use of material. Due to the increased consumption of thin-walled structural elements there has been increasing focus and need for more detailed calculations. Thus, it has been necessary to extend the classic beam theory to include the distortion of the cross section. Such an extension of the theory is considered in this paper and in a number of companion papers published by the authors [1–3], where a novel approach to generalized beam theory is formulated. A variety of other formulations and methods taking distortional displacements into account have been proposed for analysis of both open and closed cross sections. Thus, concerning analysis of thin-walled members including distortion of the cross section there are a number of methods available among which are: (i) the use of shell finite elements in the finite element method (FEM) [4,5], perhaps with utilization of recursive substructuring [6], (ii) the finite strip method (FSM) [7–11], and (iii) the use of approximate GBT-finite beam elements. Concerning approximate GBT-finite beam elements, specially the traditional first generation of generalized beam theory, known as GBT, initially proposed by Schardt in 1966 [12], has been very popular and fostered a lot of research and developments, mostly undertaken by a few independently working European groups, among others by Schardt [13], Davies [14], Lepistö [15], Simões da Silva and Simão [16], Gonçalves et al. [17], Gonçalves and Camotim [18] and Camotim and Silvestre [19].

* Corresponding author. Tel.: +45 45251707.
E-mail addresses: mican@byg.dtu.dk (M.J. Andreassen), jej@byg.dtu.dk (J. Jönsson).

0263-8231/$ - see front matter © 2012 Elsevier Ltd. All rights reserved.
http://dx.doi.org/10.1016/j.tws.2012.07.011

Silvestre and Camotim also extended the theory to include orthotropic materials, see [20,21], and experimental verifications have been presented by for example Rendek and Balaz [22]. Furthermore, Silvestre presents buckling solutions as well as non-linear post buckling solutions in [19]. For an overview and information about the research and development of GBT, see Camotim et al. [23,24].

The present novel approach to Generalized Beam Theory (GBT) involves a cross-section semi-discretization process as well as a determination of the natural cross-section eigenmodes and related axial solution functions by exact analytical solution of the related first-order GBT equations. Hereby the approach is different from the traditional GBT formulation developed by Schardt [12,13]. When Schardt uses the GBT equations to find distortional deformation modes the shear coupling stiffness terms are neglected. This corresponds to modal analysis with orthogonal (Rayleigh) damping in dynamic structural analysis. The solution of the shear coupled GBT equations for closed cross-sections was published by Hanf only in his thesis [25]. For closed (single or multi celled hollow) thin-walled cross-sections Schardt shows in his presentation of GBT [13] that the theory needs a relaxation of the Vlasov assumption of negligible shear strain in order to include the warping deformation associated with the "Bredt's shear flow" around each cell. However, it complicates the solution of the conventional GBT equations by introducing non-negligible shear coupling terms (off diagonal) in the GBT equations as can be seen in recent GBT formulations for closed thin-walled cross-sections, e.g. [26,17,27]. The present formulation therefore adheres to the definition of the warping function given by Kollbrunner and Hajdin [28], which adds the integral of the shear flow strains, see also [29–31].

The present GBT formulation for thin walled beams with both open and closed (single or multi cell) cross-sections can be regarded as an extension of classical Vlasov thin-walled beam theory to include distortional deformation modes as well as constant shear flows in the walls of the cross-section, see [32,28,33]. The innovative theoretical developments performed by introducing semi-discretization leads to a formulation, in which the rotational degrees of freedom are included, thus including local plate modes in the formulation even for the simplest discretization. It makes it possible to analyze thin-walled members with cross-section distortion and local plate behavior in a one-dimensional formulation through the linear combination of pre-established modes of deformation. In contrast to and as a considerable advance on the traditional GBT formulation this novel finite element based semi-discretization approach to generalized beam theory (GBT) solves the fourth-order differential equations to obtain the distortional displacements for a linear beam analysis. This means that we find the analytical solution to the differential GBT equations which through the magnitude of the eigenvalues gives a much better knowledge of the length scales of the modes. This also means that we find the exact mode shapes and amplitude solutions of the reduced order GBT equations related to the discretized cross section. In contrast, the conventional GBT formulation solves the equations using the approximate engineering methods, in which the shear coupling terms are neglected, producing orthogonal axial and transverse normal stress modes. In such a case the differential equations are not solved but a weak solution may be found through the introduction of the established approximate mode shapes and use of approximate modal amplitude functions. Thus the conventional GBT formulations use the produced approximated modes as shape functions in a virtual work or potential energy formulation leading to approximated finite GBT beam elements and the discretization has to be performed without proper prior knowledge of the problem length scales of the individual modes.

With respect to buckling the first application of the first generation of GBT to buckling analysis was published in 1970 by Schardt [34]. Among others also Davies [35], Simão [16] and Camotim [36] have investigated the area. Buckling analysis using GBT beam elements is an alternative to the use of finite-strip methods (FSM), see [37]. However, GBT is as its name states essentially a beam theory, whereas FSM essentially is based on plate theory. Therefore, FSM does not contain a natural decomposition into basic beam, distortional, local and other modes. Furthermore, conventional GBT does not contain other modes as mentioned above. Since the modal decomposition may lead to advantages in design of thin-walled structures using FSM a great deal of work has been performed by Ádány and Schafer to develop a constrained finite strip method (cFSM) and modal decomposition methods for open (single-branched) cross-sections, see [38–40]. The modal approaches of extended conventional GBT and cFSM formulations have been compared in [41]. The present novel developed semi-discretization approach to Generalized Beam Theory (GBT) is extended in [3] to include the geometrical stiffness terms which are needed for column buckling analysis and identification of buckling modes.

When cross sections distort, it means that they change shape. Distortional displacements can be of a local character in which the length scale is typically equal to or less than the cross section dimension or it can be non-local in which case the length scale is typically several times the cross section dimension or even longer. In the recent buckling literature and especially in codes there is a tendency, with respect to buckling, to distinguish between these two behaviors as distortional buckling and local buckling. In [1–3] we are operating with global, distortional non-local and distortional local modes when we define first-order displacement modes. However, in paper [3] which concerns buckling we have chosen to distinguish between distortional buckling and local buckling as in the recent codes and literature.

It should be noticed that shear deformation accommodating Bredt's shear flow around closed cells is included in the theory through the specific definition of the warping function, see Ref. [28]. Since we are dealing with a basic generalized beam theory and not an extended finite element formulation of an approximate beam element it makes sense to neglect the overall transverse shear deformation as in conventional beams. It is also important to note that shear lag is not included and that it would not be included even by including shear deformation as described by Kollbrunner and Hajdin [28]. Thus, we are only dealing with a beam element adhering to generalized beam theory and not an extended weak formulation of a finite beam element that allows the addition of special (transverse extension and shear lag) modes.

Let us introduce the contents of the following sections and illuminate the development. In the theories of beams, the displacements assumed are typically separated into a sum of displacement fields. In the sections involving the determination of such a displacement field, only one of these displacement fields is considered in the variational formulation. The basic kinematic assumptions of one of these displacement fields are introduced in Section 2. The displacements are separated into the product of cross-section displacement functions and the axial variation functions. Following this, the strain fields are derived. In Section 3 constitutive energy assumptions lead to the formulation of the internal and external elastic energy potential. In Section 4 the cross-section is discretized by straight wall elements in which the local transverse displacements, the warping displacements and the loads are interpolated. The element interpolation functions are introduced and the total elastic potential energy (for a single mode) is formulated in a semi-discretized form. To get a formulation resembling a generalization of Vlasov beam theory [32], Section 5 first briefly describes three main steps leading to the

derivation and solution of the full set of GBT differential equations. Following this, Section 5 briefly describes the notation and solution of the final condensed distortional differential equations of GBT. The full solution functions are assembled and the full solution along the beam is presented by nodal solution vectors. In section 6 the beam element stiffness matrix and load vector for the full solution is found. In Section 7 the introduction of the boundary conditions is described and the necessarily transformation from the degree-of-freedom finite element space to the reduced degree-of-freedom GBT space is also introduced. Section 8 is devoted to the development and assembling of the exact full generalized displacement solution along the beam element. Here the generalized displacements of the homogeneous solution and the generalized displacements of the non-homogeneous solution are assembled to describe the full generalized displacement solution along the beam element. Four illustrative examples are given in Section 9.

2. Beam kinematics of a single mode

The potential energy is expressed in terms of displacements and strains. Hereby a representation of the generalized displacement field is a part of the evaluation of the potential energy. For the present beam theory the displacement field is represented in terms of generalized displacements describing extension, flexure, torsion, warping and distortion.

The straight beam of constant cross section is described in a global Cartesian (x,y,z) coordinate system as shown in Fig. 1. From the figure it is seen that a local coordinate system (n,s,z) corresponding to the normal and tangential directions is defined. In the local coordinate system, the displacements u_n, u_s and u_z of a material point are defined as

$$u_n(s,z) = \mathrm{w}_n(s)\psi(z) \tag{1}$$

$$u_s(n,s,z) = \big(\mathrm{w}_s(s) - n\mathrm{w}_{n,s}(s)\big)\psi(z) \tag{2}$$

$$u_z(n,s,z) = -\big(\Omega(s) + n\mathrm{w}_n(s)\big)\psi'(z) \tag{3}$$

For the local transverse displacements $u_n(s,z)$ and $u_s(n,s,z)$, the corresponding displacement components $\mathrm{w}_s(s)$ and $\mathrm{w}_n(s)$ are the local displacements of the centerline and $\psi(z)$ is the function which describes the variation along the beam. For the axial displacements $u_z(n,s,z)$ generated by the out-of-plane distortional cross-sectional displacements, the axial (warping) displacement mode $\Omega(s)$ has been included with a variation corresponding to the negative axial derivative of the axial variation factor, $-\psi'$, and due consideration of local transverse variation through the term $n\mathrm{w}_n$. The local components are shown in Fig. 2. The notation indicates the two dimensions of the cross-section planes and the single dimension associated with the variation along the beam.

The strain components associated with the given displacements are found as

$$\varepsilon_z = -(\Omega + n\mathrm{w}_n)\psi'' \tag{4}$$

$$\varepsilon_s = (\mathrm{w}_{s,s} - n\mathrm{w}_{n,ss})\psi \tag{5}$$

$$\gamma_{zs} = (\mathrm{w}_s - \Omega_{,s} - 2n\mathrm{w}_{n,s})\psi' \tag{6}$$

Here the given strains are the axial strains, transverse strains and engineering shear strains.

The present approach is based on a semi-discretization process in which the thin-walled cross section is discretized in straight finite cross-sectional wall elements of constant thickness. The thickness of the individual plane cross-section element is denoted by t and the width of the wall element by b_{el}.

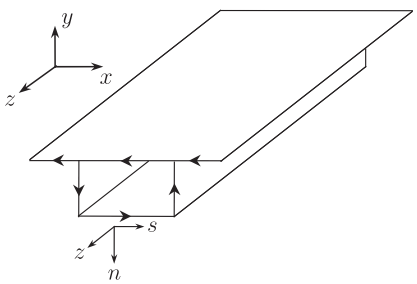

Fig. 1. Global and local Cartesian reference frames.

3. Strain energy assumptions of a single mode

In this section the internal energy potential as well as the external energy potential are derived.

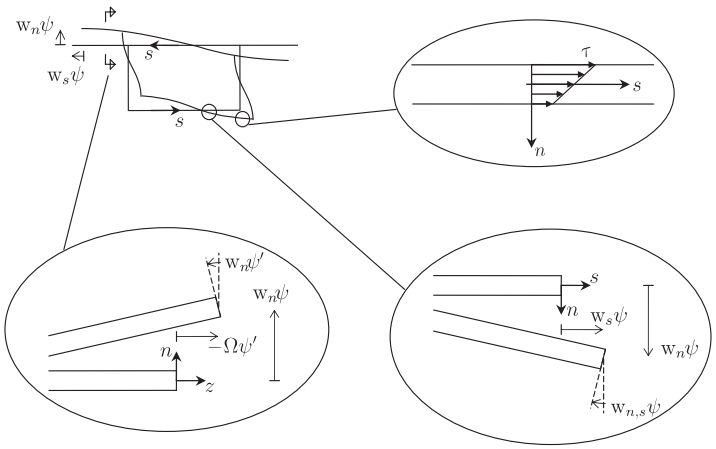

Fig. 2. Local components of the displacement field and assumed shear stresses.

3.1. Internal energy potential of a single mode

In the following we will adhere to simple constitutive relations, i.e. the material is assumed to be linear elastic with a modulus of elasticity E and a shear modulus G. In the transverse direction we will assume a plate type elasticity modulus $E_s = E/(1-\nu^2)$, in which ν represents the Poisson ratio. The axial stress is determined as $\sigma = E\varepsilon$, the shear stress as $\tau = G\gamma$ and the transverse stress as $\sigma_s = E_s\varepsilon_s$. Thus we are using non-coupling constitutive relations or in other words we neglect the coupling of axial strain ε and transverse strain ε_s. Note that this means that we also neglect the equivalent coupling between axial and transverse curvatures in the constitutive relations for the plate moments, but with some changes it is possible to include the coupling of the curvatures. With the simple constitutive relations assumed, the elastic energy potential becomes

$$\Pi_{int} = \int_V \left(\frac{1}{2}E\varepsilon^2 + \frac{1}{2}G\gamma^2 + \frac{1}{2}E_s\varepsilon_s^2\right)dV \tag{7}$$

Let us now introduce a thin-walled cross-section assembled using straight cross-sectional elements, see Fig. 3, and let us integrate through the thickness, t, across the widths, b_e, of the elements, and over the length, L, of the thin-walled beam.

The elastic potential energy takes the following form after the introduction of the strains expressed by the displacement in separated form

$$\begin{aligned}\Pi_{int} = \frac{1}{2}\int_0^L \Bigg[&\sum_{el}\int_0^{b_{el}} \Bigg\{ \left[Et(\Omega\psi'')^2 + \frac{1}{12}Et^3(\mathrm{w}_n\psi'')^2\right] \\ &+ \Big[Gt(\mathrm{w}_s\psi')^2 + Gt(\Omega_{,s}\psi')^2 \\ &-2Gt(\mathrm{w}_s\psi')(\Omega_{,s}\psi') + \frac{1}{3}Gt^3(\mathrm{w}_{n,s}\psi')^2\Big] \\ &+ \left[E_s t(\mathrm{w}_{s,s}\psi)^2 + \frac{1}{12}E_s t^3(\mathrm{w}_{n,ss}\psi)^2\right]\Bigg\} ds\Bigg] dz\end{aligned} \tag{8}$$

In Eq. (8) the elastic energy terms have been grouped in axial strain energy, shear energy, and transverse strain energy. Note that the shear constraints associated with constant shear flow and the transverse extension constraint have not been introduced yet. In the current work we wish to establish a set of displacement modes by using semi-discretization. To achieve this, the cross-section will be divided into discrete straight-line elements, in which we interpolate the transverse and axial displacements.

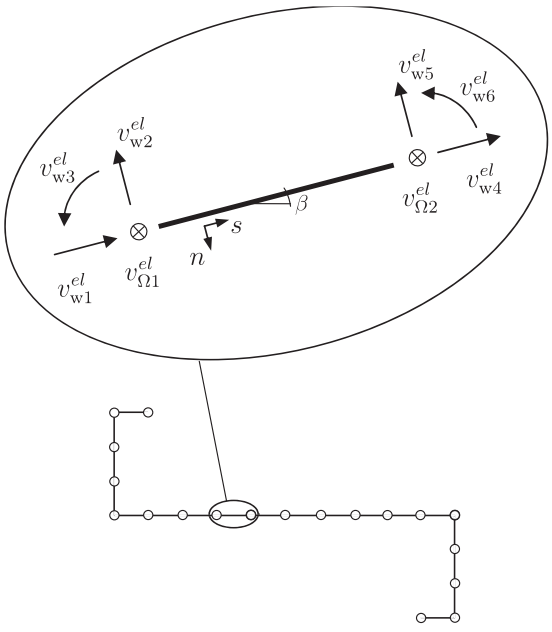

Fig. 3. Nodal components of a straight single flat element.

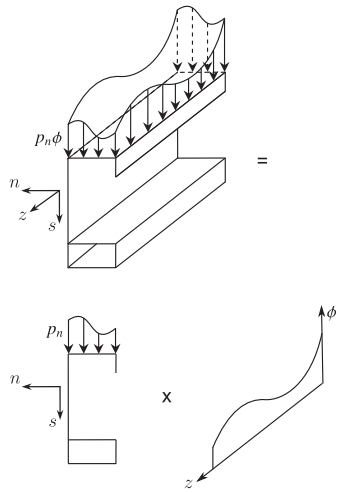

Fig. 4. Load distribution.

3.2. External energy potential of a single mode

Let us introduce three types of distributed loads q_z, q_s, q_n which act on the mid-plane of the individual walls in the z,s,n directions, respectively. The external load potential for these distributed loads can then for a single mode be found as

$$\Pi_{ext} = -\int_0^L \int_0^{b_{el}} [q_z u_z + q_s u_s + q_n u_n]\, ds\, dz \tag{9}$$

Using separation of variables for the distributed loads as for the displacements, we introduce the following load variables $q_s = p_s(s)\phi(z)$, $q_n = p_n(s)\phi(z)$, $q_z = p_z(s)\phi(z)$. In this formulation p_s, p_n, p_z represent the cross-section load distribution, and the function ϕ represents the axial variation of the loads. In the following formulation we operate with only one cross-section load distribution, which may be modified by summation of various different cross-section load distributions and axial load variation functions. The load separation is illustrated in Fig. 4 for a distributed load $q_n = p_n(s)\phi(z)$ on the upper flange of a thin-walled beam. The local components of the loads and force vectors for a cross-section wall element are shown in Fig. 5.

Hereby the contribution to the external load potential of a single wall element takes the following form:

$$\Pi_{ext,el} = -\int_0^L \int_0^{b_{el}} \phi[p_s w_s\psi + p_n w_n\psi - p_z\Omega\psi']\, ds\, dz \tag{10}$$

which is suited for adequate interpolation in the following. Note that the two first load terms perform work through the transverse displacements and the last load term performs work through the axial warping displacements.

4. Interpolations

In the present approach we introduce interpolations related to the cross-section displacements, w_s, w_n and Ω, using the nodal degrees of freedom shown in Fig. 3 and to the cross-section loads, p_s, p_n and p_z shown in Figs. 4 and 5.

4.1. Displacement interpolations

Within each single straight finite cross-section wall element the displacements are interpolated using the following interpolation functions:

$$\Omega\psi' = \mathbf{N}_\Omega \mathbf{v}_\Omega^{el}\psi' \tag{11}$$

$$\mathrm{w}_s\psi = \mathbf{N}_s \mathbf{v}_\mathrm{w}^{el}\psi \tag{12}$$

$$\mathrm{w}_n\psi = \mathbf{N}_n \mathbf{v}_\mathrm{w}^{el}\psi \tag{13}$$

in which $\mathbf{N}_\Omega(s)$ and $\mathbf{N}_s(s)$ are linear interpolation matrices and $\mathbf{N}_n(s)$ is a cubic (beam) interpolation matrix. Furthermore, the axial and transverse nodal displacement components of a straight cross-section element are defined as

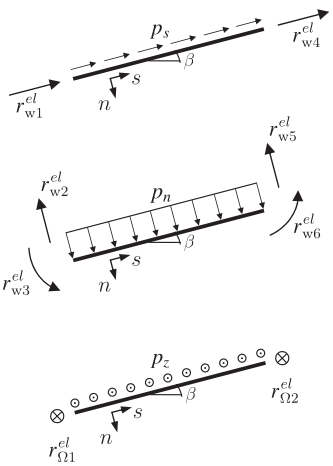

Fig. 5. Distributed loads and the resulting load vectors.

Table 1
Straight-element stiffness and load contributions.

$$\mathbf{k}^\sigma_{\Omega\Omega} = \int_0^{b_e} Et\mathbf{N}_\Omega^T\mathbf{N}_\Omega\, ds$$
$$\mathbf{k}^\sigma_{\mathrm{ww}} = \int_0^{b_e} \frac{Et^3}{12}\mathbf{N}_n^T\mathbf{N}_n ds$$
$$\mathbf{k}^s = \int_0^{b_e}\left(E_s t\mathbf{N}^T_{s,s}\mathbf{N}_{s,s} + \frac{E_s t^3}{12}\mathbf{N}^T_{n,ss}\mathbf{N}_{n,ss}\right) ds$$
$$\mathbf{k}^\tau_{\mathrm{ww}} = \int_0^{b_e}\left(Gt\mathbf{N}_s^T\mathbf{N}_s + \frac{Gt^3}{3}\mathbf{N}^T_{n,s}\mathbf{N}_{n,s}\right) ds$$
$$\mathbf{k}^\tau_{\Omega\Omega} = \int_0^{b_e} Gt\mathbf{N}^T_{\Omega,s}\mathbf{N}_{\Omega,s}\, ds$$
$$\mathbf{k}^\tau_{\mathrm{w}\Omega} = \left[\mathbf{k}^\tau_{\Omega\mathrm{w}}\right]^T = -\int_0^{b_e} Gt\mathbf{N}_s^T\mathbf{N}_{\Omega,s}\, ds$$
$$\mathbf{r}^{el}_\Omega = \int_0^{b_e}\mathbf{N}_\Omega^T\mathbf{N}_p ds\ \mathbf{p}_z^{el} + \mathbf{P}^{el}_\Omega$$
$$\mathbf{r}^{el}_\mathrm{w} = \int_0^{b_e}\mathbf{N}_s^T\mathbf{N}_p ds\ \mathbf{p}_s^{el} + \int_0^{b_e}\mathbf{N}_n^T\mathbf{N}_p ds\ \mathbf{p}_n^{el} + \mathbf{P}^{el}_\mathrm{w}$$

Table 2
Assembly into total cross-section stiffness contributions.

$\mathbf{K}^\sigma_{\Omega\Omega} = \sum_{el}\mathbf{T}^T_\Omega\mathbf{k}^\sigma_{\Omega\Omega}\mathbf{T}_\Omega$	$\mathbf{K}^\tau_{\mathrm{ww}} = \sum_{el}\mathbf{T}^T_\mathrm{w}\mathbf{k}^\tau_{\mathrm{ww}}\mathbf{T}_\mathrm{w}$
$\mathbf{K}^\sigma_{\mathrm{ww}} = \sum_{el}\mathbf{T}^T_\mathrm{w}\mathbf{k}^\sigma_{\mathrm{ww}}\mathbf{T}_\mathrm{w}$	$\mathbf{K}^\tau_{\Omega\Omega} = \sum_{el}\mathbf{T}^T_\Omega\mathbf{k}^\tau_{\Omega\Omega}\mathbf{T}_\Omega$
$\mathbf{K}^s = \sum_{el}\mathbf{T}^T_\mathrm{w}\mathbf{k}^s\mathbf{T}_\mathrm{w}$	$\mathbf{K}^\tau_{\mathrm{w}\Omega} = \sum_{el}\mathbf{T}^T_\mathrm{w}\mathbf{k}^\tau_{\mathrm{w}\Omega}\mathbf{T}_\Omega$

$$\mathbf{v}_\Omega^{el} = [v^{el}_{\Omega 1}\ \ v^{el}_{\Omega 2}]^T$$
$$\mathbf{v}_\mathrm{w}^{el} = [v^{el}_{\mathrm{w}1}\ \ v^{el}_{\mathrm{w}2}\ \ v^{el}_{\mathrm{w}3}\ \ v^{el}_{\mathrm{w}4}\ \ v^{el}_{\mathrm{w}5}\ \ v^{el}_{\mathrm{w}6}]^T \tag{14}$$

The nodal components and the direction of the section coordinates (n,s) are shown in Fig. 3.

Using the introduced interpolations for the displacements and introducing the straight-wall element stiffness contributions given in Table 1, the internal potential energy now takes the following form for a single wall element

$$\Pi_{int,el} = \frac{1}{2}\int_0^L \left\{ \begin{bmatrix} \psi\mathbf{v}_\mathrm{w}^{el^T} & \psi\mathbf{v}_\Omega^{el^T}\end{bmatrix}'' \begin{bmatrix}\mathbf{k}^\sigma_{\mathrm{ww}} & \mathbf{0}\\ \mathbf{0} & \mathbf{k}^\sigma_{\Omega\Omega}\end{bmatrix}\begin{bmatrix}\psi\mathbf{v}_\mathrm{w}^{el}\\ \psi\mathbf{v}_\Omega^{el}\end{bmatrix}'' \right.$$
$$+ \begin{bmatrix} \psi\mathbf{v}_\mathrm{w}^{el^T} & \psi\mathbf{v}_\Omega^{el^T}\end{bmatrix}' \begin{bmatrix}\mathbf{k}^\tau_{\mathrm{ww}} & \mathbf{k}^\tau_{\mathrm{w}\Omega}\\ \mathbf{k}^\tau_{\Omega\mathrm{w}} & \mathbf{k}^\tau_{\Omega\Omega}\end{bmatrix}\begin{bmatrix}\psi\mathbf{v}_\mathrm{w}^{el}\\ \psi\mathbf{v}_\Omega^{el}\end{bmatrix}'$$
$$\left. + \begin{bmatrix} \psi\mathbf{v}_\mathrm{w}^{el^T} & \psi\mathbf{v}_\Omega^{el^T}\end{bmatrix} \begin{bmatrix}\mathbf{k}^s & \mathbf{0}\\ \mathbf{0} & \mathbf{0}\end{bmatrix}\begin{bmatrix}\psi\mathbf{v}_\mathrm{w}^{el}\\ \psi\mathbf{v}_\Omega^{el}\end{bmatrix} \right\} dz \tag{15}$$

In Eq. (15) and in the following, a bold zero $\mathbf{0}$ denotes a suitable size matrix or vector of zeroes.

Assembling the local element degrees of freedom, the global displacement vectors for the total cross section are given as

$$\mathbf{v}_\Omega = [v_{\Omega 1}\ \ v_{\Omega 2}\ \ v_{\Omega 3}\ \ \ldots]^T$$
$$\mathbf{v}_\mathrm{w} = [v_{x1}\ \ v_{y1}\ \ \phi_1\ \ v_{x2}\ \ v_{y2}\ \ \phi_2\ \ \ldots]^T \tag{16}$$

where the axial displacements and the transverse displacements are separated into two vectors.

In Eq. (16) $\mathbf{v}_\Omega$ holds the local axial element degrees of freedom and $\mathbf{v}_\mathrm{w}$ holds the local transverse element degrees of freedom, corresponding to two displacements and one rotation for each node. The transformation from local to global components is performed using a formal standard transformation of the components in the cross-section plane, i.e. $\mathbf{v}_\Omega = \mathbf{T}_\Omega\mathbf{v}_\Omega^{el}$ and $\mathbf{v}_\mathrm{w} = \mathbf{T}_\mathrm{w}\mathbf{v}_\mathrm{w}^{el}$. The local stiffness matrices are given in Table 1 and the global assembly of stiffness matrices found by summation of the contribution from each element are as illustrated in Table 2.

4.2. Load interpolations

Having described the displacement interpolations for w_s, w_n and Ω as also described in the companion paper [1], the interpolation of the cross-section loads p_s, p_n and p_z are introduced in the following. The distributed load shown in Fig. 4 is defined by a linear interpolation of the load on each cross-section wall element multiplied by an axial shape function $\phi(z)$, for which we will introduce a specific interpolation later in a following section. The load interpolation in a cross-section wall is given by

$$p_s = \mathbf{N}_p\mathbf{p}_s^{el},\quad p_n = \mathbf{N}_p\mathbf{p}_n^{el},\quad p_z = \mathbf{N}_p\mathbf{p}_z^{el} \tag{17}$$

in which $\mathbf{N}_p(s) = [1-s/b_{el}, s/b_{el}]$ is the linear interpolation matrix, and where the nodal end values of a cross-section wall element are given as

$$\mathbf{p}_s^{el} = \begin{bmatrix}p_{s1}\\ p_{s2}\end{bmatrix},\quad \mathbf{p}_n^{el} = \begin{bmatrix}p_{n1}\\ p_{n2}\end{bmatrix},\quad \mathbf{p}_z^{el} = \begin{bmatrix}p_{z1}\\ p_{z2}\end{bmatrix} \tag{18}$$

Using the introduced interpolations for the displacements and the loads, the external potential energy now takes the following form

for a single wall element:

$$\Pi_{ext,el} = -\int_0^L \int_0^{b_{el}} \left[\psi \mathbf{v}_w^{el^T} \mathbf{N}_s^T \mathbf{N}_p \mathbf{p}_s^{el} + \psi \mathbf{v}_w^{el^T} \mathbf{N}_n^T \mathbf{N}_p \mathbf{p}_n^{el} - \psi' \mathbf{v}_\Omega^{el^T} \mathbf{N}_\Omega^T \mathbf{N}_p \mathbf{p}_z^{el}\right] \phi \, ds \, dz \tag{19}$$

This formulation allows us to write the element load vector in the same format as the element stiffness contributions. These are also shown in Table 1, where we have also included the nodal cross-section wall loads $\mathbf{P}_w^{el}$ and $\mathbf{P}_\Omega^{el}$ corresponding to line loads also varying along the beam with ϕ. Hereby the walls of the thin-walled beam can be loaded by line loads acting at the cross-section nodes, and by surface loads acting on the mid-plane of a cross-section wall. Both these loads are distributed along the beam as given by the ϕ-function. For a single displacement mode we can now rewrite the external load potential of a wall element as follows:

$$\Pi_{ext,el} = -\int_0^L \left[\psi \mathbf{v}_w^{el^T} \mathbf{r}_w^{el} \phi - \psi' \mathbf{v}_\Omega^{el^T} \mathbf{r}_\Omega^{el} \phi\right] dz \tag{20}$$

where we have introduced the axial and transverse nodal load components of a straight cross-section element as

$$\mathbf{r}_\Omega^{el} = [r_{\Omega 1}^{el} \;\; r_{\Omega 2}^{el}]^T \tag{21}$$

$$\mathbf{r}_w^{el} = [r_{w1}^{el} \;\; r_{w2}^{el} \;\; r_{w3}^{el} \;\; r_{w4}^{el} \;\; r_{w5}^{el} \;\; r_{w6}^{el}]^T \tag{22}$$

These components are shown in Fig. 5 along with the direction of the wall element coordinates (n,s) as well as the positive direction of the load components.

We choose to assemble the single element components into two separate global vectors containing the axial load and the transverse load, respectively. These global vectors we will write as follows:

$$\mathbf{r}_\Omega = [r_{\Omega 1} \;\; r_{\Omega 2} \;\; r_{\Omega 3} \;\; \ldots]^T \tag{23}$$

$$\mathbf{r}_w = [r_{w1} \;\; r_{w2} \;\; r_{w3} \;\; r_{w4} \;\; r_{w5} \;\; r_{w6} \;\; \ldots]^T \tag{24}$$

where the transformation from local to global components is performed using a formal standard transformation of the components in the cross-section plane, i.e.

$$\mathbf{r}_\Omega = \sum_{el} \mathbf{T}_\Omega^T \mathbf{r}_\Omega^{el} \tag{25}$$

$$\mathbf{r}_w = \sum_{el} \mathbf{T}_w^T \mathbf{r}_w^{el} \tag{26}$$

See Table 2 in paper [2] for a overview of the important transformations used in this and in the companion papers [1–3].

4.3. Total elastic energy potential of a single mode

Now we can write the total potential energy for a single mode of deformation by summation of each element contribution as

$$\Pi_{tot} = \sum_{el} (\Pi_{int,el} + \Pi_{ext,el}) \tag{27}$$

Introducing the described interpolation and matrix calculation scheme, the total elastic potential energy for a single mode now takes the following form:

$$\begin{aligned}\Pi_{tot} = \frac{1}{2}\int_0^L \Bigg\{ &\begin{bmatrix} \psi \mathbf{v}_w^T & \psi \mathbf{v}_\Omega^T \end{bmatrix}'' \begin{bmatrix} \mathbf{K}_{ww}^\sigma & \mathbf{0} \\ \mathbf{0} & \mathbf{K}_{\Omega\Omega}^\sigma \end{bmatrix} \begin{bmatrix} \psi \mathbf{v}_w \\ \psi \mathbf{v}_\Omega \end{bmatrix}'' \\ &+ \begin{bmatrix} \psi \mathbf{v}_w^T & \psi \mathbf{v}_\Omega^T \end{bmatrix}' \begin{bmatrix} \mathbf{K}_{ww}^\tau & \mathbf{K}_{w\Omega}^\tau \\ \mathbf{K}_{\Omega w}^\tau & \mathbf{K}_{\Omega\Omega}^\tau \end{bmatrix} \begin{bmatrix} \psi \mathbf{v}_w \\ \psi \mathbf{v}_\Omega \end{bmatrix}' \\ &+ \begin{bmatrix} \psi \mathbf{v}_w^T & \psi \mathbf{v}_\Omega^T \end{bmatrix} \begin{bmatrix} \mathbf{K}^s & \mathbf{0} \\ \mathbf{0} & \mathbf{0} \end{bmatrix} \begin{bmatrix} \psi \mathbf{v}_w \\ \psi \mathbf{v}_\Omega \end{bmatrix} \\ &- (\psi \mathbf{v}_w^T) \mathbf{r}_w \phi + (\psi \mathbf{v}_\Omega^T)' \mathbf{r}_\Omega \phi \Bigg\} dz \end{aligned} \tag{28}$$

The axial stiffness from transverse displacements, submatrix $\mathbf{K}_{ww}^\sigma$, has a rank deficiency equal to the number of free end nodes plus the number of "internal" nodes between corner points of the cross section. The in-plane cross-section distortional stiffness submatrix $\mathbf{K}^s$ has a rank deficiency of 3, corresponding to three in-plane "rigid body" or rather non-distortional displacements of the cross section. Finally the whole shear stiffness matrix related to torsion has a rank deficiency of 3, corresponding to the existence of pure axial extension and two pure flexural modes without shear. It turns out that since the pure axial displacement only involves the sub matrix $\mathbf{K}_{\Omega\Omega}^\tau$, this matrix has a rank deficiency of one. The first load term corresponds to the distortional moment load which performs work through the transverse displacements. The second load term corresponds to the distortional bimoment load which performs work through the axial displacements, see [30].

5. Eigenmodes and solution functions

To get a formulation resembling a generalization of Vlasov beam theory [32] the following three main steps are performed:

- In step I it is first acknowledged that the pure axial extension mode is a separate mode with only pure unit warping displacement which varies along the beam as function of the axial parameter $\zeta(z) = -\psi'(z)$. Second the shear constraint equations that bind axial, $\mathbf{v}_\Omega$, and transverse, $\mathbf{v}_w$, degrees of freedom together are used to eliminate all the axial warping degrees of freedom except from the pure axial extension. Finally variations of the condensed version of the potential energy in Eq. (28) are taken with due acknowledgement of the pure axial extension mode leading to the identification of all the general differential equations of GBT. This leads to the identification, solution and elimination of the axial extension mode as an eigenmode.
- In step II two eigenmodes corresponding to transverse translation of the cross section are identified, solved and eliminated. Also a pure rotational (torsional) eigenmode is identified for solution and elimination in the next step. Furthermore, the transverse displacement field is constrained, so that transverse normal strains in the middle surface of the cross section are zero, i.e. $w_{s,s} = 0$, see Eq. (5).
- In step III the order of the coupled fourth order differential equations is reduced by doubling the number of equations through the introduction of a state vector with components of different differentiation levels. The pure St. Venant torsion mode is identified, solved and eliminated as an eigenmode with its linear axial solution. This reveals the final set of (reduced order) distortional differential equations.

For a more elaborate description of the steps performed see the companion papers [1,2].

The four identified eigenmode vectors corresponding to the displacements of conventional beam theory are ordered consecutively in the transverse beam displacement mode matrix $\mathbf{V}_w^b$ and the beam warping mode matrix $\mathbf{V}_\Omega^b$ as

$$\mathbf{V}_w^b = [\mathbf{0} \;\; \mathbf{v}_w^{1\ \mathrm{trans}} \;\; \mathbf{v}_w^{2\ \mathrm{trans}} \;\; \mathbf{v}_w^{3\ \mathrm{rot}}] \tag{29}$$

$$\mathbf{V}_\Omega^b = [\mathbf{v}_\Omega^{3\mathrm{xial}} \;\; \mathbf{v}_\Omega^{1\ \mathrm{trans}} \;\; \mathbf{v}_\Omega^{2\ \mathrm{trans}} \;\; \mathbf{v}_\Omega^{3\ \mathrm{rot}}] \tag{30}$$

and the related homogenous analytical solutions for each of the four modes are given by

$$\psi_a(z) = -c_{a1} z - \frac{1}{2} c_{a2} z^2 = \mathbf{\Psi}_a(z) \mathbf{c}_a = [-z \;\; -\tfrac{1}{2} z^2] \begin{bmatrix} c_{a1} \\ c_{a2} \end{bmatrix} \tag{31}$$

$$\psi_1(z) = c_{11} + c_{12}z + c_{13}z^2 + c_{14}z^3 = \boldsymbol{\Psi}_1(z)\mathbf{c}_1 = [1 \;\; z \;\; z^2 \;\; z^3] \begin{bmatrix} c_{11} \\ c_{12} \\ c_{13} \\ c_{14} \end{bmatrix} \tag{32}$$

$$\psi_2(z) = c_{21} + c_{22}z + c_{23}z^2 + c_{24}z^3 = \boldsymbol{\Psi}_2(z)\mathbf{c}_2 = [1 \;\; z \;\; z^2 \;\; z^3] \begin{bmatrix} c_{21} \\ c_{22} \\ c_{23} \\ c_{24} \end{bmatrix} \tag{33}$$

$$\psi_3(z) = c_{31} + c_{32}z = \boldsymbol{\Psi}_3(z)\mathbf{c}_3 = [1 \;\; z] \begin{bmatrix} c_{31} \\ c_{32} \end{bmatrix} \tag{34}$$

To enable pre-multiplication by the beam mode matrix we assemble the beam displacement constants in $\mathbf{c}_b$ and the homogenous solution functions in the beam solution matrix $\boldsymbol{\Psi}_{bh}(z)$ as follows:

$$\boldsymbol{\Psi}_{bh}(z)\mathbf{c}_b = \begin{bmatrix} \boldsymbol{\Psi}_a(z) & \mathbf{0} & \mathbf{0} & \mathbf{0} \\ \mathbf{0} & \boldsymbol{\Psi}_1(z) & \mathbf{0} & \mathbf{0} \\ \mathbf{0} & \mathbf{0} & \boldsymbol{\Psi}_2(z) & \mathbf{0} \\ \mathbf{0} & \mathbf{0} & \mathbf{0} & \boldsymbol{\Psi}_3(z) \end{bmatrix} \begin{bmatrix} \mathbf{c}_a \\ \mathbf{c}_1 \\ \mathbf{c}_2 \\ \mathbf{c}_3 \end{bmatrix} \tag{35}$$

Note that the integral of the axial solution $\boldsymbol{\Psi}_a = [-z - \frac{1}{2}z^2]$ does not pertain to any solution; however, it allows us to use its derivative as the axial solution for extension $\boldsymbol{\Psi}'_a = [-1 \;\; -z]$.

Using the identified beam eigenmode vectors the non-homogeneous equilibrium equations can be uncoupled and the load terms identified, see [2]. With respect to the axial variation of the cross-section load we will interpolate it using the distribution function $\phi(z)$. This function varies linearly between two end values (ϕ_1 and ϕ_2) representing the values of the multiplicative function at the ends of the profile. Thus we introduce ϕ as

$$\phi = \begin{bmatrix} 1 - \frac{z}{L} & \frac{z}{L} \end{bmatrix} \boldsymbol{\phi} \quad \text{where } \boldsymbol{\phi} = \begin{bmatrix} \phi_1 \\ \phi_2 \end{bmatrix} \tag{36}$$

Using this linear interpolation of the loads we find and write a fully integrated particular beam solution matrix multiplied by the intensity load values as

$$\boldsymbol{\Psi}_{bp}(z)\boldsymbol{\phi} = \begin{bmatrix} \boldsymbol{\Psi}_{ap}(z) \\ \boldsymbol{\Psi}_{1p}(z) \\ \boldsymbol{\Psi}_{2p}(z) \\ \boldsymbol{\Psi}_{3p}(z) \end{bmatrix} \boldsymbol{\phi} \tag{37}$$

where $\boldsymbol{\Psi}_{ap}$, $\boldsymbol{\Psi}_{1p}$ … each hold the two components of the polynomial solution expressions. The polynomial expressions for the particular load contributions are derived and given in the second companion paper [2].

Following the completion of steps I–III the final distortional differential equations are solved by seeking solutions of exponential form and solving the related eigenvalue problem (giving twice as many eigenvectors as conventional GBT). Two examples of such transverse mode shapes are shown in Figs. 6 and 7 respectively. The shown mode shapes correspond to a lipped channel and a box section used in the example section.

The transverse displacements and the related warping displacements of the found distortional eigenvectors are ordered column wise in the distortional mode matrices $\mathbf{V}_{\mathrm{w}}^{d}$ and $\mathbf{V}_{\Omega}^{d}$. The ith distortional eigenvector corresponds to a solution $\psi_{d_i}(z)$ which takes the form

$$\psi_{d_i}(z) = c_{d_{2i-1}} e^{\xi_i z} + c_{d_{2i}} e^{-\xi_i z} = \boldsymbol{\Psi}_{d_i}(z)\mathbf{c}_{d_i} = [e^{\xi_i z} \;\; e^{-\xi_i z}] \begin{bmatrix} c_{d_{2i-1}} \\ c_{d_{2i}} \end{bmatrix} \tag{38}$$

in which constants $c_{d_{2i-1}}$ and $c_{d_{2i}}$ are assembled in the vector $\mathbf{c}_{d_i}$ and depend on the boundary conditions of the problem at hand. All the distortional solution functions are assembled in the homogenous distortional solution matrix $\boldsymbol{\Psi}_{dh}$ and multiplied by the assembled vector of distortional constants $\mathbf{c}_d$ as follows:

$$\boldsymbol{\Psi}_{dh}(z)\mathbf{c}_d = \begin{bmatrix} \boldsymbol{\Psi}_{d_1}(z) & \mathbf{0} & \mathbf{0} & \cdots \\ \mathbf{0} & \boldsymbol{\Psi}_{d_2}(z) & \mathbf{0} & \cdots \\ \mathbf{0} & \mathbf{0} & \boldsymbol{\Psi}_{d_3}(z) & \cdots \\ \vdots & \vdots & \vdots & \ddots \end{bmatrix} \begin{bmatrix} \mathbf{c}_{d_1} \\ \mathbf{c}_{d_2} \\ \mathbf{c}_{d_3} \\ \vdots \end{bmatrix} \tag{39}$$

The particular load contributions are found by using the state eigenvectors to decouple the equations and integrate the solutions as described in the second companion paper [2]. The particular solutions may be written as follows using the

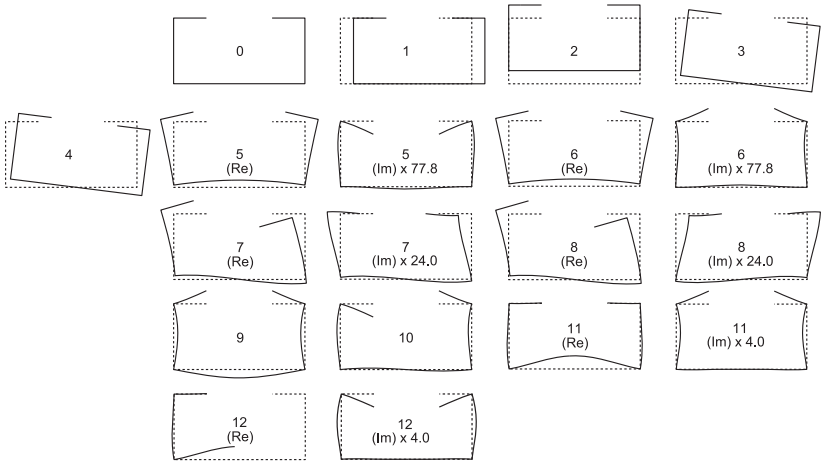

Fig. 6. Lipped channel—13 in-plane deformation mode shapes.

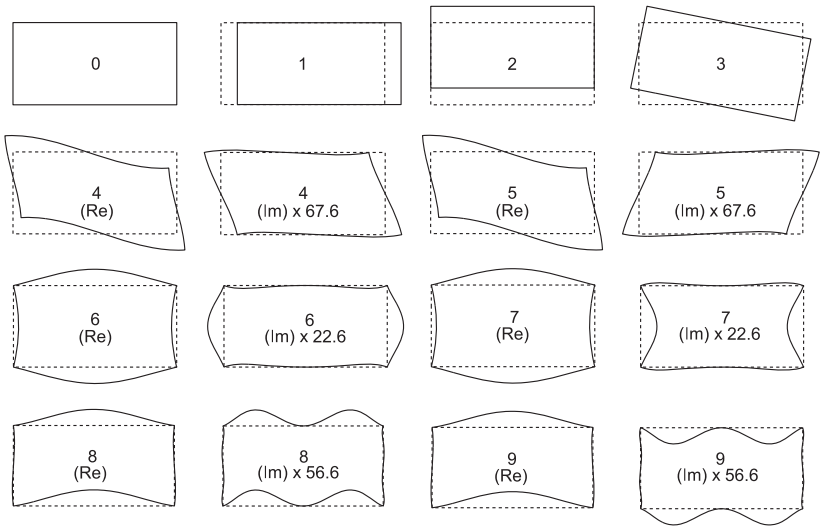

Fig. 7. Rectangular box cross-section—10 in-plane deformation mode shapes.

introduced linear cross-section load interpolation along the beam:

$$\boldsymbol{\Psi}_{dp}(z)\boldsymbol{\phi} = \begin{bmatrix} \boldsymbol{\Psi}_{dp_1}(z) \\ \boldsymbol{\Psi}_{dp_2}(z) \\ \vdots \end{bmatrix} \boldsymbol{\phi} \tag{40}$$

where $\boldsymbol{\Psi}_{dp_i}$ each hold the two components of the polynomial solution expressions. The more elaborate polynomial expressions for the particular load contribution are derived and given in the second companion paper [2].

Finally we are able to assemble the full modal matrices for the problem. The eigenmode vectors of the full solution can now be assembled from the beam eigenvectors and the distortional eigenvectors as follows:

$$\mathbf{V}_{\mathrm{w}} = [\mathbf{V}_{\mathrm{w}}^{b} \ \mathbf{V}_{\mathrm{w}}^{d}], \quad \mathbf{V}_{\Omega} = [\mathbf{V}_{\Omega}^{b} \ \mathbf{V}_{\Omega}^{d}] \tag{41}$$

The related homogenous and particular solution matrices are assembled as

$$\boldsymbol{\Psi}_{h}(z)\mathbf{c} = \begin{bmatrix} \boldsymbol{\Psi}_{bh}(z) & \mathbf{0} \\ \mathbf{0} & \boldsymbol{\Psi}_{dh}(z) \end{bmatrix} \begin{bmatrix} \mathbf{c}_b \\ \mathbf{c}_d \end{bmatrix} \tag{42}$$

and

$$\boldsymbol{\Psi}_{p}(z)\boldsymbol{\phi} = \begin{bmatrix} \boldsymbol{\Psi}_{bp}(z) \\ \boldsymbol{\Psi}_{dp}(z) \end{bmatrix} \boldsymbol{\phi} \tag{43}$$

This concludes the determination of all the solutions for all the displacement modes of GBT.

After having obtained and assembled the cross-section displacement modes in $\mathbf{V}_{\mathrm{w}}$ and $\mathbf{V}_{\Omega}$ as well as all the homogeneous and particular solution functions in $\boldsymbol{\Psi}_h$ and $\boldsymbol{\Psi}_p$ the full solution along the beam is presented using the nodal solution vectors $\mathbf{u}_w(z)$ and $\mathbf{u}_\Omega(z)$ as

$$\begin{aligned} \mathbf{u}_{\mathrm{w}}(z) &= \mathbf{V}_{\mathrm{w}}[\boldsymbol{\Psi}_h(z)\mathbf{c} + \boldsymbol{\Psi}_p(z)\boldsymbol{\phi}] \\ \mathbf{u}_z(z) &= -\mathbf{V}_{\Omega}[\boldsymbol{\Psi}_h'(z)\mathbf{c} + \boldsymbol{\Psi}_p'(z)\boldsymbol{\phi}] \end{aligned} \tag{44}$$

The constants, $\mathbf{c}$, have to be determined by the boundary conditions of the thin-walled beam.

6. Element stiffness matrix and load vector

In this section the global beam element stiffness matrix and load vector needed for the determination of the nodal element solution are found. As the load has no influence on the stiffness contributions we use the full assembled homogeneous solution along the beam found in the companion paper [1]. We also use the homogeneous displacement modes to generate the nodal load vector. Some of the distortional displacement modes found and their related eigenvalues are complex. In contrast to paper [1] where a transformation to real modes and real solutions are performed we will here continue working with complex numbers. This means that the use of compilers which include complex numbers with complex operations on matrices will lead to simple algorithms based directly on the following formulations.

The homogeneous solution vectors along the beam are given by the first part of the full solution in Eq. (44) as

$$\begin{aligned} \mathbf{u}_{\mathrm{w}}(z) &= \mathbf{V}_{\mathrm{w}}\boldsymbol{\Psi}_h(z)\mathbf{c} \\ \mathbf{u}_z(z) &= -\mathbf{V}_{\Omega}\boldsymbol{\Psi}_h'(z)\mathbf{c} \end{aligned} \tag{45}$$

where the given constants have to be determined by the GBT-space boundary conditions of the thin-walled beam as described in Ref. [1]. To establish the stiffness matrix and load vector for a single beam element the constants are viewed as temporary element degrees of freedom. The transformation between these constants and the final end displacements of the beam element will be determined by setting up the necessary GBT boundary conditions. Using the homogeneous solution vectors given in Eq. (45) the potential energy including all the homogeneous modes in Eq. (28) can be written as

$$\begin{aligned} \Pi = \frac{1}{2}\int_0^L \Bigg\{ & \mathbf{c}^T \begin{bmatrix} \boldsymbol{\Psi}_h^T\mathbf{V}_{\mathrm{w}}^T & \boldsymbol{\Psi}_h^T\mathbf{V}_{\Omega}^T \end{bmatrix}'' \begin{bmatrix} \mathbf{K}^{\sigma}_{\mathrm{ww}} & \mathbf{0} \\ \mathbf{0} & \mathbf{K}^{\sigma}_{\Omega\Omega} \end{bmatrix} \begin{bmatrix} \mathbf{V}_{\mathrm{w}}\boldsymbol{\Psi}_h \\ \mathbf{V}_{\Omega}\boldsymbol{\Psi}_h \end{bmatrix}'' \mathbf{c} \\ & + \mathbf{c}^T \begin{bmatrix} \boldsymbol{\Psi}_h^T\mathbf{V}_{\mathrm{w}}^T & \boldsymbol{\Psi}_h^T\mathbf{V}_{\Omega}^T \end{bmatrix}' \begin{bmatrix} \mathbf{K}^{\tau}_{\mathrm{ww}} & \mathbf{K}^{\tau}_{\mathrm{w}\Omega} \\ \mathbf{K}^{\tau}_{\Omega\mathrm{w}} & \mathbf{K}^{\tau}_{\Omega\Omega} \end{bmatrix} \begin{bmatrix} \mathbf{V}_{\mathrm{w}}\boldsymbol{\Psi}_h \\ \mathbf{V}_{\Omega}\boldsymbol{\Psi}_h \end{bmatrix}' \mathbf{c} \\ & + \mathbf{c}^T \begin{bmatrix} \boldsymbol{\Psi}_h^T\mathbf{V}_{\mathrm{w}}^T & \boldsymbol{\Psi}_h^T\mathbf{V}_{\Omega}^T \end{bmatrix} \begin{bmatrix} \mathbf{K}^{s} & \mathbf{0} \\ \mathbf{0} & \mathbf{0} \end{bmatrix} \begin{bmatrix} \mathbf{V}_{\mathrm{w}}\boldsymbol{\Psi}_h \\ \mathbf{V}_{\Omega}\boldsymbol{\Psi}_h \end{bmatrix} \mathbf{c} \\ & - \mathbf{c}^T(\boldsymbol{\Psi}_h^T\mathbf{V}_{\mathrm{w}}^T)\mathbf{r}_{\mathrm{w}}\phi - \mathbf{c}^T(\boldsymbol{\Psi}_h^T\mathbf{V}_{\Omega}^T)'\mathbf{r}_{\Omega}\phi \Bigg\} \, dz \end{aligned} \tag{46}$$

Table 3
Beam element stiffness contributions.

$\tilde{\mathbf{K}}^{\sigma}_{ww} = \int_0^L \boldsymbol{\Psi}_h'^T \mathbf{V}_w^T \mathbf{K}^{\sigma}_{ww} \mathbf{V}_w \boldsymbol{\Psi}_h' \, dz$	$\tilde{\mathbf{K}}^{\sigma}_{\Omega\Omega} = \int_0^L \boldsymbol{\Psi}_h'^T \mathbf{V}_\Omega^T \mathbf{K}^{\sigma}_{\Omega\Omega} \mathbf{V}_\Omega \boldsymbol{\Psi}_h' \, dz$
$\tilde{\mathbf{K}}^{\tau}_{ww} = \int_0^L \boldsymbol{\Psi}_h'^T \mathbf{V}_w^T \mathbf{K}^{\tau}_{ww} \mathbf{V}_w \boldsymbol{\Psi}_h' \, dz$	$\tilde{\mathbf{K}}^{\tau}_{\Omega w} = \int_0^L \boldsymbol{\Psi}_h'^T \mathbf{V}_\Omega^T \mathbf{K}^{\tau}_{\Omega w} \mathbf{V}_w \boldsymbol{\Psi}_h' \, dz$
$\tilde{\mathbf{K}}^{\tau}_{w\Omega} = \int_0^L \boldsymbol{\Psi}_h'^T \mathbf{V}_w^T \mathbf{K}^{\tau}_{w\Omega} \mathbf{V}_\Omega \boldsymbol{\Psi}_h' \, dz$	$\tilde{\mathbf{K}}^{\tau}_{\Omega\Omega} = \int_0^L \boldsymbol{\Psi}_h'^T \mathbf{V}_\Omega^T \mathbf{K}^{\tau}_{\Omega\Omega} \mathbf{V}_\Omega \boldsymbol{\Psi}_h' \, dz$
$\tilde{\mathbf{K}}^{s} = \int_0^L \boldsymbol{\Psi}_h'^T \mathbf{V}_w^T \mathbf{K}^{s} \mathbf{V}_w \boldsymbol{\Psi}_h \, dz$	

Table 4
Beam element load vector contributions.

$\tilde{\mathbf{r}}_w = \int_0^L \boldsymbol{\Psi}_h^T \phi \, dz \, \mathbf{V}_w^T \mathbf{r}_w$	$\tilde{\mathbf{r}}_\Omega = \int_0^L \boldsymbol{\Psi}_h' T \phi \, dz \, \mathbf{V}_\Omega^T \mathbf{r}_\Omega$

or in integrated form as

$$\Pi = \tfrac{1}{2}\mathbf{c}^T(\tilde{\mathbf{K}}\mathbf{c} - \tilde{\mathbf{r}}) \tag{47}$$

where $\tilde{\mathbf{K}}$ is the stiffness matrix and $\tilde{\mathbf{r}}$ the load vector related to the modal displacement constants $\mathbf{c}$. The stiffness matrix and the load vector are found by integration and addition of the individual sub matrix products in the potential energy equation (46) as

$$\tilde{\mathbf{K}} = \tilde{\mathbf{K}}^{\sigma}_{ww} + \tilde{\mathbf{K}}^{\sigma}_{\Omega\Omega} + \tilde{\mathbf{K}}^{\tau}_{ww} + \tilde{\mathbf{K}}^{\tau}_{w\Omega} + \tilde{\mathbf{K}}^{\tau}_{\Omega w} + \tilde{\mathbf{K}}^{\tau}_{\Omega\Omega} + \tilde{\mathbf{K}}^{S} \tag{48}$$

and

$$\tilde{\mathbf{r}} = \tilde{\mathbf{r}}_w + \tilde{\mathbf{r}}_\Omega \tag{49}$$

The stiffness matrix contributions are given in Table 3 and the two load vector contributions are given in Table 4. Let us now turn to a reformulation of eigenvectors and solution functions which enables clearer analytical integration.

6.1. Formulation enabling analytical integration

In the potential energy formulation in Eq. (46) the modal matrix of transverse displacement vectors $\mathbf{V}_w$ and the modal matrix of axial warping displacement vectors $\mathbf{V}_\Omega$ contain all the found eigenmode vectors assembled column-wise. However, each eigenvector is only represented once. To ease the integration of the products of the longitudinal amplitude functions $\boldsymbol{\Psi}_h$ we will here introduce a matrix format $\overline{\boldsymbol{\Psi}}_h$ corresponding to a diagonal representation of the solution functions. This can only be done if we also introduce an expanded representation of the eigenvectors $\overline{\mathbf{V}}_w$ and $\overline{\mathbf{V}}_\Omega$. By doing this each eigenvector is represented twice for double roots and four times for quadruple roots. To obtain this format we will use a transformation matrix $\mathbf{H}$ to expand the transverse displacement vectors $\mathbf{V}_w$ and the axial warping displacement vectors $\mathbf{V}_\Omega$ into the full space by

$$\overline{\mathbf{V}}_w = \mathbf{V}_w \mathbf{H} \tag{50}$$

$$\overline{\mathbf{V}}_\Omega = \mathbf{V}_\Omega \mathbf{H} \tag{51}$$

The transformation matrix also gives a transformation from the diagonalized solution function matrix to the original format in Eq. (42) by

$$\boldsymbol{\Psi}_h = \mathbf{H}\overline{\boldsymbol{\Psi}}_h \tag{52}$$

The transformation matrix can be subdivided into a part $\mathbf{H}_b$ related to the transformation of the classic beam modes and a part $\mathbf{H}_d$ related to the transformation of the distortional modes by

$$\mathbf{H} = \begin{bmatrix} \mathbf{H}_b & \mathbf{0} \\ \mathbf{0} & \mathbf{H}_d \end{bmatrix} \tag{53}$$

Concerning the conventional beam displacements as given in Eqs. (29) and (30) the expanding transformation matrix $\mathbf{H}_b$ takes the following form:

$$\mathbf{H}_b = \begin{bmatrix} 1 & 1 & 0 & 0 & 0 & 0 & 0 & 0 & 0 & 0 & 0 & 0 \\ 0 & 0 & 1 & 1 & 1 & 1 & 0 & 0 & 0 & 0 & 0 & 0 \\ 0 & 0 & 0 & 0 & 0 & 0 & 1 & 1 & 1 & 1 & 0 & 0 \\ 0 & 0 & 0 & 0 & 0 & 0 & 0 & 0 & 0 & 0 & 1 & 1 \end{bmatrix} \tag{54}$$

and for the distortional displacements the expanding transformation takes the form

$$\mathbf{H}_d = \begin{bmatrix} 1 & 1 & 0 & 0 & 0 & 0 & \cdots \\ 0 & 0 & 1 & 1 & 0 & 0 & \cdots \\ 0 & 0 & 0 & 0 & 1 & 1 & \cdots \\ \vdots & \vdots & \vdots & \vdots & \vdots & \vdots & \ddots \end{bmatrix} \tag{55}$$

To be clear let us repeat the formulation of the solution functions in the new diagonalized formulation. The integral of the pure axial solution in diagonalized form takes the form

$$\overline{\boldsymbol{\Psi}}_a(z)\mathbf{c}_a = \begin{bmatrix} -z & 0 \\ 0 & -\frac{1}{2}z^2 \end{bmatrix} \begin{bmatrix} c_{a1} \\ c_{a2} \end{bmatrix} \tag{56}$$

while the axial variation of the pure translational modes determined by quadruple integration as described in paper [1] is represented in diagonalized form as

$$\overline{\boldsymbol{\Psi}}_1(z)\mathbf{c}_1 = \begin{bmatrix} 1 & 0 & 0 & 0 \\ 0 & z & 0 & 0 \\ 0 & 0 & z^2 & 0 \\ 0 & 0 & 0 & z^3 \end{bmatrix} \begin{bmatrix} c_{11} \\ c_{12} \\ c_{13} \\ c_{14} \end{bmatrix}$$

$$\overline{\boldsymbol{\Psi}}_2(z)\mathbf{c}_2 = \begin{bmatrix} 1 & 0 & 0 & 0 \\ 0 & z & 0 & 0 \\ 0 & 0 & z^2 & 0 \\ 0 & 0 & 0 & z^3 \end{bmatrix} \begin{bmatrix} c_{21} \\ c_{22} \\ c_{23} \\ c_{24} \end{bmatrix} \tag{57}$$

The axial variation of the pure twist mode (St. Venant torsion) is represented by

$$\overline{\boldsymbol{\Psi}}_3(z)\mathbf{c}_3 = \begin{bmatrix} 1 & 0 \\ 0 & z \end{bmatrix} \begin{bmatrix} c_{31} \\ c_{32} \end{bmatrix} \tag{58}$$

Substituting these full diagonalized solution matrices into a diagonal block matrix formulation similar to Eq. (35) the assembled full diagonalized axial classic beam solution functions $\overline{\boldsymbol{\Psi}}_b$ are obtained.

Concerning the distortional analytical solution functions the ith eigenvalue results in following diagonal solution matrix representation:

$$\overline{\boldsymbol{\Psi}}_{d_i}(z)\mathbf{c}_{d_i} = \begin{bmatrix} e^{\xi_i z} & 0 \\ 0 & e^{-\xi_i z} \end{bmatrix} \begin{bmatrix} c_{d_{2i-1}} \\ c_{d_{2i}} \end{bmatrix}$$

The full diagonalized distortional solution functions are assembled in the (diagonal block) distortional solution matrix $\overline{\boldsymbol{\Psi}}_d$ and multiplied by the assembled vector of distortional constants $\mathbf{c}_d$ similar to Eq. (39). Finally the longitudinal classic beam amplitude solution functions as well as the longitudinal distortional amplitude solution functions are assembled using diagonal block matrices as

$$\overline{\boldsymbol{\Psi}}(z)\mathbf{c} = \begin{bmatrix} \overline{\boldsymbol{\Psi}}_b(z) & \mathbf{0} \\ \mathbf{0} & \overline{\boldsymbol{\Psi}}_d(z) \end{bmatrix} \begin{bmatrix} \mathbf{c}_b \\ \mathbf{c}_d \end{bmatrix} \tag{59}$$

where $\mathbf{c}$ are the original displacement constants. Using the transformation matrix $\mathbf{H}$ as given in Eq. (53) we can obtain the original formulation of the solution function matrix by using the transformation as shown in Eq. (52).

Introducing the transformation given in Eq. (52) of the longitudinally varying amplitude solution functions in the integrals given in Table 3, followed by the use of Eqs. (50) and (51) and noting that only the diagonal amplitude solution functions are

Table 5
Beam element stiffness contributions enabling analytical integration.

$$\tilde{\mathbf{K}}^{\sigma}_{\mathrm{ww}} = \overline{\mathbf{V}}^{T}_{\mathrm{w}}\mathbf{K}^{\sigma}_{\mathrm{ww}}\overline{\mathbf{V}}_{\mathrm{w}} \circ \int_0^L \overline{\mathbf{\Psi}}''\mathbf{J}\overline{\mathbf{\Psi}}''\,dz \qquad \tilde{\mathbf{K}}^{\sigma}_{\Omega\Omega} = \overline{\mathbf{V}}^{T}_{\Omega}\mathbf{K}^{\sigma}_{\Omega\Omega}\overline{\mathbf{V}}_{\Omega} \circ \int_0^L \overline{\mathbf{\Psi}}''\mathbf{J}\overline{\mathbf{\Psi}}''\,dz$$
$$\tilde{\mathbf{K}}^{\tau}_{\mathrm{ww}} = \overline{\mathbf{V}}^{T}_{\mathrm{w}}\mathbf{K}^{\tau}_{\mathrm{ww}}\overline{\mathbf{V}}_{\mathrm{w}} \circ \int_0^L \overline{\mathbf{\Psi}}'\mathbf{J}\overline{\mathbf{\Psi}}'\,dz \qquad \tilde{\mathbf{K}}^{\tau}_{\Omega\mathrm{w}} = \overline{\mathbf{V}}^{T}_{\Omega}\mathbf{K}^{\tau}_{\Omega\mathrm{w}}\overline{\mathbf{V}}_{\mathrm{w}} \circ \int_0^L \overline{\mathbf{\Psi}}'\mathbf{J}\overline{\mathbf{\Psi}}'\,dz$$
$$\tilde{\mathbf{K}}^{\tau}_{\mathrm{w}\Omega} = \overline{\mathbf{V}}^{T}_{\mathrm{w}}\mathbf{K}^{\tau}_{\mathrm{w}\Omega}\overline{\mathbf{V}}_{\Omega} \circ \int_0^L \overline{\mathbf{\Psi}}'\mathbf{J}\overline{\mathbf{\Psi}}'\,dz \qquad \tilde{\mathbf{K}}^{\tau}_{\Omega\Omega} = \overline{\mathbf{V}}^{T}_{\Omega}\mathbf{K}^{\tau}_{\Omega\Omega}\overline{\mathbf{V}}_{\Omega} \circ \int_0^L \overline{\mathbf{\Psi}}'\mathbf{J}\overline{\mathbf{\Psi}}'\,dz$$
$$\tilde{\mathbf{K}}^{s} = \overline{\mathbf{V}}^{T}_{\mathrm{w}}\mathbf{K}^{s}\overline{\mathbf{V}}_{\mathrm{w}} \circ \int_0^L \overline{\mathbf{\Psi}}\mathbf{J}\overline{\mathbf{\Psi}}\,dz$$

dependent on z allows us to see that the product terms become simple. Thus the individual components of the stiffness matrix only contain integrals of one product term. For example the transverse stiffness contribution is reformulated as follows:

$$\tilde{\mathbf{K}}^{s} = \int_0^L \overline{\mathbf{\Psi}}^{T}_{h}\mathbf{H}^{T}\mathbf{V}^{T}_{\mathrm{w}}\mathbf{K}^{s}\mathbf{V}_{\mathrm{w}}\mathbf{H}\overline{\mathbf{\Psi}}_{h}\,dz = \int_0^L \overline{\mathbf{\Psi}}_{h}\overline{\mathbf{V}}^{T}_{\mathrm{w}}\mathbf{K}^{s}\overline{\mathbf{V}}_{\mathrm{w}}\overline{\mathbf{\Psi}}_{h}\,dz$$
$$= \overline{\mathbf{V}}^{T}_{\mathrm{w}}\mathbf{K}^{s}\overline{\mathbf{V}}_{\mathrm{w}} \circ \int_0^L \overline{\mathbf{\Psi}}\mathbf{J}\overline{\mathbf{\Psi}}\,dz \tag{60}$$

in which $\mathbf{J}$ is a matrix of unit components (i.e. all components are equal to one) and the mathematical symbol $\circ$ represents the Hadamard product also known as the "entry-wise product" or the "Schur product". It is seen that only the diagonal matrix $\overline{\mathbf{\Psi}}$ is a function of z and that the integral of the product terms are easily solved analytically due to the simple longitudinal $\psi(z)$ solution functions. This means that the formulation of the respective beam element stiffness contributions in Table 3 can be reformulated as given in Table 5.

6.2. Generalized displacements

The generalized displacements of the present GBT formulation are determined by the first variation of the potential energy, shear constrains and the multi point constraint equations, as described in Ref. [1]. This degree of freedom space is what we refer to as the GBT-space. In this space the degrees of freedom are determined as the value of the pure axial extension $u^{a}_{z}(z)$, the values of the remaining unconstrained transverse displacements $\mathbf{u}^{g}_{\mathrm{w}}(z)$ and their axial derivatives $\mathbf{u}^{g'}_{\mathrm{w}}(z)$ as given by the expressions involving the eigenmode vectors, solution functions and solution constants

$$\begin{bmatrix} u^{a}_{z}(z) \\ \mathbf{u}^{g}_{\mathrm{w}}(z) \\ \mathbf{u}^{g'}_{\mathrm{w}}(z) \end{bmatrix} = \begin{bmatrix} -\mathbf{T}^{a^T}_{\Omega}\mathbf{V}_{\Omega}\mathbf{\Psi}'_{h}(z) \\ \mathbf{T}^{g^T}_{\mathrm{w}}\mathbf{V}_{\mathrm{w}}\mathbf{\Psi}_{h}(z) \\ \mathbf{T}^{g^T}_{\mathrm{w}}\mathbf{V}_{\mathrm{w}}\mathbf{\Psi}'_{h}(z) \end{bmatrix}\mathbf{c} \tag{61}$$

Here the transformations are taken directly from Ref. [1], which in detail describes these. As in a basic beam element formulation we will specify the boundary displacements at the two ends of the beam, i.e. at $z=0$ and at $z=L$ where L is the beam length. Denoting the assembled boundary displacement vector by $\mathbf{u}_b$ we can write the following equation for the determination of the solution constants:

$$\mathbf{u}_b = \begin{bmatrix} u^{a}_{z}(0) \\ \mathbf{u}^{g}_{\mathrm{w}}(0) \\ \mathbf{u}^{g'}_{\mathrm{w}}(0) \\ u^{a}_{z}(L) \\ \mathbf{u}^{g}_{\mathrm{w}}(L) \\ \mathbf{u}^{g'}_{\mathrm{w}}(L) \end{bmatrix} = \begin{bmatrix} -\mathbf{T}^{a^T}_{\Omega}\mathbf{V}_{\Omega}\mathbf{\Psi}'_{h}(0) \\ \mathbf{T}^{g^T}_{\mathrm{w}}\mathbf{V}_{\mathrm{w}}\mathbf{\Psi}_{h}(0) \\ \mathbf{T}^{g^T}_{\mathrm{w}}\mathbf{V}_{\mathrm{w}}\mathbf{\Psi}'_{h}(0) \\ -\mathbf{T}^{a^T}_{\Omega}\mathbf{V}_{\Omega}\mathbf{\Psi}'_{h}(L) \\ \mathbf{T}^{g^T}_{\mathrm{w}}\mathbf{V}_{\mathrm{w}}\mathbf{\Psi}_{h}(L) \\ \mathbf{T}^{g^T}_{\mathrm{w}}\mathbf{V}_{\mathrm{w}}\mathbf{\Psi}'_{h}(L) \end{bmatrix}\mathbf{c} = \mathbf{A}\mathbf{c} \tag{62}$$

This equation defines the "square" invertible matrix $\mathbf{A}$ and allows the determination of the solution constants by the beam end displacements as

$$\Rightarrow \quad \mathbf{c} = \mathbf{A}^{-1}\mathbf{u}_b \tag{63}$$

The first variation of the elastic potential energy in Eq. (47) then takes the form

$$\delta\Pi = \delta\mathbf{c}^{T}(\tilde{\mathbf{K}}\mathbf{c} - \tilde{\mathbf{r}}) \tag{64}$$

Substituting beam boundary displacements for the solution constants using Eq. (63) we redefine the formulation to include the end displacements in GBT-space as follows:

$$\delta\Pi = \delta\mathbf{u}^{T}_{b}\mathbf{A}^{-T}\tilde{\mathbf{K}}\mathbf{A}^{-1}\mathbf{u}_b - \delta\mathbf{u}^{T}_{b}\mathbf{A}^{-T}\tilde{\mathbf{r}} = \delta\mathbf{u}^{T}_{b}(\mathbf{K}_e\mathbf{u}_b - \mathbf{R}_e) \tag{65}$$

where we have introduced the beam element stiffness matrix in GBT-space as

$$\mathbf{K}_e = \mathbf{A}^{-T}\tilde{\mathbf{K}}\mathbf{A}^{-1} \tag{66}$$

and the beam element load vector in GBT-space as

$$\mathbf{R}_e = \mathbf{A}^{-T}\tilde{\mathbf{r}} \tag{67}$$

For stationarity the first variation of the potential energy must be equal to zero whereby we can write the single element equations as

$$\mathbf{K}_e\mathbf{u}_b = \mathbf{R}_e \tag{68}$$

Having a prismatic structure of multiple beam elements we have to setup a global system in which the end boundary displacements (in GBT-space) are assembled. Using a standard finite element procedure to assemble the global system we obtain

$$\mathbf{K}\mathbf{u} = \mathbf{R} \quad \Leftrightarrow \quad \mathbf{u} = \mathbf{K}^{-1}\mathbf{R} \tag{69}$$

where $\mathbf{K}$ has to be a positive definite "square" matrix and $\mathbf{R}$ is the load vector corresponding to the chosen load. However, in order to achieve a positive definite matrix it is necessary to apply boundary conditions, for example as described in the next section.

In a conventional finite element formulation the displacement field between the nodes is usually interpolated using approximated shape functions. In the present formulation we do not use approximated interpolation functions as we have found the exact shape functions as given in Eq. (61). Furthermore, we can adjust the internal displacement field to the distributed loads on the individual beam element using the particular solutions with adequate boundary conditions as described after the next section.

7. Boundary conditions and nodal loads

In the present formulation the global stiffness matrix $\mathbf{K}$ is related to sets of beam end degrees of freedom $\mathbf{u}_{\mathrm{GBT}}$ in the GBT-space and after assembling the individual element matrices this global matrix will be singular corresponding to the rigid body movements. Thus we have to specify at least six conditions to keep the beam fixed in space in order to solve the equations.

Of the methods used to introduce boundary conditions in the finite element equations (69) we have chosen the simple method of adding stiff springs. As the present formulation is in the constrained, eliminated and transformed GBT-space it is rather difficult to apply directly to the desired boundary conditions. Therefore, the boundary stiffness contributions $\Delta\mathbf{K}_{\mathrm{FE}}$ are formulated in the unconstrained FE-space $\mathbf{u}_{\mathrm{FE}}$ corresponding to all nodal degrees of freedom shown in Fig. 3 and the axial derivatives of transverse components of these. For more clarity let us show the GBT and FE-space displacement vectors and their transformation as deduced from the companion paper [1]

$$\mathbf{u}_{\mathrm{GBT}} = \begin{bmatrix} u^{a}_{z} \\ \mathbf{u}^{g}_{\mathrm{w}} \\ \mathbf{u}^{g}_{\mathrm{w}} \end{bmatrix} = \begin{bmatrix} \mathbf{T}^{a^T}_{\Omega} & \mathbf{0} & \mathbf{0} \\ \mathbf{0} & \mathbf{T}^{g^T}_{\mathrm{w}} & \mathbf{0} \\ \mathbf{0} & \mathbf{0} & \mathbf{T}^{g^T}_{\mathrm{w}} \end{bmatrix} \begin{bmatrix} \mathbf{u}_{z} \\ \mathbf{u}_{\mathrm{w}} \\ \mathbf{u}'_{\mathrm{w}} \end{bmatrix} = \mathbf{T}\mathbf{u}_{\mathrm{FE}} \tag{70}$$

Thus the beam end spring stiffness contributions $\Delta\mathbf{K}_{\mathrm{FE}}$ are transformed into GBT space by

$$\Delta\mathbf{K}_{\mathrm{GBT}} = \mathbf{T}^{T}\Delta\mathbf{K}_{\mathrm{FE}}\mathbf{T} \tag{71}$$

and the nodal loads (at beam element ends and intersections) are transformed from FE-space to GBT-space by the transformation

$$\Delta \mathbf{R}_{\mathrm{GBT}} = \mathbf{T}^T \Delta \mathbf{R}_{\mathrm{FE}} \tag{72}$$

Using this method quite a wide range of situations may be analyzed. However, other methods involving coupling with traditional finite plate elements is envisioned to be possible and should be further investigated in the future.

8. Internal element displacements

The internal beam displacements are represented by the cross-section node displacement vectors $\mathbf{u}_z(z)$ and $\mathbf{u}_w(z)$ as a function of the axial coordinate z. In the beam element these internal displacements are found by superposition of ⓐ the internal displacements induced by the nodal displacements without distributed loading and ⓑ the displacements induced by the loading on the beam with zero nodal displacements.

8.1. Nodal displacements

Adhering to this concept Eq. (73) gives us the first contribution as

$$\begin{aligned} \mathbf{u}_{\mathrm{w}}^{\textcircled{a}}(z) &= \mathbf{V}_{\mathrm{w}} \boldsymbol{\Psi}_h(z) \mathbf{c} \\ \mathbf{u}_z^{\textcircled{a}}(z) &= -\mathbf{V}_{\Omega} \boldsymbol{\Psi}_h'(z) \mathbf{c} \end{aligned} \tag{73}$$

where the constants $\mathbf{c} = \mathbf{A}^{-1}\mathbf{u}_b$ are determined by the nodal displacements of the element $\mathbf{u}_b$.

8.2. Loading induced displacements

The second contribution involves the solution of the differential equations with boundary conditions corresponding to zero nodal displacements. As the particular solution does not abide to zero displacements at the nodes, this has to be achieved by addition of a homogeneous solution. The boundary conditions for the GBT equations are formulated in the companion paper [2], which in the present complex formulation corresponds to

$$\mathbf{u}_b = \begin{bmatrix} -\mathbf{T}_{\Omega}^{a^T}\mathbf{V}_{\Omega}\boldsymbol{\Psi}_h'(0) \\ \mathbf{T}_{\mathrm{w}}^{g^T}\mathbf{V}_{\mathrm{w}}\boldsymbol{\Psi}_h(0) \\ \mathbf{T}_{\mathrm{w}}^{g^T}\mathbf{V}_{\mathrm{w}}\boldsymbol{\Psi}_h'(0) \\ -\mathbf{T}_{\Omega}^{a^T}\mathbf{V}_{\Omega}\boldsymbol{\Psi}_h'(L) \\ \mathbf{T}_{\mathrm{w}}^{g^T}\mathbf{V}_{\mathrm{w}}\boldsymbol{\Psi}_h(L) \\ \mathbf{T}_{\mathrm{w}}^{g^T}\mathbf{V}_{\mathrm{w}}\boldsymbol{\Psi}_h'(L) \end{bmatrix} \mathbf{c}_p + \begin{bmatrix} -\mathbf{T}_{\Omega}^{a^T}\mathbf{V}_{\Omega}\boldsymbol{\Psi}_p'(0) \\ \mathbf{T}_{\mathrm{w}}^{g^T}\mathbf{V}_{\mathrm{w}}\boldsymbol{\Psi}_p(0) \\ \mathbf{T}_{\mathrm{w}}^{g^T}\mathbf{V}_{\mathrm{w}}\boldsymbol{\Psi}_p'(0) \\ -\mathbf{T}_{\Omega}^{a^T}\mathbf{V}_{\Omega}\boldsymbol{\Psi}_p'(L) \\ \mathbf{T}_{\mathrm{w}}^{g^T}\mathbf{V}_{\mathrm{w}}\boldsymbol{\Psi}_p(L) \\ \mathbf{T}_{\mathrm{w}}^{g^T}\mathbf{V}_{\mathrm{w}}\boldsymbol{\Psi}_p'(L) \end{bmatrix} \boldsymbol{\phi} = \mathbf{A}\mathbf{c}_p + \mathbf{B}\boldsymbol{\phi} \tag{74}$$

which also defines the particular solution matrix $\mathbf{B}$ that gives the displacement values of the particular solutions at the beam boundaries when multiplied by the two end load intensity values in $\boldsymbol{\phi}$. Inserting that the nodal displacements are zero we find the constants $\mathbf{c}_p$, which are determine the homogeneous solutions to add to the particular solution in order to abide the boundary conditions

$$\mathbf{u}_b = 0 \Rightarrow \quad \mathbf{c}_p = -\mathbf{A}^{-1}\mathbf{B}\boldsymbol{\phi} \tag{75}$$

With this knowledge the second contribution is given by Eq. (44) as

$$\begin{aligned} \mathbf{u}_{\mathrm{w}}^{\textcircled{b}}(z) &= \mathbf{V}_{\mathrm{w}}[\boldsymbol{\Psi}_h(z)\mathbf{c}_p + \boldsymbol{\Psi}_p(z)\boldsymbol{\phi}] \\ \mathbf{u}_z^{\textcircled{b}}(z) &= -\mathbf{V}_{\Omega}[\boldsymbol{\Psi}_h'(z)\mathbf{c}_p + \boldsymbol{\Psi}_p'(z)\boldsymbol{\phi}] \end{aligned} \tag{76}$$

8.3. Superpositioned displacements

Finally we can superimpose the two solutions ⓐ and ⓑ and find the semi-analytically determined internal displacement vectors as

$$\begin{aligned} \mathbf{u}_{\mathrm{w}}(z) &= \mathbf{V}_{\mathrm{w}}\left[\boldsymbol{\Psi}_h(z)(\mathbf{c}+\mathbf{c}_p) + \boldsymbol{\Psi}_p(z)\boldsymbol{\phi}\right] \\ \mathbf{u}_z(z) &= -\mathbf{V}_{\Omega}\left[\boldsymbol{\Psi}_h'(z)(\mathbf{c}+\mathbf{c}_p) + \boldsymbol{\Psi}_p'(z)\boldsymbol{\phi}\right] \end{aligned} \tag{77}$$

where $\mathbf{c} = \mathbf{A}^{-1}\mathbf{u}_b$ and $\mathbf{c}_p = -\mathbf{A}^{-1}\mathbf{B}\boldsymbol{\phi}$. Now we are able to find displacements, strains and stress at any point in the beam element. In the next section some examples illustrating this new approach are given.

9. Example

In this section four illustrative examples are given and nodal displacement results as well as stress distribution results of GBT are compared to those found using the commercial FE program Abaqus. In the examples we consider a simple supported lipped channel beam and a box beam each with a length of 1500 mm consisting of and assembled by three single beam elements of 500 mm. The end sections are constrained against transverse displacements, but otherwise free to warp (and thus also rotate). Further, one of the ends is fixed at a single node against longitudinal translation. Different load cases have been chosen for the four examples. An elasticity modulus $E = 2.1 \times 10^5$ MPa and a Poisson ratio of $\nu = 0.3$ have been used.

The results found using Abaqus are based on isotropic material and the S4 shell element with full 4 point integration. The linear elastic finite element calculations are based on a structured rectangular mesh with a side length seed of 5 mm. The cross section is fixed in the transverse directions at both ends and fixed at a single node against longitudinal translation.

All stress comparisons between the present novel approach and the commercial FE program Abaqus are performed in relation to the given maximum stress at the cross section.

9.1. Example 1: Uniform distributed load on a simple supported lipped channel beam

In this example a simple supported lipped channel beam loaded as shown in Fig. 8 is analyzed.

Using the parameters as given in Figs. 20 and 21 and the full solution from Eq. (77) leads to the deformed configuration shown in Fig. 10 and the associated displacement values in Table 6 from the marked node at mid-span. It is seen that the main

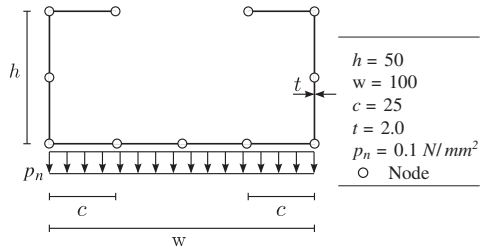

Fig. 8. Example 1: Geometry, in-plane discretization, parameter values and load for the lipped channel beam.

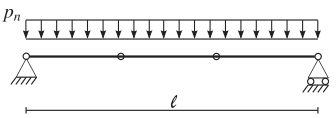

Fig. 9. Example 1: Geometry and discretization for a lipped channel beam consisting of three elements.

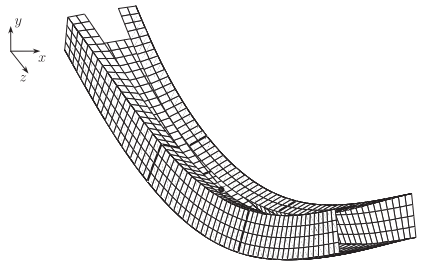

Fig. 10. Example 1: GBT plot of the lipped channel with a flexural load.

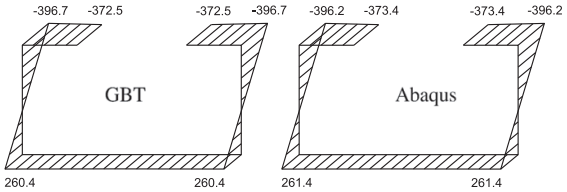

Fig. 11. Example 1: Comparison between the axial normal stress distributions obtained with GBT and Abaqus at mid-span. All values are in MPa.

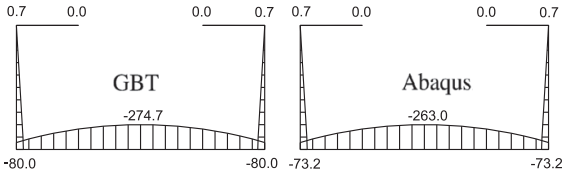

Fig. 12. Example 1: Comparison between the transverse bending stress distributions obtained with GBT and Abaqus at mid-span. All values are in MPa.

Table 6
Example 1: Nodal displacements of GBT and FE analysis.

	GBT (mm)	Abaqus (mm)	Difference (%)
u_x	2.504	2.443	2.5
u_y	−16.236	−16.378	0.9

Table 7
Example 1: Stress distributions of GBT and FE analysis.

	GBT (MPa)	Abaqus (MPa)	Difference (%)
σ_z	260.4	261.4	0.3
σ_s	−274.7	−263.0	4.3

deformation is related to flexure; however, also an in-plane deformation of the cross section becomes clear. This points out the importance of taking distortion into account in order to obtain a good approximation of the deformation shape even in simple load cases.

The bold lines shown in the figure correspond to the deformed end cross sections at the nodes of the assembled beam elements. These nodes are also shown in Fig. 9.

Comparing the nodal displacements of GBT to the one found from a model in the commercial FE program Abaqus gives the values and the corresponding deviations shown in Table 6. The values correspond to the node marked on the deformed plot of the GBT solution in Fig. 10 at mid-span of the beam. From Table 6 the deviation from Abaqus results of the displacement, u_x, in the horizontal direction is 2.5%. In contrast, the deviation for the vertical displacement, u_y, is 0.9%. Based on the poor discretization of the cross section and according to the present approach which is based on a beam theory these deviations may be expected. Having compared the nodal displacements obtained with GBT and Abaqus we take a look at the stress distributions. A comparison of the membrane stresses in the z-direction at mid-span are shown in Fig. 11. Comparing the stresses in relation to the maximum stress at the cross section a maximum deviation of 0.3% is obtained as shown in Table 7. The transverse bending stresses at mid-span are shown in Fig. 12. In this case a maximum deviation of 4.3% is obtained which is caused by the approach based on a beam theory and by the poor discretization of the cross section as well as the chosen fine mesh size used in the Abaqus model.

9.2. Example 2: Point loads on a simple supported lipped channel beam

In this example a simple supported lipped channel beam loaded by two point loads symmetrically placed in the same cross section as shown in Fig. 13 is analyzed.

Using the parameters as given in Figs. 13 and 14 and the full solution in Eq. (77) leads to the deformed configuration shown in Fig. 15. Here it is seen that the global deformation is related to flexure of the beam, non-local distortional deformation of the cross section and a very local plate deformation of the lips related to the location of the point loads. Thus three length scales are represented, the global flexural beam mode as seen in Fig. 15, the non-local distortional deformation of the lips as shown in Fig. 16 and the local distortional plate deformation of the lip as shown in

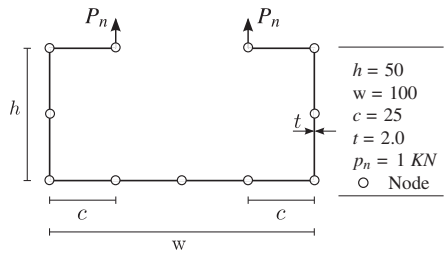

Fig. 13. Example 2: Geometry, in-plane discretization, parameter values and load for the lipped channel beam.

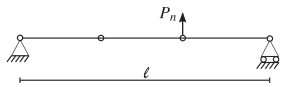

Fig. 14. Example 2: Geometry and discretization for a lipped channel beam consisting of three elements.

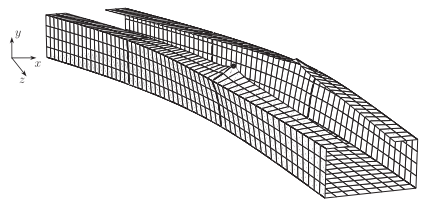

Fig. 15. Example 2: GBT plot of the lipped channel with point loads.

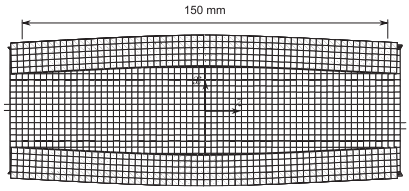

Fig. 16. Example 2: GBT plot of the lipped channel to shown the exponential decrease in the x–z-plane.

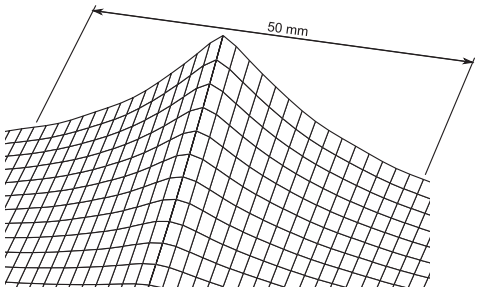

Fig. 17. Example 2: GBT plot of the lipped channel to shown the exponential decrease in the y–z-plane.

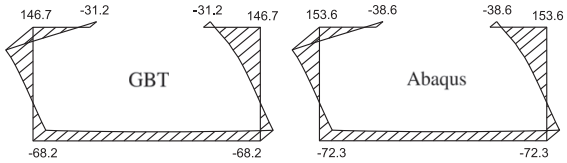

Fig. 18. Example 2: Comparison between the axial normal stress distributions obtained with GBT and Abaqus. All values are in MPa.

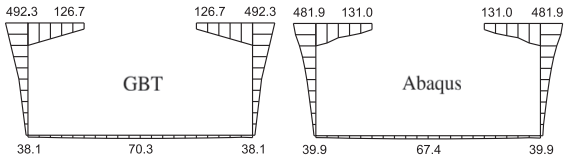

Fig. 19. Example 2: Comparison between the transverse bending stress distributions obtained with GBT and Abaqus. All values are in MPa.

Table 8
Example 2: Nodal displacements of GBT and FE analysis.

	GBT (mm)	Abaqus (mm)	Difference (%)
u_x	−1.424	−1.415	0.6
u_y	4.697	4.772	1.6

Table 9
Example 2: Stress distributions of GBT and FE analysis.

	GBT (MPa)	Abaqus (MPa)	Difference (%)
σ_z	−31.2	−38.6	4.8
σ_s	492.3	481.9	2.1

close-up in Fig. 17. This example points out the importance of taking distortion into account in order to obtain a good approximation of the deformation shape.

From Fig. 17 it is seen that the deflection in the longitudinal z-direction decreases exponentially in the y–z-plane. It should also be noted that the deformation is so local that it is difficult to see that the surface is C^1 continuous. The decreasing non-local distortion is clear in the x–z-plot shown in Fig. 16, which represents a part of the beam symmetrically about the loaded cross section. Comparing the nodal displacements of the marked node to the displacement found using a model in the commercial FE program Abaqus gives the displacement values and the corresponding deviations shown in Table 8. From Table 8 the deviation from Abaqus results of the displacement, u_x, in the horizontal direction is 0.6% while the deviation for the vertical displacement, u_y, is 1.6%. Due to the poor discretization of the cross section and the present approach which is based on a beam theory these deviations may also be expected.

Having compared the nodal displacement obtained with GBT and Abaqus we take a look at the stress distributions. A comparison of the membrane stresses in the z-direction is shown in Fig. 18. Comparing the stresses in relation to the maximum stress at the cross section a maximum deviation of 4.8% is obtained as shown in Table 9. This deviation level is expected as the chosen point is subjected to very local complex phenomena. The transverse bending stresses are shown in Fig. 19. In this case a maximum deviation of 2.1% is obtained.

9.3. Example 3: Line load on a simple supported lipped channel beam

In this example a simple supported lipped channel beam loaded as shown in Fig. 20 is analyzed. The length of the beam elements is 500 mm whereby the total beam length is 1500 mm.

Using the parameters as given in Figs. 20 and 21 and the full solution in Eq. (77) leads to the deformed configuration shown in Fig. 22. Here it is seen that the main deformation is related to flexure; however, also an in-plane deformation of the cross section becomes clear. Comparing the nodal displacements of the marked node at mid-span to the displacement found using a model in the commercial FE program Abaqus gives the displacement values and the corresponding deviations shown in Table 10. The bold lines given in the figure are describing the connection points between the assembled elements as also shown in Fig. 21.

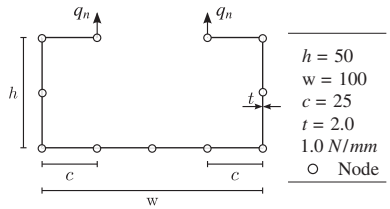

Fig. 20. Example 3: Geometry, in-plane discretization, parameter values and load for the lipped channel beam.

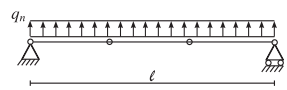

Fig. 21. Example 3: Geometry and discretization for a lipped channel beam consisting of three elements.

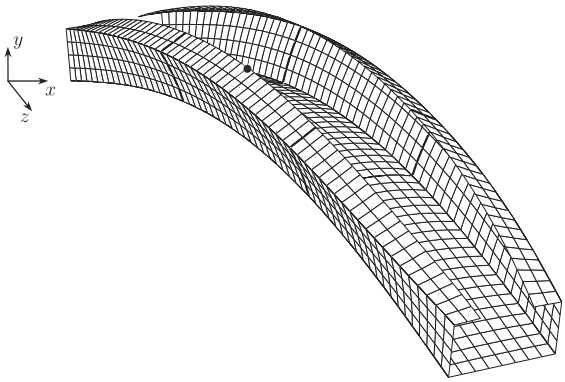

Fig. 22. Example 3: GBT plot of the lipped channel with a line load.

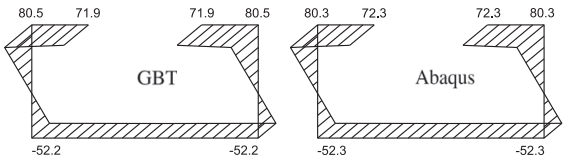

Fig. 23. Example 3: Comparison between the axial normal stress distributions obtained with GBT and Abaqus at mid-span. All values are in MPa.

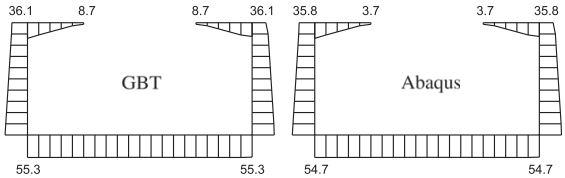

Fig. 24. Example 3: Comparison between the transverse bending stress distributions obtained with GBT and Abaqus at mid-span. All values are in MPa.

Table 10
Example 3: Nodal displacements of GBT and FE analysis.

	GBT (mm)	Abaqus (mm)	Difference (%)
u_x	−0.870	−0.853	2.0
u_y	3.634	3.657	0.6

Table 11
Example 3: Stress distributions of GBT and FE analysis.

	GBT (MPa)	Abaqus (MPa)	Difference (%)
σ_z	71.9	72.3	0.5
σ_s	8.7	3.7	9.0

The values in Table 10 corresponds to the node marked on the deformed plot of the GBT solution in Fig. 22 at mid-span of the beam. From Table 10 the deviation from Abaqus results of the displacement, u_x, in the horizontal direction is 2.0%. In contrast, the deviation for the vertical displacement, u_y, is 0.6%. Based on the chosen discretization of the cross section and according to the present approach which is based on a beam theory these deviations may be expected. Having compared the nodal displacement obtained with GBT and Abaqus we take a look at the stress distributions. A comparison of the membrane stresses in the z direction at mid-span is shown in Fig. 23. Comparing the stresses in relation to the maximum stress at the cross section a maximum deviation of 0.5% is obtained as shown in Table 11. The transverse bending stresses at mid-span are shown in Fig. 24. In this case a maximum deviation of 9.0% is obtained. This is due to the use of the minimum possible discretization of the cross section lip with only one cross section wall element.

9.4. Example 4: Flexural–torsional load on a simple supported box beam

In this example a simple supported box beam loaded as shown in Fig. 25 is analyzed.

Using the parameters as given in Figs. 25 and 26 and the full solution given in Eq. (77) leads to the deformed configuration shown

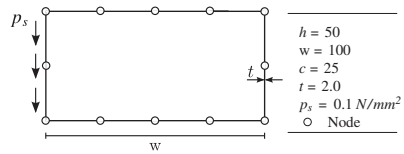

Fig. 25. Example 4: Geometry, in-plane discretization, parameter values and load for the box beam.

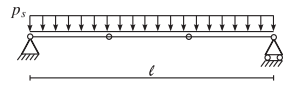

Fig. 26. Example 4: Geometry and discretization for a box beam consisting of 3 elements.

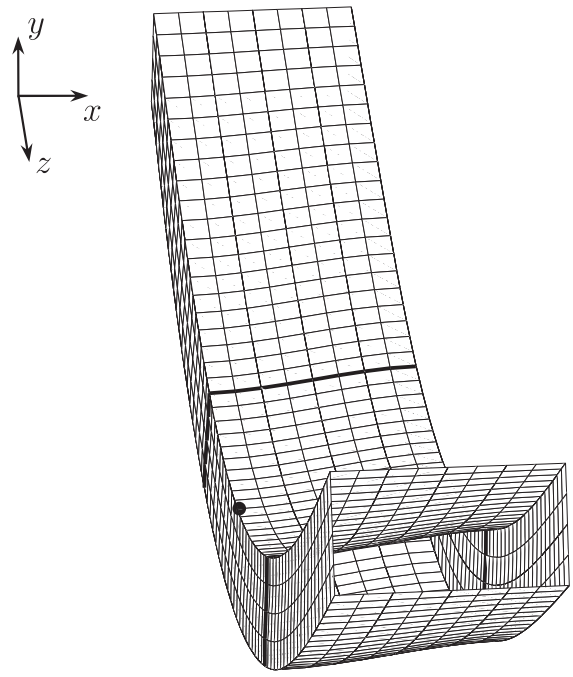

Fig. 27. Example 4: GBT plot of the box beam with a flexural-torsional load.

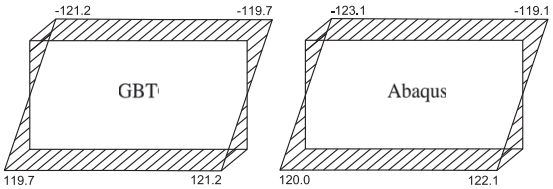

Fig. 28. Example 4: Comparison between the axial normal stress distributions obtained with GBT and Abaqus at mid-span. All values are in MPa.

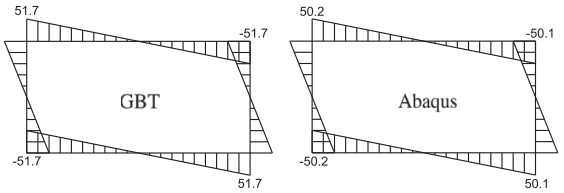

Fig. 29. Example 4: Comparison between the transverse bending stress distributions obtained with GBT and Abaqus at mid-span. All values are in MPa.

Table 12
Example 4: Nodal displacements of GBT and FE analysis.

	GBT (mm)	Abaqus (mm)	Difference (%)
u_x	−0.067	−0.068	1.5
u_y	−5.584	−5.698	2.0

Table 13
Example 4: Stress distributions of GBT and FE analysis.

	GBT (MPa)	Abaqus (MPa)	Difference (%)
σ_z	−121.2	−123.1	1.6
σ_s	51.7	50.1	3.1

in Fig. 27 and the associated displacement values in Table 12 from the marked node at mid-span. Here it is seen that the main deformation is related to flexure and torsion; however, also an in-plane deformation of the rigid box section becomes clear.

Comparing the nodal displacements of the marked node to the displacement found using a model in the commercial FE program Abaqus gives the displacement values and the corresponding deviations shown in Table 12. The deviations from the Abaqus results of the displacement, u_x, in the horizontal direction is 1.5% while the deviation for the vertical displacement, u_y, is 2.0%. Based on the chosen discretization of the cross section and according to the present approach which is based on a beam theory these deviations may be expected.

Having compared the nodal displacement obtained with GBT and Abaqus we take a look at the stress distributions. A comparison of the membrane stresses in the z-direction at mid-span are shown in Fig. 28. Comparing the stresses in relation to the maximum stress at the cross section a maximum deviation of 1.6% is obtained as shown in Table 13. The transverse bending stresses at mid-span are shown in Fig. 29. In this case a maximum deviation of 3.1% is obtained.

10. Conclusion

In this paper we have presented the formulation of a distortional semi-discretized thin-walled beam element. Using the full assembled homogenous solution along the beam, the beam element stiffness matrices have been found. From the full assembled homogenous solution as well as the full assembled non-homogeneous solution the displacements of the full semi-analytical solution along the beam have been found in the context of a beam element. Illustrative examples including both open and closed cross sections as well as different load cases have been given. The chosen examples show solutions which are applicable to the finite element formulation. The novel approach presented in this paper is a considerable theoretical achievement, since it without approximation gives the full analytical solution along the loaded beam for a given discretization of the cross section. Reasonable matches are obtained in all cases confirming that this new developed GBT approach provides reasonable results with a very small computational cost making it an alternative to the traditional finite element calculations and the other available methods.

References

[1] Jönsson J, Andreassen MJ. Distortional eigenmodes and homogeneous solutions of semi-discretized thin-walled beams. Thin-Walled Structures 2011;49:691–707.
[2] Andreassen MJ, Jönsson J. Distortional solutions for loaded semi-discretized thin-walled beams. Thin-Walled Structures 2012;50:116–27.
[3] Andreassen MJ, Jönsson J. Distortional buckling modes of semi-discretized thin-walled columns. Thin-Walled Structures 2012;51:53–63.
[4] Zienkiewicz OC, Taylor RL. The finite element method. In: Basic formulations and linear problems, fourth ed, vol. 1. UK: McGraw-Hill Book Company; 1989.
[5] Hughes TJR. The finite element method: linear static and dynamic finite element analysis. Englewood Cliffs, NJ: Prentice-Hall; 2000.
[6] Jönsson J, Krenk S, Damkilde L. Recursive substructuring of finite elements. Computers Structures 1995;54:395–404.
[7] Cheung YK. Finite strip method in structural analysis. Oxford: Pergamon Press; 1976.
[8] Cheung YK, Tham LG. The finite strip method. Boca Raton: CRC Press; 1998.
[9] Williams FW, Wittrick WH. Computational procedures for a matrix analysis of the stability and vibrations of thin flat-walled structures in compression. International Journal of Mechanical Sciences 1968;11:798–979.
[10] Loja M, Mota Soares CM, Mota Soares CA. Modelling and design of adaptive structures using B-spline strip models. Composite Structures 2002;57(1–4):245–51.
[11] Schafer BW, Ádány S. Modal decomposition for thin-walled member stability using the finite strip method. In; Advances in engineering structures, mechanics and construction. Springer; 2006. p. 411–22.
[12] Schardt R. Eine Erweiterung der technischen Biegelehre für die Berechnung biegesteifer prismatischer Faltwerke. Der Stahlbau 1966;35:161–71.
[13] Schardt R. Verallgemeinerte Technische Biegetheorie. Germany: Springer-Verlag; 1989.
[14] Davies JM, Leach P. First-order generalised beam theory. Journal of Constructional Steel Research 1994;31(2–3):187–220.
[15] Lepistö J, Nikula S, Niemi E. Optimum design of cold-formed sections using generalized beam theory. In: Rondal J, Dubina D, Gioncu V, editors, Proceedings of the second international conference on coupled instabilities in metal structures (CIMS 1996 - Liège, 05-07/09). London: Imperial College Press. p. 101–8.
[16] Simão P, Simões da Silva L. Comparative analysis of the stability of open and closed thin-walled section members in the framework of generalized beam theory. In: Lamas A, Simões da Silva L, editors, Proceedings of the third European conference on steel structures (EUROSTEEL 2002—Coimbra, Portugal, 19-20/09), vol. 1; 2002. p. 711–21.
[17] Gonçalves R, Dinis PB, Camotim D. GBT formulation to analyse the first-order and buckling behaviour of thin-walled members with arbitrary cross-sections. Thin-Walled Structures 2009;47:583–600.
[18] Gonçalves R, Camotim D. Steel-concrete composite bridge analysis using generalised beam theory. Steel and Composite Structures 2010;10:223–43.
[19] Silvestre N. Generalized beam theory: new formulations, numerical implementation and applications. PhD thesis. IST—Technical University of Lisbon, Portugal; 2005 [in Portuguese].
[20] Silvestre N, Camotim D. First-order generalised beam theory for arbitrary orthotropic materials. Thin-Walled Structures 2002;40:755–89.
[21] Silvestre N, Camotim D. Second-order generalised beam theory for arbitrary orthotropic materials. Thin-Walled Structures 2002;40:791–820.

[22] Rendek S, Baláž I. Distortion of thin-walled beams. Thin-Walled Structures 2004;42:255–77.
[23] Camotim D, Silvestre N, Gonçalves R, Dinis PB. GBT analysis of thin-walled members: new formulations and applications. In: Loughlan J, editors. Thin-walled structures: recent advances and future trends in thin-walled structures technology. Bath: Canopus Publishing Ltd.; 2004. p. 137–68.
[24] Camotim D, Silvestre N, Gonçalves R, Dinis PB. GBT-based structural analysis of thin-walled members: overview, recent progress and future developments. In: Pandey M, Xie W-C, Xu L, editors. Advances in engineering structures, mechanics & construction. Dordrecht, Waterloo: Springer; 2006. p. 187–204.
[25] Hanf M. Die geschlossene Lösung der linearen Differentialgleichungssysteme der Verallgemeinerten Technischen Biegetheorie mit einer Anwendung auf die Ermittlung plastischer Grenzlasten, vol. 9. Darmstadt: Instituts für Werkstoffe und Mechanik im Bauwesen der TU; 1989.
[26] Gonçalves R, Camotim D. GBT local and global buckling analysis of aluminium and stainless steel columns. Computers and Structures 2004;82:1473–84.
[27] Gonçalves R, Ritto-Corrêa M, Camotim D. A new approach to the calculation of cross-section deformation modes in the framework of generalized beam theory. Computational Mechanics 2010;46:759–81.
[28] Kollbrunner CF, Hajdin N. Dünnwandige Stäbe 1, Stäbe mit undeformierbaren Querschnitten. Berlin: Springer-Verlag; 1972, 1975.
[29] Jönsson J. Determination of shear stresses. Computers Structures 1998;68:393–410.
[30] Jönsson J. Distortional theory of thin-walled beams. Thin-Walled Structures 1999;33:269–303.
[31] Jönsson J. Distortional warping functions and shear distributions in thin-walled beams. Thin-Walled Structures 1999;33:245–68.
[32] Vlasov VZ. Thin-walled elastic beams. Israel program for scientific translations, Jerusalem, Israel, second ed; 1961.
[33] Kollbrunner CF, Hajdin N, Dünnwandige Stäbe 2, Stäbe mit deformierbaren Querschnitten, Nicht-elastisches Verhalten dünnwandiger Stäbe. Berlin: Springer-Verlag; 1972, 1975.
[34] Schardt R. Anwendung der Erweiterten Technischen Biegetheorie auf die Berechnung prismatischer Faltwerke und Zylinderschalen nach Theorie I. und II. Ordnung. Ordnung. IASS–Symposium on Folded Plates and Prismatic Structures, vol. 1, Wien; 1970.
[35] Davies JM, Leach P. Second-order generalised beam theory. Journal of Constructional Steel Research 1994;31:221–41.
[36] Camotim D, Silvestre N, Basaglia C, Bebiano R. GBT-based buckling analysis of thin-walled members with non-standard support conditions. Thin-Walled Structures 2008;46:800–15.
[37] Zienkiewicz OC, Taylor RL. Finite element method. In: Solid mechanics, fifth ed, vol. 2. Elsevier; 2000. p. 207.
[38] Ádány S, Schafer BW. Buckling mode decomposition of single-branched open cross-section members via finite strip method: derivation. Thin-Walled Structures 2006;44:563–84.
[39] Ádány S, Schafer BW. Buckling mode decomposition of single-branched open cross-section members via finite strip method: application and examples. Thin-Walled Structures 2006;44:585–600.
[40] Ádány S, Schafer BW. A full modal decomposition of thin-walled, signle-branched open cross-section members via the constrained finite strip method. Journal of Constructional Steel Research 2008;64:12–29.
[41] Ádány S, Silvestre N, Schafer BW, Camotim D. GBT and cFSM: two modal approaches to the buckling analysis of unbranched thin-walled members. International Journal of Advanced Steel Construction 2009;5:195–223.

Appendix F

Paper V

Michael Joachim Andreassen and Jeppe Jönsson, (2009).

Distortional Modes of Thin-Walled Beams.

Full conference paper published in Proceedings of the 7th EUROMECH Solid Mechanics Conference - Mini-Symposia (ISBN: 978-989-96264-2-3) (paperid: 0680) , pages: 11, 2009, APMTAC - Portuguese Association for Theoretical, Applied and Computational Mechanics, Laboratório Nacional de Engenharia Civil, Av. do Brasil, 101, 1700-066 Lisboa, Portugal.

Presented at ESMC2009, 7th EUROMECH Solid Mechanics Conference, 2009, Instituto Superior Técnico, Lisbon, Portugal.

7th EUROMECH Solid Mechanics Conference
J. Ambrosio et.al. (eds.)
Lisbon, Portugal, 7–11 September 2009

DISTORTIONAL MODES OF THIN-WALLED BEAMS

Jeppe Jönsson[1], **Michael Joachim Andreassen**[2]

[1]Technical University of Denmark, Department of Civil Engineering
Brovej building 118, DK-2800 Kgs. Lyngby
e-mail: jej@byg.dtu.dk

[2] Technical University of Denmark, Department of Civil Engineering
Brovej building 118, DK-2800 Kgs. Lyngby
e-mail: mican@byg.dtu.dk

Keywords: Distortion, Warping, Generalized beam theory, Thin-walled beams, Beam theory, Quadratic eigenproblem.

Abstract. *The classic thin-walled beam theory for open and closed cross-sections can be generalized by including distortional displacement modes. The introduction of additional displacement modes leads to coupled differential equations, which seems to have prohibited the use of exact shape functions in the modelling of coupled torsion and distortion. However, if the distortional displacement modes are chosen as those which decouple the differential equations as in non proportionally damped modal dynamic analysis then it may be possible to use exact shape functions and perform analysis on a reduced problem. In the recently developed generalized beam theory (GBT) the natural distortional displacement modes are determined on the basis of a quadratic eigenvalue problem. However, as in linear modal dynamic analysis of proportionally damped structures this problem has been solved approximately using linear eigenvalue analysis of modified sub problems. This seems to have worked well for open cross sections but not for closed. It will be shown that it is possible to solve the distortional quadratic eigenvalue problem and find the natural distortional displacement modes using a method equivalent to that used for non proportionally damped (linear) dynamic modal analysis. The beam displacement field is separated into a sum of products of the cross-section displacement modes and their axial variation. This displacement field will then be constrained to follow the shear assumptions made in Vlassov beam theory, which condenses the problem considerably and reduces the number of possible eigen modes.*

1 INTRODUCTION

Thin-walled structural beams are extremely efficient due to the minimizing of the thickness to width ratio of the cross-section walls. The thin walls are a primary aspect of the behavior and design. Thin-walled structures are everywhere and include high rise industrial and residential buildings, storage racks, box girder bridges, ship hulls, aircraft skins, silos, tanks, pipes, wind turbine towers and wings and many others. Current practice of maximum strength at minimum cost drives classic engineering materials such as concrete, steel and aluminium as well as newer materials such as fibre reinforce materials (glass and carbon fibres in polyester or epoxy resin) to be used as thin-walled structures.

Several formulations have been developed to study the behavior of thin-walled members, some of them with respect to the distortion of the cross section, e.g. the Generalized beam theory (GBT).

Generalized beam theory (GBT) is a theory devoted to the analysis of thin-walled members, and proposed first by Schardt [1] in 1966, and have since fostered a lot of research, e.g. by Schardt [2], Davies [3], Jönsson [4] and Camotim & Silvestre [5]. Also Hanf [6], Rendek & Balaz [7], and Simao & Silva [8] has investigated the area. For further information about the research development see e.g. [9], [10] and [11]. The theory can be regarded as a fusion between the classical Vlasovs theory for thin-walled members and the plate theory [12], [13], and is an alternative to the classical finite strip and finite element methods. It enables the analysis of thin-walled members with the allowance of cross-section distortion and local plate behavior, in a one-dimensional formulation through the linear combination of pre-established deformation patterns - the modes of deformation.

2 BASIC AND KINEMATICS ASSUMPTIONS

The prismatic thin-walled beam is described in a global Cartesian (x, y, z) coordinate system where the z-axis is in the longitudinal direction of the beam, see Figure 1. A cross-section coordinate s is introduced as a curve parameter, which runs through the section along the center line and n is the coordinate along the local normal. Subscripts n and s are used for the components in the local coordinate system corresponding to the normal and tangential directions. Subscripts following a comma are used for derivatives, for example $u_{n,ss} = d^2u_n(s)/ds^2$ or $u_{s,n} = \partial u_s(s,n)/\partial n$. A prime, ', is used for the axial derivative, d/dz.

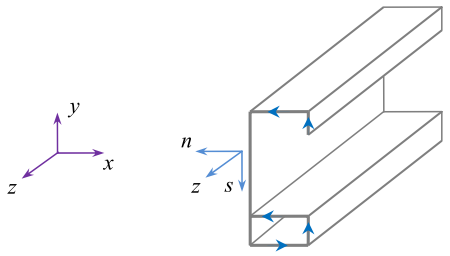

Figure 1: Global and local Cartesian reference frames of the thin-walled beam. Modified from [4].

The theories of beams are derived on the basis of assumed displacement fields, which correspond to extension, flexure, torsion, warping and distortional displacements. The main idea is to separate the cross section displacements into axial and transverse displacement fields. Each of these transverse or axial displacement fields are factorized in a displacement mode, which is a function of the in-plane coordinates, multiplied by a function of the axial coordinate, which describes the axial variation of the mode. In the following we will propose a method for finding the natural distortional displacement modes. In the definition of the displacements and strains the influence of curved cross section walls is neglected and it is assumed that the radius of curvature is sufficiently large, so that curvature effects vanish. The local effects at corners and joints are also neglected. Only shear contributions from torsion and shear flow around cells will be allowed. The components u_n and u_s of the in-plane cross section displacements in the local coordinate system at a point (n, s) in the cross-section are introduced as

$$u_n(s,z) = \mathrm{w}_n\psi \tag{1}$$

$$u_s(n,s,z) = (\mathrm{w}_s - n\mathrm{w}_{n,s})\psi \tag{2}$$

where $\mathrm{w}_s(s)$ and $\mathrm{w}_n(s)$ are the local displacements of the centre line as shown in Figure 2 and $\psi(z)$ is the function, which describes the axial variation of the in-plane distortional displacements. The axial displacements $u_z(n,s,z)$ generated by the in-plane distortional displacements are introduced as

$$u_z(n,s,z) = -(\Omega + n\mathrm{w}_n)\psi' \tag{3}$$

Here the axial displacement mode $\Omega(s)$(warping) has been included with a variation corresponding to the axial derivative of the axial variation factor ψ and due consideration of local transverse variation. Thus neglecting shear deformation. The corresponding axial strains are

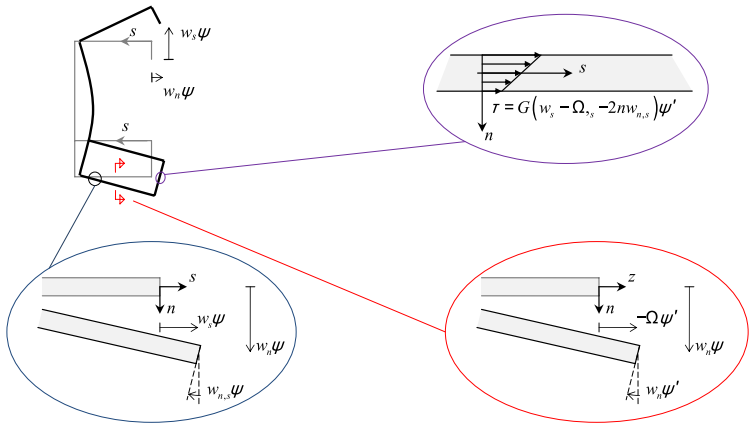

Figure 2: Local components of displacements and assumed shear stresses. Modified from [14] and [15].

$$\varepsilon = u_z' = -(\Omega + n\mathrm{w}_n)\psi'' \tag{4}$$

The cross section distortional strains are

$$\varepsilon_s = (\mathrm{w}_{s,s} - n\mathrm{w}_{n,ss})\psi \tag{5}$$

The engineering shear strain in the walls of the cross section becomes

$$\gamma = \gamma_{zs} = u_{z,s} + u_{s,z} = (\mathrm{w}_s - \Omega_{\prime s} - 2n\mathrm{w}_{n,s})\psi' \tag{6}$$

In order to cope with the shear flow around closed cells we introduce the shear strain in the middle of the wall as

$$\bar{\gamma}_d = (\mathrm{w}_s - \Omega_{\prime s})\psi' \tag{7}$$

Bernoulli beam theory is based on the assumption of negligible shear strain and sets the shear strain equal to zero and thus determines the warping displacements (flexural modes) by the differential equation $\Omega_{\prime s} = \mathrm{w}_s$. The weak formulation of Bernoulli beam theory does therefore not include shear contributions and the axial equilibrium equation of a section cut-out is not fulfilled, thus leading to the use of Grashofs method for determination of the shear stresses. However if we are to analyse closed cross sections as in Vlasow beam theory we have to allow for a constant shear flow around the cells and the warping of the cross section then has to be determined by the differential equation $\Omega_{\prime s} = \mathrm{w}_s - \bar{\gamma}_d$ as

$$\Omega(s) = \int_0^s \mathrm{w}_s ds - \int_0^s \bar{\gamma}_d ds + \Omega_0 \tag{8}$$

In the current context the warping function will be determined from a weak formulation of the assumption of a constant shear flow $\bar{T}_d$ in the walls of the cross section, (where $\bar{T}_d = Gt\bar{\gamma}_d$). The strong formulation of the constraining assumption is that the contribution of the shear flow to the axial equilibrium equation of a section cut-out is zero, i.e.

$$\bar{T}_{d,s} = 0 \tag{9}$$

Multiplying by a virtual centreline axial displacement $\delta\bar{u}_z$ and integrating over the cross section we find the virtual work of the shear stresses in a cross section as

$$\int_C \bar{T}_{d,s}\delta\bar{u}_z ds = 0 \tag{10}$$

Performing a partial integration and noting that the shear stress flow is zero at all free edges we find the weak formulation that will be used to determine the warping function

$$\left[\bar{T}_d\delta\bar{u}_z\right]_{\text{free edges}} - \int_C \bar{T}_d\delta\bar{u}_{z,s} ds = 0 \quad \Rightarrow \quad \int_C \bar{T}_d\delta\bar{u}_{z,s} ds = 0 \tag{11}$$

This equation is the constraint equation that we will use to enforce the assumption of zero axial work performed by the shear flow around the cells.

3 STRAIN ENERGY ASSUMPTIONS

In the following we will adhere to simple constitutive relations, i.e. the material is assumed to be linear elastic with a modulus of elasticity E and a shear modulus G. The axial stress is determined as $\sigma = E\varepsilon$, the shear stress as $\tau = G\gamma$ and the transverse stress as $\sigma_s = E\varepsilon_s$. Thus the coupling of axial strain ε and transverse strain ε_s is neglected. The elastic energy potential thus becomes

$$\Pi = \int_V \left(\tfrac{1}{2}E\varepsilon^2 + \tfrac{1}{2}G\gamma^2 + \tfrac{1}{2}E\varepsilon_s^2\right)dV \tag{12}$$

Let us introduce a thin-walled cross section assembled using straight cross sectional elements, see Figure 3, and let us integrate through the thickness t, across the widths, b_e, of the elements,

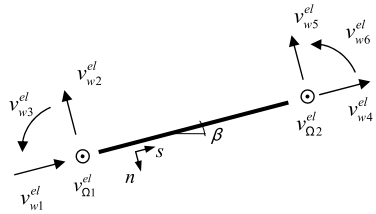

Figure 3: Components of the displacements vectors of a straight cross section element.

and over the length, L, of the thin-walled beam. The elastic potential energy takes the following form after introduction of the strains expressed by the displacement in separated form

$$\Pi = \tfrac{1}{2}\int_0^L \left[\sum_{el}\int_0^{b_{el}} \begin{Bmatrix} Et(\Omega\psi'')^2 + \frac{Et^3}{12}(\mathrm{w}_n\psi'')^2 \\ +Gt(\mathrm{w}_s\psi')^2 + Gt(\Omega_{,s}\psi')^2 - 2Gt(\mathrm{w}_s\psi')(\Omega_{,s}\psi') + \frac{1}{3}Gt^3(\mathrm{w}_{n,s}\psi')^2 \\ +Et(\mathrm{w}_{s,s}\psi)^2 + \frac{Et^3}{12}(\mathrm{w}_{n,ss}\psi)^2 \end{Bmatrix} ds\right] dz \tag{13}$$

In equation 13 the elastic energy terms have been grouped in axial strain energy, shear energy and transverse strain energy. In conventional beam theory we usually introduce rigid cross sectional displacement modes and the elastic energy will be described by a summation of the energy stored in all displacement modes. However we have to remember the shear constraints induced on our formulation from a constant shear flow assumption. In the current work it is the goal to establish a natural set of displacement modes. To achieve this, the cross section will be divided into discrete straight line elements in which we interpolate the transverse and axial displacements.

4 INTERPOLATION WITHIN CROSS SECTION ELEMENTS

The axial displacements Ω within each flat element will be interpolated linearly corresponding to a linear variation of the warping functions, the in-plane transverse displacement of the elements will also be interpolated linearly (although a constant displacement might be more appropriate) and finally the transverse displacement will be interpolated by cubic interpolation

corresponding to beam elements. The displacements in a flat element are thus interpolated as follows

$$\begin{aligned}
\Omega\psi' &= \mathbf{N}_\Omega \mathbf{v}^e_\Omega \psi' \quad , \quad \text{where } \mathbf{N}_\Omega(s) \text{ is a linear interpolation matrix} \\
\mathrm{w}_s\psi &= \mathbf{N}_s \mathbf{v}^e_\mathrm{w} \psi \quad , \quad \text{where } \mathbf{N}_s(s) \text{ is a linear interpolation matrix} \\
\mathrm{w}_n\psi &= \mathbf{N}_n \mathbf{v}^e_\mathrm{w} \psi \quad , \quad \text{where } \mathbf{N}_n(s) \text{ is a cubic (beam) interpolation matrix}
\end{aligned} \tag{14}$$

where we in equation 14 have introduced the axial and transverse nodal displacement components of a straight cross section element as

$$\begin{aligned}
\mathbf{v}^e_\Omega &= [\Omega(0), \Omega(b_e)]^T \\
\mathbf{v}^e_\mathrm{w} &= [\mathrm{w}_s(0), -\mathrm{w}_n(0), -\mathrm{w}_{n,s}(0), \mathrm{w}_s(b_e), -\mathrm{w}_n(b_e), -\mathrm{w}_{n,s}(b_e)]^T
\end{aligned} \tag{15}$$

Here b_e is the width of the flat element. Nodal components and the direction of the section coordinates (n,s) are shown in Figure 3.

The element stiffness contributions to the axial strain, shear strain and transverse strain energy can now be found using the displacement interpolations. The found stiffness contributions are shown in Table 1 in which the left column holds two axial stiffness contributions and the transverse distortional stiffness term, whereas the second column holds the shear strain stiffness contributions. Let us prepare for the formulation of the total cross section elastic energy by intro-

$\mathbf{k}^\sigma_{\Omega\Omega} = \int_0^{b_e} Et\mathbf{N}^T_\Omega \mathbf{N}_\Omega ds$	$\mathbf{k}^\tau_{\mathrm{ww}} = \int_0^{b_e} \left(Gt\mathbf{N}^T_s \mathbf{N}_s + \frac{Gt^3}{3}\mathbf{N}^T_{n,s}\mathbf{N}_{n,s} \right) ds$
$\mathbf{k}^\sigma_{\mathrm{ww}} = \int_0^{b_e} \frac{Et^3}{12}\mathbf{N}^T_n \mathbf{N}_n ds$	$\mathbf{k}^\tau_{\Omega\Omega} = \int_0^{b_e} Gt\mathbf{N}^T_{\Omega,s}\mathbf{N}_{\Omega,s} ds$
$\mathbf{k}^s = \int_0^{b_e} \left(Et\mathbf{N}^T_{s,s}\mathbf{N}_{s,s} + \frac{Et^3}{12}\mathbf{N}^T_{n,ss}\mathbf{N}_{n,ss} \right) ds$	$\mathbf{k}^\tau_{\mathrm{w}\Omega} = \left[\mathbf{k}^\tau_{\Omega\mathrm{w}} \right]^T = -\int_0^{b_e} Gt\mathbf{N}^T_s \mathbf{N}_{\Omega,s} ds$

Table 1: Straight element stiffness contributions.

$\mathbf{K}^\sigma_{\Omega\Omega} = \sum_{el} \mathbf{T}^T_\Omega \mathbf{k}^\sigma_{\Omega\Omega} \mathbf{T}_\Omega$	$\mathbf{K}^\tau_{\mathrm{ww}} = \sum_{el} \mathbf{T}^T_\mathrm{w} \mathbf{k}^\tau_{\mathrm{ww}} \mathbf{T}_\mathrm{w}$
$\mathbf{K}^\sigma_{\mathrm{ww}} = \sum_{el} \mathbf{T}^T_\mathrm{w} \mathbf{k}^\tau_{\mathrm{ww}} \mathbf{T}_\mathrm{w}$	$\mathbf{K}^\tau_{\Omega\Omega} = \sum_{el} \mathbf{T}^T_\Omega \mathbf{k}^\tau_{\Omega\Omega} \mathbf{T}_\Omega$
$\mathbf{K}^s = \sum_{el} \mathbf{T}^T_\mathrm{w} \mathbf{k}^s \mathbf{T}_\mathrm{w}$	$\mathbf{K}^\tau_{\mathrm{w}\Omega} = \sum_{el} \mathbf{T}^T_\mathrm{w} \mathbf{k}^\tau_{\mathrm{w}\Omega} \mathbf{T}_\Omega$

Table 2: Assembly into total cross section stiffness contributions.

ducing global displacement vectors as an assembly of the local element degrees of freedom. The axial displacements and the transverse displacements are separated into two vectors as follows:

$$\begin{aligned}
\mathbf{v}_\Omega &= \begin{bmatrix} \mathrm{v}_{\Omega 1} & \mathrm{v}_{\Omega 2} & \mathrm{v}_{\Omega 3} & \dots \end{bmatrix}^T \\
\mathbf{v}_\mathrm{w} &= \begin{bmatrix} \mathrm{v}_{x1} & \mathrm{v}_{y1} & \phi_1 & \mathrm{v}_{x2} & \mathrm{v}_{y2} & \phi_2 & \dots \end{bmatrix}^T
\end{aligned} \tag{16}$$

The transformation from local to global components is performed using a standard transformation of the components in the cross section plane, i.e. $\mathbf{v}_\Omega = \mathbf{T}_\Omega \mathbf{v}^{el}_\Omega$ and $\mathbf{v}_\mathrm{w} = \mathbf{T}_\mathrm{w} \mathbf{v}^{el}_\mathrm{w}$. The global

assembly of stiffness matrixes are found by summation of the contribution from each element as illustrated in Table 2. Introducing the described interpolation and matrix calculation scheme the elastic potential energy in equation 13 now takes the following form,

$$\Pi = \frac{1}{2}\int_0^L \left\{ \begin{bmatrix} \psi \mathbf{v}_{\mathrm{w}}^T & \psi \mathbf{v}_{\Omega}^T \end{bmatrix}'' \begin{bmatrix} \mathbf{K}_{\mathrm{ww}}^{\sigma} & \mathbf{0} \\ \mathbf{0} & \mathbf{K}_{\Omega\Omega}^{\sigma} \end{bmatrix} \begin{bmatrix} \psi \mathbf{v}_{\mathrm{w}} \\ \psi \mathbf{v}_{\Omega} \end{bmatrix}'' \right. \\ + \begin{bmatrix} \psi \mathbf{v}_{\mathrm{w}}^T & \psi \mathbf{v}_{\Omega}^T \end{bmatrix}' \begin{bmatrix} \mathbf{K}_{\mathrm{ww}}^{\tau} & \mathbf{K}_{\mathrm{w}\Omega}^{\tau} \\ \mathbf{K}_{\Omega\mathrm{w}}^{\tau} & \mathbf{K}_{\Omega\Omega}^{\tau} \end{bmatrix} \begin{bmatrix} \psi \mathbf{v}_{\mathrm{w}} \\ \psi \mathbf{v}_{\Omega} \end{bmatrix}' \\ \left. + \begin{bmatrix} \psi \mathbf{v}_{\mathrm{w}}^T & \psi \mathbf{v}_{\Omega}^T \end{bmatrix} \begin{bmatrix} \mathbf{K}^{s} & \mathbf{0} \\ \mathbf{0} & \mathbf{0} \end{bmatrix} \begin{bmatrix} \psi \mathbf{v}_{\mathrm{w}} \\ \psi \mathbf{v}_{\Omega} \end{bmatrix} \right\} dz \tag{17}$$

In equation 17 the $\mathbf{0}$ denotes a suitable size matrix of zeroes. The axial stiffness from transverse displacements sub matrix $\mathbf{K}_{\mathrm{ww}}^{\sigma}$ has a rank deficiency equal to the number of free end nodes plus the number of "internal" nodes between corner points of the cross section. The in cross section plane distortional stiffness sub matrix $\mathbf{K}^{s}$ has a rank deficiency of 3 corresponding to 3 in plane "rigid body" or rather non distortional displacements of the cross section. Finally the shear stiffness matrix $\mathbf{K}^{\tau}$ has a rank deficiency of 3 corresponding to the existence of pure axial extension and two pure flexural modes without shear. It turns out that since the pure axial displacement only involves the sub matrix $\mathbf{K}_{\Omega\Omega}^{\tau}$ this matrix has a rank deficiency of 1.

To find the natural displacement modes we will investigate the first variation of the elastic potential energy by making variations in the complete displacement field. We will denote the virtual variation of a property by a δ in front of the varied property, such as for example $\delta(\mathrm{v_w}\psi)'$ as the variation of the first derivative of the transverse displacement expressed by the product of the transverse displacement and the axial variation. After using integration by parts twice we find the following expression for the first variation of the elastic potential energy:

$$\delta\Pi = \int_0^L \delta \begin{bmatrix} \psi \mathbf{v}_{\mathrm{w}}^T & \psi \mathbf{v}_{\Omega}^T \end{bmatrix} \left\{ \begin{bmatrix} \mathbf{K}_{\mathrm{ww}}^{\sigma} & \mathbf{0} \\ \mathbf{0} & \mathbf{K}_{\Omega\Omega}^{\sigma} \end{bmatrix} \begin{bmatrix} \mathbf{v}_{\mathrm{w}} \\ \mathbf{v}_{\Omega} \end{bmatrix} \psi'''' - \begin{bmatrix} \mathbf{K}_{\mathrm{ww}}^{\tau} & \mathbf{K}_{\mathrm{w}\Omega}^{\tau} \\ \mathbf{K}_{\Omega\mathrm{w}}^{\tau} & \mathbf{K}_{\Omega\Omega}^{\tau} \end{bmatrix} \begin{bmatrix} \mathbf{v}_{\mathrm{w}} \\ \mathbf{v}_{\Omega} \end{bmatrix} \psi'' + \begin{bmatrix} \mathbf{K}^{s} & \mathbf{0} \\ \mathbf{0} & \mathbf{0} \end{bmatrix} \begin{bmatrix} \mathbf{v}_{\mathrm{w}} \\ \mathbf{v}_{\Omega} \end{bmatrix} \psi \right\} dz \\ + \left[\delta \begin{bmatrix} \psi \mathbf{v}_{\mathrm{w}}^T & \psi \mathbf{v}_{\Omega}^T \end{bmatrix}' \begin{bmatrix} \mathbf{K}_{\mathrm{ww}}^{\sigma} & \mathbf{0} \\ \mathbf{0} & \mathbf{K}_{\Omega\Omega}^{\sigma} \end{bmatrix} \begin{bmatrix} \mathbf{v}_{\mathrm{w}} \\ \mathbf{v}_{\Omega} \end{bmatrix} \psi'' \right. \\ \left. + \delta \begin{bmatrix} \psi \mathbf{v}_{\mathrm{w}}^T & \psi \mathbf{v}_{\Omega}^T \end{bmatrix} \left\{ - \begin{bmatrix} \mathbf{K}_{\mathrm{ww}}^{\sigma} & \mathbf{0} \\ \mathbf{0} & \mathbf{K}_{\Omega\Omega}^{\sigma} \end{bmatrix} \begin{bmatrix} \mathbf{v}_{\mathrm{w}} \\ \mathbf{v}_{\Omega} \end{bmatrix} \psi''' + \begin{bmatrix} \mathbf{K}_{\mathrm{ww}}^{\tau} & \mathbf{K}_{\mathrm{w}\Omega}^{\tau} \\ \mathbf{K}_{\Omega\mathrm{w}}^{\tau} & \mathbf{K}_{\Omega\Omega}^{\tau} \end{bmatrix} \begin{bmatrix} \mathbf{v}_{\mathrm{w}} \\ \mathbf{v}_{\Omega} \end{bmatrix} \psi' \right\} \right]_0^L \tag{18}$$

The last terms in the bracketed parenthesis correspond to the boundary loads and boundary conditions, which will not concern us in the current presentation.

For internal variations in the displacement fields $\delta[\psi \mathbf{v}_{\mathrm{w}}^T \quad \psi \mathbf{v}_{\Omega}^T]$ the elastic potential energy should be stationary and therefore its first variation must be equal to zero. Taking internal variations reveals the following fourth order coupled homogeneous differential matrix problem for determination of the transverse and axial displacement modes:

$$\begin{bmatrix} \mathbf{K}_{\mathrm{ww}}^{\sigma} & \mathbf{0} \\ \mathbf{0} & \mathbf{K}_{\Omega\Omega}^{\sigma} \end{bmatrix} \begin{bmatrix} \mathbf{v}_{\mathrm{w}} \\ \mathbf{v}_{\Omega} \end{bmatrix} \psi'''' - \begin{bmatrix} \mathbf{K}_{\mathrm{ww}}^{\tau} & \mathbf{K}_{\mathrm{w}\Omega}^{\tau} \\ \mathbf{K}_{\Omega\mathrm{w}}^{\tau} & \mathbf{K}_{\Omega\Omega}^{\tau} \end{bmatrix} \begin{bmatrix} \mathbf{v}_{\mathrm{w}} \\ \mathbf{v}_{\Omega} \end{bmatrix} \psi'' + \begin{bmatrix} \mathbf{K}^{s} & \mathbf{0} \\ \mathbf{0} & \mathbf{0} \end{bmatrix} \begin{bmatrix} \mathbf{v}_{\mathrm{w}} \\ \mathbf{v}_{\Omega} \end{bmatrix} \psi = \begin{bmatrix} \mathbf{0} \\ \mathbf{0} \end{bmatrix} \tag{19}$$

In order to get a formulation resembling a generalization of Vlasov beam theory the following three main steps must be performed:

- In step I we introduce the shear constraint equations that bind axial and transverse modes together and at the same time simplifies or condenses equation 19. In this process we need to eliminate the singularity in the shear stiffness matrix related to pure axial extension.
- In step II we will constrain the transverse displacement field, so that we do not allow transverse normal strains in the middle surface of the cross section, i.e. we will enforce $\mathrm{w}_{s,s} \equiv 0$, see equation 5 .
- In step III we will condense our eigenvalue problem by removing singularities due the two remaining shear stiffness singularities belonging to pure flexural deformation without shear.

Hereby the following condensed version of equation 19 is obtained,

$$\bar{\mathbf{K}}^{\sigma}_{ee}\mathbf{v}^{ue}_{\mathrm{w}}\psi'''' - \mathbf{K}^{\tau}_{ee}\mathbf{v}^{ue}_{\mathrm{w}}\psi'' + \mathbf{K}^{s}_{ee}\mathbf{v}^{ue}_{\mathrm{w}}\psi = \mathbf{0} \tag{20}$$

This concludes the three steps and now the solution of this quadratic matrix equation is wanted.

5 THE DISTORTIONAL QUADRATIC EIGENVALUE PROBLEM

We will start the solution of the final condensed differential equation 20 by seeking solution to this fourth order matrix equation by guessing that the solutions are of the form

$$\psi(z) = e^{\xi z} \tag{21}$$

where ξ is a length scale parameter which may be complex. Inserting the guess leads to a quadratic eigenvalue problem, which we choose to write in the following form to illuminate the next transformation of the problem:

$$\xi^2\bar{\mathbf{K}}^{\sigma}_{ee}(\xi^2\mathbf{v}^{ue}_{\mathrm{w}}) - \xi^2\mathbf{K}^{\tau}_{ee}\mathbf{v}^{ue}_{\mathrm{w}} + \mathbf{K}^{s}_{ee}\mathbf{v}^{ue}_{\mathrm{w}} = \mathbf{0} \tag{22}$$

This quadratic eigenvalue problem may be transformed into a linear eigenvalue problem of double size by introducing the following "state" vector $\mathbf{v} = [\mathbf{v}^{ue}_{\mathrm{w}} \quad \xi^2\mathbf{v}^{ue}_{\mathrm{w}}]^T$. There are a number of different possible formulations of this eigenvalue problem however we choose to keep a symmetric formulation and formulate the problem as the following symmetric generalized eigenvalue problem:

$$\begin{bmatrix} \mathbf{K}^{s}_{ee} & \mathbf{0} \\ \mathbf{0} & -\bar{\mathbf{K}}^{\sigma}_{ee} \end{bmatrix} \begin{bmatrix} \mathbf{v}^{ue}_{\mathrm{w}} \\ \xi^2\mathbf{v}^{ue}_{\mathrm{w}} \end{bmatrix} - \xi^2 \begin{bmatrix} \mathbf{K}^{\tau}_{ee} & -\bar{\mathbf{K}}^{\sigma}_{ee} \\ -\bar{\mathbf{K}}^{\sigma}_{ee} & \mathbf{0} \end{bmatrix} \begin{bmatrix} \mathbf{v}^{ue}_{\mathrm{w}} \\ \xi^2\mathbf{v}^{ue}_{\mathrm{w}} \end{bmatrix} = \begin{bmatrix} \mathbf{0} \\ \mathbf{0} \end{bmatrix} \tag{23}$$

Solving the symmetric generalized eigenvalue problem in equation 23 leads to a number of modes corresponding to the number of degree of freedom. Some of the relevant eigenvalues are shown in Table 3, and the corresponding modes are shown in Figure 4.

Mode	Eigenvalue ξ^2	Length scale parameter ξ
1	$3.3573 \cdot 10^{-6} - 2.6519 \cdot 10^{-5}i$	$\pm(3.8787 \cdot 10^{-3} - 3.4186 \cdot 10^{-3}i)$
2	$3.3573 \cdot 10^{-6} + 2.6519 \cdot 10^{-5}i$	$\pm(3.8787 \cdot 10^{-3} + 3.4186 \cdot 10^{-3}i)$
3	$4.2311 \cdot 10^{-6} - 5.0044 \cdot 10^{-5}i$	$\pm(5.2180 \cdot 10^{-3} - 4.7954 \cdot 10^{-3}i)$
4	$4.2311 \cdot 10^{-6} + 5.0044 \cdot 10^{-5}i$	$\pm(5.2180 \cdot 10^{-3} + 4.7954 \cdot 10^{-3}i)$
5	0.00082381	± 0.028702
6	0.00095079	± 0.030835
7	0.00179050	± 0.042315
8	0.00333320	± 0.057734

Table 3: Eigenvalues ξ^2 and corresponding length scale parameters ξ.

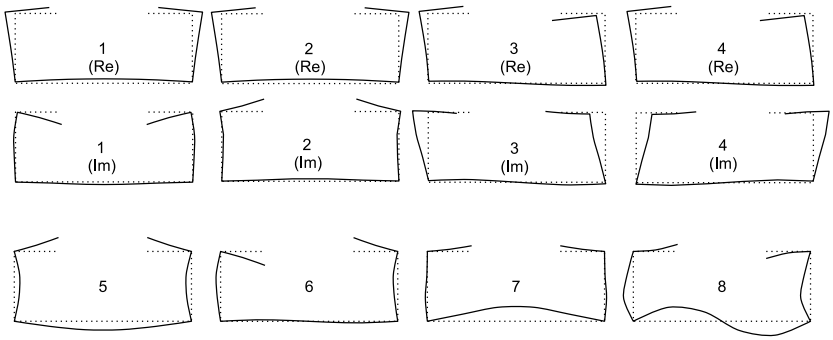

Figure 4: Lipped channel 8 in-plane deformation mode shapes.

From Table 3 and Figure 4 it is seen that some of the solutions give complex eigenvalues, which leads to length scale parameters that becomes complex, and to modes containing both a real part and an imaginary part. The eigenvalues of mode 2 and mode 4 are complex conjugated eigenvalues of mode 1 and 3. To handle the complex solutions we use Euler's formula and some boundary conditions to find the constants, which will combine the real part and the imaginary part.

6 CONCLUSION

As shown in Figure 4 relevant deformation modes have been found by formulating and solving the distortional quadratic eigenvalue problem. Hereby it is shown that it is possible to solve the distortional quadratic eigenvalue problem and find the natural distortional displacement modes using a method equivalent to that used for non proportionally damped (linear) dynamic modal analysis. The beam displacement field has been separated into a sum of products of the cross-section displacement modes and their axial variation. This displacement field has been constrained to follow the shear assumptions made in Vlassov beam theory, which has condensed the problem considerably and reduced the number of possible eigen modes.

Having solved the distortional quadratic eigenvalue problem allows us to sort and arrange the

calculated modes and enables the formulations of a generalized one dimensional beam element which can handle the extra distortional contributions. Afterwards, the generalization of the formulation have to be extended to perform stability– and dynamic analysis of advanced issues by the formulation of advanced dimensional bar elements.

REFERENCES

[1] R. Schardt, Eine Erweiterung der technischen Biegelehre für die Berechnung biegesteifer prismatischer Faltwerke. *Der Stahlbau*, **35**, 161–171, 1966.

[2] R. Schardt, *Verallgemeinerte Technische Biegetheorie*. Springer-Verlag, Germany, 1989.

[3] J.M. Davies, Recent research advances in cold-formed steel structures. *Journal of Constructional Steel Research*, **55**, 267–288, 2000.

[4] J. Jönsson, Distortional theory of thin-walled beams. *Thin-Walled Structures*, **33**, 269–303, 1999.

[5] N. Silvestre and D. Camotim, First-order generalised beam theory for arbitrary orthotropic materials. *Thin-Walled Structures*, **40**, 755–789, 2002.

[6] M. Hanf, Die geschlossene Lösung der linearen Differentialgleichungssysteme der Verallgemeinerten Technischen Biegetheorie mit einer Anwendung auf die Ermittlung plastischer Grenzlasten. *Instituts für Werkstoffe und Mechanik im Bauwesen der TU Darmstadt*, **9**, 1989.

[7] S. Rendek and I. Baláž, Distortion of thin-walled beams. *Thin-Walled Structures*, **42**, 255–277, 2004.

[8] P. Simão and L. Simões da Silva, A unified energy formulation for the stability analysis of open and closed thin-walled members in the framework of the generalized beam theory. *Thin-Walled Structures*, **42**, 1495–1517, 2004.

[9] D. Camotim, N. Silvestre, R. Gonçalves and P.B. Dinis, GBT analysis of thin-walled members: new formulations and applications. J. Loughlan eds. *Thin-Walled Structures: Recent Advances and Future Trends in Thin-Walled Structures Technology*, Canopus Publishing Ltd., Bath, 137–168, 2004.

[10] D. Camotim, N. Silvestre, R. Gonçalves and P.B. Dinis, GBT-Based Structural Analysis of Thin-Walled Members: Overview, Recent Progress and Future Developments. M. Pandey, W.-C. Xie and L. Xu eds. *Advances in Engineering Structures, Mechanics & Construction*, Springer (Dordrecht), Waterloo, 187–204, 2006.

[11] J. Rondal, Cold formed steel members and structures - General Report. *Journal of Constructional Steel Research*, **55**, 155–158, 2000.

[12] V.Z. Vlasov, *Thin-walled elastic beams*, 2nd ed. Israel Program for Scientific Translations, Jerusalem, Israel, 1961.

[13] C.F. Kollbrunner and N. Hajdin, *Dünnwandige Stäbe 2, Stäbe mit deformierbaren Querschnitten, Nicht-elastisches Verhalten dünnwandiger Stäbe.* Springer-Verlag, Berlin, 1975.

[14] J. Jönsson, Determination of shear stresses, warping functions and section properties of thin-walled beams using finite elements. *Computers & Structures*, **68**, 393–410, 1998.

[15] J. Jönsson, Distortional warping functions and shear distributions in thin-walled beams. *Thin-Walled Structures*, **33**, 245–268, 1999.

Appendix G

Paper VI

Michael J. Andreassen and Jeppe Jönsson, (2011).

Distortional eigenmodes and solutions for thin-walled beams.

Full conference paper published in Thin-Walled Structures, Recent Research Advancences and Trends (ISBN: 978-92-9147-102-7), 2011, ECCS - European Convention for Constructional Steelwork.

Presented at the International Conference on Thin-Walled Structures (ICTWS) - 6, 2011, Timisoara, Romania

DISTORTIONAL EIGENMODES AND SOLUTIONS FOR THIN-WALLED BEAMS

Michael J. Andreassen and Jeppe Jönsson

Technical University of Denmark, Department of Civil Engineering, Kgs. Lyngby, Denmark

Abstract: This paper presents a generalization of the classic theory for thin-walled beams by including distortional displacements. A condensed presentation of the novel finite-element-based displacement approach in [1,2] is given, where specific distortional displacement fields, which decouple the differential equations for generalized beam theory (GBT), are determined via a semi-discretization procedure. The distortional displacement fields are found as solutions to a distortional homogeneous eigenvalue problem which produce distortional displacement eigenmodes. Using the distortional modal matrix found for the homogeneous system the final uncoupled set of distortional differential equations including the load terms are presented and the full solution is given, including an illustrative example. This new approach is an alternative to the traditional first order GBT method.

1. INTRODUCTION

A number of formulations have been developed to study the behavior of thin-walled members, some of them including the distortion of the cross-section, e.g. the Generalized beam theory (GBT), a designation which is associated with a modal discretization performed at the cross-section level. GBT is a theory devoted to the analysis of thin-walled members, proposed first by Schardt [3], and has led to a lot of research, for example by Schardt [4], Davies [5], Jönsson [6], Camotim & Silvestre [7] and Hanf [8]. The theory can be considered as an extension of classical Vlasov theory for thin-walled members [9] and is an alternative to the classical finite strip and finite element methods. It enables the analysis of thin-walled members with the allowance of cross-section distortion and local plate behaviour, in a one-dimensional formulation through the linear combination of pre-established modes of deformation.

In the present paper a new and alternative approach [1,2] to traditional GBT will shortly be presented. Via this new approach it is possible to determine specific distortional displacement fields which decouple the differential equations for generalized beam theory (GBT) via a semi-discretization procedure. Here the cross-section is discretized into finite elements, and the axial variation of the displacement functions are solutions to the established coupled fourth order differential equations. This novel finite-element-based displacement approach is introduced in combination with a weak formulation of the shear constraints and constrained wall widths.

The order of the distortional homogeneous equations is reduced, and the related distortional homogeneous eigenvalue problem of double size is solved as in non-proportionally damped structural dynamic analysis. From the distortional homogeneous eigenvalue problem the eigenvalues and the corresponding distortional displacement eigenmodes are found. Some

of the distortional displacement modes found and their related eigenvalues are complex but rewritten into real quantities. The distortional differential equations including the load terms are presented. Transforming these distortional differential equations into the eigenmode space, by using the distortional modal matrix found for the homogeneous system, the final diagonalized and thus uncoupled set of differential equations including the load terms are obtained. The full solution to these uncoupled linear second order differential equations is given.

2. BASIC ASSUMPTIONS AND KINEMATIC RELATIONS

In [1,2] the prismatic thin-walled beam is described in a global Cartesian (*x, y, z*) coordinate system where the *z*-axis is in the longitudinal direction of the beam, see Fig. 1. A cross-section coordinate *s* is introduced as a curve parameter, which runs through the section along the centreline and *n* is the coordinate along the local normal. Subscripts *n* and *s* are used for the components in the local coordinate system corresponding to the normal and tangential directions.

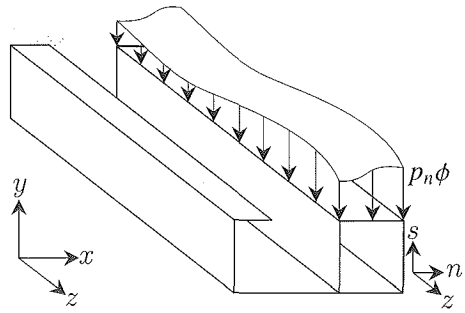

Fig. 1: Global and local Cartesian reference frames of the thin-walled beam including load distribution

The components of the cross section displacements in the local coordinate are introduced as:

$$u_n(s,z) = \mathrm{w}_n(s)\psi(z) \tag{1}$$

$$u_s(n,s,z) = (\mathrm{w}_s(s) - n\mathrm{w}_{n,s}(s))\psi(z) \tag{2}$$

$$u_z(n,s,z) = (\Omega(s) + n\mathrm{w}_n(s))\psi'(z) \tag{3}$$

Here $\mathrm{w_s(s)}$ and $\mathrm{w_n(s)}$ describes the local displacements of the centreline as shown in Fig. 2, ψ(z) describes the function which defines the axial variation of the in-plane distortional displacements and Ω(s) (warping) describes the axial displacement mode.

The corresponding strains appears as:

$$\varepsilon = u_{z'} = -(\Omega + n\mathrm{w}_n)\psi'' \tag{4}$$

$$\varepsilon_s = (\mathrm{w}_{s,s} - n\mathrm{w}_{n,ss})\psi \tag{5}$$

$$\gamma = \gamma_{zs} = u_{z,s} + u_{s,z} = (\mathrm{w}_s - \Omega_{,s} - 2n\mathrm{w}_{n,s})\psi' \tag{6}$$

For a greater explanation and description see paper [1,2].

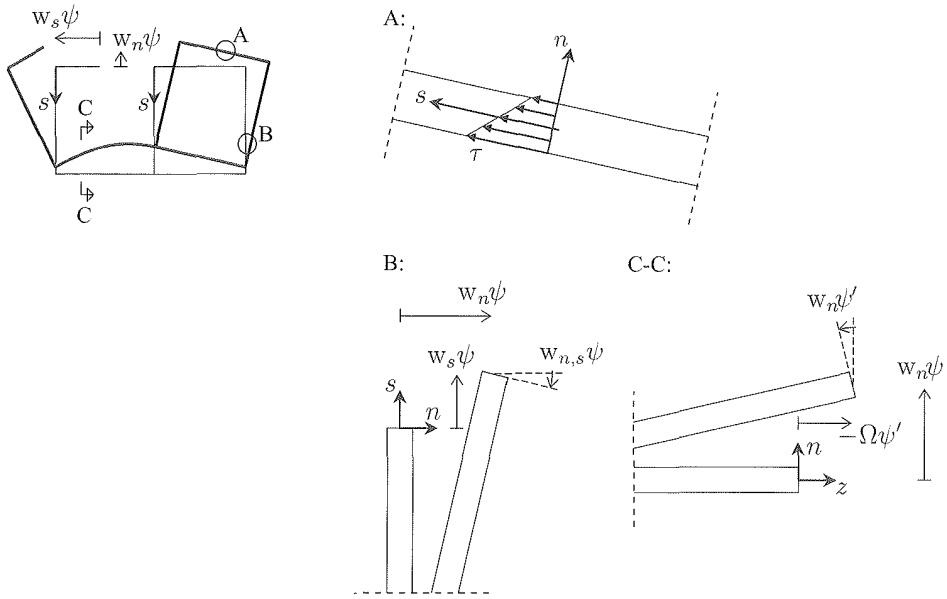

Fig. 2: Local components of displacements and assumed shear stresses

3. ENERGY POTENTIAL

The total energy potential can be expressed as

$$\Pi_{tot} = \Pi_{int} + \Pi_{ext} \tag{7}$$

Here Π_{int} is the contribution to the potential energy from the internal properties, see paper [1], and Π_{ext} is the contribution from the external loads, see paper [2].

Introducing the strains expressed by the separated displacement functions, the total potential energy takes the following form:

$$\begin{aligned}\Pi_{tot} = \tfrac{1}{2}\int_0^L [\ \sum_{el}\int_0^{b_{el}} \{\ [Et(\Omega\psi'')^2 + \tfrac{1}{12}Et^3(\mathrm{w}_n\psi'')^2] + [Gt(\mathrm{w}_s\psi')^2 + Gt(\Omega_{,s}\psi')^2 \\ - 2Gt(\mathrm{w}_s\psi')(\Omega_{,s}\psi') + \tfrac{1}{3}Gt^3(\mathrm{w}_{n,s}\psi')^2] + [E_s t(\mathrm{w}_{s,s}\psi)^2 + \tfrac{1}{12}E_s t^3(\mathrm{w}_{n,ss}\psi)^2] \\ - \varphi[p_s w_s\psi + p_n w_n\psi - p_z\Omega\psi']\ \}ds\ ]dz\end{aligned} \tag{8}$$

The interpolations connected to the cross-section are the displacement interpolations for $\mathrm{w_s}$, $\mathrm{w_n}$ and Ω which is described in [1]. The interpolation of the cross-section loads p_s, p_n and p_z are introduced in [2]. Introducing these interpolations and the calculation scheme as described in [1,2] we can write the total potential energy as

$$\begin{aligned}\Pi_{tot} = \tfrac{1}{2}\int_0^L \{[\psi\mathbf{v}_{\mathrm{w}}^T \quad \psi\mathbf{v}_{\Omega}^T]''\begin{bmatrix}\mathbf{K}^{\sigma}_{\mathrm{ww}} & \mathbf{0}\\ \mathbf{0} & \mathbf{K}^{\sigma}_{\Omega\Omega}\end{bmatrix}\begin{bmatrix}\psi\mathbf{v}_{\mathrm{w}}\\ \psi\mathbf{v}_{\Omega}\end{bmatrix}'' + [\psi\mathbf{v}_{\mathrm{w}}^{\mathrm{T}} \quad \psi\mathbf{v}_{\Omega}^{\mathrm{T}}]'\begin{bmatrix}\mathbf{K}^{\tau}_{\mathrm{ww}} & \mathbf{K}^{\tau}_{\mathrm{w}\Omega}\\ \mathbf{K}^{\tau}_{\Omega\mathrm{w}} & \mathbf{K}^{\tau}_{\Omega\Omega}\end{bmatrix}\begin{bmatrix}\psi\mathbf{v}_{\mathrm{w}}\\ \psi\mathbf{v}_{\Omega}\end{bmatrix}' \\ + [\psi\mathbf{v}_{\mathrm{w}}^{\mathrm{T}} \quad \psi\mathbf{v}_{\Omega}^{\mathrm{T}}]\begin{bmatrix}\mathbf{K}^{s} & \mathbf{0}\\ \mathbf{0} & \mathbf{0}\end{bmatrix}\begin{bmatrix}\psi\mathbf{v}_{\mathrm{w}}\\ \psi\mathbf{v}_{\Omega}\end{bmatrix} - (\psi\mathbf{v}_{\mathrm{w}}^{\mathrm{T}})\mathbf{r}_{\mathrm{w}}\varphi - (\psi\mathbf{v}_{\Omega}^{\mathrm{T}})'\mathbf{r}_{\Omega}\varphi\}dz\end{aligned} \tag{9}$$

To get a formulation resembling a generalization of Vlasov beam theory [9] the following three main steps are performed:

- In step I the shear constraint equations that bind axial and transverse modes together are introduced and at the same time Eq. (9) are simplified or condensed. In this process the singularity in the shear stiffness matrix related to pure axial extension is needed to be eliminated.
- In step II two eigenmodes corresponding to transverse translation of the cross section are identified and eliminated. Also a pure rotational eigenmode is identified for elimination in the next step. Furthermore the transverse displacement field is constrained, so that transverse normal strains in the middle surface of the cross section are not allowed, i.e. $w_{n,ss}=0$ is enforced, see Eq. (5).
- In step III the order of the coupled fourth order differential equations is reduced and the eigenvalue problem is condensed by removing singularities due pure St. Venant torsion.

Hereby the following condensed version of the final distortional differential equations is obtained:

$$\begin{bmatrix} \mathbf{K}^{s}_{uu} & \mathbf{0} \\ \mathbf{0} & -\mathbf{K}^{\sigma}_{ee} \end{bmatrix} \begin{bmatrix} \mathbf{v}^{u}_{w}\psi \\ \mathbf{v}^{e}_{w}\psi'' \end{bmatrix} - \begin{bmatrix} \overline{\mathbf{K}}^{\tau}_{uu} & -\overline{\mathbf{K}}^{\sigma}_{ue} \\ -\overline{\mathbf{K}}^{\sigma}_{eu} & -\overline{\mathbf{K}}^{\sigma}_{ee} \end{bmatrix} \begin{bmatrix} \mathbf{v}^{u}_{w}\psi \\ \mathbf{v}^{e}_{w}\psi'' \end{bmatrix}'' = \begin{bmatrix} \mathbf{r}^{\alpha u3}_{w} \\ \mathbf{r}^{e3}_{w} \end{bmatrix} \varphi + \begin{bmatrix} \mathbf{r}^{\alpha u3}_{\Omega} \\ \mathbf{r}^{e3}_{\Omega} \end{bmatrix} \varphi' \tag{10}$$

The block matrices and the transformed stiffness matrices, $\mathbf{K}$, are introduced in paper [1] while the load vectors, $\mathbf{r}$, are introduced in paper [2].

4. SOLUTION OF DISTORTIONAL EQUATIONS

The solution of the final condensed differential Eq. (10) is obtained by first seeking a solution to the homogeneous part of this fourth order matrix equation. In this context the following form of the solutions are postulated:

$$\psi(z) = e^{\xi z} \tag{11}$$

where ξ is a length scale parameter which may be complex. Inserting the postulated solution leads to the following homogeneous generalized linear matrix eigenvalue problem, in which the eigenvalues are ξ^2 and the eigenvectors are the searched distortional modes:

$$\begin{bmatrix} \mathbf{K}^{s}_{uu} & \mathbf{0} \\ \mathbf{0} & -\mathbf{K}^{\sigma}_{ee} \end{bmatrix} \begin{bmatrix} \mathbf{v}^{u}_{w} \\ \xi^2 \mathbf{v}^{e}_{w} \end{bmatrix} - \xi^2 \begin{bmatrix} \overline{\mathbf{K}}^{\tau}_{uu} & -\overline{\mathbf{K}}^{\sigma}_{ue} \\ -\overline{\mathbf{K}}^{\sigma}_{eu} & -\overline{\mathbf{K}}^{\sigma}_{ee} \end{bmatrix} \begin{bmatrix} \mathbf{v}^{u}_{w} \\ \xi^2 \mathbf{v}^{e}_{w} \end{bmatrix} = \begin{bmatrix} \mathbf{0} \\ \mathbf{0} \end{bmatrix} \tag{12}$$

Now the found eigenvectors are used to decouple the system of equations in (10). Transforming the distortional differential equations into the eigenmode space, by using the distortional modal matrix, $\mathbf{V}^{T}$, found for the homogeneous system, we get the final diagonalized and thus uncoupled set of differential equations of GBT (reduced system) including the load terms as

$$\begin{aligned} &\begin{bmatrix} \mathbf{v}^{u}_{w} \\ \mathbf{v}^{e}_{w}\xi^2 \end{bmatrix}_i^T \begin{bmatrix} \mathbf{K}^{s}_{uu} & \mathbf{0} \\ \mathbf{0} & -\mathbf{K}^{\sigma}_{ee} \end{bmatrix} \begin{bmatrix} \mathbf{v}^{u}_{w} \\ \mathbf{v}^{e}_{w}\xi^2 \end{bmatrix}_i \psi_{di} - \begin{bmatrix} \mathbf{v}^{u}_{w} \\ \mathbf{v}^{e}_{w}\xi^2 \end{bmatrix}_i^T \begin{bmatrix} \overline{\mathbf{K}}^{\tau}_{uu} & -\overline{\mathbf{K}}^{\sigma}_{ue} \\ -\overline{\mathbf{K}}^{\sigma}_{eu} & -\overline{\mathbf{K}}^{\sigma}_{ee} \end{bmatrix} \begin{bmatrix} \mathbf{v}^{u}_{w} \\ \mathbf{v}^{e}_{w}\xi^2 \end{bmatrix}_i \psi_{di}'' \\ &\qquad = \begin{bmatrix} \mathbf{v}^{u}_{w} \\ \mathbf{v}^{e}_{w}\xi^2 \end{bmatrix}_i^T \begin{bmatrix} \mathbf{r}^{\alpha u3}_{w} \\ \mathbf{r}^{e3}_{w} \end{bmatrix} \varphi + \begin{bmatrix} \mathbf{v}^{u}_{w} \\ \mathbf{v}^{e}_{w}\xi^2 \end{bmatrix}_i^T \begin{bmatrix} \mathbf{r}^{\alpha u3}_{\Omega} \\ \mathbf{r}^{e3}_{\Omega} \end{bmatrix} \varphi' \end{aligned} \tag{13}$$

which is abbreviated as

$$K^{g}_{ii}\psi_{di} - K^{d}_{ii}\psi_{di}'' = r^{d}_{w\,i}\phi + r^{d}_{\Omega\,i}\phi' \tag{14}$$

Normalizing Eq. (14) and specifying that the eigenvalue ξ_i^2 is equal to K^{g}_{ii}/K^{d}_{ii}, the following standard form is obtained:

$$\psi_{d\,i}{}''-\xi_i^{\,2}\psi_{d\,i}=-\frac{1}{K_{ii}^{d}}(r_{\mathrm{w}\,i}^{d}\phi+r_{\Omega\,i}^{d}\phi') \tag{15}$$

The introduced distortional stiffness and load terms are given in [2]. It should be noticed that $r_{\mathrm{w}\,i}^{d}\phi$ is the distortional moment load and $r_{\Omega\,i}^{d}\phi'$ is the distortional bimoment load.

Now the full solution of each of the uncoupled non-homogeneous linear 2. order differential equations in (15) is given by

$$\begin{aligned}\psi_{d\,i}(z) \;=\; & c_1e^{\xi_i z}+c_2e^{-\xi_i z}-\frac{1}{2\xi_i}e^{\xi_i z}\int e^{-\xi_i z}\frac{1}{K_{ii}^{d}}(r_{\mathrm{w}\,i}^{d}\varphi+r_{\Omega\,i}^{d}\varphi')\,dz\\ & +\frac{1}{2\xi_i}e^{-\xi_i z}\int e^{\xi_i z}\frac{1}{K_{ii}^{d}}(r_{\mathrm{w}\,i}^{d}\varphi+r_{\Omega\,i}^{d}\varphi')\,dz\end{aligned} \tag{16}$$

This concludes the determination of all the solutions for all the displacement modes of GBT. After having obtained and assembled all the full solution functions in $\widetilde{\boldsymbol{\Psi}}$ and in-plane modes in $\widetilde{\mathbf{V}}$, the full solution along the beam is presented in real numbers using the nodal solution vectors $u_{\mathrm{w}}(z)$ and $u_{\Omega}(z)$ as

$$\begin{aligned}\mathbf{u}_{\mathrm{w}}(\mathrm{z}) &= \widetilde{\mathbf{V}}_{\mathrm{w}}[\widetilde{\boldsymbol{\Psi}}_{\mathrm{h}}(\mathrm{z})\,\widetilde{\mathbf{c}}+\widetilde{\boldsymbol{\Psi}}_{\mathrm{p}}(\mathrm{z})\boldsymbol{\varphi}]\\ \mathbf{u}_{\mathrm{z}}(\mathrm{z}) &= -\widetilde{\mathbf{V}}_{\Omega}[\widetilde{\boldsymbol{\Psi}}'_{\mathrm{h}}(\mathrm{z})\,\widetilde{\mathbf{c}}+\widetilde{\boldsymbol{\Psi}}'_{\mathrm{p}}(\mathrm{z})\boldsymbol{\varphi}]\end{aligned} \tag{17}$$

The constants, $\widetilde{\mathbf{c}}$, have to be determined by the boundary conditions of the thin-walled beam.

5. BOUNDARY CONDITIONS

To determine the constants using displacement boundary conditions as in finite element formulations, the displacements at the boundary at the ends of the beam are needed, i.e. at $z=0$ and at $z=L$, where L is the length of the beam. As in [1,2] the assembled boundary displacement vector is denoted by u_b. Hereby the following equation for the determination of the solution constants is obtained:

$$\mathbf{u}_b=\begin{bmatrix}u_z^{a}(0)\\ \mathbf{u}_{\mathrm{w}}^{\mathrm{g}}(0)\\ \mathbf{u}_{\mathrm{w}}^{\mathrm{g}}{}'(0)\\ u_z^{a}(\mathrm{L})\\ \mathbf{u}_{\mathrm{w}}^{\mathrm{g}}(\mathrm{L})\\ \mathbf{u}_{\mathrm{w}}^{\mathrm{g}}{}'(\mathrm{L})\end{bmatrix}=\begin{bmatrix}-\mathbf{T}_{\Omega}^{\mathrm{a}\,\mathrm{T}}\widetilde{\mathbf{V}}_{\Omega}\widetilde{\boldsymbol{\Psi}}'_{\mathrm{h}}(0)\\ \mathbf{T}_{\mathrm{w}}^{\mathrm{g}\,\mathrm{T}}\widetilde{\mathbf{V}}_{\mathrm{w}}\widetilde{\boldsymbol{\Psi}}_{\mathrm{h}}(0)\\ \mathbf{T}_{\mathrm{w}}^{\mathrm{g}\,\mathrm{T}}\widetilde{\mathbf{V}}_{\mathrm{w}}\widetilde{\boldsymbol{\Psi}}'_{\mathrm{h}}(0)\\ -\mathbf{T}_{\Omega}^{\mathrm{a}\,\mathrm{T}}\widetilde{\mathbf{V}}_{\Omega}\widetilde{\boldsymbol{\Psi}}'_{\mathrm{h}}(\mathrm{L})\\ \mathbf{T}_{\mathrm{w}}^{\mathrm{g}\,\mathrm{T}}\widetilde{\mathbf{V}}_{\mathrm{w}}\widetilde{\boldsymbol{\Psi}}_{\mathrm{h}}(\mathrm{L})\\ \mathbf{T}_{\mathrm{w}}^{\mathrm{g}\,\mathrm{T}}\widetilde{\mathbf{V}}_{\mathrm{w}}\widetilde{\boldsymbol{\Psi}}'_{\mathrm{h}}(\mathrm{L})\end{bmatrix}\widetilde{\mathbf{c}}+\begin{bmatrix}-\mathbf{T}_{\Omega}^{\mathrm{a}\,\mathrm{T}}\widetilde{\mathbf{V}}_{\Omega}\widetilde{\boldsymbol{\Psi}}'_{\mathrm{p}}(0)\\ \mathbf{T}_{\mathrm{w}}^{\mathrm{g}\,\mathrm{T}}\widetilde{\mathbf{V}}_{\mathrm{w}}\widetilde{\boldsymbol{\Psi}}_{\mathrm{p}}(0)\\ \mathbf{T}_{\mathrm{w}}^{\mathrm{g}\,\mathrm{T}}\widetilde{\mathbf{V}}_{\mathrm{w}}\widetilde{\boldsymbol{\Psi}}'_{\mathrm{p}}(0)\\ -\mathbf{T}_{\Omega}^{\mathrm{a}\,\mathrm{T}}\widetilde{\mathbf{V}}_{\Omega}\widetilde{\boldsymbol{\Psi}}'_{\mathrm{p}}(\mathrm{L})\\ \mathbf{T}_{\mathrm{w}}^{\mathrm{g}\,\mathrm{T}}\widetilde{\mathbf{V}}_{\mathrm{w}}\widetilde{\boldsymbol{\Psi}}_{\mathrm{p}}(\mathrm{L})\\ \mathbf{T}_{\mathrm{w}}^{\mathrm{g}\,\mathrm{T}}\widetilde{\mathbf{V}}_{\mathrm{w}}\widetilde{\boldsymbol{\Psi}}'_{\mathrm{p}}(\mathrm{L})\end{bmatrix}=\widetilde{\mathbf{A}}\widetilde{\mathbf{c}}+\widetilde{\mathbf{B}} \tag{18}$$

$$\Rightarrow\quad \widetilde{\mathbf{c}}=\widetilde{\mathbf{A}}^{-1}(\mathbf{u}_b-\widetilde{\mathbf{B}})$$

Here the matrices $\widetilde{\mathbf{A}}$ and $\widetilde{\mathbf{B}}$ are introduced, were $\widetilde{\mathbf{A}}$ is an invertible positive definite matrix. In the following example all boundary displacements are chosen to be zero. This is to compare the influence of the load with a similar finite element context with built in edges. Hereby Eq. (18) is presented as

$$\mathbf{u}_b^{T}=[0\quad 0\quad 0\quad 0\quad 0\quad 0]^{T} \tag{19}$$

which is used in the following example.

6. EXAMPLE

By using an example, some nodal displacement results of GBT will now be compared to results found using the commercial FE program Abaqus. A lipped channel beam is considered with a load as shown in Fig. 3.

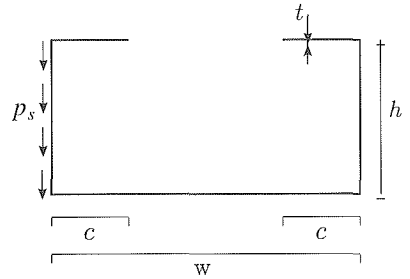

Fig. 3: Geometry, parameter values and load for the lipped channel

The load is 0.1 N/mm, uniformly distributed as shown in Fig. 3 and hereby given by a cross-section load distribution multiplied by $\varphi(z)=1$. The dimensions of the cross-section are w=100 mm, h=50 mm, c=25 mm and t=2 mm. Furthermore the beam has a length of L=2000 mm, an elasticity modulus $E=2.1\cdot10^5$ MPa and a Poisson ratio of ν=0.3. The comparison results found by using Abaqus are based on isotropic material and the S4 shell element with full 4 point integration. The linear elastic finite element calculations are based on a structured rectangular mesh with a side length seed of 10 mm.

First the solution of the final condensed differential equation is found by solving the homogeneous generalized linear matrix eigenvalue problem in Eq. (12) including the geometry and parameter values as described above. Solving the eigenvalue problem leads to a number of modes corresponding to the number of degree of freedom. Some of the relevant eigenvalues are shown in Table 1, and the corresponding modes are shown in Fig. 4.

Table 1: Eigenvalues ξ^2 and corresponding length scale parameters ξ

Mode	Eigenvalue ξ^2	Length scale parameter ξ
0	0	0
1	0	0
2	0	0
3	0	0
4	$0.37\cdot10^{-6}$	$0.61\cdot10^{-3}$
5	$3.36\cdot10^{-6}-2.65\cdot10^{-5}i$	$\pm(3.88\cdot10^{-3}-3.42\cdot10^{-3}i)$
6	$3.36\cdot10^{-6}+2.65\cdot10^{-5}i$	$\pm(3.88\cdot10^{-6}+3.42\cdot10^{-3}i)$
7	$4.23\cdot10^{-6}-5.00\cdot10^{-5}i$	$\pm(5.22\cdot10^{-3}-4.80\cdot10^{-3}i)$
8	$4.23\cdot10^{-6}+5.00\cdot10^{-5}i$	$\pm(5.22\cdot10^{-3}+4.80\cdot10^{-3}i)$
9	$825.6\cdot10^{-6}$	$\pm28.7\cdot10^{-3}$
10	$951.1\cdot10^{-6}$	$\pm30.8\cdot10^{-3}$
11	$1823\cdot10^{-6}$	$\pm42.7\cdot10^{-3}$
12	$3359\cdot10^{-6}$	$\pm58.0\cdot10^{-3}$

Here mode 0-3 are global beam modes, mode 4-8 are non-local distortional modes and mode 9-12 are local distortional modes. From table 1 it is seen that some of the important distortional modes and related eigenvalues are complex, come in pairs and that the imaginary

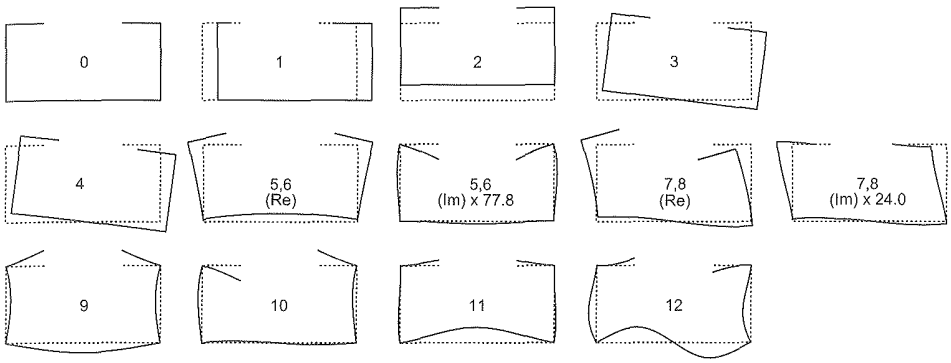

Fig. 4: Lipped channel – 13 in-plane deformation mode shapes.

part of the conjugated mode changes sign. It is also observed that all the eigenvalues concerning the distortional local modes (9-12) are real. However, also complex solutions for a few high number local distortional modes are obtained and it is not known whether other cross-sections may produce real distortional modes.

Using the found eigenvectors to decouple the system of equations in (10), it is possible to find the full solution of each of the uncoupled non-homogeneous linear 2. order differential equations in Eq. (16). Having obtained and assembled all the full solution functions and in-plane modes, the full solution along the beam can be presented in the nodal solution vectors $\mathbf{u}_w(z)$ and $\mathbf{u}_\Omega(z)$ using (17). Using the full solution in Eq. (17) with parameters, discretization and distributed cross-section load as given and shown in Fig. 3 leads to the deformations shown in Fig. 5 and table 2.

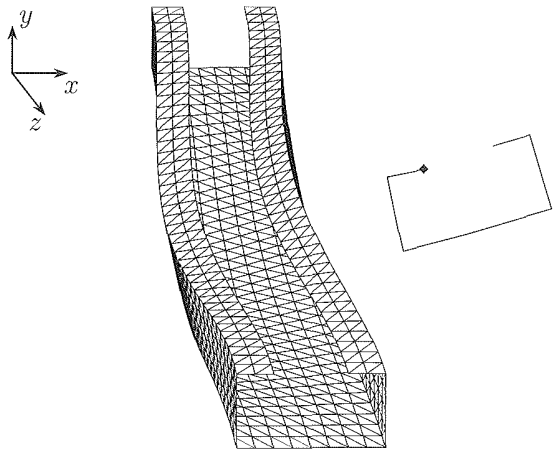

Fig. 5: GBT plot of the lipped channel with a torsional load

Table 2: Nodal displacements of GBT and FE analysis

	GBT (mm)	Abaqus (mm)	Diff. (%)
u_x	-4.719	-4.824	2.2
u_y	-6.892	-7.135	3.4

Comparing a nodal displacement of GBT to the one found from a model in the commercial FE program Abaqus, gives the values and the corresponding deviations shown in Table 2. The

value corresponds to the node marked on the deformed cross-section plot of the GBT solution in Fig. 5 at mid-span of the beam. From table 2 the deviation from Abaqus results of the displacement, u_x, in the horizontal direction is 2.2% and the deviation for the vertical direction, u_y, is 3.4%. These deviations can be explained by the formulation of the present theory, which is based on a beam theory where the shear deformations are neglected.

7. CONCLUSIONS

A novel finite-element-based displacement approach is shortly presented, where specific distortional displacement fields, which decouple the differential equations for generalized beam theory (GBT), was determined via a semi-discretization process. The distortional displacement fields were found as solutions to a distortional homogeneous eigenvalue problem which produce distortional displacement eigenmodes. Using the distortional modal matrix found for the homogeneous system the final uncoupled set of distortional differential equations including the load terms was formulated and the full solution was given, including an illustrative example. The presented approach is a theoretical improvement of the traditional GBT approach, in view of the fact that the obtained GBT equations are now solved analytically and the formulation is valid for open as well as closed single or multi cell cross-sections without special attention.

References

[1] Jönsson J, Andreassen MJ. "Distortional eigenmodes and homogeneous solutions for semi-discretized thin-walled beams", *Thin-Walled Structures,* doi:10.1016/j.tws.2010.12.009, 2011.

[2] Andreassen MJ, Jönsson J. "Distortional solutions for loaded semi-discretized thin-walled beams", *Thin-Walled Structures*, Submitted, 2010.

[3] Schardt R. "Eine Erweiterung der technischen Biegelehre für die Berechnung biegesteifer prismatischer Faltwerke", *Der Stahlbau*, 35, 161–171, 1966.

[4] Schardt R. "Verallgemeinerte Technische Biegetheorie", *Springer-Verlag*, Germany, 1989.

[5] Davies JM, Leach P. "First-order generalised beam theory", *J. Construct. Steel Research*, 31(2-3), 187–220, 1994.

[6] Jönsson J. "Distortional theory of thin-walled beams", *Thin-Walled Structures*, 33, 269–303, 1999.

[7] Silvestre N, Camotim D. "First-order generalised beam theory for arbitrary orthotropic materials", *Thin-Walled Structures*, 40, 755–789, 2002.

[8] Hanf M. "Die geschlossene Lösung der linearen Differentialgleichungssysteme der Verallgemeinerten Technischen Biegetheorie mit einer Anwendung auf die Ermittlung plastischer Grenzlasten", *Instituts für Werkstoffe und Mechanik im Bauwesen der TU Darmstadt*, 9, 1989.

[9] Vlasov VZ. "Thin-walled elastic beams", 2nd ed., *Israel Program for Scientific Translations*, Jerusalem, Israel, 1961.

Appendix H

Paper VII

Jeppe Jönsson and Michael Joachim Andreassen, (2012).

A semi-discretization approach to generalized beam theory and analytical solutions of the generalized column equations.

Full conference abstract published in Proceedings of the 8th EUROMECH Solid Mechanics Conference - Mini-Symposia, Graz, Austria.

A Semi-Discretization Approach to Generalized Beam Theory and Analytical Solutions of the Generalized Column Equations

Jeppe Jönsson[†], **Michael Joachim Andreassen**[†]

[†]DTU Civil Engineering, Technical University of Denmark,
Brovej Building 118, DK-2800 Kgs. Lyngby, Denmark
jej@byg.dtu.dk

ABSTRACT

A generalized beam theory can be formulated based on the assumption that the displacements can be described as a sum of displacement fields. These displacement fields are each assumed to be separable into the products of functions of the local transverse coordinates and functions of the axial coordinate z. Thus in a single displacement field as shown in Fig. 1 the transverse displacements are described by the product of a transverse displacement mode $\mathrm{w}_n(s)$, $\mathrm{w}_s(s)$ and a function $\psi(z)$ of the axial coordinate. Further more due to shear constraints the related axial warping of the transverse displacement is described by the product of the related warping function $\Omega(s)$ and the derivative $\psi\,'(z)$ of the axial function. To establish these displacement

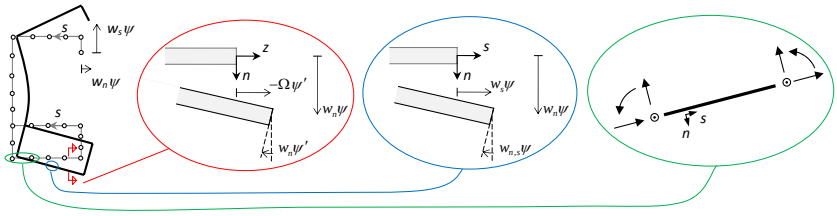

Figure 1: Displacement assumptions and discretization of the cross section in a straight elements.

fields the thin-walled cross section is discretized in elements in which the displacement modes and warping functions are interpolated. Introducing the constraining assumptions of beam theory the remaining degrees of freedom of the interpolated functions are $\tilde{\mathbf{v}}_\mathrm{w}$. Thus the thin-walled beam has been semi-discretized and the governing differential equilibrium equations for determination of the transverse displacement modes $\tilde{\mathbf{v}}_\mathrm{w}$ and the axial variation $\psi(z)$ takes the following form

$$\widetilde{\mathbf{K}}^{\sigma}\tilde{\mathbf{v}}_\mathrm{w}\psi'''' - \left[\widetilde{\mathbf{K}}^{\tau} + \lambda\widetilde{\mathbf{K}}^{0}\right]\tilde{\mathbf{v}}_\mathrm{w}\psi'' + \widetilde{\mathbf{K}}^{s}\tilde{\mathbf{v}}_\mathrm{w}\psi = \mathbf{0} \tag{1}$$

in which the matrices $\widetilde{\mathbf{K}}^{\sigma}$, $\widetilde{\mathbf{K}}^{\tau}$, $\widetilde{\mathbf{K}}^{0}$ and $\widetilde{\mathbf{K}}^{s}$ correspond to axial stiffness, shear stiffness, initial stress influence and transverse stiffness respectively. The magnitude of the initial stress is governed by the λ factor. The semi-discretization approach treated in this paper is developed in [1]-[3]. In the classic stability theory the solution functions $\psi(z) = e^{\xi z}$ are normally assumed to be trigonometric functions, $\psi(z) = e^{i\mu z} = \sin\mu z = \sin(n\pi z/L)$, in order to satisfy

suitable simple boundary conditions. These solutions are illustrated as the conventional half wavelength buckling curves or so called cross section signature curves in the upper left part of Fig. 2. On the other hand seeking general solutions to the differential equations it is necessary to fix the initial stress level and thus perform calculations with fixed values of λ. Furthermore it is necessary to reduce the order of the differential equations and introduce a state vector with twice the number of dof. Through solution of the related linear eigenvalue problem of double size the state space displacement solutions are identified. The eigenvalues ξ are functions of the initial stress level and correspond to complex solution length scales (π/ξ) plotted in the upper right part of Fig. 2. The changes in solution modes and length scales are shown in the lower part of the figure.

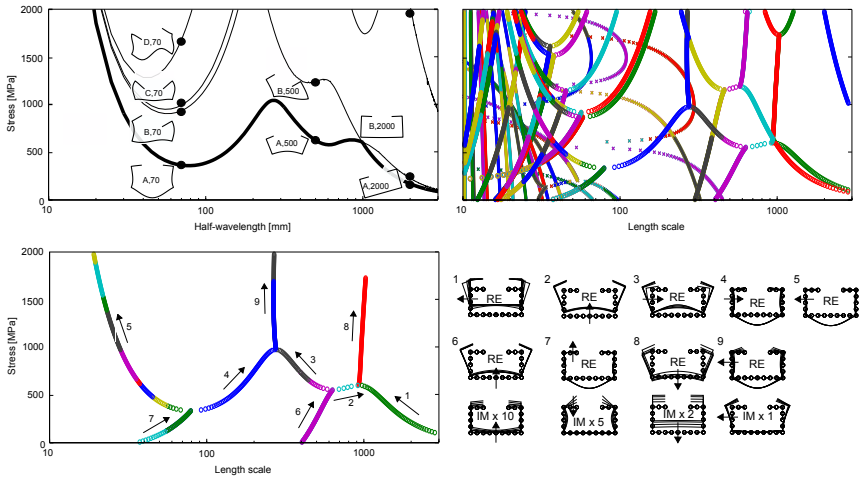

Figure 2: Signature curves, solution length scale curves and solution mode development.

References

[1] J. Jönsson and M.J. Andreassen. Distortional eigenmodes and homogeneous solutions of semi-discretized thin-walled beams. *Thin-Walled Structures* **49**: 691–707, 2011.

[2] M.J. Andreassen and J. Jönsson. Distortional solutions for loaded semi-discretized thin-walled beams. *Thin-Walled Structures* **50**: 116-127, 2012.

[3] M.J. Andreassen and J. Jönsson. Distortional buckling modes of semi-discretized thin-walled columns. *Thin-Walled Structures* **51**: 53-63, 2012.

In several industries such as the civil, mechanical and aerospace, thin-walled structures are often used due the high strength and effective use of the materials. Because of the increased consumption there has been increasing focus on optimizing and more detailed calculations. However, more detailed calculations are very time consuming, if not impossible, due to the large amount of degrees of freedom needed.

This thesis deals with a novel mode based semi-discretization approach concerning more detailed calculations in the context of distortion of the cross section and model distortion by a limited number of degrees of freedom. This new approach is a considerable theoretical and practical development, since the obtained differential equations of generalized beam theory are now solved analytically and the formulation is valid without special attention and approximation also for closed single or multi-cell cross sections.

DTU Civil Engineering
Department of Civil Engineering
Technical University of Denmark

Brovej, Building 118
2800 Kgs. Lyngby
Telephone 45 25 17 00

www.byg.dtu.dk

ISBN: 9788778773555
ISSN: 1601-2917